

# Green Building, Environment, Energy and Civil Engineering

---

Editors: Jimmy C.M. Kao & Wen-Pei Sung







**Taylor & Francis**

Taylor & Francis Group

<http://taylorandfrancis.com>

PROCEEDINGS OF THE 2016 INTERNATIONAL CONFERENCE ON GREEN BUILDING,  
MATERIALS AND CIVIL ENGINEERING (GBMCE2016), HONG KONG, CHINA, 26–27  
APRIL 2016

# Green Building, Environment, Energy and Civil Engineering

*Editors*

**Jimmy C.M. Kao**

*Institute of Environmental Engineering, National Sun Yat-Sen University,  
Kaohsiung, Taiwan*

**Wen-Pei Sung**

*Department of Landscape Architecture,  
Integrated Research Center for Green Living Technologies,  
National Chin-Yi University of Technology, Taichung, Taiwan*



**CRC Press**

Taylor & Francis Group

Boca Raton London New York Leiden

---

CRC Press is an imprint of the  
Taylor & Francis Group, an **informa** business

A BALKEMA BOOK

Description of cover illustration: blue\_science\_building

Year: 2014

copyright holder: Wenli Yao

*CRC Press/Balkema is an imprint of the Taylor & Francis Group, an informa business*

© 2017 Taylor & Francis Group, London, UK

Typeset by V Publishing Solutions Pvt Ltd., Chennai, India

All rights reserved. No part of this publication or the information contained herein may be reproduced, stored in a retrieval system, or transmitted in any form or by any means, electronic, mechanical, by photocopying, recording or otherwise, without written prior permission from the publisher.

Although all care is taken to ensure integrity and the quality of this publication and the information herein, no responsibility is assumed by the publishers nor the author for any damage to the property or persons as a result of operation or use of this publication and/or the information contained herein.

Published by: CRC Press/Balkema  
P.O. Box 11320, 2301 EH Leiden, The Netherlands  
e-mail: [Pub.NL@taylorandfrancis.com](mailto:Pub.NL@taylorandfrancis.com)  
[www.crcpress.com](http://www.crcpress.com) – [www.taylorandfrancis.com](http://www.taylorandfrancis.com)

ISBN: 978-1-138-02964-4 (Hbk)

ISBN: 978-1-315-37510-6 (eBook)

## Table of contents

Preface	xi
Committee	xiii
Board members	xv
Safety problems and control measures in the construction of the building project <i>M.-L. Guo &amp; S.-P. Huang</i>	1
Study on protecting and inheriting the traditional crafts and the contemporary design education <i>L.-S. Hao &amp; L.-L. Chen</i>	5
Financial accounting of long-term equity investment <i>J. Wu</i>	11
Workflow design and analysis of the function of a PLC ship power station management system <i>S.-C. Jiang, X.-P. Sui, Z.-Z. Liu, S. Wu &amp; Y.-Z. Geng</i>	15
Suitability of electrochemical methods to evaluate the corrosion of reinforcing steel in micro-cell and macro-cell states <i>Z.-L. Cao, H.-Y. Chen, Z.-C. Su, S.-D. Mi, L.-Y. Wei &amp; M. Hibino</i>	19
Green consumption attitudes of the tourists lodging in resort hotels <i>C.-C. Lin &amp; W.-T. Wu</i>	25
Comparison of prediction models for shrinkage and creep of high-strength, lightweight aggregate concrete <i>S.-Q. Mei, H.-B. Xie, L. Su, J. Gong, K. Guo &amp; Y.-F. Wang</i>	31
Social impact assessment of green residential district in China <i>L. Fan, Y.-X. Zhang, Y.-R. Zhang, B. Pang, J.-J. Wang &amp; W. Luo</i>	37
Problems of and strategies for financial fund management of enterprises <i>J. Wu</i>	41
Mono-layer reticulated shell structure design <i>L. Mi</i>	45
Research on the neural network based on an improved PSO algorithm <i>J. Liu</i>	49
Study of the consolidation effect of a marginal bank by vacuum preloading based on a network <i>C.-H. Wang</i>	55
Design of the man-machine interface for the operating system of two-for-one twister <i>Q. Shen, Y.-B. Ni &amp; Q.-H. Zhou</i>	59
Design of the measurement standard for ultrasonic PD tester <i>Q. Wang, J. Zhang, W. Zhou, B. Lu &amp; X.-C. Rao</i>	65
Summary of the research on a network fault prediction method <i>W.-Q. Xu, G.-S. Chen, G. Niu &amp; W.-G. Chen</i>	71
Study of the green design strategies of the senior housing in Wuhan <i>J. Lu</i>	77

Survey and analysis of intellectual capital of scientific research team <i>F.-L. Chen</i>	81
A fuzzy DEMATEL method to analyze the criteria for sustainable supplier selection <i>X.-L. Jiang, Z.-B. Wu &amp; Y. Yang</i>	85
Research on ecological reconstruction strategies for the Shanghai Shendu Building <i>M. Gao</i>	93
Applications of the passive solar energy technology in office buildings in Changchun <i>J. Qiu &amp; T.-L. Zhao</i>	99
Study of the effects and applications of fiber art on the indoor space <i>H.-B. Sun</i>	103
Finite element analysis on shear lag effect of concrete curved box girder under moving loads <i>H.-L. Lu, C.-Y. Wan, X.-L. Zhou, J.-Q. Qian, B. Chen &amp; S.-B. Zhu</i>	107
Application of soundscape in city parks by case study <i>J.-L. Zhou &amp; L.-F. Xie</i>	113
RCS terminal test <i>X.-F. Ren &amp; J.-F. Zhao</i>	119
Research on Shanghai ecological residence green ecological technology <i>M. Gao</i>	125
Study on the modern dilemma of the Chinese traditional literati painting <i>Z.-H. Zhang</i>	129
Reliability analysis of pre-stressed concrete continuous girder bridges using the incremental launching method on Chinese code and BS5400 <i>C.H. Lou &amp; F.H. Dong</i>	133
Stability analysis of underground roadways in large fault zones <i>Y.-F. Su, P. Wang &amp; J. Zhai</i>	137
Effect of sputtering time on the micro-hardness of QC-10 alloy <i>M. Hu, X.-X. Ren, Y.-L. Zhang, J. Gao &amp; P.-L. Ding</i>	141
Automatic incident detection algorithm based on under-sampling for imbalanced traffic data <i>M.-H. Li, S.-Y. Chen &amp; Y.-C. Lao</i>	145
Stress calculation and analysis of cut-off wall in the sand gravel foundation <i>X.-M. Dong, Z.-Z. Wei, J.-T. Niu &amp; W.-L. He</i>	151
Stress distribution of anchor bolts due to empty pulp defects <i>S. Zeng, J. Zhang &amp; B. Sun</i>	155
Damage laws of layered and jointed rock mass under the impact of cyclic loading <i>B. Sun, X.-S. Deng, J.-H. Xie &amp; S.-Q.-Y. Zhang</i>	159
Heating characteristics of microwave-absorbing asphalt mixture <i>W. Liu, P.-H. Miao &amp; S.-Y. Wang</i>	163
Numerical analysis of the influence range of a tunnel ventilation resistance grid <i>Y.-X. Xin, Y.-Q. Wang &amp; K. Lai</i>	169
Degradation of benzo[a]pyrene (BaP) in clay soil by electro-bioremediation <i>D.N. Huang, Z.S. Ai, J. Tan, Y.J. Zhao &amp; J.X. Fu</i>	175
Study of the cable breaking effect on the structural characteristics of cable-stayed bridges <i>W.-F. Tang</i>	181
Passive and energy-efficient house design based on the climate of Tianjin <i>Y.F. Zhao, Z.R. Wang &amp; Y.X. Tian</i>	185
Location information provider framework using the open IoT technology <i>N. Kim, J. Park &amp; E. Choi</i>	191

Review of three-dimensional braided piezoelectric ceramic matrix composite <i>X. Ma &amp; G.-F. Wei</i>	195
Analysis of deformation of a transmission tower by vacuum-combined surcharge preloading <i>B.B. Xu &amp; W. Si</i>	199
Numerical modeling of air flow and pollutant distribution in industrial workshop with different solar chimney on the roof <i>Y.-F. Xue, X.-Z. Zhang, Y.-X. Su &amp; W.-Y. Deng</i>	203
Test and analysis of hydration heat for the zero block of a continuous rigid frame bridge <i>H.B. Zhang, C.L. Lv, M. Ma, S.B. Chai &amp; X. Ren</i>	209
A review on load forecasting of town gas: Methods, applications, and analyses <i>H. Y. Tan, N. Li &amp; C. Y. Tang</i>	215
Distributed temperature sensor- and fiber Bragg grating sensor-based method for gas pipeline leakage detection <i>T. Li, H.-D. Gong, L.-C. Su &amp; Q. Li</i>	219
Study on the re-utilization of wasted civil air defense project <i>X.-Y. Zu &amp; L.-C. Su</i>	223
GPR scan assessment of pressure mortar quality in a tunnel vault <i>S.-L. Tian &amp; M. Cui</i>	227
Research on existing residential building refurbishment in the urban area of cold climate region in China based on the aging population trend <i>Z.-G. Chen &amp; Y. Zhang</i>	233
Assessment of isolation methods for the erected tower near soft road embankment <i>B.B. Xu &amp; W. Si</i>	237
Research on variable water volume collaborating with a variable water temperature operation scheme <i>H. Y. Tan &amp; F. Cai</i>	241
Corrosion resistance of a plasma ion-implanted QC-10 alloy <i>M. Hu, X.-X. Ren, Y.-L. Zhang, J. Gao &amp; P.-L. Ding</i>	245
Exploring research theories and methods of rural settlement landscape from a multidisciplinary perspective <i>N.-X. Wang &amp; Q. Lu</i>	249
Research on reinforced methods for a concrete structure <i>M.-X. Zhang, B. Sun &amp; X.-Y. Zhang</i>	253
Analysis of the factors influencing energy consumption of a passenger transport station <i>X.-K. Meng, Z. Yan, W.-W. Heng &amp; C. Zeng</i>	257
Environmental development of the reading room in the university library based on human factors engineering <i>C.-J. Xu</i>	261
A study on the optimization of green light sources in subway stations <i>Z.-C. Zhao</i>	265
A study on the mechanical properties of mechanism sand mortars subjected to different temperatures <i>H.-J. Xu &amp; C.-X. Cen</i>	269
Study on numerical simulation of three-dimensional viscoelastic mechanics for steel deck asphalt pavement <i>W.-K. Huang, X.-N. Zhang, H.-L. Rong &amp; S.-F. Cai</i>	273
Analysis of fluctuation in China's remaining recoverable oil reserves <i>L. Wang &amp; J.S. Zhang</i>	279

Research on the recycled brick concrete technology <i>M.-X. Zhang, X.-Y. Zhang &amp; B. Sun</i>	285
A comprehensive information system for landslide monitoring based on a three-dimensional geographic information system <i>M.-W. Xie, Y.-C. Jia, F.-X. Lv &amp; S.-X. Chang</i>	289
Study on the compatibility of the art design major and the Chinese language course in the colleges and universities of fine arts <i>M.-Y. Liang &amp; Z.-X. Ge</i>	295
The calibration of refinery wastewater treatment process <i>D.-L. Cheng &amp; L.-H. Yan</i>	299
Relationship between microcell corrosion and macrocell corrosion of reinforcing steel in concrete structures <i>Z.-L. Cao, S.-D. Mi, H.-Y. Chen, Z.-C. Su, L.-Y. Wei &amp; M. Hibino</i>	303
The application of an active filter based on FPGA in a large building <i>Y. Lou &amp; X.-J. Wang</i>	309
Crouching suspicions, hidden potential: A literature review on US–China clean energy cooperation since 2009 <i>Y.-N. Ding &amp; J. Shi</i>	313
Research on the crack resistance ability of hybrid fiber reinforced concrete <i>X.-K. Liu, Z.-Q. Du, J.-X. Hui &amp; Y. Gao</i>	317
Fabrication and characterization of B <sub>4</sub> C ceramics with Al <sub>2</sub> O <sub>3</sub> -La <sub>2</sub> O <sub>3</sub> aids <i>Y.-L. Zhang, Y.-M. Zhang, X.-S. Ding, M. Hu, C.-L. Ma &amp; C.-H. Li</i>	321
An experimental study on eccentric compression reinforced concrete columns strengthened with HDPFs <i>Y. Qiao, C.Z. Sun, Z.B. Wang &amp; G. Zuo</i>	325
Road traffic conflict prediction model based on speed dispersion in mixed traffic environment <i>X. Xia &amp; J.-Y. Gai</i>	331
A review on the current development and debate of the global green new deal <i>Y.-N. Ding &amp; J. Tang</i>	337
Toward a more compact and sustainable city—the use of underground space for Chinese mainland cities <i>J.-Y. Chen, L.-M. Huang &amp; L.-C. Su</i>	341
Natural ventilation and seismic performance analysis of the special L-shaped spiral layout green building <i>X.-D. Li, W.-J. Li, H. Yang &amp; Z.-T. Chen</i>	345
Effect of freezing and thawing on the physical properties of red sandstone <i>H.-M. Zhang, X.-N. Liu, C. Peng &amp; X.-Z. Meng</i>	351
Effect of surface microstructural features of injection-molded zirconia on the construction of dental implants <i>C.-C. Wang, M.-H. Lin, S.-L. Chen, C.-C. Lin, Y.-C. Liu &amp; C.-Y. Lin</i>	355
Application of the catenary method and FBG sensors to monitoring ice thickness of power transmission lines <i>L.-M. Li, Z.-M. Liu, Z.-G. Zhang &amp; C.-L. Liu</i>	359
Low temperature synthesis of CNTs on the micron-sized Cu <sub>p</sub> surface <i>P.-L. Ding, Y.-L. Zhang, M. Hu &amp; J. Gao</i>	363
An experimental study on stiffness degradation of reinforced concrete columns strengthened with HDPF <i>Y. Qiao, C.Z. Sun, Z.B. Wang &amp; G. Zuo</i>	367



Architectural design strategies of zero-energy houses in a solar decathlon competition <i>C. Chen &amp; X.-P. Liu</i>	373
Hot pressure sintering of BN-SiC composites with $\text{La}_2\text{O}_3$ - $\text{Al}_2\text{O}_3$ aids <i>Y.-L. Zhang, Y.-M. Zhang, Z.-H. Shao, M. Hu, Y. Li, J.-P. Gong, B. Li &amp; Y.-H. Zhang</i>	379
Optimization of electric vehicle charging infrastructure and model simulation through the Jeju electric vehicle demonstration project <i>J. Gu, J. Lee &amp; J. Lee</i>	383
Research on the impact of the fault's thickness on underground roadways <i>M.-H. Zhang, P. Wang &amp; L.-L. Shao</i>	387
Study on the selection of adaptable plants in the area polluted with lead-zinc tailings in Hunan Province <i>Q. Wang, W. Sun &amp; L.-L. Wu</i>	391
Research on development and utilization of the empty layer space of Nanjing Weisanlu Yangtze River Tunnel <i>L.-C. Su, X.-P. Zhu, X.-Y. Zu &amp; W.-N. Hou</i>	397
Study of rural landscape design ideas <i>X.-Y. Zhang</i>	403
Author index	407



**Taylor & Francis**

Taylor & Francis Group

<http://taylorandfrancis.com>

## Preface

On the successful basis of GBMCE 2011, 2012, 2013, 2014, the 5th International Conference on Green Building, Materials and Civil Engineering (GBMCE) was held in Hong Kong, on April 17–18, 2016. The conference aimed mainly at promoting the development of green building, energy, environmental and civil engineering, strengthening the international academic cooperation and communications, and exchanging research ideas.

Energy and environmental problems have become more and more serious in recent years, so energy and environmental problems must be considered in construction and civil engineering. This book brings together about 85 peer-reviewed papers on Green Building, Energy, Environment, Materials and Civil Engineering and provides the readers a broad overview of the latest advances in the field of Energy, Environment and Civil Engineering.

On behalf of the guest editor for this conference book, I would like to thank the conference organization staff, and the members of the International Technological Committees for their hard work. We look forward to seeing all of you next year at GBMCE 2017.

October, 2016

Wen-Pei Sung  
*National Chin-Yi University of Technology*



**Taylor & Francis**

Taylor & Francis Group

<http://taylorandfrancis.com>

## Committee

### CONFERENCE CHAIRS

Prof. Wen-Pei Sung, *National Chin-Yi University of Technology, Taiwan*  
Prof. Jimmy C.M. Kao, *National Sun Yat-Sen University, Taiwan*

### INTERNATIONAL TECHNOLOGICAL COMMITTEES

Prof. Yu-Kuang Zhao, *National Chin-Yi University of Technology, Taiwan*  
Prof. Ron Chen, *Chung Hua University, Taiwan*  
Prof. Wen-Sheng Ou, *National Chin-Yi University of Technology, Taiwan*  
Yoshinori Kitsutaka, *Tokyo Metropolitan University, Japan*  
Nasrudin Bin Abd Rahim, *University of Malaya, Malaya*  
Yan Wang, *The University of Nottingham, UK*  
Zhi Jian Wang, *China Academy of Science, China*  
Darius Bacinskas, *Vilnius Gediminas Technical University, Lithuania*  
Qing-Lin Meng, *South China University of Technology, China*  
Li-Xin Guo, *Northeastern University, China*  
Cheer Germ Go, *National Chung Hsing University, Taiwan*  
Liu Yunan, *University of Michigan, USA*  
Ye-Cai Guo, *Nanjing University of Information Science and Technology, China*  
Wang Liying, *Institute of Water Conservancy and Hydroelectric Power, China*  
Chenggui Zhao, *Yunnan University of Finance and Economics, China*  
Rahim Jamian, *Universiti Kuala Lumpur Malaysian Spanish Institute, Malaysia*  
Gang Shi, *Inha University, South Korea*  
Bhagavathi Tarigoppula, *Bradley University, USA*  
Yean-Der Kuan, *National Chin-Yi University of Technology, Taiwan*  
Chen Wang, *University of Malaya, Malaya*  
Fu-Jen Wang, *National Chin-Yi University of Technology, Taiwan*  
Wei Song, *Minzu University of China, Tsinghua University, China*  
Shyr-Shen Yu, *National Chung Hsing University, Taiwan*  
Shen-Chuan Tai, *National Cheng Kung University, Taiwan*  
Jzau-Sheng Lin, *National Chin-Yi University of Technology, Taiwan*  
Rong-Chang Jou, *National Chi Nan University, Taiwan*  
Jeng-Min Huang, *National Chin-Yi University of Technology, Taiwan*  
Jiunn-Min Chang, *National Chin-Yi University of Technology, Taiwan*  
Hua-Zhi Hus, *National Kaohsiung Marine University, Taiwan*  
Shih-Heng Tung, *National University of Kaohsiung, Taiwan*  
Chi-Wun Lu, *National Chin-Yi University of Technology, Taiwan*  
Yu-Lieh Wu, *National Chin-Yi University of Technology, Taiwan*  
Chau-Cho Yu, *National University of Kaohsiung, Taiwan*  
Kuo-Tsang Huang, *National Taiwan University, Taiwan*  
Hsueh-Chun Lin, *China Medical University, China*  
Yao-Chiang Kan, *Yuan Ze University, Taiwan*  
Yao-Ming Hong, *Ming Dao University, Taiwan*  
Rey-Chue Hwang, *I-Shou University, Taiwan*  
Dyi-Cheng Chen, *National Changhua University of Education, Taiwan*

Shao-Wen Su, *National Chin-Yi University of Technology, Taiwan*  
Yi-Ying Chang, *National Chin-Yi University of Technology, Taiwan*  
P.S. Pa, *National Taipei University of Education, Taiwan*  
Cheng-Yi Yu, *National Chin-Yi University of Technology, Taiwan*  
Jun-Hong Lin, *Nanhua University, Taiwan*  
Lei Wei, *National Chin-Yi University of Technology, Taiwan*  
Kuang-Cheng Yu, *National Chin-Yi University of Technology, Taiwan*  
Ting-Yu Chen, *National Chin-Yi University of Technology, Taiwan*

CO-SPONSORED BY

National Chin-Yi University of Technology, Taiwan  
National Cheng Kung University, Taiwan  
National Sun Yan-Sen University, Taiwan  
National Chi Nan University, ChienKuo Technology University, Taiwan  
Control Engineering and Information Science Research Association, China  
International Frontiers of science and technology Research Association, China  
Trans Tech Publications, China

## Board members

Jimmy Kao, Ph.D., P.E., DEE, P.H., CGWP, D.WRE, F.ASCE, F.AAAS, F.EWRI, F.EASA

*Distinguished Professor and Academician*

*Institute of Environmental Engineering*

*National Sun Yat-Sen University*

*Kaohsiung, Taiwan*

*email: jkao@mail.nsysu.edu.tw*

Wen-Pei Sung, Ph.D., F.IET, F.ICDM, F. IETI, BCEEM, D.WRE, MASCE

*Distinguished Professor and Dean*

*College of Humanities and Creativity*

*National Chin-Yi University of Technology*

*Taichung, Taiwan*

*email: wps@ncut.edu.tw*

Y.K. Zhao, Ph.D.

*Professor*

*Department of Air Conditioning and Energy*

*National Chin-Yi University of Technology*

*Taiwan*

*email: zhao@ncut.edu.tw*

K.F. Chen, Ph.D.

*Profesor*

*Department of Civil Engineering*

*National Chi Nan University*

*Taiwan*

*email: kfchen@ncnu.edu.tw*

T.Y. Chen, Ph.D.

*Professor*

*Department of Landscape Architecture*

*National Chin-Yi University of Technology*

*Taiwan*

*email: tychen@ncut.edu.tw*

J.Y. Chen, Ph.D.

*Senior Researcher*

*Formosa Petrochemical Co.*

*Taiwan*

*email: d933030006@student.nsysu.edu.tw*

S.H. Liang, Ph.D.

*Biotechnology R&D Office*

*Taiwan VCM Corp.*

*Taiwan*

*email: shuhao@tvc.com.tw*



C.C. Chien, Ph.D.  
*Senior Researcher*  
*Green energy and Eco-system Center*  
*Industrial Technology Research Institute*  
*Taiwan*  
*email: varian@itri.org.tw*

Y.T. Sheu, Ph.D.  
*Researcher*  
*Institute of Environmental Engineering*  
*National Sun Yat-Sen University*  
*Taiwan*  
*email: ytsheu727@gmail.com*

Y.T. Tu, Ph.D.  
*Researcher*  
*Institute of Environmental Engineering*  
*National Sun Yat-Sen University*  
*Taiwan*  
*email: todow119@gmail.com*

# Safety problems and control measures in the construction of the building project

Mei-ling Guo & Shui-ping Huang

*Guangdong University of Science and Technology, Guangdong, P.R. China*

**ABSTRACT:** The building industry is an emerging pillar industry in China and is also a high-risk industry. Owing to the imperfect laws, low personnel quality, insufficient attention attached to the managers, backward technological equipment, etc., inevitably, the safety accidents have frequently taken place on the building industry, which have seriously affected the economic benefit and image of the enterprise, damaged the personal rights of the construction personnel, and hindered the timely completion of the project's construction tasks. Therefore, during the process of the project construction, strengthening the safety construction measures can effectively ensure that the project construction can be implemented step by step in accordance with the schedule and the project's construction tasks can be completed on time at required volume.

**Keywords:** construction of building project; safety; accident types; causes; control measures

## 1 INTRODUCTION

The building industry is one of the important industrial sectors of a country; however, the safety level for the building industry of various countries in the world is all lower than the average safety level for the industrial sectors of the country. In 2011, only 8% of the labor force in the United States was engaged in the building industry, but among the national industrial accidents of the year, the fatal accidents and the disability accidents from the building projects were as high as 18% and 12% respectively; in 2011, the casualty accidents from the building projects accounted for 28.8% of those from all the industrial sectors; in the same year, the accident death toll of per one hundred thousand people was about 30; however, the occurrence rate of the building project's safety accidents in Hong Kong was unexpectedly up to 20 times of that in Japan.

With the increasing the construction scale in China, the building industry has become an emerging pillar industry. Compared with the past, the building construction is featured by higher technology content, larger construction difficulty, and more urgent schedule, so that the risk in the project construction has also been increased accordingly, which thus inevitably will lead to the occurrence of the safety accidents in the process of construction. In recent years, along with the mass development of the building projects, the safety accidents have taken place frequently so that the situation has become more serious. In 2009, totally 673 casualty

accidents related to the building projects occurred in China, which led to a death toll of 794 people; in 2010, totally 756 casualty accidents related to the building projects occurred in China, which led to a death toll of 1225 people; in a word, the safety situation in the building project's construction is gloomy, to which we shall attach great importance.

## 2 TYPES OF SAFETY ACCIDENTS INVOLVED IN THE BUILDING PROJECT'S CONSTRUCTION

The building industry is a high-risk industry, which is prone to multiple types of safety incidents. For example, in 2009, the safety accidents involved in the building project's construction of China mainly include the following five types.

### 2.1 *Falling accident from high place*

Totally, 356 falling accidents from high place took place and 382 people died in consequence, which accounted for 52.7% and 48.1% of the total number of accidents and deaths, respectively.

### 2.2 *Collapse accident*

Totally, 94 collapse accidents took place and 161 people died in consequence, which accounted for 14.2% and 20.2% of the total number of accidents and deaths, respectively.

### 2.3 *Object strike accident*

Totally, 86 object strike accidents took place and 91 people died in consequence, which accounted for 12.7% and 11.3% of the total number of accidents and deaths, respectively.

### 2.4 *Electric shock accident*

Totally, 29 electric shock accidents took place and 32 people died in consequence, which accounted for 4.1% and 4.2% of the total number of accidents and deaths, respectively.

### 2.5 *Lifting injury accident*

Totally, 42 lifting injury accidents took place and 52 people died in consequence, which accounted for 6.5% and 6.6% of the total number of accidents and deaths, respectively.

## 3 CAUSES FOR THE FREQUENT SAFETY ACCIDENTS IN THE BUILDING PROJECT'S CONSTRUCTION

Frequent safety accidents in the building project's construction not only will bring about the enormous economic loss and reputational damage to the enterprise, but also will generate the misfortune for the families of the accident victims and such events might affect the social harmony and stability. Specifically, the causes for the frequent safety accidents in the building project's construction of China mainly include the following aspects.

### 3.1 *Both of the law and system involved in the building project are imperfect*

Although China has enacted *The Law on Safety in Production*, *The Safety Production Management Regulations for Building Project*, and other laws and regulations, in the aspects of the supporting system construction and the connection among various specialized laws, there are still many imperfections urgently requiring further establishment and improvement.

### 3.2 *The quality of the personnel engaged in the building construction is not high*

According to the statistics, at present, the number of people engaged in all kinds of building projects' construction in China is more than 300 million, of which more than 200 million are the migrant workers. Having not accepted the formal professional education and training, they lacking in proper safety knowledge, so that they are weak in safety awareness, which thus easily leads to the safety accidents involving themselves or others.

### 3.3 *The materials, equipment, and construction technology are backward while the protection facilities are incomplete*

Some construction enterprises are characterized by weak safety production foundation, backward materials, equipment, and construction technology, as well as uncertain target management. Moreover, during the building project's construction, the safety facilities and safety protection articles fail to get enough attention. For example, the manual hole digging pile works easily lead to the collapse and poisoning accidents; affected by the materials, the large template support system, bamboo scaffold, etc., are low in safety and reliability; the derrick, gantry, and other construction machineries are backward, which will easily lead to the mechanical damage and falling accident from a high place and which, thus, shall be restricted for use or just be eliminated.

### 3.4 *The construction unit ignores the safety management and supervision*

Some leaders of the construction enterprise are lacking proper knowledge over the laws and regulations on safety in production, as well as cannot put the relationship of safety with production, efficiency, and progress correctly, so that when there is a contradiction between the production, efficiency and progress, and the safety, they often will sacrifice the safety and fail to take safety as an important issue to cope with. The safety production supervision institutions for the construction project in some places are featured by personnel vacancy, insufficient fund sources, lacking in punishment basis, and other problems, so that the safety supervision functions of the safety supervision station fail to be fully played. At present, the safety management concepts held by most of the project construction enterprises are backward and they cannot effectively use the advanced management technology and information technology to improve the safety management level.

### 3.5 *The construction unit has blindly cut down its costs for safety measures*

Owing to the fierce competition of the building market, the development organization will often reject to pay the construction enterprise with enough expenses for the safety measures. Actually, there are serious illegal phenomena in all kinds of development zones, industrial parks, investment attraction projects, individual investment projects, and former renovation projects, for which no high attention has been paid to the safety production. Some construction units even believe that the safety in production is a kind of unprofitable input, which will only lead to the increase in the

unit cost and the enterprise burden. The popularity of this kind of wrong safety concept definitely will lead to the serious shortage of the fund input for the safety production at the construction site, the aging of the safety protection equipment, and other safety facilities and devices, as well as the substandard, safety protection.

#### 4 CONTROL MEASURES FOR THE SAFETY PROBLEMS OF THE BUILDING PROJECT'S CONSTRUCTION

Owing to the frequent occurrence of safety problems in construction, the construction units must strengthen the construction safety measures in the construction process, so as to ensure that the project construction can be implemented step by step in accordance with the schedule.

##### 4.1 *Electricity management measures*

- i. The general distribution box of the construction site, the switch box, and the terminals of the equipment's load line shall be set up with the two-level leakage protector, in order to make them hold the grading protection function to prevent the occurrence of the accidental injury.
- ii. The power cable at the construction site shall be buried into the ground at a depth of 50 cm; the circuit shall adopt the three-phase five-wire system with the protective connecting neutral conducted; meanwhile, the repeat grounding shall be carried out for the terminals of all the guard wires.
- iii. The construction site shall carry out the grading power distribution; meanwhile, the power distribution box and the lighting distribution box shall be set respectively. Moreover, the distance between the distribution box and the switch box shall not be more than 30 m, while the horizontal distance between the switch box and its controlling equipment shall not be more than 3 m.
- iv. One electrical appliance and one knife switch shall be equipped inside the switch box and every single electrical appliance shall have its own switch box.
- v. The distribution box at the construction site shall be installed in place and firmly; the mobile distribution box of the floor shall be installed on the fixed bracket; meanwhile, the distance from the fixed distribution box to the ground shall be 1.8 m, while that from the mobile distribution box to the ground shall be 1.6 m.
- vi. All kinds of electrical appliances in the distribution box shall be fixed on the mounting plate; meanwhile, both of the overhead lines outside the box and the lines inside the box shall adopt the insulated conductors, which shall be bound into a bundle and then be fixed on the plate.

##### 4.2 *Fire safety measures at the construction site*

- i. Establish a responsibility system for fire prevention; during the organization of construction, it is necessary to implement the requirements over the fire safety, carry out the fire prevention measures, define the responsibilities, and distribute them to the specific person.
- ii. In the process of construction, it is necessary to implement the fire safety disclosure system and put it in writing.
- iii. To carry out the site layout, the construction road will also be taken as the fire fighting access so that its width shall be not less than 3.5 m and both sides of the road shall not be stacked with materials.
- iv. There shall be enough fire extinguishing tools and devices available for the temporary facilities, warehouses, and material yards within the scope of the project's plane layout. The fire-fighting equipment shall be managed and inspected on a regular basis by the specially assigned personnel. Meanwhile, as for the inflammable and explosive goods, it is necessary to set up the warehouse for safekeeping.
- v. Pay attention to the fire prevention requirements at different construction stages, especially the last stage of decoration; meanwhile, it is necessary to strengthen the management over the materials and electro-gas welding.

##### 4.3 *Safety measures for the mechanical equipment at the construction site*

- i. The safety of the on-site mechanical equipment shall conform to the relevant acceptance criteria.
- ii. The application and operation over the on-site mechanical equipment shall comply with the relevant operational procedures.
- iii. The operating personnel of the mechanical equipment shall only be appointed if they have work license.
- iv. It is necessary to carry out inspection, repair, and maintenance for the on-site mechanical equipment; the fault-carrying and timeout operation of the mechanical equipment are strictly prohibited.
- v. Ensure that the lightning protection devices and lightning arresters for the on-site tower cranes and construction derricks are effective and complete.
- vi. As for the personnel operating all kinds of machinery and small electric tools, it is necessary to adhere to the principle of training first and operating second; meanwhile, it is necessary to appoint the specially assigned personnel to head for the construction site for instruction: as for the personnel violating the rules and regulations, they shall be required to stop immediately and be criticized seriously.

- vii. The project manager shall organize the relevant construction personnel to carry out inspection over the implementation of the safety measures to the mechanical equipment at the construction site every week.

#### 4.4 *Safety measures for the building construction*

- i. The on-site management personnel at all levels shall conscientiously implement the policy of “prevention foremost and safety first”, strictly abide by the various safety technical measures, carry out the safety education for the on-site construction personnel, and establish the concept of safety first.
- ii. The construction personnel entering into the construction site shall wear the “three safety protection articles”. Meanwhile, the construction personnel not wearing a helmet shall not be allowed to enter the construction site.
- iii. As for the “four openings” of the project, it is necessary to weld the iron fences or use the steel frames for retaining and it is necessary to hang the warning signs at the same time.
- iv. The stair step and stair landing shall be set up with the protective railing, the front of which shall be suspended with the safety net.
- v. The bottom surroundings of the project and the entrance/exit of the building shall be erected with the protective shed.
- vi. During the high-place operation, it is strictly not allowed to throw down the materials.
- vii. Before the construction for the sub-division and sub-item works, it is necessary to carry out the written safety technical disclosure; meanwhile, on a weekly basis, the project manager shall organize a safety education and safety production inspection and appraisal activity.

#### 4.5 *Safety measures for the frame works*

- i. The steel pipes, fasteners, and other materials adopted by the external frame shall conform to the requirements of the relevant standards; the overload operation is not allowed for the external frame; before the demolition of the external frame, it is necessary to carry out the written safety technical disclosure.
- ii. The external frame’s bottom layer and the construction layer shall be erected with the framing plate and the safety net, the outer sides of which shall be suspended with the dense mesh net for closure.
- iii. The scaffold and derrick steep pipe shall be padded with the board in accordance with the provisions, which meanwhile shall be tamped; the three meters distance shall adopt the inclined strut to strengthen the intensity; it is

not allowed to climb the scaffold and to go up/down by the vertical hanging basket; it is necessary to check the scaffold frequently in order to prevent the tilt and other conditions. If any one of the above circumstances is found, it shall be corrected immediately.

- iv. All the personnel working at high levels above the ground shall wear the safety devices in accordance with the provisions and shall conduct the operation in strict accordance with the safety disclosure; as for the personnel violating the safety operation, the criticism and correction shall be put forward or the economic punishment shall be made in a timely manner.
- v. In case of the high wind at the Level Five or above and the rain and snow weather, the external frame works shall be stopped; the frame erection shall not be carried out at night; the foreman and safety personnel for the frame shall carry out inspection and acceptance over the erection of the frame, as well as filling in the acceptance sheet.

## 5 CONCLUSIONS

The building industry is a high-risk industry. Owing to the imperfect laws, low personnel quality, backward technological equipment, etc., inevitably the safety accidents have frequently taken place in the building industry, which have seriously affected the economic benefit and image of the enterprise, and hindered the timely completion of the project’s construction tasks. Therefore, during the process of the project construction, strengthening the safety construction measures, such as electricity management, on-site public security defense, fire safety at the construction site, mechanical equipment safety, building construction safety, and frame works safety, can effectively ensure that the project construction can be implemented step by step in accordance with the schedule and the project’s construction tasks can be completed on time at required volume.

## REFERENCES

- [1] Luo Kai. Handbook of Safety Technical Disclosure for Building Project. Beijing: China Market Press, 2004.
- [2] Hong Liang. Safety Knowledge over Construction for Building and Public Projects. Beijing: China Labor Social Security Publishing House, 2006.
- [3] Liu Jia-Fu. Building Construction Safety Technology. Beijing: China Building Industry Press, 2004.
- [4] Pan Quan-Xiang. Data Handbook of Safety Production and Civilization Construction for Building Installation Works. Beijing: China Building Industry Press, 1995.

# Study on protecting and inheriting the traditional crafts and the contemporary design education

Ling-sheng Hao & Ling-ling Chen

*Hebei Academy of Fine Arts, Shijiazhuang, Hebei, China*

**ABSTRACT:** A change in the age makes the slow pace of the rural pastoral life go away from us, and the word of the traditional craft is also gradually seldom mentioned in our ears. However, in recent years, with the development of the global informatization, the global culture homogeneity becomes more and more serious. People pay more and more attention to the protection and inheritance of the regional traditional culture. The traditional crafts are recognized by more and more consumers. The article discusses the traditional crafts in the point of view of the traditional crafts orientation, the analysis of the objective death cause, the practical significance of protecting and inheriting the traditional crafts, and the combination of the traditional crafts and the contemporary design education. It also explores how to do a good job of protecting the traditional crafts under the contemporary design education system.

**Keywords:** traditional crafts; protection; inheritance; the contemporary design education

## 1 INTRODUCTION

The traditional crafts mentioned here are the development products of the human in the feudal era before the industrial revolution. This kind of skill is the survival root of the people. It is a production mode, which is adapted to the development of the social productive forces. Its characteristics of the times are particularly obvious.

## 2 THE GRADUALLY DISAPPEARING TRADITIONAL HANDICRAFTS

At present, many old traditional handicrafts, even some childhood memories of the people who were born in the 1970s and the 1980s, also have disappeared or are about to disappear in our modern society. Such as the cotton and linen manual textile manufacture, the traditional way of printing and dyeing, and the brocade way have begun to disappear.

Now for the traditional wooden sugar machine, let us take a look at what makes the traditional handicraft disappear. The wooden sugar machine, which was earliest recorded in the book of 《Tian Gong Kai Wu》, was invented by the Han nationality. It may be the earliest sugar machine in the world. In the 17th century, as the book of 《Tian Gong Kai Wu》 was introduced to Yunnan, now we can also find it in some ancient towns or ancient villages, which are far away from the cities and are less

influenced by the modern civilization. The authors have the opportunity to see the old wooden sugar machine in a Dai nationality subline in Mangyun village, Menglian county, Yunnan province located in the Sino-Burmese border area. It is still used to make sugar by a few people.

The crafts in the region can be influenced by the geographical conditions, the social structure, and the farming methods of the region. A particular way of life determines the specific products. The village of Mangyun belongs to the subtropical mountain basin and is suitable for sugarcane growth. About a few decades ago, the people in the Dai villages in Zhennan all used their sugar machines to make sugar. However, in recent years, many mechanical sugar-houses are mostly built in every region of the Zhennan sugarcane. Sugaring using the wooden gear can only be seen in the villages of Mengma, and only a few of the old men master this skill. Therefore, the development of the modern science and technology has changed our way of life. The new technology replaced the old technology, and the mass standardized and mechanized production replaced the original small batch and manual production. This is the main reason for the traditional craft dying. Second, owing to the lack of raw materials, some raw materials used in the traditional handicrafts are hard to find in our modern society. As the timbers for making traditional wooden sugar machine are the hard water teak woods of more than 50 years. For the Dai stockaded village where the deforestation behavior was prohibited since the ancient times, even in the

original forest around, the raw materials are also difficult to be found. Moreover, it usually takes you at least a few years learning the production craft of the traditional wooden sugar machine. In the process, you need to use your body, mind, and hands to memory. However, in this era of the rapid economic development, young people are more interested in some economic return quickly work than learning the traditional things.

On the other hand, a change in the city residential structure changed the life style of the people. With the development of the economy and the improvement of the modernization degree, some old folk-customs have been far away from us, which eventually lead some traditional handicrafts in line with them to be also far away from us. For the traditional Spring Festival, we should be able to feel that the atmosphere of the year becomes more and more light in some more developed areas, whether in the cities or the countryside. With the change in the age, many spring festival customs are also weakened. Many families in the cities choose to go to the supermarket and buy the mechanized and mass produced special products for the Spring Festival. They hardly imagine that the purchases taking you a little time buying lack the flavor of the year and the milk of human kindness. The pictures posted in the Spring Festival before also gradually disappeared in the modern decoration buildings.

### 3 PROTECTING AND INHERITING THE TRADITIONAL CRAFTS HAS VERY IMPORTANT PRACTICAL SIGNIFICANCE

The traditional crafts have the function of spreading the culture literature. The big handicrafts are called the small traditional culture in the literature. They have the function of spreading the culture and education. The inheritance way of the traditional handicrafts often uses the way of “pass on by the word and teach by the heart from the teachers to the pupils”. Every word of the handicraftsmen will have their own language. For example, the carpenters have the carpenters’ language, and even the boatmen all have their own language. Where do the original words used by the various handicraftsmen actually come from? The simple language used by the handicraftsmen when they are working is also a part of the handicrafts heritage, and also can say it is a kind of culture. The small handicrafts contain the great wisdom. Many jargons of the handicraftsmen have become the proverbs in our today’s life, such as “Skill is no burden”, “Three hundred and sixty line, line out of the top”, and “ Families with money enormously inferior to slight skill in the body”.

The traditional handicraft can be a refuge for the thoughts of people. We temporarily escape from the mechanization and the automation brought by the modern society and the social reality, which is too organized and standardized for the life, and seek a kind of peace, simplicity, and beauty. Living for long time in the developed and high technological place, people often yearn for those rough, simple, primitive, and original products and life. When we see the sugar paint, the dough figurine and the soup woman, and when we walk in the ancient quaint town, which is with many traditional handicrafts, such as the Smithys and the MieJiang shop, if the heart is full of peace and contentment. It will be a very beautiful enjoyment. When we see a tool left by the old handicraftsman, perhaps we can feel the marks of the gone time from the rusty tool.

The traditional handicrafts can become the foundation of developing the design with Chinese characteristics. Our design starts relatively late, and the design education is largely influenced by the western countries. Therefore, our current design and design education almost has no relation with the traditional handicrafts. However, it does not like this in the western countries. In the early 1860s, the time of the rapid industrialization development, the British designers were aware of the significance of the handicrafts in daily life. In the industrialized society with the handicrafts, the life will not be single and the ethos like the arts and crafts movement appeared. Although the design history world has different viewpoints for the movement, in a sense, it deserves our contemporary people to think. In Italy, in the southern Europe, the combination of the traditional handicrafts and the modern design is more prominent and it creates its own design and manufacture road. The Italian designers put the emotive factors of the traditional handicrafts as the basis of the product design and create a kind of classic fashion combining the tradition with the modern, which becomes the famous brand in Europe, even in the world. The development of the design process in these countries all can be our reference model. Especially in the gradually diversified society, the supply of the current industrial products is beyond the requirements, and hence, it has very important practical significance to rethink the traditional handicrafts and meet the consumers’ cultural appeal for the products.

The traditional handicrafts can relieve our mental environment and physical environment. The emotional sustenance is the accumulated precious spiritual wealth of the traditional handicraft during the long-term development process of the human, which is the lack of our design work in the fast-paced society. As the crystal of the human manual labor, the traditional handicraft is the organic combination of the technology and the art and it



has the abundant creativity and imagination of the craftsmen. It is also the main characteristic which is different from the modern industrial production. The process of doing the handicraft works includes their understanding of the life, the cultural heritage, and the character and temperament of the traditional craftsmen. Therefore, the traditional handicraft can mostly arouse the identity sense of the people to the traditional culture and the humanity atmosphere. On the other hand, the Chinese traditional handicrafts specially focus on the use of the original ecological resources and have formed the green ecological art system in harmony with the environment. It is the biggest reflection of the Taoist ideas advocating that man is an integral part of the nature. Moreover, it totally accords with the sustainable development and the low-carbon life, which is the current national advocacy.

#### 4 THE TRADITIONAL HANDICRAFT IS THE INSPIRATION SOURCE OF THE CONTEMPORARY DESIGN EDUCATION CARRYING FORWARD THE NATIONAL CULTURE

The economy of our country has made a boom after the reform and opening-up policy, but the designs are always weak. The word of cheap copy can summarize the design status now. Their innovation is seldom and blindly imitate or copy others. Therefore, the designs of our country always cannot get the international recognition. When our applications of taking part in an exhibition are turned away by the international furniture fairs in Milan repeatedly, whether there is a reflection to our design and education. Study and imitation is not terrible, because any things should have a process of development. Germany has faked the British products, and Japan also has imitated and learned Germany. It is terrible that we have no innovation, and cannot create our own design road. Chinese design education began in the last century in the early 1980s, with the development of recent decades, and has become a large art design education system containing dozens of kinds of designs. However, the foundation of our design education is the western education, and greatly influenced by the western education mode. Then, based on this, how to draw the nutrition from the Chinese traditional craft to improve our design education mode and cultivate the true Chinese designers is a problem worth we are thinking about. As the chairman of the Milan international furniture fair, Carlo Guye Mi, said that “for made in China, the most important thing is to develop the product system with the Chinese culture, and not only to imitate and copy like before. Because they are the prod-

ucts from the different cultures”. China’s industrial design leader, Professor Liu Guanzhong, also once said that “the reason of the design not developing is that we don’t steadfastly study our own life”. Chinese should form our own characters and soul from our own life and the successive tradition, and turn them into our own design. In this way, our designs can go towards the international markets. Now, there are some designers starting to create our own brands, walking in the road of innovation, and also getting some international recognition, which is very delightful.

To protect the traditional craft is not to copy the elements, but to continue the culture of our nation. The traditional culture is our culture gene pool. The use of the simple folk elements is not equal to the brand innovation of our country and integrates our own characters into the products. If we want to innovate and create our own brand image, we will deeply study our tradition, really study our own life and put our soul into our own design. Therefore, for the design of the contemporary education, we should adjust the idea instead of only blindly looking at the west and having the things of our ancestors as a burden, and we will stand in the point of view of the current era to perceive the tradition. Admittedly, the current culture is diversified. Many young people hold the strong rebellion consciousness and think that the tradition should be discarded. This is an extremely shallow view. From another point of view, only when we have understood the national tradition of the world, can we dialogue with the world. Just as the famous conductor Seiji Ozawa evaluated that the erhu music of a bing was the music of heaven, but we rarely perceive the creation of a folk artist in such a height level. Therefore, we should have the mentality of revering our own culture to understand the national tradition and strengthen the cultural self-confidence.

In the process of the specific implementation, I think we should appropriately adjust and strengthen the traditional knowledge structure. Such as the major of arts and crafts, now the knowledge of drawings, design principle, and picture composition mostly is the modern architecture system, but it does not systematically reflect the thoughts of the sculpt, the creation, and the statues in ancient China. Therefore, many traditional education contents in the aspects of the curriculum provision or the textbook compilation in the future are worth studying. The schools should also spread the charm of the traditional crafts to the students in the way of establishing the museums, the galleries, and the data repositories. In this way, the students who receive the modern design education will visit and study the old items and the old tools in the traditional view.

In addition, we should also set up the folk art research course and organize the students to go deeply into the folk life to understand the society. We often say that the masters are often in the folk. The students should study in the social practice and from the old actors and experience more traditional culture. Therefore, they can understand the traditional handicrafts, fully understand the connotation of it, and apply it into practicing the design works. For example, we think that many things have disappeared, but, in fact, they may still exist in every corner. Like the folder valerians, we think that they have lost for millennium, but they actually resurge in the hands of a folder valerian artist in Wenzhou, Zhejiang Province. The financial support for the traditional handicraft recovery is from a Japanese, Kubo ma. Her blue calico shed on the road of Change in Shanghai especially sells the blue calicos printed using the traditional printing technology by the Wenzhou artist. In the process of the design teaching, we should make full use of this part of the education resources, integrate it, constantly improve it, and form a complete set of the education system.

## 5 TAKE THE DESIGN EDUCATION AS A FUNDAMENTAL STARTING POINT TO INHERIT THE TRADITIONAL HANDICRAFT

Many traditional handicrafts are mastered by a few old handicraft men, even only one person, and this is a very terrible reality. The death of an old handicraft man is equivalent to a museum destroyed in the fire. Therefore, I think the most important point to protect the traditional handicraft is to go into the schools and the scientific research institutions and let more people master them. Then, we cannot close, and we need a living traditional craft skill. Therefore, the best way to make the traditional handicraft alive is to combine with the modern market and go on the road of industrialization. On the other hand, we should set up the system and conditions for protecting the folk handicraft inheritors in the design education. At present, our country shows great importance to protect the intangible cultural heritage and the traditional culture. The country is our strong background to protect the traditional handicraft and the traditional culture. When President Xi Jinping took office, he explicitly pointed out: “we should be familiar with the national traditional culture, study and respect it. In order to make the Chinese civilization radiate the new splendor in the new one thousand years and walk in the forefront of the human civilization, we should truly take its essence, discard the dregs and innovate comprehensively”. Therefore, since

the protection of the non-material cultural heritage is brought up, our traditional handicrafts and folk arts receive much attention. Many non-material cultural heritages have been commented and many old handicraft men or inheritors have been judged to be the masters of the arts and crafts. To a certain degree, they promote the development of the traditional handicrafts. Some traditional arts and crafts even become the very popular commodities, and are loved by the consumers. Many traditional arts have developed very well, such as the traditional toy monkeys of the old Beijing, the scissor-cuts in the county of Wei, the clay figurines of Tianjin, and the New Year pictures of Yang Liuqing. For those who hold the folk arts, our country can bring them into the technical position evaluation category, establish the assessment evaluation criteria of the folk art heritage, and set up the professional title accrediting agencies paralleling with the teachers in universities and colleges. In this way, a group of people can go into the colleges and universities, and let the traditional folk handicrafts pass down from generation to generation by the schools or the scientific research institutions. The school is built into an important propaganda tool and position to protect the traditional handicrafts.

Look around the world, Japan is far ahead in the aspect of the education and thinking of the traditional handicrafts. As early as the Second World War had just ended in 1945, the Japanese government revitalized the industry in the face of the scarred country. They firstly recognized that the protection of the traditional handicrafts had the important development significance on the Japan's future and organized the experts to demonstrate their importance. They carried out the movement of “one village one art” and strived to develop the traditional folk arts. They also spread the thought that the improvement of the national spiritual life is built based on the creation of the traditional materials. In this way, the Japanese people can recognize the mutually beneficial relationship between the traditional handicrafts and the industrial production, and the Japanese traditional handicrafts were protected from the corrosion of the modern industrial civilization in the ideology. Hence, it ensured that the Japanese in the era of industrialization could use the commodities with emotional hopes to relieve the coldness of the modern industrial civilization and to arouse their pride of the national culture.

As the social productive forces of the traditional society, the handicraft was inseparable with the food, clothing, living, and vehicle in the ancient society. However, in the current society after the industrial revolution, the traditional handicraft carries more the meaning of the national culture and the national spirit. Especially, now the

modern culture is homogenized, and it has been an involuntary behavior for the people to pursue and consume the spirit of the traditional handicrafts. Their arts have become a particular cultural phenomenon and exceeded the value of the productions themselves. In addition, this kind of cultural phenomenon has the potential market, and will become a kind of consumption factors beyond the substance itself.

The traditional handicrafts disappeared because of the transformation of the productivity. It is a pity that the cultural spirit conveyed by the traditional handicrafts has been submerged by the flood of the times. In the contemporary society, if we want to find the traditional handicrafts again, we need to find the cultural spirit conveyed by the traditional handicrafts instead of developing the backward productivity. It is our national comprehension for the behavior of "Creation" for thousands of years. Today when many of the standardized industrial products are full of the markets, the cultural spirit is particularly important. It is probably a key to open the design nationalization. It is of vital significance for promoting the national design. To solve the problem and pass the values is the core of the traditional handicrafts. It contains the double meanings of the human demands for the nature and the spirit of the materials. As the purpose of the human creation, the material demand is simple and clear, and hence, we will not talk about it here. The spiritual demand is the feelings of the people for the age, the morality, and the nature, and has the strong emotional significance. Today, the design and the consumer group are increasingly diversified and the professional boundary is blurred, and therefore, we need the emotional supplement of the traditional handicrafts for a mass and standardized production mode. In other words, it is the emotional regression of the products. Therefore, manufacturing is no longer the purport of the handicraft arts and the traditional ideas of creation will be inherited as the core. Therefore, in the diversified era, our designers choose to "redesign" using the traditional thought and skills, and the purpose is to awaken the approval of the modern consumers for the traditional culture and aesthetic. "Redesign" cannot completely copy the traditional designs, but have to reinterpret the traditional handicrafts in the present social environment and design a double art form which both adapts to the current consumer psychology and conforms to the traditional aesthetic modeling. We can create a new design with the aesthetic characteristics of the age through the traditional concept of creation and the application of the technical materials and the technology. The process is complex and involves the materials, the shapes, the functions, and many other factors,

which needs to spend a lot of energy and labor to explore. Under the current material interest development, we need to carefully study, and explore in a quiet environment, to solve these problems, and the schools and the scientific research institutes are undoubtedly the best choices. It is the main reason that the traditional handicrafts must set the design education as the fundamental starting point. From the point of view of reviving the ethnic traditional culture, the government agency should take out the special funds and support the restudy of the traditional handicrafts. In this way, the traditional handicrafts of our ancestry will reveal the new charm in the new era.

The traditional crafts and designs are the different appellation for the creation activity in the different stages of the human development. Studying the contemporary designs, we must study the designs in the past. If we want to design in China, we must know the design condition of the past handicrafts. Therefore, the traditional craft education in the contemporary design education is indispensable. Both are interdependent on time and are inseparable. As the gene pool of the Chinese traditional culture is a treasure house belonging to all humankind, only when transfusing the traditional quintessence, can the Chinese design be recognized by the world. The age of the earth village is coming. However, the earth culture village will be the incomplete world without the Chinese and the Chinese culture. Only by transfusing the accumulation of the Chinese culture and wisdom for thousands of years, the earth cultural village can present a colorful appearance. In the 21st century, the folk art movement in Japan entered into a new development period. Designer Kenya Zai in 2003 launched the culture promotion activity called "redesign", which caused the strong reaction in the design world. The main core tenet of the movement was to analyze the creation concept of the traditional handicrafts again based on the concept of the modern market and apply it into the specific design practice. It was an important step that the traditional handicrafts are created in the current social development and changes.

## REFERENCES

- Daoyi Zhang. The Folk Arts Theory of Zhang Daoyi. Shandong: Shandong Art Prss. 2008. 5. (In Chinese).
- Hangjian. Handicraft Thoughts. Shandong: Shandong Pictorial Prss. 2003. 1. (In Chinese).
- Lusheng Pan. The Guiding Principle Of The Folk Arts Study. Beijing: Beijing Arts and Crafts Press. 1998. 10. (In Chinese).
- Shengzhong Lu. Goodbye, tradition. Beijing: Sanlian Bookstore. 2004. 5. (In Chinese).



**Taylor & Francis**

Taylor & Francis Group

<http://taylorandfrancis.com>

# Financial accounting of long-term equity investment

Jie Wu

Langfang Polytechnic Institute, Langfang, China

**ABSTRACT:** In 2006, People's Republic of China issued a new "Enterprise Accounting Standards", which made adjustments for enterprise amalgamation and long-term equity investment and mainly focused on scientific and reasonable standardizing of the accounting standards of long-term equity investment. Compared with the existing equity investment standards, the new ones have been improved comprehensively. Financial accounting of long-term equity investment has been further applied by long-term research and analyses.

**Keywords:** long term; equity investment; financial accounting

## 1 INTRODUCTION

On 15 February 2006, China's fiscal institutions issued new accounting standards, mainly focusing on scientific and reasonable standardizing of the financial accounting of long-term equity investment. Compared with the existing accounting standards, the new ones have changed the provisions of the financial accounting of long-term equity investment considerably. Therefore, it is necessary to study the accounting of long-term equity investment, which is the aim of this paper. This paper will introduce the theories of long-term equity investment first, analyze the accounting methods of the long-term equity investment based on both the old and new accounting standards, and then study the measurement of the accounting of long-term equity investment. The author believes that this paper will help the readers understand the new accounting standards.

## 2 THEORIES OF LONG-TERM EQUITY INVESTMENT

### 2.1 *Definition of long-term equity investment*

Long-term equity investment is a type of equity investment in subsidiary companies, cooperative enterprises, and joint ventures. Before studying the long-term equity investment, it is necessary to determine its limitations. The following are the four types of long-term equity investment. First is investment in subsidiary companies. By adopting this type of investment, the investing company may have control over the invested enterprise. Second is investment in cooperative enterprises. By adopting

this investment method, the investing enterprise will have control over the invested enterprise, which is only partial. In the process of production and operation of the invested enterprise, the investing enterprise and other cooperative enterprises shall be responsible for the management of the invested enterprise. Third is investment in joint ventures. By adopting this type of investment, the investing enterprise will have a significant influence on the invested enterprise. Fourth is equity investment methods other than the above three types. By adopting this method, the investing enterprise will have no control or significant influence on the invested enterprise.

### 2.2 *Initial recognition of long-term equity investment*

The initial cost measurement of long-term equity investment includes the following three cases. The first is the enterprise merger under the same control. In this case, the initial cost of the long-term equity investment should be equal to the book value made by the merging party. The initial cost of the merging party may be acquired by cash payment, incurring debts with the merged enterprise, or transferring non-cash assets. Differences between the initial costs of long-term equity investment and the value of funds generated by the merging party (if any) can be dealt with by adjusting fund surplus. The second is the enterprise merger under non-unified control. In this case, the merging party still invests by providing funds and incurring debts, but the investment of the merging party should be dealt with by fair value. The difference between the book value and fair value of the capital or assets provided by the merging party shall be included in

the current profits and losses. All other forms of long-term equity investment constitute the third category, which should be based on specific circumstances. For example, if the long-term equity investment is carried out by paying cash, the payment of cash shall be regarded as initial investment costs. If the long-term equity investment is carried out by issuing equity securities, the initial costs of the long-term equity investment should be the fair value by issuing equity securities. If other long-term equity investment methods are adopted, the initial cost of the long-term equity investment shall be determined in accordance with relevant provisions.

### 3 RESEARCH ON THE ACCOUNTING OF LONG-TERM EQUITY INVESTMENT BASED ON THE NEW AND OLD ACCOUNTING STANDARDS

As early as 2001, China's financial sectors improved part of the old accounting standards to clarify some basic concepts and theories. Accounting methods of investment were also reformed and innovated and the costs of long-term equity investment, earnings, and accounting information were standardized comprehensively. Research and analyses have found that there are some problems in accounting of the long-term equity investment due to the old accounting standards.

#### 3.1 *From the perspective of the entry value of investment*

According to the old accounting standards, investment valuation mainly includes the book value of the investment company. This approach will reduce the operative power on profitability of the fair value, which makes the company's own investment value not match its actual value. Part of the book value is reserved by the principle of historical costs, which makes it difficult to reflect legitimate rights and interests between the investors and the invested company, especially for the company with a long-term investment. Economic value and book value cannot be effectively connected, and the rights and interests of the invested company cannot be truly reflected.

#### 3.2 *From the perspective of cost accounting*

According to the old accounting standards system, an enterprise's long-term equity investment needs to carry out accounting based on the law of costs, which does not include the additional and recovering investment. The book value of the long-term equity investment remains stable, and the aggregate investment only covers the allocation of net profits

of the invested company. In other words, even the net profit increase of the invested company cannot record the investment income as long as allocation is not carried out. Therefore, once the company reduces its rate of income on investment without obtaining any equity profit, it will affect the scientific and reasonable analysis of investment.

#### 3.3 *From the perspective of equity method of accounting*

The rights and interests enjoyed by the invested company are not clear in the process of long-term equity investment.

First, the investing company should enjoy shares of rights and interests allocated by historical data and associated less with information data. Although the application of historical data is very simple, these data do not accord with actual situations.

Second, to determine the difference of the long-term equity investment that cannot help implement the basic concepts of investment costs, the accounting method of amortizing the difference of the long-term equity investment also lacks corresponding theories. Once the operation is run in this way, it will make prospective earnings gradually decline and will not make a scientific and reasonable judgment.

#### 3.4 *From the perspective of terminal impairment of accounting*

According to the standards system, profit and loss of the current investment are because the recoverable amount of assets is less than the book value of the long-term equity investment. The higher value between a company's net amount of sales and the expected amount of assets can be viewed as recoverable amount. The future trends of expected asset flows make it difficult for both investing companies and invested companies to fully grasp the investment value, and they also lack the corresponding theories for their judgment.

The new accounting standards system has revised and supplemented the accounting of long-term equity investment. Scientific and reasonable measurement of the initial investment costs has been made together with fair value to eliminate the assets difference in the long-term equity investment. The study and analyses of the problems described above improve and standardize the standards system of long-term equity investment. The company's financial status can be better developed, and the quality and efficiency of its financial information can be improved.

#### 3.5 *Reducing scale to match the risk features*

According to the new accounting standards, investors should bear with main investment

management risks in the long-term equity investment, which include asset price change risks, investee's credit risks, and other influential investment risks. Different types of investment need to implement different risk control methods, and the corresponding provisions are mentioned in the new accounting risk standards.

#### 4 MEASUREMENTS OF ACCOUNTING OF LONG-TERM EQUITY INVESTMENT

##### 4.1 *Improvement of law of cost and equity*

The new accounting standards facilitate the invested companies to obtain long-term equity investment from the investing company. They do not need to be managed and influenced by the investing company, to have quotation and fair value in market economy, or to rely on reliable measurement of long-term equity investment, which generally uses the law of cost. On the contrary, if the investing company has a unified control over the invested company and a certain impact on long-term equity investment, it will adopt the equity law.

Under the old accounting standards, the investing companies usually implement the corresponding equity law for accounting in the invested company. Furthermore, time point of the investment income accounted by the cost law is generally similar to the time point of cash inflow, so the computing information on the rate of return on investment and other rate of return is more comprehensive and authentic.

##### 4.2 *Further improvements of accounting methods*

On the basis of new accounting standards, corresponding accounting methods are established for each investment type.

First, the accounting method of fair value is applied to investment types. Cash dividends need to be directly brought into profits and losses of this period when the dividends are distributed. Then, investment needs to be valued by using accounting method of the fair value. Changes in the fair value can bring a series of changes, which can go directly to the holder's rights and interests.

Second, the investing company can have control over the invested company, which needs to apply the cost accounting method, draw up financial statements, combine different works, and strictly abide by the equity method of accounting to make scientific and effective adjustment.

When a company uses the equity method of accounting, it needs to determine the difference between the long-term equity investment and measurements after the investment. On the basis

of the new accounting standards, when the initial investment amount is higher than the actual investment amount, the investing company can gain the fair value of the invested company, and its initial investment cost for the long-term equity investment does not need to be adjusted again. If the cost of the long-term equity investment is less than the investment amount, the investment difference can be included in the current profit and loss, and the initial investment cost for the long-term equity investment can be adjusted scientifically to match the real value.

##### 4.3 *Reasonable suggestions on accounting of long-term equity investment*

Under the requirements of the new accounting standards, it is necessary to sum up and adjust the investment before. At the same time, accounting subjects need to be constructed. The accounting of long-term equity investment will be standardized reasonably, and its demand can be met. Long-term equity investment made by the merger of companies should make unified management to have assets difference sterilized and income situation retained. On the contrary, when using equity methods for the accounting of long-term equity investment, it is required to allocate the holder's rights and interests in accordance with the corresponding proportion and to timely go to the current profit and loss, which will reasonably adjust the current profits and losses of long-term equity investment.

If the value of long-term equity investment tends to decrease, the enterprise should formulate measures to deal with it in advance and make corresponding adjustments to the investment in the subsidiary companies, joint ventures, and so on. On the basis of the equity law for accounting, changes in the investing companies' ownership of the invested enterprise should depend on the investing companies' proportion of holding shares and the invested companies' profits and losses in the premise of holding the same shares. At the same time, the book value of the long-term equity investment should be adjusted, to increase or decrease the capital reserve. In practice, if the enterprise has investment losses, it should debit "income on investment" and credit to "long-term equity investment (profit and loss adjustment)".

#### 5 CONCLUSION

The purpose of accounting of long-term equity investment is to improve the quality of accounting information. On the basis of investment accounting, the accounting measurement method should be used to ensure the authenticity and accuracy

of the accounting information. The investors and the investees' legitimate rights and interests can be guaranteed by a series of reasonable adjustments. The accounting of long-term equity investment can also be improved.

## REFERENCES

[1] Cheng Huiling. A brief analysis of accounting of long-term equity investment under new accounting

standards [J]. *Investment and Cooperation*, 2012, (8): 138-139.

[2] Zhu Beibei. A brief analysis of the changes in accounting of long-term equity investment under new accounting standards [J]. *Modern Business*, 2015, (9): 206-207.

[3] Hu Yingying. The change and thinking of the accounting of long-term equity investment under new standards [J]. *China Business Monthly*, 2015, (15): 232.



# Workflow design and analysis of the function of a PLC ship power station management system

Shu-cui Jiang, Xiu-ping Sui, Zhuan-zhao Liu, Shuo Wu & Yun-zi Geng

*Maritime College, Shandong Jiaotong University, Weihai, Shandong, China*

**ABSTRACT:** On the basis of PLC control technology, the ship power station management system with advantages of perfect function and advanced technology is widely applied on board ship. The rational design of the workflow of PLC ship power station management system has practical significance in analyzing and solving problems in the operation of the power station and improving the independent innovation ability of the ship power plant control technology.

**Keywords:** automatic control system; ship power station; PLC; system module

## 1 FUNCTION OF PLC SHIP POWER STATION MANAGEMENT SYSTEM

### 1.1 Control function of ship generator

In order to improve the continuity and reliability of power supply, ships are often equipped with a number of generating units. With the change of working condition, there are several combinations of the unit operation modes. A single diesel generator can supply power to a whole ship, and two diesel generators may parallel to serve this purpose. Sometimes, a diesel generator may parallel with a shaft generator transiently for operating mode switching. All these can be used to perform control functions, such as starting and stopping, paralleling, load distribution, load transferring, and splitting. In general, these functions are implemented by controlling the speed and voltage of the generator.

When one generator could not meet the requirements of power supply, it is necessary to start another one in parallel to supply power. Therefore, paralleling operation is fundamental. When paralleling, the frequency, voltage, and phase angle of the in-coming generator should be adjusted to be consistent with the on-line generator (within the permitted deviation range). The adjustment of frequency and phase angle is realized by controlling the speed of the generator through the grid-connected controller. Voltage is regulated by the grid controller through adjusting the excitation current. However, in many cases, the voltage will be regulated automatically, depending on the type of excitation of the generator set. When paralleling, the running speed of the in-coming generator is slightly higher than the on-line generator. The phase of the in-coming generator is slightly ahead. This is because when the switch is closing, the

in-coming generator will share part of line load, and the speed will reduce due to the reaction force generated by the rotor cutting the magnetic lines. Therefore, if it does not happen, the in-coming generator will be damaged by reverse power. For the paralleling of diesel generator and shaft generator, the former should be adjusted to meet the requirements of frequency and phase angle, because the speed of the latter is not adjustable (the speed of the shaft generator is controlled by the main engine remote control system).

When the paralleling operation is finished, if the load of two or more paralleled generators cannot be evenly distributed, one of them may overload and the other remains in low-load condition. For this reason, load distribution control mode is used, that is, the load will be distributed according to the capacity of each generator. The speed of the shaft generator is not adjustable, and thus the load distribution between diesel generator and shaft generator is not needed. Only when working status is switching, the transitional and transient paralleling of these two generators is needed.

If the power consumption is reduced, one generator can supply the required power. In order to optimize the operation, it is necessary to transfer the load from one generator to the other, cut off the switch, and stop the engine. These are the control functions of load transfer and splitting, and often are combined to perform together.<sup>[1]</sup>

### 1.2 Ship power station management system

In accordance with load variation, the generators will parallel in and off. Therefore, high-performance management system of automatic ship power station is demanded. The main contents include:

1. Preliminary work before starting generator sets: The relevant provision of the China Classification Society on ship automation is that the power of the ship should be restored within 45 s after loss (provision of some foreign countries is 30 s). Therefore, the standby generator set of the automatic power station should be prepared in advance. The key preparation work is pre-heating and pre-lubrication for diesel engine.
2. Automatic starting of generator set: When the load increases and fixes the on-line generator in heavy-load status, mechanical and electrical failures of the running generator occurs, the starting of one generator fails or the main switch fails to close, and the power station management system is able to automatically send out a start command to start the standby set quickly and automatically, build up voltage, and put into line to supply power.
3. Automatic paralleling: Through collecting and computing the basic parameters of voltage and frequency, some instructions, including frequency adjusting and switch closing, are sent out to parallel the generators.
4. Power distribution and frequency adjustment of generators in parallel: When two generators are in parallel to supply power, the governors and automatic frequency load regulators of prime movers cooperate to maintain a stable frequency and make generators undertake proportional loads based on different capacities.
5. The number management of running sets: On the basis of the premises of meeting power supply quality requirements, the generator sets should run in the most economical mode, make full use of the power of each set, and reduce the cost of power generation.
6. Heavy-load starting query: When the heavy-load device is about to be started, the management system will estimate whether the load adding of the power grid will exceed the permitted maximum load or not. If not, the device is allowed to start; otherwise, another standby generator set should be started first and paralleled in automatically. Then, it will be allowed to start.
7. Automatic handling of failures and automatic unloading by steps: The system is equipped with failure-handling mode corresponding to failures and automatic unloading by steps to ensure the continuous power supply of important equipment and cut off the unimportant load automatically in case of overload.
8. Control of automatic splitting, failure splitting, and failure shutdown: When the generator sets are under low-load or failure condition, and need to shut down, the load on paralleled sets will be transferred automatically, and then the sets will be split in order and shut down.
9. Safeguard to the generator sets: Besides overload, short circuit, under-voltage, and reverse-power protection, automatic power station has under-frequency protection, high-voltage protection, and the function of minor device unloading by steps. Thus, the power supply quality is increased and continuous power supply is ensured.
10. Running status display and failure monitoring: On modern electronic touch screen, the status of main distribution panels, generator sets, main switches, and other electrical components can be shown. In addition, switches and buttons are built in and shown by programming. Briefly, the touch screen has not only the display function but also the operating function.<sup>[2,3]</sup>
11. Monitoring and modification of the given parameters of the operating system: System offers the function of parameter monitoring and online modification, and the PLC technology can store designed programs and parameters into Random Access Memory (RAM), which is convenient for online modification.

On the basis of the requirements of power station management system, the functions of PLC power station management system can be divided into different modules. The modules are set as subprograms and the flow diagrams of implementing these subprograms are designed. The main program will combine these subprograms properly to perform the automated management of power station. The main modules designed include automatic start module, parallel module, frequency and load adjustment module, heavy-load start inquiry module, auto-split module, and auto-shutdown module.

The block diagram of the PLC ship automation power station system is shown in Fig. 1.

The main program of management system will scan main parameters and working status automatically, make logical analysis and comprehensive computing according to different parameters and

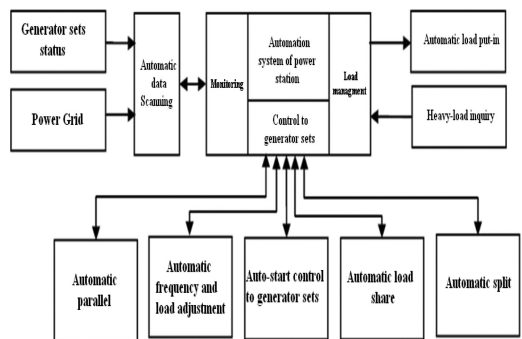


Figure 1. Block diagram of PLC automatic power plant system.

status, and determine which function subprogram to be called to perform the work. Once the called function subprogram finishes the work, it will return to the main program to continue scanning. The system works in such a repeated operation. This thesis takes heavy-load start inquiry module, auto-split module, and auto-stop module as examples to proceed workflow design and analysis.<sup>[4]</sup>

## 2 HEAVY-LOAD START INQUIRY MODULE AND FLOW DIAGRAM

Heavy-load start inquiry function module is a processing module to deal with heavy load. It aims at inquiring before heavy-load device starts and taking surplus power as criteria to decide on whether to start the load or standby generator set first.

### 2.1 Input signal for heavy-load start inquiry module

1. Heavy-load inquiry signal (to determine whether it needs to be handled as heavy load) (interface signal)
2. Feedback signal for switch closing (to determine whether the switch closing is successful) (signal interface)
3. Status marking signals of each set (to determine whether the generator is running and the power should be calculated in the total power)
4. Output and rated power signals of sets online (for calculating the surplus power to decide whether to start the heavy-load device) (items mentioned above are inputting signals on CAN).

Input information from heavy-load start inquiry module is expressed in binary codes. For example: signal of no heavy-load inquiry is 1 and signal of heavy-load inquiry is 0. Heavy-load inquiry signals come from external heavy-load inquiry button input, external closing feedback signal, the set status identification register (CAN upload), and the set output power register (CAN upload).

### 2.2 Output signal of heavy-load start inquiry module

1. Heavy-load start signal (for heavy-load switch closing) (signal interface)
2. Generator set adding signal (to start the standby set and increase the surplus power) (the upload signal of CAN)
3. Closing failure alarm signal on heavy load (the upload signal of CAN).

The output of the heavy-load start inquiry is expressed in binary codes. For example: the response signal of allowing is 1, no response signal of allowing is 0, the signal of generator adding is 1, and the signal of no generator adding is 0.<sup>[5]</sup>

### 2.3 The flow diagram design of heavy-load start inquiry module is shown in Fig. 2

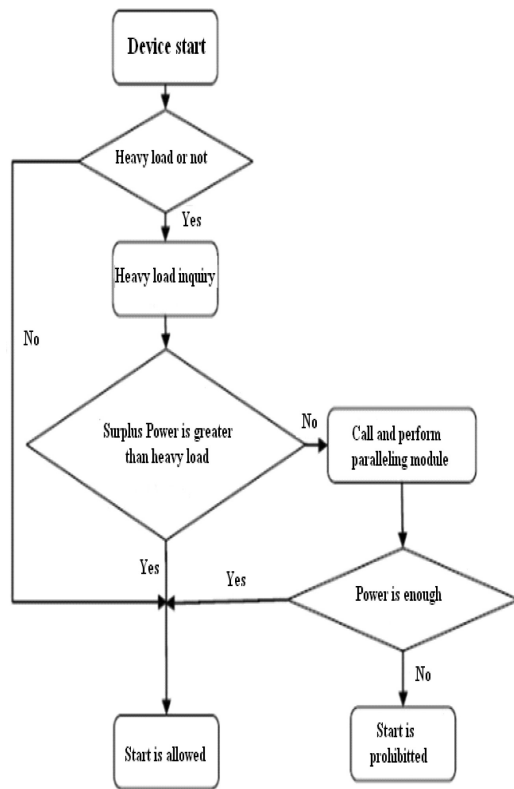


Figure 2. Heavy-load start inquiry flow diagram.

## 3 AUTO-SPLIT MODULE AND AUTO-SHUTDOWN MODULE AND FLOW DIAGRAM

The conditions for the formation of the auto-split of the ship power station include: (1) the set is operating online and (2) the load is too low or set failure. When the set is sure to be split, the load will be transferred first. When the load of the set to be split is reduced to about 10% of the rated load, the main switch is open and separated. At the same time, the upper computer is informed. After splitting, the system judge current condition of power station is delayed. If the load on station does not change, the shutdown operation will be implemented. If the load is increased to heavy-load limit in the delay, the parallel program will be implemented again.

Auto-split and auto-parallel are interrelated and are combined by the program. In this program, when the load of paralleled sets is less than 25%  $P_e$ , one

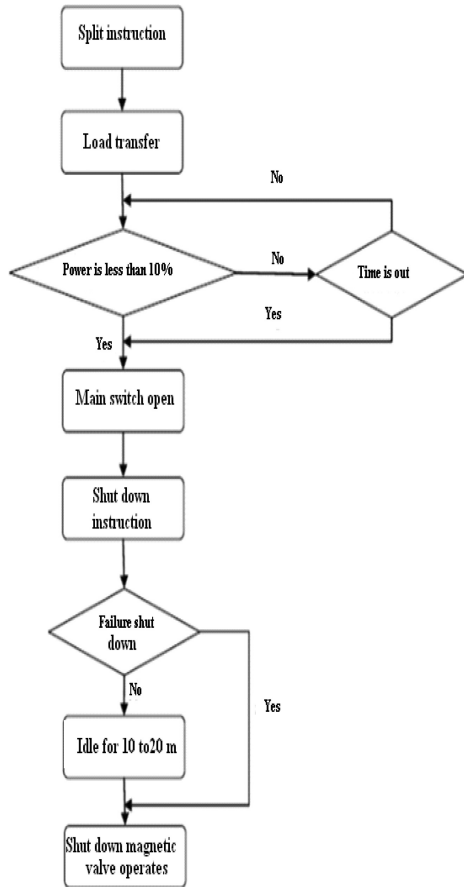


Figure 3. Flow diagram of auto-split and failure shutdown.

set will implement split operation. When the load is transferred to 10%  $P_e$ , the switch of the splitting set will be taken off. If the load on station increases to heavy-load limit in 10 s, the system will call the

parallel program and parallel the split set again to the line. Otherwise, it will split and shut down.

The flow diagram of auto-split and failure shutdown is shown in Fig. 3.

#### 4 CONCLUSION

With the development of automatic control technology of ship, the automatic ship power station has been widely used on board. In this paper, workflow of automatic ship power station based on PLC control is designed and analyzed. This has practical significance in analyzing and solving problems in the operation of the power station and improving the independent innovation ability of ship power plant control technology.

#### REFERENCES

- [1] Zhao Dianli. Marine Electric Installations and System[M]. Dalian: Dalian Maritime University Press, 2009:334–335.
- [2] Liu Xianqiang, Shi Weifeng, Li Weixiang, Monitoring and Control System based on Touch-screen and PLC for Shipboard Power Station[J]. Chinese Journal of Power Sources, 2014(4):89–91.
- [3] LI Wei-xiang, SHI Wei-feng, Zhang Wei, et al. Design of shipboard electrical propulsion monitoring control device based on PLC and touch screen [EB/OL]. Beijing: Sciencepaper Online, 2014-04-25.
- [4] Ye Jiying. Design of Automatic Control System of Marine Ship Power Station Base on PLC[D]. Hangzhou: Zhejiang University of Technology, 2011.
- [5] Pang Kewang, Liang Boning, Liu Weiting. Research on the design of monitoring system on modern shipboard power station [J]. Ship Engineering, 2010(5):27–29.

## Suitability of electrochemical methods to evaluate the corrosion of reinforcing steel in micro-cell and macro-cell states

Zhong-Lu Cao

*Tianjin Port Engineering Institute Ltd. of CCCC First Harbor Engineering Company Ltd., Tianjin, China*  
*School of Civil Engineering, Hebei University of Technology, Tianjin, China*  
*Department of Civil Engineering, Kyushu Institute of Technology, Kitakyushu-shi, Japan*

Hao-Yu Chen, Zhong-Chun Su & Sheng-Dong Mi

*Tianjin Port Engineering Institute Ltd. of CCCC First Harbor Engineering Company Ltd., Tianjin, China*

Lian-Yu Wei

*School of Civil Engineering, Hebei University of Technology, Tianjin, China*

Makoto Hibino

*Department of Civil Engineering, Kyushu Institute of Technology, Kitakyushu-shi, Japan*

**ABSTRACT:** The suitability of using half-cell potential and corrosion rate to evaluate the probability and degree of corrosion of steel in reinforced concrete structure was investigated by comparing and analyzing the values in micro-cell and macro-cell states. The results indicated that the use of half-cell potential to determine the corrosion probability of steel was effective in micro-cell corrosion state, but not suitable in macro-cell corrosion state. With the presence of macro-cell corrosion, some areas in a reinforced structure, where the steels were in a passive state, could be assigned a high corrosion probability when they were corroding at a low rate. The use of corrosion rate calculated by the Stern–Geary equation was reliable and feasible in distinguishing the corrosion degree of steel in both micro-cell and macro-cell corrosion states and therefore was more useful than that of the half-cell potential.

**Keywords:** reinforcing steel; corrosion; suitability evaluation; half-cell potential; corrosion rate

### 1 INTRODUCTION

For chloride-induced corrosion in reinforced concrete structure, half-cell potential and corrosion rate are the commonly used electrochemical parameters to evaluate the state or degree of corrosion in steel bar. The half-cell potential based on ASTM C876 standard only provides a probability judgment on whether the steel is in passive or corroded state, and the decision is significantly affected by the environment. Besides, this standard is not suitable for carbonated concrete and may lead to misjudgment when macro-cell corrosion is present (Cao, Hibino & Goda, 2014a; Cao, Hibino & Goda, 2015). The corrosion rate usually obtained by Linear Polarization Resistance (LPR) or Electrochemical Impedance Spectrum (EIS) is generally considered as micro-cell corrosion rate, and is close to the true corrosion rate only when macro-cell corrosion is

negligible. As the true corrosion rate is equal to the sum of micro-cell and macro-cell corrosion rates, and macro-cell corrosion is very common in reinforced concrete structures, the use of LPR and EIS may lead to underestimation of true corrosion rate. Therefore, whether the determination of corrosion based on half-cell potential and corrosion rate is effective or not to distinguish the probability and degree of corrosion of steel attracts research interest.

For this purpose, the passive steel and rusted steel were cast in two separated cement mortar blocks, and were connected or disconnected by means of a lead wire to simulate the macro-cell or micro-cell corrosion. The half-cell potential and corrosion rate of steels in micro-cell and macro-cell corrosion states were measured and investigated. The suitability of the use of half-cell potential and corrosion rate to determine the probability and degree of corrosion of steel was analyzed and discussed.

## 2 EXPERIMENTAL

### 2.1 Materials

Plain round mild steel bars of diameter and length 19 and 180 mm, respectively, were used in the experiment. The chemical composition of the steel was (wt%): 0.146 C%, 0.223 Si%, 0.521 Mn%, 0.019 P%, 0.010 S%, and the remaining Fe. On one end of the steel bar, a lead wire was fixed by means of a screw and the connection area was sealed by PS resin. In order to prevent atmospheric corrosion and enhance the reliability and accuracy of measurement, the two bare ends of the bars were coated with epoxy resin for a length of 40 mm. The exposed area of the steel was 59.7 cm<sup>2</sup>. The surface of the exposed area was polished by sandpaper No.180 and cleaned with acetone just before placing it in the mold to ensure maximum accuracy of the experimental results. Rusted steel was artificially produced to clarify the suitability of half-cell potential and corrosion rate in determining its probability and degree of corrosion. The rusted steel was usually generated during the production, transportation, and fabrication of reinforcing steel, and therefore was commonly found in reinforced concrete structures just before the concrete was poured or cast. The pre-rusted surface was obtained by spraying tap water on the surface of polished steel once every 2 weeks for 104 days in a room maintained at a constant temperature of 20°C. Finally, the surface of Water-Rusted (RW) steel was covered by yellow-brown oxides with a density of 8.3 mg/cm<sup>2</sup>.

The corrosion behaviors of the steel bars were investigated in cement mortar blocks of dimension 80 × 80 × 160 mm. For each cement mortar specimen, the mix proportion of water/cement/sand was 0.7:1:5. Ordinary Portland cement that met the specification requirements of JIS R5210 and had a density of 3.15 g/cm<sup>3</sup> was used. Sea sand that passed through JIS A 1102 sieve No.4 (4.75 mm opening) and washed by tap water was selected as the fine aggregate. Its density and water absorption were 2.58 g/cm<sup>3</sup> and 1.53%, respectively. For some specimens, chloride ions (3 wt% of cement) were added into the cement mortar at the time of casting as NaCl dissolved in the mix water. All the specimens were allowed to set and harden in the mold for 1 day before being de-molded and then cured for the next 2 weeks in water. After that, they were allowed to dry under laboratory conditions for another 2 weeks, prior to the beginning of experimental measurements.

### 2.2 Methods

The experimental design is shown in Table 1. Each case in Table 1 consists of two specimens defined as A-side and B-side. For specimens in A-side, steels

with polished surface were used, and the chloride content was 0 wt% of cement. On the contrary, for specimens in B-side, steels with RW surface were used, and the chloride content was 0 or 3 wt% of cement. The experimental process is depicted in Figure 1. First, the specimens in A-side and B-side were disconnected for 2 weeks and then they were connected for another 2 weeks. This constitutes one cycle and seven such cycles were performed in this study.

During the whole experimental procedure, half-cell potential referenced to Ag/AgCl electrode, resistance of reinforcing steel (unit: Ω), and resistance of concrete (unit: Ω) were measured at pre-determined intervals using CM-SE1, a device for detecting corrosion developed by Nippon Steel Techno Research. As the current imposed by the device was not uniformly distributed on the surface of steel and was significantly affected by the thickness of concrete cover and the diameter of reinforcing steel, the resistivities of steel and concrete (unit: kΩ cm<sup>2</sup>) would be a function of concrete cover thickness and steel diameter. In this study, these values were calculated by the auxiliary soft switching of this device, which fully considered the influence of concrete cover thickness and steel diameter. Before the measurement, water-saturated cotton was placed between the electrode

Table 1. Experimental design of this study.

Case No.			Surface condition	
	A-Side	B-Side	A-Side	B-Side
5-1	P70-0-33	RW70-0-1	Polished	Water rusted
5-2	P70-0-34	RW70-0-2	Polished	Water rusted
6-1	P70-0-39	RW70-3-1	Polished	Water rusted
6-2	P70-0-40	RW70-3-2	Polished	Water rusted

\*Note: In this table, the steel with initial polished surface was marked as P, the steel with initial water-rusted surface was marked as RW, and the w/c ratio of specimen was marked 70. The chloride content (wt% of cement) of the specimen was marked as 0 and 3. The serial number of specimens was marked as 1, 2, 33, 34, 39, and 40. For example, in P70-0-33, P indicates that the steel had polished surface, 70 shows that the w/c ratio of specimen was 0.70, 0 indicates that the chloride content of specimen was 0 wt% of cement, and 33 indicates that the serial number of specimens was 33.

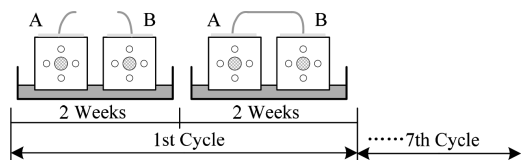


Figure 1. Experimental process of this study.

of the device and the surface of the specimen to ensure good current transmission (Cao, Hibino & Goda, 2014b).

In order to distinguish the micro-cell and macro-cell corrosion current densities, the corrosion current density of steel in the disconnected periods was defined as the micro-cell corrosion current density of steel (Poursaei, Laurent, & Hansson, 2010; Hansson, Poursaei, & Laurent, 2006; Maruya, Takeda, Horiguchi, Koyama, & Hau, 2007; Andrade, Maribona, Feliu & González, 1992). It was calculated by the Stern–Geary equation:  $i_{\text{corr-mi}} = B/R_p$ , where  $R_p$  denotes the resistivity of steel and  $B$  is a constant, whose value is 26 mV for steel in corroded state and 52 mV for steel in passive state.

In the connected periods of each cycle, the macro-cell current flowing between A-side and B-side was measured by a zero-resistance ammeter. The macro-cell corrosion current density of steel was calculated by the equation:  $i_{\text{corr-ma}} = I_{\text{ma}}/A_a$ , where  $I_{\text{ma}}$  is the macro-cell current (unit:  $\mu\text{A}$ ) and  $A_a$  is the surface area of steel (unit:  $\text{cm}^2$ ) acting as anode specimen. The anode specimen was defined as the specimen producing electrons, and it could be judged from the direction of current flow.

### 3 RESULTS AND DISCUSSION

The time evolution curves of half-cell potential and micro-cell and macro-cell corrosion current density of reinforcing steel for cases 5 and 6 are shown in Figures 2 and 3, respectively. As can be seen from Figure 2, with the absence of chloride ions in cement mortars, in the disconnected periods, there was no significant difference between the half-cell potential of steel with polished surface in A-sides and the half-cell potential of steel with RW surface in B-sides. After the steel in A-side was connected with the steel in B-side, a weak macro-cell current flowing between A-side and B-side was detected, and some small changes in the half-cell potential of steels in A-side and B-side were also observed. The formation of the weak macro-cell current was mainly attributed to the imbalance of electrochemical potential of steels in A-side and B-side. The potential imbalance was due to the non-uniform distribution of voids at the steel–mortar interface, the varying diffusion rates of oxygen, the different moisture content, and the various steel surface conditions. The changes in the half-cell potential of steels in A-side and B-side were related to the redistribution of electrons on the surface of steel and the rebalance of electrochemical reactions. With the increase of cycle numbers, the half-cell potential of steel in both A-side and B-side had a tendency to increase as a result of the further passivation of steel.

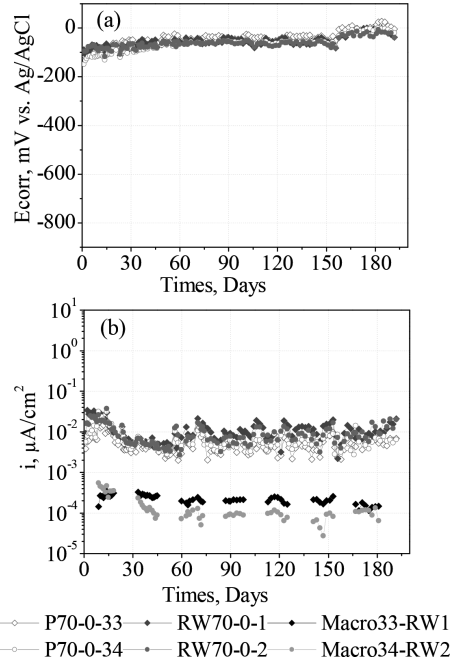


Figure 2. Time evolution curves of (a) half-cell potential and (b) micro-cell and macro-cell current density of steels for case 5.

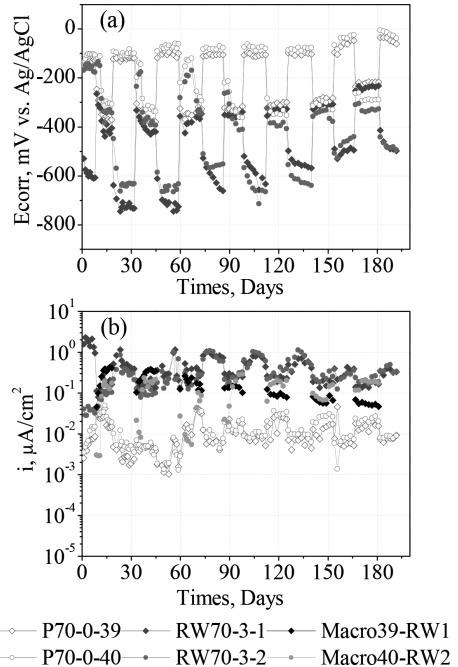


Figure 3. Time evolution curves of (a) half-cell potential and (b) micro-cell and macro-cell current density of steels for case 6.

With the presence of chloride ions (3 wt% of cement) in the specimens of B-side, as shown in Figure 3, the dissolution of steel in B-side was promoted by chloride ions, which resulted in the decrease of half-cell potential of steel in B-side. Therefore, in the disconnected periods, there was a distinct difference between the half-cell potential of steel with polished surface in A-sides and the half-cell potential of steel with RW surface in B-sides. The micro-cell corrosion current density of steel between A-side and B-side can also be obviously distinguished in the disconnected periods. After the steel in A-side was connected with the steel in B-side, under the action of electric potential, the electrons on the surface of the steel in B-side were transferred to the surface of steel in A-side. This transfer of electrons from B-side to A-side not only resulted in the formation of macro-cell current, but also led to the decrease of half-cell potential of steel in A-side and the increase of half-cell potential of steel in B-side. The instantaneous macro-cell current was relatively large when the steel in A-side was connected with the steel in B-side, and subsequently, it decreased quickly to a relatively small value in several seconds, continued to decrease slowly in the next few hours, and finally reached a relatively stable value within 24 h. Corresponding to the change of macro-cell current, similar behaviors were also observed on the half-cell potential of steel in both A-side and B-side. Because of the limitation of the experimental device in our laboratory, continuous measurement of half-cell potential and macro-cell current was impossible. All the data presented in Figures 2 and 3 were measured artificially at predetermined intervals, and the data given in the connected periods were stable values.

The significant change of half-cell potential caused by macro-cell corrosion in the connected periods attracted our attention to discuss the suitability of using ASTM C876 standard to determine the probability of corrosion of steel. According to this standard, when the reference electrode is Ag/AgCl electrode, if the potential of steel is higher than  $-80$  mV, the probability of corrosion of steel is  $<10\%$ . If the potential of steel is less than  $-230$  mV, the probability of corrosion of steel is  $>90\%$ . The corrosion probability of steel is uncertain when the half-cell potential is in the range of  $-80$  to  $-230$  mV. As can be seen from Figure 3, in the disconnected periods, the half-cell potential of steel in A-side ranged from about  $-100$  to  $140$  mV in the first cycle and  $9$  to  $57$  mV in the seventh cycle, which indicated that the corrosion probability of steel improved gradually from the uncertain state to the state of passivation with  $90\%$  probability. However, in the connected periods, because of the influence of macro-cell current, the half-cell poten-

tial of steel in A-side decreased to a value less than  $-230$  mV, which led to the change of judgment on the corrosion probability of steel in A-side. The corrosion probability of steel in A-side changed from the uncertain or passivation state during the disconnected periods into the state of active corrosion with  $90\%$  probability during the connected periods. The different states of steel corrosion probability in the disconnected and connected periods indicated that the macro-cell current has a significant effect on the qualitative judgment of steel corrosion. Therefore, when macro-cell current was present, the qualitative judgment of steel corrosion based on the ASTM C876 standard might be not suitable. Another interesting finding from Figure 3 was that, in the connected periods, the half-cell potential of steel in A-side was very close to that of steel in B-side, although a small potential difference induced by mortar resistance was present. The small half-cell potential difference between steel in A-side and B-side indicates that, in the presence of macro-cell current, the distinction of passive steel and active steel was difficult based on measured half-cell potential values. In real reinforced structures, the steels usually contacted with each other, which was similar to the situation that the steel in A-side was connected with the steel in B-side. By the effect of macro-cell current, some areas in a reinforced structure where the steels were in a passive state could be assigned a high corrosion probability when they were corroding at an insignificant rate. Therefore, when the steel corrosion probability was determined by using ASTM C876 standard, significant attention should be paid to the conclusion, which might be erroneous and misled by the macro-cell corrosion.

As discussed above, the half-cell potential of reinforcing steel only gave the qualitative information, which was prone to be misled by the macro-cell corrosion. Corresponding to the qualitative information, the quantitative information was another important way to evaluate the corrosion state of steel. The effect of the macro-cell corrosion on the qualitative information of steel corrosion has been confirmed, but its effect on the quantitative information of steel corrosion remains unknown. Therefore, whether the quantitative information of steel corrosion was misled or not by the macro-cell corrosion is another area that the author was interested in.

In this study, the quantitative information of steel corrosion was related to the corrosion current density calculated by using the Stern–Geary equation. As described in the experimental section, this corrosion current density was defined as the micro-cell corrosion current density of reinforcing steel, and its time evolution curves are also presented in Figures 2 and 3. According



to the standard for evaluating the corrosion state of reinforcing steel, the steel was in passive state when its corrosion current density was  $<0.1 \mu\text{A}/\text{cm}^2$ ; the corrosion extent of steel was low to moderate in the range of  $0.1\text{--}0.5 \mu\text{A}/\text{cm}^2$ ; moderate to high in the range of  $0.5\text{--}1.0 \mu\text{A}/\text{cm}^2$ ; and the corrosion extent of steel was high when the corrosion current density of steel was  $>1.0 \mu\text{A}/\text{cm}^2$ . As can be seen from Figure 2, in the absence of chloride ions in cement mortars, no significant difference in the corrosion current density of steel between A-side and B-side could be observed, irrespective of whether they were connected or not. The micro-cell current densities of steel in A-side and B-side were about two orders of magnitude lower than  $0.1 \mu\text{A}/\text{cm}^2$ , while the macro-cell current flowing between A-side and B-side was about one order of magnitude lower than the micro-cell current density. Therefore, the very small macro-cell current flowing between steels had little effect on the corrosion state of steel. As can be seen from Figure 3, in the presence of chloride ions (3 wt% of cement) in the mortars of B-side, the micro-cell current density of steel in B-side increased to a value  $>0.1 \mu\text{A}/\text{cm}^2$  and about two orders of magnitude higher than that of steel in A-side. Therefore, in the disconnected periods, the steel in B-side was in the active corrosion state, the steel in A-side was in the passive state, and the use of micro-cell current density to distinguish the passive and corrosion state was reliable. When the steel in A-side was connected with the steel in B-side, an increase of the micro-cell current density of steel in A-side and a decrease of the micro-cell current density of steel in B-side could be observed. The increment and decrement of the micro-cell current density were not significant. The micro-cell current density of steel in A-side was still  $<0.1 \mu\text{A}/\text{cm}^2$  and the micro-cell current density of steel in B-side was still  $>0.1 \mu\text{A}/\text{cm}^2$ . Thus, in the connected periods, using the micro-cell current density of steel to distinguish the passive and corrosion states was possible. This could also be understood that when the passive and active corrosion states coexisted on the surface of steel, the micro-cell current density of steel was more useful than the half-cell potential for distinguishing the corrosion areas. It was worth noting that this conclusion was obtained mainly based on the condition that the area ratio of steel in A-side (passive state) to steel in B-side (active corrosion state) was equal to 1. For conditions in which the area ratio of steel in A-side to steel in B-side was higher or smaller than 1, whether this conclusion was supported or not would be further investigated. The increase of the micro-cell current density of steel in A-side and the decrease of the micro-cell current density of steel in B-side were mainly attributed to the redistribution of electri-

cal signals at the time of measuring the resistivity of steel. Because of the condition that steel in A-side (passive state) was connected with that in B-side (active corrosion state), the electrical signals imposed on the steel in A-side could be partially distributed or transferred to the steel in B-side, which led to the increase of polarization current for unit overpotential and thus resulted in the decrease of polarization resistance of steel in A-side and consequently caused the increase of the micro-cell current density of steel in A-side. Similarly, the electrical signals imposed on the steel in B-side could be partially distributed or transferred to the steel in A-side, which led to the decrease of polarization current for unit overpotential and thus resulted in the increase of polarization resistance of steel in B-side and consequently caused the decrease of the micro-cell current density of steel in B-side. Besides this, the distribution of free electrons on the surface of steels was responsible for the observed changes in micro-cell current density and was just probably a contributory factor. Therefore, attention should be paid to the fact that, when the macro-cell corrosion occurred, the micro-cell current density calculated by using the Stern–Geary equation might be overestimated for the steel in passive state and underestimated for that in active corrosion state.

#### 4 CONCLUSIONS

In micro-cell corrosion state, the use of half-cell potential was very effective in determining the corrosion probability of steel, but in macro-cell corrosion state, the qualitative determination of steel corrosion based on the ASTM C876 standard was not suitable. The distinction of passive steel and active steel was difficult based on the measured half-cell potential values. In the presence of macro-cell corrosion, some areas in a reinforced structure where the steels were in a passive state could be assigned a high corrosion probability when they were corroding at a low rate. Therefore, when the steel corrosion probability was determined by the use of ASTM C876 standard, significant attention should be paid to the conclusion, which might be erroneous and misled by the macro-cell corrosion.

In both micro-cell and macro-cell corrosion states, the use of corrosion rate calculated by the Stern–Geary equation to distinguish the passive state and corrosion state of steel was reliable and more useful than that of the half-cell potential. However, attention should be paid to the fact that, when the macro-cell corrosion occurred, the corrosion rate might be overestimated for the steel in passive state and underestimated for the steel in active corrosion state.

## REFERENCES

- Andrade C., Maribona I.R., Feliu S. & González J. A.. 1992. The effect of macrocells between active and passive areas of steel reinforcements. *Corrosion Science* 33(2): 237–249.
- Cao Z.L., Hibino M., & Goda H. 2014a. Effect of water-cement ratio on the macrocell polarization behavior of reinforcing steel. *Journal of Engineering* (2014): 1–11.
- Cao Z.L., Hibino M., & Goda H. 2014b. Effect of Steel Surface Conditions on the Macro-Cell Polarization Behavior of Reinforcing Steel. *Applied Mechanics and Materials* 584–586: 1771–1779.
- Cao Z.L., Hibino M., & Goda H. 2015. Effect of Nitrite Inhibitor on the Macrocell Corrosion Behavior of Reinforcing Steel. *Journal of Chemistry* (2015): 1–15.
- Hansson C.M., Poursae A., & Laurent A. 2006. Macro-cell and microcell corrosion of steel in ordinary Portland cement and high performance concretes. *Cement and Concrete Research* 36(11): 2098–2102.
- Maruya T., Takeda H., Horiguchi K., Koyama S., & Hau K.L.. 2007. Simulation of steel corrosion in concrete based on the model of macro-cell corrosion circuit. *Journal of Advanced Concrete Technology* 5(3): 343–362.
- Poursae A., Laurent A., & Hansson C.M. 2010. Corrosion of steel bars in OPC mortar exposed to NaCl, MgCl<sub>2</sub> and CaCl<sub>2</sub>: Macro-and micro-cell corrosion perspective. *Cement and Concrete Research* 40(3): 426–430.

## Green consumption attitudes of the tourists lodging in resort hotels

Chia-Chia Lin

*Department of Tourism and Leisure Management, WuFeng University, Minxiong, Taiwan*

Wen-Tan Wu

*Institute of Leisure Recreation and Travel Management, ToKo University, Chiayi County, Taiwan*

**ABSTRACT:** The purpose of this study was to investigate the green consumption attitudes of resort hotel tourists. In this survey research, questionnaires were distributed to tourists derived from non-probability convenience sampling. A total of 360 tourists from resort hotels of Alishan area were surveyed, and 274 questionnaires were given back at a return rate of 76%. Descriptive statistics, independent t-test, and one-way Analysis of Variance (ANOVA) are further used to analyze the collected data.

The results showed that no significant difference exists between genders regarding green consumption attitude. However, significant difference did exist among different age and marital status groups ( $p < .05$ ). Results of a comparative analysis showed that individuals in the 30–39 and 40–49 age groups paid higher attention to “green concept” than those in the 20–29 age group.

Finally, further suggestions were made according to the research results. This study suggested that the government department of environmental protection should strengthen the promotion and guidance of the green concept and legislate related laws to strengthen the consumers’ cognition of environmental protection.

**Keywords:** green consumption attitudes, consumer behavior, resort hotel

### 1 INTRODUCTION

At present, Taiwan is becoming one of the developed countries because of its high socioeconomic performance. Therefore, its citizens demand a better living quality and have a great concern toward the environment. Green consumption is doubtlessly a must in this trend.

Recently, international hotel entrepreneurs have been paying an increasing attention to this issue. They have built green hotels or green buildings to offer tourists a new alternative of accommodations.

Taiwan government is rapidly promoting the ecological tour. In 2000, the Outline of Sustainable Development of R.O.C. indicated that government should present a tourism white paper and eco-tour development policy, and build an eco-tour accreditation system to point out a direction for eco-tour work. Unfortunately, a perfect plan for its execution is still not available to the environmental management, regulations, and system of hotels (Su & Liao, 2005). In particular, in domestic hotel enterprises, the concept of green hotel is still in its initial stage. Only a few hotels are under the green hotel procession by saving energy or reducing the use of chemical detergents. Their purpose is to lower the

management costs. Therefore, realizing the concept of green hotel is actually difficult for hotels that have been in business for several years.

A hotel is a large place suitable for living, whose energy consumption and pollutant emission are very high. To follow the trend of eco-tourism and sustainable tourism, the system of green hotel and accreditation means has been recently built, including environmental hotels guide published by Green Seal in the United States, environmental hotel evaluation system built by Canada, and green hotel leveling regulations provided by Mainland China. Taiwan, however, has not yet had any plan and preparation with the related policy. Therefore, to assure the hotel service and management corresponding to the spirit of sustainable tourism, building hotel management policy, setting up a hotel environment protection valuation system, and promoting the accreditation assistance work are necessary.

Alishan is an area rich in natural scenery, attracting a large number of tourists throughout the year. Thus, there exists a high demand for accommodation. The primary purpose of this study was to discuss tourists’ green consumption attitude. In addition, the researchers intended to test whether any significant difference is found between the

different personal variables such as gender, age, marital status, and educational background.

The results of this study could effectively predict tourists' option of hotel accommodation. They could provide a foundation for hotel entrepreneurs to evaluate the possibility of running a green building as well. Furthermore, the results could serve as a valuable reference for government authorities to be engaged in the green marketing.

## 2 LITERATURE REVIEW

### 2.1 *Green consumption attitude*

According to a report on human development by the United Nations in 1996, individual consumption of energy in industrial countries is nine times higher than that in the commercial ones, although the corresponding population was only one-fifth of the global population. World Wild Fund for Nature (WWF), the most well-known environmental conservation organization, made an announcement 1 day before the world environment day of 2000. According to that report on earth life, in Taiwan, individual average energy consumption was 3.42 times higher than the average global value, and it ranked second in the world. This evidenced that environmental problems in Taiwan are more serious than that of most other countries of the world. The average energy consumption in the United States was high, but it ranked sixth. Its pressure value was less than two-thirds of Taiwan's. Mainland China ranked 60 with a pressure value of 0.86. This aim of this study was to analyze the environment pressure caused by the consumption of natural resources.

Green consumption attitude is a combination of special environmental characters and a belief coming from a direct relationship of the entire environment with people and objects. Such a combination includes cognition of the environment and an overall evaluation leads to a sustainable behavior inclination (Hines, et al., 1987). Accordingly, green consumption attitude means an individual's conception of the overall environment and his/her viewpoints of the human responsibilities and roles in the environment. Earlier studies on the behaviors of the environmental responsibilities usually hypothesized that knowledge affects attitude in a linear model and attitude will influence the thought of the behaviors (Cottrell & Graefe, 1997).

### 2.2 *Consumer behavior*

The study of consumer behavior as a separate marketing discipline began when marketers realized that consumers did not always act or react as marketing theory suggested they would (Leon G. & Leslie Lazar,

2000). Despite a sometimes "me too" approach to fads and fashions, many consumers rebelled at using the products identical to that others used. Many early theories concerning consumer behavior were based on economic theory, on the notion that individuals act rationally to maximize their benefits (satisfactions) in the purchase of goods and services. Later research discovered that consumers are likely to purchase impulsively, and to be influenced not only by family and friends, advertisers, and role model, but also by mood, situation, and emotion. All of these factors combine to form a comprehensive model of consumer behavior that reflects both the cognitive and emotional aspects of consumer decision making.

The study of culture includes all aspects of a society. Language, knowledge, laws, and customs give a society its distinctive character and personality. In the context of consumer behavior, culture is defined as the sum of learned beliefs, values, and customs that serve to regulate the consumer behavior in a particular society. Beliefs and values are guides for consumer behavior; customs are usual and accepted ways of behaving (Leon G. & Leslie Lazar, 2000).

### 2.3 *Resort hotel*

With the increasing awareness of global environmental protection, the concept of environmental protection hotel and eco-hotel is gradually attracting attention worldwide. Tourism Council Australia (1998) claimed that green hotels are tourism hotels depending on the nature; they run in an environment-sensitive way, maintaining an environment where green products and green services are provided for tourists. Moreover, they are an eco-like environment, making tourists feel healthy, fresh, and comfortable. Tourists, during their stay in the hotel, can enjoy nature, and the process and education of nature protection (Guo & Chen, 2003). Green Mountain State (2002) stated that a green hotel attempts to create an environment with the participation of staff members and tourists. Therefore, it is necessary to make a careful observation into every operational procedure to realize the least significant impact on the environment, search ways to educate tourists and hotel staff and faculty, and remind everybody to work hard and stick to the promise to offer a service that tourists expect and desire.

## 3 RESEARCH METHODOLOGY

### 3.1 *Research participants and sampling method*

A total of 10 resort hotels in Alishan were chosen: Alishan House, Gau Shan Ching Hotel, Alishan Shermuh International Tourist Hotel, Ho Fong Villa Hotel, Gau Shan Ching Hotel, Dafeng Hotel,

Alishan Youth Activity Center, Alishan Gou Hotel, and Ying Shan Hotel. Study participants were 40 hotel residents from each resort hotel. Questionnaires were distributed to them from 21 June 2015 to 20 July 2015. A total of 360 questionnaires were filled out. After removing the invalid ones, 274 copies were analyzed. The valid return rate was 76%. Non-probability convenience sampling method was adopted in this study.

### 3.2 Research tools

#### 3.2.1 Questionnaire designing and scoring

Questionnaires were used to collect data in this survey research. After reviewing the literature, the researchers compiled a questionnaire entitled "Questionnaire of Resort Hotel Tourists' Attitude toward Green Consumption". There were two parts in the questionnaire. The first part included questions regarding the personal background of resort hotel tourists, such as gender, marital status, and occupation. The data were measured according to the nominal levels. As for educational background, age, and individual income, the data were measured based on the ordinal levels. The second part concerned tourists' attitude toward green consumption. It was a modified version of Pong's (2002), Lee and Gan's (2007) questionnaires. A total of 14 questions were asked and answered on a five-point Likert scale: 5 – strongly agree, 4 – agree, 3 – neutral position, 2 – disagree, and 1 – strongly disagree. Participants filled up the questionnaire based on their current situation. The higher scores the participants received on the scale, the more positive attitude they held or vice versa.

#### 3.2.2 Factor analysis

After compiling the questionnaire, it was pre-tested by distributing to 90 tourists. Then, an item analysis and factor analysis were conducted to modify inappropriate statements before a formal questionnaire was established. In the factor analysis of tourists' attitude toward green consumption, statements were categorized into three factors: green conception, purchasing behaviors, and negative disappointment. The total explanation variance was 60%. The first factor was therefore named green conception, and the factor explanation variance reached 30.1%. The second factor covered the tourists' green attitude of purchasing behavior. For example, when staying in a hotel, tourists would consider environment protection to make or reject a purchase. The explanation variance in the factor "purchasing behavior" was 16.9%. As for the third factor, the statements in this category were more negative ones.

#### 3.2.3 Validity and reliability

After compiling the questionnaire, to assure its appropriateness, it was given to eight environmental

educators and scholars to review the content validity. Moreover, the three sub-scales, green conception, purchasing behavior, and negation and disappointment, were analyzed to determine the internal consistency of each item in order to test the reliability of the questionnaire. The corresponding Cronbach  $\alpha$  coefficients were 0.845, 0.676, and 0.612.

## 4 STUDY RESULTS

### 4.1 Description of the personal background of tourist interviewees

Results of descriptive statistic analysis revealed that female visitors (N = 217, 59%) are more than male visitors (N = 147, 40.4%) and married tourists (N = 235, 64.6%) are more than the single ones (N = 129, 35.4%). The age distribution data are as follows: there are 73 tourists (20.2%) in the age range of 20–29 years; 132 (36.6%, the highest percentage) in the 30–39 age-group; 101 (28.0%) in the 40–49 range; and 55 tourists (15.2%) from age 50 to 59. Regarding the tourists' educational background, it was found that 223 people were university or college graduates with the highest percentage of 61.3%. Followed were high school graduates or below (N = 120, 32.9%). Finally, graduates above university level constituted 21 people with the least proportion of 5.8%.

### 4.2 Tourists' attitude toward green consumption

#### 4.2.1 A significant difference test on different genders of tourists' green consumption attitude

Table 1 summarizes the results of difference test on different genders of tourists' attitude toward green consumption on three categories: green conception, negation and disappointment, and purchasing behaviors. No significant difference was found between them.

#### 4.2.2 A significant difference test on different marital statuses of tourists' green consumption attitude

Table 2 summarizes the difference test on different marital statuses of tourists' attitude toward green consumption on three categories: green conception, negation and disappointment, and purchasing behaviors. Significant differences were found in the category of green conception ( $p < .05$ ).

#### 4.2.3 Attitude toward green consumption of tourists of different ages

Table 3 summarizes the attitude toward green consumption of tourists of different ages. Significant differences were still found in the

Table 1. Attitude toward green consumption of different genders.

Attitude toward green consumption	Sex	Number	Mean	S.D.	t-value	p-value
Green conception	Male	113	4.65	0.42	-0.611	0.542
	Female	161	4.67	0.39		
Negation and disappointment	Male	113	2.74	0.87	1.677	0.094
	Female	161	2.59	0.84		
Purchasing behavior	Male	113	4.11	0.55	1.253	0.211
	Female	161	4.03	0.60		

\*p<.05.

Table 2. Attitude toward green consumption of tourists of different marital statuses.

Attitude toward green consumption	Sex	Number	Mean	S.D.	t-value	p-value
Green conception	Male	181	4.69	0.35	2.217	0.034*
	Female	93	4.60	0.47		
Negation and disappointment	Male	181	2.60	0.88	-1.554	0.121
	Female	93	2.74	0.81		
Purchasing behavior	Male	181	4.10	0.57	1.542	0.124
	Female	93	4.00	0.59		

\*p<.05.

Table 3. Attitude toward green consumption of tourists of different ages.

Attitude toward green consumption	Age	Number	Mean	S.D.	t-value	p-value	Post-hoc test
Green conception	20–29	56	4.50	0.51	5.574	0.001*	2 > 1 3 > 1
	30–39	101	4.73	0.35			
	40–49	78	4.68	0.38			
	>50	39	4.67	0.33			
	Total	274	4.66	0.40			
Negation and disappointment	20–29	56	2.80	0.84	1.147	0.330	
	30–39	101	2.58	0.89			
	40–49	78	2.62	0.82			
	>50	39	2.65	0.85			
	Total	274	2.65	0.86			
Purchasing behavior	20–29	56	4.03	0.59	0.444	0.721	
	30–39	101	4.10	0.59			
	40–49	78	4.03	0.60			
	>50	39	4.2	0.51			
	Total	274	4.06	0.58			

\*p<.05.

category of green conception (p<.05) among the three factors. The results of post hoc test reveal that people in the age range of 30–39 hold stronger attitude than those in the 20–29 range, and tourists ranging from age 40 to 49 hold stronger attitudes than those in the age range of 20–29.

#### 4.2.4 Attitude toward green consumption of tourists with different educational background

Table 4 summarizes attitude toward green consumption of tourists with different educational background. No significant difference was found among the three factors.

Table 4. Attitude toward green consumption of tourists of different educational background.

Attitude toward green consumption	Educational level	Number	Mean	S.D.	t-value	p-value
Green conception	Below high school	92	4.67	0.39	1.81	0.835
	Univ. or college	171	4.66	0.40		
	Graduate school	11	4.61	0.45		
	Total	274	4.66	0.40		
Negation and disappointment	Below high school	92	2.65	0.81	1.114	0.320
	Univ. or college	171	2.62	0.90		
	Graduate school	11	2.92	0.64		
	Total	274	2.65	0.86		
Purchasing behavior	Below high school	92	4.02	0.62	0.604	0.547
	Univ. or college	171	4.09	0.55		
	Graduate school	11	4.00	0.67		
	Total	274	4.06	0.58		

## 5 CONCLUSION

This study investigated the personal background differences of tourists visiting Alishan. Similar to Chen's (2001) study results, no difference was found regarding genders. It implies that gender difference will not lead to different attitude toward green consumption.

The results of this study on the effect of marital status on the green consumption indicated a significant difference between married and single participants in the factor of green conception ( $p < .05$ ). This indicates that people of different marital statuses will hold different green conception attitudes. The attitude of the married peoples is more positive than that of the single. This could be because the former have a family and children. They have to play the role of parents and educators. Therefore, their attitude is stronger than the single ones. Concerning the effect of age difference on the attitude, a significant difference was also found, especially in the factor of green conception ( $p < .05$ ). The result of the post hoc test was also consistent with Chen's (2001) research findings: the attitude of people in the age range of 30–49 is stronger than that found in the age range of 20–29. This may be attributed to life habits, family education, and personal education. Tourists in the age group of 30–49 seem to emphasize green conception more, as they were still under school education when government was highly promoting environmental protection.

Besides, the results show that no significant difference toward the attitude of green consumption was found in the different educational background. Thus, educational background will not affect tourists' green consumption attitude.

The findings of this study indicate that differences in age and marital status cause significant differences of tourist attitude, particularly green conception. Consequently, it is suggested that authorities of environmental protection should strengthen their promotion. Knowledge of environmental protection should be included in the school curricula by educational authorities to build a correct green consumption attitude among people. Through the promotion of green consumption, environment pollution can be reduced. Moreover, legislative authorities should establish laws and regulations to enhance people's awareness on environmental protection.

## REFERENCES

- [1] Cottrell, S. P. & Graefe, A. R., 1997, Testing a conceptual framework of responsible environment behavior. *Journal of Environmental Education*, Vol.29 No. 1, pp. 17–27.
- [2] Elkington, J., Hales, J., & Makower, J., 1990, *The green consumer*, New York: Penguin Books.
- [3] Gilg, A., Barr, S., & Ford, N., 2005, Green consumption or sustainable lifestyles? Identifying the sustainable consumer, *Futures*, Vol. 37, pp. 481–504.

- [4] Green Hotels Association, What are green hotels?, 2002 Retrieved June 5, 2008, from <http://www.green-hotels.com/whatare.htm>
- [5] Guo, N. W. & Chen, Y. S., 2003, Sustainable tourism management: Suggestions of green hotel develop in Taiwan, Presented at The 3rd Session Tourism leisure and Hospitality industry Sustainable Management Academic Conference.
- [6] Hines, J. M., Hungerford, H. R., & Tomera, A. N., 1987, Analysis and synthesis of research on responsible environment behavior: A meta-analysis, *Journal of Environmental Education*, Vol. 18 No. 2, pp. 1–8.
- [7] Leon G. Schiffman & Leslie Lazar Kanuk, 2000, *Consumer Behavior*, 7th ed, Upper Saddle River, NJ: Prentice Hall.
- [8] Lu, C. C., 1994, A study of green consumer behavior for homemaker union in Taiwan, Master Thesis of the Department of Commerce, National Taiwan University.
- [9] Peng, W. C., 2002, Relationships between personal value, product attributes, green attitude and green consumer behavior, Master Thesis of the Department of Business Administration, National Cheng Kung University.
- [10] Philip Kotler, 1997, *Marketing Management Analysis: Planning and Control*, 9th ed. Upper Saddle River, NJ: Prentice Hall. pp.4–11.
- [11] Republic of China People: Green Hotel Grading Rules, 2004. Retrieved Feb. 5, 2008, from <http://big5.huaxia.com/xw/dl/00050560.html>
- [12] Shrum, L. J., McCarty, J. A., & Lowrey, T. M., 1995, Buyer characteristics of the green consumer and their implications for advertising strategy, *Journal of Advertising*, Vol. 24 No. 2, pp. 71–82.
- [13] The State Economic and Trade Commission., Standards for green hotels promulgated, 2008. Retrieved June 5, 2008, from <http://www.cenews.com.cn>.
- [14] Wang, J. C., 2005, Constructing a mechanism for green hotel certification in Taiwan, Master Thesis of the Graduate Institute of Environmental Education, National Taiwan Kaohsiung Normal University.
- [15] Weber, A. L., 1991, *Introduction to psychology*, New York: Harper Perennial.
- [16] Yu, N. & Lai, M. S., 2000, Origin, present situation and future of the green consumption movement, *Journal of Environmental Engineer*, Vol. 11 No.3, pp. 6–15.



## Comparison of prediction models for shrinkage and creep of high-strength, lightweight aggregate concrete

Sheng-qi Mei, Hui-bing Xie, Li Su, Jian Gong, Kun Guo & Yuan-feng Wang

*School of Civil Engineering, Beijing Jiaotong University, Beijing, China*

**ABSTRACT:** The significance of shrinkage and creep in long-term deformation and mechanical state of concrete structures is widely recognized. However, creep and shrinkage of lightweight aggregate concrete with high moisture content is not the same as normal aggregate concrete. On the basis of the summary of Chinese regulation model, MC2010 model, ACI209 model, B3model, and combination of the existing literature data, the applicability of these models in predicting creep and shrinkage of High-Strength, Lightweight Aggregate Concrete (HSLWAC) is analyzed. The results indicate that MC2010 and ACI209 models have good precision for basic creep, but not for shrinkage because of the high water content in lightweight aggregate. Therefore, a modified MC2010 model considering the effect of aggregate moisture content is presented in this paper. Comparing with the experimental data shows that the modified model is more feasible for predicting shrinkage of HSLWAC.

**Keywords:** high-strength, lightweight aggregate concrete; shrinkage; creep; prediction models

### 1 INTRODUCTION

Regulations of technology of lightweight aggregate concrete in China (2002) defines Lightweight Aggregate Concrete (LWAC) as a mixture of light aggregate, light sand or ordinary sand, cement, and water with dry apparent density not exceeding 1950 kg/m<sup>3</sup>. With the advantages of lightweight, the presence of environment protecting materials, and cost saving, LWAC has been widely applied in the field of modern civil engineering (Alduaij et al. 1999, Liu et al. 2010). High-Strength, Lightweight Aggregate Concrete (HSLWAC) refers to strength grade more than LC40 mixture with high-strength, lightweight aggregate (mainly ceramsite) (Ye et al. 2007). Lightweight aggregate is about 25–30% lighter than normal aggregate in the same concrete strength grade.

Creep is the increase of strain under continuous stress (Neville et al. 1983). Accumulated effect of concrete creep can lead to slope, excessive deformation of structure, and even catastrophic accident (Qi et al. 2011, Bazant et al. 2012). Hence, so far, researchers have conducted several experimental studies and theoretical analyses of creep in different types of concrete, and proposed the corresponding calculation models (Bazant & Baweja 2000, ACI 1992, CEB-FIP 2010). To date, researchers have conducted several experimental research works on the basic performance and engineering application of High-Strength, Lightweight Aggregate

Concrete (HSLWAC) (Jiao et al. 2014, Sun et al. 2007, Tang 2013, Song et al. 2002). Among them, Sun et al. (2007) found that the early shrinkage of high-strength, lightweight aggregate is smaller than that of ordinary high-strength concrete because of the difference in the moisture content of the aggregate. With the loss of aggregate moisture content by hydration and drying effect, the late shrinkage increases gradually. On the basis of the test results, researchers only analyzed the phenomenon, and did not put forward prediction models of shrinkage and creep of high-strength lightweight aggregate.

Although Regulations of technology of lightweight aggregate concrete in China put forward the calculation model (hereinafter referred to as JGJ51-2002 model) for light sand concrete, the grade scope is only up to LC55 and LC60 (corresponding to axial compressive strengths of 35.5 and 38.5 MPa, respectively), and the drying shrinkage and autogenous shrinkage considered no details, which obviously cannot meet the demand of the application of high-strength, lightweight aggregate concrete.

First, this paper summarizes the application scope and calculation process of the JGJ51-2002, MC2010, ACI209, and B3 models. Then, prediction accuracies for shrinkage and creep of HSLWAC were compared. Finally, the MC2010 model was corrected by considering the effect of aggregate moisture content.

## 2 SUMMARY OF MODELS

### 2.1 Applicable scope

The applicable scopes of Chinese regulations model, MC2010 model, ACI209 model, and B3 model are shown in Table 1, where C and LC represent the normal concrete and lightweight concrete grades,  $\bar{f}_c$  is the mean compressive strength, and  $\sigma$  is the loading stress.

### 2.2 Calculation process

#### JGJ51-2002 model

In the *Regulations of technology of lightweight aggregate concrete*, shrinkage  $\omega(t)$  calculation equation is shown as follows:

$$\omega(t) = \omega(t)_0 \beta_1 \cdot \beta_2 \cdot \beta_3 \cdot \beta_5 \quad (1)$$

$$\omega(t)_0 = \frac{t}{a + bt} \times 10^{-3}, \quad (2)$$

where  $\omega(t)$  is the shrinkage value of light sand concrete;  $\omega(t)_0$  is the change value of shrinkage with time;  $t$  is the loading age (d);  $\beta_1$ ,  $\beta_2$ ,  $\beta_3$ , and  $\beta_5$  are correction coefficients; and  $a$  and  $b$  are the calculating parameters.

The creep coefficient can be calculated as:

$$\phi(t) = \phi(t)_0 \cdot \xi_1 \cdot \xi_2 \cdot \xi_3 \cdot \xi_4 \cdot \xi_5 \quad (3)$$

$$\phi(t)_0 = \frac{t^n}{a + bt^n}, \quad (4)$$

where  $\xi_1$ ,  $\xi_2$ ,  $\xi_3$ ,  $\xi_4$ , and  $\xi_5$  are correction coefficients.

Table 1. Applicable scope.

Prediction model	Year	Applicable scope
JGJ51-2002	2002	LC15–LC60; Aggregate density: 600–1900 kg/m <sup>3</sup> ; other same as normal concrete.
MC2010	2010	C20–C130, LC8–LC80; Aggregate density: 800–2600 kg/m <sup>3</sup> .
ACI209	1992	Applied for normal weight, light sand, and all light concretes; Type I and III ce-ment; Cement density. 279–446 kg/m <sup>3</sup> .
B3	1995	$\bar{f}_c$ : 17–70 MPa; Aggregate/cement weight ratio 2.5–13.5; Type I, II, and III cement.

#### MC2010 model

Concrete shrinkage in MC2010 model is divided into basic shrinkage  $\varepsilon_{cas}(t)$  with no moisture loss and dry shrinkage  $\varepsilon_{cds}(t, t_s)$ , as shown in Equation 5:

$$\varepsilon_{cs}(t, t_s) = \varepsilon_{cas}(t) + \varepsilon_{cds}(t, t_s), \quad (5)$$

where  $t$  is the concrete age,  $t_s$  is the drying age, and  $t-t_s$  is the drying time.

Shrinkage of LWAC in MC2010 model is of high strength corresponding to the correction coefficient based on normal concrete, as shown in Equation 6:

$$\varepsilon_{lcs} = \eta \cdot \varepsilon_{cas}(t, t_s), \quad (6)$$

where  $\eta = 1.5$  for LC8, LC12, and LC16 and  $\eta = 1.2$  for LC20 and higher strength grade.

Creep coefficient in MC2010 is also divided into basic creep  $\phi_{bc}(t, t_0)$  and drying creep  $\phi_{dc}(t, t_0)$ , as shown in Equation 7:

$$\phi(t, t_0) = \phi_{bc}(t, t_0) + \phi_{dc}(t, t_0), \quad (7)$$

where  $t$  is the concrete age and  $t_0$  is the loading age.

For lightweight aggregate concrete, the creep coefficient can be obtained by multiplying density correction coefficient based on normal concrete:

$$\phi_l = \eta_E \cdot \phi(t, t_0), \eta_E = (\rho / 2200)^2, \quad (8)$$

where  $\rho$  is the dry density.

#### ACI 209-92 model

The equations to calculate the total shrinkage are as follows:

$$\varepsilon_{sh}(t, t_c) = \frac{(t - t_c)^a}{f + (t - t_c)^a} \cdot \varepsilon_{shu} \quad (9)$$

$$\varepsilon_{shu} = 780 \gamma_{sh} \times 10^{-6} \quad (10)$$

$$\gamma_{sh} = \gamma_{sh,dc} \gamma_{sh,RH} \gamma_{sh,vs} \gamma_{sh,s} \gamma_{sh,\psi} \gamma_{sh,c} \gamma_{sh,a}, \quad (11)$$

where  $t_c$  is drying age,  $f$  and  $a$  coefficients,  $\gamma_{sh,dc}$ ,  $\gamma_{sh,RH}$ ,  $\gamma_{sh,vs}$ ,  $\gamma_{sh,s}$ ,  $\gamma_{sh,\psi}$ ,  $\gamma_{sh,c}$ , and  $\gamma_{sh,a}$  are parameters for loading age, related humidity, size, slump, aggregate content, and air content, respectively.

The equations to calculate creep compliance are as follows:

$$\phi(t, t_0) = \frac{(t, t_0)^\psi}{d + (t, t_0)^\psi} \phi_u \quad (12)$$

$$\phi_u = 2.35 \gamma_c \quad (13)$$

$$\gamma_c = \gamma_{c,t0} \gamma_{c,RH} \gamma_{c,vs} \gamma_{c,s} \gamma_{c,\psi} \gamma_{sh,a}, \quad (14)$$

where  $d = 10$  and  $\gamma_{c,t0}, \gamma_{c,RH}, \gamma_{c,VS}, \gamma_{c,s}$  and  $\gamma_{c,a}$  are parameters for loading age, related humidity, size, slump, aggregate content, and air content, respectively.

### B3 model

The creep compliance equations for B3 model are:

$$J(t, t') = q_1 + C_0(t, t') + C_d(t, t', t_0) \quad (15)$$

$$q_1 = 0.6 \times 10^6 / E_{28} \quad (16)$$

$$C_0(t, t') = q_2 Q(t, t') + q_3 \ln[1 + (t - t')^n] + q_4 \ln\left(\frac{t}{t'}\right) \quad (17)$$

$$C_d(t, t', t_0) = q_5 [\exp\{-8H(t)\} - \exp\{-8H(t_0)\}]^{1/2}, \quad (18)$$

where  $E_{28} = 57000 \sqrt{f_c}$  is the elastic modulus and  $q_2, q_3, q_4,$  and  $q_5$  are the coefficients considering the influence of cement content, water-cement ratio, aggregate cement ratio, and final shrinkage, respectively.

## 3 MODEL VALIDATION

### 3.1 Shrinkage

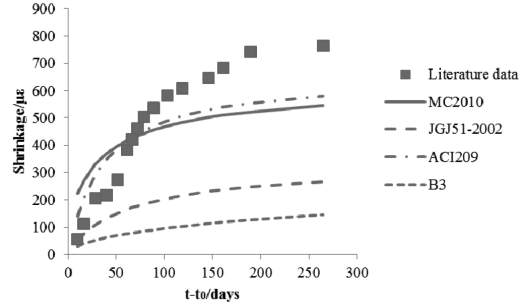
Comparison of two groups' shrinkage data of HSLWAC specimen in Sun et al. (2007) and calculation results are shown in Figure 1, where  $t-t_0$  is the drying time of shrinkage.

It can be seen from Figure 1 that the JGJ 51-2002 and B3 models seriously underestimated the shrinkage deformation of HSLWAC. Although the precision of MC2010 and ACI209 models is good initially, they did not respond to the development trend well. The reason is that more pore water exists in LWAC, which reduces hydration and dry shrinkage in the early stage. As the hydration reaction continues, water consumption increased and gradually exceeded the aggregate moisture content, and hence shrinkage increased rapidly. Although a correction coefficient is multiplied in the MC2010 model for lightweight aggregate shrinkage, the comparison indicates that simple parameters cannot accurately reflect the shrinkage characteristics of LWAC.

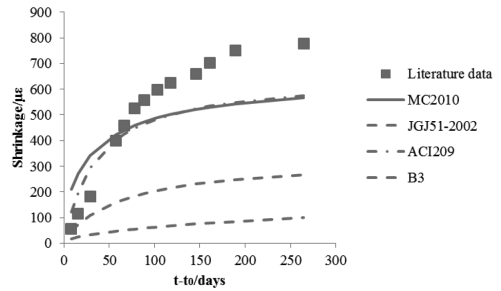
### 3.2 Creep

Comparison of the creep experimental data of HSLWAC specimens in Sun et al. (2007) and calculation results are shown in Figure 2, where  $t-t'$  is the drying time of creep.

Figure 2 shows that the B3 and JGJ 51-2002 models overestimate the creep of HSLWAC, while the MC2010 and ACI209 models are of higher prediction accuracy. It is worth noting that the

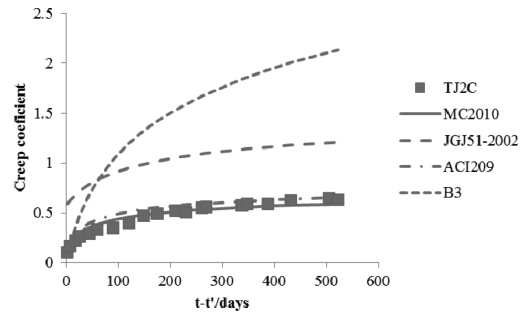


(a) The first group data

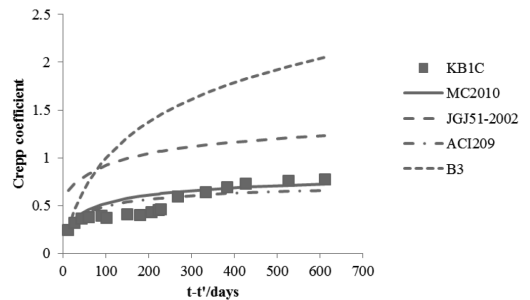


(b) The second group data

Figure 1. Comparison analysis of shrinkage of HSLWAC.



(a) The first group data



(b) The second group data

Figure 2. Comparison analysis of creep of HSLWAC.

calculation results in this paper did not multiply the correct coefficient for the MC2010 model. This is because the selected creep data were basic creep, which eliminated the effect of aggregate moisture content. Engineers should pay attention to actual calculation, and decide whether to use the model correction coefficient based on real conditions.

#### 4 MODEL MODIFICATION

According to the above calculation analysis, the results show that the MC2010 and ACI209 models have a poor prediction for shrinkage of HSLWAC.

To validate the performance of the MC2010 model for normal aggregate high-strength concrete, data of two groups were selected in Sun et al. (2007) for analysis. The MC2010 model separates the drying shrinkage from autogenous shrinkage even more tallies with the development of high-strength concrete shrinkage deformation.

The results show that the MC2010 model has a good prediction for shrinkage of normal high-strength concrete. MC2010 specification also

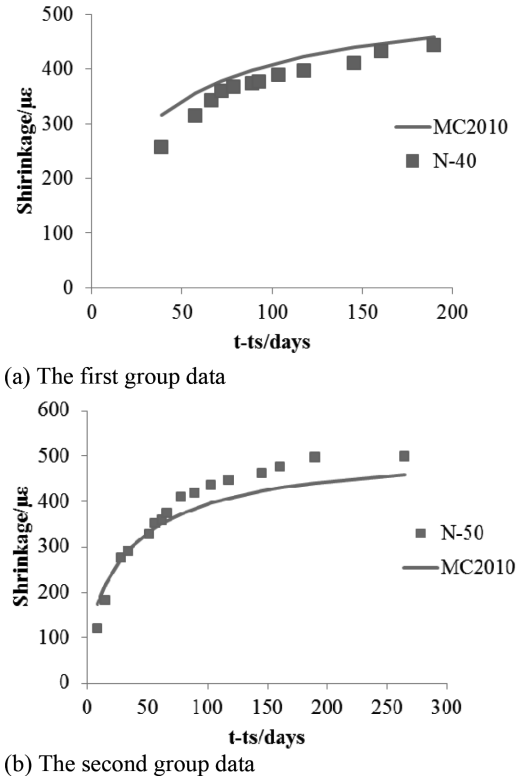
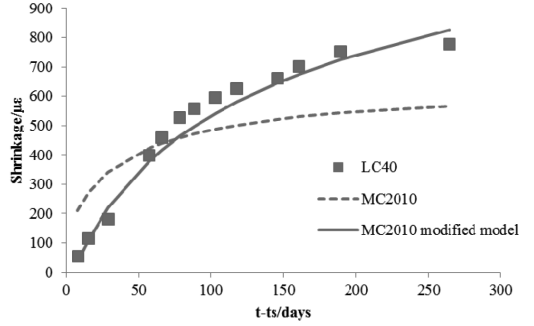
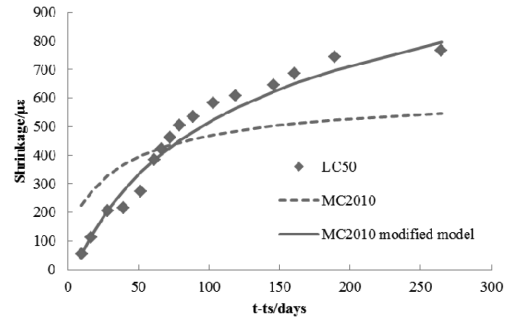


Figure 3. Comparison analysis of shrinkage of normal high-strength concrete.



(a) The first group data



(b) The second group data

Figure 4. Validation of the modified MC2010 model.

showed that the influence of the moisture content of lightweight aggregate should be considered. In order to compute preferably the result, the MC2010 model was modified by considering the influence of moisture content of aggregate.

As aggregate moisture content will gradually decrease with the hydration reaction, this paper defines the moisture content in raw material preparation phase as the initial moisture content, and the power function multiplied by the corresponding form of logarithmic function over time is used to characterize the changing of moisture content during service stage. The correction model form is shown below:

$$\epsilon_{ts} = \beta(Z) \cdot \epsilon_{cs}(t, t_s) \quad (19)$$

$$\beta(Z) = a \cdot (100Z)^b \cdot (c \cdot \ln(t - t_s) - d), \quad (20)$$

where  $\epsilon_{ts}$  is the total shrinkage calculated by the modified model,  $\beta(Z)$  is the coefficient of the influence of moisture content in lightweight aggregate,  $\epsilon_{cs}(t, t_s)$  is the total shrinkage calculated by the MC2010 model, and  $a$ ,  $b$ ,  $c$ , and  $d$  are all constant coefficients.

By combining test data of seven groups with different moisture content in Sun et al. (2007), the function parameters have been fitted by using SPSS software as:

$$\beta(Z) = 2.5 \cdot (100Z)^{-0.3} \cdot (0.43 \cdot \ln(t - t_s) - 0.7), \quad (21)$$

where  $Z$  is the percentage of moisture content,  $t - t_s$  is the drying time of shrinkage.

Validation of the modified model is shown in Figure 4. It can be found that the modified MC2010 model has higher prediction accuracy for shrinkage of HSLWAC.

## 5 CONCLUSIONS

This paper analyzed the prediction accuracy of the JGJ 51-2002 model, MC2010 model, ACI209 model, and B3 model for creep and shrinkage of HSLWAC, and proposed a modified model by considering the influences of moisture content of lightweight aggregate. Comparison analysis results showed that the MC2010 and ACI209 models have high precision for predicting basic creep of HSLWAC. All the above models have poor precision for prediction shrinkage of HSLWAC because of the high water content in the lightweight aggregate. By considering the influence of aggregate moisture content changes over time, the MC2010 model is modified. Compared with the actual experimental process, the results show that the prediction accuracy of the MC2010 model for shrinkage of HSLWAC has improved significantly. In addition, it should be carefully decided whether to use aggregate density correction coefficient of the MC2010 model during the actual structure analysis.

## REFERENCES

- ACI Committee 209R1. 1992. *Prediction of creep, shrinkage and temperature effects in concrete structures. Manual of concrete practice part 1*. American Concrete Institute.
- Alduaij, J. et al. 1999. Lightweight concrete in hot coastal areas. *Cement and Concrete Composites* 21:435–458.
- Bazant, Z. P. & Baweja, S. 2000. Creep and shrinkage prediction model for analysis and design of concrete structures: Model B3. *ACI Special Publications* 194: 1–84.
- Bazant, Z. P., et al. 2012. Excessive long-term deflections of Prestressed box girder. Part I: record-span bridge in Palau and other paradigms. *ASCE Journal of Structure Engineering* 138(6):676–686.
- CEB-FIP. 2008. *Constitutive modelling of high strength/high performance concrete*. State-of-art report prepared by Task Group 8.2.
- CEB-FIP. *Model Code 2010 First Complete Draft—Volume 1*. Lausanne, Switzerland. 146–150.
- Jiao C. J. et al. 2014. Overview of study on lightweight aggregate concrete. *Concrete* 08:111–114.
- Liu, Z. F. et al. 2010. Seismic performance analysis of lightweight aggregate and ordinary concrete frame structures. *Building Structure* 40(2):22–24.
- Ministry of housing and urban-rural development of the People's Republic of China. 2002. *Technical specification for lightweight aggregate concrete JGJ 51–2002*. Beijing: China Architecture & Building Press.
- Neville, A. M. et al. 1983. *Creep of plain and structural concrete*. Construction Press.
- Qi, X. Y. et al. 2011. Effect analysis of deformation difference between vertical members of the Shanghai Tower. *Journal of Building Structures* 32(7):15–21.
- Song Y. P. et al. 2002. Study on the quantity and arraying of the reinforcement bars in the prestressed lightweight-high strength concrete platform. *Journal of Southeast University* 32(5):775–778.
- Sun, H. L. et al. 2007. Shrinkage and creep of high-strength lightweight aggregate concrete. *Journal of Tsinghua University* 47(6): 765–767+780.
- Tang J. 2013. *Experiment study on mechanical performance and analysis bond anchorage performance of high-strength lightweight concrete*. Xi'an: Chang'an University.
- Ye, L. P. et al. 2007. Time dependent prestress losses due to creep and shrinkage in high-strength lightweight concrete beams. *Journal of Southeast University* 37(1):94–99.



**Taylor & Francis**

Taylor & Francis Group

<http://taylorandfrancis.com>

# Social impact assessment of green residential district in China

Lei Fan, Yu-xiong Zhang, Yu-rong Zhang, Bo Pang, Jing-jing Wang & Wei Luo

Beijing Jiaotong University, Beijing, P.R. China

**ABSTRACT:** In this paper, a social and cultural evaluation method of China's green residential district based on Social Impact Assessment (SIA) was proposed to counter the common defects of the current Chinese and foreign green building evaluation methods in social and human levels. Besides, according to the three important principles of social investigation as well as the method of SIA, a survey list for buildings' SIA was provided. Moreover, this paper summarizes and expounds the process of social and cultural evaluation of China's green residential quarter based on SIA, in order to enrich the evaluation dimensions of green residential district and expand its connotation and denotation.

**Keywords:** social impact assessment, green residential district, social and humanity demand

## 1 INTRODUCTION

The social and humanity demand of green residential district planning is of paramount importance as it involves social, cultural, and other aspects of knowledge in the social sciences. However, only few related studies have been conducted in China. At present, the comprehensive evaluation index systems of green residential districts in China and some developed countries have focused on two factors: resource and environment (Liu, 2014). In the implementation stage of the evaluation, humanity demand evaluation is often neglected and considered as a non-important index of planning and construction. Consequently, there are gross defect losses in planning content, and many security and social psychological problems appeared in the area that is already in use. Therefore, it is necessary to innovatively improve and complete it based on the social and humanity demand.

Social Impact Assessment (SIA) is a tool for assessing the social impact of planning projects or policies (Frank, 2003). Application of the evaluation method of SIA to the evaluation of green building residential areas in China will enrich the contents of the social and humanity demands, so that the evaluation system of the latter becomes more complete, which will promote the harmony and equality between human and community by more extensive public participation.

On the basis of the SIA system, we proposed a method to evaluate the social and humanity demands of Chinese green building residential district. The evaluation of the social and humanity factors in the residential area of green building is able to suffice the social and cultural needs of the

green building residential area in China and guide the planning and design of green building area in the long term.

## 2 SURVEY OF THE SOCIAL AND CULTURAL NEEDS OF CHINESE GREEN BUILDING RESIDENTIAL DISTRICTS BASED ON SIA

### 2.1 *Object and principle*

The survey includes the basic research work on the social and humanity demand of different types of buildings such as housing, hotels, and commercial buildings. The research objects include the designer of green building city, experts and scholars from universities and science institutes, students who are going to be graduated from school, and people of different age groups. The investigation is also carried out according to the importance of different social factors.

During the investigation, we use the following principles:

1. Objective principle, which requires that the social investigation of the green building community planning and design should observe the social problems in general community planning based on actual situation and analyze specific problems.
2. Scientific principle, which requires a comprehensive survey in the social investigation of the humanity demands on the green building community planning and design. The content of this survey should cover the whole process of building planning. The survey scope should

include experts, scholars, ordinary construction consumers, and the public.

3. Systematic principle, which requires that the social investigation list as well as the elements system of the green building community planning and design, as a whole, should be able to reflect the characteristics of green building community planning and social humanity demands comprehensively.

## 2.2 Survey list

SIA is based on the necessary analysis and evaluation of investigations and interviews. Therefore, it is necessary to confirm the investigation contents and formulate the survey list. The social and humanity evaluation survey list of green building residential districts, which is based on SIA (Y. Tang et al. 1989), is divided into four major categories: population impact, community system, infrastructure needs, and cultural heritage.

### 2.2.1 Population influence

The different composition of the community population has an important impact on the human and social activities of the residential district. The investigation should include the current population status and expectations in variations of the green building residential district, which are intended to evaluate the ethnic and racial diversity, the flow of residents, and the emergence of temporary residents and tourists. During the investigation of the social and cultural needs of the green building residential districts, the main contents can be listed as follows: (1) population variation; (2) the flow of temporary workers; (3) the resettlement of individuals and families; and (4) the composition of age, gender, and nationality.

### 2.2.2 Community and institutional structure

Community structure and institution mean the scale, structure, scope, and level of the local organization. It is a prerequisite to understand and contact the social organizations and the interest groups through the investigation in social and humanity evaluation of green building residential districts. The main contents of the evaluation should be: (1) the formation of the attitude on the project; (2) the activities of the interest groups; (3) the incomes of families; and (4) the diversity of the industry.

### 2.2.3 Demands for infrastructure

The quality and cost of infrastructure and public services are vital to the welfare and satisfaction of community residents. Living infrastructure and social services are not only the fundamental aspects for meeting the basic needs of the people, but also quantifiable measurement and assessment. The

main contents of the evaluation are: (1) commercial facilities; (2) fitness and recreational facilities; (3) education facilities and the ratio of teachers to students; (4) medical facilities and the ratio of doctors to 1000 people; and (5) urban life garbage treatment facilities.

### 2.2.4 Cultural heritage

The negative impact on the natural landscape, natural heritage, cultural landscape, and historical and cultural environment should be considered. In addition to environmental protection, we should deepen the understanding on the inheritance of cultural heritage as well as the protection of social culture. The main contents of the evaluation of the social and cultural demand of green building residential district should be: (1) natural landscapes and relics and (2) cultural, historical, religious, and cultural landscape.

## 3 EVALUATION PROCESS OF SOCIAL AND HUMANITY DEMAND ON CHINESE GREEN RESIDENTIAL DISTRICTS BASED ON SIA

According to the SIA process proposed by the *Principles and Guidelines for Social Impact Assessment in the United States (Environmental Impact Assessment Review, 1995)* and the contents of the social and humanity evaluation system of green residential districts in other countries, the evaluation process of social and humanity demand about Chinese green residential districts based on SIA could be generalized into four main steps: (1) the definition of goal and scope; (2) the survey of baseline conditions of residential districts to be evaluated; (3) identification of major social impact factors and establishment of evaluation index system of social impact about green building settlements; and (4) comprehensive analysis of the social impact of green building residential district.

### 3.1 Definition of goal and scope

Scope definition is the initiation of SIA, which involves the determination of the scope of the evaluation and identification of key stakeholders and the pivotal issue of evaluation confirmed by the means of data access and interview.

The goal of the evaluation on green residential district is to bring the negative social impact down to a minimum level, serve all the residents in the district, and create a harmonious living environment. In this paper, the key stakeholders in the evaluation of green building residential district are divided into four categories: owners, construction enterprises, community residents, and government.



Affected areas include the community to be evaluated and the nearby region.

### 3.2 Survey of baseline conditions

The aim of the baseline study is to investigate basic environmental elements initially in the evaluated region. Initially, the evaluation of social and humanity demand in green residential districts should focus on the collection of related information and data to perform a comprehensive analysis.

Baseline study should focus on the historical background, population characteristics, attitude of the stakeholders, construction of community infrastructure, and the natural landscape of the

community. Then, initial investigation should be carried out through listing and numbering.

### 3.3 Establishment of the evaluation index system of social impact on green residential district

It is a fundamental requirement for SIA to establish an evaluation index system of green residential district, which is the basis and standard of social impact analysis and evaluation. Some SIA index systems have been proposed, such as the guidelines and principles of the American social impact assessment index system by the Inter-organizational Committee (Bryan Tilt et al, 009). Adjustments should be made according to the actual situation because of different situations and the differences

Table 1. Index system of green residential district in China based on SIA.

First-level indicator	Weights	Second-level indicator	Weights	Introduction
Population influence A1	0.24	Population change B1	0.23	The scale of population change, the density of population in the affected areas, and the ratio of floating population
		Temporary workers' movement B2	0.35	Inflow and outflow of temporary workers
		Replacement of individuals and families B3	0.24	Population and distance of migration
		Age, gender, and ethnic composition B4	0.18	Age, gender, and national characteristics
Community system A2	0.33	The formation of the attitude to the project B5	0.38	Positive or negative attitude of residents toward residential districts.
		Activities of interest groups B6	0.13	Attitude of stakeholders
		Family income B7	0.20	Employment rate, major economic sources, and income levels of residents
		Industry diversification B8	0.29	The number and type of private sector (manufacturing, retail, and service) in the community
Demand for infrastructure A3	0.36	Commercial facilities B9	0.21	Commercial facilities richness and distance
		Fitness, entertainment facilities B10	0.16	Convenient places for sports and entertainment
		Educational facilities B11	0.22	Kindergarten, primary school, middle school, high school, library, the ratio of teachers to students
		Medical facilities B12	0.17	Medical construction, public health welfare propaganda, the ratio of doctors to 1000 people
		Domestic waste treatment facilities B13	0.24	Capacity and disposal of urban life garbage
Cultural heritage A4	0.17	Natural landscapes and relics B14	0.34	Protection of nonrenewable natural heritage resources
		Culture, history, religion, and cultural landscape B15	0.66	Protection of the social and humanity environment

of evaluation objects (Li Qiang, 2010). Therefore, the content of the impact should be classified and analyzed systematically. Then, a hierarchical index system about the social and humanity demand evaluation of green residential district should be established, which includes two types of content: quantitative and qualitative.

According to the information collected in the aforementioned survey list, a questionnaire was designed and distributed to the aforementioned stakeholders. A total of 323 questionnaires were finally distributed and 305 copies were returned, while 276 of them were valid. The social and humanity demand evaluation index system of green residential district based on the SIA was established through the data processing and analysis of the questionnaire results, taking into account the importance of various factors. In this paper, the index system based on SIA was divided into two levels. The first level indicators are composed of four aspects, population influence, community system, demand for infrastructure, and cultural heritage, each of which in turn contains a number of second-level indicators. The social impact assessment index system of green residential district in China based on SIA is shown in Table 1.

### 3.4 Results analysis

#### 3.4.1 Weight analysis

Analytical hierarchy process (T.L.Saaty,1980) was used to conduct weight analysis of first—and second-level indicators.

The established evaluation system contains qualitative and quantitative indicators, which are difficult to quantify. Therefore, they need to be necessarily graded by the experts based on the indicators' influence to obtain the original data of weight. Finally, weights of all the indicators can be obtained by calculation, which are shown in Table 1.

#### 3.4.2 Final score

According to the weights of the indicators obtained from the analysis above, every indicator was assigned a point and a questionnaire survey was conducted on the stakeholders. Then, summation of the points with weights provided comprehensive evaluation scores. According to the final comprehensive evaluation score, the evaluation result is shown in Table 2.

Table 2. Evaluation results of social and humanity demand evaluation based on SIA.

Reviews	100–80	80–60	60–40	Under 40
Evaluation results	A	B	C	D

## 4 SUMMARY

On the basis of China's current situation, it can be seen that there is defect in the evaluation system of green residential district; therefore, an evaluation method based on SIA was proposed in this paper. It is a manifestation of a people-centered concept of sustainable development to bring social humanity demand into evaluation on green residential district. The government should strengthen the work for social and humanity demand evaluation on green residential district. At present, the environmental impact assessment for the project has been growing, but the impact on social and humanity aspects still lacks attention. This paper is a valuable tool to promote the evaluation of social and humanity demand on green residential district.

## ACKNOWLEDGMENT

The authors gratefully acknowledge the financial support of 12th Five-Year National Science and Technology Support Programs of China (Grant No.: 2012BAJ12B03-02).

## REFERENCES

- Bryan Tilt et al, 2009. Social impacts of large dam projects: A comparison of international case studies and implications for best practice. *Journal of Environmental Management*, (90): 249–257.
- Li Qiang, Li Lin, 2010. The Index System of Social Influence Evaluation Adaptable to China's Situation, *Hebei Academic Journal*, 30 (1): 106–112.
- Liu Qibo, 2004. Study on Synthetic Assessment to Green Residential Quarters, *Xi'an University of Architecture and Technology*.
- Saaty, T.L. 1980. *The Analytic Hierarchy Process*, New York: McGraw-Hill.
- Tang, Y., Y. Xu, 2007.5. Summaries and studies about Social Impact Assessment, *Urban Planning Forum*, 73–77.
- The Inter-organizational Committee on Principles and Guidelines for Social Impact Assessment, 1995. Guidelines and principles for social impact assessment. *Environmental Impact Assessment Review*, Vol.15(1):11–43.
- Vanclay Frank, 2003. International Principles For Social Impact Assessment, *Impact Assessment and Project Appraisal*, Vol.21(1):5–12.

# Problems of and strategies for financial fund management of enterprises

Jie Wu

Langfang Polytechnic Institute, Langfang, China

**ABSTRACT:** Financial management of enterprises focuses on the study of how individuals and institutions under uncertain conditions optimally allocate funds across time and space. Financial management is very important for any enterprise, and hence the author wishes to study the issues related to the financial management of enterprises, which can not only save cost and reduce opportunity cost, but also make them generate income from investment. In this paper, problems related to the financial fund management of enterprises are studied, aiming at reducing their management and production cost and realizing the maximization of the enterprise value.

*Keywords:* enterprise; financial funds; management

## 1 INTRODUCTION

All goods and materials have a certain value in the market, which is related to the amount of necessary social labor consumed in them. The monetary expression of the material value in the process of social reproduction is the fund, which is an essential condition for the processes of production and operation. The production and operation of an enterprise, on the one hand, are presented by the continuous purchase and sale of goods and materials; on the other hand, they are presented by the expenditure and recovery of funds. In general, income and expenses of funds result from business activities. These constitute the economic activities of an enterprise, that is, its financial activities. Therefore, when an enterprise performs well in business finance, its value is maximized in the market. In the following part, an enterprise's financial fund management.

## 2 SOME ASPECTS RELATED TO AN ENTERPRISE'S FINANCIAL FUND MANAGEMENT

To analyze the problems existing in the financial fund management of enterprises, it is necessary to understand all aspects involved in financial funds of an enterprise and know the ongoing financial activity and problems that require special attention. With the use of relevant materials, the author makes a summary of these problems and believes that the majority of financial personnel would supplement if there are some shortcomings.

### 2.1 *Financial activities caused by financing in the enterprise's financial fund management*

Enterprises mainly engage in operating activities. However, before carrying out the operating activities, funds should be raised. An enterprise's financial fund management should solve problems such as in what ways the enterprise can raise funds and how much money should be raised during a certain period. In general, raising funds includes issuing stocks, bonds, and absorbing direct investment. Enterprises can be based on their own arrangements for reasonable financing.

### 2.2 *Financial activities caused by investment in the enterprise's financial fund management*

Funds raised by an enterprise can be used to purchase fixed assets, intangible assets, and so on for its own operation, which forms its inward investment. Funds raised by the enterprise can be used to invest in other enterprises' stocks, bonds, investment for joint operation, to purchase another enterprise, and so on, which forms the enterprise's foreign investment. Because funds are limited, how to carry out the effective investment with limited resources is a problem to be solved by the enterprise's financial fund management.

### 2.3 *Financial activities caused by operation in the enterprise's financial fund management*

Enterprises in their daily business activities will have a series of income and expenses of funds. The expenses mainly include purchasing and paying

wages; the main source of income includes selling goods. The problem of how to accelerate the turnover of funds should be solved by the enterprise's financial fund management.

#### 2.4 *Financial activities caused by distribution in the enterprise's financial fund management*

In the operating process, enterprises will produce profits and may also share them because of foreign investment, which indicates that they have had the capital appreciation or obtained investment returns. The profits of an enterprise shall be allocated according to established procedures. Therefore, enterprises should pay attention to the relationship between distribution and investment in the process of distribution.

### 3 SOME PROBLEMS EXISTING IN AN ENTERPRISE'S FINANCIAL FUND MANAGEMENT

Inaccurate information of an enterprise's financial fund management will lead to some problems, which are discussed as follows.

#### 3.1 *Asymmetric information*

In financial activities, information is wealth. Getting a solid message will seize an opportunity and win a chance. However, in real economic activities, it is very difficult to obtain real information. Information of many enterprises is not completely disclosed, which leads to wrong judgment, because financial managers during decision-making process cannot grasp the real situation of enterprises. In addition, subordinates may conceal the truth which makes it more likely that top managers will make mistakes in decision making.

#### 3.2 *Enterprises are not strict enough in their financial supervision*

It is very important for the enterprise to set up strict supervision and regulatory agencies. However, in fact, supervision in many enterprises has not played a role in the enterprise management. Funds have been diverted during cash flow. For example, the bankruptcy of Barings Bank was caused by its supervision mechanism, providing the staff a loophole to exploit. Eventually, the bank was heavily in debt and unable to repay the debts. In reality, some enterprises do not pay much attention to financial supervision, and the supervision mechanism is only nominal. In addition, there is another problem of supervision, that is, when enterprises make a major decision, there is no effective mechanism for its

assessment and control. Only a few top managers have the right to make decisions, and there is possibility for them to make mistakes.

#### 3.3 *The rate of capital turnover is not high*

Some enterprises do not optimally utilize funds and funds have not been best used. According to the author, the main reasons are the following: (1) The enterprise's decision making is not rigorous; there is no strategic planning for the enterprise's overall funds, making investment get into a difficult position. (2) The purchasing process is not well planned, resulting in overstocked products, which will increase the opportunity cost of funds and inventory costs.

#### 3.4 *Disordered fund management and lack of an effective fund management model*

There are two types of funds involved in the process of an enterprise's production and operation, namely fixed funds and circulating funds. Fixed funds include plant buildings and production equipment; circulating funds include funds for purchasing materials and equipment. The object of the enterprise fund management mainly refers to the circulating funds. Effective management of the circulating fund can make it retain its value and upvalue. However, the majority of enterprises, especially small and medium-sized enterprises, do not pay enough attention to the circulating fund management, which is presented by non-formulation of proper management system and standards. It will lack guidance for the management of funds and lead to disordered management, which cannot fully achieve the value of funds. In some large companies, there is no unified financial accounting standards between parent and subsidiary companies, and they lack specialized fund management departments and personnel.

#### 3.5 *Financial information distortion makes it difficult for the enterprise's decision making*

In order to achieve an effective management of the enterprise's financial funds, the most direct means is to collect financial information and then collate and analyze it properly. It is becoming difficult for an enterprise to collect and check its financial information, because the its production scale is continuously expanding, the management type is increasing gradually, and the amount of financial information is unceasingly increasing. In addition, some units will provide false financial information to obtain more economic benefits, which will further increase the difficulty of checking financial information, and ultimately lead to erroneous decisions in the enterprise investment.

#### 4 A SOLUTION TO THE PROBLEM OF AN ENTERPRISE'S FINANCIAL FUND MANAGEMENT

Some problems in an enterprise's financial fund management have been listed in the above part, whose solutions will be provided in the following part, according to the author's viewpoint.

##### 4.1 *To implement internal control*

Internal control is implemented by the board of directors, the board of supervisors, the managers, and the staff aiming to control objectives. The problem of information asymmetry in an enterprise arises due to the poor internal control. The author believes that the implementation of internal control in the enterprise should do at least two things: (1) Separation of incompatible posts. For example, the accountant and the cashier cannot be the same person. (2) Implementation of important posts rotation system will effectively prevent the formation of informal organizations.

##### 4.2 *To enhance the enterprise's risk awareness*

Risk management is very important for any enterprise. Some of the problems are caused by inadequate assessment of risks. According to the author, an enterprise should improve its risk prevention awareness and establish specialized risk management departments to predict and respond to each risk.

##### 4.3 *To set the enterprise's strategic objectives*

Some enterprises do not have a clear strategic planning, and hence they do not have a clear direction of development. The author thinks that the enterprise needs to set specific goals for its development and figure out its core advantage in order to avoid blind investment.

##### 4.4 *To strengthen the supervision system*

Financial supervision is necessary. Effective supervision measures can avoid the diversion of funds in the enterprise, mistakes in decision making, and damage to the interests of creditors. The author holds that the supervision system should be changed from the higher level to the lower level. First of all, supervision will be reformed to make it play a supervisory role.

##### 4.5 *To devote major efforts to promoting online business bank settlement center*

In recent years, online banking has been developing rapidly. The establishment of the online bank settlement center can significantly improve the efficiency

of the use of enterprise funds and ensure the safety of enterprise funds. At the same time, it can also achieve the purpose of unified management of funds. The main services provided by the online business bank settlement center include the following: First of all, online business bank settlement center can have centralized management of the enterprise accounts. This is easy not only to manage the enterprise accounts, but also to trace the funds in the account. Online business bank settlement center will have a detailed list of all the accounts that can effectively avoid the abuse of enterprise funds. Second, the online business bank settlement center can have unified management of enterprise funds. Banks will formulate fund management system according to the requirements of the enterprise; thus, enterprises can have unified scheduling and management of the funds by banks, which can not only save the cost of fund management, but also improve the utilization rate of funds. Finally, online business bank settlement center can control the powers of the enterprise financial personnel. It can restrict financial staff's access rights. Only those financial personnel who have gained their access rights can obtain financial information. This can not only avoid the disclosure of the financial information, but also make the financial personnel's responsibilities clear and fall on each individual.

##### 4.6 *To formulate financial fund management system based on the enterprise's actual situations*

Management by objectives is an important management method in modern management. The implementation of management by objectives in enterprises can indicate a right direction for their development. In the process of the enterprise's financial fund management, we should also adopt this method to set a specific goal for its financial fund management activities and make all the financial activities focus on this goal. After setting the objective of the enterprise's financial fund management, the enterprise should establish a financial fund management system based on its actual situations. The purpose of establishing the financial fund management system is to better achieve the objective of the financial fund management. Therefore, the establishment of the objective should take full account of the enterprise's current financial management status and its financial development in the future to make the enterprise's financial fund management system conform to its actual situations.

##### 4.7 *To refine the enterprise's financial fund management*

An enterprise's financial fund management is not only related to the financial situation of the

enterprise, but it also affects its development, because financial statements are also the main reference for decision making. The enterprise's financial personnel did not realize the importance of financial fund management before producing unsatisfactory results. Therefore, it is necessary to change the current situation of the enterprise's financial fund management and refine the level of its financial management. The key to improve the level is to introduce a budget model through rigorous mathematical methods to figure out the budget of the enterprise. At the same time, it should also strengthen the management of the enterprise's operating costs to improve its economic benefits.

## 5 CONCLUSION

It is of paramount importance for any enterprise to carry out reasonable financial fund management. Only by carrying out effective financial fund

management, enterprises can achieve the optimal allocation of resources and have better development. Of course, problems are inevitable in the process of financial fund management; however, the author believes that effective internal control, reasonable assessment of market risks, and increase of the utilization rate of funds will solve these problems and achieve the best results in the enterprise's financial fund management.

## REFERENCES

- [1] Mo Lijun. Analysis of problems and measures of the enterprise's financial funds management system [J]. *New Finance and Economics (THEORY EDITION)*, 2013, (7): 218–218, 220.
- [2] Wang Zheng. The analysis of how to improve the enterprise's financial funds management [J]. *China Management Informationization*, 2013, 16 (6): 4–5.
- [3] Zhang Limin. Centralized financial management of settlement in the business group [J]. *Business*, 2015, (25): 23–23.

# Mono-layer reticulated shell structure design

Lan Mi

*Environmental Management College of China, Qinhuangdao, Hebei Province, China*

**ABSTRACT:** According to the *Regulations of technology of space grid structure* (JGJ7-2010), this paper analyzes the linear bearing capacity, stability, deflection, and nonlinear overall stability of the top spherical reticulated shell of the 44 m circular pool using SAP2000 program. Through the finite element analysis of geometric nonlinearity, it accurately calculates the critical load limit of reticulated shell and thus provides a reference for future reticulated shell design.

**Keywords:** spherical single-layer reticulated shell; SAP2000

## 1 DESIGN OVERVIEW

In this paper, structure design of a spherical reticulated shell at the top of a circular pool is described. The biting + sunflower hybrid grid shows that the structure has a span of 44 m and height of 7.5 m, which is about 1/6 of the span. It adopts the embedded hub node, with fixed hinge support on top of the tank wall. The reticulated shell uses a cold bending thin-walled rectangular steel tube, with the steel type Q235C. As a result of the embedded hub nodes, the connection between the network shell bars just outside the shell surface contact and the inner surface of the shell can be considered to be articulated, and the model will be calculated according to rigid connection. All bar specification is  $120 \times 80 \times 4$ . The bar slenderness ratio is 150. The basic wind pressure is  $0.7 \text{ kN/m}^2$  and the basic snow pressure is  $0.5 \text{ kN/m}^2$ . Temperature changes of  $+20$  and  $50^\circ\text{C}$  are considered. The calculation model is shown in Figure 1.

Modeling and calculation need the joint effort of MST and SAP2000. As nonlinear analysis cannot be performed by MST, problems exist in the

calculation of internal forces of beam rods. Therefore, only MST is used in quick modeling, and then SAP2000 is imported for calculations.

## 2 STRUCTURAL CALCULATION

The structural calculation mainly consists of two parts. The first is a linear analysis, which calculated the relevant lever strength, deflection, and stability. The second is a nonlinear buckling analysis (also known as load–displacement of the whole process of analysis), which calculated the overall stability of the reticulated shells, in which the reticulated shell only considers geometric nonlinearity, regardless of material nonlinearity. The surface mounting errors of initial installation should be taken into consideration in the overall process analysis of reticulated shell. (As the reticulated shell is very sensitive to initial defects, the design should consider the effect of the installation error on the overall stability). According to the provisions of section 4.3.3 in *Regulations of technology of space grid structure* (JGJ7-2010), the lowest buckling mode can be adopted as initial defect modal distribution, based on which the whole process is analyzed, and the load–displacement curve can be drawn, with the first extreme point as the ultimate capacity of reticulated shell. This requires that the carrying capacity should not be less than 4.2 times of the 1.0 constant + 1.0 live. The nonlinear buckling analysis of the structure is focused below.

### 2.1 Linear buckling analysis

Before the nonlinear buckling analysis, first, a linear buckling analysis should be performed. The so-called linear buckling analysis is the calculation

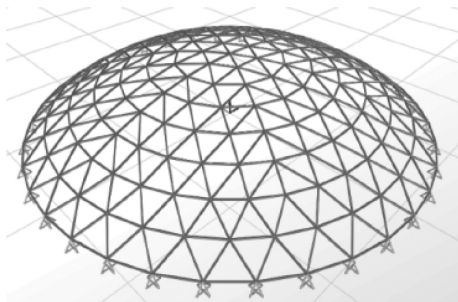


Figure 1. The calculation model of reticulated shell.

of matrix eigenvalue in mathematics, and thus it is also called the eigenvalue buckling. It is mainly used to solve the first type of stability problems of the structure. The nonlinearity of a structure cannot be considered in calculation. In SAP2000, it simply needs to define buckling analysis (buckling) conditions. The condition uses constant 1.0 + 1.0 live to load. Figure 2 shows the first-order buckling mode of the structure, and the structural maximum displacement point is No.101 node. The buckling coefficient  $K = 15.999$ , which means that in ideal state (that is, the bar does not have geometric defects), when the load reaches  $K \times$  live constant (1.0 + 1.0), the structure will lose its stability.

### 2.2 Application of defects

In SAP2000, the application of initial defects to the structure can be mainly summarized by the following steps:

1. Calculate the maximum initial defects according to specifications.  $\text{Max} = \text{span}/300$ . The maximum of this project is 146.7 mm.
2. Calculate the ratio of the maximum value of initial defects and the maximum value of the vector buckling defects.
3. Multiply all buckling volume by this ratio, and then get the initial defect of each node.
4. Add the initial defects and the coordinates of undeformed reticulated shell nodes to change the coordinates of each node.
5. Import the coordinates of the changed nodes to SAP2000, and the new model is the one with initial defects. The above operation is preferably conducted in EXCEL; otherwise, there will be a huge workload.

### 2.3 Nonlinear buckling analysis

In SAP2000, nonlinear buckling problem can be solved by defining a nonlinear static analysis case

(NLSTAT1). Consider P- $\Delta$  effect and large displacement of the structure in analysis. The basic method of nonlinear buckling analysis can be expressed as follows: A constant load increment is applied to the structure until the structure does not converge. The so-called non-convergence structure means zero stiffness matrix structure, that is, the whole structure loses its stability.

In SAP2000, there are two ways of load control in nonlinear analysis: load control and displacement control. For the structure whose ultimate strength of load is unknown, usually it is easier to obtain the ultimate capacity through displacement control.

In the nonlinear static analysis case, the amount of applied load usually takes  $K \times (1.0 + 1.0$  constant live), and the monitoring nodes usually take the maximum displacement point of linear buckling analysis. The monitoring node of this project is No.101. The maximum displacement monitoring needs to be calculated repeatedly until the structure is not converged. The monitoring displacement of this project takes 400 mm. In continuing the loading process, when the node 101 reaches the displacement 400 mm, the program terminates the iterative calculations.

The substrate reaction force of drawn structure (Uz) and 101 node displacement curve are shown in Figure 3.

Drawing data of the extraction section is as follows:

```

Joint101 Base shearing resistance Z
8 - 362.50000 7969.06681
9 - 375.00000 8017.46216
10 - 378.12500 8023.56824
11 - 381.25000 8019.03488
12 - 382.03125 8009.73635
13 - 382.42188 7993.98556
14 - 382.43408 7989.50047

```

It can be seen that with the increasing displacement of No.101 node, at the 10th load step, the structure reaches the maximum carrying capacity of 8023 kN. Then, as the nodal displacement continues to

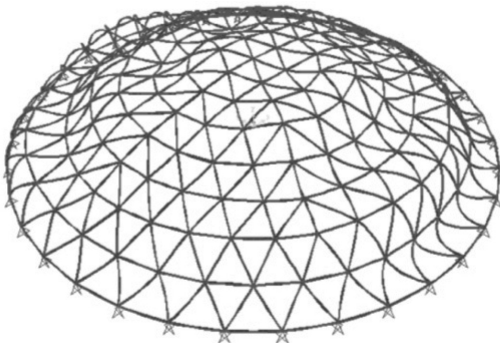


Figure 2. The first-order buckling mode.

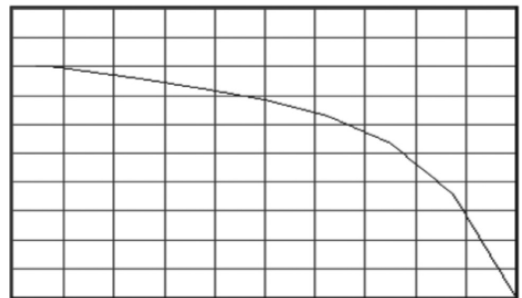


Figure 3. Substrate reaction force–displacement curve.



increase, the bearing capacity of the structure begins to fall, which shows that the structure has already lost its stability. The value 8023 kN represents the ultimate stability or bearing strength of the structure.

According to specifications, the stability allowable bearing capacity of reticulated shell is calculated by dividing the ultimate capacity by 4.2, that is, 1910 kN. Constant substrate reaction force with read structure at 1.0 + 1.0 live is 1550 kN, less than 1910 kN; therefore, the overall stability of the structure meets regulatory requirements.

The ultimate bearing capacity of linear buckling analysis is  $15.99 \times 1550 = 24,645$  kN, and the ultimate load capacity obtained by nonlinear buckling analysis is 8023 kN, only about 1/3 of the former. Thus, the initial defects have a significant impact on the stability ultimate capacity of reticulated shells.

### 3 CONCLUSION

Practice shows that bars of reticulated shell are mainly under pressure, with a high efficiency of

span. As the amount of steel for this project is only  $16.9 \text{ kg/m}^2$ , there must be stable problems on pressure. The control factor in shell design is usually the stability ultimate capacity and slenderness ratio; therefore, it is of vital importance to make buckling analysis of the entire process considering initial imperfections of reticulated shells. This paper focuses on the application of SAP2000 for a large-diameter spherical lattice shell nonlinear buckling analysis of the entire process. The author believes that this paper can serve as a reference for the following reticulated shell design.

### REFERENCES

- [1] JGJ7-2010 spatial grid structure Technical Specification Beijing: China Planning Press, (2010).
- [2] Yin Deyu, Liu Shanwei, Qian Ruojun. Reticulated Shell Design. Beijing: China Building Industry Press, (1996).



**Taylor & Francis**

Taylor & Francis Group

<http://taylorandfrancis.com>

# Research on the neural network based on an improved PSO algorithm

Jiang Liu

Electronic Information Vocational Technology College, Tianjin, China

**ABSTRACT:** A modified particle swarm optimization is proposed for artificial neural network studying, in which a window is introduced to detect the change of environment. Through reinitializing the parameters, the modified particle swarm optimization can enhance the diversity of the particles and solve the problems in the determination of the convergence result by the distribution of the particles when they are initialized. The particle swarm optimization often converges prematurely in solving problems under complex background. Another parameter will be tuned according to the condition of the search process, and this tuning will balance the global search capability and the local search capability. Experiments were conducted to illustrate the effectiveness of this new algorithm, and the results showed that the modified particle swarm optimization is advantageous over the unmodified technique.

**Keywords:** Particle Swarm Optimization (PSO); Artificial Neural Network (ANN); swarm intelligence

## 1 INTRODUCTION

The Particle Swarm Optimization (PSO), introduced by Kennedy and Eberhart, draws inspiration from social behavior of bird flocking or fish schooling, and has been successfully applied in many areas. Different from traditional search algorithms, PSO, like other evolutionary computation techniques, works on a population of potential solutions in the search space. Through cooperation and competition among the potential solutions, this technique can often find optima more quickly when applied to some optimization problems. Furthermore, unlike Genetic Algorithm (GA), PSO has no evolution operators such as crossover and mutation; therefore, it is easy to implement and there are few parameters to adjust. The neural network application described in ref.<sup>[1]</sup> showed that the particle swarm optimizer could train Artificial Neural Network (ANN) weights as effectively as the usual error backpropagation method. Intriguing informal indications are that the trained weights found by particle swarms sometimes generalize from a training set to a test set better than solutions found by gradient descent<sup>[2]</sup>. However, this network studying algorithm based on PSO is still in its development stage. In some special fields, experiments show that using PSO to train ANN is not an efficient way for optimization. For example, it failed to perform global search in nearly each run using this way to determine the cement quality. Therefore, a modified PSO is presented and introduced to train ANN. Its application shows that the new algorithm gives some balance between global

and local search capability and results in a high convergence rate.

## 2 NETWORK STUDYING ALGORITHM BASED ON PSO

Consider the solution of every optimization problem as a point of  $d$ -dimensional space, namely call it particle. For each particle, iterative search is updated according to equations (1) and (2), namely it follows two optimal points (or two extrema ) to refresh itself until the destination is reached<sup>[3]</sup>:

$$v_i = w \cdot v_{i-1} + c_1 \cdot r_1 \cdot (pbest - x_{i-1}) + c_2 \cdot r_2 \cdot (gbest - x_{i-1}) \quad (1)$$

$$x_i = x_{i-1} + v_i, \quad (2)$$

where  $pbest$  and  $gbest$  are the current individual extreme point and swarm's extreme point, respectively;  $v_i$  and  $v_{i-1}$  are the current and previous move velocities of the particles, respectively;  $r_1$  and  $r_2$  are random numbers between 0 and 1;  $c_1$  and  $c_2$  are learning factors; and  $w$  is inertia weight factor. In addition, the regulation of velocity is shown as follows:

$$\begin{cases} v_i = V_{\max}, & \text{if } v_i > V_{\max} \\ v_i = -V_{\max}, & \text{if } v_i \leq -V_{\max} \end{cases} \quad (3)$$

Selection of proper parameter guarantees iterative convergence<sup>[4]</sup>. The concrete steps of training neural network by using PSO are as follows:

1. Random initiation of species swarm. Suppose there are  $d$  weight values and threshold values that need to be determined in a neural network with only one hidden layer. Then, considering each particle as a point in  $d$ -dimensional space, the number of particles is  $K$ . Initiate the velocity  $v_i = (v_{i,1}, v_{i,2}, \dots, v_{i,d})$  and destination  $x_i = (x_{i,1}, x_{i,2}, \dots, x_{i,d})$  of each particle, whose values are random numbers between 0 and 1. The initial value of  $pbest$  for each particle is the initial value of  $x_i$ .
2. Calculate the fitness value of every particle. The fitness function is the following error function. The smaller the error, the larger the fitness value is:

$$E \equiv \frac{1}{P \cdot N} \sum_{p=1}^P \sum_{i=1}^N (y_i - \bar{y}_i)^2, \quad (4)$$

where  $P$  is the number of sample,  $N$  is the number of output layer nodes, and  $\bar{y}$  is the expected output.

3. Copy the species swarm according to fitness value. First search the destination of global extreme point, namely  $gbest$ . If the individual error function  $E(x_i)$  is smaller than the individual extreme value  $E(pbest)$ , then order  $pbest = x_i$ ,  $E(pbest) = E(x_i)$ .
4. Refresh the output of the destination of particle swarm. Refresh according to equations (1) and (2). If  $E(gbest)$  is smaller than the control value  $\epsilon$  or the iterative times is equal to the given evolutionary times  $T$ , stop refreshing, and the searching process finishes, and output the result. Otherwise, go to step (2).

However, there are problems associated with this algorithm. It does not detect the environment changes automatically; for example, the search is trapped in local optima. A further discussion is developed in the following section. The algorithm needs some outside information about the changes. These requirements are usually not available in real-world problems. Some kind of automatic environment sensing technique should be used to solve the problem<sup>[5]</sup>. Therefore, a modified PSO is proposed.

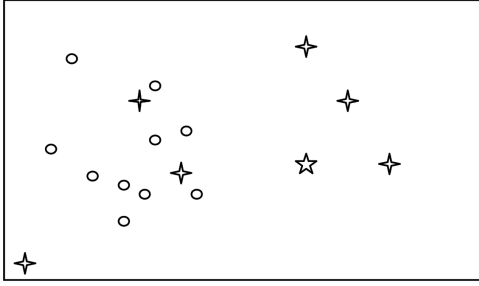
### 3 MODIFIED PSO

PSO is a population-based stochastic optimization technique. It begins the search for optimum solution from a group of dispersed solutions in the solution space, which makes PSO feature good global convergence. In general, there is high probability of PSO converging to the global optimum solution when initial solutions, generated stochastically,

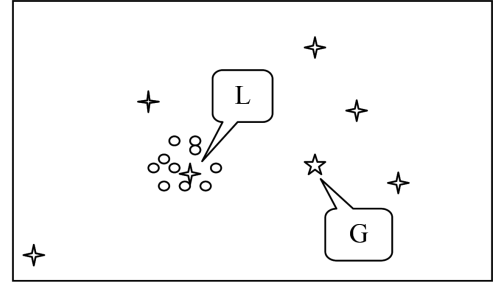
are dispersed in the solution space. However, if the solution space is so large that initial solutions occupy a comparative small corner, through “flying”, the particles will stop once they find the local optima. This phenomenon results from the lack of diversity, which restrains the particles’ capability of jumping out of local optima when the scale of particle swarm is small. Figure 1 illustrates this point in a two-dimensional space. The dots represent the particles, the cross stars represent the local optima (L), and the pentagrams represent the global optima (G). However, it will consume unacceptable time cost if diversity is enhanced by enlarging the scale of particle swarm. Second, particle swarm will converge toward local optima or global optima at the late stage of evolutionary computation, here every particle’s  $pbest$ ,  $gbest$ , and current position would tend to the same point and every particle’s velocity would tend to become zero. In this case, the point of the particle swarm tends to become the limit value of the ultimate solution of the PSO algorithm<sup>[6]</sup>. Because several local minima exist in practical problems under complex backgrounds, the probability that the solution obtained by PSO algorithm is the local optimum will be greater than that of the solution is a global optimum. This is also illustrated in Figure 1, in which the local optima are much more than the global optima. In addition, for the whole particle swarm fly toward the optimum solution according to the search experience of other particles and themselves, particle swarm may miss the optimum solution, disperse in the space far away from the optimum solution, and make the algorithm not converge in the condition of large momentum item. Under the condition of convergence, since all the particles fly toward the optimum solution, they tend to sameness, lost the diversity of the solutions among particles, and obviously reduce the speed of later-stage convergence. Figure 2 simply shows the relationship between search ability and momentum item (d). For example, if the velocity is too large, the particles will jump over the global optima and cannot get a satisfied precision. Reversely, if the velocity is rather small, the particles will not jump out of local optima. Therefore, a balance between global search capability and local search capability should be made to arrive at the global optima rapidly and at the same time obtain a better precision.

On the basis of the above consideration, a modified PSO was proposed, which could be used for training ANN efficiently. Below is the modified algorithm:

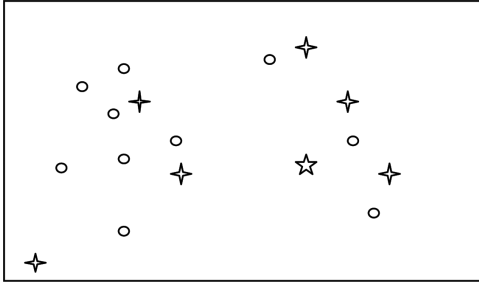
1. Initialize the species swarm randomly and set a positive integer called window scale represented by  $W$ .



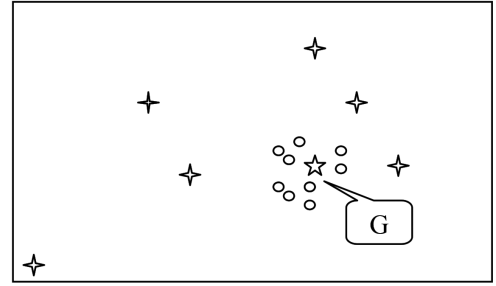
1.1(a)



1.1(b)



1.2(a)



1.2(b)

Figure 1. The effect of convergence resulting from the distribution of the particles when they are initialized.

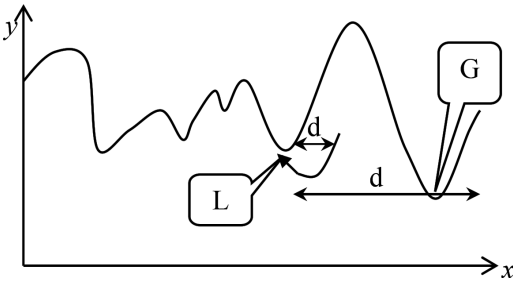


Figure 2. Relationship between search ability and momentum item (d).

2. Calculate the fitness value of every particle.
3. For each particle, if the fitness value is better than the best fitness value ( $pbest$ ) in history, set current value as the new  $pbest$ .  
Choose the particle with the best  $pbest$  value among all the neighbors as the  $gbest$ .  
All the above must obey regulation (3).
4. Update particles' positions according to equations (1) and (2).
5. Monitor the change in the window in which  $W$  iteration results are recorded. If there is continuous unchanging in this window, do as follows and then go to step (2):  
Initialize the species swarm's positions, velocities, and  $pbest$  randomly, keep the record of

$gbest$  of the last iteration and set  $T_{iter}$  to 1. The parameter " $T_{iter}$ " represents a variable associating the iterative times and is used in the formula below:

$$w = w_{max} - \frac{(w_{max} - w_{min}) \cdot T_{iter}}{T}, \quad (5)$$

where  $w_{max}$  is usually set to 0.9,  $w_{min}$  to 0.4, and  $T$  is an iteration time set according to the special problems.

6. If  $E(gbest)$  is smaller than the control value  $\varepsilon$  or the iterative times is equal to the given evolutionary times  $T_{max}$  (notice that  $T_{max}$  is not equal to  $T$  here, but they are same in the original PSO), stop refreshing, and the searching process finishes, and output the result. Otherwise, go to step (2).

There are two versions of PSO algorithm: local version and global version. The global version is faster while the local version is better in avoiding local optima<sup>[2]</sup>. In fact, this modified PSO algorithm integrates the advantages of the two versions of PSO algorithm. A small window will affect local optimization, whereas a large one may pay time cost in a region that does not have the optimum solution. Therefore, a reasonable window size will guarantee the balance between global and local

search capability, and result in a high convergence rate.

Compared to other improvement measures, this approach has the following advantages:

1. It is simple. It is not much different from the original algorithm, but performs efficiently. The rules underlining this algorithm can be easily understood.
2. It is faster. It saves more time in local optimum regions and accelerates the exploring speed by setting  $T_{iter} = 1$ , which provides a large inertia weight factor.
3. It is efficient. In the original PSO algorithm, all the particles are apt to converge to the same point, trapped in local optima, and won't optimize any more when solving a complex problem. This modified algorithm gives some balance between global and local search capability.

Conclusions should state concisely the most important propositions of the paper as well as the author's views of the practical implications of the results.

#### 4 EXPERIMENTS AND DISCUSSION

We introduce this modified PSO to train ANN and use it to determine the cement quality. The data are taken from ref. [7]. The professional background about cement bond log and cement quality can also be found in ref. [7]. In this experiment, the input vectors are four first-wave amplitudes  $A_{11}$ ,  $A_{12}$ ,  $A_{22}$ ,  $A_{21}$  (Unit: mV). Output vectors are good cement, medium cement, and poor cement. Design a three-layer forward neural network, and there are four nodes in the input layer according to this problem. For the three types, good, medium, and poor, there are three output layer nodes. The expected output of good cement is (1,0,0), medium cement is (0,1,0), and poor cement is (0,0,1). The node number of the hidden layer is set to 4.

The test examples use a population of 10 particles. Each particle is initialized with position (within the range of (-100, +100)) and velocity vectors (within the range of (-10, +10)) of 35 elements.  $T$  is set to 500,  $T_{max}$  to 1000, and  $W$  to 50. The required fitting error, namely the control value  $\epsilon$ , is  $<10^{-6}$ . By training the ANN using the samples listed in Table 1, it can automatically determine the cement quality. Table 2 is the recognition result of cement quality at typical depth points from certain experimental well.

From the result of the experiment, it can be concluded that the network studying algorithm based on the modified PSO performs well. In order to compare the modified PSO with the original one, a comparative experiment is conducted. Figure 3

Table 1. Cement quality sample for network studying.

Cement	$A_{11}$ (mV)	$A_{12}$ (mV)	$A_{22}$ (mV)	$A_{21}$ (mV)	$(d_1, d_2, d_3)$
Good	31.5	18.7	29.9	19.2	(1,0,0)
Good	42.1	22.1	42.5	22.8	(1,0,0)
Good	50.2	27.6	49.6	24.7	(1,0,0)
Medium	54.6	28.5	55.7	20.9	(0,1,0)
Medium	64.1	32.6	64.4	33.2	(0,1,0)
Medium	71.4	35.7	70.6	36.2	(0,1,0)
Poor	74.5	48.3	74.3	37.8	(0,0,1)
Poor	84.2	43.5	85.7	44.1	(0,0,1)
Poor	96.6	50.9	92.7	50.3	(0,0,1)

Table 2. Recognition result of cement quality.

Depth no	$A_{11}$	$A_{12}$	$A_{22}$	$A_{21}$	Actual	Forecast
1	75.4	37.6	76.5	38.3	Poor	Poor
2	70.5	28.9	71.2	28.1	Medium	Medium
3	119.4	71.6	121.5	71.5	Poor	Poor
4	78.8	41.8	83.6	40.7	Poor	Poor
5	39.8	19.1	41.5	21.1	Good	Good
6	49.5	24.7	48.7	25.6	Good	Good
7	32.1	10.3	33.2	11.2	Good	Good
8	89.5	44.8	90.1	43.6	Poor	Poor
9	80.1	37.6	81.1	38.2	Poor	Poor
10	67.6	33.8	68.3	34.2	Medium	Medium

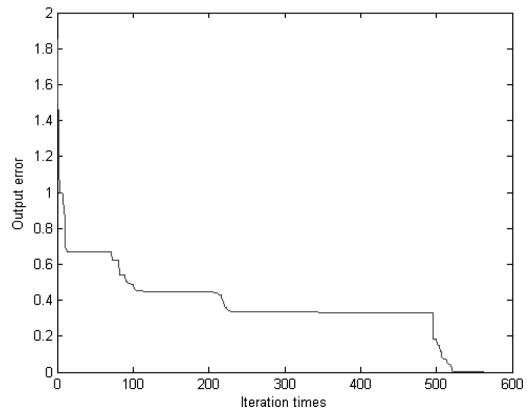


Figure 3. Error curve of modified PSO algorithm.

shows the output error with the iteration times, which was recorded in the above test. Figure 4 shows the output error with the iteration times in the same condition, but using original PSO other than the modified PSO. From the comparative experiment, it can be concluded that the modified PSO is indeed advantageous over the original one.

We can also find that the special problem has several local optima that output the fitting errors

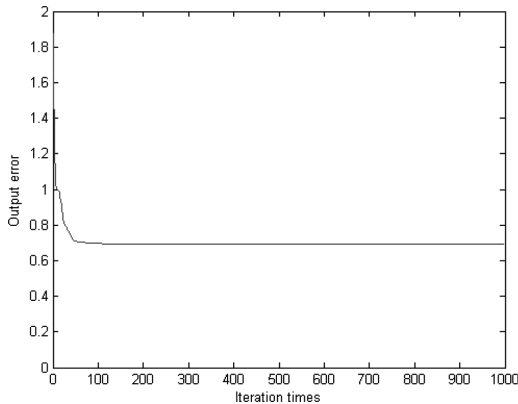


Figure 4. Error curve of original PSO algorithm.

as about 0.6667, 0.4207, and 0.3333. Because the original PSO algorithm is prone to converge prematurely, it is often trapped in local optima. This is partly because the diversity of particle swarm becomes worse with iteration time increasing. In the convergence of original PSO algorithm, all the particles trend to the same point, which can be tested in the experiment, and make the second and third parts of equation (1) equal to zero. Without these two parts, the particles will keep on “flying” at the current speed in the same direction until they hit the boundary. PSO will not find an acceptable solution unless there are acceptable solutions on their “flying” trajectories. However, that is a rare case<sup>[8]</sup>. Therefore, it loses the significance of swarm.

Through setting  $W$  suitably, particles can become diverse by initiating the species swarm’s positions, velocities, and  $pbest$  randomly again. Moreover, it can enhance the global search capability by setting  $T_{iter}$  to 1, which makes a large  $w$ , and jump out of local optima. Meanwhile, a suit  $W$  will make  $T_{iter}$  not refreshed too frequently to lose the local search capability. Therefore, the modified PSO algorithm overcomes the drawbacks discussed in section 3.

However, there are still shortcomings in the modified PSO algorithm. Because PSO is a stochastic optimization technique, although it is advantageous over the original PSO algorithm in solving complex problems, it is not so successful in

every run. Figure 3 is just the result of one run and others may consume more time at the local optima. Therefore, a further development should be made on this algorithm.

## 5 CONCLUSIONS

In this paper, we proposed a modified PSO and introduced it as an ANN studying algorithm. It is simple, fast, and efficient. In the special field, it overcomes the problems encountered by the original PSO. Experiment has been conducted to illustrate the advantages of this new PSO algorithm. It is concluded that the modified PSO shows a better performance.

## REFERENCES

- [1] Eberhart R. C. and Kennedy J. A new optimizer using particle swarm theory. Proceedings of the Sixth International Symposium on Micromachine and Human Science. Nagoya, Japan. pp. 39–43. 1995.
- [2] Kennedy J, Eberhart R C. Particle swarm optimization [A]. Proc. IEEE Int. Conf. Neural Networks. Piscataway, NJ: IEEE Press. pp. 1942–1948. 1995.
- [3] Xia Kewen, Zhang Zhiwei, Liu Mingxiao, Yang Ruixia. A Recognition Method of Reduced Evolutionary Neural Network and Its Application, ICNN&B ’05, IEEE press. pp. 343–348. 2005.
- [4] E Ozcan, C Mohan. Particle swarm optimization: Surfing the waves. In: Proc of the Congress on Evolutionary Computation. Piscataway, NJ: IEEE Service Center. pp. 1939–1944. 1999.
- [5] Xiaohui Hu and Russell C. Eberhart. Adaptive Particle Swarm Optimization: Detection and Response to Dynamic Systems, CEC ’02, IEEE press. pp. 1666–1670. 2002.
- [6] FU Guo-jiang, WANG Shao-mei, LIU Shu-yan, LI Ning. A PSO with dimension mutation operator. Engineering Journal of Wuhan University, Vol. 38, No. 4, pp. 79–83, 2005.
- [7] Xia Kenwen, Song Jianping. Identification of Cement Quality by Neural Network with Nonlinear Connected Weights [J], Journal of Xi’an Jiaotong University, Vol. 37, No. 2, pp. 192–195, 2003.
- [8] Shi, Y. and Eberhart, R. C. A modified panicle swarm optimizer. Proceedings of the IEEE Congress on Evolutionary Computation (CEC 1998). Piscataway, NJ. pp. 69–73, 1998.



**Taylor & Francis**

Taylor & Francis Group

<http://taylorandfrancis.com>



# Study of the consolidation effect of a marginal bank by vacuum preloading based on a network

Chang-Hong Wang

Tianjin Research Institute for Water Transport Engineering, Tianjin, China

**ABSTRACT:** In this paper, the method and application situation of a neural network is introduced briefly. Datum of project and monitoring from a project of soft foundation by vacuum preloading in Tianjin was filtrated and summarized. After analysis and comparison, optimization of the neural network model was established to evaluate the consolidation effect. Then, it was analyzed that the main parameter of soft foundation consolidation process is the sensitivity of impact factors.

**Keywords:** Neural network; Vacuum preloading; Consolidation effect

## 1 RESEARCH AND APPLICATION OF NEURAL NETWORKS

A mathematical model of distributed parallel information processing is proposed by imitating the behavior of animal's neural network. This type of network depends on the complexity of the system, through adjusting the relationship between the large number of nodes, so as to achieve the purpose of processing information. At present, neural network learning algorithm has been widely used in pattern recognition, data prediction, system identification, image processing, speech understanding, function fitting, and other fields<sup>[1,2]</sup>. Artificial neural networks have been applied in civil engineering since the late 1980s, such as the simulation of the construction process, the construction cost budget, the earthquake hazard prediction, the stress-strain relationship of soil, the hardening and softening of residual soil during loading, and the bearing capacity of the pile<sup>[3-8]</sup>. The wide application of neural network is sufficient to explain its practical significance in solving the problem of rock and soil.

The following are the characteristics of artificial neural network: nonlinearity, non-limitation, highly qualitative, and non-convex. The vacuum preloading process is affected by many factors, and the natural law of the reinforcement effect is difficult to be described by the known mathematical expression. This nonlinear problem is well suited for artificial neural networks to deal with.

## 2 NEURAL NETWORK MODELING OF SOFT FOUNDATION REINFORCEMENT EFFECT

### 2.1 Basic principles

In this study, a BP network model was used to train the multilayer feedforward network trained by the error backpropagation algorithm. The BP network can store and learn several input and output mode mapping relations without having to understand the mathematical equation of the mapping relationship. S (Sigmoid)-type function is generally used in the function of each layer:

$$f(x) = \frac{1}{1 + e^{-x}}. \quad (1)$$

The accuracy of the network is evaluated by the global error E, which is the sum of the output errors of all the input samples, expressed as:

$$E = \sum_n E_n \quad (2)$$

The standard deviation of  $E_n$  for the first n samples is

$$E_n = \frac{1}{2} \sum_{k=1}^l (Y_k - t_k)^2, \quad (3)$$

where  $Y_k$  is the output value of K,  $t_k$  is the ideal output value of K, and L is the number of nodes.

Thus, the steps of the BP algorithm can be summarized as follows: the initial value of the selected weight coefficient; forward propagation, E; back-propagation, correction weight:

$$w_{ij}(r+1) = w_{ij}(r) - \mu \frac{\partial E}{\partial w_{ij}}, \quad (4)$$

The condition  $u > 0$  denotes the step size and R denotes the first R iterations, until convergence. The network can be realized by NeuroSolutions software, which is a highly graphical neural network development tool.

## 2.2 Input and output parameters

The evaluation index of vacuum preloading effect should be the most direct in situ test or soil test. In situ testing of the reinforcement zone involves cross-plate shear test and plate-loading test. The index of soil testing is often concerned with water content, because it can reflect the degree of saturation of the saturated soft soil. In this paper, the original soil above the vane strength average value was studied as the output parameter. Many factors affect the strength and moisture content of the cross plate, such as reinforcement time, field parameter, blowing earth parameter, and observation data. In addition, the construction quality factor is also an important index in the project management. For the research object of this paper, we make a comprehensive evaluation of the index, such as drainage board, sand cushion quality, membrane surface sealing, and open pump, which can be quantified by the supervision log 0–100 value index.

## 2.3 Model structure

The convergence speed and the convergence of network training depend on the topological structure of the network (the hidden layer number, the hidden layer node number). The network topology is not appropriate when the training is too long or during the oscillation, and may even lead to network paralysis. At present, the three-layer BP neural network has been considered the most mature and widely used algorithm, which is most suitable for simulating the input and output of the neural network.

The generalization ability and training speed of the network are influenced by the number of nodes in the hidden layer. Selecting the appropriate number of hidden layer nodes plays a key role in constructing a neural network model. Implicit nodes usually follow experience selection method and formula selection method. The commonly used formula is:

$$o = \sqrt{n + m} + l, \quad (5)$$

where  $n$  is the number of nodes,  $m$  represents the number of output nodes,  $o$  represents the number of hidden layer nodes, and  $l$  takes 1 to 20 arbitrary natural number<sup>[9]</sup>.

## 3 ENGINEERING PRACTICE

### 3.1 Sample processing

In this study, a vacuum preloading area in Tianjin was used as the sample source to extract the sample. The total reinforcement area of the project is 4 million 700000 square meters, the area is 178, the foundation is reinforced with a depth of 20 m, and the thickness of blow fill up to 10 m. According to construction, supervision, and monitoring data and the contents of the upper section, select the thickness of the fill soil, construction days, the average value of pre-engineering, pre-engineering plastic index, the amount of settlement during the period, the average vacuum, the pre-pressure area of the shape factor (i.e., the area in addition to the perimeter), and construction quality index data as the input parameters, and the cross-plate strength mean as the output parameter. A total of 60 groups of data were selected, of which 55 groups were used as training data and 5 groups were used as test data. Because of the difference of the numerical value of each physical quantity, the normalized treatment should be taken to avoid the slow training and the weakening of the small numerical influence:

$$X_i = \frac{x_i - x_{\min}}{x_{\max} - x_{\min}} \times 0.9 + 0.05 \quad (6)$$

### 3.2 Sample training and testing

In practical applications, the convergence is slow, and the BP algorithm is used to adjust the momentum terms when the weights are corrected. That is, the number of the previous weight adjustment is multiplied by the number of the product of the error calculation. From the experience gained by this training, the learning step is 5, and the momentum is 0.5. According to formula (5), the number of hidden nodes is between 4 and 23. For selection of different node numbers of training comparison, see Table 1. According to the mean square error, 12 hidden nodes are chosen as the optimal test network.

### 3.3 Results of application and analysis

By optimizing the training network, the effect of the vacuum preloading area near the sample area is evaluated (Table 2). It was predicted that, after

Table 1. Mean square error of training with different hidden nodes.

Hidden node number	Frequency of training	Mean square error
4	40,000	0.0081
7	40,000	0.005
8	40,000	0.0033
9	40,000	0.0029
10	40,000	0.0054
11	40,000	0.0055
12	40,000	0.0025
13	40,000	0.0063
23	40,000	0.0062

Table 2. Prediction of the neural network in the project.

Blow fill thickness (m)	8.1	8.5
Construction days (d)	96	101
Pre-engineering water content mean (%)	57.11	44.91
Pre-engineering plastic exponential mean	24.26	21.11
Settlement amount during play (m)	1.04	0.81
Sedimentation rate during vacuum pumping (m)	1.02	0.84
Average vacuum degree (kPa)	82.49	77.65
Shape factor of pre-pressure region	40.05	40.05
Construction quality index	70	74
Cross-plate strength (kPa)	21.7	30.4

stopping the construction after detection, the experimental value will be less than the predicted value of about 3 kPa.

The sensitivity of each input parameter has different effects on the prediction results. The sensitivity measurement method is the average value of each input data. A small proportion (0.1–0.5%) is fixed to increase or decrease the value of one of the parameters, with other parameters unchanged, through the network to get an output value. The operation is repeated to obtain 100 output values, and the standard deviation of the 100 output values is the network sensitivity to change parameters. NeuroSolutions software can be directly used in the sensitivity analysis module; vacuum degree, shape factor, and construction quality index are relatively sensitive factors. Vacuum degree in engineering practice is also an important part of the guarantee, and the shape coefficient is more reflected in the boundary conditions, to ensure that the vacuum degree and the construction quality index, on the one hand, contain the vacuum degree guarantee, and, on the other hand, it is also a reflection of the drainage channels. Based on relatively sensitive

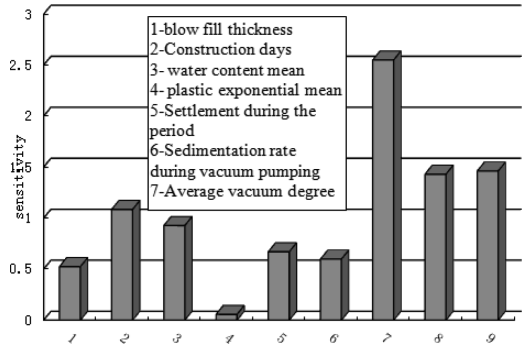


Figure 1. Sensitivity analysis chart of impact factors.

and weak factors such as the thickness of the soil, the number of days before construction, the water content of the workers, the amount of precipitation during the period, and the sensitivity of the water cut, high water content requires more drainage time, and thus the corresponding vacuum degree will also be higher. While the plastic index is the lowest, due to its inherent characteristics in the soil, it will not change much because of environmental change. Sensitivity analysis shows that the prediction error is more affected by the vacuum degree and the construction quality index value is not accurate.

The sensitivity analysis module can be used directly in NeuroSolutions software, and the calculation results are shown in Figure 1. The vacuum degree, shape factor, and construction quality index are relatively sensitive.

#### 4 CONCLUSION

1. Combined with the strengthening mechanism of the soft foundation, the neural network has a reference value to the effect of vacuum preloading, and it can avoid the detection of the broken film. Compared with the traditional degree of consolidation, it is more intuitive and reliable.
2. The sensitivity analysis of the influence factors of this study provides a good guidance to the key index of the vacuum preloading.
3. The selection of indicators is too concentrated, and hence their application may be limited to the surrounding area. For a network with a wider application effect, more in-depth research is needed, especially the impact factor selection and processing. A large number of samples not only increases the burden on the BP neural network training, but also increases the need for more efficient learning rules. Neural network is a summary of the data, and will not analyze the nature of the link; therefore, engineering applications need to be cautious.

## REFERENCES

- [1] Li Yibao, Zhang Xueyong, Ma Jianguo, Wang Lijun. Study of improving algorithms based on the BP neural network. *Journal of Hefei University of technology*, 2005, 28(6): 668–671.
- [2] Ghaboussi J, Sidatra D E. New method of material modeling using neural networks. *Numerical models in Geomechanics*, 1997, 393–400.
- [3] Ellis G W, Yao C, Zhao R, Penumadu D. Stress-strain modeling of sands using artificial neural networks. *Geotechnical Engineering*, 1995, 121(5): 429–435.
- [4] Zhu J H, Zaman M M, Anderson S A. Modeling of soil behavior with a recurrent neural network. *Canada Geotechnic*, 1998, 35: 858–872.
- [5] Kiefa M A A. General regression neural networks for driven piles in cohesion less soils. *Geotechnical Engineering*, 1998, 124(12): 1177–1185.
- [6] Zhang Dexian. A New Approach for the Efficient Estimation of the Number of Hidden Units for Feed forward Neural Networks. *Computer engineering and applications*, 2003, 39(5): 21–23

## Design of the man–machine interface for the operating system of two-for-one twister

Qiong Shen, Yan-bo Ni & Qi-hong Zhou

*College of Mechanical Engineering, Donghua University, China*

**ABSTRACT:** Compared with the high degree of automation of foreign two-for-one twisters, which have produced modularization and intelligence, the study of such twisters has a late start, simple interface, single function, and poor expandability. In order to solve the above issues, improve production efficiency, reduce labor costs, improve the working environment, design man–machine interface for the operating system of two-for-one twisters, through preliminary investigation and analysis of domestic and foreign textile industry status and twisting industry production environment issues, we have conducted a research on twisting and textile industry workers and design students and analyzed user needs, objectives, expectations, preferences, and so on, and finally designed a two-for-one twister interactive interface. Finally, the eye tracker experiment was conducted to test the feasibility of the design.

**Keywords:** interfacial design; man–machine interaction; user research; eye tracker experiment

### 1 RESEARCH BACKGROUND AND PURPOSE

Nowadays, as a realization of a twist yarn twisting two-revolution textile equipment, two-for-one twisters also need a large amount of labor. Recently, foreign two-for-one twister mechatronics equipment has been developed with high degree of automation, which initially produced modularization and intelligence [1]. The study of domestic two-for-one twister has a late start, simple interface, single function, and poor expandability, and some devices are even still using the traditional physical key. With the development of science and technology, intelligent twister will become a mainstream trend. On the basis of the relationship between twister operating system interface and user psychology, behaviors, needs, we conducted a research on textile workers, students and related professional textile design students; analyzed the user habits, order of operations, cognitive mode, and degree of comfort and satisfaction; obtained user needs, goals, expectations, preferences, and so on; analyzed the positioning of the operation interface; and designed a two-for-one twister interactive interface to meet the needs of users. Finally, through the eye tracker device, we tested and analyzed the feasibility of the design.

Several problems exist in the working environment of a twisting workshop. To better understand the working environment and problems of the twisted silk industry workers, we conducted a field

visit on Jiangsu Zhengda twisted yarn companies and found the following problems in twisting silk industry production environment:

#### 1. Severe noise pollution

The tangential belt of twister causes high mechanical losses, high power consumption, large variation in the speed of different spindles, and severe noise. Long-term exposure to noise will have a severe negative effect on the human auditory system, non-auditory system, and work efficiency, and produce symptoms of tinnitus, memory loss, dizziness, headache and insomnia on the workers. With prolonged exposure to noise, aural loss becomes more severe [2].

#### 2. Hot and humid, unventilated

The temperature of a twisted workshop is generally 2–3°C higher than the outdoor temperature. As the work environment is often closed, the temperature in summer is unbearably high. In order to safeguard themselves from such high temperatures, workers typically wear long-sleeved pants, which in turn make them streaming with sweat.

#### 3. Work intensity

In general, the work mode of the twisting industry is 8 h in three shifts, basically in the state of standing or walking around. Night shift work does not provide rest to workers rest, thereby damaging their body severely.

Two-for-one twister interactive interface could rise the degree of intelligence of machines,

and taking advantage of the network system to remotely control, it can reduce the amount of labor and labor costs. This type of interface could alleviate the disadvantages of twisting wire industry such as high pollution, high temperature, high humidity, and high work intensity. Workers can use this system to constantly monitor the status of the machine and time the workshop to process, thereby reducing the time they spend in the workshop and avoiding the damage to their health caused by the noisy, hot, and humid work environment.

However, there are many problems in its structure. It requires a man-machine interface for the twister structure to improve the design. To alter the twist of two-for-one twisters, the gearbox behind the twist gear should be adjusted, and because of the structural design requirements, twist gears do not have high anti-load capacity. Thus, low-twist activities or large load could easily damage the gear. Meanwhile, oil can pollute the tangential belt, causing it to slip. In order to solve the above issues, two-for-one twisters were designed, which do not require a gearbox. Without gearbox, spindle speed, winding speed, and traverse speed are controlled separately, thus requiring a central control unit PLC (programmable logic controller)—a man-machine interface.

At present, a decentralized production equipment monitoring scheme based on interconnection of things has been proposed on the market. Programs aim to study twister, loom, and other major production equipment in textile enterprises and develop the integration of financial-line real-time monitoring, statistical analysis, and decision support for intelligent monitoring systems. It aims to enhance the level of automation of production and management and achieve effective integration of enterprise management information systems and on-site control systems. The textile production process monitoring and management system has been formally applied in Huzhou city, Zhejiang Province, by a textile group. The system monitors the production process, for two-for-one twister's downtime, break time, down times, break times, operation rate, and other parameters of statistical analysis [3].

Because the textile production process monitoring and management systems are mainly used in two-for-one twister, textile machinery, and other production equipment, it only makes parameter statistical analysis to twister production downtime, break time, down times, break times, operation rate and so on, and lacks analysis and intelligent design for concrete steps and operational problems during twisting. The human-computer interface design applies design psychology, ergonomics, and other knowledge from the user's needs, preferences, and expectations, to make intelligent and detail-oriented design of each operation during the

production process, thereby making the user interface design more suitable to the behavioral habits. Therefore, in order to improve workers' working conditions, increase productivity, and reduce labor costs, a questionnaire survey was conducted on 10 workers and 30 industrial design, textile, and related professional students. To obtain their needs for operator interface, expectations, and preferences, we proposed a design program of the twister interactive interface.

## 2 RESEARCH METHODS

### 2.1 *Questionnaire*

Through designing "on twister usage questionnaire" and conducting the aforementioned questionnaire survey, we summarized the current problems in operation and their needs, expectations, and preferences for twister interface.

### 2.2 *Design proposal*

Ergonomics, design psychology, graphic design school, user behavior science, and other knowledge were comprehensively used to synthetically analyze human-computer interface design principles, graphics, color, user behavior, and psychological method and provide a theoretical basis for user interface design by

1. comprehensively applying software packages such as Adobe Photoshop and Adobe Dreamweaver for designing and
2. converting the optimization program into a HTML page format [4].

### 2.3 *Eye tracker experiment*

Eye tracker test was conducted on 30 industrial design and textile students to evaluate the operating system interface, and the final evaluation data were adapted to reflect the user's adaptation to interface operation. Then, the level of usability of user interface was assessed and the program was optimized [4].

## 3 RESULT ANALYSIS

To further understand the users' problems in using two-for-one twisters and the demand, expectation, and preference of this twister interface, a questionnaire survey on the use of two-for-one twisters was designed. A detailed investigation of the questionnaire was carried out to solve the problems existing in the operation of the two-for-one twisters, which included users' demand and preference, as well as

the function, font, and icon of the two-for-one twister interface.

On 13 October 2015, 10 twisting workers, aged 45–55 years, in Zhengda Throwster, Qidong city, Jiangsu Province, were investigated. From 20 October 2015 to 22 October 2015, 30 industrial design and textile professional undergraduate students and graduate students from Donghua University, aged 18–22 years, were investigated. The demand, preference, and expectation of the two-for-one twister interface were assessed. During the investigation, most respondents expressed the expectation of the two-for-one twister man–machine interface and were willing to use it. Respondents expressed the expectation that they hoped the interface icon to be clear and intuitive, twisting parameter settings to be convenient, and the cylinder fault to be directly displayed during the process of winding yarn. For the text, icon size of the interface is supposed to be moderate and bright in showing, and develop the emergency brake operation.

#### 4 OPERATING SYSTEM INTERFACE DESIGN

The position design of the two-for-one twister man–machine operation interface must consider ergonomics, design psychology, graphic design, user behavior, and other related requirements. As the interface is the medium of communication and exchange between human and machine, in order to pay attention to both the user-oriented principle and the principle of easy operation, we need to define the main operation steps of the two-for-one twister, link the main steps of the operation to be ordered, and clarify the relationship between the front and rear tasks and several major modules, so that the operation becomes more smooth [4]. However, the current interface design is common in the main problems such as incompatible color, unknown character of the signal, and the function zoning chaos [5]. Therefore, during the interface designing, the color tone, primary and secondary colors, icon size and semantics, text size and reading ability, and so on, need be repeatedly tested and adjusted, also taking into account the interface needs and preferences of respondents in the previous research.

##### *Man–machine interactive interface operation procedures of the two-for-one twister*

1. Set outline. There are four major modules, all of which are confirmed by the list: yarn-winding process, broken yarn joint process, troubleshooting instructions, and the setting of the double-twist parameter.
2. Yarn-winding process. Users can conveniently monitor the operation of the machine at any

time. If the yarn is broken in the process of winding, users acquire the information of the interface feedback to determine the location of the fault, and process it in time.

3. Broken yarn joint process. This module will reflect the condition of the user to process the broken ends of the yarn. It mainly presents the number of processed and non-processed yarn breakage and detailed processing information, including the concrete position of the processed and non-processed yarn.
4. Troubleshooting instructions. This module contains two parts of gear fault and bearing fault. The main forms of fault in the two-for-one twister machine gear are fatigue, indentation, corrosion, bonding, wear, and fracture. The main forms of fault in the two-for-one twister machine bearing are the fatigue fracture, abrasive wear, wear, or abrasion and desquamate of the bearing. The user can judge and locate the concrete fault caused by the module in the machine fault.
5. The setting of double-twist parameter. When the products of different varieties are produced, the different times and twist parameters need to be set. This module contains the component parameter setting and process parameter setting. Users can modify the parameters according to the actual needs and find the history record of the parameter setting.
6. Compulsorily stop. When a severe breakdown of the machine occurs, it should be stopped compulsorily to safeguard the user.

#### 5 EXPERIMENTAL RESULTS

To verify the feasibility of the design scheme, 30 undergraduate and graduate industrial design and textile students (10 male and 20 female) from Donghua University aged from 18 to 22 years were selected for eye tracking test of the man–machine interface of two-for-one twisters in the laboratory of Donghua University on 13 October 2015 and 20 October 2015. The main targets of this test are the hotspot view of the static state, the distribution map of sight, and Area of Interest (AOI)[6].

##### *5.1 Hotspot view of the static state*

The residence time in a region and the degree of concentration of the subjects can be analyzed through the hotspot view, in which red represents the long fixation time and green the short fixation time. In the login interface of the design scheme, eyes of the subjects were mostly focused on the OK button in the login screen, that is, the current region that should be operated; meanwhile, only a small

part of the view focus on other areas of operation. This showed that the design could better concentrate their attention, as shown in Figure 1. In the parameter setting interface of the design scheme, eyes of the subjects were basically focused on the historical records, changing the parameters or historical records of the parameter setting, which shows that the program design allowed users to correctly find the area of changing parameters and that the test results were consistent with the users' demand, as shown in Figure 2.

It can be drawn through the analysis that the design scheme can clearly divide the functional area and the main button, and the design objective is consistent with the needs of users. Plan design reasonably set up the important icon and button clarified whether the functional partition was in line with the intelligent demand of the two-for-one twister man-machine interface from the design psychology and ergonomics.



Figure 1. Hotspot view of the login interface in program.



Figure 2. Hotspot view of the parameter setting interface in program.

## 5.2 The distribution map of sight

Gaza plot can view the subjects' gaze point. The number in dot represents the order of subjects viewing pictures. The size of dot indicates the fixation time, that is, the larger the dot, the longer the time and vice versa [7]. The distribution map of sight mainly presents the changes of the path and diameter of the gaze point of subjects, to analyze the operation behavior of each subject. If the sequence of viewing the image and the fixation point is mainly concentrated in the target operation area, then the design and layout of the interface becomes reasonable, thereby better understanding the interface, and making the interface design meet the needs of users.

As shown in Figure 3, in the second interface of the setting parameters of the design scheme, on clicking the process parameter setting button, users can switch to the process parameter setting interface from the component parameter setting interface, thereby successfully modifying process parameters. In their distribution map of sight, the gaze point of the subject is largely concentrated near the component parameters and the process parameters key, less concentrated on other areas, and the most concentrated area is the process parameters key area. This shows that the gaze point of the subject is focused on the target functional area of the interface.

The user demand is consistent with the interface function. At the same time, the distribution of track of subjects is concentrated around the gaze point, moving slightly. The line of sight path of the conner is: component parameters—the right-hand side of process parameters—near the process parameters—the process parameters button. The conner first stays in the current sight of the interface icon and then switches from the current



Figure 3. The distribution map of sight of the parameter setting interface.



interface to the process parameter setting interface. The line of sight of the conner soon moves to the correct target area, that is, process parameters button, and does not stay there too long. The moving range of the tracking point is small, which indicates that the target function keys can be found quickly and the operation is completed.

## 6 CONCLUSION

Through the analysis of problems in textile industry environment and twisting industry production and the existing intelligent two-for-one twisters, a questionnaire survey was conducted on 40 textile workers and industrial design and textile students. Using the knowledge of ergonomics, design psychology, graphic design, user behavior, and so on, the man-machine interface of two-for-one twisters was designed. An eye tracking test was conducted on 30 industrial design and textile majors to verify the feasibility of the design scheme and the adaptability of the user to the design scheme. The intelligence of the textile machinery can not only improve the level of the information of the future development of the textile industry, but also greatly improves the production efficiency and reduce labor costs. In the follow-up study, the details of the interface and the detailed function of the two-for-one twisters will be further studied and more functional setup and interface analysis will be performed, so that the interface design is more in line with the needs and expectations of users.

## ACKNOWLEDGMENTS

This study was sponsored by the Fundamental Research Funds for the Central Universities (Grant No. 2232015G1-54) and Science and Technology Project of China Textile Industry Association (20121116).

## REFERENCES

- [1] Yuan Song, Zhang Jianyi, Yuan Yanhong. Design of Human-Machine Interactive Intelligent System of Two-For-One Twister [J]. Modern Textile Machinery Technology, 2013.
- [2] Zhao Yanfang, Fu Xue, Jiang Yueming, Yao Jianhua. The Effects of the Noises of Textile Industry On Health of Weavers [J]. Suzhou University Journal of Medical Science 2005; 25(5).
- [3] Niu Zhiyun, Xu Jingyun. Gu Yuxiang. Use Textile Production Process Monitoring and Management System on the Twister Loom [J]. Science and Technology Information.
- [4] Shen Qiong, Chen Bei, Zhang Lu. Human-Machine interaction design on operation system interface of roving-spinning machine [J]. Journal of Machine Design, 2014, 31(9).
- [5] Wu Jiang, Zeng Lifei. The Study of Design of the Human-computer Interactive Interface of Flat-panel TV [J]. Machinery Design & Manufacture, 2010.
- [6] Hu Fengpei, Han Jianli, Ge Liezhong. The Research Summary of the Eye Tracking and the Usability Test [J]. Human ergonomics, 2005(2):52-54
- [7] Chen Zailiang. Research on the Method of Extracting Region of Interest [D]. Hunan: Central South of University, 2012.



**Taylor & Francis**

Taylor & Francis Group

<http://taylorandfrancis.com>

# Design of the measurement standard for ultrasonic PD tester

Quan Wang, Jun Zhang, Wei Zhou & Bing Lu

*China Electric Power Research Institute, Wuhan, China*

Xi-Cheng Rao

*State Grid Information and Telecommunications Branch, Wuhan, China*

**ABSTRACT:** The measurement standard of the ultrasonic PD (Partial Discharge) tester applied to the laboratory environment is introduced in this paper, in order to effectively improve the measurement technology and the traceability reliability of the ultrasonic PD tester. The standard of measurement is composed of ultrasonic signal source, power amplifier, data processing module and standard microphone. The Direct Digital frequency Synthesis (DDS) technology is used in the ultrasonic signal source, which can transmit the ultrasonic signals such as continuous wave and sharp pulse according to the demand. The high speed A/D converter is used in the data processor. The ultrasonic signal can be collected from 20 kHz to 200 kHz at least 10 MS rate. The measurement standard can be used to detect the sensitivity and frequency of the ultrasonic PD tester in the experimental environment.

**Keywords:** ultrasonic PD tester; measurement standard; direct digital frequency synthesis; sensitivity

## 1 INTRODUCTION

The partial discharge is an important index to reflect the insulation performance of electrical equipment. The ultrasonic signals generated by the board can be used to check the location of the discharge [1]. The ultrasonic method is seldom used in partial discharge test because of its low sensitivity. But the sensitivity of ultrasonic measurement has been greatly improved since the improvement of the sensitivity of energy exchange components and the application of low noise integrated amplifier in the last twenty years [2]. In addition, the ultrasonic tester can eliminate the external electromagnetic interference and can effectively determine the part of the partial discharge. Therefore, the ultrasonic testing method has been widely used in the high voltage electrical equipment with complex structure.

The ultrasonic partial discharge tester can extract the amplitude, frequency, waveform and other characteristics of the signal through the detection of ultrasonic signal, in order to determine whether there has been the phenomenon of partial discharge of power equipment and the type and the location of the discharge. However, these factors that the ultrasonic partial discharge detection technology started late and the related technology is not mature enough limit the continued promotion of ultrasonic partial discharge detection technology in

the state maintenance of power equipment [3]. At present, the performance parameters, the manufacturing standards and the testing indicators of the ultrasonic partial discharge tester are not uniform in all over the world. There is little research about the measurement standard of ultrasonic partial discharge tester in China. China Electric Power Research Institute has made a preliminary research of the ultrasonic partial discharge tester. But the research is mainly about the performance testing of the ultrasonic partial discharge tester from an acoustic point of view. The testing index is mainly focused on the acoustic performance of the sensor head, but it has not been related to the electrical properties of the detector.

## 2 WORKING PRINCIPLE OF THE ULTRASONIC PARTIAL DISCHARGE TESTER

### 2.1 *Ultrasonic propagation characteristics*

The sound wave of partial discharge can be transmitted to the transducer of the receiving acoustic wave through a variety of media in the insulation structure. For example, the sound wave can reach the transducer on the surface of the shell through the solid medium, liquid medium and metal shell when the phenomenon of the partial discharge in the air gap of the solid medium happen in the

transformer. The sound waves will be reflected, reflected and attenuated in the process of propagation. The speed of sound wave propagation in various media is shown in Table 1.

The relationship formula between incidence angle  $\phi_0$  and refraction angle  $\phi_1$  [4]:

$$\sin \phi_0 / \sin \phi_1 = C_0 / C_1$$

In the formula,  $C_0$  and  $C_1$  is the speed of sound wave of the incidence angle and the refraction angle.

The ultrasound has many characteristics, such as amplitude, energy, duration, frequency, average frequency, rise time and so on. When the real discharge quantity of the partial discharge is changed, three parameters that contain signal amplitude, frequency and duration of the signal will change. Under a certain partial discharge condition, the amplitude of the ultrasonic signal is proportional to the discharge of the partial discharge. At the same time, the ultrasonic frequency spectrum moves to the low frequency with the increase of the discharge.

### 2.2 Composition of the ultrasonic partial discharge tester

At present, there are a lot of applications of the ultrasonic partial discharge tester in the electrical equipment condition-based maintenance and fault diagnosis. Its structure is basically the same. The tester can be divided into the sensor, data acquisition, data processing and display according to the angle of the measuring device. As shown in Fig. 1, it can be divided into ultrasonic sensor and ultrasonic testing host according to the spatial structure of the tester.

Table 1. The speed of sound wave propagation in the medium.

Material	Speed (m/s)
Transformer oil	1400
Oil paper	1420
Oil immersed electrical board	2300
Copper	3580
Steel	6000
Silicon steel sheets	5050

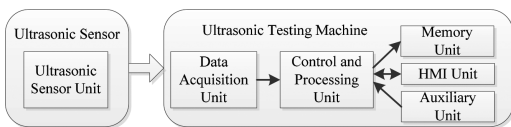


Figure 1. Structure of the ultrasonic partial discharge tester.

### 3 DESIGN OF ULTRASONIC PARTIAL DISCHARGE MEASUREMENT STANDARD

The standard device for the ultrasonic partial discharge measurement is mainly composed of standard ultrasonic signal source, broadband power amplifier, ultrasonic transducer, standard microphone, data processing and host computer. The standard ultrasonic signal source is the core module of standard device. The ultrasonic signal source is mainly used to generate the standard ultrasonic power signal which is needed for calibration. The frequency range of ultrasonic power signal is from 20 kHz to 200 kHz. The function of the broadband power amplifier is to amplify the standard ultrasonic power signal generated by the power source according to the requirement. The power amplifiers have a wide frequency band, to ensure that the ultrasound signal has a low distortion. The ultrasound transducer includes an impedance matching device and an electroacoustic converter. The function of the impedance matching device is to improve the efficiency of the acoustic electric conversion, so that the active power can be transmitted to the electroacoustic converter as much as possible. The main function of the standard microphone is to measure the standard ultrasonic signal generated by the impedance matching device. The function of the data processing is to sample the output signal of the standard microphone. It can convert analog signal to digital signal. At the same time, it can also export the data of the ultrasonic partial discharge tester. The function of the upper computer is to calculate and compare the number of data processing module, and display the test indexes of the tester.

#### a. Ultrasonic signal source

The ultrasonic signal source is composed of the stable programmable power and the standard ultrasonic transducer. The programmable power uses the control core FPGA and the D/A converter. The total technique project is as follows. Firstly, the sine single of range from 20 kHz to 200 kHz is stored in FPGA. Then

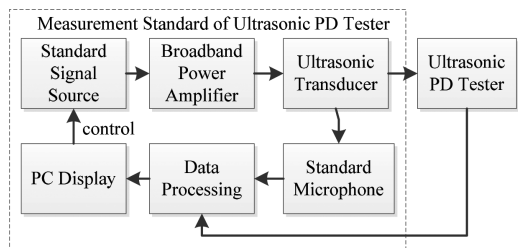


Figure 2. The block diagram of the measurement standard of the ultrasonic partial discharge tester.

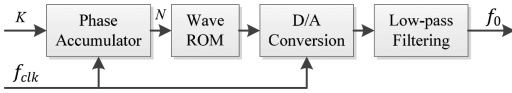


Figure 3. Schematic diagram of the DDS.

the corresponding waveform parameters are selected to output by the host computer. And the output digital signal is converted to analog signal by D/A converter. Finally, the analog signal will be filtered by the low-pass filter, to filter the high order harmonic generation from the discrete digital quantity into continuous analog quantity. The output waveforms are designed by the Direct Digital Frequency Synthesis (DDS) technology. DDS technology is that generate waveform through the search method according to Nyquist sampling theorem. Then the analog signals are discretized and stored in memory in binary form. When the signal is needed, the data is taken out from the memory at a certain speed. In order to get the desired waveform, the signal needs to be sent to the D/A converter. Then the high frequency component is filtered out by the low pass filter. And the output signal becomes smooth.

b. Power amplifier module

The power amplification section is based on the minimum driving power of the ultrasonic transducer. The power of the driving transducer must be 5 W, and the voltage of the driving transducer must be 16 V through the calculation of subsequent transducer. So the power amplifier chip of the APEX Company's PA75 chip is selected. The chip can be output  $\pm 40$  V voltage. The maximum current of the chip can be up to 2.5 A. The gain bandwidth of the chip is 1.4 MHz. And the upper limit power of the chip is 60 W. The output voltage of the front function generator is 5 V. The sine signal of 16 V and 5 W is output after the power amplifier chip amplification.

c. Impedance matching module

The impedance matching of ultrasonic transducers is carried out in a wide frequency band. Thus, the reactive power loss caused by the impedance parameter of the transducer itself can be reduced. The energy conversion efficiency is improved, and the input power of the ultrasonic transducer is stabilized. In order to obtain the maximum transmission power gain TPG in the frequency band range from 20 kHz to 200 kHz, the transducer can be matched with the broadband impedance in the desired frequency band. The impedance characteristic of the ultrasonic transducer in the frequency band is measured by the impedance analyzer, to obtain the impedance

characteristic curve of the transducer. Then, the impedance matching is carried out by using the simplified real frequency method. Finally, a matching network is obtained by the optimization algorithm. If the final selection of the passive impedance matching network is the four order network, you can get an impedance matching network as shown below.

The TPG is expressed as a function of frequency  $\omega$ , load impedance  $Z$  and vector  $h$ . Namely, TPG can be expressed as the form  $T(\omega, Z, h)$ . Generally, the reflection of the load side is as small as possible and the TPG is as large as possible. The next job is to find the maximum  $h$  in the given frequency range TPG. The problem becomes the design optimization problem of the matching network. Given a target power gain  $T_0$  that we need to achieve, the optimization of the objective function is the following.  $\varepsilon = T(\omega, Z, h) - T_0(\omega)$ .

The  $h$  that makes the objective function minimum can be found by a computer program, to ensure that is obtained in the specified frequency.

#### 4 TRACEABILITY OF KEY PARAMETERS

In order to test the reliability and accuracy of the measurement data of the ultrasonic partial discharge tester, the reasonable traceability should be considered. The design of the measurement standard of the ultrasonic partial discharge tester can be more specific to the current ultrasonic partial discharge tester. Because the current ultrasonic partial discharge tester is still lack of effective measurement standards. The measurement standard is based on the Enterprise Standard *Technical Specification for Ultrasonic Partial Discharge Tester* of China State Grid Corp and the Industry Standard *General Technical Requirements for Ultrasonic Partial Discharge Tester* of Chinese Electric Power, which needs to trace the ultrasonic signals and electrical signals. The comparison method is used to trace the reference sensor of the acoustic emission sensor and the Measurement Institute of China. The amplification and acquisition system of electrical signals can be traced back to the precision pulse amplitude meter and frequency meter of the National High Voltage Metering Station. Thus, the problem of the lack of measurement standard for ultrasonic partial discharge tester is solved.

##### 4.1 Traceability of acoustic signal sensor

According to the national measurement technical specification JJF1337-2012 "*Acoustic Emission Sensor Calibration Specification (Comparison Method)*", the block diagram of the sound signal sensor traceability is as follows.

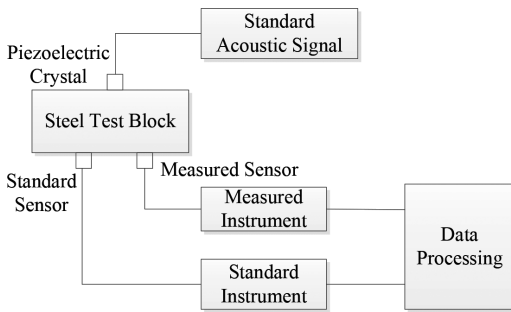


Figure 4 The block diagram of the Comparison calibration device of the sensitivity. 1-Reference sensor; 2-Sensor to be measured; 3-Transmitting transducer; 4-Pre-amplifier.

The reference sensor used in this paper is the standard sensor of the Chinese Academy of metrology. The sensor can be traced back to the United States NIST standard sensor, which used to be the source of the United States acoustic emission sensor. According to the standard requirement, the pulse signal source uses the sound wave generated by the capillary glass tube broken or the pulse waveform generated by HB pencil core fractured.

#### 4.2 Traceability of electric signal acquisition system

There are precision pulse amplitude measuring instrument and frequency meter in national high voltage metering station. The standard table method is used to calibrate the electrical signal acquisition system. The source of the electrical signal acquisition system is as follows.

### 5 EXPERIMENTAL RESULTS AND ANALYSIS

Stability is one of the important indexes of ultrasonic standard source. The output voltage stability test of the standard output voltage of the ultrasonic partial discharge measurement standard is shown in Figure 5. The S9208 of the PAC Company's was chosen as an ultrasound transducer. The working resonance frequency of the S9208 is 500 kHz. The working frequency band of the S9208 has a range from 20 kHz to 1000 kHz. The peak sensitivity of the S9208 is 45 dB/V/(m/s). The R15D of the PAC Company's was chosen as a Standard microphone. The working frequency band of the R15D has a range from 100 kHz to 200 kHz. The resonance frequency of the R15D is 75 kHz. The peak sensitivity of the R15D is 69 dB/V/(m/s). The acquisition card has a sampling rate of 10 MS/s per channel in the device.

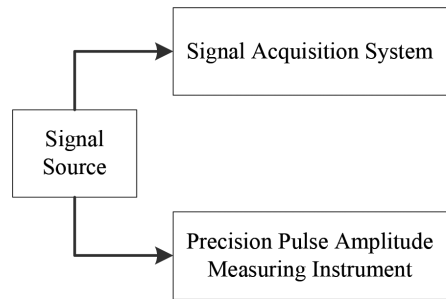


Figure 5. The traceable amplitude figure of electric signal acquisition system.

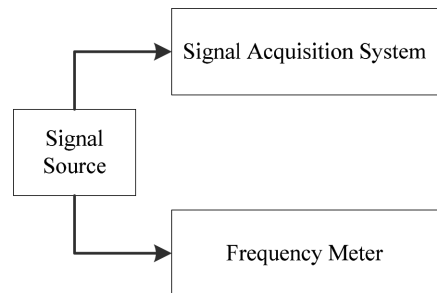


Figure 6. The traceable frequency figure of electric signal acquisition system.

The resonant frequency of the R15D type AE sensor used for the project of the ultrasonic partial discharge measurement standard is 156.35 kHz. Its maximum sensitivity is -60.51dB. According to the resonant frequency of the R15D of the standard output voltage stability test of ultrasonic partial discharge measurement standard, the stability test frequency has a range from 100 kHz to 200 kHz. The output voltage of the AE type R15D sensor measured by the 34411 Multicenter are shown in Table 1, if the amplitude of the transducer's front power is not changed, the output frequency is changed, and each frequency measurement point is constantly output every 5 min.

According to the output stability test of the standard output of the ultrasonic partial discharge measurement standard, the test frequency has a range from 100 kHz to 200 kHz; the test time is 5 min, the maximum acoustic output stability of the measurement standard is 1.75%, and the minimum value is 0.24%. According to Table 2 and Figure 7, the stability and sensitivity of the standard microphone device is proportional when the test frequency is near the resonant frequency of the standard microphone except the test frequency in

Table 2. Standard output voltage stability test of ultrasonic partial discharge measurement standard.

Frequency/ kHz	Minimum Output/Vrms	Maximum Output/Vrms	Instability/ ±%
100	0.134	0.136	0.74
110	0.121	0.123	0.82
120	0.09	0.091	0.55
130	0.0185	0.0189	1.07
140	0.028	0.029	1.75
150	0.196	0.2	1.01
160	0.261	0.265	0.76
170	0.207	0.208	0.24
180	0.207	0.209	0.48
190	0.229	0.234	1.08

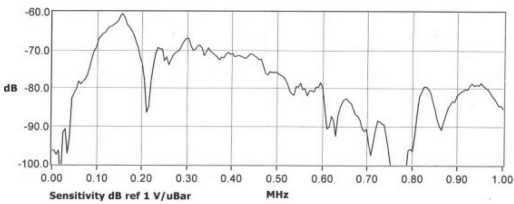


Figure 7. Relationship between frequency and sensitivity of R15D.

the 190 kHz. In order to avoid that the stability of the measurement device does not generate large fluctuations and the output signal is stable, the sensitivity of the standard microphone should be better than 45dB and the test frequency should be selected in the sensitivity stable region. Only in this way can we effectively improve the output stability of the measurement standard.

## REFERENCES

- [1] Yu Xiegen. New progress in the research and measurement techniques of partial discharge [J]. *Electric World*, 1997, 04: 4–6.
- [2] Maimaiti Nur, Shi Haizhen, Qi Tiedong. Application Research on the technology of partial discharge charging inspection [J]. *Scientific and Technological Innovation and Application*. 2013 (02).
- [3] Huang Xingquan, Tang Zhiguo, Li Chengrong, Zhang Yuxiao, Wang Wei. High frequency partial discharge of power transformer on line detection of [J]. *High Voltage Technology*. 2003 (04).
- [4] Li Dajian, Ji Chong Liang, Kewei, Jing Gang Yang, Li Yanming. Typical defects in GIS Partial Discharge Ultrasonic testing [J]. *High Voltage Apparatus*. 2009 (01).



**Taylor & Francis**

Taylor & Francis Group

<http://taylorandfrancis.com>



# Summary of the research on a network fault prediction method

Wei-qiang Xu

*School of Ordnance Engineering College, Shijiazhuang, China*

Guo-shun Chen, Gang Niu & Wei-guo Chen

*Institute of Ordnance Technology, Shijiazhuang, China*

**ABSTRACT:** In this paper, the significance of Prognostics and Health Management (PHM) applied in network maintenance support was analyzed and the key techniques of network PHM based on the core of fault prediction were shown. In order to understand the present research situation, network fault prediction methods and the development direction of network fault prediction methods were summarized, which had important guiding significance for the research of network fault diagnosis and related work.

**Keywords:** network diagnosis, fault prediction, network PHM

## 1 INTRODUCTION

With the rapid development of information technology, the network has gradually become one of the most important infrastructures, whose reliability has attracted increasing attention. People's increasing needs in network application have resulted in the expansion of the scale and complex structure of network, thereby increasing the network maintenance cost. At the same time, because of the growth of network composition and influence factors, fault occurrence and failure probability have increased gradually. Network fault diagnosis and maintenance is becoming the major focus of researchers nowadays. In the field of military, war has entered the era of information warfare. Information control and reliable transmission have become the keys of victory in wartime. Considering the network reliability, security, cost, and other issues, the application of Prognostics and Health Management (PHM) in network provides a new way to improve network maintenance support.

## 2 NETWORK FAULT CLASSIFICATION

Network fault is defined as the deterioration in the performance of network system. For failures in computer and communication network, faults can be broadly divided into two categories: catastrophic failure and gradual failure. There is no obvious sign of abrupt fault before failure, and it is difficult to predict it by early measurement and monitoring. The network throughput can instantly be reduced

to zero when abrupt fault occurs. Such failure is usually caused by network communication equipment, featured with destruction, caused by force majeure (major) such as war or natural disasters. Gradual fault refers to the situation where the network can still work and provide the expected service, but with a declined performance and Quality Of Service (QOS). Because of improper operation and aging of equipment, some link nodes result in network congestion and other faults. Some faults such as bandwidth loss and delayed deterioration are usually gradual processes, which usually result from aging of the equipment, improper application, or hidden factors. Such failures can generally be predicted through the measurement and monitoring of network state parameters. Most of unknown faults originate from the gradual faults of the system. The research of network fault prediction is mainly aimed at the detection of gradual failure.

Network fault diagnosis means discovering the cause of abnormal network system and state deterioration parts in the work environment and forecasting the development trend of the network status. One of the difficulties in network fault management is the degradation of system performance and trend prediction. Real-time service in the network has aroused the requirement for continuous monitoring and prediction of system performance and reliability. Although fault is an unusual event, its occurrence will lead to many undesired consequences. Decrease of network performance could be regarded as a precursor of an upcoming fault. Effective treatment for performance decline can help solve the network fault prediction problem.

### 3 MEASURING NETWORK SYSTEM PERFORMANCE INDEX SELECTION PRINCIPLE

Strictly speaking, measuring the performance parameters of network system should include all state information of all modules in the network system. However, the network system structure is complex and the evaluation parameters of network system health and performance are complicated and fuzzy. The primary and secondary indicators of the parameters are difficult to determine, making it difficult to establish a unified network health assessment and fault prediction model. If the selected indicators cannot meet the test requirements of a specific network system, ideal prediction will not be achieved.

Different network systems are measured by different indicators and factors, but they generally follow three principles: The first one is the principle of completeness, namely choosing parameters in the network core function module, making the selection of parameters reflect the network performance as much as possible. The second is the secondary principles, whose parameters must be set in a suitable range and have the difference of superiority, which is determined according to the importance of network health effect. The third is the principle of independence, which means that there should be no overlap between the selected parameters, in order to avoid repeated use of the same parameter. According to the above principles index, the test index selected can accurately evaluate and concisely predict the actual situation network.

### 4 NETWORK PHM SYSTEM

PHM is a comprehensive fault detection, isolation, prediction, and state management technology. It represents the change of maintenance strategy, namely from the traditional diagnosis to predictions based on the intelligent system and from maintenance dominated by events or time-related maintenance on a regular basis to the Condition-Based Maintenance (CBM). The transformation is the development direction of modern equipment support. A large proportion of the unit or scholars launched an in-depth research on PHM and certain achievements have been made in the theory.

A complete network PHM system should include the following functions theoretically: network health assessment, fault diagnosis, fault prediction, fault location, health management, and service life tracking. Information consistency problem caused by the heterogeneity of network should be taken into account in the construction of the network PHM system. As is shown in Fig 1, the

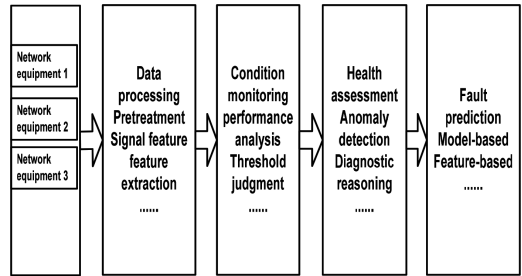


Figure 1. Fault prediction module of network PHM system.

PHM architecture based on Mobile Agent (MA) is constructed to realize the basic operation of surveillance, interactive, prediction, and diagnosis. This architecture can be used to solve the problem of large server load and network congestion caused by the centralized fault management mode.

As can be seen in the figure above, PHM system based on the core of fault prediction is mainly composed of the following six parts:

1. Data collection: Data collection is the basic module, and only relevant parameters of the system will be collected. Data analysis is the base of evaluation and forecast of the system.
2. Data processing: This aims at selecting the appropriate database for the storage of the collected data, as a guarantee for the data query. The data were processed in data format and the corresponding data fusion was specified by the subsequent modules.
3. Condition monitoring: This aims at monitoring the status of the network, and data will be compared with the threshold value.
4. Health assessment: This uses the data processed, such as early warning information, performance degradation information, and other historical data, and then provides guidance for fault prediction.
5. Fault prediction: This aims at predicting the overall development trend of the network system and possible failure assessment by using appropriate prediction algorithms. Measures are taken to ensure that the system is monitored before failure.
6. Reasoning and decision making: This section will use the results of (4) and (5) to provide maintenance recommendations. In addition, there is an inevitable link between the PHM modules, whose boundaries are not obvious because of data transmission and feedback cross between the modules.

This paper focused on the research of network fault prediction method. Monitoring present state

of the network system is the initial step in fault prediction. By combining recent network health degree, characteristic parameters, and historical data, the health status of the network was analyzed through the corresponding pre-algorithm. Then, the future working state was obtained and fault prediction was realized, which ensure to take effective measures promptly to guarantee the smooth working of the network before the occurrence of the failure.

## 5 NETWORK FAULT PREDICTION METHOD

The causes of network failures are complex and diverse, and the focus of research varies in different needs. Therefore, network fault prediction can be divided into the following situations:

### 5.1 Prediction of single-component network equipment

Although initially it is difficult to use a mathematical model to describe the status of network devices, after considerable practice and observation, some rules could be followed:

1. In a relatively short period of time, the influence factor of the network equipment parameter is relatively fixed.
2. There is a certain relationship between the next moment of network equipment and the last moment.
3. In a certain period of time, the change of the network equipment parameter value will be in accordance with the continuation of a certain trend.

Therefore, in a relatively short period of time, the network device state parameters can be predicted by the linear model. A combined regression model proposed a polynomial of individual component failure rate in the network regression prediction model. The prediction equation is obtained by transforming the polynomial regression model into multiple linear regression model to solve the parameters. New prediction equation is obtained with the actual failure data by using the significance of test regression equation and regression coefficient, fitting better than the original equation. The prediction equation could be verified by using a group of network component failure rate data. The results show that, in accordance with the <2% prediction error of the requirements to determine the prediction interval, the method can estimate the decision basis for the single-component failure rate.

### 5.2 Network traffic prediction

The operational status of network in the future can be obtained intuitively through the prediction of

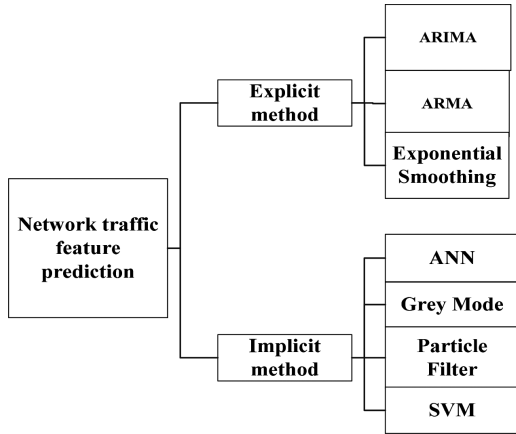


Figure 2. Prediction method of flow characteristics.

flow characteristics and then the network fault will be predicted. The prediction method of network traffic characteristics is summarized as shown in Figure 2. Explicit method to establish a linear model to achieve prediction is simple but less accuracy. The implicit method can better adapt to the network state parameters' high-dimensional and nonlinear characteristics and has good prediction effect. This method follows empirical risk minimization principle, using the learning method as representative of the neural network. Sufficiently large sample data are needed, but learning problems may appear, which lead to poor generalization model of defects. The Support Vector Machine (SVM) based on the structural risk minimization principle ensures maximum theoretical model generalization ability and solves the practical problems of small, nonlinear, high-dimensional, and local minimum samples better, which is now considered a more advanced and better method of prediction.

### 5.3 Prediction of network performance

In network fault prediction, single parameter tends to have a certain one-sidedness and cannot fully reflect the network's operation, generally for particular system with a higher requirements index. Comprehensive indices are often obtained from the MIB of network management center, and the format of the standard MIB variable is complex. The differences and range between raw data are relatively large, and hence the data are usually quantified and value ratio is adjusted before processing. In order to keep each attribute value in small range, a study proposed an intelligent network performance management method based on statistical analysis. In network performance monitoring, network throughput, delay, and the change

of equipment use rate can significantly affect the performance. Correlation analysis was used to identify three performance indicators relating with different factors (for example, the protocol of the data packet and packet length), and then further reasons for the fault and potential network problems will be found.

#### 5.4 *Fault prediction based on network alarm*

A warning by means of an alarm notifies the incident report when some specific abnormal events occurred in the system. Alarm generation indicates that the system temporarily has some kind of abnormality [14], which is detected by the system equipment manufacturer or system management personnel. Each warning has a specific meaning. Warning generation does not necessarily mean failure, but it indicates that there is an abnormal "situation". In fact, warning information significantly increased the network fault probability.

According to the network warning correlation analysis, the idea is to delete, merge, or transform multiple alarm information and generate a warning with more information. According to the corresponding relationship between the network fault and the historical warning, the current warning may mean the appearance of network fault. This approach is essentially pattern recognition and the key is how to build a knowledge base. Generally speaking, because of the delay of the network and failure of the alarm, warning signs often fail to reach the network management system in the right time. The time window indicates the difficulty of acquiring knowledge. The research focuses on how to deal with the network delay, the determination of the time window, and the method of pattern recognition. Alarm data pre-processing includes analyzing and summarizing the characteristics of the alarm data, designing a reasonable alarm filtering mechanism and implementation scheme to reduce the number of alarms to be analyzed, so as to improve the efficiency of mining.

## 6 DEVELOPMENT TRENDS

The network management system based on traditional expert system is difficult to handle the rapid changes in the dynamic network environment because of failure in learning. Knowledge acquired from experts in the field is featured with strong subjectivity and randomness. Therefore, traditional expert system was limited in the further application in fault management, because knowledge is difficult to acquire and maintain, practicability is poor, and exact inference is not suitable to solve

fuzzy problems and deficiencies. The development trend of network fault prediction technology is reflected in the following aspects:

### 6.1 *Integrated Intelligent Fault Prediction System (IIFPS)*

Single intelligent prediction technology cannot achieve the conversion between linguistic variables and fuzzy number or explain the difference for knowledge. Therefore, it is difficult to meet fault forecast demand of complex system. Integrated intelligent system was integrated by various fault forecast technologies effectively. It overcomes the limitations of the existing single prediction technology and makes full use of the advantages of each technology. Furthermore, it improves the intelligence of prediction and enhances the ability of machine learning and accuracy and stability of the prediction in complex system.

### 6.2 *Analog Fault Prediction System (AFPS)*

In order to make full use of virtual reality technique, which is a new way of visualization and interaction of complex data, comprehensive analysis, simulation, and forecast decision for data information are carried out. The prediction technique considers technical personnel, forecast object, and computer as a whole system. Computers are used to generate a 3D virtual information space and users achieve intuitive operation and computer control in the virtual space, thereby significantly improving the prediction efficiency. The application of virtual reality technology for intelligent prediction technology development has revolutionized the technology.

### 6.3 *Remote distributed intelligent forecast system (RDIFS)*

RDIFS is a system based on the combination of distributed network technology and the fault prediction technique, which is based on comprehensive fault prediction technology, communication, and computer technology. It has obvious advantages in resource sharing and real-time forecast. RDIFS can use multiple systems together as a device to realize prediction. On the contrary, the system can also provide predictive diagnosis service for a plurality of devices. Its characteristics can be summarized for multi-system cooperation and multi-equipment adaptability. This method effectively solves the problems existing in fault diagnosis and maintenance. The cost of network maintenance support would be significantly reduced by overcoming the maintenance time and geographical limitations.

## 7 CONCLUSION

With the continuous progress of science and technology, network equipment structure is becoming increasingly complex, automated, and the integrated degree continuously increases. Therefore, the causes and characteristics of fault become more complex than before, which has brought great challenges to fault prediction. Therefore, relevant new thinking and methods should be introduced in fault prediction, especially integration of different forecasting technologies. The intelligent prediction method based on computer, including state management and fault diagnosis, needs further development and improvement. IIFPS, AFPS, and RDIFS will have a wide application prospect in the future.

## REFERENCES

- Basak, J., & Krishnapuram, R. (2005). Interpretable hierarchical clustering by constructing an unsupervised decision tree. *IEEE Transactions on Knowledge & Data Engineering*, 17(1), 121–132
- Cao, J., Liu, Y., & Dai, Y. (2007). Network Traffic Prediction Based on Error Advanced DGM (1,1) Model. *Wireless Communications, Networking and Mobile Computing, 2007. WiCom 2007. International Conference on* (pp. 6353–6356). IEEE.
- Deng, L., Fan, G., & Liu, Z. X. (2012). Network fault prediction based on regression analysis method. *Computer Engineering*, 38(20), 251–255.
- Ghosh, A., & Kanjilal, M. (2012). Throughput prediction for tcp bulk transfers. *Lap Lambert Academic Publishing*.
- Maxion R A, Feather P E. (1990). A Case Study of Ethernet Anomalies in a Distributed Computing Environment [J]. *IEEE Trans. on Reliability*, 39(4): 433–443.
- Ma, H. L. Z. (2006). Network fault prediction based on alarm correlation. *Computer Engineering & Applications*.
- Mirza, M., Sommers, J., Barford, P., & Zhu, X. (2010). A machine learning approach to tcp throughput prediction. *Networking IEEE/ACM Transactions on*, 18(1), 1026–1039.
- Ni, N. Y. P. X. D. (2003). Network performance management and fault prediction based on statistical analysis. *Computer Engineering*.
- Shan, X., Zhu, Y. X., & Guo, J. (2007). Network alarm prediction knowledge discovery based on support vector machine. *Microelectronics & Computer*, 24(6), 35–39.
- Wen, X. X. (2012). Survey on key technologies of network prognostic and health management. *Systems Engineering-Theory & Practice*, 32(1), 146–154.



**Taylor & Francis**

Taylor & Francis Group

<http://taylorandfrancis.com>

# Study of the green design strategies of the senior housing in Wuhan

Jun Lu

Hubei Institute of Fine Arts, Wuhan, China

**ABSTRACT:** With the rapid growth of the elderly population in China, the market requirements for buildings for the elderly have become very high. As an important type of buildings for the elderly, the senior housing will be greatly concerned. According to the climatic characteristics of the hot summer and cold winter in Wuhan, this paper discusses the strategic problems of the green design for the senior housing in Wuhan and proposes green strategies, which are adapted to the climate conditions in Wuhan, such as the building site selection, building layout, building orientation, daylight of the sunshine, building shading, natural ventilation, heat preservation, and heat insulation.

**Keywords:** Senior housing, Green design, Building layout, Three-dimensional green

## 1 INTRODUCTION

### 1.1 Current situation

The total registered population of Wuhan by the end of 2014 is 8.27 million, of which 1.56 million (19%) are elderly people, that is, one-fifth of the total population. Besides, the number of people aged over 80 years has reached 0.21 million. By 2020, the elderly population in Wuhan will reach 1.9 million, which will exceed 21% of the total population. Although most of the elderly realize home-based care, some others badly need professional care because of their diseases or the unwillingness of their children to provide care to them. This raises a huge demand for buildings for the elderly. The buildings for the elderly will become the main building type throughout the main residential area in the future.

### 1.2 The green senior housing

Promoting the development of buildings for the elderly in the direction of the green buildings will not only help to increase profitability, but also can provide a healthy and comfortable living space for them. As an important type of buildings for the elderly, the senior housing will be greatly concerned. On the basis of the characteristics of the local climate environment, this paper discusses the green design strategies of the senior housing in Wuhan.

## 2 THE DEFINITION AND THE EPITAXY OF THE SENIOR HOUSING

In the book “*Code for design of residential building for the aged*”, senior housing is defined as the elderly apartment house in which the elderly can live in together and which conforms to the physical and mental characteristics of the old people, and the synthetically managerial housing types with the service systems of catering, clean sanitation, entertainment, and health care. According to the difference between the service objects and service facilities, the senior housing is divided into three types: independent apartments, caring-type apartments, and nursing apartments.

The development of the Chinese contemporary facilities for the elderly is in the initial stage. Compared with other types of the green public buildings in China, the green senior housing is still in the relatively blank state. The design of the green senior housing is guided by the green concept. According to its own conditions and the operating features of the apartment in various regions and the physical and mental characteristics of the elderly, we could set the green building technology as the main investment target, because its investment is relatively lower and the development is relatively mature. In the architectural design, through the reasonable use of the location planning, orientation, separation distance, layout, and some energy-saving technologies, we can possibly create a healthy

and comfortable indoor and outdoor environment for the elderly by constructing a building with natural lighting and natural ventilation, and by saving land, energy, water, and materials.

### 3 INVESTIGATION OF THE SENIOR HOUSING IN WUHAN

#### 3.1 *The starlight senior housing on Luonan Street, Hongshan District in Wuhan*

The starlight senior housing is a private institution for the elderly, which is located on the intersection of Shi PaiLing road and Xiongchu Street and near the former site of the civil affairs bureau in Hongshan District. The surrounding traffic is very convenient, but the service facilities are insufficient. The apartment is rebuilt from the old office building in the flourishing section of the city, which is composed of the third and fourth floors. It is a social endowment institution with residence and entertainments together, which is rebuilt to serve both the urban and rural elderly. It has about 20 rooms and can accommodate more than 30 old people. The occupancy rate has now reached 98%. The old people are mostly the surrounding elderly or the parents of migrant workers nearby. The rent of a bed in the apartment ranges from 1300 to 2000 yuan per month, including the expenses of eating, living, and the different-level daily nursing, but it does not include the medical treatment costs. It is specially designed for the low-income people. There are several such small apartments in the different communities of Wuhan. The spatial layout of Wuhan's facilities for the elderly (2012–2020) estimated that the number of senior housing in Wuhan would exceed 169 by 2015. Because the urban area is very limited, all aspects of the conditions are indeed to be improved.

Since it is a reconstruction project, the design is not all based on the stipulation in *Code for Design of Building for elderly Persons*. The design of the corridor and bathroom is barrier-free; for example, the corridor is equipped with handrails. However, the activity room, staircase, and the outdoor space environment are not barrier-free, which is inconvenient for the elderly. The hallway is toward the south, and its area is narrow. Because the indoor corridors are too long, the ventilation and the natural lighting conditions are not very good. The building exterior walls do not have thermal insulation measures and the windows are made of aluminum alloy without sunshades, and hence the heat preservation and heat insulation performances of the building external envelope system are poor.

Therefore, the Starlight Senior Housing reconstruction project was employed. Because of its own conditions, the internal environment needs to be improved, and there are many problems in

various aspects of the apartment layout design and the landscape planning.

#### 3.2 *The senior housing in Jiangnan District in Wuhan*

The senior housing in Jiangnan District in Wuhan is one of the largest public institutions for the elderly in central China with functions of living, medical treatment, recovery, and entertainment. It covers an area of 3.79 acres with 370 rooms and 800 beds. The senior housing consists of three parts of buildings: Yishou garden, Yiyang garden, and Fu Hui hospital. Yishou garden is a new high-end hotel-style senior housing. It has 17 floors and an area of 15,680 square meters, accommodating more than 300 elderly. The lower floors of the apartment are the public service area, such as the public restaurant, the chess and card room, the music hall, the painting and calligraphy studio, and the Internet bar. The middle and higher floors consist of the standard rooms. The standard room in the new building is designed for two old persons. Yiyang garden is an old senior housing with three buildings uniting seven floors. Its balconies are annular and the aisles are connected. In the old building, there are rooms for three people or two rooms with one hall for two elderly.

The barrier-free design in the apartment meets the requirements of the specification. The handrails are set up in the corridors and staircases so that it is convenient and safe for the elderly to walk in. There is a laundry room, barbershop, and supermarket in the apartment, which provide a certain social intercourse space for the old people. Each floor has a treatment room for medical services. The rooms also have balconies for the elderly to dry their clothes. The building exterior walls have thermal insulation measures and the windows are made of aluminum alloy without sunshades, and hence the heat preservation and heat insulation performances of the building external envelope system are poor.

In conclusion, because of their unique geographical location and good medical conditions in the senior housing in Jiangnan District, the medical binding mode and the auxiliary services of the university of old age are welcomed by the elderly. However, air conditioners to keep cool in summer and supply heat in winter increases the energy consumption of the building, thereby costing the old people an extra amount of 200 yuan per month.

### 4 THE GREEN DESIGN STRATEGY OF THE SENIOR HOUSING IN WUHAN

Building the senior housing and creating a healthy and comfortable living environment for the elderly



is important to support old people in China. Results of research found that the current senior housing in Wuhan cannot meet the requirements of the green energy-saving buildings. Wuhan is characterized by hot summers and cold winters. For the special characteristics of the old people, the implementation difficulty and emphasis of the green energy-saving building should ensure cool conditions in summer and warm conditions in winter. And according to our own situation, the buildings for the elderly need to minimize the costs to become high-quality green buildings.

#### 4.1 Site selection

The senior housing is mostly located in the urban community, city, or the suburban scenic area. It exhibits different characteristics at different locations. Because of the physical and psychological needs of the elderly, regardless of the type of the senior housing, several key points should be considered when the building site is selected.

1. Respect the principle of the upper-level planning: The apartment must be located on the direction of the city master planning. The local reconstruction project should choose buildings that are close to the senior housing space requirements, such as hotels, offices, or other suitable space for the elderly.
2. Flat terrain: The base terrain should be as flat as possible. It must avoid steep walks and steep stairs to facilitate the activities of the elderly.
3. Surrounding environment: It requires quiet environment, adequate sunlight, good ventilation, and fresh air.
4. Auxiliary facilities: Because of the decline of their physical function and their small living range, the senior housing should be equipped with complete supporting facilities. The residential auxiliary facilities can be shared with the senior housing in the community.
5. Convenient transportation: It should not only be convenient for the elderly to get around, but also facilitate visiting by their children.

#### 4.2 Building layout

Reasonable layout of the building is a prerequisite to provide good sunshine and wind environment, so that it can have good ventilation and lighting. The sunshine time through the windows of the bedroom in the senior housing should be more than 2 h in the winter solstice. According to the characteristics of the elderly, the senior housing is generally located in the lower and multi-floor. This building layout type is divided into centralized layout and decentralized layout. The centralized layout mainly has the corridor-style and courtyard-style layout, which is suitable for small apartment

buildings. The centralized layout is also divided into three styles of the central emanant layout, blade layout, and hybrid layout, which is suitable for large apartment buildings. The distributed layout should connect the functions in the apartment using the corridors and the ramps. This layout is flexible and has good orientation, ventilation, and lighting. However, it covers a large area and needs to be built in the scenic area in the suburbs.

#### 4.3 The orientation and daylight of the buildings

When designing the green building, the most important factor to be considered is the selection of the appropriate construction direction. Wuhan is characterized by hot summers and cold winters, so the best orientation for the buildings in Wuhan is 10 degrees south by east and 10 degrees south by west. The suitable orientation is 20 degrees south by east and 15 degrees south by west. It is unfavorable toward the west and northwest. This type of orientation could avoid too much exposure to the sun and improve ventilation in summer; furthermore, it facilitates the maximum solar radiation and avoids the entry of cold air into the room in winter. Therefore, when we design the senior housing, the best orientation of the elderly bedroom should be carried out, that is, toward the south and the auxiliary function room can be set in the northern side.

#### 4.4 Building shading and natural ventilation

Because the temperature is high in summer in Wuhan, we have to consider architectural shading and natural ventilation in the architectural design. The building shading can be divided into architectural form shading, glass skin material shading, highlighted components wall shading, solar photovoltaic panels shading, combined vertical green shading, and so on. The main purpose is to adjust the indoor temperature of the apartment and reduce the air-conditioning load. At the same time, the architectural shading can also effectively prevent the glare phenomenon and material deteriorating and aging phenomenon caused by the direct light.

The natural ventilation can maintain good indoor air quality by eliminating the indoor waste heat and importing fresh air. In the building, there are four common natural ventilation implementation modes: thermal pressure ventilation, wind pressure ventilation, natural ventilation under the simultaneous action of the wind pressure, and thermal pressure and the natural ventilation of the mechanical auxiliary type. In some senior housing in Wuhan, air ventilation in the room is poor, especially in the corridors. As both sides of the room are closed, the indoor ventilation is not free without effectively organizing the draught. There-

fore, in the building design of the senior housing in Wuhan, we can choose the thermal pressure ventilation and organize the ventilation by using the vertical space in the building, such as the staircase, atrium, and air shaft. The bedroom of the elderly is normally exposed to the sun and wind in summer. Thus, natural lighting and ventilation can be obtained by opening the window directly, especially in the bathroom. If the building condition does not favor this, an exhaust fan should be set in the bathroom to improve ventilation.

#### 4.5 Heat preservation and heat insulation

In order to prevent cold air from entering the rooms in winter, we need to take measures for the senior housing envelope to ensure the basic thermal environment quality in the room and prevent the large room temperature fluctuations. Research findings showed that heat insulation is not efficient in the senior housing in Wuhan. The main manifestation is that the effect of the heat insulation of the external envelope structure is poor and the indoor comfort is adjusted mainly relying on air-conditioning and heating installation without considering energy saving. The energy consumption of the envelope system is mainly through the exterior wall, doors, windows, roof, and ground. Their heat dissipation is different: the heat dissipation of the exterior wall is 25–28%. The door and window penetration is 23–25%. The heat dissipations of the roof and ground are 8% and 3%, respectively, while the partition wall of the stairs is 10%. Therefore, the walls of the senior housing should be built using hollow bricks and composite wall material. The external wall heat insulation system should be used and more attention should be paid to the safety and fireproofing of the thermal insulation materials. The commonly used thermal insulation materials are EPS, XPS, and PUR.

The energy-saving design of doors and windows in the senior housing is mainly embodied in the choice of the materials and the construction methods. The doors of the senior housing are often divided into two types: vertical-hinged doors and sliding doors. The thermal resistance of the door is higher than that of the window, but smaller than that of the exterior wall and roof. Therefore, doors should be made of materials with good thermal insulation properties. An anteroom should be designed in the hall to reduce heat loss in winter. The windows in the senior housing should be

double-layer hollow glass window or low-E glass window. The window frame should be made of plastic–steel, steel–wood, wood–plastic, and other low-thermal conductivity materials. The ratio of the window and the wall should meet the requirement of *Design standard for energy efficiency of residential building in Hubei*.

#### 4.6 Other strategies

Three-dimensional afforesting of the senior housing plays an important role in the elderly living environment atmosphere, and the green design directly affects the daily life and the physical and mental health of the elderly. Therefore, the three-dimensional green design should be used sensibly according to the climate characteristics, the plant distribution, the surrounding environment of the building, and special use requirements of the old people in Wuhan.

## 5 CONCLUSION

According to the climatic characteristics of hot summer and cold winter in Wuhan, this paper mainly discusses the strategic problems of the green design for the senior housing in Wuhan. First, when selecting the architectural site, we need to consider the characteristics of the elderly. Second, building layout, building orientation, and daylight of the sunshine were considered. These factors should ensure a good sun and wind environment. Third, we discussed building shading, natural ventilation, heat insulation, and other three-dimensional green strategies.

## REFERENCES

- Bin Ma. The Research of Green Design for Apartments for the elderly in Jinan. Jinan, Shandong Jianzhu university. 2013.
- Chen Yuqing. Design with Climate-The Research of the Bio-climatic Design Approach. Wuhan. Huazhong university of science and technology. 2005.
- Min Jia Encouraging the Development of Sustainable Building for the elderly Under the Ageing Before Getting Rich Social Background. *City and House*. 2015. 8: 19–23.
- Wei Tian, Zhan Chen, Wujie Rong. Sustainable Building Design Strategy in Region Where Has Hot Summer and Cold Winter. *Architecture Technique*. 2011. 12: 59–63.

# Survey and analysis of intellectual capital of scientific research team

Feng-Lin Chen

*Nanjing Jincheng College, Jiangsu, China*

**ABSTRACT:** In order to clarify the current situation of intellectual capital of scientific research team, we carried out a special research by conducting personnel interview and questionnaire survey. This paper discusses the purpose, significance, theoretical basis, main content, method, and process of the research, provides research results, and concludes that the intellectual capital of the teams is overall strong.

**Keywords:** intellectual capital; survey; analysis; scientific research team

## 1 INTRODUCTION

Senior (1836) argues that intellectual capital refers to the sum of all knowledge and ability that could bring competitive advantage to the organization. Regarding the structure of intellectual capital, there are three types of views: binary thinking, trialistic thinking, and pluralistic thinking. The most common is trialistic thinking argued by Seemann (1997), which divides intellectual capital into human capital, structural capital, and social capital. Therefore, scholars usually measure the overall value of intellectual capital through the measurement of human capital, structural capital, and social capital.

Human capital is summarized into comprehensive knowledge, technology, innovation ability, values, culture, and philosophical thinking to solve the problem of work for employees proposed by Edvinsson and Malone (1997). Sveiby (2001) also argues that human capital should include skills, education level, experience, values, and motivation;

Capital structure includes the physical content, such as the self-built database and independent research scientific equipment, and the content of the system and culture, such as team management system and team culture.

Social capital is reflected by the following four variables, which are the major stakeholders of scientific research team: government, academia, industry, and the social public.

In conclusion, the various parts of intellectual capital are as follows: human capital considers members as the carrier, and it could be divided into the following five variables: basic knowledge, academic vision, team cooperation,

innovation motivation, and shared vision; structure capital considers organization as the carrier, and it could be divided into the following three variables: material platform, system platform, and culture platform; and social capital between organization and various stakeholders, and it could be divided into relationship between the government, academia, industry, and the social public.

## 2 EVALUATION INDEX SYSTEM

To collect information about the current situation of the intellectual capital of the domestic scientific research team through interviews and questionnaires, the problem of the composition of intellectual capital should be resolved first.

Because there is no ready-made, scientific measurement scale of intellectual capital of scientific research team in the literature, we adopt the following steps and methods to build an intellectual capital scale.

First step: We start from the essential characteristics of the scientific research team and design the initial measurement scale of intellectual capital of the team based on literature data.

Second step: In order to optimize the above index system, we make the empirical test on the scientific nature and effectiveness of the index system by membership degree analysis, correlation analysis, and discrimination analysis. Then, we modify and perfect the index system based on the inspection results in order to construct a more scientific and practical intellectual capital scale of the scientific research team.

Table 1. Index system of intellectual capital.

Primary index	Secondary index	Three-grade index
Human capital	Team structure	Age distribution V1
		Degree distribution V2
		School distribution V3
	Overall capacity	Turnover rate V4
		Annual number of published papers V5
		Reference of each paper V6
Structure capital	Research resources	The key instruments and equipment V7
		The key database V8
		Interdisciplinary papers V9
	Knowledge sharing	Team work papers V10
		The team atmosphere V11
		Understanding of the members V12
Social capital	Team leadership	Credibility V13
		Organizing ability V14
		Domestic cross-team cooperation V15
	Collaborative research	International cooperative papers V16
		Number of members be in office every year tenure V17
		Number of members obtained title overseas V18
Academic participation	Number of international conference members attent V19	
	International relations	Domestic spending V20
		International cooperative project V21
	Budget devotion	

### 3 MEASURE OF INTELLECTUAL CAPITAL

We select 22 teams from the research team randomly as research objects in the factor analysis and comprehensively analyze intellectual capital of the 22 teams according to the result of factor analysis.

#### 3.1 Standardization and source of data

The 22 scientific research teams mainly come from colleges and research institutes. The data used in this study have been mainly obtained from the research results and public information of the teams in recent 5 years. In addition, some indicator data are obtained by questionnaire and simple calculation.

Because of the dimension of each evaluation, index data are different, and hence it is necessary to carry out the data dimensionless processing.

At present, the globally used index standardization processing method is the Z score method. The index standardization conversion formula is:

$$X'_{ij} = \frac{X_{ij} - \bar{X}_j}{S_j} \quad (i = 1, 2, \dots; j = 1, 2, \dots) \quad (1)$$

#### 3.2 Factor analysis process and result

Before factor analysis, it is necessary to determine whether the measurement data for factor analysis through sampling suitability test statistic are KMO or Bartlett sphere test index. A small KMO value shows that the common factor between the observed variables is less, which not suitable for factor analysis.

The judging standard of index is: KMO > 0.9 – very suitable; 0.7 – general; 0.6 – does not suit; 0.5 – highly fit, the specific output as shown in Table 2.

From Table 2, the chi-square approximation of Bartlett sphere inspection is 678.429, the corresponding probability (p value) is 0.000, less than the significant level (0.01), the null hypothesis is rejected, and the correlation coefficient matrix has statistical significance.

However, KMO value is 0.867, which is in good agreement with the KMO metrics given by Kaiser. As a result, the original variables are suitable for factor analysis.

If the accumulation contribution rate of factor reaches or exceeds 80% of the numbers of factors, we use principal component analysis to extract “public factor”. Load factor eigenvalues and rotation sum of squares loaded are shown in Table 3.

The cumulated variance contribution ratios of the former four factors extracted are shown in Table 3. It is evident that the first four factors can explain 85.092% of the original data information, so we select four common factors that are more reasonable.

The purpose of factor analysis is not just to find the common factor, but to make certain the meaning of each public factor, in order to analyze the practical problems. However, the result of the principal component factor analysis shows that the common factor of load is more dispersed and the typical representative of the variable is not very outstanding. The meaning of the factor is fuzzy and the actual

Table 2. KMO and Bartlett test.

Kaiser-Meyer-Olkin		0.867
		678.429
Bartlett	df	210
	Sig.	0.000

problem is difficult to analyze. Therefore, we adopt orthogonal rotation method to orthogonal rotation factors and make the absolute value of new factor loading close to 0 or 1 as soon as possible.

Table 4 shows that the first factor F1 has high factor loading on seven indicators: V7, V5, V8, V6, V11, V9, and V10. These indicators fully embody the intellectual capital of scientific research team, so we name F1 “management factor”.

The factor loading of F2 is higher on four indicators: V12, V2, V13, and V1. These indicators reflect the intellectual capital of the domestic scientific research team, so we named F2 “output factor”.

The factor loading of F3 is higher on six indicators: V16, V17, V14, V15, V4, and V3. These indicators reflect resources of investment in the intellectual capital of the domestic scientific research team, so we named F3 “inputs”.

The factor loading of F4 is higher on four indicators: V21, V18, V19, and V20. These indicators

reflect marketing ability of the intellectual capital of the domestic scientific research team, so we named F4 “marketing factor”.

The factor score coefficient matrix values calculated by SPSS are shown in Table 5.

Set F1 to F4 for the score of four factors in various companies:

$$\begin{aligned} F_1 &= -0.148V1 - 0.154V2 + 0.063V3 + \dots + 0.075V21 \\ F_2 &= 0.016V1 + 0.271V2 + 0.183V3 + \dots - 0.157V21 \\ F_3 &= 0.352V1 + 0.077V2 - 0.177V3 + \dots + 0.202V21 \\ F_4 &= -0.139V1 - 0.113V2 - 0.047V3 + \dots + 0.004V21 \end{aligned}$$

Let variance contribution ratio of each factor denote the weight to calculate the weighted sum and abstain the comprehensive evaluation score:

$$F = (32.635F_1 + 25.714F_2 + 18.918F_3 + 7.825F_4) \div 85.092$$

Table 3. Results of principal component analysis.

Ingredients	Initial eigenvalue			Rotation sum of squares loaded		
	Total	Variance (%)	Accumulation (%)	Total	Variance (%)	Accumulation (%)
1	13.67	65.09	65.09	6.85	32.63	32.63
2	1.82	8.69	73.79	5.40	25.71	58.34
3	1.27	6.09	79.88	3.97	18.91	77.27
4	1.09	5.20	85.09	1.64	7.82	85.09

Table 4. Rotating component matrix.

	Component			
	1	2	3	4
v7	0.822	0.402	0.259	0.135
v5	0.811	0.450	0.227	0.133
v8	0.804	0.381	0.283	0.158
v6	0.803	0.429	0.300	0.096
v11	0.802	0.264	0.419	0.004
v9	0.793	0.381	0.305	0.088
v10	0.779	0.304	0.396	0.192
v12	0.290	0.840	0.222	0.152
v2	0.373	0.838	0.163	0.005
v13	0.305	0.782	0.353	0.182
v1	0.546	0.738	0.005	0.039
v16	0.322	0.196	0.879	0.109
v17	0.300	0.216	0.865	0.221
v14	0.554	0.077	0.653	0.146
v15	0.732	0.373	0.469	0.065
v4	0.360	0.464	0.290	0.204
v3	0.209	0.222	0.237	0.181
v21	0.351	0.828	0.361	0.742
v18	0.251	0.489	0.156	0.607
v19	0.347	0.565	0.101	0.548
v20	0.468	0.492	0.313	0.460

Table 5. Component score coefficient matrix.

	Component			
	1	2	3	4
v1	-0.148	0.016	0.352	-0.139
v2	-0.154	0.271	0.077	-0.113
v3	0.063	0.183	-0.177	-0.047
v4	-0.097	0.276	-0.043	-0.067
v5	0.217	-0.041	-0.121	-0.014
v6	0.203	-0.050	-0.074	-0.046
v7	0.228	-0.068	-0.103	-0.015
v8	0.216	-0.074	-0.086	0.003
v9	0.212	-0.070	-0.066	-0.050
v10	0.140	-0.062	0.044	-0.072
v11	0.230	-0.130	0.005	-0.120
v12	0.191	-0.108	-0.015	0.026
v13	-0.188	0.259	0.072	0.065
v14	0.013	0.162	0.040	-0.512
v15	-0.074	0.146	-0.096	0.361
v16	-0.036	0.070	-0.003	0.268
v17	-0.173	0.296	0.002	0.050
v18	-0.046	-0.010	0.007	0.472
v19	-0.140	-0.040	0.389	-0.016
v20	-0.166	-0.026	0.379	0.073
v21	0.075	-0.157	0.202	0.004

Table 6. Scores of intellectual capital in 22 teams.

Team	Score	Score	Score	Score	Score
Team 1	0.9623	-0.315	2.8338	1.5041	1.172
Team 2	0.7715	-0.023	1.3327	0.7071	2.3951
Team 3	0.5253	1.0301	0.7541	1.4273	-0.942
Team 4	0.4405	0.2906	1.2244	-0.046	-0.333
Team 5	0.4314	0.3603	0.657	0.7988	-0.902
Team 6	0.3619	0.3984	-0.294	0.6896	1.5728
Team 7	0.3207	1.6525	-0.197	-1.267	0.3057
Team 8	0.2822	0.6389	-1.249	1.4869	0.9158
Team 9	0.2713	0.9816	0.7173	-0.791	-1.588
Team 10	0.2268	1.1082	0.0262	-0.907	-0.049
Team 11	0.2186	0.7111	-0.304	0.5121	-0.828
Team 12	0.0867	-0.04	-0.215	0.8543	-0.25
Team 13	-0.018	0.7619	-1.792	-1.241	1.9385
Team 14	-0.138	-1.002	0.0734	0.856	0.3691
Team 15	-0.15	0.8431	-0.178	-1.469	-1.004
Team 16	-0.273	0.1615	-1.012	-0.221	0.22
Team 17	-0.523	-0.826	-0.589	0.0118	-0.331
Team 18	-0.575	-1.568	0.1693	-0.079	-0.079
Team 19	-0.591	-0.586	-1.027	-0.045	-0.503
Team 20	-0.652	-0.92	-0.16	-1.188	0.1482
Team 21	-0.753	-1.44	-0.821	0.1194	0.222
Team 22	-1.227	-2.22	0.0501	-1.713	-0.106

The factors and the negative comprehensive score must be clarified as not indicating that the intellectual capital of the team is negative, but that it is lower than the average sample. We can see that the intellectual capital of the teams is overall strong from all the scores, and rankings were analyzed.

## REFERENCES

- [1] Davenport. T H, and Prusak. L. Working knowledge: How organizations manage what they know [M]. Boston: Harvard Business School Press, 1998.
- [2] Ulrich. D. Intellectual capital = competence commitment [J]. Sloan Management Review, 1998, 39(2):15-26.
- [3] Burt, R S. The contingent value of social capital [J]. Administrative Science Quarterly, 1997, 42(2):339-365.
- [4] Barathi G Kamath. The intellectual capital performance of Indian banking sector [J]. Journal of Intellectual Capital, 2007, 8(1):96-123.

# A fuzzy DEMATEL method to analyze the criteria for sustainable supplier selection

Xiang-lan Jiang

*Business School, Sichuan University, Chengdu, P.R. China*  
*Sichuan Technology and Business College, China*

Zhi-bin Wu & Yao Yang

*Business School, Sichuan University, Chengdu, P.R. China*

**ABSTRACT:** Academic and corporate interest in sustainable supplier selection has risen considerably in recent years. This paper first reviews the existing criteria for sustainable supplier selection and then develops a criteria set which has in three aspects: economic, environmental and social. The fuzzy Decision Making Trial and Evaluation Laboratory (DEMATEL) approach is then introduced to find the key influence criteria. The applicability of proposed method is demonstrated by a case study of a Chinese chemistry organization. The results from causal diagram divided the criteria into two groups: cause criteria and effect criteria. The cause group (C2, C3, C4, C5, C6, C7, C11, C13) should be controlled and paid more attention to, while the effect group (C1, C8, C9, C10, C12, C14, C15) need to be improved. Among those, C1 (Quality) and C2 (Delivery) would take into further consideration.

**Keywords:** supplier selection; sustainable; supply chain management; fuzzy DEMATEL

## 1 INTRODUCTION

The concept of sustainable supply chain management has been of great interest among academics and practitioners in recent years due to rising awareness of environment protection and social well-being while supporting the economic goal of organizations [1, 2, 3]. To increase competitive advantage of the companies, supplier selection is an important operational and strategic task for sustainable supply chain partnership development. Sustainable supplier performance evaluation and selection plays a significant role in establishing an effective sustainable supply chain management. To achieve a sustainable supply chain, all of the members in the chain must carry on sustainable strategy [28, 29, 30]. Supplier selection techniques can be used to select suppliers of raw materials to end-of-life service providers. Supplier selection problems deal with both tangible and intangible factors [12].

### 1.1 Literature review on sustainable supply chain management

Sustainable development is defined as “development that meets the needs of present without compromising the ability of future generations to meet

their own needs” [13]. Supply Chain Management (SCM) is defined as the management of exchanges of material, capital and information flows in the logistics process stretching from the purchasing of raw materials to the delivery of end-products to end customers [14]. Linton et al. [15] combined the concepts of sustainability and supply chains. They believed that sustainability must integrate issues and flows that extend beyond the core of supply chain management. Seuring and Müller [1] defined sustainable supply chain management as the management of material, information and capital flows as well as cooperation among companies along the supply chain, which taking goals from all three dimensions of sustainable development, i.e., economic, environmental and social, into account which are derived from customer and stakeholder requirements. In sustainable supply chains, environmental and social criteria need to be fulfilled by the members to remain within the supply chain, while it is expected that competitiveness would be maintained through meeting customer needs and related economic criteria. While Carter and Rogers [16] defined SSCM as the strategic, transparent integration and achievement of an organization’s social, environmental, and economic goals in the systemic coordination of key inter-organizational business processes for improving the long-term

economic performance of the individual company and its supply chains. We are now ready to provide a unified definition for sustainable supply chain management as the management of supply chain operations, resources, information, and funds in order to maximize the supply chain profitability while at the same time minimizing the environmental impacts and maximizing the social well-being.

### 1.2 Literature review on supplier selection

Industrial production can have a great impact and damage on the sustainability of the natural environment and human life such as the impacts include depletive resource use, global environmental impacts, local environmental impacts, health impacts, and safety risks [18]. Many factors affect a supplier's performance. Dickson [4] identified 23 criteria that have been considered by purchasing managers in various supplier selection problems. Weber et al. [8] found that 47 of the 76 articles reviewed addressed more than one criterion. Following this exploratory study, a great number of articles focused on SCM and supplier selection criteria specifically. Sustainable supplier selection is a multi-criteria decision making problem which includes both qualitative and quantitative factors and it is necessary to employ MCDM methods to handle it appropriately [5].

Sustainable purchasing has significant implications for the firms implementing it, especially when it comes to the criteria used in supplier selection [6, 7]. Until the early 1990 s, it emphasized the strategic importance of the supplier selection process and evaluated the relative importance of quality, cost, delivery, service performance, and other supplier attributes in the supplier selection process [4, 8]. Green purchasing, however, requires the inclusion of environmental criteria in supplier selection, which leads us to the concept to green supplier selection [9]. With the development of global economy and international cooperation, more and more firms from SCM integrate economic performance, environmental protection and social well-being to achieve sustainable development, which is called sustainable supplier selection [1, 30, 10].

There are lots of reviews about supplier selection. William et al. [22] reviewed multi-criteria supplier evaluation and selection approaches in international journals from 2000 to 2008. Kannan et al. [23] examined green supplier selection papers that appeared from 1996 to 2011 in international scientific journals. Wu and David [24] reviewed the literature on supply partner decision-making published between 2001 and 2011. Chai et al. provided a systematic literature review on articles published from 2008 to 2012 on the application of DM techniques for supplier selection [25].

### 1.3 Motivation

Lots of methods are used for evaluating suppliers, such as Analytic Hierarchy Process (AHP), fuzzy AHP, TOPSIS, Fuzzy TOPSIS, Data Envelopment Analysis (DEA), Analytic Network Process (ANP), fuzzy ANP, Genetic Algorithm (GA) in literature. However, those methods about supplier selection in the supply chain management require extra data and hardly consider the relationship among criteria. The DEMATEL method has been considered one of the best approaches to deal with the importance and causal relationships among the evaluation criteria [21, 23]. It does not need mass data and fits the problem examined in this research. The DEMATEL can find key criteria to improve performance and provide decision-making information in supplier selection in the supply chain management [27, 28].

The DEMATEL method originated from the Geneva Research Centre of the Battelle Memorial Institute is especially pragmatic to visualize the structure of complicated causal relationships [17, 18]. DEMATEL is a comprehensive tool for building and analyzing a structural model involving causal relationships between complex factors. It can clearly see the cause-effect relationship criteria when measuring a problem [19]. In DEMATEL method the criteria are divided into the cause group and the effect group. The cause group has an influence on the effect where such an influence is used to estimate the criteria weights [20, 21]. The mathematical concepts are then evolved and adapted in many academic fields, such as industrial strategy analysis, competence evaluation, solution analysis, selection, and etc. It has been proven as a useful method to solve complicated problems. Sustainable supplier selection is an important aspect of supply chain management. It is of great theoretical and practical significance to develop research on this subject.

The aim of the paper is to explore an efficient framework for the evaluation of supplier sustainability to improve supply chain performance. Sustainable supplier selection requires the evaluation of suppliers' performance with respect to several metrics. There are complex relationships among these metrics [26]. Environmental, social and economic supplier characteristics are necessary considerations for effective sustainable supplier evaluation and selection. Supplier selection is a Multi-Criteria Decision Making (MCDM) problem. Human judgement in decision making is often unclear and therefore it is hard to estimate these judgements by exact numerical values [27, 28, 29]. Hence fuzzy logic is necessary for handling problems characterized by vagueness and impression [30]. This paper utilized Decision Making Trial and



Table 1. Sustainable supplier performance criteria ([30, 18, 22, 23, 27]).

Dimension	Economic (Eco)	Environmental (Env)	Social (Soc)
Criteria	Quality (C1) Delivery (C2) Service (C3) Price (C <sub>4</sub> ) Flexibility (C5)	Resource consumption (C6) Pollution control (C7) Environmental management system (C8) Green product (C9) Environmental competencies (C10)	Stakeholders' rights (C11) Health and safety (C12) Technology improvement (C13) Wealth created (C14) Respect for the policy (C15)

Evaluation Laboratory (DEMATEL) to find key influence criteria in selection suppliers, which can help enterprises to forecast suppliers in terms of the observation on influence of criteria [27]. Lastly, an empirical case study is presented to demonstrate the application of the proposed framework.

The paper is organized as follows: In section 2, the assessment criteria of sustainable supplier selection are presented. In section 3, the proposed model is presented. In section 4 an application is provided illustrate how the framework can work in practice. Section 5 concludes the study.

## 2 SUSTAINABLE SUPPLIER PERFORMANCE CRITERIA

Sustainable supplier selection is one of the key measures for modern management which emphasizes on sustainable development. In this paper, potential feasible suppliers' performances are identified based on social, environmental and economic considerations. Inspired by [30, 18, 22, 23, 27], we suggest a model considering fifteen criteria to cover the three dimensions, five for each dimension. (Table 1).

## 3 FUZZY DEMATEL METHODOLOGY

In the real world there are many situations in which problems must deal with vague and imprecise information that usually involves uncertainty in their definition frameworks. It is hard to provide numerical precise information when the knowledge is vague. The use of linguistic modelling in problems dealing with non-probabilistic uncertainty seems logic and has produced successful results in different fields. This success would not have been possible without methodologies to carry out the processes of Computing with Words (CW) that implies the use of linguistic information. Decision making is very difficult for vague and uncertain environment. This vagueness and uncertainty can be handled by using fuzzy set theory, which was proposed by Zadeh [11].

Fuzzy DEMATEL is built on the basis of graph theory which analyzes and solves problems by

Table 2. The fuzzy linguistic scale.

Linguistic variable	Corresponding triangular fuzzy numbers
No influence	(0,0.1,0.3)
Very low influence	(0.1,0.3,0.5)
Low influence	(0.3,0.5,0.7)
High influence	(0.5,0.7,0.9)
Very high influence	(0.7,0.9,1.0)

visualization method [28]. It analyzes the influential status and strength between the factors and converts them into an explicit structural model of a system [21].

The modified fuzzy DEMATEL method is summarized in the following:

### Step 1: Generating the average matrix.

Suppose we have  $H$  experts to offer their suggestions and  $n$  factors to consider. Each stakeholder is asked to indicate the degree to which he or she believes the factor  $i$  affects the factor  $j$ . Their pairwise comparison between any two factors are denoted as  $x_{ij}^k$ , which takes an integer score ranging from 0 to 4, representing "No influence (0)," "Low influence (1)," "Medium influence (2)," "High influence (3)," and "Very high influence (4)." respectively [1]. In the fuzzy context, the linguistic scale is shown in Table 2. The scores given by each expert will form a  $n \times n$  non-negative answer matrix  $X^k = [x_{ij}^k]$ , with  $k = 1, 2, \dots, H$ . Thus,  $X^1, X_2, \dots, X^H$  are the answer matrices of  $H$  experts. The diagonal elements of each answer matrix  $X^k = [x_{ij}^k]_{n \times n}$  are all set to 0, which means no influence is given by itself. The  $n \times n$  average matrix  $A$  for all expert opinions can be calculated by averaging the scores of the  $H$  experts as follows:

$$a_{ij} = \frac{1}{H} \sum_{k=1}^H x_{ij}^k \quad (1)$$

The average matrix  $A = [a_{ij}]_{n \times n}$  is also called the initial direct relation matrix. Furthermore, we can map out the causal effect between each pair of factors in a system by drawing an influence map. Fig. 1 expresses an example of such an influence map. Each letter represents a factor in the system.

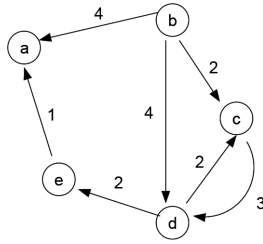


Figure 1. Example of an influence map.

An arrow from c to d shows the effect that c exercises on d, and the strength of its effect is three. DEMATEL can convert the structural relations among the factors of a system into an intelligible map of the system.

**Step 2:** Normalizing the direct relation matrix.

The normalized initial direct-relation matrix  $D = [d_{ij}]_{n \times n}$  is obtained by normalizing the average matrix  $A$  in the following method:

Let

$$s = \max \left( \max_{1 \leq i \leq n} \sum_{j=1}^n a_{ij}, \max_{1 \leq j \leq n} \sum_{i=1}^n a_{ij} \right) \quad (2)$$

Then

$$D = \frac{A}{s} \quad (3)$$

Note that the sum of each row  $j$  of matrix  $A$  represents the direct effects that factor exert on the other factors. Thus  $\max_{1 \leq i \leq n} \sum_{j=1}^n a_{ij}$  represents the factor of the highest direct influence on other factors. Likewise, the sum of each column  $i$  of matrix  $A$  represents the direct effects received by factor  $i$ . Thus  $\max_{1 \leq j \leq n} \sum_{i=1}^n a_{ij}$  represents the factor which is the most influenced factor by other factors. The positive scalar  $S$  takes larger of the two extreme sums, and the matrix  $D$  is obtained by dividing each element of  $A$  by the scalar. Note that each element  $d_{ij}$  of matrix  $D$  is between 0 and 1.

**Step 3:** Obtaining the total-relation matrix.

The total-relation matrix  $T = [t_{ij}]_{n \times n}$ ,  $i, j = 1, 2, \dots, n$  can be obtained by using Eq. (4)

$$T = \lim_{m \rightarrow \infty} (D + D^2 + \dots + D^m) = D(I - D)^{-1} \quad (4)$$

where  $I$  denotes the identity matrix.

**Step 4:** Computing the dispatcher group and receiver group.

The vectors  $R = (R_1, R_2, \dots, R_n)$  and  $C = (C_1, C_2, \dots, C_n)$  represent the sum rows of and the sum of columns of matrix  $T$  respectively.

$$R_i = \sum_{j=1}^n t_{ij} \quad (5)$$

$$C_i = \sum_{i=1}^n t_{ij} \quad (6)$$

$R+C$  named “Prominence” which indicates the degree of importance that the corresponding criteria plays in the entire system. The factor having greater value of  $R-C$  has more interrelationships with other factors. Similarly,  $R-C$  named “Relation” which may group criteria into a cause group if  $R-C$  is positive. Or, if  $R-C$  is negative, the criteria will be grouped into the effect group.

**Step 5:** Producing the causal diagram.

The causal diagram can be obtained by mapping the dataset of the ( $R+C$ ,  $R-C$ ) where the horizontal axis is  $R+C$  and the vertical axis is  $R-C$ .

#### 4 APPLICATION OF THE PROPOSED METHOD

The case study is carried out at a medium chemistry company in China. There are one vice president and two purchasing managers with extensive consulting experience who constitute a decision group in the company. Through a detailed and through analysis of the relative literature and in-depth interviews with the decision group, 15 criteria were recognized as bases for formulating the framework for selecting for sustainable suppliers which has been shown in Table 1.

Fifteen evaluation criteria for sustainable supplier selection were addressed. We use the fuzzy DEMATEL to establish the influence map in accordance with the real situation in which criteria should be interdependent. The three experts were invited to fill out expert questionnaires using the five linguistic terms: 0 (No influence), 1 (Low influence), 2 (Medium influence), 3 (High influence), and 4 (Very high influence). The linguistic scale is presented in Table 2.

Using the pairwise comparisons, the averages of their opinions were calculated in accordance with Eq. (1). The normalized initial direct-relation matrix was generated by using Eqs. (2) and (3). Through transforming the crisp values into TFNs, the obtained DEMATEL initial direct relation matrix was shown in Table 3. The total relation matrix was computed by using Eqs. (4)-(6) as produced in Table 4. Final results of computations were obtained in Table 5. The influence map of the criteria was depicted in Fig. 2.

Considering the significance of criteria in supplier selection, as presented in Table 5, the importance is identified as  $C1 > C2 > C6 > C4 > C3 > C10 > C5 > C11 > C15 > C8 > C12 > C7 > C9 > C14 > C13$  according to

Table 3. The triangular fuzzy numbers.

	C1	C2	C3	C4	C5	C6	C7	C8
C1	(0,0,1.0,3)	(0,5,0,7,0,9)	(0,3,0,5,0,7)	(0,5,0,7,0,9)	(0,7,0,9,1,0)	(0,3,0,5,0,7)	(0,5,0,7,0,9)	(0,7,0,9,1,0)
C2	(0,7,0,9,1,0)	(0,0,1,0,3)	(0,5,0,7,0,9)	(0,7,0,9,1,0)	(0,3,0,5,0,7)	(0,3,0,5,0,7)	(0,3,0,5,0,7)	(0,5,0,7,0,9)
C3	(0,5,0,7,0,9)	(0,3,0,5,0,7)	(0,0,1,0,3)	(0,3,0,5,0,7)	(0,5,0,7,0,9)	(0,5,0,7,0,9)	(0,3,0,5,0,7)	(0,7,0,9,1,0)
C4	(0,7,0,9,1,0)	(0,7,0,9,1,0)	(0,5,0,7,0,9)	(0,0,1,0,3)	(0,5,0,7,0,9)	(0,7,0,9,1,0)	(0,5,0,7,0,9)	(0,3,0,5,0,7)
C5	(0,5,0,7,0,9)	(0,5,0,7,0,9)	(0,3,0,5,0,7)	(0,5,0,7,0,9)	(0,0,1,0,3)	(0,5,0,7,0,9)	(0,3,0,5,0,7)	(0,3,0,5,0,7)
C6	(0,7,0,9,1,0)	(0,5,0,7,0,9)	(0,5,0,7,0,9)	(0,3,0,5,0,7)	(0,5,0,7,0,9)	(0,0,1,0,3)	(0,5,0,7,0,9)	(0,5,0,7,0,9)
C7	(0,3,0,5,0,7)	(0,5,0,7,0,9)	(0,7,0,9,1,0)	(0,3,0,5,0,7)	(0,5,0,7,0,9)	(0,3,0,5,0,7)	(0,0,1,0,3)	(0,5,0,7,0,9)
C8	(0,5,0,7,0,9)	(0,7,0,9,1,0)	(0,3,0,5,0,7)	(0,5,0,7,0,9)	(0,3,0,5,0,7)	(0,3,0,5,0,7)	(0,1,0,3,0,5)	(0,0,1,0,3)
C9	(0,5,0,7,0,9)	(0,5,0,7,0,9)	(0,7,0,9,1,0)	(0,5,0,7,0,9)	(0,1,0,3,0,5)	(0,5,0,7,0,9)	(0,3,0,5,0,7)	(0,1,0,3,0,5)
C10	(0,3,0,5,0,7)	(0,5,0,7,0,9)	(0,3,0,5,0,7)	(0,3,0,5,0,7)	(0,3,0,5,0,7)	(0,7,0,9,1,0)	(0,5,0,7,0,9)	(0,3,0,5,0,7)
C11	(0,5,0,7,0,9)	(0,5,0,7,0,9)	(0,5,0,7,0,9)	(0,3,0,5,0,7)	(0,7,0,9,1,0)	(0,3,0,5,0,7)	(0,5,0,7,0,9)	(0,3,0,5,0,7)
C12	(0,5,0,7,0,9)	(0,3,0,5,0,7)	(0,3,0,5,0,7)	(0,3,0,5,0,7)	(0,1,0,3,0,5)	(0,1,0,3,0,5)	(0,3,0,5,0,7)	(0,5,0,7,0,9)
C13	(0,3,0,5,0,7)	(0,5,0,7,0,9)	(0,3,0,5,0,7)	(0,7,0,9,1,0)	(0,5,0,7,0,9)	(0,3,0,5,0,7)	(0,1,0,3,0,5)	(0,3,0,5,0,7)
C14	(0,5,0,7,0,9)	(0,3,0,5,0,7)	(0,3,0,5,0,7)	(0,3,0,5,0,7)	(0,1,0,3,0,5)	(0,3,0,5,0,7)	(0,3,0,5,0,7)	(0,3,0,5,0,7)
C15	(0,7,0,9,1,0)	(0,3,0,5,0,7)	(0,5,0,7,0,9)	(0,1,0,3,0,5)	(0,5,0,7,0,9)	(0,5,0,7,0,9)	(0,3,0,5,0,7)	(0,1,0,3,0,5)

	C9	C10	C11	C12	C13	C14	C15
C1	(0,5,0,7,0,9)	(0,3,0,5,0,7)	(0,3,0,5,0,7)	(0,5,0,7,0,9)	(0,7,0,9,1,0)	(0,3,0,5,0,7)	(0,7,0,9,1,0)
C2	(0,5,0,7,0,9)	(0,7,0,9,1,0)	(0,3,0,5,0,7)	(0,5,0,7,0,9)	(0,5,0,7,0,9)	(0,3,0,5,0,7)	(0,5,0,7,0,9)
C3	(0,5,0,7,0,9)	(0,7,0,9,1,0)	(0,5,0,7,0,9)	(0,3,0,5,0,7)	(0,3,0,5,0,7)	(0,3,0,5,0,7)	(0,5,0,7,0,9)
C4	(0,3,0,5,0,7)	(0,3,0,5,0,7)	(0,3,0,5,0,7)	(0,5,0,7,0,9)	(0,5,0,7,0,9)	(0,5,0,7,0,9)	(0,3,0,5,0,7)
C5	(0,3,0,5,0,7)	(0,5,0,7,0,9)	(0,5,0,7,0,9)	(0,5,0,7,0,9)	(0,1,0,3,0,5)	(0,5,0,7,0,9)	(0,5,0,7,0,9)
C6	(0,5,0,7,0,9)	(0,5,0,7,0,9)	(0,5,0,7,0,9)	(0,5,0,7,0,9)	(0,3,0,5,0,7)	(0,7,0,9,1,0)	(0,5,0,7,0,9)
C7	(0,3,0,5,0,7)	(0,1,0,3,0,5)	(0,3,0,5,0,7)	(0,3,0,5,0,7)	(0,1,0,3,0,5)	(0,5,0,7,0,9)	(0,5,0,7,0,9)
C8	(0,1,0,3,0,5)	(0,5,0,7,0,9)	(0,3,0,5,0,7)	(0,3,0,5,0,7)	(0,3,0,5,0,7)	(0,5,0,7,0,9)	(0,7,0,9,1,0)
C9	(0,0,1,0,3)	(0,3,0,5,0,7)	(0,1,0,3,0,5)	(0,1,0,3,0,5)	(0,3,0,5,0,7)	(0,3,0,5,0,7)	(0,5,0,7,0,9)
C10	(0,5,0,7,0,9)	(0,0,1,0,3)	(0,5,0,7,0,9)	(0,3,0,5,0,7)	(0,3,0,5,0,7)	(0,1,0,3,0,5)	(0,3,0,5,0,7)
C11	(0,3,0,5,0,7)	(0,5,0,7,0,9)	(0,0,1,0,3)	(0,3,0,5,0,7)	(0,3,0,5,0,7)	(0,5,0,7,0,9)	(0,3,0,5,0,7)
C12	(0,3,0,5,0,7)	(0,5,0,7,0,9)	(0,5,0,7,0,9)	(0,0,1,0,3)	(0,3,0,5,0,7)	(0,3,0,5,0,7)	(0,3,0,5,0,7)
C13	(0,3,0,5,0,7)	(0,5,0,7,0,9)	(0,3,0,5,0,7)	(0,7,0,9,1,0)	(0,0,1,0,3)	(0,1,0,3,0,5)	(0,3,0,5,0,7)
C14	(0,3,0,5,0,7)	(0,5,0,7,0,9)	(0,7,0,9,1,0)	(0,5,0,7,0,9)	(0,1,0,3,0,5)	(0,0,1,0,3)	(0,3,0,5,0,7)
C15	(0,3,0,5,0,7)	(0,3,0,5,0,7)	(0,3,0,5,0,7)	(0,3,0,5,0,7)	(0,3,0,5,0,7)	(0,3,0,5,0,7)	(0,0,1,0,3)

Table 4. Total relation matrix.

	C1	C2	C3	C4	C5	C6	C7	C8	C9	C10	C11	C12	C13	C14	C15
C1	0.421	0.457	0.407	0.412	0.435	0.391	0.375	0.425	0.385	0.419	0.379	0.412	0.382	0.370	0.464
C2	0.502	0.385	0.422	0.428	0.388	0.388	0.352	0.401	0.383	0.455	0.375	0.406	0.359	0.364	0.437
C3	0.461	0.412	0.338	0.367	0.392	0.392	0.336	0.405	0.367	0.438	0.381	0.367	0.321	0.350	0.420
C4	0.508	0.476	0.426	0.344	0.413	0.431	0.376	0.386	0.366	0.419	0.380	0.412	0.361	0.391	0.420
C5	0.445	0.415	0.369	0.373	0.311	0.376	0.325	0.349	0.333	0.401	0.368	0.375	0.288	0.358	0.402
C6	0.520	0.466	0.437	0.398	0.423	0.354	0.386	0.416	0.396	0.450	0.412	0.420	0.347	0.422	0.453
C7	0.393	0.386	0.385	0.327	0.352	0.330	0.254	0.347	0.308	0.333	0.322	0.328	0.265	0.335	0.377
C8	0.426	0.418	0.351	0.359	0.341	0.340	0.288	0.287	0.296	0.385	0.331	0.339	0.297	0.341	0.406
C9	0.400	0.373	0.374	0.337	0.299	0.341	0.291	0.293	0.254	0.340	0.287	0.296	0.279	0.301	0.363
C10	0.395	0.390	0.347	0.331	0.334	0.375	0.325	0.327	0.333	0.309	0.343	0.330	0.289	0.295	0.357
C11	0.442	0.414	0.389	0.353	0.398	0.355	0.344	0.349	0.332	0.401	0.301	0.354	0.307	0.357	0.381
C12	0.380	0.337	0.314	0.302	0.284	0.282	0.277	0.320	0.284	0.345	0.316	0.256	0.266	0.286	0.326
C13	0.394	0.389	0.342	0.373	0.352	0.332	0.280	0.325	0.309	0.376	0.322	0.373	0.244	0.291	0.353
C14	0.392	0.346	0.325	0.310	0.293	0.312	0.287	0.308	0.293	0.355	0.348	0.332	0.252	0.251	0.335
C15	0.416	0.349	0.348	0.293	0.340	0.336	0.289	0.291	0.297	0.337	0.308	0.315	0.276	0.299	0.294

R+C. According to the analysis of fuzzy DEMATEL method, quality (C1), delivery (C2), resource consumption (C6), and price (C4) are the top four

most important criteria with the values of 12.627, 12.062, 11.635, and 11.417, respectively. Technology improvement (C13) and wealth created (C14) are

Table 5. Final results of the analysis.

Criteria	R	C	R+C	R-C
Quality (C1)	6.134	6.493	12.627	-0.359
Delivery (C2)	6.047	6.015	12.062	0.032
Service (C3)	5.746	5.575	11.320	0.171
Price (C4)	6.110	5.308	11.417	0.802
Flexibility (C5)	5.487	5.355	10.841	0.132
Resource consumption (C6)	6.301	5.334	11.635	0.967
Pollution control (C7)	5.042	4.785	9.827	0.257
Environmental management system (C8)	5.206	5.229	10.435	-0.023
Green product (C9)	4.826	4.936	9.762	-0.110
Environmental competencies (C10)	5.079	5.763	10.842	-0.684
Stakeholders' rights (C11)	5.477	5.174	10.650	0.303
Health and safety (C12)	4.576	5.315	9.891	-0.739
Technology improvement (C13)	5.055	4.531	9.586	0.524
Wealth created (C14)	4.737	5.010	9.747	-0.273
Respect for the policy (C15)	4.789	5.788	10.577	-0.999

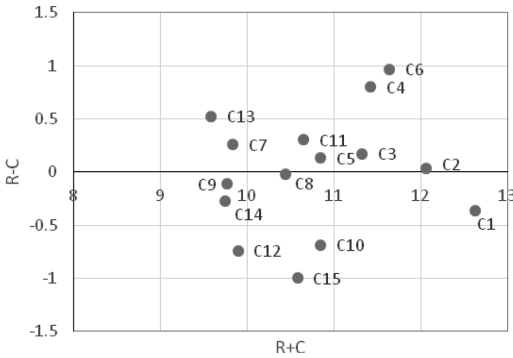


Figure 2. The causal diagram.

the least important criteria with the values of 9.586 and 9.747, respectively. As shown in Fig. 2, the main criteria were divided into clusters, namely cause cluster with positive  $R-C$  values, which includes delivery (C2), service (C3), price (C4), flexibility (C5), resource consumption (C6), pollution control (C7), stakeholders' rights (C11), and technology improvement (C13). While the effect cluster was composed with negative  $R-C$  values, which includes quality (C1) environmental management system (C8), green product (C9) environmental competencies (C10), health and safety (C12), wealth created (C14), and respect for the policy (C15).

This research plans to improve sustainable supplier performance through three dimensions and 15 criteria. Following the study, several managerial implications are derived. Managers should pay attention to four factors in supplier selection which are quality (C1), delivery (C2), resource consumption (C6), and price (C4). The results from causal diagram shows that C2 is taken into account the

highest intensity of relation to other criteria and C1 is the most influencing factor.

## 5 CONCLUSIONS

This study suggests a novel fuzzy DEMATEL approach to evaluate sustainable suppliers for the need of improving SSCM initiatives. Based on the literature survey and the validated preferences of industrial experts, possible sustainable supplier evaluation criteria were defined. Furthermore, a new evaluation model namely the fuzzy DEMATEL was adopted to explore the relationships among the criteria. The proposed model was implemented in a Chinese company, which is one of the pioneering companies about sustainable subjects in China.

The fuzzy DEMATEL approach used in this study offered a more precise and accurate analysis by integrating interdependent relationships within and among a set of criteria. This paper provides critical criteria among various influencing elements. The results from causal diagram divided the criteria into two groups: cause criteria and effect criteria. The cause group (C2, C3, C4, C5, C6, C7, C11, C13) should be controlled and paid more attention to, while the effect group (C1, C8, C9, C10, C12, C14, C15) need to be improved. Among those, C1 and C2 would take into further consideration.

This paper proposed a framework for sustainable supplier selection in the supply chain management which can serve as foundation for further study. Combining with other multiple attribute decision making methods such as TOPSIS, VIKOR and outranking approach would give a more comprehensive analysis to the sustainable supplier selection problem.

## ACKNOWLEDGEMENT

This work was supported by National Natural Science Foundation of China (71301110) and the Humanities and Social Sciences Foundation of the Ministry of Education (3XJC630015) and also supported by Research Fund for the Doctoral Program of Higher Education of China (20130181120059) and supported by the Fundamental Research Funds for the Central Universities (skqy201525).

## REFERENCES

- [1] Seuring S, Müller M (2008) From a literature review to a conceptual framework for sustainable supply chain management. *Journal of Cleaner Production* 16:1699–1710.
- [2] Hassini E, Surti C, Searcy C (2012) A literature review and a case study of sustainable supply chain with a focus on metrics. *International Journal of Production Economics* 140:69–82.
- [3] O'Rourke D (2014) The science of sustainable supply chains. *SCIENCE* 344:1124–1127.
- [4] Dickson, GW (1966) An analysis of vendor selection systems and decisions. *Journal of Purchasing* 2:5–17.
- [5] Xia WJ, Wu ZM (2007) Supplier selection with multiple criteria in volume discount environments. *Omega* 35:494–504.
- [6] Van der Rhee B, Verma R, Plaschka G (2009) Understanding trade-offs in the supplier selection process: The role of flexibility, delivery, and value-added services/support. *International Journal of Production Economics* 120:30–41.
- [7] Igarashi M, Boer L de, Fet AM (2013) What is required for greener supplier selection? A literature review and conceptual model development. *Journal of Purchasing & Supply Management* 19:247–263.
- [8] Weber CA, Current JR, Benton WC (1991) Vendor selection criteria and methods. *European Journal of Operational Research* 50:2–18.
- [9] Noci G (1997) Designing green vendor rating systems for the assessment of a supplier's environmental performance. *European Journal of Purchasing and Supply Management* 3:103–114.
- [10] Elkington J (1997) *Cannibals With Forks: the Triple Bottom Line of 21st Century Business*. Oxford.
- [11] Zadeh LA (1965) Fuzzy sets. *Information and Control* 8:338–353.
- [12] Bai C, Sarkis J (2010) Integrating sustainability into supplier selection with grey system and rough set methodologies. *International Journal of Production Economics* 124:252–64.
- [13] WCED (1987) *Our common future*. Oxford, United Kingdom: Oxford University Press.
- [14] Cooper MC., Lambert DM., Pagh JD (1997) Supply chain management: More than a new name for logistics. *International Journal of Logistics Management* 8:1–14.
- [15] Linton JD, Klassen R, Jayaraman V (2007) Sustainable supply chains: An introduction. *Journal of Operations Management* 25:1075–1082.
- [16] Carter CR, Rogers DS (2008) A framework of sustainable supply chain management: moving toward new theory. *International Journal of Physical Distribution & Logistics Management* 38:360–387.
- [17] Gabus A., Fontela E (1972) World problems. An invitation to further thought within The Framework of DEMATEL. Geneva: Battelle Geneva Research Centre.
- [18] Lin RJ (2013) Using fuzzy DEMATEL to evaluate the green supply chain management practices. *Journal of Cleaner Production* 40:32–39.
- [19] Wu WW., Lee YT (2007) Developing global managers' competencies using the fuzzy DEMATEL method. *Expert Systems with Applications* 32:499–507.
- [20] Dalalah D., Hayajneh M., Batieha F (2011) A fuzzy multi-criteria decision making model for supplier selection. *Expert Systems with Applications* 38:8384–8391.
- [21] Uygun Ö, Kaçamak H, Kahraman ÜA (2015) An integrated DEMATEL and Fuzzy ANP techniques for evaluation and selection of outsourcing provider for a telecommunication company. *Computers & Industrial Engineering* 86:137–146.
- [22] Ho W, Xu X, Dey PK (2010) Multi-criteria decision making approaches for supplier evaluation and selection: A literature review. *European Journal of Operational Research* 202:16–24.
- [23] Govindan K, Rajendran S, Sarkis J, Murugesan P (2015) Multi criteria decision making approaches for green supplier evaluation and selection: a literature review. *Journal of Cleaner Production* 98:66–83.
- [24] Wu C, Barnes D (2011) A literature review of decision-making models and approaches for partner selection in agile supply chains. *Journal of Purchasing and Supply Management* 17:256–274.
- [25] Chai J, Liu JNK., Ngai EWT (2013) Application of decision-making techniques in supplier selection: A systematic review of literature. *Expert Systems with Applications* 40:3872–3885.
- [26] Büyüközkan G, Çifçi G (2011) A novel fuzzy multi-criteria decision framework for sustainable supplier selection with incomplete information. *Computers in Industry* 62:164–174.
- [27] Hsu CW, Kuo TC, Chen SH, Hu AH (2013) Using DEMATEL to develop a carbon management model of supplier selection in green supply chain management. *Journal of Cleaner Production* 56:164–172.
- [28] Chang B., Chang CW, Wu CH (2011) Fuzzy DEMATEL method for developing supplier selection criteria. *Expert Systems with Applications* 38:1850–1858.
- [29] Orji IJ, Wei S (2015) An innovative integration of fuzzy-logic and systems dynamics in sustainable supplier selection: A case on manufacturing industry. *Computers & Industrial Engineering* 88:1–12.
- [30] Amindoust A, Ahmed S, Saghafinia A, Bahreininejad A (2012) Sustainable supplier selection: A ranking model based on fuzzy inference system. *Applied Soft Computing* 12:1668–1677.



**Taylor & Francis**

Taylor & Francis Group

<http://taylorandfrancis.com>

# Research on ecological reconstruction strategies for the Shanghai Shendu Building

Ming Gao

*School of Civil Engineering and Architecture, Southwest University of Science and Technology, Sichuan, China*

**ABSTRACT:** Using the ecological reconstruction theory of old industrial architectures, this paper analyzes advanced experience in ecological reconstruction project of the Shanghai Shendu Building from the perspective of ecological technology. It also discusses site environment rectification, formal space transformation as well as passive technology, resource utilization, and other reconstruction strategies in old industrial architecture reconstruction, in order to develop ecological design methods that can be applied to old industrial architecture reconstruction.

**Keywords:** ecology; old industrial architectures; strategy of reconstruction

## 1 INTRODUCTION

As the problem of fog and haze is becoming increasingly serious in China, environmental issues could not be avoided, and the application of ecological technology in architectural design is a type of essential remedy, which is still in its initial stage. Old industrial architectures in China have large stock, and are faced with problems such as high energy consumption, poor indoor and outdoor environment, and less use of ecological building materials. Old industrial architecture reconstruction in China has started late, and lacks in-depth and systematic study in the aspect of ecological reconstruction technology integration. Architectural energy-saving reconstruction is urgent, and the research on ecological reconstruction strategies suitable to the national conditions for old industrial architectures is of utmost importance.

## 2 RESEARCH BACKGROUND

### 2.1 *Old industrial architectural reconstruction and development of ecological theory*

In the 1960 s, the reconstruction of old industrial architectures was originated from the protection of industrial heritage. From Brownfield reconstruction in Germany's Ruhr industrial region to artistic revival in Chinese 798 factory, reconstruction of China's existing buildings had experienced three stages, namely "energy-saving reconstruction", "comprehensive reconstruction", and "green reconstruction". Together with the development and drive of foreign ecological ideas, ecological

reconstruction of architectures will become the important approach and key link to solve problems related to resources and environment, and it will effectively alleviate the pressure of energy conservation and emission reduction potential in China. Therefore, the ecological reconstruction of old industrial architectures will be the trend of times.

### 2.2 *The concept of ecological reconstruction*

"Ecological reconstruction" is not only the reconstruction design in function, appearance, natural environment, structure, energy use, materials used, and other aspects of old industrial architectures, but also the factor for comprehensive ecological concept improvement in construction, management, evaluation, and many other aspects. In order to make buildings possess a healthy and comfortable ecological environment both inside and outside, "ecological reconstruction" advocates to reconstruct under the premise of reducing energy consumption and environmental pollution as far as possible, and supports the reconstruction mode of "passive priority, initiative optimization", low cost, and conventional technologies.

## 3 ECOLOGICAL RECONSTRUCTION STRATEGIES

### 3.1 *Rectification strategies of site environment*

Because the characteristics of old industrial architectures are existing location and outdoor sites, and landform, body mass, and orientation have

been fixed, a few places can be changed, and they tend to be in a poorer environment. The harsh environment directly affects comfort and human health of building indoors. Therefore, it is essential to conduct optimization and rectification as well as ecological restoration on site environment. Through reasonable planting of woods or green belts, replacement of ground materials, and so on, wind can be guided around buildings to adjust and slow down cold wind and reduce heat loss of buildings in winter. Reasonable layout of trees and plants can increase sunlight's irradiation on buildings to reduce heat in micro-environment, such as shading the radiation of sunlight, reducing the heat gain of buildings, and reducing sound and noise. In addition, water body could better maintain the environment temperature and humidity than greenbelt; therefore, a combined layout of water body and greening on the site will better improving indoor and outdoor environment [1].

### 3.2 *Reconstruction strategies of formal space*

The major factors of plant reconstruction are building size and inner space. Reasonable formal space reconstruction should adapt to the local climate characteristics, strengthen natural lighting and ventilation of the building, and reduce solar radiation heat gains. The following three methods are used to reconstruct formal space: figure reconstruction, atrium implantation, and space restructuring.

Figure reconstruction states that under the premise of meeting functions as well as healthy and comfortable indoor environment, outside climate conditions and other factors should be comprehensively considered and internal natural ventilation should be guided through the increase in bump changes of exterior structure of building and use of unevenness of building size. Simultaneously, architectural shaded area and heat radiating area should be increased and self-shading of building should be used to reduce its active heat gain and improve indoor natural lighting.

Atrium implantation is a traditional and effective method for ecological reconstruction. It alleviates the effect of external climate changes on internal environment of buildings through courtyard adjustment. Buildings can form hot-pressing draft channel and generate the effect of strengthening natural ventilation through atrium. Natural ventilation effect is especially good in the transition season. Industrial plants have a large depth, and hence the method of atrium implantation can significantly improve internal lighting of building. Adumbral solar photovoltaic panels can also be set at the top of atrium to effectively block direct solar radiation heat gains and reduce energy consumption.

Space restructuring aims at meeting functional requirements and ecological concepts, focusing on the consideration of the integration of internal space and external environment, and reconstructing and re-dividing the space with different requirements for indoor thermal environment. The original spatial organizing forms can be broken by means of restructuring and replacement to form some new spatial forms in order to improve natural ventilation, lighting, and indoor thermal environment.

### 3.3 *Passive technology strategies*

Passive technology is the one that achieves energy saving completely through its own form, maintenance structure, and structural details of building, but not depending on energy-intensive building equipment system. Compared with advanced high ecological technology, although passive energy-saving technology has relatively low energy efficiency, its methods for improving natural ventilation, lighting, and heat insulation of building are simple, easy to apply, of low cost, and can provide ecological benefits as well. Passive technology is developed because its economy and environmental protection are superior to active energy-saving technology.

Exterior enclosure of building mainly includes building exterior walls (including doors and windows attached to external walls, ornamental components, and functional components), roof, and so on. The external wall materials of old industrial architectures are mostly concrete or brick wall materials. At that time, the consideration of thermal performance design of building envelope was less, and exterior enclosure surface was the main portal of building energy consumption. The ecological reconstruction of exterior enclosure plays an important role in improving energy saving and human comfort of buildings.

Exterior walls of buildings are directly exposed to outdoor environment, and they generate energy exchange being influenced by natural factors such as outdoor wind, light, and heat. Improvement and strengthening of thermal performance of enclosure system is an important link of energy conservation reconstruction. The strategies include improving heat preservation, thermal insulation, sunshading, ventilation, and other performances of building envelope. For example, reconstruction of architectural surface into a hollow one is called as "breathing-type curtain wall" double-layer external wall system. Adjustable shading facilities must be set on the architectural surface or architectural surface material and angle variation of mechanism must be used to achieve the effect of sunshading; shading facilities must be used to gen-



erate refraction, interference, diffraction, and other phenomena on the architectural surface system to reduce direct solar radiation heat gains and adjust natural lighting. The strategies for energy-saving reconstruction of external windows are energy-efficient double window, LOW-E glass and glass films, hollow-glass built-in shutters, and so on.

The thermal performance of roofing is most affected by solar radiation, and hence the reconstruction of thermal insulation of roofing is particularly important. The major reconstruction strategies are setting of overhead ventilation layer or water surface on the roof to reflect solar radiation and planting and greening the roof, which can play a role in heat insulation as well as makes the environment look pleasant.

### 3.4 Resource utilization strategies

In view of the current energy crisis and environmental crisis, the development and utilization of renewable energy sources have become inevitable. Conventional renewable resources include wind energy development and solar energy and geothermal energy utilization. The utilization of solar energy is divided into natural light utilization and solar energy utilization. The former includes skylight design, facade daylighting design, and light duct system. The utilization of solar energy and natural light will be affected by the characteristics of light climatic regions. In areas with strong sunlight and rich sunshine, the use of solar energy collecting system should be fully considered, and relevant shading facilities should be adopted. In areas with little solar radiation, the key of strategy is to guide limited sunlight into indoor.

## 4 EXAMPLE ANALYSIS OF THE RECONSTRUCTION—PROJECT OF THE SHANGHAI SHENDU BUILDING

### 4.1 Project overview

The project is the plant of Shanghai No.5 Scarf Factory built in the 1970 s, and rebuilt into a six-story office building with semi-basement in 1995. Later, with the widening of the public project—South Xizang Road and demolition of residential buildings in the east, the building has become one among other buildings along the street. In view of the current situation of old façade and crowded internal space, it could not meet the needs of modern office, and it is essential to re-position and conduct old building reconstruction. After project reconstruction, there are six floors aboveground and one underground. The underground room is air-conditioned room, and serves as garage and accessory room for other mechanical equipment;

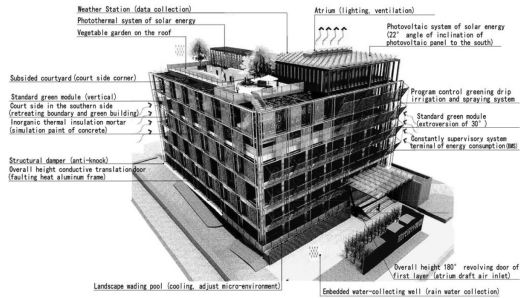


Figure 1. Ecological reconstruction system diagram.

the first story aboveground serves as lobby, exhibition room, restaurant, and room for logistics; and the main utilization function of second floor to sixth floor is office space. The aboveground area of the building is 6231 m<sup>2</sup>, underground area is 1070 m<sup>2</sup>, and the building height is 23.75 m.

The building is L-shaped, the east and west depth of the building on the northeastern side and the north and south depth on the southwestern side are larger with nearly 20 m, the direction is roughly from north to south, and figure coefficient value is 0.23. Improvement and energy conservation reconstruction are conducted on the enclosure system according to the energy-saving design standard for public buildings; planted roof, flat roof, metal roofing, and other forms are adopted in the aspect of house roof; internal and external insulation energy-saving measures are taken in the aspect of external walls; thermal insulation, sunshading, lighting, and other factors are comprehensively considered in the aspect of glass doors and windows; and high-permeability faulting heat aluminum alloy and low-E hollow glass windows have been adopted<sup>[2]</sup> (as shown in Figure 1).

### 4.2 Examples of ecological reconstruction strategies

#### 4.2.1 Strategies of site rectification—healthy and applicable

The project has complicated the regional environment; it is in the adverse environment with three sides enclosed—facing the main street. It faces the main street of South Xizang Road in the east, which is seriously affected by sight and noise due to high traffic flow. It is adjacent to the community center in the north and old multi-story residential building in the south and west, and there are disturbances of direct-view of residents such as bathroom and other aspects of logistical privacies.

It should be ensured that the south area of the building is the reconstruction priority, the original architectural style is retained in the north, and west

is restricted by conditions. Through the analysis of site environment, computer simulation software, and other methods; analysis of ventilation, lighting, noise, and other conditions, and through retreating, setting up, breaking, shading, and other design methods, the adverse impact of the building on surrounding environment could be minimized. Regional greening treatment includes innovative designs such as “breaking wall to present greening”, “retreating wall and green building”, and “flattening house and paving greening” to realize a “healthy, applicable, and efficient” location space.

#### 4.2.2 Strategies of formal space reconstruction—sharing and symbiosis

Determine architectural form and structure as well as the location of principal and subordinate space by virtue of use function, and make full use of lateral daylighting and locally embedded atrium to improve the conditions of internal lighting and ventilation of building. Southern façade reconstruction is mainly to solve mutual interference contradiction with less than 10 m with adjacent residential buildings. Embed court side and atrium between office area and residential buildings, and use the remaining interlayered floor slab to form an interlayer staggered design of “retreating boundary and green building”. Metal mesh and vertical greening attached to southern façade are scattered layer-to-layer, and indoor work places and opposite houses can share the green landscape; thus, it effectively solves the mutual interference between office space and residential buildings. In order to improve the poor draft effect of existing atrium, space has been stretched by setting up court side to combine court side wind and flue wind to enhance ventilation effect [2].

Natural ventilation is much affected by climate and environment, and the passive ventilation design of each building has its special characteristics due to objective factors. Replace old windows in the northern and western facades of building to increase ventilation area. Set up openable draft outlet protruding house roof in the corresponding part of roof atrium, which can play a certain role in hot-pressing draft in summer; however, as its base is located in dense city and building height is not high, the effect of hot-pressing draft of atrium is very limited.

#### 4.2.3 Passive technology strategies

##### 1. Natural light—bright and sharing balanced advantages

Reconstruct external windows in the east and south into openable French windows and adopt standard greening module in external walls to control the indoor lighting intensity, make incident light be guided to indoor softly with sharing balanced advantages, and reduce

artificial lighting lamps indoor. Continue to use traditional windows in the plant room of building, bathroom as well as the north and west sides of the building to protect from wind in winter.

In view of the current situation of larger depth of the main entrance in the northeastern side, coupled with lower story height of the first and second floors of the building and poor lighting, locally implant atrium in the first story of building and open windows through the main entrance and guide natural light into indoor to improve internal lighting. Implant connected court side up and down in the second to sixth floors of the south side of the building, divide the additional atrium space into two combining with transportation linkage, set up openable skylight and external shadings on the top to strengthen top daylighting and ventilation of building, and improve indoor physical environment of the building depth part. Through the reflection between slant sunshading baffle, light rays form a soft light [3].

##### 2. Natural wind—passive ventilation

Natural ventilation is much affected by climate and surrounding environment. Set up a 29.4 m overall height of glass daylighting atrium in the position of being adjacent to elevator hall and set up coordinated type of draft outlet of openable fan in the corresponding upper part of the atrium. The “passive ventilation system” (as shown in Figure 2) is formed to increase the overall indoor comfort degree using a series of small space collaboration. It can play a certain role in hot-pressing draft in summer and reducing the mechanical load of air conditioner. Especially in the transition season of spring and autumn, the draft effect of skylight is the best. Because the prevailing wind direction of transition season and summer in Shanghai is mostly southeaster, adopt mobile glass doors to increase the openable area in the eastern and southern facades, and set up ground glass windows that

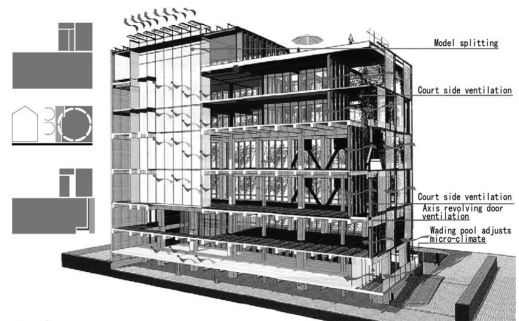


Figure 2. Analysis of passive natural ventilation system.

can effectively increase ventilation area in the eastern façade to increase the opening area of windows on both sides, and be conducive to ventilation effect. Sunshade in the east inclines 30° outward for ventilation purpose and forms an effective ventilation duct. Set up court side in the south to expand the openable area of windows and guide cross-ventilation<sup>[4]</sup>.

3. Ecological house roof—combine with nature  
Surrounding buildings facing the site are intensive and greening environment is modest. Building is added with an open-hall space on the roof by using photovoltaic panel system. Design roof balcony and vegetable garden outside the open hall. The vegetable garden is divided into massive and diversified vegetable area, climbing plants area, lawn and aquatic plants area, so that people can directly observe the growth process of fruits and vegetables on the site and can practice cultivation and taste, which draws human closer to nature.

4. Architectural shading—three-dimensional innovation

On the basis of the climate characteristics of areas with hot summer and cold winter, relieve the contradiction between sunshading in summer and heat gains in winter, and take environment characteristics outside site and block of surrounding buildings on old buildings in winter into account. Set up 30° outward-inclined stretch mesh backing greening cling mesh module in the east to meet the requirements of too high temperature in summer and sunshading, and not affect that winter sunlight shines indoors. The use of components in plant greening not only enhances shaded effects in summer, it also effectively increases incident sunlight after leaves falling in winter and achieves reasonable visual design of “shading” and “penetrating”. Setting 3.9-m-wide structure aside horizontally in the southern façade has a very good effect on sunshading, and the structure is used as outdoor traffic space<sup>[4]</sup> (as shown in Figure 3).

5. Ecological greening—greening around  
Set up vertical greening separately in the building’s south area with strong sunshine and east area along the main street and implant greening court side in the southern facade in order

to increase transitional buffer indoors and outdoors and prevent glare. Integrate the measures for building energy saving, greening, sunshading, ventilation, anti-noise, and so of building and set up standardized compound system of vertical greening decoration. Mainly adopt deciduous climbing plants and evergreen climbing plants in vertical greening to block direct light from south and east sides of the building, and deciduous plants set increase the guiding of direct sunlight in winter. Indoor solid green space, joyful office garden and vivid outdoor urban landscape are created.

#### 4.3 Resources utilization strategies

Under the condition of compact existing architectural space and environment space, comprehensively consider the requirements of roof activity area for sheltering from rain and sunshading, increasing the construction of recycling system of recycling resources, and reconstructing and designing solar energy photothermal system and solar energy photovoltaic system to enhance the utilization efficiency of solar energy; weather station and constant supervisory system terminal of energy efficiency; and rainwater recycling system for outdoor landscape planting irrigation, vehicle cleaning, road cleaning.

## 5 CONCLUSION

Through the analysis of ecological strategies in aspects such as Shendu Building reconstruction project’s construction of ecological environment, application of passive low ecological reconstruction mode, effective utilization of resources, green materials and recycling, and so on, several types of strategies have been summarized in the ecological reconstruction of old industrial architectures. Currently, faced with the situation of large stock of domestic old industrial architectures, high energy loss and being in urgent need for energy-saving reconstruction, ecological reconstruction technology will make architecture run in a new and sustainable way, and will become the mainstream of architectural reconstruction in the future. At the same time, ecological reconstruction strategy should also be a constantly broken and constantly improved practice engineering.

## PROJECT SOURCE

Key Research Base of Humanities and Social Sciences of Sichuan Provincial Department of Education—Topic in the 2015 of Sichuan Circular Economy Research Center, project number: XHJJ-1516.



Shaded effect in the south side and diagrammatic cross section  
Shaded effect in the east side and diagrammatic cross section

Figure 3. Shading analysis in the south and east sides.

## REFERENCES

- [1] Editorial Board of *Retrofitting of Existing Buildings Yearbook*, *Retrofitting of Existing Buildings Yearbook* (2012) [M], China Architecture & Building Press, 2013.
- [2] Xia Lin, Tian Hui. *Shanghai Modern Shendu Mansion Reconstruction Project* [J], *Construction Science and Technology* 2014(10), 57–61.
- [3] Tian Hui, Xia Lin, An Dongya. *Green Regeneration of Shendu Building* [J], *Architectural Technique* 2013(02), 71–74.
- [4] Li Qun. *Establishing Environment by Nature, Creating Green by Space—Green Remodeling for the Existing Building of Shanghai Shendu Mansion*, *Architectural Journal*, 2013(07), 75–77.

# Applications of the passive solar energy technology in office buildings in Changchun

Ju Qiu & Tian-Lun Zhao

*School of Architecture and City Planning, Jilin Jianzhu University, Changchun, China*

**ABSTRACT:** With the constant development of China's economy, energy shortage has become a prominent problem. Hence, energy conservation by buildings is increasingly important for the development of national economy. As a sustainable energy source, solar energy has found wide applications recently, showing advantages of extensiveness, durability, and environment-friendliness. Thus, this paper mainly discusses and studies the applications of the passive solar energy technology in office buildings.

**Keywords:** passive solar energy technology; office buildings; energy conservation

## 1 INTRODUCTION

Office buildings not only provide a comfortable working environment for people, but also beautify streets. In recent years, together with the constant development of building techniques and the increasing concerns of people over indoor environment comfort degree, energy consumption of office buildings has also marked an annual increase, thus aggravating environmental and energy issues. Currently, it has become one of the major problems inhibiting development of the building industry. Adopting feasible methods to cut energy consumption has been an issue of increasing concern. Although various techniques have popped up in response to the necessity of building energy conservation, capital cost and operating cost of these techniques are often extremely high, which are not suitable for some areas due to the local economic conditions. Adopting proper techniques for proper utilization of social energy resources in office building design has become one of the efficient methods to reduce office building energy consumption.

## 2 ANALYSES OF ADVANTAGES OF SOLAR ENERGY RESOURCES AND SOLAR ENERGY APPLICATION STATUS IN CHANGCHUN

### 2.1 *Advantages of solar energy resources*

As a renewable clean energy, which has emerged as the major energy resource in recent years, solar energy has striking advantages compared with other traditional energy sources. In particular, its advantages are reflected in the following aspects:

1. A huge reserve: The energy contained in solar radiation in a year is twice higher than the annual energy consumed worldwide. If properly utilized, solar energy can fully meet the current energy requirements.
2. Universality: Various resources for buildings call for immediate supply and update to meet daily demands. For example, electricity is produced from urban power grids, domestic water comes from the urban underground water supply system, and the winter heating is supplied collectively in a city. As an open energy, solar energy is free of cost for supply and transportation. This is the unique advantage of solar energy.
3. Pollution-free: Environmental issues brought by buildings are well known. The emergence of solar energy as a clean energy can definitely well alleviate the contradictions between buildings and environment.

### 2.2 *Analysis of solar energy application status in Changchun*

Located in Jilin, one of the three provinces in Northeast China, Changchun belongs to the B zone of the severe cold area according to the national climate division, where the total solar radiation averages at 4787.4 MJ/m<sup>2</sup> and the annual sunshine duration is 2,200–3,000 h. From this perspective, Changchun is an area with medium light resources, with a high probability of solar energy utilization and can achieve remarkable progress. For example, anti-season planting relying on absorption of solar energy by the exterior and thin-film materials is a proper means of utilizing solar energy. However, despite the rich solar energy resources

of Changchun, the current utilization methods do not optimally utilize its advantages. Application of solar energy technology to the building area to solve the issue of energy consumption facing buildings is of vital significance to the sustainable development of buildings.

### 3 ENERGY CONSUMPTION CHARACTERISTICS OF OFFICE BUILDINGS

Office buildings are a special building type, which differ from other types of building with its unique use and energy consumption characteristics. Lighting energy consumption, air-conditioning and heating energy consumption, and water supply and drainage power energy consumption are the main sources of energy consumption in office buildings. Among them, heating energy consumption accounts for nearly 41.4% of the total energy consumptions. Considering the special climate conditions in severe cold areas and in order to guarantee a comfortable indoor temperature, it is necessary to combine air-conditioning equipment with other heating equipment. As a result, the heating energy consumption of buildings in Changchun is the highest. Thus, it is of positive significance to study how to adopt proper techniques and measures to solve the energy consumption issue in the area. Besides, the operation of office buildings has its own characteristics. In the daytime, there are many personnel working within, thus the requirement of the indoor temperature is high. Hence, the energy consumption of the corresponding equipment is relatively high during daytime. At night, with only few personnel overworking, the demand for the corresponding equipment is decreased. The energy consumption and use characteristics are in line with the application principles of the solar energy technology. Therefore, there is a huge development space for solar energy technology to be applied to reduce office building energy consumption.

### 4 APPLICATIONS OF THE PASSIVE SOLAR ENERGY TECHNOLOGY TO OFFICE BUILDINGS IN CHANGCHUN

The application methods of the passive solar energy technology vary depending on the different structures and functions of office buildings in Changchun. In general, the passive solar energy technology can be divided into four types: immediate benefiting type, heat-collecting and heat-storing wall type, extra sunshine room type, and the combinational type.

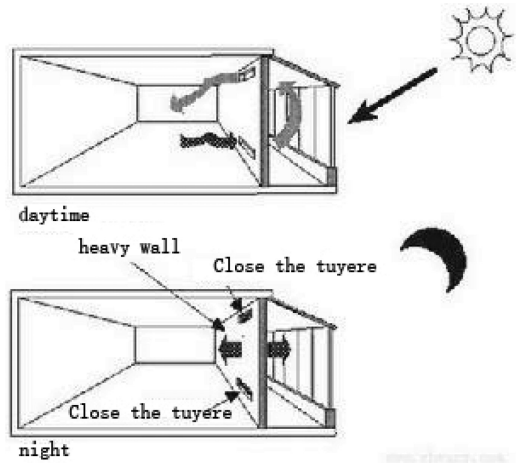


Figure 1.

#### 4.1 Direct benefiting type

The principle of the direct benefiting type is to add transparent materials to the glass. In that way, when the solar radiation is sufficient in the daytime, the indoor walls and floors can fully absorb and store it. At night, when the indoor and outdoor temperatures decrease, the internal heat gives off to maintain the indoor temperature at certain level. (See Fig. 1) Office buildings featuring the direct benefiting type require favorable lighting conditions. Besides, the requirement of maintaining the structure's thermal resistance is high, which can help reduce the natural loss of indoor heat.

#### 4.2 Heat-collecting and heat-storing wall type

The principle of the heat-collecting and heat-storing wall type is to enhance heat absorption and reduce radiation-induced heat loss by coating the sunward side of the wall with a dark selective layer. In this way, the wall is turned into a heat collector, and it can release heat when required. Glass or transparent plastic slice can be equipped about 10 cm away from the surface, thus forming an air layer between walls. The indoor temperature can be adjusted by the closing and opening of the gas holes and the moving of the movable heat-insulating layer. During the daytime of winter, the greenhouse effect is adopted to heat up the heat-collecting wall and the air interlayer. The air hole is opened to provide heating through convection. At night, the air hole is closed; there are heat-insulating curtains or shutters between the glass and walls, and the walls transfer heat through radiation to the indoor. The function is the reverse in summer. The heat-insulating layer is launched in the daytime and turned off at night.

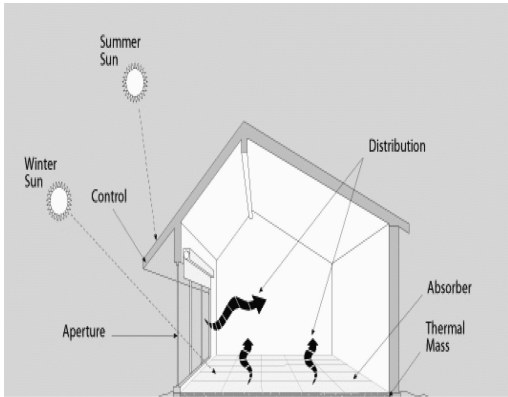


Figure 2.

#### 4.3 Extra sunshine room type

The working principle of the extra sunshine room is to add a glasshouse outside the southward rooms in the office building. Then, a heat-storing wall is adopted to separate the normal office space. Because the temperature within the sunshine room is relatively high, when the normal office space temperature is relatively low, the door can be opened to have heat exchange with the indoor. Apart from storing heat, the sunshine room also has other functions, such as displaying plants and holding entertainment facilities, which can beautify the office space.

#### 4.4 Combinational type

As its name implies, the combinational type refers to the combination of the above three types. Since every type is targeted at different office buildings, the integrated type can help to more flexibly utilize the solar energy. The above three types can be properly combined according to different heating requirements of different office buildings.

### 5 FACTORS TAKEN INTO CONSIDERATION DURING OFFICE BUILDING DESIGN WITH THE APPLICATION OF THE PASSIVE SOLAR ENERGY TECHNOLOGY

When the passive solar energy technology is adopted, office building designers should consider two aspects: design of the surrounding layout and the building itself.

#### 5.1 Building layout

The overall layout of office buildings should make full use of solar energy resources. Besides, the rela-

tionship among the building complex type, the functions, and the heat-collecting style should be coordinated. The plane layout of buildings and the heat-collecting surface should have the most favorable orientation. It is preferred for office buildings that are in use mostly in the daytime to be located within 15° south by east. Besides, surrounding landforms and surface features (including surrounding buildings) should be avoided from blocking the south orientation and the orientation scope within 15° south by east or west. Furthermore, the major part of office buildings should be away from pollutants as they could affect the transmitting surface of the heat-collecting components. Office buildings should not be set in the downwind direction of the surrounding pollution sources.

#### 5.2 Office building design

In terms of office building design, different parts of an office building should not block the sunshine for itself, such as the blocking of the heat-collecting surface by the protruding part of the office building in the coldest month. The office building structure should be concise with preferably being square or nearly square. Besides, the temperature partition principle is used to properly distribute the functional space of the office building according to different functional demands. The major space in use should face the south. Rooms or passages without strict temperature requirements can be put in the north or outside. Finally, office buildings adopting the passive solar energy technology should not be too high, because the energy-saving efficiency is reduced in tall buildings. The solar energy heat utilization efficiency will be satisfying for buildings with depth  $\leq 2.5$  times of the floor height.

### 6 CONCLUSIONS

Environmental pollution problems and energy consumption problems have seriously impeded the development of the building industry, thus making development and utilization of new resources inevitable. The emergence of relevant concepts, such as “green buildings” and “sustainable buildings”, also requires designers to make full utilization of local materials and proper selection of building techniques to achieve proper utilization of energies. Overall, building energy conservation is the top priority. From the current technical cases, it can be seen that the passive solar energy technology has made remarkable achievements in energy conservation. If properly used, it can further reduce the energy consumption of office buildings and play a more significant role in more practical projects.

## REFERENCES

- [1] LONG Weiding. Prospects of China building energy efficiency [J]. *Energy Engineering*, 2001 (2): 1–6.
- [2] ZHU Wei. Several measures for building energy-saving technology [J]. *Gansu Science and Technology*, 2002 (2): 37.
- [3] LIU Jiaping. New energy utilization in architectural energy conservation and design [J]. *Energy Engineering*, 2001 (2): 12–15.
- [4] ZHOU Zhennan. *Applications of Solar Energy Technology to German Buildings* [M]. Beijing: Tsinghua University Press, 2008: 56–78.
- [5] WANG Yanhong. Solar thermal utilization technology integrated with building [J]. *Energy Technology*, 2010, 31 (1): 45–48.



# Study of the effects and applications of fiber art on the indoor space

Hai-bo Sun

*College of Environment and Art, Hebei Academy of Fine Arts, Hebei, China*

**ABSTRACT:** As an important part of the indoor space, fiber art can make the modern design fuse into the city and give birth to a new concept. Fiber art can be applied to the indoor space in different styles blending the indoor design principle to make our living space look beautiful. The application of fiber art in the modern indoor space can accelerate the development of the fiber art itself. The traditional and the modern fiber art show that fiber art has the scope of being promoted and blended in the indoor space environment by using new materials and new technologies and combining the concept of the modern indoor design. Therefore, fiber art can definitely meet the needs and feasibility of the indoor design.

**Keywords:** fiber art; the modern indoor design; artistic design

## 1 INTRODUCTION

With the continuous development of science and technology, the indoor environment of buildings has improved together with people's understanding of the environment as well as the aesthetic standards. Several decorative elements can be blended in the indoor space, such as ceramics, glass, and iron art. Because the fibrous materials have high plasticity, soft and pendent texture, compatibility, simplicity, and natural availability, they are extensively used in the indoor space. They transform the material problems of stiff and gray, create different visual aesthetic art, and convey the consciousness emotions of humans.

## 2 CHARACTERISTICS OF THE FIBER ART

The fiber art has different qualities, colors, shapes, and textures. In addition, it conforms to the corresponding use in aesthetic decoration, as well as it is more abundant. To a certain extent, it reduces the hardness and apathy caused by the currently used hard materials and let the people feel the true emotions of the human again. The fiber art has the following aesthetic characteristics:

### 2.1 *Beauty of the materials*

The fiber art materials consist of animal and plant fiber materials, synthetic fiber materials, and physical materials. Different materials exhibit different physical properties and have different psychological inductions as visualized by humans. The difference

of the physical properties between the materials will produce different aesthetic feelings through the treatment of the artists. Metal substances can make people have the sense of purity; wood materials can provide the plain affinity; and fabrics can build sweet and amiable feelings in them. With elastic light, artificial fibers do not only possess flexible universal beauty, but also have the unique beauty of the different texture.<sup>[1]</sup>

### 2.2 *Form beauty*

Because an object's form or appearance gives people a harmonious visual experience, we call this the form beauty. Form is divided into external form and internal form. The external form refers to the space characteristics, and it usually refers to the appearance of the form. The internal form reflects the form boundaries between the parts in the form, which is also called as the structure form. The external and internal forms are similar to local and overall and background and foreground, and they both foil each other. The tension between the external form and the internal form achieves the balance in the interaction. The external shape can reflect the structure outline of the internal form.

The different material textures can change the texture of the contour line of the external and internal structures, and then enrich the form beauty in the visual aspects. Similar to bamboos and rattans, their elastic tension constitutes a relatively distinct structure outline because of the structure combination of the appearance and the inner figure. Thus, they have tall and spiffy form beauty.<sup>[2]</sup>

### 2.3 *Texture beauty*

As the fiber materials are soft, different textures can be processed artificially and freely, thereby creating a kind of visual state with the protean beauty, called the texture beauty. This makes the unique space beauty of the fiber art.

First, the texture beauty belongs to the visual form. The material tendentiousness tension extending in the organizational structures is the representation element that creates the texture beauty and influences the psychological feelings of the people. The texture beauty is the visual feeling in the texture form and the connotative mind feeling constituted by the materials.

Second, the texture beauty has a different sense of quality. Integrating with color, light shadow, and form, the texture produces a quality sense of the beauty different from that of the physical properties. The texture with a dim appearance, weak reflective light, and rough surface can produce massive and contractive psychological feelings. On the contrary, it will generate lively and expansive psychological feelings.

### 2.4 *Space beauty*

No matter they are in the two-dimensional state or three-dimensional space state, the state, color, and texture of the fiber artistic works all have contact with the surrounding space factors. The artists must have a balance and make people have aesthetic association in the visual psychology, so that they can finally complete the overall space beauty.

The creation of the space beauty is inseparable from the specific lighting of the fiber art works. Almost all excellent indoor wall hangings are inseparable from the specific lighting. It can not only make the works look bright, with full texture and the plump hierarchies, but also make them have a casual visual effect, which the morphological structures do not have.

### 2.5 *Color beauty*

The ultimate goal of the color beauty creation should be based on the people, and build aesthetic psychology of the integral space color. Color is an important composition language. It creates the space beauty of the fiber arts by the combination of materials and qualities and the reflection of shapes and colors. The color performance of the modern fiber art has two characteristics. The first is to form the language by using natural colors or adjacent colors, which are suitable for expressing the convex obviously, thick texture, and abstract style fiber arts. The second is to form the language by using material contrast colors, which are suited to express the fiber arts with rich decorative style.

### 2.6 *Surface layer aesthetics*

The surface layer aesthetics is the combining reflection of the form beauty, including the preliminary judgment, and the fundamental experience of the people to the visual forms of the fiber art works in the visual factors' aspect of the shape, light, texture, and color and luster. The modern fiber arts show their unique aesthetic features through their own material textures combined with their unique personalities.

### 2.7 *Deep-layer aesthetics*

Both the modern indoor designs and fiber arts have influence on people's psychology. It includes cultural identity of the people and the continuity and permeability of the city environment. In this way, the characteristics of nationality, regional-ity, and the times of the fiber arts can be showed vividly.

## 3 THE INFLUENCE OF THE FIBER ART ON THE INDOOR SPACE

As an important part of the modern indoor space environment, the fiber art becomes an affectional tie between the indoor space and the people with soft materials full of natural breath and various art forms. The fiber art exists in the buildings and has some effects on the building environment.

### 3.1 *The influence of the material texture of the fiber art on the indoor space environment design*

The fiber art is a kind of goods with performance texture and manufacture texture. No matter it is in the visual sense or tactile sense, they both have incomparable visual appeal. The same materials have different expression forms, and different materials can produce different textures through different processing technologies or by adopting different structures. The indoor fiber decorations can give people different feelings by the tactile senses. Different tactile feelings, such as hard and soft, thick and thin, and hot and cold, have significant influence on people's psychological feelings. The pursuit of the modern fiber arts is beyond the painting and focuses focus on the beauty of the materials themselves. The application of the natural forms and the rich texture of the fiber materials and the contrast of tough and soft, straight and curved, mixed and pure, bright and dark, and light and heavy between different fiber materials in the indoor space environment bring rich aesthetic feelings.

### 3.2 *The influence of the expression forms of the fiber art on the indoor space environment design*

The indoor space environment design is a creative activity which expresses the theme through people's behavior. When fiber creation is carried out on a specific environment, the style and the expression form of the fiber art will have an effect on that environment. For example, the fiber wall hanging "alive" of the new Baiyun Airport in Guangzhou, which was designed by the artist Ms Li Fengwen, has gorgeous colors. Its vivid style has the stereo feeling, and it is both abstract and enjoyable. The design is large but not loose, and hence it attracts many viewers. The fiber art with the strong visual effect has a very strong adornment effect on the surrounding environment. It fully shows the humanistic color of the people in Lingnan and the time spirit of advance with the times.

### 3.3 *The influence of the colors of the fiber art on the indoor space environment design*

The indoor environmental color has great influence on the indoor space, comfort level, environmental atmosphere, use efficiency, and Person's psychology and physiology. The color of the indoor environment is the soul of the indoor environment design. Different colors can cause different psychological feelings, and a good color environment is an ideal combination of these feelings.

The modern indoor environment color is mainly from three aspects: light color, display color, and environmental color. A good fiber color can compromise and match colors to the indoor space and make the whole space harmonious and comfortable. Under the condition of the monotonous indoor environment color, rich-colored fiber art can give the indoor space more taste and enrich the whole indoor color perception. For example, the overall environment color of the landmark center in Nashville is gray. Its indoor suspensory fiber artworks use a few strong and saltatory colors such as red, blue, green, and white. In this way, color of the indoor environment is much abundant, and the environment has the harmonious feelings of calm and brightness. Therefore, no matter in what form the fiber art appears, the impact of color change on the indoor environment should not be ignored.

### 3.4 *The influence of the fiber art forms on the indoor space environment design*

The indoor space is the place that shows the use functions and people's activities. While meeting the use functions, diversification of the space form is required to satisfy the constantly increased aesthetic value. Overall coordination

of the fiber art with the space is also required. If we use the inappropriate fiber artwork, we will have incongruous feelings on the indoor environment. In particular, the performance of the size, shape, and color use of the fiber art is the necessary way to reconcile the indoor space form. If smaller fiber arts are set in a larger indoor space, there will be an imbalance between them and loss of embodiment of the space beauty. Meanwhile, they still can make the indoor space environment look drab and empty. For example, the soft sculpture "flowing" designed by the famous fiber artist Professor Lin Lecheng is hanging in the coffee house in Tongcheng International Hotel. Its size is harmonious on the scale with the environment space and the wool texture is soft. The warmth of the anaglyph effect makes the coffee house comfortable and warm, and the lively and rich color makes the indoor space environment wide and bright. Use the fiber artwork, the space form will become more vibrant with effectively guiding and reconciling the indoor space.

## 4 APPLICATION OF THE FIBER ART IN THE INDOOR SPACE

As the main content of the indoor space, the fiber art plays an important role in the indoor environment; furthermore, its effect is very important. The fiber art can not only make the space more rich, but also combine with the material, color, and lighting of the indoor space of the buildings. It combines people's artistic atmosphere and architectural design ideal, and then makes the indoor environment of the building warmer. Meanwhile, it also creates more abundant humanity space<sup>[3]</sup>.

### 4.1 *Application of different colorful fiber art in the indoor space*

As the important part of the fiber art, color is also a basic element of the indoor mass-tone attune. When we use fiber art, we should pay attention to its consistency with the indoor mass-tone attune. The fiber art can make the mass-tone attune of the indoor environment color more bright and clear simply by using color collocation and combination. The color of the indoor space should keep harmony and unity with the pure color in the room. At the same time, we should also find the subtle changes among the various colors on the details. However, if we use too much colorful fiber art products, it will affect the overall effect of the indoor environment. Therefore, we must place special emphasis on the color contrast.

#### 4.2 *Application of different texture fiber art in the indoor space*

The fiber art belongs to the material art. The different qualities of the materials have different effects, and they are different in both the tactile sense and visual sense. For example, both linen and silk exhibit abundant mechanism and their forms are natural. These materials themselves have high aesthetic value, and they happen to have the same view with people's aesthetic feelings in the indoor environment designs. When we design the indoor environment, skillfully using the characteristics of the fiber arts, creativity, richness, and a reasonable combination of them with the room can properly reflect the charm of the fiber art.

#### 4.3 *Application of different design forms of the fiber art in the indoor space*

According to its application forms, the fiber art can be divided into three-dimensional form and plane form. The three-dimensional form mainly includes fiber installation art blending into the indoor environment and soft sculpture of the stereo modeling. The fiber art in the plane form has a raised effect and it mostly displays its artistic effect in the form of hanging. This is a new type of cultural phenomenon and art behavior. It transcends the traditional fiber art and exhibits the characteristics of the strong subjective cognition and aesthetics of the designers.

## 5 CONCLUSION

Both fiber arts and the indoor space designs come from the long river of human history. The rich heritage of human civilization shows abundant culture and unique art connotation. Because the fiber art is very abundant in the content and its style and texture are diverse, it can be effectively combined in a different environment space and becomes a whole. And because most of the fiber materials have relatively soft texture, they can combine with the environment space. In the future, we need to continually exploit and keep forging ahead. In this way, the ancient and warm art can be well combined with the modern decoration and blend into more vigor and vitality to resonate with people's hearts.

## REFERENCES

- Chen Xuemiao. The effects and the utilization principles of the fiber arts in the indoor environment. *Art sea*. 2012(11): 89–91. (In Chinese).
- Huang Jie, Xie Bing, Li Yan. The creation study of the fiber art decoration in the modern architectural space. *Journal of Lanzhou Institute of Technology*. 2013(5): 175–176. (In Chinese).
- Hao Wei. The balance beauty of the material and the space—the psychological construction of the modern fiber art in architectural indoor space. *Journal of Yibin University*. 2011(11): 130–132. (In Chinese).

## Finite element analysis on shear lag effect of concrete curved box girder under moving loads

Hai-lin Lu, Chong-yong Wan, Xiao-long Zhou & Jia-qi Qian

*School of Resource and Civil Engineering, Wuhan Institute of Technology, Wuhan, China*

Bin Chen

*Architectural Design Institute of China First Metallurgical Group Co. Ltd., Wuhan, China*

Song-bo Zhu

*Hainan Yingda Real Estate Development Co. Ltd., Haikou, China*

**ABSTRACT:** The general software of the finite element ANSYS is used to analyze the shear lag effect of concrete curved box girder under the moving loads. Under the action of the same load, three different moving load speed and two different positions were set to investigate the distribution of shear lag effect of the cross-section when the loads moved to the mid-span. The results show that when the loads move along the inside web, in a certain range, the shear lag coefficient at the junction of the roof and web plate decreases with the increasing of speed; when the speed is greater than 15 m/s, the shear lag coefficient increases with the increasing of speed. When the loads move along the outside web, in a certain range, the shear lag coefficient at the junction of the roof and web plate increases with the increasing of speed, when the speed is greater than 15 m/s, the shear lag coefficient decreases with the increasing of speed. When the moving load is at the same speed, the load location has an effect on the shear lag coefficient of box girder cross-section, the shear lag coefficient of load side is greater than that of the other side, and it presents the positive shear lag phenomenon.

**Keywords:** moving load; concrete; finite element; curved box girder; shear lag effect

### 1 INTRODUCTION

With the development of traffic construction in China, curved box girder bridges have been widely applied to the construction of highways and bridges, especially to construction of the overhead viaducts and flyovers in urban areas. Curved box girder has such advantages as great bending rigidity and torsional stiffness, good mechanical performance, large span capacity as well as broad bridge view, so it is widely used at present [1]. In curved box cross-section girder because of the nonuniform distribution [2] of shear deformation along the width of flange plate of the box girder the longitudinal displacement of the flange plate distancing rib plate is slower than that of the flange plate nearing rib plate while bending transverse distribution of bending normal stress takes on curve shape. The phenomenon is called “Shear Lag Effect” [3]. If influences brought by shear lag is neglected in curved box girder, the actual stress and deflection at the junction of structural web plate and flange plate will be underrated, leading to insecurity in

structure and engineering accidents. To reduce the incidence of those accidents, it is of critical importance to ensure the safety and endurance of bridges in heavy traffic by in-depth research into shear lag effect in concrete curved box girder bridges to prevent the box girder from being damaged.

J. Senthilvasan [4] conducted an experiment on continuous bending concrete bridges to deepen people’s understanding in bridge dynamic responses and calibration analysis. By keeping the record of strain and deflection of double room box-shaped bridges when the heavy vehicles were driving at different speeds, J.S analysed the data and the experiment results comparatively agreed with those predictive results made by bridge design regulations, therefore the experiment proved to be feasible. SUN Zhao-yu [5] analysed the influences that vehicle load longitudinal action position and transverse action position exerted on continuous box girder shear lag effect of through adopting FEM. LU Hai-lin [6] made use of ANSYS, a large-scale general finite element software, to build cantilever curved box girder model, and analysed



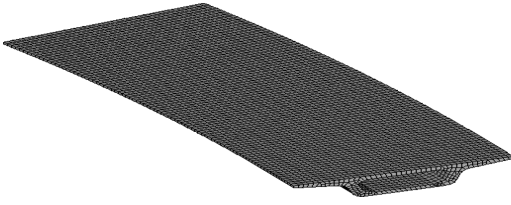


Figure 4. Finite element model of curved box girder.

range, well reflect the nonlinearity [10] of concrete structure. In this thesis the finite element model is divided into 11,340 units, 17,765 nodes in total, and the boundary constraint conditions adopt surface constrain, which restrains UX, UY, UZ on the one side and restrains UX, UY on the other side.

### 3 NUMERICAL RESULT AND ANALYSIS

#### 3.1 Roof and bottom shear lag coefficient of mid-span cross-section of box girder under moving load

When the load moves from the starting point to the end point and the calculation process finishes, post-processing can be started. Count the total moving load step as N and adjust the load step of the result to N/2, and take the mid-span of the box girder as study object, and now the action influence effects of the cross-section are most evident [11]. Get the roof and bottom stress values of the cross-section and then convert them into shear lag coefficient. Define shear lag coefficient as the ratio of normal stress considering shear lag effect in the cross-section to the stress calculated based on elementary girder theory. Finally analyse the obtained data to get the shear lag coefficient curve distribution under each work condition respectively, as is shown from Fig. 5–Fig. 14.

#### 3.2 Result analysis

From Fig. 5 to Fig. 14, it can be noted that because of the adoption of the curved box girder model in this dissertation, the data obtained through calculation has no symmetry. The conclusion can be got below:

1. From Fig. 5 and Fig. 6 it can be seen that the roof shear lag coefficient of the box girder ranges from 0.14 to 3.0 and it is distributed on the two sides of 1.0, which displays certain regular patterns. From Fig. 5 it can be known that when the load moves along the inside web with its speed in the scope of 10–15 m/s, the shear lag coefficient at the junction of the roof and

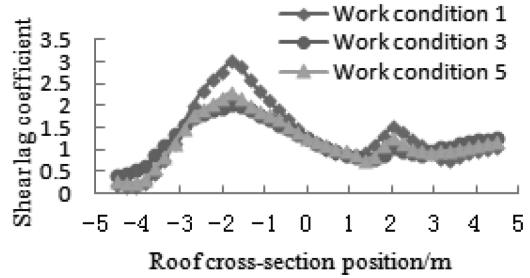


Figure 5. Shear lag coefficient of the mid-span cross section of the roof when the load is on inside web.

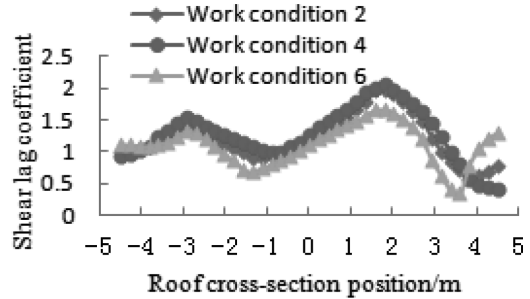


Figure 6. Shear lag coefficient of the mid-span cross section of the roof when the load is on outside web.

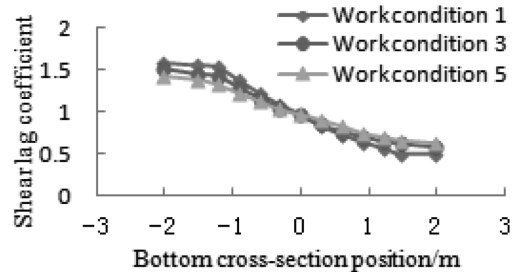


Figure 7. Shear lag coefficient of the mid-span cross section of the bottom when the load is on inside web.

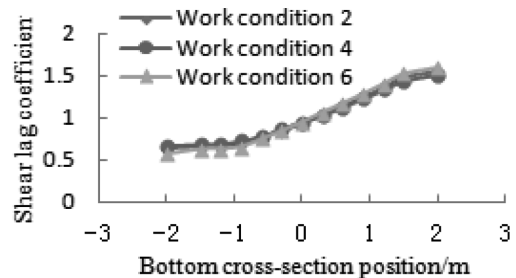


Figure 8. Shear lag coefficient of the mid-span cross section of the bottom when the load is on outside web.

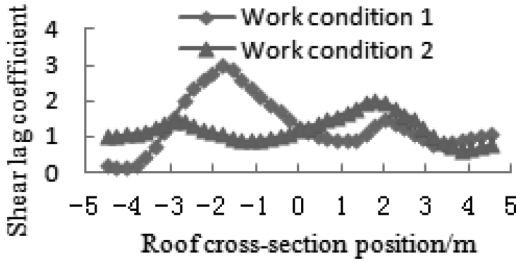


Figure 9. Shear lag coefficient of the mid-span cross section of inside and outside webs roof when  $V = 10$  m/s.

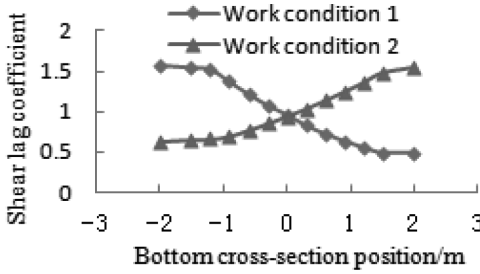


Figure 10. Shear lag coefficient of the mid-span cross section of inside and outside webs bottom when  $V = 10$  m/s.

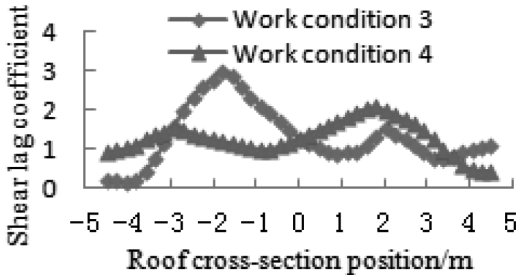


Figure 11. Shear lag coefficient of the mid-span cross section of inside and outside webs roof when  $V = 15$  m/s.

the web plate decreases as the speed increases, while when in the scope of 15–20 m/s, shear lag coefficient increases as the speed increases. From Fig. 6 it can be known that when the load moves along the outside web, the distribution law of shear lag at the junction of the roof and web plate is opposite to that of the load moving along the inside web.

2. From Fig. 7 to Fig. 8 it can be seen that the bottom shear lag coefficient of the box girder ranges from 0.48 to 1.6 and it is distributed on the two sides of 1.0, which displays apparent regular pattern. From Fig. 7 it can be known

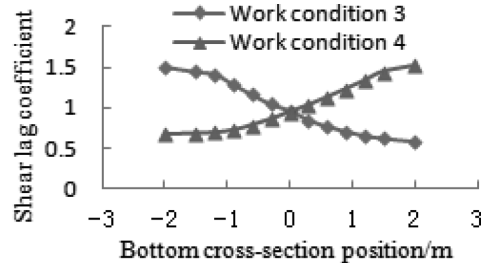


Figure 12. Shear lag coefficient of the mid-span cross section of inside and outside webs bottom when  $V = 15$  m/s.

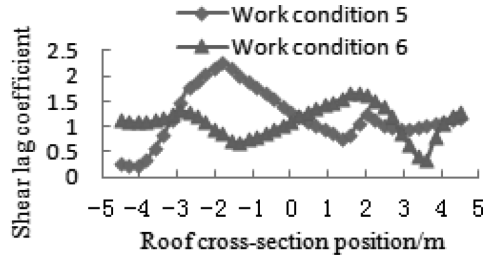


Figure 13. Shear lag coefficient of the mid-span cross section of inside and outside webs roof when  $V = 20$  m/s.

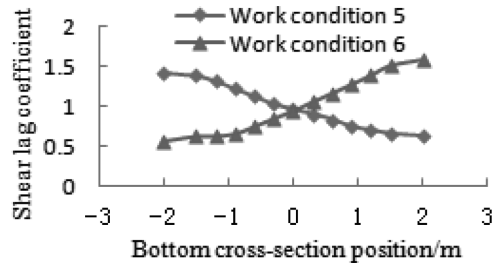


Figure 14. Shear lag coefficient of the mid-span cross section of inside and outside webs bottom when  $V = 20$  m/s.

that when the load effect is on the inside web, bottom shear lag coefficient near the inside web side, ranging from 10 m/s to 20 m/s, decreases as the speed increases while the bottom shear lag coefficient near the outside web side, ranging from 10 m/s to 20 m/s, increases as the speed increases. From Fig. 8 it can be known that when the load effect is on the outside web, bottom shear lag coefficient near the inside web side, ranging from 10 m/s to 20 m/s increases as the speed increases while the bottom shear lag coefficient near the inside web side, ranging



from 15 m/s to 20 m/s, decreases as the speed increases. But the distribution law of bottom shear lag coefficient near the outside web side is opposite to that near the inside web side.

3. From Fig. 9, 11, 13 it can be noted that under the same speed when the load moves along the inside web, the shear lag coefficient at the junction of the inside web roof and the web plate is significantly greater than that of the load moving along the outside; when the load moves along the outside web, the obtained regular pattern is similar to that of the load moving along the inside web.
4. From Fig. 10, 12, 14 it can be noted that under the same speed when the load moves along the inside web, the bottom shear lag coefficient near the inside web side is significantly greater than that of the load moving along the outside web; when the load moves along the outside web, the similar regular pattern can be obtained too.

#### 4 CONCLUSION

The three-dimensional finite element software ANSYS is adopted in this paper to analyse the mid-span cross-section shear lag effect distribution regular pattern of concrete curved box girder under the influence of two different positions and three different speeds. The analytical result shows that when the load moves along the box girder inside web, the shear lag coefficient at the junction of inside web roof and web plate is significantly greater than that of load moving along the outside web. At the junction of the roof and the web plate, it displays evident positive shear lag effect and at the central position of the web plate reaches the maximum value and the whole diagram takes on M-shape, which is in accordance with the theoretical results. When the load effect is on the inside web, bottom shear lag coefficient on the inside web is bigger than that on the outside web and decreases in descending number from the inside web to the outside web. At this moment the bottom on the inside web will display positive shear lag effect. When the load effect is on the outside web, bottom shear lag coefficient on the outside web is bigger than that on the inside web and increases in ascending order. At this moment the bottom on the outside web will display positive shear lag effect.

Although the above-stated conclusions are reached in the thesis, there remains much to be improved. For example, the cross-section is not inconclusive for it only covers the single box and single room cross-section; the number of vehicle load is not sufficient without the consideration of the moving multi-vehicle load; researches on pre-stress have not been conducted yet; it is hoped

that relevant researches into the above-mentioned matters can be performed.

#### ACKNOWLEDGEMENTS

This study was supported by the Natural Science Foundation of China (project approval no. 51378404) and the Graduate Student Education Innovation Fund of Wuhan Institute of Technology (project approval no. CX2013115). And the Transportation Research Center of Wuhan Institute of Technology provided software to help for this study. I expressed thanks for them here.

#### REFERENCES

- [1] Liu Hui. Finite element analysis of shear lag effect for curved box girder [J]. *China water transport*, 2007, 7(2):85–86.
- [2] Lu Hailin, Zhu Songbo, Zhou Xiaolong, Qian Chaobang, Wan Chongyong. Shear lag effect of straight box girder under different loads [J]. *Journal of Wuhan institute of technology*, 2014, 36(12):39–43.
- [3] Xiang Haifan, Yao Lingsen. *The theory of higher bridge structure* [M]. Beijing: China communications press, 2001.
- [4] J. Senthilvasan, D.P. Thambiratnam, G.H. Brameld. Dynamic response of a curved bridge under moving truck load [J]. *Engineering Structures*, 2002, 24:1283–1293.
- [5] Sun Zhaoyu, Liu Jianxun, Zhao Wenbin. Shear Lag Effect of Continuous Box Girder Bridges under Vehicle Load [J]. *Journal of Lanzhou institute of technology*, 2015, 22(5):27–31.
- [6] Lu Hailin, Zhang Wei, Yan Changxiong. Moving load speed on shear lag effect of cantilever curved box girder [J]. *Journal of Wuhan institute of technology*, 2014, 36(3):18–21.
- [7] Sang-Youl Lee, Sung-Soon Yhim. Dynamic behavior of long span box girder bridges subjected to moving loads: Numerical analysis and experimental verification [J]. *International Journal of Solids and Structures*, 2005, 42:5021–5035.
- [8] Zhao Yunan, Wang Yan. Analysis of the shear lag effect in curved continuous box girder bridge under the vehicle load [J]. *Railway Engineering*, 2013, 2:9–11.
- [9] Wang Xinmin. *ANSYS numerical analysis of engineering structural* [M]. Beijing: China Communications Press, 2007.
- [10] Lu Hailin, Chen Lipeng, Zhu Songbo, Wan Chongyong, Qian Jiaqi. Analysis of effect factors about shear lag in curved box girder under seismic loads [J]. *Advanced Materials Research*, 2014, 926–930:505–510.
- [11] Lu Hailin, Nan Zijun, Zhang Wei. Shear lag effect of curved box girder under moving load [J]. *Journal of Wuhan institute of technology*, 2015, 37(5):23–27.



**Taylor & Francis**

Taylor & Francis Group

<http://taylorandfrancis.com>

# Application of soundscape in city parks by case study

Jun-ling Zhou

*School of Design, Shunde Polytechnic, Foshan, China*

Ling-feng Xie

*The School of Architecture, South China University of Technology, Guangzhou, China*

**ABSTRACT:** Through comparative analysis of identifying today with historical experience, this paper makes an exploration of auditory sense from the altitude of eastern and western philosophy as well as the aesthetic angle of “interesting philosophy” and “silence”, thus laying an aesthetic foundation for soundscape in city parks. It also dissects the content and meaning of soundscape and explains the great significance of soundscape design. At last, it takes the design of Beck Park as the research and practice case of soundscape in city parks to demonstrate that the design law of classical gardens is still valuable and deserves learning nowadays.

**Keywords:** city park; classical garden; artistic conception; modern application

## 1 INTRODUCTION

The concept of soundscape is first clearly put forward by the Canadian composer R. Murray Schafer in 1960 s, and it is also called sound landscape. The word soundscape is analogized from landscape, which is a compound of stem “sound” and affix “scape”. Corresponding to landscape, soundscape means “the scenery captured by ears” or “auditory scenery”.

For a long time, landscape architects have put their attention on visual elements and functional qualities. They always seek for greater perfection especially on spatial form, functional layout, material texture and color composition while neglecting perception and experience of landscape through organs based on auditory sense, sense of touch, sense of smell, etc. Therefore, we hope to introduce the design concept of using five sense organs to conduct an omni-directional and multi-perspective feeling and take the auditory element which is often neglected as an entry point to have a comprehensive grasp and recognition of sound environment with the concept of “soundscape”. At the same time, through the active attempt of soundscape design’s application in landscape planning, this paper also discusses the design considerations, functional characteristics and design methods of soundscape in order to bring richer design elements and new entry points into landscape planning.

## 2 THE RESEARCH STATUS OF INTERNATIONAL AND DOMESTIC SOUNDSCAPE

### 2.1 Canada—World Soundscape Project

World Soundscape Project (WSP for short) is created by the Canadian scientist and professor R. Murray Schafer from Simon Fraser University in the late 1960 s and early 1970 s. It is an organization with purpose of educating and studying sound environment.

In 1975, Professor Schafer led a massive academic report group to make a European trip, during which they did academic reports and held symposiums in some major big cities. They also made a detailed survey of soundscape information in five villages of each country including Sweden, Germany, Italy, France and Scotland.

This European trip records a large amount of sound material and builds a stereo simulation audiotape database, of which more than 300 Canadian and European sounds are stored. Two books are also published about this trip. One is called European Sound Diary that narrates this trip. The other one is called Five Village Soundscapes that specifically analyzes soundscape.

### 2.2 Japan—Soundscape Action

“Soundscape” is called “sound landscape” in Japan where sound environment is studied from different sides of natural science, sociology and

the humanities and new sound awareness is established. It takes sound and relative issues as new entry points to expect new development in the fields of environmental science, cultural anthropology, acoustics, noise control, environment design, etc.

1.2.1. As required by the “basic environment program” of EPA, various local public groups and residents took part in the activity of reviewing and selecting the existing “100 soundscapes of Japan” in order to preserve good sound environments. This activity collects local sound environments (soundscapes) which are recommended by the people all over the country. In the process of keeping these sound environments, 100 soundscapes are judged out.

1.2.2. As regard to the recommendation and collection of the existing “100 soundscapes of Japan”, besides the selection and presentation from towns and villages in city proper based on actual conditions, other individuals and groups that care about sound environment can also recommend to EPA. Application paper should be filled as required when recommending and reasons should also be specified to preserve the sound.

1.2.3. The collected soundscapes would be reviewed, decided and published results by “Japan Soundscape Research Institute” (chairman: Mitsuyasu Yamashita, president of Kobayasi Institute of Physical Research)

1.2.4. For detailed announcement information, please contact with the EPA (noise control office) or atmospheric protection agency of each prefecture (12 designated cities).

### 2.3 *The report of Wang Junxiu, a Tsinghua student from Hsinchu, Taiwan*

Urban expressions of soundscape: the imagination of environmental sociology in two cities. Wang attempted to compare the two transnational cities of Hsinchu city and Vancouver from the

perspective of environmental sociology and explore how soundscape transforms to urban expressions. He also adopted the analysis matrix composed of Ecological Triangle and Soundscape Triangle and then went to Canada during his summer vacation to do a common research together with professors of Simon Fraser University, expecting soundscape to be another part of urban expressions.

### 3 THE APPLICATION MEANING OF SOUNDSCAPE IN CITY PARKS

The city park in modern sense originates from USA. Frederick Law Olmsted (1822–1903), the founder of American landscape architecture, came up with the great idea of building parks in cities. He and Calvert Vaux (1824–1895) commonly designed New York Central Park (1858–1876) as early as 100 years ago. This event is not only a precedent of modern landscape architecture. What’s more important, it marks the advent of city public life. Park is no longer a luxury enjoyed by few people but a space for general public to be physically and mentally delighted.

The traditional function of city parks is to satisfy urban residents’ leisure need as a site to rest, go sightseeing, exercise, communicate and hold various collective cultural activities. In recent years, city parks get enhanced in improving eco-environment and preventing disasters. Modern cities are filled with all kinds of architectures and have problems of being over-crowded and lacking isolation space and rescue paths, so the construction of city parks is a resolution that can serve multiple purposes. In addition, with the rise of city tourism, many famous large comprehensive parks take the lead in becoming an important urban tourism attraction with their unique tastes. City parks become the center of city tourism. City parks are also an important carrier of afforesting and beautifying cities and improving eco-environment. What is more special is that the construction of massive park green space not only visually brings people aesthetic enjoyment but also has obvious effects in the modification of partial microclimates and effective control of dust and automobile exhaust. It plays a significant role in improving the ecology and living environment of modern cities.

However, as people tend to be no longer satisfied with transient visual enjoyment but turn to pay more attention to art and spiritual life, people’s expectation and hope of city parks also goes for a deeper level. People do not passively adapt to the environment any more, instead, they hope to positively join the interactive experience with environment while sound is a very good carrier without any doubt.

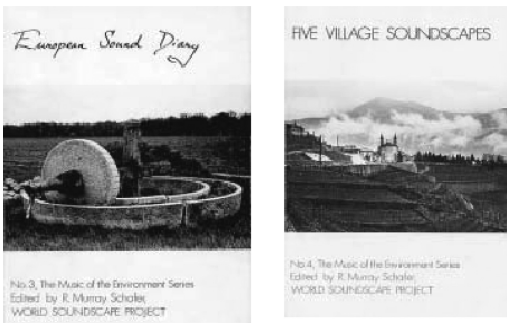


Figure 1.

We used to be charmed by bird songs and chirps, contemplated by ancient temples and bells and traditional rites and moved by children's frolics. But these nice sounds in our childhood memories are gradually losing their vigor and fascination during the swelling development of cities. Thus landscape design should not merely perform the single function of passively removing or isolating some sounds but should also consciously plan and guide with a more positive attitude, such as positively designing listening contents and creating listening "sites" to refresh people's nice and special memories, making a special emotion and atmosphere of a locality or space and turning "passive listening" to be "active listening" and "active feeling and connecting".

With the speed-up development of urbanization, noise has become an increasingly severe problem in city landscape. And at the same time, we can feel through our own experience that the natural sound of bird songs and chirps, the historical sound of ancient temple bells and traditional rites and the life sound of children's frolics are gradually losing or have lost their vigor. Therefore, stressing research on soundscape and intensifying research and design of sound environment which is often neglected in landscape provides a carrier for better interaction between people and the environment.

#### 4 THE APPLICATION OF SOUNDSCAPE IN CHINESE CLASSICAL GARDENS

The winter mountain area of Four Seasons Rockeries in Yangzhou Geyuan Garden reflects certain acoustic rationalities. It is a landscape composed of rockeries piled by white Xuan stones against the wall and white snow stones with veins of ice cracks used to pave the ground, and winter ornamental plants are matched around such as wintersweet and asparagus fern. As the area is located in the shade of north wall with an all-seasons coldness sense, it fully expresses a strong winter scene of un-melted accumulation of snow and chilliness. What shows more ingenuity is that the "leaking wind and moon" background wall opens rows of scenery-admiring windows with diameter more than one foot. It connects winter mountain area with spring mountain area though a wall is set between them, forming a temporal connotation of "spring coming after winter" and "spring coming back to the earth". On the other hand, it also increases air flowing and air velocity, which creates a whistling of wind, thus a vivid scene of chilly winter with roaring north wind is coming out. Wu Zhaozhao once made an analysis of its acoustic effect: the outside is narrow alley and high wall. According to the Bernoulli's principle



Figure 2.

(Professor Gao Deyu from University of Kentucky thinks that Venturi Effect is more accurate), the small holes sharply increases air flowing velocity and under the suction of narrow alley and high wall, wind whirs through the holes. As the holes are arranged like a harmonica, the wind velocity at each hole differs, so wind sound at each hole is also quite different. Landscape architects set a road in the northeast of the holes to leave an empty site (the prevailing wind direction all year round in Yangzhou is northeasterly wind) so that the artificial north wind can keep running throughout the year, which is quite skillful and impressive. It has both superb art form and rich scientific knowledge that can evoke people's visual, auditory and sensory feeling within a narrow space. This is a very rare technique of building landscape in China. After confirming the soundscape theme of a park, architects generally will organize relevant landscape elements on the basis of artistic conception. Though the organization of these landscape elements is launched around the humanistic theme of artistic conception, the law of managing humanism contains rational technical logic. Since these technical experiences of soundscape can't separate from personal practical experience, it restricts the formation of quantitative technology system based on objective laws of physics. But it is just because of this technical mode of knowledge and action being one that these technical experiences of soundscape can achieve consistence with certain basic elements of architects themselves. So it goes beyond the control of common number and quantity to directly connect the expression of inner heart and ensures the transformation from various sound artistic conceptions to garden physical landscape. Rational technical logic is the guarantee and foundation for soundscape to convey the conception it wants.

## 5 PRACTICE CASE OF SOUNDSCAPE IN CITY PARKS

The Beck Park in the city proper of Dallas is built to commemorate Henry C. Beck Jr., the founder of Beck Architecture and Engineering Firm. Entrusted by the Beck family, the park design combines the building materials and methods used in Beck's life as a symbol of remembrance, while it also provides a comfortable and elegant space for the city. Landscape architects communicate with customers and fuse the rectangular geometrical concept to the design. In this rectangular square, two concrete walls divide the square into four proportional small rectangular squares. At the intersection of walls, a unique waterscape design becomes the visual focus, which is a sharp contrast to the noisy and crowded transportation nearby. In order to make a bigger rectangular area in the square, landscape architects arrange a vertical array of cob walls that enlarges the gap space with neighboring architecture. On the basis of the geographical advantage of the square, the architects design a comfortable entrance that coordinates with surrounding sidewalks. The design of the square tries to avoid removing original trees, thus ensuring the completeness of original green areas. The sidewalks into the square clearly separate small spaces of the square and the connecting passage through walls is also quite special.

This design also provides fresh, joyful and fascinating public activity space for residents in the city proper. It shows as well that Beck's building technology with decades' profession leads the development direction of park construction. The design of concrete walls is not only elegant but also highlights edges and corners. Landscape architects, architectural engineers and structural engineers cooperate closely to achieve a high quality concrete structure and ensure the perfect combination of focus situation and wall intersection and other corresponding

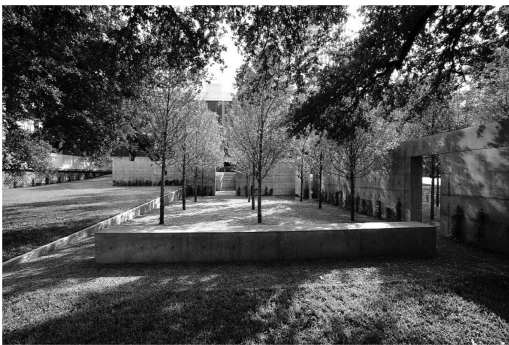


Figure 3.



Figure 4.

sceneries. The side revetment design uses blue-stones and the architecture intersection inside the revetment uses concrete material.

The waterscape design aims to highlight the motion of water and its melodious rippling sound. The intersection of concrete walls and two horizontal lines create a specialty and constitute the essential condition of completing the design. The pool with high water level has a skillful design as its water level keeps the same with the square horizon. The pool with low water level receives water from the channel of the pool of high water level and top wall intersection. The main attraction of waterscape is the source nappe in the contrary direction of concrete walls. The pools with high and low water level are both covered with Pennsylvania gravels, which hide the source and make a mysterious sense. In order to ensure night activity and safety as well as convenience, lighting design is added in the city park.

There are downward mercury vapor illuminants around oak trees, creating a "moonlit" sense. Designers use upward lighting in the inner side of the square. Metal halogenated compound gives out warm light color, adding a tone of autumn red maple. The downward metal halogenated compound chooses surrounding oaks as illuminants to provide light for the sidewalks.

The design of soundscape in Beck City Park, Heavy partition wall; cross-separated geometrical courtyard; tranquil atmosphere of oriental artistic conception.

Although it uses modern simple design method, it contains the quintessence of building classical gardens.

By analyzing and understanding soundscape—an important component which is often neglected in landscape planning and taking Yangzhou Geyuan Garden and Beck Park as practice cases, this paper analyzes the design elements, design

phases and design methods of park soundscape with the intention of introducing the concept of soundscape to landscape design and bringing a new entry point to landscape research. The quantitative analysis of natural sound, background sound, artificial sound and action sound in the process of human getting knowledge of landscape enriches and completes human's cognitive methods and subjective experience of objective environment.

## REFERENCES

- [1] Naveh, Lieberman. Landscape Ecology: Theory and Application [M]. Springer-Verlag, 1984.
- [2] Yu Kongjian, The Meaning of Landscape [J]. Time Architecture, 2002.
- [3] Kangjian, Yangwei, Soundscape in Urban Public Open Space, World Architecture, 2002
- [4] Li Jinbo, Bai Yanlin, Discuss of Controllability of Green and Ecological Residential Environment Design [J]. Engineering Construction and Design, 2003
- [5] Jin Xuezhi, China Park Thesis, China Architecture & Building Press, 2005.
- [6] Zhang Daoyong, Chenjian, Xu Xiaojun, Analysis of Soundscape Concept, Journal of Hefei University of Technology, 2007.



**Taylor & Francis**

Taylor & Francis Group

<http://taylorandfrancis.com>



## RCS terminal test

Xiao-fang Ren

CTTL (China Telecommunication Technology Labs)—Terminals Test Lab, Beijing, China

Jian-feng Zhao

CTTL (China Telecommunication Technology Labs)—Systems Test Lab, Beijing, China

**ABSTRACT:** We studied the test standard of the Rich Communication Services (RCS) terminal in detail and developed a set of test system to test the same. This paper first introduces the definition of RCS, architecture, standard development process, present situation of global development, the development of China Mobile, and test standard of the RCS terminal. Then, as shown in Figure 3, we set the test environment of the RCS terminal. Server in the test system was provided by a German instrument company, which is worldwide famous in the field of terminal Application Enabler (AE) test. At present, this paper has developed 17 test cases (as shown in Table 5), covering the five big aspects of RCS terminal test. After system development is complete, we will submit it to GCF platform certification immediately. Then, the system can provide GCF certification test. At present, very few test systems capable of testing the RCS terminal have appeared on the market. This study provides a test method of RCS terminal.

**Keywords:** RCS; GSMA; standard; test

### 1 RCS INTRODUCTION

#### 1.1 Definition

Rich Communication Services (RCS) is the platform that enables the delivery of communication experiences beyond voice and SMS, providing consumers with instant messaging or chat, live video and file sharing—across devices, on any network. RCS marks the transition of messaging and voice capabilities from circuit switched technology to an all-IP world—and it shares the same IMS investment as Voice over Long Term Evolution (VoLTE).

In addition to providing the original SMS and voice services, RCS can facilitate instant messaging/chat (one to one chat or group chat), file transfer, pictures and video sharing, and other businesses. Enhanced message, rich voice, and enhanced address book are the characteristic features of RCS. Enhanced message can provide users with a more diverse chat experience, such as file transfer in the chat process. Rich voice can provide users with pictures, video, and other content sharing in the process of communication. Enhanced address book can be used to easily gain access to social networks by mobile address book, and network interoperability can be achieved between different countries and mobile operators.

#### 1.2 Architecture

Taking GSMA (Global System for Mobile Communications Assembly) RCS5.1 version as an example, we briefly introduce the architecture of RCS.

Figure 1 shows a simplified example of two RCS service providers exchanging traffic with each other using the standard Network-to-Network Interface (NNI) mechanisms (IPX, IP Packet Exchange). RCS compliant access networks include, but are not limited to, those illustrated in Figure 1<sup>[1]</sup>. Architecture terminologies are presented in Table 1.

#### 1.3 Standard development process

In May 2007, Initiative RCS as a working group was set up. Later, Initiative RCS were formally incorporated into the GSMA standard organization in July 2008. Up to now, the RCS standard

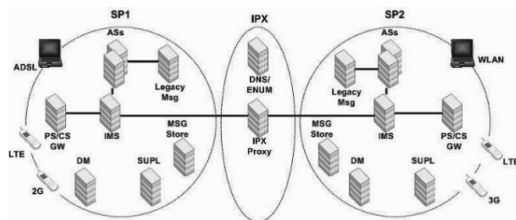


Figure 1. RCS simplified architecture.

Table 1. Architecture terminology.

Name	Paraphrase
PS/CS gateway (GW)	Used for interworking between Circuit Switched (CS) and Packet Switched (PS) voice, for example, Voice over Long Term Evolution (VoLTE).
IMS	IP Multimedia Subsystem
Legacy Msg	Refers to the Short Message Service (SMS)/Multimedia Message Service (MMS)
Ass	Application Servers, for example: Presence Server Messaging Server XML (Extensible Markup Language) Document Management (XDM) Server (XDMS) Multimedia Telephony (MMTEL) Application Server Video Share Application Server ...
Msg Store	Relates to the CPM (Converged IP Messaging) Message Storage Server.
SUPL	Indicates the Secure User Plane Location element to support exchanging geolocation information as part of Social Presence Information (SPI) and Geolocation PUSH and PULL.
DM	Device Management
IPX Proxy	Internet Protocol Packet eXchange Proxy
DNS/ENUM	Domain Name Server/Electronic Numbers to URI Mapping Server ENUM, Telephone Number Mapping working group
SP	Service Provider

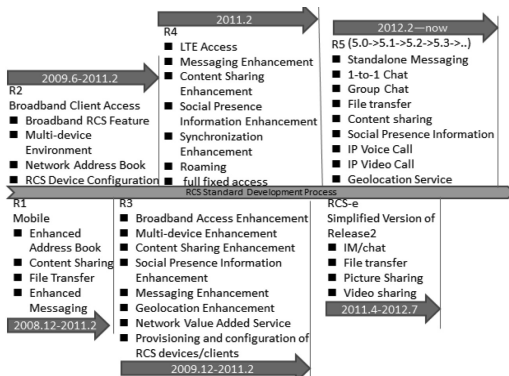


Figure 2. RCS standard update process.

has experienced six development stages, Release 1, Release 2, Release 3, Release 4, RCS-e, Release 5 (5.0, 5.1, 5.2, 5.3...) (see Figure 2). The latest version is RCS 5.3, while the RCS 5.1 and RCS-e

(a simplified version of Release2) is currently recognized as a relatively stable version of the industry.

#### 1.4 Present situation of global development

In order to ensure the global interoperability of RCS services and to give user a unified perception, GSMA in 2012 in the World Communications Conference proposed brand “Joyn”, which is based on RCS-e standard. “Joyn” is divided into the certification of the terminal and the certification of the network. For users, all the terminal or operator’s network that has the use right of “Joyn” brand have the ability of interworking with the other “Joyn” terminal or network. In this way, RCS can quickly get the user’s recognition of the world, and can ensure what business can be consistently used by which user.

In over 3 years, “Joyn” has been from the initial version “joyn Hot Fixes” into the second product phase “joyn Blackbird”. The version “joyn Hot Fixes” was formally transferred to the European operators Certificated Forum GCF in December 2013 to be responsible for the certification test work. Certification requires becoming a member of GCF (client vendor) first, and then testing by the GCF-certified RTO (Recognized Testing Organization). GCF “Joyn” certification needs to be tested in three authenticated networks and requires the test with three certified clients to ensure their interoperability performance. In September 2014, “joyn Blackbird” has been handed over to the GCF certification body too.

The current terminal manufacturers through the “Joyn” certification are: SONY, Samsung, HTC, HUAWEI, NOKIA, LG. Blackberry and ZTE will receive this certification soon. In addition, in 18 December 2014, Microsoft became the first company through the “joyn Blackbird” test certification. Until November 2015, HTC, Samsung, SONY, HUAWEI, and DT Network have also passed the “joyn Blackbird” test certification. Until December 2015, there have been 78 terminals through the certification and 47 operators in 34 countries in the world launched RCS services.

#### 1.5 Development and challenge of China Mobile

In the 2014 World Mobile Congress (MWC), Li Yue, President of China Mobile formally announced the plan of the RCS development. In February and June 2014, he released two versions of white paper *Next-Generation Converged Communication*<sup>[2]</sup>. On the 19 December 2014 China Mobile Worldwide Partner Conference, China Mobile released “three new ‘and’ mobile phone”. The “new message” is based on RCS, seamless integration of a variety of media and message format, seamlessly with the traditional SMS/MMS intercommunication.

In March 2015, the MWC conference site, half of China Mobile's booth, is related to the RCS, including on-site business presentation and terminal display. And China Mobile is put forward, with the hope that the RCS business can be carried out through terminal native method (i.e. mobile phone has RCS function in the factory), the user without the need for ordering business and downloading application can not perceive the use of calls, text messages, and contacts conveniently.

At present, China Mobile is facing the following five aspects of challenge:

1. Native mode. The terminal manufacturers need to develop the corresponding interface, and not only increases the development costs, but also will influence the consistency of RCS business experience to a certain extent.
2. No perception. No perception brings convenience to users and, at the same time, will challenge the consumer's right to know, which will bring a series of problems such as billing, authentication, and service.
3. User experience. OTT service providers improve the user experience through fast iterative version. In this aspect in the current view, the mechanism, talent, and motivation of the mobile operators do not match with the Internet company. If mobile operators want to develop the RCS, it is bound to grasp the principles underlying the development of mobile Internet, to simulate the thinking of OTT service providers to operate, improve user experience, and increase users' degree of interest.
4. Service quality. China Mobile as a telecom operator will certainly be able to provide users with high quality of service as an opportunity, but the corresponding hardware conditions should also be keeping pace with the development of RCS. On the one hand, in the communication network aspect, in order to meet the needs of RCS business development and ensure service quality of RCS, it needs to further enhance communication network coverage ability in depth and breadth. On the other hand, in the terminal aspect, in order to provide more choices to the user, the joint terminal manufacturers should support the research of RCS terminal, which can support a variety of systems, and will avoid possible influence due to the lagging development of terminal.
5. Interoperability. As can be seen in the commercial RCS of various countries, the interoperability of the operators provides a large-scale application environment to the RCS user. At present, the attitude of China Telecom and China Unicom to treat the development of RCS has not unified. We are afraid that achieving interoperability between the two operators with China Mobile in a short time is still a problem.

## 2 RCS TEST STANDARD AND TEST SYSTEM

### 2.1 Test standard

#### 1. GCF

In January 2013, RCS test was added to the GCF certification test. The standard is *OMA-ETS-RCS-V1\_2*<sup>[3]</sup>. In January 2014, the standard *3GPP TS 34.229-1*<sup>[4]</sup> was added to the GCF certification test too. The current test standard of RCS certification test is *OMA-ETS-RCS-V5\_1*. The latest version of this standard is *OMA-ETS-RCS\_CON-V5\_1-20150526-C*<sup>[5]</sup>. GCF chooses part of this standard's test cases, eight parts and 21 test cases. The specific test cases are shown in Table 2.

Table 2. GCF certification test cases.

GCF		
No.	Test content	Items
1	Configuration	2
2	Mobile Originated Capability Discovery	1
3	Mobile Terminated Capability Discovery	2
4	Capability update	2
5	Mobile Originated one-to-one Chat	6
6	Mobile Terminated one-to-one Chat	6
7	Mobile Originated Group Chat	1
8	Mobile Terminated Group Chat	1

#### 2. GSMA

Here, test case information is listed on two stable versions of the GSMA, RCS5.1 (i.e. joyn Blackbird) and RCS-e (i.e. joyn Hot Fixes). RCS5.1 has a total of seven parts and 77 test cases. RCS-e has a total of four parts and 24 test cases. See Table 3.

Table 3. GSMA RCS5.1 and RCS-e test cases.

GSMA		
No.	RCS 5.1	Items
1	Capability exchange	10
2	Registration	3
3	Configuration	32
4	File transfer using http	14
5	Group Chat	10
6	IM/chat	3
7	RCS in-call services	5
No.	RCS-e	Items
1	Configuration	2
2	File transfer	3
3	IM/chat	17
4	Multi-device	2

### 3. China industry standard

The current China industry testing standard is *TC11-WG3-2014-073-Test Specification for RCS Device - Draft V2 (20150603)* [6]. This standard is still a draft and not an officially released version. It has 11 parts and 98 test cases. See Table 4.

Table 4. GSMA RCS5.1 and RCS-e test cases.

China industry standard		
No.	Test content	Items
1	Configuration	16
2	Capability discovery	14
3	Social presence	4
4	IM/chat	4
5	Content sharing	2
6	File transfer	27
7	RCS multi-task concurrent test	11
8	RCS and other business concurrent test	4
9	RCS protocols	6
10	Network compatibility(with Joyn Hot Fixes network)	6
11	Performance test	4

By the above three parts, we can see that currently RCS test mainly focuses on the following aspects: terminal configuration, registration, capability exchange, one-to-one chat, group chat, file transfer, content sharing, and so on.

In addition to these standards, some mobile operators formulate test standards by themselves to require terminal manufacturers support, such as Verizon, AT&T, and China Mobile. Verizon is fully formulated by itself. AT&T formulates its test standards based on GSMA test standards. China Mobile formulates its test standard based on GSMA RCS5.1. North American carrier certification organization PTCRB has not yet introduced test standards related to RCS.

#### 2.2 Test system

The RCS terminal test environment/system is as shown in Figure 3[6]. Test terminal is arranged in 2G/3G/LTE/WiFi network environment, through the IMS core network access to the RCS server, to test the related functions.

Server in the test system is manufactured in a German instrument company, which is worldwide famous in the field of AE (application enabler) test. This server can realize a series of functions, Radio Frequency (RF), IMS core network, Ass, and so on, and provides a basic framework. According to the standard, we can write the required program to invoke the corresponding module and repeat test validation.

At present, test system is built according to the GSMA RCS5.1 and RCS-e standards. We have developed and tested 17 test cases (see Table 5),

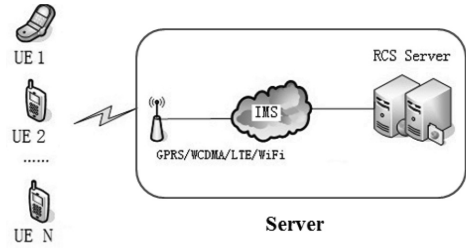


Figure 3. RCS terminal test environment/system map.

Table 5. Test cases that have been developed.

No.	Test content	
1	ID_RCS_4_4_1	Capability query in addressbook (new tags available)
2	ID_RCS_4_4_2	Capability query in addressbook (RCS contact currently not registered)
3	ID_RCS_6_10_1	Video share: sending video
4	ID_RCS_6_10_2	Video share: receiving video
5	ID_RCS_7_7_2	Behalf of legacy devices
6	ID_RCSE_3_1_1	User discovery in addressbook: Initial check of capabilities
7	ID_RCSE_4_1_3	Unsuccessful capability query during a call due to one of the handsets is not reporting
8	ID_RCSE_4_2_2	Capability query in addressbook (RCSe contact currently not registered)
9	ID_RCSE_4_2_3	Capability query in addressbook (polling)
10	ID_RCSE_5_1_3	Successful file transfer (one-to-one)
11	ID_RCSE_7_1_1	Chat 1 to 1 IM-SESSION-START parameter
12	ID_RCSE_7_1_7	“Is Composing” Notification/Typing info
13	ID_RCSE_7_4_2	Initiating a chat/adding a new participant
14	ID_RCSE_7_4_3	Typing text / notifications
15	ID_RCSE_7_4_4	Closing a group chat (initiator)
16	ID_RCSE_7_4_5	Closing a group chat (other than initiator)
17	ID_RCSE_7_4_6	Re-join to the multichat

and our test focuses on the consistency of the interaction protocol between the test terminal and the RCS server. Test covers in five aspects: capability discovery, video sharing, address book, one-to-one chat, and group chat. The test system is still

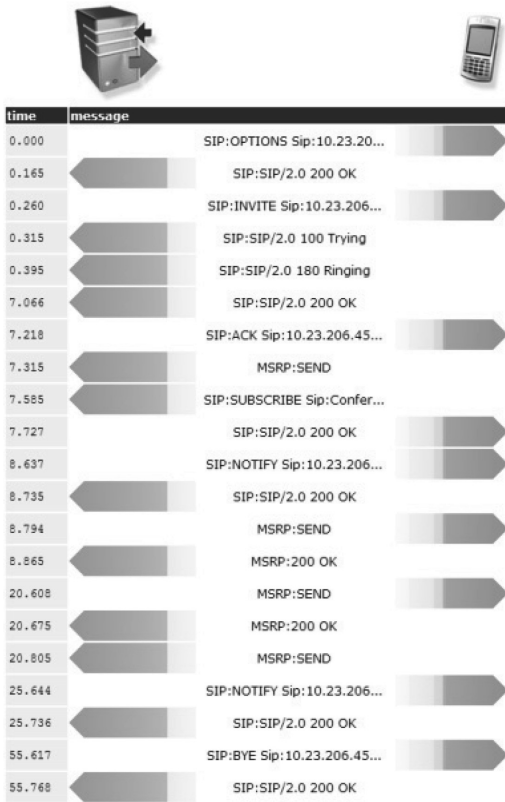


Figure 4. Initiating a chat/adding a new participant message flow.

in the development process. Immediately after the completion of system development, we will submit it to GCF platform certification. Then, the system can provide GCF certification test.

Here is an example. Test case: Initiating a chat/adding a new participant, see Figure 4.

Message flow in detail:

(

DUT is IMS REGISTERED

Step 1: User A selects users B and C from IM/chat application to start a chat (DUT is User B)

Step Verdict: PASSED

SIP 200 OK is received from the DUT for SIP OPTIONS

Step Verdict: PASSED

a first query to know users B's real-time RCS-e capabilities is performed

Step 2: user A sends a message to invite B and C to the chat

Step Verdict: PASSED

SIP 180 RINGING is received from the DUT for SIP INVITE

Step 3: user B and C accepts the invitation. User A sends them a message.

Step Verdict: PASSED

200 OK received for SIP INVITE

Connecting to DUT at 10.23.206.45:20000

Step Verdict: PASSED

SIP SUBSCRIBE is received from the DUT

Step Verdict: PASSED

Users A, B, and C have established a multichat session between them.

Step Verdict: PASSED

IM chat message received from User A

Step 4: User A search for a new participant (user D) in the phonebook or IM/chat application (user D's RCS-e capabilities previously detected) and sends an invitation to join the multichat)

Step Verdict: PASSED

Users B (DUT remains unaware unless the new invited user accepts the group chat invitation

Step 5: User A search for a new participant again (user E) in the phonebook or the IM/chat application and sends him/her an invitation (user E is RCS-e registered).

Step Verdict: PASSED

User E is added to the participant list

Step 6: Closing the chat session

Closing the chat session toward DUT

Final Verdict: PASSED

)

After the completion of the test, test logs and test results are given. From the test logs, we can see the test purposes in detail for each step in the process. Judgment can be given for each step for testers to pinpoint the steps in which problems occurred.

In addition, China Mobile is currently in the preparation stage before the RCS storage test. From the internal news, we learned that China Mobile RCS test currently focuses on three aspects: server registration, group chat, and file transfer. Specific test cases are related to SMS over IMS, registration, address book, instant messaging, group chat, one-to-one chat, burn after reading, and so on. The other functions of RCS will be gradually achieved later.

### 3 TEST SUMMARY

Together with the rapid development of RCS, RCS terminal test is very important, on the one hand in order to maintain the consistency of the RCS terminal, on the other hand in order to ensure the interoperability of RCS terminal in the world. At present, for most parts in China, terminal achieves the RCS by the way of downloading the APP client, and testing situation is not optimistic. RCS terminal joined in native way will also bring more challenges to the test work.

## ACKNOWLEDGMENT

This paper is sponsored by Major projects of Ministry of industry and information technology, project name:TD-LTE/FDD-LTE/TD-SCDMA/WCDMA/GSM Multi mode commercial baseband chip development (No. 2013ZX03001007).

## REFERENCES

- [1] GSMA. 2013. GSMA Rich Communication Suite 5.1 Advanced Communications Services and Client Specification Version 4.0 28 November 2013.
- [2] CMCC. 2014. Next-Generation Converged Communication.
- [3] OMA. 2014. OMA-ETS-RCS\_CON-V1\_2\_2-20141107-C.
- [4] 3GPP. 2015. 3GPP TS 34.229-1.
- [5] OMA. 2015. OMA-ETS-RCS\_CON-V5\_1-20150526-C.
- [6] CCSA. 2015. TC11-WG3-2014-073- Test Specification for RCS Device—Draft V2 (20150603).

# Research on Shanghai ecological residence green ecological technology

Ming Gao

*School of Civil Engineering and Architecture, Southwest University of Science and Technology, Sichuan, China*

**ABSTRACT:** This paper takes “Shanghai ecological residence” in the Best City Practices Area of the 2010 Shanghai World Expo as an example. It provides an analysis summary of ecological low-technology strategy from folk houses and the integrated use of “wind, light, shadow, green, and waste”, the five types of “ecological” elements integration design on structure and technology. This technology is of low cost, easy to implement, and its marketing development is conformed to the national conditions.

**Keywords:** green residence; ecological low-technology strategy

## 1 INTRODUCTION

With the rapid development of China’s economy, energy consumption has shown a rapid growth trend, and more than 90% of the buildings are high-energy buildings in China. According to the energy efficiency standards established by the Ministry of Construction, by the end of 2000, only 5% of the buildings achieved energy efficiency standards. In the early 2005, this figure rose to 15–20%, still being low. Faced with such a huge amount of high-energy consumers, how to use new technological means to reduce building energy consumption has become the focus of architectural design field. And how to set up building energy-efficient policy has become an urgent need in China.

“Shanghai ecological residence” as green residence experience pavilion in the 2010 Shanghai World Expo China City Practices Area based on the geographical, cultural, and climatic characteristics derives Jiangnan residential architectural elements, alley, Patio, Shikumen, dormers, and gables, and other traditional cultures and ecological methods. It includes natural light, cross-ventilation, courtyard green plant, shading, and other functions, given a new ecological connotation and fully embodies the adjusting measures to differing conditions, ecological construction concepts, and sustainable development of green innovative ideas.

## 2 PROJECT PROFILE

The project is located in the northern blocks of Puxi Region of the Urban Best Practices Area in 2010 Shanghai World Expo Park, site select waste plant. It is concentrated in residential, commercial, and office buildings as main function, including

more than a dozen real cases of different countries, with common analog block of life. It reflects the “Urban Environment with Science and Technology Innovation”, which has brought a better urban life (Figure 1). Above the entrance plaza residential groups at the North Square, there is a brick white wall with characteristics of the Jiangnan residential four-storey building, which represents the Shanghai Real case “Shanghai ecological residence” (Figure 2).

“Shanghai ecological residence” covers an area of 1300 m<sup>2</sup>, and has a construction area of 3020 m<sup>2</sup>, with four layers on the ground and one layer under the ground. Its roof construction height is 18.9 m during the Shanghai World Expo, and has “zero carbon pavilion” from London, “bamboo pavilion” from Madrid, and other cases constitute living groups, all of which will be converted into permanent work groups after the Expo.

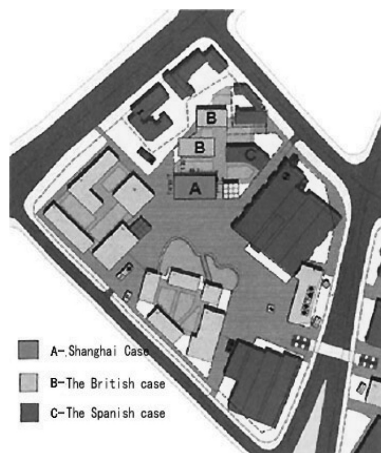


Figure 1. “Shanghai ecological residence” location.



Figure 2. “Shanghai ecological residence” reality images.

### 3 GREEN ECOLOGY TECHNOLOGY

#### 3.1 Wind power utilization

##### 3.1.1 Natural ventilation

The arrangement of building masses as north–south strips is to meet the summer monsoon direction of Shanghai, and design multi-channel through air duct. The bottom layer has an empty waiting area leading to traditional alley space and angularly formed wind wall. The north side of the building implants “eco Atrium” to form a vertical pull air duct, surrounding the arranged planting module to purify air. Underground space through north–south water features and courtyards forms an air duct. Facade doors and windows are designed with ventilation features to fit various weather conditions. The first floor south facade has the design of a wind sash. North of the interior design, “eco Atrium”, forms the hot-pressing air duct of natural ventilation. The roof is designed as an open-and-close type, which can be controlled according to the external climatic conditions (Figure 3).

##### 3.1.2 Eco Atrium

“Eco Atrium”, in accordance with the direction of rotation of the airflow, makes the module planting area to enhance air movement trend and purify indoor air. The two sides of the eco Atrium have potential energy recycle elevator and variable speed elevator with vertical motion to save energy and activate air movement.

To enhance the driving of the top of the air flow in the atrium, the side higher than the roof is designed with a window joint control by machinery from the roof vertical-axis silent wind power generation system and the wind turbine to increase natural ventilation efficiency. The roof can be controlled according to the external climatic conditions by opening and closing. North of the “eco Atrium”

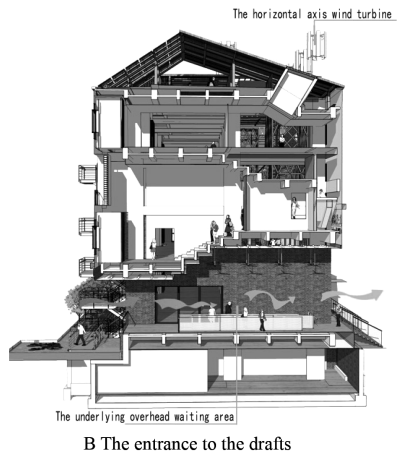
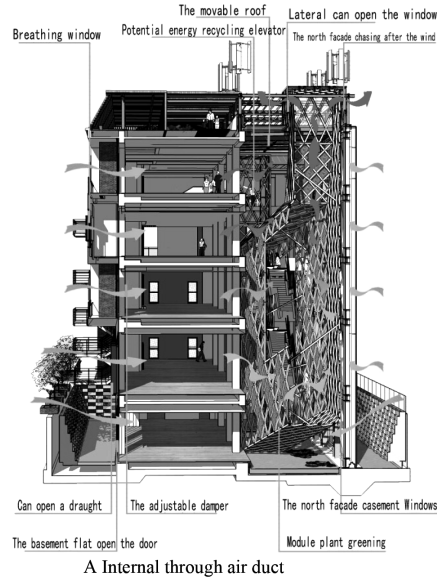


Figure 3. Analysis of natural ventilation of “Shanghai ecological residence”.

has six “wind catchers” and interactions with north adjustable vents of lower face to increase the “eco Atrium” delivery volume (Figure 4).

#### 3.2 Light utilization

The use of modern architectural language in the traditional Shanghai house ecological approach can improve lighting. Through intelligent control systems, integrated shading systems, and artificial lighting, sunlight can be utilized to provide most of the interior lighting. North and south sides of the sink court side, supplemented with the landscape pond surface-reflected light, improve the lighting



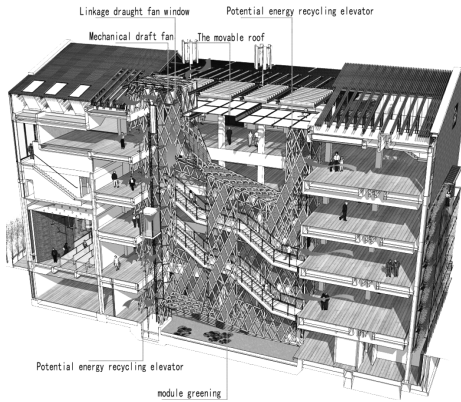


Figure 4. “Ecological atrium” ventilation effect.

of the underground region. Both building exterior floodlighting and indoor public lighting adopt LED lighting technology, which is highly efficient, energy-saving, and long-lasting. Southern sloping roof set BIPV amorphous silicon thin-film photovoltaic systems and solar hot water flat collector system with the role of rooftop garden awnings offer architectural lighting electricity and hot water, respectively.

### 3.2.1 Natural light

The following features of the building improve indoor natural lighting effects and underground space illumination: north-south layout; reasonable building depth and window-wall ratio; knowledge from Shanghai traditional houses translucent atrium, dormer windows, skylights, and other natural lighting techniques; setting lighting atrium in the middle of the north side of the building from the basement to the fourth floor with height and area of about 22 m and 120 square meters, respectively; passing of natural light through the skylight and glass curtain wall on the north side into the room; setting the south side of the building with ground subsidence waterscape courtyard at a depth of 4.5 m; and high surface reflectivity facilitating the reflection of natural light to the interior ceiling. The south facade increases transparent window area and direct entry of sunlight (Figure 5).

### 3.2.2 Solar energy utilization

Southward sloping roof and balcony combining thin-film photovoltaic solar panels has good geographical applicability, and is convenient for building integrated design, installation, and commissioning with a conversion of 8.5%. Furthermore, it integrates solar water heating system.

### 3.2.3 LED energy saving

The use of different colors illuminates the walls with different materials and emphasizes the massing sense of the facade. Large constructions that do

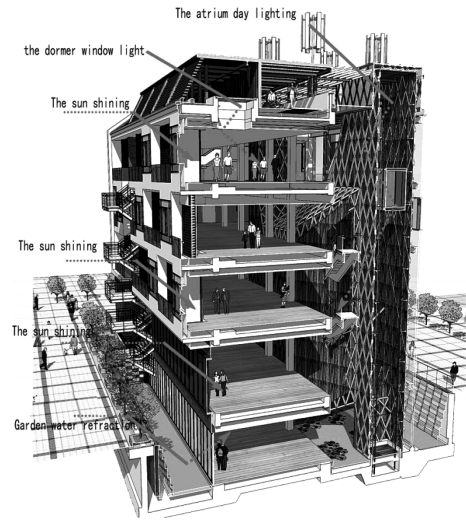


Figure 5. “Shanghai ecological residence” natural lighting analysis.

not affect residents and have sufficient brightness at night attract people. Simple appearance of exhibition buildings and bright interior courtyard and interior space reflected through the grid, indoor, and outdoor formation of “opposite scenery” improve the attractiveness and intimacy of the building. Important features of the building such as deepening porch, entrance, and grill top positions deepen processing and attention and improve construction quality.

### 3.3 Shading technology

South facade latticed windows and recessed balconies are well proportioned, and self-shading effect of the building is obvious. Ground floor entrance waiting area is empty, forming a large shaded area to address the sunstroke problem of the waiting crowd. Planted tank, combined with polycarbonate visor, of the western wall design green vines constitute double-shading system. South outwardly windows have center sunshade and roof-mounted shutters to flexibly change the angle and maintain a reasonable indoor illumination.

Roof lighting Atrium design of external blinds consists of an electric shutter; scattered south facade balcony, facilitating self-shading; adjustable doors and windows in the south at specific locations in the home using electric sunshade; west facade planting cavity design; the outer perforated design polycarbonate visor; the cavity layer design planting trough; west facade double-shading systems; and east facade design recycling the old brick wall empty bucket respiratory system.

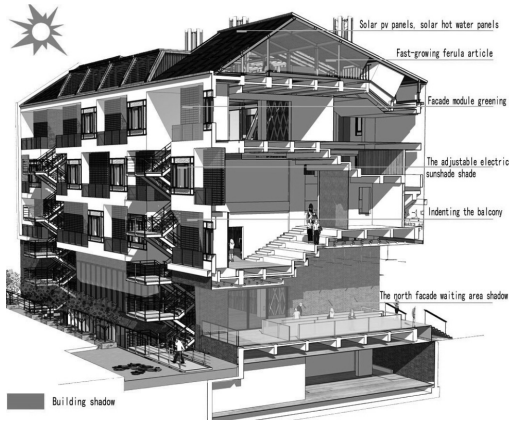


Figure 6. Building self-shading analysis.

Roof architectural form is regular. South facade latticed windows and recessed balconies are well proportioned, and the self-shading effect of the building is remarkable. Ground floor entrance waiting area is empty, forming a large shaded area to address the sunstroke problem of the waiting crowd (Figure 6).

### 3.4 Greening technology

Greening species select native plants that fit Shanghai soil conditions, planting with lightweight nutritive soil. Constituting the facade shading and environmental cleanup, the whole assembly outside and inside “eco Atrium” forms a comprehensive greening system.

Relying on the “eco Atrium” grid structure, the south facade wall is a built-up module, the west facade planting vines, and the roof module assembly is a planted roof garden. After collecting rainwater in the roof landscape pool, the ecological floating bed system is planted in the filtration water to improve water quality. It not only facilitates landscaping, but also enhances the performance of building insulation. In addition to conventional landscaping, planting purifies water and improves the design of ecological floating bed system. The atrium space grid is combined, and a duplex unit modular green land is designed according to the airflow analysis result.

### 3.5 Waste technology

Although advocacy saving utilizes old building material, comprehensive utilization of urban solid waste changes “waste” to treasure.

With about 150,000 Shikumen-style building facade with “breathing wall”, stair stepping, rainwater recycling ponds, and other landscape, demolition of the old plant re-welding recycled steel is processed

into “eco Atrium” and steel stairs. The main structure of construction adopts high-performance recycled aggregate concrete, using slag powder, fly ash, and other industrial wastes instead of cement, with the old concrete replacing gravel as the concrete aggregate wall materials using Yangtze River silt hollow bricks and fly ash to build blocks, and inorganic insulation mortar and gypsum composite thermal insulation systems to build interior partition wall using all waste materials and renewable materials, such as autoclaved sand-lime brick, gypsum lightweight partition board, and concrete blocks. Construction waste after screening compaction is directly used as a under layer. Fast-growing bamboo is used in the southern region to replace wood products, because of its less impact and damage on the environment as well as recycling properties.

## 4 CONCLUSION

“Shanghai ecological residence” combines environmental protection and historical and cultural protection to achieve dual conduction of local cultural value of information and ecological technology, showing the warm summer and cold winter urban areas of developing countries, ecological technology, and development trends of green ecological residential development concept. China will face enormous quantity of energy-saving targets on Old Town transformation of 230 million m<sup>2</sup> of existing residential ownership. “Shanghai ecological residence” provides great inspiration and practice experience for its transformation.

## PROJECT SOURCE

Key Research Base of Humanities and Social Sciences of Sichuan Provincial Department of Education—Topic in the 2015 of Sichuan Circular Economy Research Center, project number: XHJJ-1516.

## REFERENCES

- [1] Fan Yifei, Cao Jiaming, urban green house—Shanghai ecological residence [J] *Building Technology*, 2010 (8), 29–32.
- [2] Fan Yifei, natural way—Interpretation of Shanghai ecological residence [J] *building skills*, 2010 (9), 60–67.
- [3] Han Jihong, Wang Wei, Zhang Ying. China 2010 Shanghai World Expo Urban Best Practices Area of “Shanghai ecological residence” [J]. *Green Building*, 2010 (5), 61–66.
- [4] Han Jihong, Wang Wei, Zhang Ying smart ecological housing.—Shanghai ecological residence [J] *Construction Science and Technology*, 2010 (5), 75–79.

## Study on the modern dilemma of the Chinese traditional literati painting

Zi-han Zhang

*Hebei Academy of Fine Arts, Shijiazhuang, Hebei, China*

**ABSTRACT:** The Chinese traditional literati painting is a kind of unique art system originated in ancient China, which is mainly composed of the literati. This kind of art provides a large number of extraordinary works for the mankind in its long development process. However, in the recent years, it has gradually declined because of the disappearance of the literati class, the pause of the theory research, and the rapid change of the social ideology. In the current historical conditions, the traditional Chinese literati painting should face more challenges and innovate in all directions to revive and develop.

**Keywords:** The Chinese traditional literati painting; the art form; the art development

### 1 FORMATION OF THE TRADITIONAL LITERATI PAINTING

As a kind of independent system art style, the literati painting was introduced in the Northern Song Dynasty. In the middle of the Northern Song Dynasty, a group of literati began to treat the form and spirit and the form and meanings in a different way. Su Shi explicitly put forward the concept of “literati painting”. He fully illuminated the theory of literati painting, which played a decisive role in the formation of the literati painting system. He strongly encouraged the combination of poetry and paintings and advocated the concept of “one body of the poetry and the painting”, which became one of the basic characteristics of the literati paintings.

In the Yuan Dynasty, because of the cancellation of the imperial examination system, the top elite status of the literati suddenly slid and a large number of literati expressed their emotions by calligraphy and paintings. Several literati in the elite class engaged in the art creation and formed a peak of the creation and research of the literati paintings. The maturity of the literati paintings in the Yuan Dynasty was marked by the summary and perfection of three aspects: the literati painting language system, which prioritized Dong Yuan and Ju Ran and also considered Li Cheng, Guo Xi, and other masters in the Tang Dynasty, the Five dynasties, and the Northern Song Dynasty; the content system, which mainly described the Jiangnan landscape and the interest of flowers and birds and expressed poetic and personal feelings; and the aesthetic system, which pursued the pen and ink forms and emphasized the performance instead

of the recurrent interest and the combination of poem, calligraphy, painting, and seal.

In the Yuan Dynasty, four masters, Huang Gongwang, Ni Zan, Wang Meng, and Wu Zhen, promoted the literati landscape paintings to attain full mature condition. Their creation marked the literati paintings really view the creation from the values of the art itself and completely abandoned the function of the political ethics imposing upon the art, so that the truly independent mature system of the art was formed.

### 2 THE UNIQUE EXPRESSION FORM OF THE TRADITIONAL CHINESE LITERATI PAINTING

On the technique of the art, since Xie He in the Southern Dynasty put forward the theory of “using the brush in the bone method”, the brush was always at the centre of the painting and the lines became the modeling foundation of the Chinese painting. In the theory of the literati paintings, the beauty of the painting is not only to describe the nature, but also to describe the line color and the brush and ink of the painting itself. Since the Yuan Dynasty, the literati painters have begun introducing the skills of using brushes and the lines of the calligraphy into the literati paintings, and the literati painters were almost all the calligraphers. Generations of painters mostly used calligraphy in the paintings, and practiced and developed the ink painting skills, which enriched the expression forms and formed the artistic characteristics of the literati paintings. The calligraphy is the unique art form in China and constitutes the unique plane

modeling using the emotional lines. The combination of points, lines, and strokes in the calligraphy is not only the basic element to constitute the artistic image, but also the important appreciative object with independent aesthetic value.

In the Yuan Dynasty, when the literati paintings rose, they attracted much interest of the literati and became a kind of comprehensive platform, which could exhibit the talent of the authors. Besides implying the meanings by drawing the objects, the literati also wrote poetry on the paintings to explain the artistic inspiration and express their emotions. Some painters simply wrote some words or postscripts to express their thoughts. The inscription can explain the intention of the authors or express their feelings as well as show their calligraphy level at the same time. After the inscription, the author often needed to stamp on the paintings. As a kind of unique traditional Chinese literati art, the seals have the effect of signature on the picture. However, it is important that the seals themselves also become the important composition factors, because they can flexibly choose the stamped place and there are various types and styles of seals. On an integrated literati painting, the poetry, calligraphy, painting, and seal supplement each other as well as mark the high improvement of the expression forms of the literati paintings.

### 3 REVIEWING THE TRADITIONAL LITERATI PAINTING IN THE CONTEXT OF THE CONTEMPORARY CULTURE

In today's society, the traditional Chinese literati arts still exist in form, and even fairly attract much attention in some aspects. However, overall, the style, form, and the theory of the traditional literati art had larger disconnection with the society. For example, in the aspect of industrial and architectural design, the applied art and life aesthetics, the theory supply, and the support and guidance of the style and technology of the traditional literati art are becoming decreasingly small.

Today, we can say that the traditional Chinese literati art exists sequentially and continues to play a role in some ways only with the powerful inertia, which is caused by the long history and complex system. However, we should clearly recognize that the continued development of the traditional literati art and its cultural tradition has begun to come apart and the participation and influence of the traditional literati art for the social life decreases every day. In 100 years of social change in China, the development of the traditional Chinese literati art cannot keep up with the process of modernization like other aspects, so it sadly developed into a relatively closed and entertaining circle. Because of this, the influence of the traditional Chinese

literati art on the society decreased gradually and it became increasingly distant with the life of the ordinary people.

The weakness of the traditional literati art in the modern society is a complex process. It not only reflects in the decline from the dominant position and exit from the social mainstream life stage, but also in the decline of the theoretical research. The Chinese traditional literati art is based on the Chinese traditional philosophy and the global view. Compared with the Western philosophy, the Chinese traditional philosophy is a completely different system that is very different in the starting point, methods, and forms. On the basis of this, the traditional literati art naturally presents a completely different characterization with the Western art in the theory, the forms, and the methods.

The theoretical basis is the foothold of an art form. Since the modern times, although the traditional literati art has explored and moved forward in technology, it is almost entirely in pause in the theory research. The pause refers to the pause of the research, which is based on the Chinese traditional theoretical method and the starting point of the philosophy. Similarly to the Chinese traditional literati art, the ancient Chinese philosophy system is a kind of special and complex existence. The ancient Chinese philosophy and its theory method habitually use the intuitive and perceptual way and mostly use the suppositional and analogical method. This method may not be enough "scientific", but it is very suitable in the research of the art theory. Furthermore, in the development of the Chinese art history, under the guidance of this method, numerous masterpieces have appeared and continued to provide one after another new fulcrum for the traditional literati artistic development in the development process of the thousands of years.

After entering the modern times, because of the national needs, the Chinese society quickly accepted the Western philosophy and science system and explained all problems with the Western philosophy and scientific method in more than a century. So the traditional Chinese philosophy method was largely forgotten. The reflection in the art is that the research methods of the traditional art theory were completely given up, and the Chinese traditional philosophy stopped to supply blood to the art. The direct consequence caused by the ischemia in theory is the technical pause.

The society has entered the information age, and the renewal speed of the art is unprecedented. In this aspect, the modern art style from the Western society certainly has much more superior characteristics than the traditional literati art, such as flexibility, diversity, development with age, and good at using the new media and communication methods. In this case, the means, methods, style,

technology, and even the ideas of the traditional literati art undoubtedly fall behind the Western art in the entire range. How to catch up the West is the first big problem faced by the traditional literati art. Even without external pressure, according to the development logic of the art itself, the Chinese traditional literati art also has reached the point where it must change after 1,000 years. When the theoretical source has dried up and the technical means have been exhausted, and if the traditional literati art does not take the initiative to change, only death awaits it.

#### 4 RESUMPTION AND FUSION

As mentioned above, an important feature of the traditional literati art is closeness, which forms the good qualities of the traditional literati art. For example, it is good at introspecting and paying attention to feelings, and it also has the qualities of intuition and sensibility. However, this closeness in the new era has become a fatal weakness of the traditional literati art. In today's society which faces the huge transformation, because of the disappearance of the literati class, the huge change of the society, and the complete change of the art survival mode, the only way for the traditional literati art to survive is to take the initiative to adapt the change and envisage the social needs.

During the period of the social transition, the Chinese culture changes rapidly, so how should we treat the literati art? In allusion to the alienation and anomie phenomenon, which is caused by the modern transformation hysteresis of the current literati art, how to realize the roles change of the modern literati art and how to globalize the literati art and realize the internationalization development of the literary art?

Under the condition of the new era, because of the disappearance of the literati class, an issue immediately faced by the literati art is that the author is no longer equal to the reader. The former literati gathering will no longer exist, or at least no longer as the main platform of the works published. The publishing of the literary works will have to enter the public exhibition space and face the people who have entirely different culture background, artistic accomplishment, and aesthetic orientation. The modern audiences are not possible to enjoy the works as the original scholar-officials, and the closeness of the literati paintings will inevitably be completely broken. In such conditions, if we continue to maintain the aesthetic characteristics of the literati paintings, such as introspection and restraint and closeness to the personal feelings and experiences, we need to revolutionize on the style and the technique of the works.

Is it possible in the technology? In addition to the traditional style, such as the new literati paintings that are created by the new literati painting faction represented by Zhu Xinjian and Zhou Jingxin, we can also see some possible directions through the efforts of some avant-garde artists in recent years. Lu Shengzhong used the folk paper-cut as the creation factor and created many devices and behavior art works. For the Great Wall and the Chinese characters as his source of the inspiration and main expression object, Xu Bing created a series of works, such as "a sealed book" and "ghost strike wall". Using the traditional Chinese garden as a subject matter, Zhan Wang created "Rockery Design" in the form of the device. Although these traditional or innovative approaches are different in style, the spirit qualities of the traditional literati art are consistent. We cannot assert that these innovations must represent the development direction of the traditional art, but their spiritual core is positive. We should insist the aesthetic taste and the spiritual quality of the traditional literati art and flexibly and proactively connect with the modern technology and modern forms. Also, we should always make the literati feelings and the aesthetic values as the purpose and not refuse to try any possibilities of the art in the form.

#### 5 CONCLUSION

The traditional art must provide the society with more aesthetic experience and materials of the art application as well as provide more ideas and methods. The traditional art must learn to adapt to the modern society in harmony.

From this point, the urgent affair of the traditional Chinese literati art now is to make itself become a new art, rather than be the opposite of the new art. While retaining its own spiritual core, it should have an omnibearing reform and face the world with a new look.

#### REFERENCES

- Lanxin Xiang. The traditional and foreign relations: The evaluation of the ideological background of China-US relations. Shanghai. Shanghai Sanlian Bookstore. 2007(5). (In Chinese).
- Wolfflin Heinrich. Artistic stylistics. China's National People's Congress press. 2004 (1).
- Wuchang Zheng. The whole history of the traditional Chinese painting. The Eastern Publishing Company. 2008(1). (In Chinese).
- Yanyuan Zhang. Notes of past famous paintings (Tang). Jinghua Press. 2000(5). (In Chinese).
- Zhirong Zhu. Research on the Chinese aesthetic. Shanghai. Shanghai Sanlian Bookstore. 2006(5). (In Chinese).



**Taylor & Francis**

Taylor & Francis Group

<http://taylorandfrancis.com>

# Reliability analysis of pre-stressed concrete continuous girder bridges using the incremental launching method on Chinese code and BS5400

C.H. Lou

Department of Bridge Engineering, Chang'an University, Xi'an, Shaanxi, China

F.H. Dong

Department of Bridge Engineering, Tongji University, Shanghai, China

**ABSTRACT:** The aim of this paper is to analyze the reliability level of pre-stressed concrete continuous girder bridges designed with the Chinese code (JTG D62-2004) and BS5400 using incremental launching method at construction stage. Typical cross-sections used in the example bridge are considered at construction stage. Load and resistance parameters are treated as random variables. The statistical parameters are based on the available literature, test data, and survey results. Reliability indices are calculated by iterations using the first-order second-moment method. The calculated results indicate that the reliability indices of JTG D62-2004 are larger than that of BS5400, which could provide references for the bridges constructed using the incremental launching method in overseas construction and competition.

**Keywords:** pre-stressed concrete; girder bridge; incremental launching construction; chinese code; BS5400; reliability

## 1 INTRODUCTION

Over the last five decades, a large number of pre-stressed concrete bridges have been built or are under construction worldwide. This rapid increase of this kind of bridges is mainly due to their excellent mechanical properties and practical advantages in construction. The incremental launching method is an important construction method, which should be considered in designing such structures. This method for bridge construction may offer advantages over conventional construction, including causing minimal disturbance to the surroundings, providing a more concentrated work area for superstructure assembly, and possibly increasing worker safety, given the improved erection environment.

It is estimated that more than 1,000 bridges worldwide have been constructed by the incremental launching method [1,6], the vast majority of which have been post-tensioned concrete box girder bridges. So far, to the best of the authors' knowledge, the reliability analysis has not been applied to the pre-stressed concrete continuous girder bridges using incremental launching method. This study focuses on analyzing the reliability indices of pre-stressed concrete continuous girder bridges designed with the Chinese code (JTG D62-2004) [2] and BS5400 [3] using incremental launching method at construction stage.

## 2 BASIC INFORMATION OF THE BRIDGE

The bridge, which is a double-parallel pre-stressed concrete post-tensioned continuous girder bridge with dimensions of  $30\text{ m} + 3 \times 40\text{ m} + 30\text{ m}$ , is constructed by incremental launching method in the highway, and its total length is 180 m. The length of the center of the side pier and the beam-ends is 0.45 m; in addition, the length of the side span is 29.55 m. The launching nose is 25 m long and the ratio of it to main span is 5/8. The geometry of girder is shown in Figure 1, in which all dimensions are in centimeters.

The bridge is calculated by the finite element procedure. The length of the side span is 29.55 m, which is rounded off to 30 m. There are 72 elements and 73 nodes in the total bridge. The length of the calculated element is 2.5 m, which includes 10 elements and 11 nodes of the launching nose

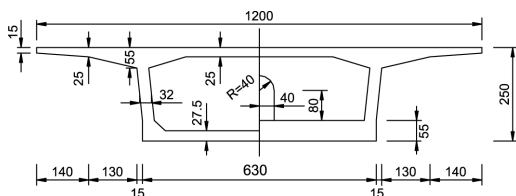


Figure 1. Girder geometry (unit: cm).

Table 1. The construction stage division.

Number of construction stage	Installing of elements	Construction illustration
1	1~14	Casting No. 1 segment-10m
2	15~16	Casting No. 2 segment-5m
3	17~20	Casting No. 3 segment-10m
17	73~76	Casting No. 17 segment-10m
18	77~78	Casting No. 18 segment-5m
19	79~82	Casting No. 19 segment-10m
20		Temperature piers removed
21	1~10 deleted	The launching nose removed
22		Second pre-stressed tendons were drawn
23		Deck pavement and attached facilities

with the length of 25 m. The numbers of nodes and elements of the launching nose are 1–11 and 1–10, respectively, and the main girders are 11–83 and 11–82, respectively. The segments of incremental launching are 10m + 5m + 15 × 10m + 5m + 10m. Table 1 indicates the construction stage division.

### 3 LOAD MODEL

The major load components for highway bridges are dead load, live load, dynamic load, environment loads (temperature, wind, earthquake), and other loads (collision, braking). In this study, only the first load and pre-stressing are considered, and the load models are based on the available statistical data, surveys, inspection reports, and analytical simulations. The load variation is described by Cumulative Distribution Function (CDF), mean value or bias factor (ratio of mean value to nominal value), and coefficient of variation.

Dead load is the gravity load due to the self-weight of structural and non-structural elements (pre-stressing force in this study) permanently connected to the bridge. Two components are considered:  $D_1$  = dead load due to cast-in-place materials (bridge girder) and  $D_2$  = dead load due to asphalt overlay. All components of the dead load are typically treated as normal random variables. The bias factor (ratio of mean value to nominal value) is  $\lambda = 1.03$ , and the coefficient of variation is  $V = 0.08$  for  $D_1$  and  $\lambda = 1.05$  and  $V = 0.10$  for  $D_2$  [4]. For asphalt-wearing surface, it is assumed that mean thickness is 80 mm.

In concrete structures, pre-stressed effects are generally considered as a force being applied to the structure. A pre-stressed force  $P(x, t)$  at a distance

Table 2. Coefficient of variation for pre-stressed losses and pre-stressed force.

Parameter	Mean value	Variation coefficient	
		$t = t_0$	$t = \infty$
Pre-stressed losses $\Delta P(x, t)$	1	0.3	0.3
Pre-stressed force $P(x, t)$	1	0.04	0.06

of  $x$  from the anchorage at time  $t$  may be expressed by the following equation [7]:

$$P(x, t) = P_0 - \Delta P(x, t), \quad (1)$$

where  $P_0$  and  $\Delta P(x, t)$  are the initial pre-stressed force and pre-stressed loss, respectively. JCSS [5] proposes that we retain the value given by the standard or regulation as a mean value for the losses, and to take the coefficients of variation presented in Table 2.

### 4 RESISTANCE MODEL

Resistance is a variable representing the load carrying capacity. The type of distribution is based on the observed shape of CDFs for presenting steel and concrete. Resistance is calculated as the product of three factors representing strength of materials, dimensions, and analysis. The stress of cross-section is considered to calculate the reliability index in the construction stage according to the codes of JTG D62-2004 and BS5400. The results shows that the stresses of all cross-sections in the bridge are compressive stresses.

According to the JTG D62-2004 code, the compressive stress  $\sigma'_{cc}$  in the construction stage must meet the following minimum requirements:

$$\sigma'_{cc} \leq 0.70 f'_{ck}, \quad (2)$$

where  $f'_{ck}$  is the standard value of the compressive strength of concrete at the center of the axis at various stages such as manufacture, transportation, and hoisting.

According to the BS5400 code, the compressive stress  $\sigma'_{cc}$  in the construction stage must meet the following minimum requirement:

$$\sigma'_{cc} \leq 0.67 f'_c, \quad (2)$$

where  $f'_c$  is the specified compressive strength of concrete for use in design.

The resistance model statistics for the codes JTG D62-2004 and BS5400 are shown in Table 3.



Table 3. The construction stage division.

Specifications	Probabilistic distribution	Compressive strength	Variation coefficient	Ref.
JTG D62-2004	Normal distribution	24.4 MPa (C50)	0.137 4	[2]
BS5400	Normal distribution	24.6 MPa (C50)	0.12	[7]

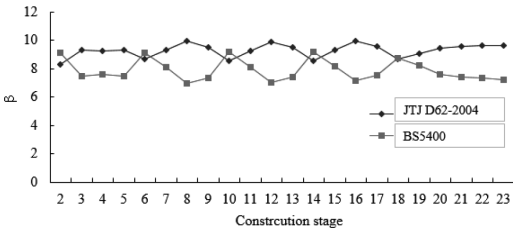


Figure 2. The upper flange reliability index of the cross-section of No. 16.

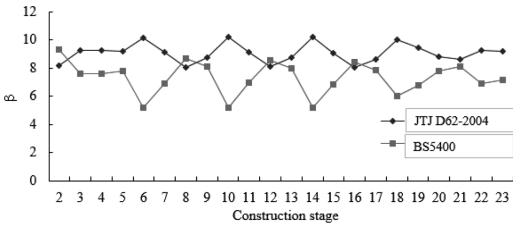


Figure 3. The bottom flange reliability index of the cross-section of No. 16.

## 5 RELIABILITY ANALYSIS

Reliability analysis is performed for pre-stressed concrete bridge girders designed according to the considered codes. The reliability index ( $\beta$ ) is defined as the function of probability of failure ( $P_F$ ):

$$\beta = -\Phi^{-1}(P_F), \quad (4)$$

where  $\Phi^{-1}$  is the inverse standard normal distribution function. An iterative procedure is used to calculate the reliability index, as described by Ming Zhang [8].

Because of the force at the construction stage of the pre-stressed concrete continuous girder bridge using incremental launching method, two cross-sections, which include the maximum moment and the minimum moment, were chosen according to the bending moment diagrams of the construction stage to calculate the reliability index.

The bending moment diagram of the cross-section in the construction stage are drawn according to the code of JTG D62-2004, from which, No. 17

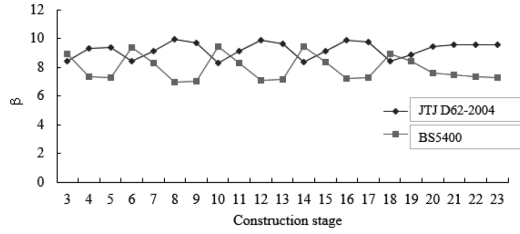


Figure 4. The upper flange reliability index of the cross-section of NO.17.

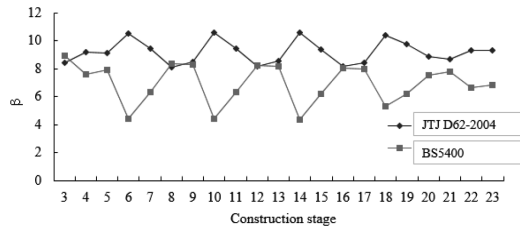


Figure 5. The bottom flange reliability index of the cross-section of No. 17.

Table 4. The average reliability of the cross-section of No. 16 in the construction stage.

Cross-section of No. 16			
Upper flange		Bottom flange	
JTG	BS5400	JTG	BS5400
9.27	8.71	9.05	8.62

Table 5. The average reliability of the cross-section of No. 17 in the construction stage.

Cross-section of No. 17			
Upper flange		Bottom flange	
JTG	BS5400	JTG	BS5400
9.22	8.82	9.18	8.78

is the minimum moment value ( $-30470.4 \text{ kN} \cdot \text{m}$ ) and No. 16 is the maximum moment value ( $18754.76 \text{ kN} \cdot \text{m}$ ). As calculation needs, the cross-sections of No. 16 and No. 17 were chosen to calculate and analyze the reliability index in the construction stage.

As for the construction stage, the reliability index of both upper and bottom flanges of cross-sections of No. 16 and No. 17 is shown in Figures 2–5 according to the codes of JTG D62-2004 and BS5400. In addition, Tables 4 and 5 show

the average reliability index of the cross-sections of No. 16 and No. 17 in the construction stage.

## 6 CONCLUSIONS

Reliability analysis is performed for pre-stressed concrete girder bridges designed using the incremental launching construction method using two codes: JTG D62-2004 and BS5400. The load and resistance parameters are treated as random variables, and the statistical parameters are taken from the available literature, test data, and survey results. Subject to the limitations of the assumptions and parameters in the study, the following conclusions can be obtained:

1. The calculated reliability indices vary considerably on the construction stage for the two considered codes.
2. At the construction stage, generally, the calculated reliability indices of the JTG D62-2004 code are larger than that of the BS5400 code.

## REFERENCES

- [1] Gohler, B. & Pearson, P. 2000. Incrementally launched bridges design and construction, Berlin: Ernst and Sohn.
- [2] The Code for Design of highway reinforced concrete and Pre-stressed concrete bridges and culverts of JTG D62-2004. Beijing: People's Communication Press. (In Chinese)
- [3] British Standard 5400. Steel concrete and composite bridges [S] 2006.
- [4] Nowak A.S. 1995. Calibration of LRFD bridge code. *J Struct Eng* 121(8):1245–1251.
- [5] JCSS, Joint Committee on Structural Safety, Probabilistic model code [S] 2001.
- [6] Li Y.H, Bao W.G, Guo X.W & Cheng X.Y. 1997. Reliability and probability limit state design of highway bridge structure. Beijing: China Communications Press. (In Chinese)
- [7] Christian, C. 2011. Structural performance probability-based assessment. Hoboken: Wiley.
- [8] Ming Z. 2009. Structure reliability analysis-method and procedures. Beijing: Science Press. (In Chinese)

## Stability analysis of underground roadways in large fault zones

Yue-feng Su, Pan Wang & Ji Zhai

*School of Civil and Environmental Engineering, University of Science and Technology Beijing, Beijing, China*

**ABSTRACT:** The geological condition in mining areas is complex, and some roadways have to be constructed in fault zones. By analyzing the engineering geological condition of a roadway in a large fault zone, we built a mechanical model to simulate the displacement and block state of rock mass around the roadway. Comprehensive support measures are designed in this model. The results of numerical simulation show that the maximum displacement of floor is in the roadway, which is about 7.3 cm; the plastic failure zone is mainly concentrated in the floor of the roadway. The existed support measure could ensure the stability of roadway, but the floor of the roadway should be a reinforced support.

**Keywords:** Underground roadway; fault; displacement; plastic zone

### 1 INTRODUCTION

Fault zones are composed of rocks in variable degrees of deformation states, often with a lower strain fracture-dominated “damage zone” surrounding a more highly strained heterogeneous “core zone” containing one or several slip zones, gouges, breccias, and oblique Riedel shears (Zoe K. Shipton 2010, D.R. Faulkner et al. 2010). Fault zones control a wide range of crustal processes and they have a controlling influence on the crust’s mechanical properties (Cox et al. 2001, Sibon 2001, Aydin et al. 2004, Seokwon et al. 2004, Zhong et al. 2008). Because of the geological structure and the complexity of the rock mass in the mining area, some roadways have to be placed in fault zones (Xun Xi et al. 2015). Engineering practice shows that when roadways are excavated in fault zones, large deformations, supporting structural damage and the whole roadway instability failure, often occur, which endangers personal safety and results in direct economic losses. There is a large fault zone in a gold mine in east of China, which is across the entire mining area, with an average thickness of about 10–25 m and a dip of nearly 90°. To ensure the stability of roadways in the large fault zone, comprehensive support measures should be taken.

Numerical simulation is an effective method to solve geotechnical engineering problems (Gong Jiwen et al. 2002). With the development of the numerical simulation method, the numerical simulation, as a tool for mechanical analysis, is often used in the numerical calculation and analysis of underground engineering construction to guide the reliable design of large underground projects

(Liu Chuanxiao et al. 2004). The paper tried to analyze the displacement and block state of rock mass around the roadways in the fault. The results of numerical simulation could be used to guide the support of roadways to ensure their stability.

### 2 ENGINEERING CONDITIONS AND DESIGN OF SIMULATION MODELS

The fault zone is located in a gold mine in the eastern part of China, which is 1500 m long in the mining area. It strikes 290°–300° with a dip of nearly 90° and an average thickness of about 10–25 m. Long-term persistence of groundwater in the fracture zone deteriorates the physical and mechanical properties of the rock and fault gouge. The mechanical properties of the broken pieces deteriorate too, which threatens the safety of mining activities.

Near the fault zone, affected by the tectonics, structural fissures are well developed. Fracture frequency is generally lower than 4 and Rock Quality Designation (RQD) value is generally higher than 75%. At the rooftop, which is far from the fault, the rock is complete, the fracture is not developed, and the RQD value is more than 75%. In the floor, which is far from the main fault, the rock is complete, the fracture is not developed, and the RQD value is more than 90%. The hardness of the rock is high, and the engineering geology conditions are very good. Depending on the construction experience, through-fault roadways need leading pre-support, U steel support, and concrete support.

Mohr–Coulomb tunnel excavation model is built using a kind of numerical software FLAC3D, which has become one of the most important tools

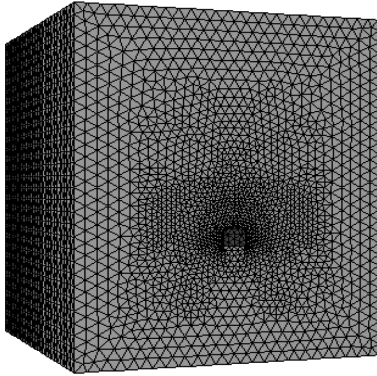


Figure 1. Numerical simulation mode.

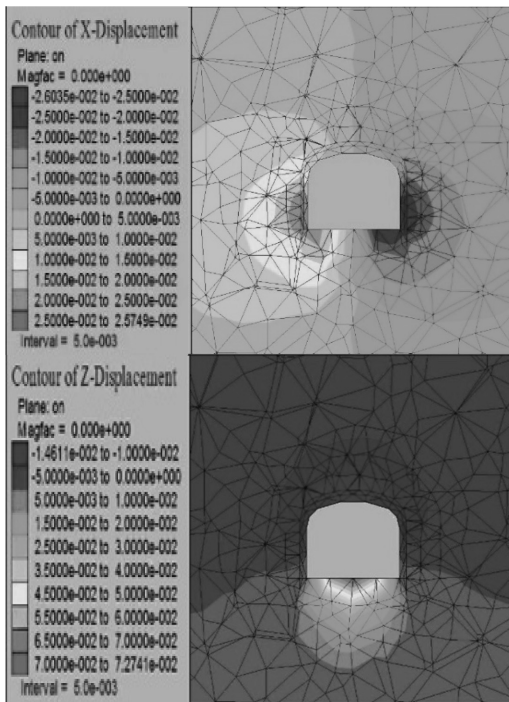


Figure 2. Contour figures of X-Displacement and Z-Displacement (in fault zones).

Table 1. Parameters of rock and fault.

Group	Density/ ( $\text{kg} \cdot \text{m}^{-3}$ )	Bulk modulus/ GPa	Shear modulus/ MPa	Internal friction angle/( $^{\circ}$ )	Cohesion/ MPa	Tensile strength/ MPa
Fault	1,707	0.221	0.113	14.6	0.0901	0.0164
Rock	1,595	2.33	1.18	28.1	33.2	5.11

in calculating rock mechanics problems since it was introduced by ITASCA Company. The Mohr–Coulomb model is suitable for analyzing the mechanical behavior of normal soil and rocks.

The numerical simulation model is 60 m high, 50 m wide, and 50 m long (Figure 2). It is divided into 2,15,345 zones and 39,203 grid-points. The shape of the roadway is a three-centered arch. The width of the fault zone is 15 m. The parameters of the fault and rock are presented in Table 1. The stress conditions in this model is as follows:  $S_{XX} = 30$  MPa,  $S_{YY} = 25$  MPa, and  $S_{ZZ} = 20$  MPa.

### 3 NUMERICAL SIMULATION AND ANALYSIS

The contour figures of displacement can reflect the stability of the roadway in the model. The lateral displacement and vertical displacement are the most important indices to analyze the effect of fault on underground roadways. So we list the figures of contour of X-displacement and Z-displacement. We divide the analyzed rock mass into fault zones and across fault zones. The width of the rock mass in fault zones is 15 m.

The displacement of the roof, floor, and two sides of the excavation roadway is obtained by simulation. The contour figures of the displacement of roadway in fault zones and across fault zones are shown in Figures 2 and 3, respectively. The midpoint displacement of the roof of the roadway across the fault zones is about 6.7 mm, and the displacement of the middle point of the left- and right-hand sides of the roadway across the fault zones is not more than 8.7 mm. In the fault zones, the displacement volume is increased, but due to the leading anchor support, log cushion, U-shaped steel frame, and the role of concrete, the roof and two sides of the roadway had been effectively controlled, and the maximum displacement within the fault area is no more than 2.3 cm.

The largest displacement of rock mass around the roadway occurred on the floor, and the maximum displacement is nearly 7.3 cm. The reasons are as follows: During the excavation of the tunnel, the stress released is borne only by the floor, thereby causing a large displacement on it. Therefore, in the process of roadway excavation, more

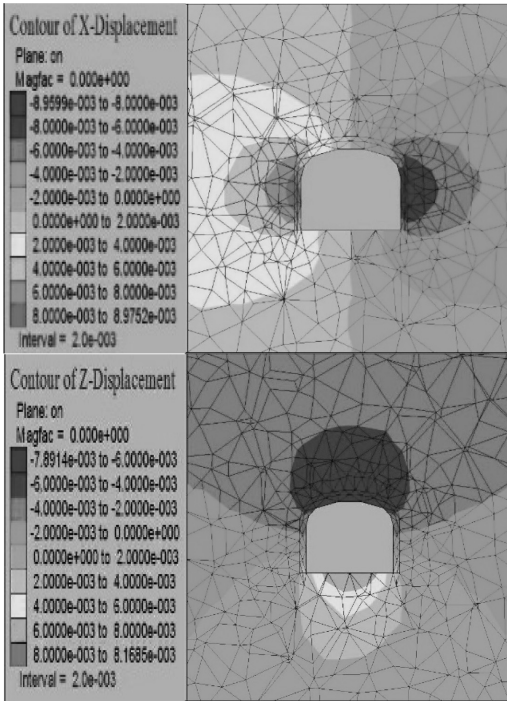


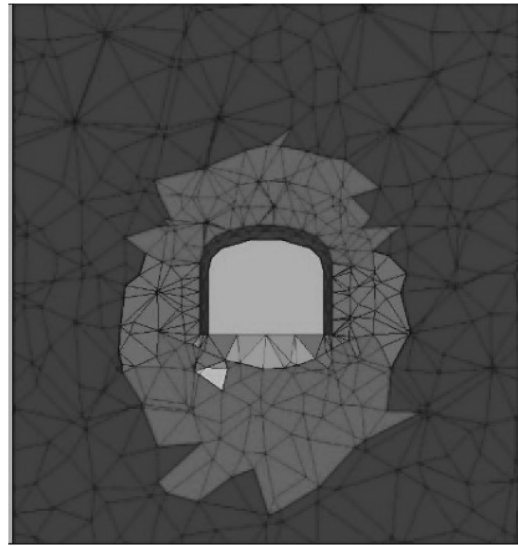
Figure 3. Contour figures of X-Displacement and Z-Displacement (across fault zones).

attention should be paid to the floor displacement, and appropriate support measures should be taken in the easily damaged and large deformation zone. Closed-loop support can enhance the integrity of the supporting system.

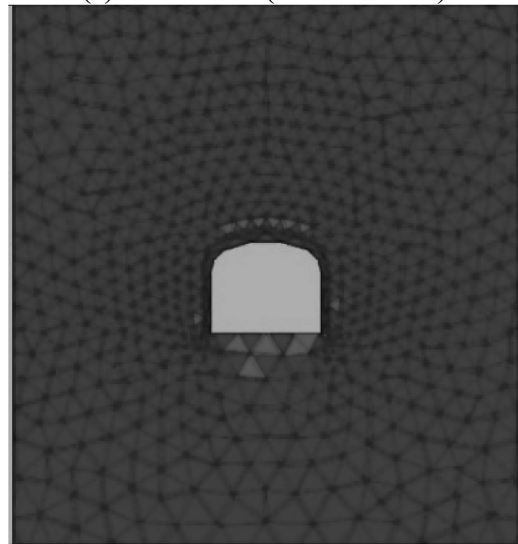
The block state of the rock mass around the roadway in fault zones and across fault zones is depicted in Figure 4.

From the distribution figure of the plastic damage area, we can find that the supporting system using leading anchor and U-shaped steel frame as main supports can play a more reliable supporting role when the surrounding rock mass failure occurs. The plastic damage zone of the roadway in roof and two sides is controlled in a reasonable range. The plastic failure zone is mainly concentrated in the position of the floor.

Through the results of the numerical simulation analysis of roadway excavation process, we can find that when the roadway uses advanced support anchor, U-shaped steel frame, and concrete as supporting system, the leading anchor laid embedded in the surrounding rock body and formed a structure similar to the shell by linking the surrounding rock. In the process of roadway excavation, anchor will bear most of the load, thereby playing an important role in supporting the surrounding rock.



(a) Block state (in fault zones)



(b) Block state (across fault zones)

Figure 4. Block state of rock mass around roadway.

#### 4 CONCLUSIONS

The roadway is in the deep area of mine roadway, and under high *in situ* stress condition, the hydrogeological conditions are more complex. The stability of roadway in fault zones plays a key role in the mining process. By numerical simulations of roadway excavation in a large fault zone and analyzing the displacement and block state of roadway, some conclusions were obtained:

1. Because of the leading anchor support, log cushion, U-shaped steel frame, and concrete role, roof and two sides of the roadway had been effectively controlled, and the maximum displacement within the fault area was no more than 2.3 cm.
2. The maximum displacement of rock mass around the roadway occurred on the floor, which is nearly 7.3 cm. More attention should be paid to the floor displacement, and appropriate support measures should be taken in the easily damaged and large deformation zone.
3. The supporting system using leading anchor support and U-shaped steel frame as main supports can play a more reliable supporting role when the surrounding rock mass failure occurs. The plastic damage zone of roadway in roof and two sides is controlled in a reasonable range. The plastic failure zone is mainly located on the floor.

## REFERENCES

- Aydin A., A. Ozbek., I. Cobanoglu. 2004. Tunneling in difficult ground: a case study from Dranaz tunnel, Sinop, Turkey. *Engineering Geology* 74(3–4): 293–301.
- Cox, S.F. et al. 2001. Principles of structural control on permeability and fluid flow in hydrothermal systems. *Reviews in Economic Geology* 14, 1–24.
- Faulkner D.R. et al. 2010. A review of recent developments concerning the structure, mechanics and fluid flow properties of fault zones. *Journal of Structural Geology* 32(11): 1557–1575.
- Gong Jiwen et al. 2002. Flac method for numerical modeling and its geological application. *Geotectonic et Metallogenia* 26(3): 321–325.
- Liu Chuanxiao et al. 2004. Numerical simulation on fractured zone of roadway in high stress area by 3dec and its gpr verification in site. *Chinese Journal of Rock Mechanics and Engineering* 23 (14): 2413–2416 (In Chinese).
- Seokwon Jeon et al. 2004. Effect of a fault and weak plane on the stability of a tunnel in rock—a scaled model test and numerical analysis. *International Journal of Rock Mechanics & Mining Sciences* 41(S1): 486.
- Xun Xi et al. 2015. Comprehensive monitoring and stability assessment of roadway with water gushing in a fault zone. *Electronic Journal of Geotechnical Engineering* 20 (9): 9685–9700.
- Zhong Nong et al. 2008. Geological guarantee and construction controlling technique of main roadway crossing fault zone with 435 m fall. *Chinese Journal of Rock Mechanics and Engineering* 27 (Supp.1): 3292–3297 (In Chinese).
- Zoe K. Shipton. 2010. Fault zones: A complex issue. *Journal of Structural Geology* 32(11): 1554–1556.

## Effect of sputtering time on the micro-hardness of QC-10 alloy

Ming Hu, Xiao-xue Ren, Yun-long Zhang, Jing Gao & Pei-ling Ding

College of Materials Science and Engineering, Jiamusi University, P.R. China  
Institute of Applied Materials and Technology, Jiamusi University, P.R. China

**ABSTRACT:** The Ti/TiN/CrN coatings were fabricated on the QC-10 surface by magnetron sputtering technology. The effect of thickness of Ti/TiN/CrN coatings on the microstructure and hardness of QC-10 alloy was studied. The results showed that Ti/TiN/CrN coatings were sputtered as modified layer on the QC-10 surface. The thickness of Ti/TiN/CrN coatings and the micro-hardness of QC-10 alloy increased with the increase of magnetron sputtering time. Simultaneously, appropriate thickness of CrN coatings was necessary for QC-10/Ti/TiN/CrN composites to facilitate tribology application.

**Keywords:** Magnetron sputtering; Ti/TiN/CrN coatings; QC-10 alloy

### 1 INTRODUCTION

Recently, surface treatment techniques have been developed for Al alloy and the coatings deposited by magnetron sputtering have distinct predominance because of the better adhesive and mechanical properties<sup>[1,2]</sup>. Nitride coatings can provide better protection because of their better mechanical properties and high corrosion resistance. The fundamental factors affecting deposition were deposition process parameters, surface crystallographic structure, and substrate surface roughness. The basic parameters of the technique included deposition temperature, gas pressure, and incidence angle of deposition flux<sup>[3-4]</sup>. The mechanical properties of CrN<sub>x</sub> coatings have been investigated since the 1980s, and Cr<sub>2</sub>N showed predominantly higher hardness and CrN exhibited better oxidation resistance and lower friction coefficient. However, reports on surface coatings of QC-10 alloy are scarce. In this study, Ti/TiN/CrN coatings were fabricated by magnetron sputtering and the effect of thickness of Ti/TiN/CrN coatings on microstructure and hardness of QC-10 alloy was investigated. The effects of sputtering time on the cross-section morphology evolution were discussed.

### 2 EXPERIMENTAL PROCESS AND CHARACTERIZATION

The CrN coatings were sputtered on QC-10/Ti/TiN by magnetron sputtering system. The vacuum system with internal dimensions of  $\Phi 450 \text{ mm} \times 300 \text{ mm}$  was a single wall of stainless steel cylinder, and cape hood could be elevated by

lifting arm. A 2 kW direct current and 2 kW direct current bias voltage supply power. A FP93-type heating source was used to control work piece temperature. A round planner magnetron with a size of  $\Phi 60 \text{ mm}$  was water-cooled and used to create the deposition gas phase. The sample holder fixed on cape hood faces the magnetron and substrate-to-target distance. First, the QC-10 alloy was machined and polished, and then specimens were fixed in a specimen holder after being ultrasonically cleaned in acetone for 10 min. Before deposition, the chamber base pressure was pumped to  $3.0 \times 10^{-4} \text{ Pa}$ , and then the interface of QC-10 was pre-sputtered and cleaned for about 20 min at minimum current after inputting Ar. To increase the adhesion force, a metallic Ti adhesive layer with thickness of about 120 nm was deposited prior to deposition of CrN coatings. The CrN coatings were deposited in an atmospheric mixture of Ar and N<sub>2</sub> using a metal Cr target with a purity of 99.95%. Subsequently, N<sub>2</sub> was inputted with different time. The distance between the substrate and target was 40 mm. The phase structure was investigated by X-ray diffraction. The morphology of QC-10/Ti/TiN/CrN was observed by an scanning electron microscope (SEM, JMS-6360 LV, Japan).

### 3 RESULTS AND DISCUSSION

#### 3.1 XRD pattern of Ti/TiN/CrN coating

Fig. 1 showed X-Ray Diffraction (XRD) patterns of the QC-10 alloy and sputtering specimens with different sputtering times. For the QC-10 alloy, Al phase was the main crystal phase. After magnetron sputtering, the diffraction peak of Al phase

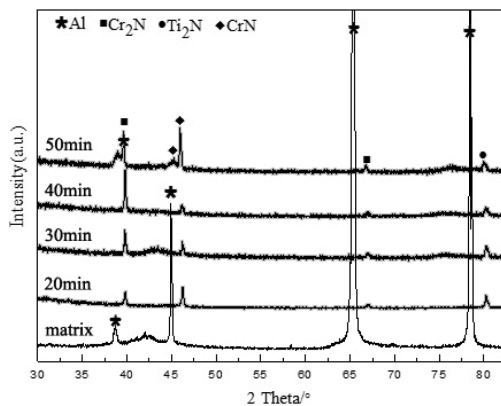


Figure 1. XRD pattern of Ti/TiN/CrN coating under different sputtering times.

disappears while that of the CrN phase became stronger with the increase of sputtering time. At the same time, Cr<sub>2</sub>N and Ti<sub>2</sub>N phases can be detected in X-ray diffraction pattern at sputtering time shorter than 30 min. This was the possible reason for the formation of thermodynamically unstable Cr<sub>2</sub>N and Ti<sub>2</sub>N phases in the early stages of sputtering CrN coating. During next reaction, N<sub>2</sub> would react with Ti and Cr layer to form thicker CrN coatings with prolonged sputtering time. The results were similar to those obtained for Mg alloy<sup>[5]</sup>. A transitional layer was formed between Cr and CrN layers, which explained the facts that chemical bond affected the out-plane growth and diffusion was sufficient to overcome the self-shadowing effect.

### 3.2 Morphology of QC-10/Ti/TiN/CrN coating

The cross-section morphologies of QC-10/Ti/TiN/CrN composites under different sputtering times are shown in Fig. 2. Ti/TiN/CrN coatings are more uniform and compact even under different sputtering times. When sputtering time was shorter than 40 min, the Ti/TiN/CrN coatings became thinner, which proves the relationship between QC-10 substrate and Ti/TiN/CrN coatings. Mutual diffusion had occurred between Ti/TiN/CrN coating and QC-10 substrate. The effect of magnetron sputtering time on the thickness of CrN coatings on the QC-10/Ti/TiN composites was also investigated. When sputtering time was 20 min, the thickness of the CrN coatings was about 1.8 μm, which increases gradually with extended time. When sputtering time was 50 min, the thickness of CrN coatings was about 5.2 μm. The evolution trend of coating thickness and micro-hardness depended on sputtering time.

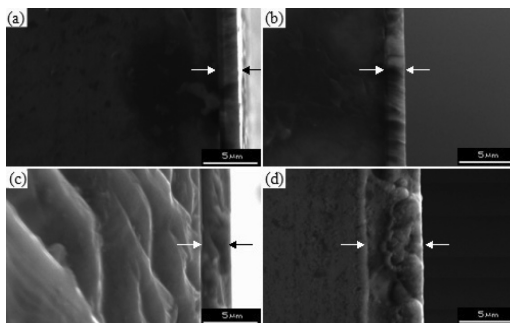


Figure 2. Section of Ti/TiN/CrN coating with different sputtering times.

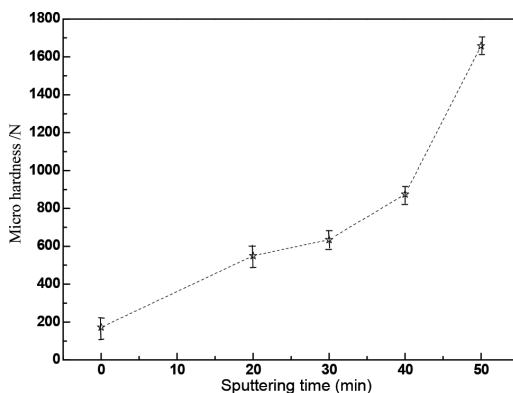


Figure 3. The curve of micro-hardness versus sputtering time of Ti/TiN/CrN coating.

### 3.3 Micro-hardness and scratch morphology analysis

The relative curve of micro-hardness versus sputtering time of Ti/TiN/CrN coating is given in Fig. 3. The QC-10/Ti/TiN composites had been fabricated by the magnetron sputtering treatment. We put emphasis on the effect of magnetron sputtering time on Ti/TiN/CrN coating. The microhardness value of QC-10/Ti/TiN composite increased gradually with prolonged sputtering time. It is important to note that bearing capacity was decided by the synergistic effect of Ti/TiN/CrN coatings, matrices of the composite, and the integrated state of the interface.

The scratch morphology of Ti/TiN/CrN coating on the QC-10/Ti/TiN surface coating composites is shown in Fig. 4, in which panels (a), (b), (c), and (d) represent scratch morphologies under different sputtering times of 2, 30, 40, and 50 min, respectively. Ti/TiN/CrN coatings began to fall off the QC-10 surface with the increased application of dynamic loads. During the application of dynamic



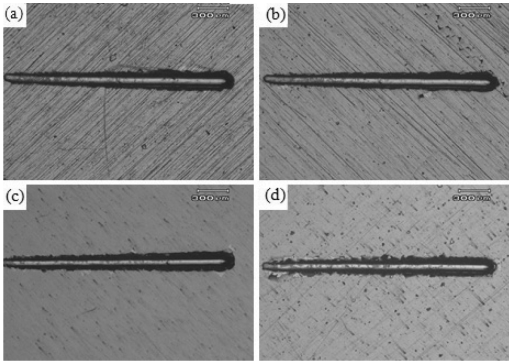


Figure 4. Scratch morphology of CrN coating on QC-10/Ti/TiN under different sputtering times.

loads, falls-off phenomenon of large-area coating did not occur. This proved that better interface bonding state condition existed between QC-10 alloy and Ti/TiN/CrN coatings. When sputtering time was increased beyond 50 min, the thickness of CrN coatings became larger, so interface bond force became weaker than that in the sputtering time of 40 min. Therefore, appropriate thickness of CrN coatings was necessary for QC-10/Ti/TiN/CrN composites to facilitate tribology application.

#### 4 CONCLUSION

The magnetron sputtering technology was used to fabricate Ti/TiN/CrN coatings on the surface of QC-10 alloy. The effect of magnetron sputtering time on Ti/TiN/CrN coating thickness and

micro-hardness of QC-10 alloy was investigated. The thickness and micro-hardness of Ti/TiN/CrN coatings increased with prolonged magnetron sputtering time. A transitional layer can be formed between Ti and CrN, which proved that appropriate thickness of CrN coatings was necessary for QC-10/Ti/TiN/CrN composites to facilitate tribology application.

#### ACKNOWLEDGMENT

The authors are grateful to the support of the Science and Technology Innovation Team of Jiamusi University (No.CXTD-2013-03).

Correspondence should be addressed to Yun-Long ZHANG; ylzhdr@126.com

#### REFERENCES

- [1] P.J. Kelly, R.D. Arnell. Magnetron sputtering: a review of recent developments and applications. *Vacuum*, 2000 (56):159–172.
- [2] Geory Merges. *Injection mold manufacturing engineering*. Chemical Industry Press, 2003: 17–20.
- [3] J. Lin, Z.L. Wu, X.H. Zhang, et al. A comparative study of CrN<sub>x</sub> coatings Synthesized by dc and pulsed dc magnetron sputtering [J]. *Thin Solid Films*. 2009, Vol. 517(6): 1887–1894.
- [4] S.S. Kumari, U.T.S. Pillai, B.C. Pai. Synthesis and characterization of in-situ Al–AlN composite by nitrogen gas bubbling method [J]. *Journal of Alloys and Compounds*, 2011: 2503–2509.
- [5] Yongjing Shi, Siyuan Long, et al. Effects of N<sub>2</sub> content and thickness on CrN<sub>x</sub> coatings on Mg alloy by the planar DC reactive magnetron sputtering. *Applied Surface Science*, 2009: 6515–6524.



**Taylor & Francis**

Taylor & Francis Group

<http://taylorandfrancis.com>

## Automatic incident detection algorithm based on under-sampling for imbalanced traffic data

Miao-hua Li, Shu-yan Chen & Ye-chun Lao

*Jiangsu Key Laboratory of Urban ITS, Southeast University, Nanjing, China*

**ABSTRACT:** Traffic data are highly skewed with rare traffic incidents in the real world, while most of the existing Automatic Incident Detection (AID) algorithms suffer from many limitations because of their inability to detect incidents under imbalanced traffic data set condition. Feasible AID algorithms based on under-sampling were proposed to process the imbalanced traffic data. An improved under-sampling method based on the nearest-neighbor cleaning rule and Support Vector Machine (SVM) are combined to detect incidents. In terms of the optimization of SVM parameters, grid search method and Particle Swarm Optimization (PSO) algorithm were compared to obtain better detection performance. In addition, the effect of the number of nearest neighbors on detection performance was investigated. The I-880 data set was finally used in experiments to verify the proposed algorithms. The experimental results indicate that PSO algorithm is more competitive than grid search method for SVM parameter optimization. Moreover, the proposed AID algorithm based on under-sampling can achieve better performance.

**Keywords:** Automatic incident detection; imbalanced traffic data set; under-sampling; parameter optimization

### 1 INTRODUCTION

The rapid increase in the economy and ownership of car has resulted in the increased growth of demand of transportation system. As a result, traffic operation conditions deteriorate and traffic incidents occur in an increasing frequency. Unexpected traffic incidents, especially secondary traffic incidents usually result in undesirable traffic congestion and higher probability of severe accidents. Automatic Incident Detection (AID), as an important component of Nation's Intelligent Transportation Systems (ITS) (JEONG, Y, et al., 2011), has great significance on reducing the delays and congestion.

To date, numerous studies have been conducted on incident detection, primarily including pattern recognition, statistical technique, traffic flow model, artificial intelligence, and wavelet analysis theory (ZHANG, J, et al., 2005). Recently, application of advanced technologies to AID models has attracted much research interest, such as neural network, fuzzy theory, Support Vector Machine (SVM), partial least square regression, and decision tree learning (CHEN, S, et al., 2009; HAWAS, Y E, 2007). Although their performance is claimed to be nearly perfect, there are some critical drawbacks. First, practical traffic data cannot always meet the training requirements for these algorithms. Traffic data are highly skewed with rare traffic incidents

in the real world and traffic data are imbalanced. However, the typical classifiers such as decision tree or neural networks are designed to optimize overall accuracy without accounting for the relative distribution of each class (KOTSIANTIS, S, et al., 2006). Although different AID models have been developed for incident detection, the application of class imbalance on AID, which is suitable for imbalanced traffic data, is not common. Considering the fact that incident detection is essentially a class imbalance problem with much fewer incident cases than incident-free cases (ANGUITA, D, et al., 2003), and to overcome the defect of poor predictive accuracy over the minority one with traditional AID models (LIPITAKIS, A D, et al., 2014), this paper proposes a novel AID model to handle imbalanced traffic data.

Many solutions to the class imbalance problem have been previously proposed at both the data and algorithmic levels. Previous studies illustrated that it is an effective way to solve the class imbalance problem from data level (KOTSIANTIS, et al., 2006). An AID algorithm based on Synthetic Minority Over-Sampling Technique (SMOTE) algorithm was proposed to address the imbalanced traffic data problem (ZHENG, W, et al., 2012). SMOTE, as an over-sampling method, usually causes over-fitting problems due to the abundant useless information obtained while increasing minority class instances (CHOI, J M, 2010). Therefore, a new AID

algorithm based on under-sampling was proposed to handle the imbalanced traffic data problem. First, it is a relatively easier task to solve class imbalance through under-sampling method instead of algorithm adjustment. Second, the improved under-sampling method, which removes majority class instances in view of the nearest-neighbor cleaning rule (QUAGLINI, S, et al., 2001), can avoid missing valuable information. Moreover, the application of under-sampling can alleviate the overfitting problem caused by SVM and improve the efficiency of SVM. The proposed AID algorithm is designed to address the class imbalance problem to enhance incident detection performance and will have significantly valuable theoretical and practical applications in this field.

## 2 UNDER-SAMPLING

As the amount of traffic incident data is rarer than the large amount of normal traffic state data in the real world, an improved under-sampling method is proposed to reconstruct the training set to obtain a relatively balanced data set.

The improved under-sampling method removes majority class instances in training set referring to the idea of Edited Nearest Neighbor (ENN) algorithm developed by Wilson (WILSON, D, et al., 2000). In ENN, the instance is removed if it does not agree with the majority of its  $k$  nearest neighbors (with  $k = 3$ , typically). In contrast to ENN, the proposed under-sampling method only removes majority class instances in training set to retain all the minority class instances. The application of nearest-neighbor cleaning rule removes noisy instances as well as close border cases, leaving smoother decision boundaries. It also retains most of the internal points, which keeps it from reducing the storage requirements as much as most other reduction algorithms.

For AID (a two-class problem), the basic ideal of this under-sampling method can be described in the following way: for each sample  $x_i$  in the training set, three nearest neighbors are found. If  $x_i$  belongs to the majority class and two or three samples in its three nearest neighbors are minority classes, then  $x_i$  is removed. If  $x_i$  belongs to the minority class and two or three samples in its three nearest neighbors are majority classes, then the nearest neighbors that belong to the majority class are removed. In this paper, normal traffic state data are regarded as the majority class.

Compared to random under-sampling, the proposed under-sampling method is an improved technique, which emphasizes data cleaning more than data reduction. In random under-sampling (CATENI, S, et al., 2014), a sample is selected

randomly from the original data set. Unfortunately, it may miss some important information of the majority class and cannot take full advantage of the available information. To avoid such problems, the improved under-sampling method divides the majority class samples into "noise sample", "border sample", and "safe sample" through the means of seeking nearest neighbors, and then removes "noise sample" and "border sample". In such a way, the more the effectiveness of the information retention, the more desirable classification result is obtained.

## 3 METHODOLOGY

The objective of this study is to develop a feasible AID model for imbalanced traffic data. A new SVM-AID model based on under-sampling method was proposed owing to the fact that incident detection is essentially a class imbalance problem. The methodology mainly consists of three stages: pre-processing of traffic data, building of SVM-AID model, and decision output.

### 3.1 Data pre-processing

In order to improve the classification performance of SVM, the raw traffic data are pre-processed before being used to train the model, including traffic dataset normalization and training set reconstruction. All of the traffic data are normalized by the maximum and minimum normalization method, and then the training set is reconstructed using the improved under-sampling method.

### 3.2 SVM-AID model building

The traffic incident detection based on SVM, in fact, is the feature extraction of traffic parameters under incident and non-incident states. These extracted traffic parameters are composed of certain dimensional feature vectors and imputed into SVM for optimized calculation. Then, to get an optimized classification based on the principle of maximum interval, it is important to achieve the purpose of traffic incident detection.

This part is the core of AID algorithm, including SVM kernel function selection, parameter optimization of SVM, and model training for incident detection. Radial Basis Function (RBF) is adopted as the SVM kernel function, and grid search method and Particle Swarm Optimization (PSO) approach are compared to determine the optimal parameter combination of SVM. Thereafter, the processed training set obtained in the first stage is inputted into SVM with the optimal parameters to train the incident detection model.

### 3.3 Decision output

The SVM–AID model constructed in the second stage is used to detect traffic incidents with the test set. The statistical evaluation criteria obtained from the output of SVM–AID model are used to verify the detection performance.

To evaluate incident detection performance of the constructed SVM–AID model, some common indexes, such as Detection Rate (DR), False Alarm Rate (FAR), Mean Time To Detection (MTTD), and Classification Rate (CR), are adopted as performance measures.

In order to make a better comparison of the detection performance of different detection models, we use an integrated Performance Index (PI) that combines DR, FAR, MTTD, as well as CR. A lower PI value indicates better detection performance.

## 4 CASE STUDIES

I-880 real traffic data in California are selected in experiments to verify the performance of the proposed algorithms. MATLAB R2009a is used to write programs for under-sampling algorithm and SVM parameter optimization algorithm, and the LIBSVM toolbox is used for SVM training and classification.

### 4.1 Data description

The data set used in experiments is the loop detector data collected at the I-880 Freeway in the San Francisco Bay area, California (PETTY, K F, et al., 1996). The database has been used in many similar research works (JEONG, Y, CASTRO-NETO, M, JEONG, M K and HAN, L D, 2011; LIU, Q, et al., 2014; XIAO, J, et al., 2012). The loop detector data, in the form of traffic parameters such as volume, average speed, and occupancy were collected at a fixed time interval of 30 s.

In order to study the effect of under-sampling on detection performance, different proportions of incident instances in training set were designed. Instances of training set and test set used in the experiment are described in Table 1.

Table 1. Traffic data instances used in experiments.

Data set	Data reconstruction	Incident instances	Non-incident instances	Total number	Incident instances' proportion (%)
Training set 1	None	762	5,272	6,034	12.63
Training set 2	Under-sampling	762	2,610	3,372	22.60
Training set 2	Under-sampling	762	2,610	3,372	22.60
Training set 3	Under-sampling	762	1,504	2,266	33.63

### 4.2 Parameter optimization of SVM

RBF was adopted as the SVM kernel function in the experiment and its parameters were optimized by grid search method and PSO algorithm.

For grid search method, first, C and g were changed with a step of 1.0 within a larger range ( $C = [2^{-10}, 2^{10}]$ ,  $g = [2^{-10}, 2^{10}]$ ) to determine the approximate range of optimal C and g, and the contour curve of classification accuracy during the process is shown in Figure 1(a). Then, the best C and g were determined with a narrower step of 0.5 within a narrower range ( $C = [2^{-10}, 2^0]$ ,  $g = [2^0, 2^{10}]$ ), and the

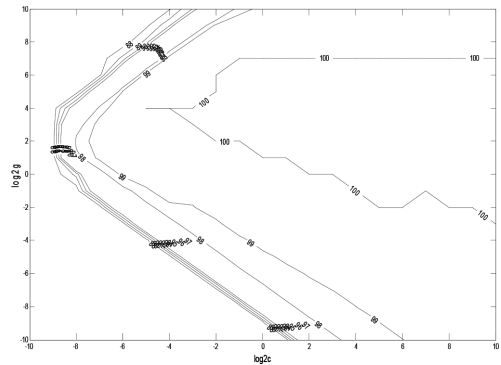


Figure 1(a). Finding the optimal C and g in a wider range.

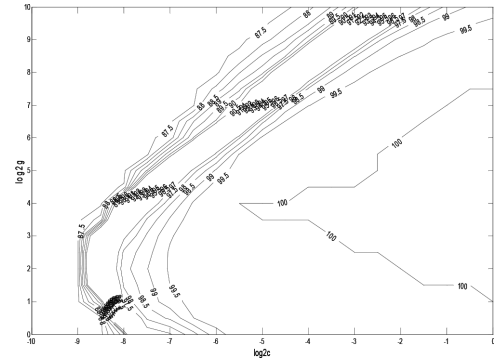


Figure 1(b). Finding the optimal C and g in a narrower range.

contour curve of classification accuracy during this process is shown in Figure 1(b).

Figure 1(a) and (b) depict the contour curves of classification accuracy to determine the best  $C$  and  $g$  using the grid search method, where the horizontal axis represents the logarithmic value of regular constant  $C$  (the base is 2) and the vertical axis represents the logarithmic value of the width of RBF  $g$  (the base is 2). The curve is the contour line of classification accuracy; figures in the curve represent the corresponding classification accuracy CR.

The optimal parameter combination for the original training set is  $C = 0.022097$ ,  $g = 16$  PSO is used for feature selection while SVM is used to predict the results. PSO is used to find the optimal parameters for SVM automatically, and the prediction accuracy serves as the fitness function for the PSO method. The fitness curve of the process to select optimal parameter combination is shown in Figure 2, where the horizontal axis represents the evolutionary generation and the vertical axis represents the fitness. The terminate generation is 200 and the population is 20 in this experiment. The optimal parameter combination for the original training set is  $C = 0.0392$ ,  $g = 15.9963$ .

These two parameter combinations obtained from grid search method and PSO algorithm were inputted into the SVM separately, and then the model performance was examine with the same test set. The experimental results are shown in Table 2.

The results indicate that both PSO and grid search methods are fairly comparable in terms of CR and MTTD, and the PSO approach can result in a higher DR and FAR. Considering the fact that the cost of missing incident inspection is far greater than that of the false alarm incident, a higher DR is usually regarded to be more meaningful in reality. In addition, PSO method achieves a lower PI value, which shows a better comprehensive

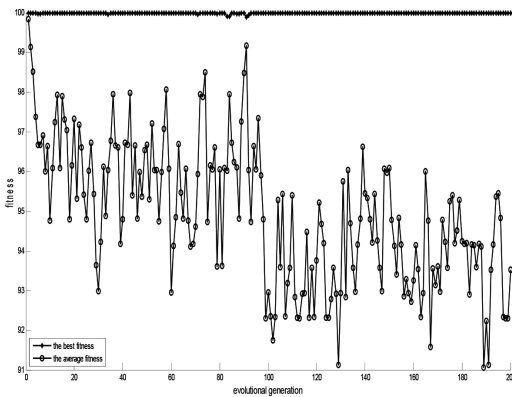


Figure 2. Fitness curve during the process to select optimal parameter combination.

Table 2. Experimental results of different parameter optimization methods.

Optimization method	DR (%)	CR (%)	FAR (%)	MTTD (min)	PI
Grid search method	85.71	92.29	0.48	3.30	0.142
PSO method	88.57	92.15	0.62	3.31	0.134

detection performance. Therefore, the PSO approach is capable of searching for the optimal parameters of SVM, and the optimal parameter combination obtained by PSO method was adopted in following experiments.

#### 4.3 Effect of under-sampling on detection performance

SVM was trained with the data presented in Table 1. On this base, the trained SVM models were used to detect traffic incidents in the same test set. The experimental results are shown in Table3.

Comparing the PI values in Table 3, SVM–AID models trained by relatively balanced training sets exhibit better detection performance in terms of DR, CR, and MTTD. With the increase in the proportion of the incident instances, DR increases from 88.57% to 91.43% and 94.29%, MTTD decreases significantly from 3.31 min to 2.08 min and 0.83 min, as well as a superior CR. In addition, PI obtained by reconstructed training sets also increases to a larger extent, although FAR is slightly inferior to that yield by the SVM–AID model trained by original training set.

It is evident from the table that incident detection performance becomes better with the proportion of incident instances increases, and DR especially achieves the largest point of 94.29%. It is also observed that training set 3 is faster in detecting incidents, but obtains a higher FAR, which indicates that it is more sensitive to detect incidents in a more balanced training set.

#### 4.4 Impact of the number of nearest neighbors in under-sampling

Typically, the number of nearest neighbors is three in data reduction technique, as suggested in WILSON, D, RANDALL and MARTINEZ (2000). In this experiment, we changed the number of nearest neighbors from three to seven in under-sampling algorithm, attempting to investigate its influence on incident detection performance. According to the demonstrated conclusion that a more balanced training set can achieve a more desirable detection performance, we assumed a proportion of incident instances at 33.63% in accordance with training

Table 3. Experimental results of different proportions of incident instances.

Training set	DR (%)	CR (%)	FAR (%)	MTTD (min)	PI
Training set 1	88.57	92.15	0.62	3.31	0.134
Training set 2	91.43	95.10	1.07	2.08	0.090
Training set 3	94.29	95.17	1.74	0.83	0.052

Table 4. Experimental results of different numbers of nearest neighbors.

Number of nearest neighbors	DR (%)	CR (%)	FAR (%)	MTTD (min)	PI
3	94.29	95.17	1.74	0.83	0.052
5	94.29	95.17	1.76	0.83	0.052
7	94.29	95.43	1.94	0.77	0.050

set 3. Moreover, we kept the same proportion of incident instances in reconstructed training sets together with the change of the number of nearest neighbors. The experimental results are shown in Table 4.

The aim of application of the nearest-neighbor cleaning rule in under-sampling algorithm is to increase the probability of obtaining inner “safe sample” and improve the data cleaning quality simultaneously. There is no rule as to how many nearest neighbors should be used to achieve a good performance. Experimental results show that no obvious difference exist between different numbers of nearest neighbors, and they yield the same DR and similar PI as well as other performance measures. However, a larger number of nearest neighbors in under-sampling algorithm can remove more majority class instances each time, while a smaller number of nearest neighbors must iterate more times to achieve the target incident instance proportion. Therefore, we consider that it is beneficial to keep the number larger (such as 7) to reduce the times of iterations.

## 5 CONCLUSION

In order to solve the imbalanced traffic data problem and improve the efficiency of SVM to detect incidents, this study developed a feasible AID model for imbalanced traffic data. In contrast to random under-sampling, the improved under-sampling method removes majority class instances in view of the nearest-neighbor cleaning rule, thus improving the data reduction quality. In addition, the application of under-sampling can alleviate the overfitting problem caused by SVM and improve

the efficiency of SVM, as the rebalanced training set is relatively small. The results implied that the proposed AID algorithm based on under-sampling is an effective method for imbalanced traffic data and can greatly improve the incident detection performance. Furthermore, different proportions of incident instances in training set were selected to investigate its effect on detection performance, and findings showed that a more balanced training set can achieve a more desirable detection performance.

Although SVM has been demonstrated to be a superior pattern classifier, it is still a challenging task to determine the optimal parameter of SVM. This study made a comparison between grid search method and PSO algorithm to determine the optimal parameter combination for better incident detection performance. The experimental results revealed that PSO approach is slightly competitive than grid search method in parameter optimization of SVM.

In addition, we investigated the effect of the number of nearest neighbors on detection performance. Analysis of the results suggested that no obvious performance difference exist between different numbers of nearest neighbors in under-sampling algorithm. Considering the fact that a larger number of nearest neighbors need a shorter iterate time under the same data reduction number, we show that it is beneficial to keep the number larger (such as 7) in under-sampling algorithm.

## ACKNOWLEDGMENTS

This work was supported by the National Natural Science Foundation of China under Grant No.61374195, the “Fundamental Research Funds for the Central Universities”, and the “Research and Innovation Project for College Graduates of Jiangsu Province” No. SJLX15\_0064.

## REFERENCES

- Anguita D, Boni A, Ridella S. 2003. A digital architecture for support vector machines: theory, algorithm, and fpga implementation [J]. *IEEE Transactions on Neural Networks*, 14(5): 993–1009.
- Cateni S, Colla V, Vannucci M. 2014. A method for resampling imbalanced datasets in binary classification tasks for real-world problems [J]. *NEUROCOMPUTING*, 135(SI): 32–41.
- Chen S, Wang W. 2009. Decision tree learning for freeway automatic incident detection [J]. *Expert Systems with Applications*, 36(2): 4101–4105.
- Choi J.M. 2010. A selective sampling method for imbalanced data learning on support vector machines [D]. ProQuest, UMI Dissertations Publishing.

- Hawas Y.E. 2007. A fuzzy-based system for incident detection in urban street networks [J]. *Transportation Research Part C: Emerging Technologies*, 15(2): 69–95.
- Jeong Y, Castro-Neto M, Jeong M.K, Han L D. 2011. A wavelet-based freeway incident detection algorithm with adapting threshold parameters [J]. *Transportation Research Part C: Emerging Technologies*, 19(1): 1–19.
- Kotsiantis S, Kanellopoulos D, Pintelas P. 2006. Handling imbalanced datasets: A review [J]. *GESTS International Transactions on Computer Science and Engineering*, 30(1): 25–36.
- Lipitakis A.D, Kotsiantis S. 2014. A hybrid Machine Learning methodology for imbalanced datasets [C]// *Chania*: 252–257.
- Liu Q, Lu J, Chen S, Zhao K. 2014. Multiple Naïve Bayes Classifiers Ensemble for Traffic Incident Detection [J]. *Mathematical Problems in Engineering*, 2014: 1–16.
- Petty K F, Noeimi H, Sanwal K. 1996. The Freeway Service Patrol Evaluation Project Database Support Programs, And Accessibility [J]. *Transportation Research Part C: Emerging Technologies*, 2(40): 71–85.
- Quaglini S, Barahona P, Andreassen S, Laurikkala J. 2001. Improving Identification of Difficult Small Classes by Balancing Class Distribution [M]//Quaglini S, Barahona P, Andreassen S. *Artificial Intelligence in Medicine*. Springer Berlin Heidelberg: 63–66.
- Wilson D, Randall, Martinez. 2000. Reduction Techniques for Instance-Based Learning Algorithms [J]. *Machine Learning*, 38(3): 257–286.
- Xiao J, Liu Y. 2012. Traffic Incident Detection Using Multiple-Kernel Support Vector Machine [J]. *Transportation Research Record: Journal of the Transportation Research Board*, 2324(-1): 44–52.
- Zhang J, Wang X. 2005. Research Progress of Traffic Incident Automatic Detection Algorithms [J]. *Journal of Wuhan University of Technology (Transportation Science and Engineering)*, 29(2): 215–218.
- Zheng W, Chen S, Wang X. 2012. Imbalanced Datasets Based SMOTE-SVM-AID Algorithm [J]. *Journal of Wuhan University of Technology*, 34(11): 58–62.



# Stress calculation and analysis of cut-off wall in the sand gravel foundation

Xin-mei Dong, Zhao-zhen Wei & Jing-tao Niu

*Water Resources Research Institute of Shandong Province, Jinan, Shandong, China*

Wen-long He

*Yellow River Dongming Bureau, Dongming, Heze, Shandong, China*

**ABSTRACT:** Mengjiagou Reservoir is a new medium reservoir, and the project consists of bounded bank, flood discharge gate, outbound culverts, and so on. The permeability coefficient of medium sand, sand gravel, and sand pebble layers in dam foundation of bounded bank is so large that anti-seepage measure has to be adopted, and the plastic concrete cut-off wall is selected for the dam foundation anti-seepage in design project. The stress condition of concrete cut-off wall is complex in sand gravel foundation, and we introduced the stress calculation method of concrete cut-off wall briefly in this paper.

**Keywords:** Mengjiagou reservoir, anti-seepage of dam foundation, concrete cut-off wall, stress analysis

## 1 PROJECT PROFILE

Mengjiagou Reservoir is located in the midstream of Jiaohe River, which in the west of Mengjiagou village, Paicheng town, Gaomi city, China, with a control area of 459.1 km<sup>2</sup> and utilizable capacity of 17.30 million m<sup>3</sup>. The project construction is planned to begin at the end of 2014, and the project consists of bounded bank, flood discharge gate, outbound culverts, and so on.<sup>[1]</sup> The filling material of the dam body is sand gravel, the total length of the bounded bank is 10,347 m, the total width of the dam crest is 8 m, the upstream dam slope is 1:3, and the downstream dam slope is 1:2.5. The unconsolidated formation of dam foundation mainly includes loam, medium sand, and sand gravel, which belong to strong permeable layers and their permeability coefficient is large; therefore, anti-seepage measure has to be adopted. Through comparison and selection of technical and economical indices for different schemes, the plastic concrete cut-off wall is adopted for dam foundation seepage control, with wall thickness of 30 cm, the bottom of wall going deep into strongly weathered bedrock above 0.5 m, and wall maximum depth of 13.20 m. The stress condition of concrete cut-off wall is complex in sand gravel foundation, and we introduced the stress calculation method of concrete cut-off wall briefly in this paper.

## 2 STRESS CALCULATION METHOD OF CONCRETE CUT-OFF WALL FOR DAM FOUNDATION

Finite element method is used to analyze the stress and strain of concrete cut-off wall in this project. In 1967, Clough and Woodward in the United States used finite element method first for nonlinear analysis of earth-rock dam [2], and calculated dam stress through simulating the staged-loading during the construction period, and in subsequent earth-rock dam stress and strain analysis, nonlinear finite element method is widely used. This method can simulate the construction process more truly and has higher calculation accuracy, which is mostly used for earth-rock dam stress and strain analysis at home and abroad.

The aim of soil stress and strain analysis is to determine the material stress-strain relations and the calculation model. In this analysis, the Duncan-Zhang double-curve calculation method, which is currently mature and has higher calculation accuracy, is adopted for nonlinear analysis of dam body and foundation soil and concrete cut-off wall.

### 2.1 Tangent modulus<sup>[3]</sup>

$$E_t = KP_a \left( \frac{\sigma_3}{P_a} \right)^n \left[ 1 - \frac{R_f (1 - \sin \varphi) (\sigma_1 - \sigma_3)}{2c \cos \varphi + 2\sigma_3 \sin \varphi} \right]^2, \quad (1)$$

where  $E_t$  – soil tangent modulus;  
 $\sigma_1$  and  $\sigma_3$  – small and large principal stress,  
 respectively;  
 $c$  and  $\varphi$  – soil cohesion and internal friction angle,  
 respectively;  
 $K$  and  $n$  – soil modulus coefficient and modulus  
 index, respectively;  
 $R_f$  – break ratio; and  
 $P_a$  – atmospheric pressure.

Incremental method is adopted in soil non-linear analysis, and amendment of pull crack and shear failure, consolidation pressure history, and unloading effect are considered in calculation.

## 2.2 Tangent Poisson's ratio

Based on previous experiment results, there is a hyperbolic relationship between the Doucan–Zhang biaxial strain and lateral strain:

$$\varepsilon_n = \frac{\varepsilon_r}{f + d\varepsilon_r}, \quad (2)$$

where  $f$  and  $d$  are undetermined coefficients.

From this, the tangent Poisson ratio can be deduced:

$$\mu_t = \frac{g - F \cdot \lg\left(\frac{\sigma_3}{p_a}\right)}{(1-A)^2} \quad (3)$$

$$A = \frac{D(\sigma_1 - \sigma_3)}{kp_a \left(\frac{\sigma_3}{p_a}\right)^n \left[1 - \frac{R_f(1 - \sin\varphi)(\sigma_1 - \sigma_3)}{2c \cos\varphi + 2\sigma_3 \sin\varphi}\right]}, \quad (4)$$

where  $g$  and  $F$  are testing constants.

The relationship between stress increment and strain increment is

$$\begin{cases} d\sigma_x \\ d\sigma_y \\ d\sigma_z \end{cases} = \frac{E_t}{(1 + \mu_t)(1 - 2\mu_t)} \times \begin{bmatrix} 1 - \mu_t & \mu_t & 0 \\ \mu_t & 1 - \mu_t & 0 \\ 0 & 0 & 1 - 2\mu_t \end{bmatrix} \begin{cases} d\varepsilon_x \\ d\varepsilon_y \\ \frac{1}{2}d\gamma_{xy} \end{cases}. \quad (5)$$

## 2.3 Staged-loading in construction

Incremental method is applied to consider staged-loading, and the stress and strain of each step in

the construction period are calculated. This calculation method of staged-loading in construction can not only simulate the stress variation of dam body during construction process, but also reflects the stress variation of concrete cut-off wall during the reservoir excavation and with the increase of dam height, and can simulate the water level lowering in reservoir area during excavation.

## 2.4 Calculation software

The stress and strain analysis module of geotechnical engineering design and analysis software *Geo-Studio* is used for the calculation.

# 3 STRESS ANALYSIS OF CONCRETE CUT-OFF WALL FOR DAM FOUNDATION

## 3.1 Calculated working condition

The calculated working condition divides into construction period and operation period.

The dam body is mainly filled with excavated soil, underground water level is high around the dam, underground water level outside the dam is 30.0 m during the construction period, the water level inside dam is controlled not to exceed excavation face through lowering water level, and the concrete cut-off wall is used to interdict the seepage of groundwater outside the dam to inside. Therefore, construction order is determined as follows: first fill the part of dam to the top elevation of concrete cut-off wall to 33.50 m, then excavate the reservoir area, and finally fill the dam to above 33.50 m. Assume irrigation level as the reservoir level in the operation period to calculate stress condition of concrete cut-off wall. According to dam layout and engineering geological condition, take E0+136, which has high cut-off wall depth and complex foundation soil layers as typical calculating cross-section.

## 3.2 Calculating parameters

The stress and strain analysis mainly adopts the Duncan–Zhang dual model based on the cut-off wall thickness. Wall unites is divided into five layers horizontally with the thickness of 0.06 m for each layer, and divided vertically according to the thickness of each soil layer; the unite size is not more than 0.5 m in controlling depth direction. The Duncan–Zhang dual model parameters of the dam and each foundation soil layer are as follows: cut-off wall elasticity modulus is 800 Mpa, elasticity modulus of foundation of completely weathered rock is  $5.0 \times 10^4$  MPa, and elasticity modulus of foundation of strongly weathered rock is  $1.0 \times 10^5$  MPa (see Table 1).

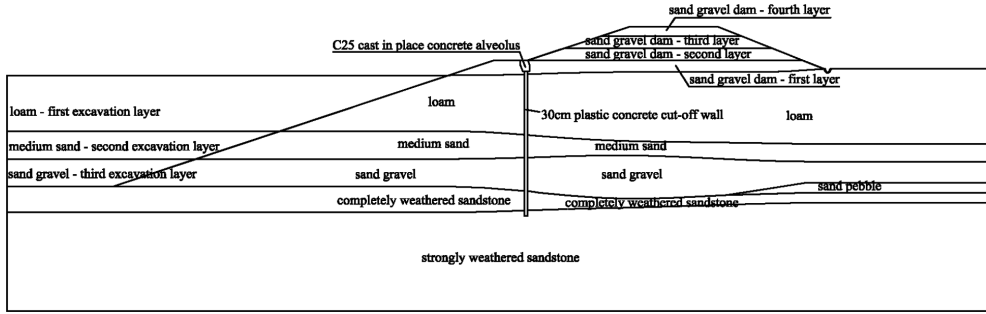


Figure 1. E0+136 dam cross-section.

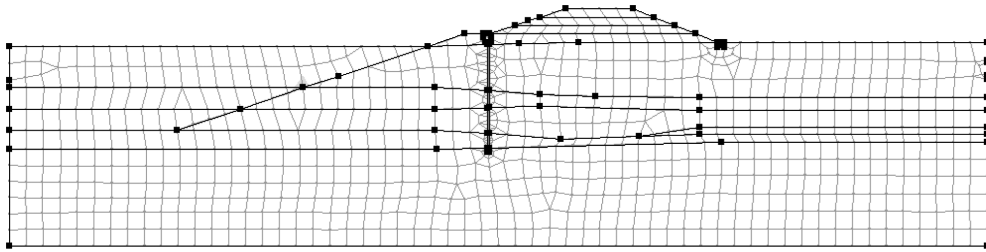


Figure 2. Calculating section meshing figure.

Table 1. 8 Duncan model parameters of dam foundation and dam body soil layers.

Duncan model parameter		Dams and gravel			
		Loam	Medium sand	Sand gravel	
Cohesion	$C_d$	0	0	0	
Internal friction angle	$\phi_d$	35	28	30	
Break ratio	$R_f$	0.97	0.81	0.87	
Modulus parameter	$k$	425	138	310	
	$n$	0.39	0.57	0.403	
Poisson's ratio parameter	$D$	3.96	2.3	3.95	
	$G$	0.37	0.35	0.361	
	$F$	-0.20	-0.15	-0.19	
				-0.2	

### 3.3 Calculation results

#### 3.3.1 Operation period

Stress distributions of the foundation concrete cut-off wall in the operation period are shown in Figures 3–8. Cut-off wall stress consists of upstream face and downstream face: X positive direction is the downstream face and Y positive direction is the upstream face.

By the stress calculation results shown above, we draw the following conclusions:

1. In operation period, the maximum principal stress of concrete cut-off wall is 0.38 Mpa at the upstream face and 0.32 Mpa at the downstream

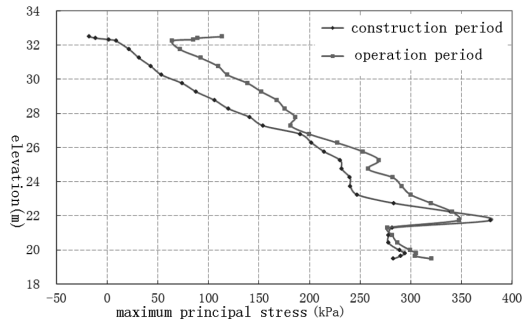


Figure 3. Upstream maximum principal stress distribution.

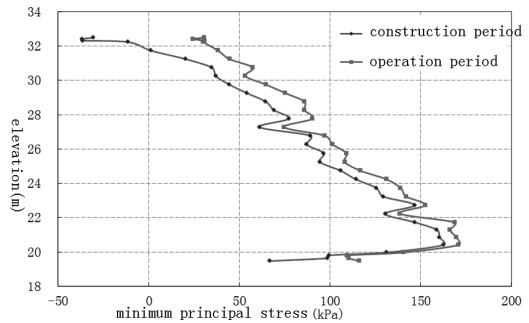


Figure 4. Upstream minimum principal stress distribution.

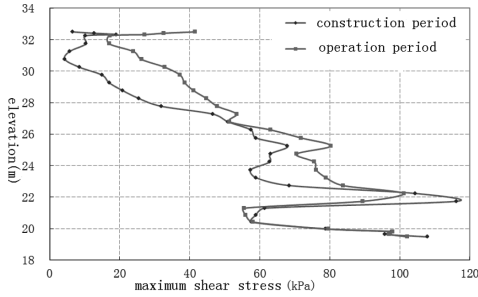


Figure 5. Upstream maximum shear stress distribution.

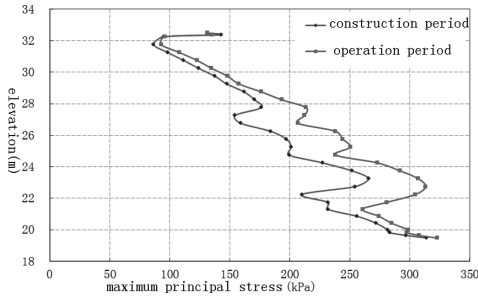


Figure 6. Downstream maximum principal stress distribution.

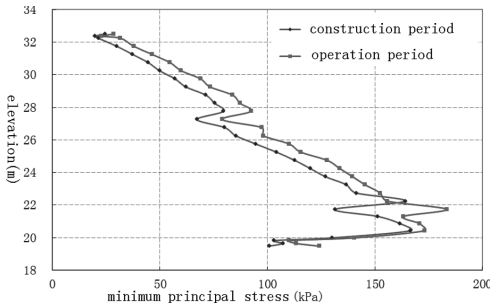


Figure 7. Downstream minimum principal stress distribution.

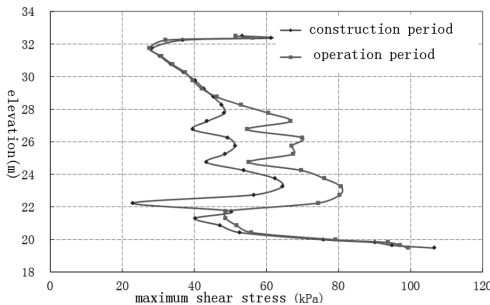


Figure 8. Downstream maximum shear stress distribution.

face, both of which are smaller than compressive strength design value of cut-off wall, that is, 3.0 Mpa. The maximum principal stress is shown at the height of 21.74 m at the upstream face and 22.74 m at the downstream face. These heights are located in the range above the completely weathered layer of bedrock, that is, at 0.5–1.5 m, it shows that the bedrock's imprison effect on cut-off wall is very significant.

2. In the operation period, maximum principal stress, minimum principal stress, and shear stress of concrete cut-off wall are all small, and the cut-off wall is in safe condition.
3. The maximum principal stresses are all greater than zero. This shows that the concrete cut-off wall will not have tensile stress, which meets design requirement.

### 3.3.2 Construction period

The calculated maximum principal stress of concrete cut-off wall is 0.41 Mpa at the upstream face and 0.34 Mpa at the downstream face in the construction period; the maximum principal stress, minimum principal stress, and shear stress of concrete cut-off wall are all small; the maximum principal stresses are all greater than zero. These show that the concrete cut-off wall is safe in the construction period and it meets design requirement.

## 4 CONCLUSIONS

Mengjiagou Reservoir is a rain and flood resource utilization plan project in Shandong Province. As a medium reservoir of hilly areas, dam foundation seepage control is critical and directly affects the reservoir's normal storage after completion. In this project, the plastic concrete cut-off wall measure is used for dam foundation seepage control, with wall thickness of 30 cm. In this paper, concrete cut-off wall stress condition is complex in sand gravel dam foundation, and the stress analysis measure of dam foundation concrete cut-off wall is briefly introduced based on the Mengjiagou Reservoir dam project, which will be instructive for similar designs.

## REFERENCES

Shangdong Province Keyuan Water Survey and Design Consultation Center. 2014. *preliminary design report of Mengjiagou Reservoir*, Gaomi [R]. 221–226.

Qingyou Wang, Wangong Sun & Huan Xiong. 2008. *Plastic concrete cut-off wall* [M]. Beijing: WaterPower Press, 35.

Jiahuan Qian & Zongze Yin. *Geotechnical principle and calculation* [M]. 1996. Beijing: Water Conservancy and Electric Power Press, 12–26.

Shangdong Province Keyuan Water Survey and Design Consultation Center. 2014. *Geological survey report in preliminary design section of Mengjiagou Reservoir*, Gaomi [R]. 67.

## Stress distribution of anchor bolts due to empty pulp defects

Sheng Zeng & Jing Zhang

*Nuclear Resources Engineering College, University of South China, Hengyang, China*

Bing Sun

*Institute of Urban Construction, University of South China, Hengyang, China*

**ABSTRACT:** In order to study the stress distribution and development of the empty pulp defects in anchor bolts, we carried out an experiment on an empty pulp defective bolt. The dynamic testing signals were obtained by non-destructive testing, and test signals under different loads were analyzed. Research shows that in the defective bolt, the strain and load show a linear trend before the empty pulp defect. In the empty pulp defective section, the strain will not have obvious change until the load reaches a certain value. After the empty pulp defect, stress redistribution occurs with the increase of load.

**Keywords:** Geotechnical engineering; defective bolt; non-destructive testing; single empty pulp

### 1 INTRODUCTION

Rock and soil anchoring technology has the advantages of ingenious structure, simple technology, low cost, and unique effect, and has been widely used in various fields of civil engineering (Cheng L.K. 2001). At present, many scholars have adopted a variety of research methods and means to obtain a series of research results on the stress distribution of anchor bolts. Jiru Zhang et al. proposed a theory to construct the anchorage shear stress distribution function curve (Zhang J.R. & Tang B.F. 2002, Phillips S.H.E. 1970). Wenwu Jiang et al. used a numerical simulation technique to analyze the mechanical effect and factors affecting anchorage. It is shown that the numerical simulation of anchor rod drawing process is feasible, and the process of pulling out the anchor rod gradually leads to the sudden instability of the whole process (Jiang W.W. et al. 2009, Pang Y.S. et al. 2009). Delhomme et al. studied the effect of bolt drawing and creep through experiments and numerical simulation. Under the rock creep mass, the changing trends of the stress and deformation of the anchor rod are closely related (Delhomme F. & Debicki G. 2010, Yang M.J. 2014). The research of defects in anchor bolt is few. Yongxing Zhang et al. set up the mathematical model of the longitudinal vibration of the defective anchor bolt. The dynamic response of rock bolts under different conditions was studied (Zhang Y.X. & Chen J.G. 2005). Jian Duan et al. studied the effect of parameters on the

anchoring properties of the soil cavity defective anchor bolts. The results showed that the existence of the cavity has a significant influence on the anchorage segment of the defective anchor bar, and the latter is less affected (Duan J. et al. 2012). Jianhui Yang et al. used the wavelet analysis method to carry out the contrast analysis of the vibration wave. It is found that the dynamic response of different anchorage states can be correctly reflected by the time domain waveform and time frequency spectrum (Yang J.H. et al. 2014).

Several domestic and foreign scholars have conducted studies on complete bolts and defective bolts. It is concluded that the mechanical properties and working principle of a defective anchor are slightly different from the intact rock bolt, and the stress development process and the stress wave propagation process are different from those of the intact rock bolt too. In order to study the dynamic response of the whole bolt and the defective anchor, and discuss the effect of the load on the dynamic test signal of the single empty slurry, an experiment for the step loading of a single air plasma defective anchor bolt was conducted. The non-destructive test was conducted on the single empty slurry defective anchor rod under different loads to obtain its dynamic test signals. Through the analysis of the dynamic test signals at all levels of load, the distribution and development of stress in the anchor bolts are obtained, which can provide some reference values for the evaluation of the quality of the anchor bolts.

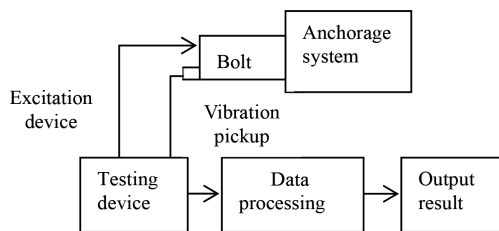


Figure 1. Non-destructive testing of bolt quality.

## 2 BASIC PRINCIPLE OF NON-DESTRUCTIVE TESTING

The theoretical basis of anchorage quality non-destructive detection is the transmission mechanism of elastic wave in one-dimensional viscoelastic rod. The moment impact force is applied at the end of the anchor rod along its axial direction, the stress wave signal is generated. When the signal is transmitted into the wave impedance interface along the depth of the anchor solid, the energy of the signal will be divided. A part of the energy is transmitted through the wave impedance interface to the deep part of the anchor, and the transmission wave is formed. Another part of the energy will return along the original path, forming a reflection wave. The particle vibration caused by a reflected wave is received by the source sensor with high sensitivity, transformed into electrical signals, and transmitted to the mainframe. The non-destructive testing of anchor bolts is shown in Figure 1 (Xiao G.Q. et al. 2012).

## 3 MODEL TESTING

### 3.1 Model making

In the bolt indoor model experiment, two bolts were made. The length of the anchor rod was 2.4 m, and the exposed length of reinforcement was 0.5 m. The construction method was to insert rod before grouting, and the mortar to slurry ratio was 1:2:4. The rebar bolts were of 28 mm in diameter. In order to complete the experimental model, 200 mm diameter PVC drainage pipe was used as template. The built-in defects used 75 mm of PVC drainage pipe. The specific setting of the defect is shown in Table 1. The anchor structure diagram is shown in Figure 2.

### 3.2 Measuring point layout

The main research object is the LM-2 bolt. The strain gauges were pasted on the corresponding part of the sensor. The influence of load on the

Table 1. Design parameters of bolt model test.

Anchor number	Construction technology	Defect setting
LM-1	First, insert bar and then pour concrete	Complete bolt, uniform and compact
LM-2	Reserve holes, reinsert steel bars, and finally cast concrete	The void, which is 50 mm in diameter at the distance of 0.70–1.30 m from the anchor end, is used as a defect

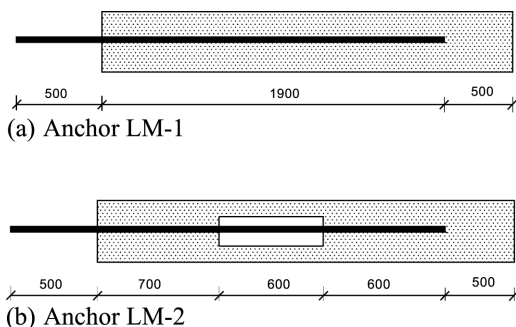


Figure 2. Sketch of bolt structure.

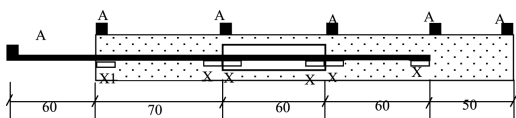
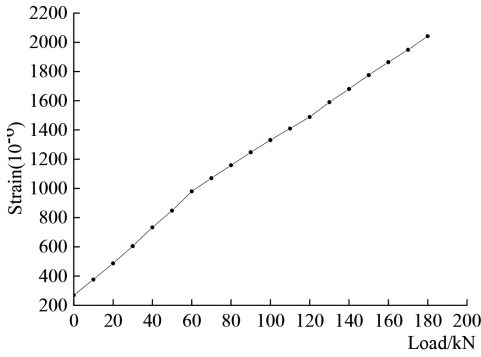


Figure 3. Layout of the strain gauges and sensors.

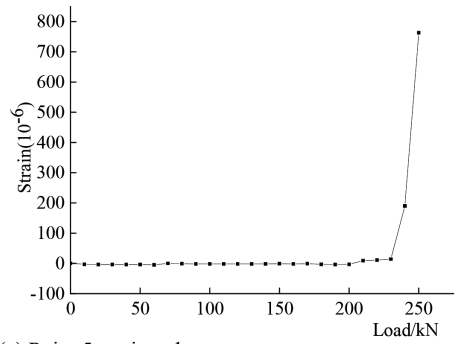
dynamic test signal and the development process of anchor stress during the loading process were discussed. The arrangement of strain gauges and sensors is shown in Figure 3, where  $a_i$  ( $i = 1, 2, 3, 4, 5, 6$ ) are sensors, and  $x_i$  ( $i = 1, 2, 3, 4, 5, 6$ ) are strain gauges. The product model of the strain gauge is BX120-100 AA.

## 4 RESULT ANALYSIS AND DISCUSSION

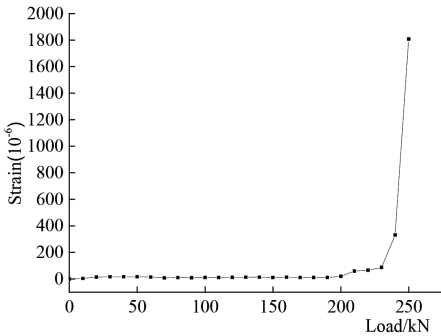
In this paper, original strain analysis of strain gauge with different measuring points of LM-2 under different loads was made. When the load is 0, the strain of each measurement point is 0. The strains under different loads are subtracted from the initial value. Strains at different points of the LM-2 under different loads and changes in the measured points under different loads are obtained as shown in Figure 4.



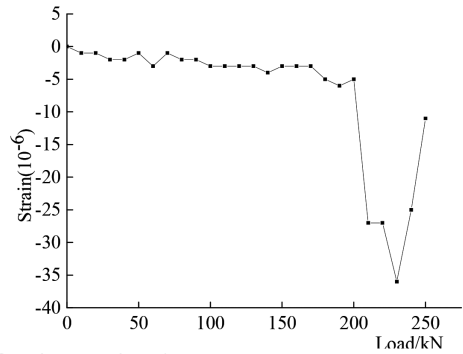
(a) Point 1 strain value



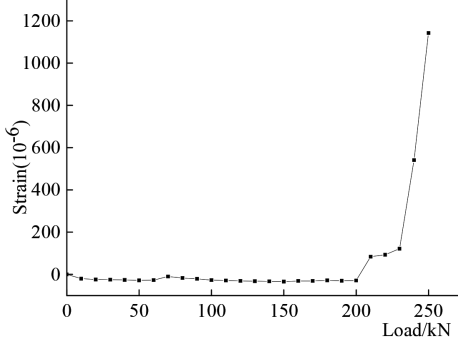
(e) Point 5 strain value



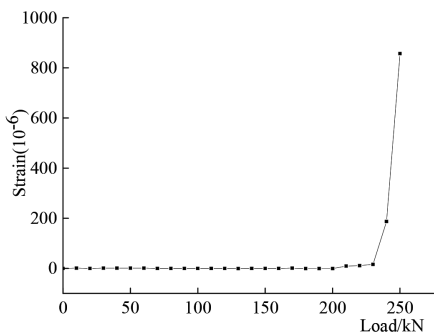
(b) Point 2 strain value



(f) Point 6 strain value



(c) Point 3 strain value



(d) Point 4 strain value

Figure 4. Strain values of each measuring point under different loads.

The failure of anchor rod occurs in three stages: viscoelastic, clay, and failure. The distribution form of the shear stress and the position of the peak points are different in each stage. From the shear stress distribution and the development of the force, the concentration degree of shear stress distribution plays a role in the end slip to the threshold in the control of shear stress. When the stress develops into the beginning of the space of the empty single slurry section anchoring the defective bolt LM-2, the stress through the steel bar is directly transferred to the air plasma segment at the end, because the air plasma interface cannot shear. The strain of bolt LM-2 is larger than that of the complete bolt LM-1, and the stress concentration is relatively small. It can be seen from Figure 4 that the variation of strain with load can be analyzed in the defective anchor LM-2.

1. The strain of point 1 increases with the increase of the load, and the curve shows a linear relationship between them. When the load reaches a certain value, the strain gauge reaches the limit and is susceptible to damage, but the steel strain has not yet reached the limit.

Figure 4. (Continued).

2. The variation trends of points 2, 4, 3, and 5 are different from that of point 1. When the load reaches a certain value, the strain will be changed obviously. Under the same load, the strain at different points of measurement will be reduced. With the development of stress to the next section, a certain amount of stress persists in the previous section. The cohesive strength of anchorage medium for anchoring steel bar is limited. When the force exceeds the limit value, it becomes debonding force. The points 2, 3, 4, and 5 will increase with the increase of the pulling force.
3. With the increase of the load, the strain changes of point 6 obviously show that the change process is from pressure to pulling. It is a more obvious stress redistribution process.
4. The shear strain effect of the defective section of the anchor rod is not affected by the anchoring medium. The stress transfer length of the anchor strain is increased and the strain variation is increased too.

## 5 CONCLUSIONS

In this article, the following conclusions can be drawn through the processing and analysis of the test data of the anchor bolt of the air plasma defect:

1. The stress of the defective anchor bolt develops into the beginning of the space. The interface of air plasma can not be cut. The stress of the reinforcement is higher and is directly transferred to the air at the end section of the slurry, and the stress concentration is relatively small.
2. Before the air plasma defect, the strain and load have a linear relationship. In the empty pulp defect section, the strain will be changed obviously when the load reaches a certain value. After the air plasma defects are formed, stress redistribution phenomenon occurred with the increase of the load.
3. In each measuring point, the change tendency and the range of the strain in the defective anchor bolt increase more than those in the complete anchor bolt. Anchoring defects also increase the anchor segment of the stress level to a certain extent, and the stress concentration becomes small.

## ACKNOWLEDGMENTS

The authors would like to acknowledge the support of the Scientific Research Fund of the National Natural Science Foundation of China (NO.51204098), the Natural Science Foundation of Hunan Province of China (NO.11 JJ6045), and the Research and Development Plan of Hunan Province of China (NO. 2015SK2058-4).

## REFERENCES

- Cheng L. K. 2001. Present situation and development of rock and soil anchoring [J]. *Civil Engineering Journal* 34(3): 7–16.
- Delhomme F. & Debicki G. 2010. Numerical modeling of anchor bolts under pullout and relaxation tests [J]. *Constr Build Mater* 24(7): 1232–1238.
- Duan J., Yan Z.X. & Guo R.J. et al. 2012. Analysis of anchorage characteristics and parameter influence of soil imperfect anchor [J]. *Journal of Central South University (Natural Science Edition)* 43(8): 3209–3215.
- Jiang W.W., Xu G.Y. & Changnian Ma. 2009. Numerical simulation on pull-tests of a cable by FLAC\_3D [J]. *Journal of Harbin Institute of Technology* 41(10): 129–133.
- Pang Y.S., Liu H.L. & Chen Y.Y. 2009. Numerical simulation of removable anchor pullout test and influence factors [J]. *Journal of PLA University of Science and Technology* 10(2): 170–174.
- Phillips S.H.E. 1970. Factors affecting the design of anchorages in rock [R]. *London: Cementation Research Ltd* 29(3): 1–10.
- Xiao G.Q., Wu J.C. & Zhou L.M. et al. 2012. Method of extracting defective information in non-destructive detection of anchor quality [J]. *Journal of Yangtze River Scientific Research Institute* 29(11): 73–76.
- Yang J.H., Qu X. & Tang X.F. et al. 2014. Assessment of anchoring quality and defects of mortar bolt based on wavelet analysis [J]. *Industrial Building*, 44(4): 157–161.
- Yang M.J., Zhao Y.M. & Zhang N. 2014. Creep behavior of epoxy-bonded anchor system. *International Journal of Rock Mechanics and Mining Sciences* 67: 96–103.
- Zhang J.R. & Tang B.F. 2002. Hyperbolic function model to analyze load transfer mechanism on bolts [J]. *Chinese Journal of Geotechnical Engineering* 24(2): 183–192.
- Zhang Y.X. & Chen J.G. 2005. Model for Longitudinal Vibration of Defective Anchor Bar and Its Solution [J]. *Journal of underground space and Engineering* 1(1): 62–66.



## Damage laws of layered and jointed rock mass under the impact of cyclic loading

Bing Sun, Xian-shi Deng, Jie-hui Xie & Song-qiu-yang Zhang

*Institute of Urban Construction, University of South China, Hengyang, China*

**ABSTRACT:** In order to study the accumulative damage laws on the jointed rock mass under the impact of cyclic and dynamic loading, one to three specimens, including layered and jointed rock mass, were precast separately, which are made of cement-mortar used as similar material. Ultrasonic wave velocity of each specimen could be measured every time by conducting shock loading one to five times separately. On the basis of ultrasonic wave velocity, the damage variable of the specimen is defined. Meanwhile, both the effect of shock damage degree on rock mass under the shock frequency and sets of joint could be obtained. The results show that under the same shock energy, the damage degree is closely related to sets of joint and shock frequency. In addition, when the shock frequency was small, the specimen only produced micro-cracks and gradually formed macro-destruction with the increase of accumulative shock frequency.

**Keywords:** rock mechanics; jointed rock mass; cyclic shock; damage law

### 1 INTRODUCTION

The joint is a widespread defect in rock mass, and it often parallels arrangement. Under the external load, two sides of joint surface will produce comparative sliding, closing splaying, and other nonlinear mechanic behaviors. In practical engineering, it is found that the existence of discontinuous structural plane significantly affects the structural stability of rock mass, mechanic property, and fatigue damage under the impact of cyclic loading, of which, the most obvious effect is fatigue damage. Researchers have adopted theories and test and numerical methods to prove that the existence of joint and cracks in macro-defects will lead to evident anisotropies in the mechanical properties of the rock mass (Wang T.T. & Huang T.H. 2009, Halakatevak is N. & Sofianos A. L. 2010, Liu H.Y. et al. 2013). First, in order to describe the damage of rock mass, the concept of damage variable is put forward. It is defined mainly depending on the change of elasticity modulus, and Lemaitre adopted this method to denote the same (Xie H.P. 1990). On the basis of damage variable, Miner came up with the linear damage model based on the cyclic loading cycles and fatigue life (Yao W.X. 2003). However, the formula of the model is simple and it has more differences than practice. Xiao J.Q. et al. considered the initial damage variable of rock mass to build a fatigue damage model based on the deformation characteristics under cyclic loading (Xiao J.Q. 2009). According to the theory of solid mechanics, scholars put forward the dynamic damage constitutive model of rock mass

(Sazid M. & Singh T.N. 2013, Jia P. & Zhu W.C. 2012). Zhu J.J. et al. built the dynamic damage constitutive model of rock mass by using the theory of Weibull distribution and put forward accumulative damage formula under the impact of cyclic loading (Zhu J.J. et al. 2013). Random distribution of micro-cracks and other defects will make the inner rock mass produce isotropic damage, thereby decreasing its strength and stiffness (Xie N. et al. 2011). Zhao Y.Q. et al. adopted Lemaitre deformation's equivalent assumption to build a damage constitutive model under the precondition of considering joint defect and defect of the rock mass (Zhao Y.Q. et al. 2015). In addition, the model's accuracy is verified by means of a test. Lin D.N. et al. analyzed that the damage degree of rock mass is influenced by impact energy, confining pressure, and shock frequency, by testing its ultrasonic wave velocity under different impact conditions (Lin D.N. & Chen S.R. 2005). On the basis of shear failure criteria, Liu H.Y. et al. constructed a damage constitutive model of across-jointed rock mass for uniaxial compression considering the shear strength of the joint (Liu H.Y. et al. 2014). Experts focus mainly on the damage failure mechanism for no and single set of joints under different conditions of loading. However, the study of dynamic accumulative damage laws, including several sets of joints, is relatively rare.

In practical engineering, various rock masses suffer from dynamic vibration interference repeatedly. Thus, on the basis of similar principle, in this study, one to three jointed specimens of rock mass were precast separately. Ultrasonic wave

velocity can be measured after shock loading through shock-testing machine, and different sets of joint rock mass for damage laws can be analyzed in different shock conditions.

## 2 THEORY ANALYSIS

Rock mass damage refers to inner micro-cracks and other mesoscopic defects. However, it is not fairly easy to measure damage from macro-defects. Ultrasonic waves are sound waves with frequency higher than 2000 Hz, which have the following advantages: better direction, stronger penetrating ability, and high sound energy, as their wavelength is shorter than that of general sound waves. Therefore, they can also penetrate opaque materials with longer distance of propagation in high-density solid and liquid materials. Because of this property, it is widely used to detect cracks, measure depth and distance, and inspect industrial materials. This test adopts ZBL-U520 (a non-metal ultrasonic detector) to inspect the ultrasonic wave velocity of specimens after blast. The average velocity of propagation  $v$  in the media is given by

$$v = \frac{L}{t}, \quad (1)$$

where  $L$  denotes the tested length of the specimen and  $t$  denotes the tested specimen's duration of propagation related to ultrasonic wave velocity.

As the joint of rock mass contains jointed cracks and other micro-cracks, it is not a homogeneous material. Ultrasonic wave velocity will pass through two types of media (solid and gas) during the process of propagation. Its propagation velocity  $v_r$  in the jointed specimen of rock mass is given by

$$v_r = \frac{L_s + L_q}{\frac{L_s}{v_s} + \frac{L_q}{v_q}}, \quad (2)$$

where  $L_s$  and  $L_q$  denote the length of the specimen in solid and gas media, respectively, and  $v_s$  and  $v_q$  denote the velocity of propagation in the solid and gas media, respectively.

Because the prefabricated specimen of jointed rock mass has higher density, compact structure, and smaller reserve joint width, the length of the gas media can be ignored in the process of calculation. Thus, the length can be expressed as

$$L_s + L_q \approx L_s. \quad (3)$$

Using formulas (2) and (3), the approximate wave velocity of the ultrasonic wave in jointed rock mass is as given by

$$v_r = \frac{L_s}{\frac{L_s}{v_s} + \frac{L_q}{v_q}}. \quad (4)$$

It is obvious that when initial micro-cracks, defects, or joint fissure in the jointed rock mass become larger, the propagation velocity of ultrasonic waves will decrease. Therefore, it can analyze the degree of damage under the effect of impact loading using a non-metal ultrasonic detector to measure the ultrasonic wave velocity in jointed rock mass after blast. In order to analyze the inner damage degree conveniently, damage variable  $D$  is defined based on the concept of ultrasonic wave. The formula is as follows:

$$D_n = 1 - \left( \frac{v_{rn}}{v_{r0}} \right)^2, \quad (5)$$

where  $v_{r0}$  denotes the tested ultrasonic wave velocity of jointed rock mass without impact loading and  $v_{rn}$  denotes the tested  $n$ th ultrasonic wave velocity after blast.

## 3 EXPERIMENT RESEARCH

### 3.1 Experimental specimen prefabrication

Because the defect of practical rock mass is complicated, it cannot be tested by measuring natural rock mass. Thus, this test simulates the rock mass, taking advantage of cement mortar with similar mechanical parameters. The test adopts ordinary Portland cement with 32.5 degree, medium sand with moisture content of 3%, and city water as the material to prefabricate the side length of 150 cubic specimens with one to three joints. Their mass ratio (cement:sand:water) is 1:4.5:0.9 and their strength degree will reach M15. After specimen fabrication and vibrating the model, 0.3-mm-thick aluminum sheet was wrapped over the specimen (Figure 1). Then, it was pulled out after initial set and different joint sets of specimens

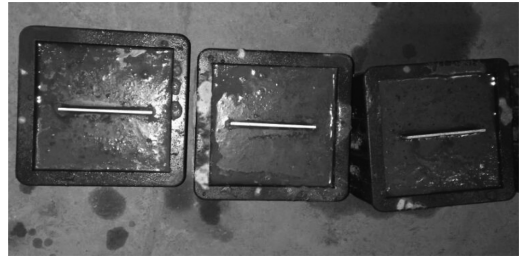


Figure 1. Pouring experiment model.

were shaped (Figure 2). The tested relative physical and mechanical parameters are as follows: mass density, 19.8 kN/m<sup>3</sup>; elasticity modulus, 2.72 GPa; and Poisson's ratio, 0.27.

### 3.2 Experimental methods

In this experiment, a 4 kg drop hammer is used, and impact loading experiment is carried out separately by using XJL-98 fall-hammer impact testing machine, including one to three jointed rock mass under the height of 2000 mm. During the process of fall-hammer, this test ignores air resistance and considers the motion of a free-falling body. Further, the impact loading experiment is conducted five times. Because fall-hammer is made of steel and its size is proper, deformation of fall-hammer in the contact process is comparatively smaller, especially it can be ignored and have a rebound. In other words, this is a perfect elastic process. Therefore, according to the law of energy conservation, the falling height  $h$  can be calculated. The exchange relationship of energy is

$$E = m_d gh, \quad (6)$$

where  $E$  denotes the impact energy of the jointed rock mass. After blast, ultrasonic wave velocity can be measured under different impact energies and cyclic shock frequencies by adopting ZBL-U520 (a non-metal ultrasonic detector, Figure 3). Then,

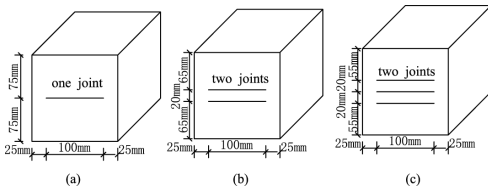


Figure 2. Different arrangement sets of jointed rock mass.



Figure 3. Non-metal ultrasonic detector.

the damage degree of each specimen can also be analyzed.

## 4 EXPERIMENTAL RESULT ANALYSIS

Under the impact height of 2000 mm, per shock input energy is calculated as 80 J using formula (6). The tested specific groups of ultrasonic wave velocity penetrating different jointed rock masses are shown in Table 1.

It is evident from Table 1 that different sets of jointed rock mass about the tested ultrasonic wave velocity decreases with the increase of shock frequency. Furthermore, the wave velocity decreases with the increase of the sets of joints. It is also evident that the increasing sets of joint will increase the size of contacting with air and decrease the compressive impact strength of the jointed specimen. It is easy to produce micro-cracks with the same impact energy. With the increase of shock frequency, ultrasonic wave velocity decreases. On the basis of the data presented in Table 1 and formula (5), the damage degrees  $D_n$  of different shock frequencies under the impact energy of 80 J are shown in Table 2.

In order to present intuitively the change law of damage degree  $D_n$ , the line chart can be drawn as follows based on the data of Table 2.

Figure 4 shows that the damage degree of the specimen increases gradually with the increase of groups of joint under the same shock frequency. When the shock frequency increases, its damage degree will also increase. When the shock frequency decreases, the added speed of damage degree gradually increases. However, when the shock frequency increases to three to five times, the damage degree of the jointed rock mass will increase rapidly. This result is attributed to two aspects. First, when the cyclic shock frequency is smaller, micro-cracks will be produced in the inner rock mass, which has little effect on ultrasonic wave velocity. Second, the accumulative damage degree of the jointed specimen increases with the increase of shock frequency, and then it will produce larger cracks by means of joining of smaller cracks.

Table 1. Ultrasonic wave velocity of jointed specimen under the impact height of 2000 mm /ms<sup>-1</sup>.

Shock frequency	One joint	Two joints	Three joints
0	3,165	3,138	3,099
1	3,138	3,121	3,022
2	3,099	3,074	2,963
3	3,024	2,998	2,743
4	2,774	2,683	2,398
5	2,445	2,291	1,949

Table 2. Damage degree  $D_n$  of jointed specimen under the impact height of 2000 mm.

Shock frequency	One joint	Two joints	Three joints
0	0.000	0.000	0.000
1	0.017	0.028	0.049
2	0.041	0.040	0.086
3	0.087	0.087	0.217
4	0.232	0.269	0.401
5	0.403	0.467	0.604

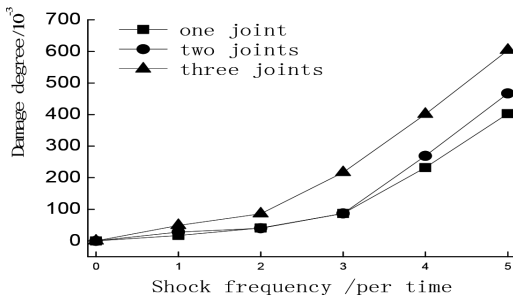


Figure 4. Relationship between damage degree and shock frequency under the impact height of 2000 mm.

## 5 CONCLUSIONS

- As shock frequency increases, the tested ultrasonic wave velocity for different sets of joint decreases gradually, so does the wave velocity with groups of joints increasing. The degree of damage of the specimen can be analyzed by using a non-metal ultrasonic detector.
- From the variables responsible for damage based on the ultrasonic wave definition and experimental results, it can be known that the degree of damage of the specimen is directly proportional to the groups of joints. Meanwhile, it increases with the increase of shock frequency.
- When the cyclic shock frequency is smaller, micro-cracks will be produced in the inner rock mass, which has little effect on the ultrasonic wave velocity. The macro-defects will appear in the specimen together with the increase of shock frequency.

## ACKNOWLEDGMENTS

The authors would like to acknowledge the support of the Scientific Research Fund of the

National Natural Science Foundation of China (NO.51204098), the Natural Science Foundation of Hunan Province of China (NO.11JJ6045), and the Research and Development Plan of Hunan Province of China (NO. 2015SK2058-4).

## REFERENCES

- Halakatevak is N. & Sofianos A.L. 2010. Strength of a blocky rock mass based on an extended plane of weakness theory [J]. *International Journal of Rock Mechanics & Mining Sciences* 47: 568–582.
- Jia P. & Zhu W.C. 2012. Dynamic-static coupling analysis on rock burst mechanism in jointed rock mass [J]. *Journal of Central South University* 19(11): 3285–3290.
- Liu D.N. & Chen S.R. 2005. Experimental study on damage evolution law of rock under cyclic impact loading [J]. *Chinese Journal of Rock Mechanics and Engineering* 24(22): 4094–4098.
- Liu H.Y., Huang S.S. & Li G.B. et al. 2013. Test study of strength and failure mode of pre-existing jointed rock mass [J]. *Rock and Soil Mechanics* 34 (5): 1235–1241.
- Liu H.Y., Lu S.R. & Zhang L.M. 2014. Dynamic damage constitutive model for persistent jointed rock mass based on combination model method [J]. *Chinese Journal of Geotechnical Engineering* 36(10): 1814–1821.
- Sazid M. & Singh T.N. 2013. Two-dimensional dynamic finite element simulation of rock blasting [J]. *Arab J Geosci* 6(10): 3703–3708.
- Wang T.T. & Huang T.H. 2009. A constitutive model for the deformation of a rock mass containing sets of ubiquitous joints [J]. *International Journal of Rock Mechanics & Mining Sciences* 46: 521–530.
- Xiao J.Q. 2009. Theoretical and experimental investigation on fatigue properties of rock under cyclic loading [D]. Changsha: *Central South University*.
- Xie H.P. 1990. Rock damage mechanics of concrete [M]. Xuzhou: *China University of Mining and Technology Press*: 152–166.
- Xie N., Zhu Q.Z. & Xu L.H. et al. 2011. A micromechanics-based elastoplastic damage model for quasi-brittle rocks [J]. *Computers and Geotechnics* 38: 970–977.
- Yao W.X. 2003. Fatigue life prediction of structures [M]. Beijing: *National Defense Industry Press*.
- Zhao Y.Q., Liu H.Y. & Lu S.R. et al. 2015. Damage constitutive model of jointed rock mass based on coupling macroscopic and mesoscopic flaws [J]. *Journal of Central South University (Science and Technology)* 46(4): 1489–1496.
- Zhu J.J., Li X.B. & Gong F.Q. et al. 2013. Dynamic characteristics and damage model for rock under uniaxial cyclic impact compressive loads [J]. *Chinese Journal of Geotechnical Engineering* 35(3): 531–539.

## Heating characteristics of microwave-absorbing asphalt mixture

Wei Liu, Peng-hui Miao & Sheng-yue Wang

*School of Transportation, Southeast University, Nanjing, P.R. China*

**ABSTRACT:** Microwave heating technology has been applied in pavement maintenance for years. In this paper, two different methods are considered to improve the efficiency of microwave heating. Steel slag and Carbonyl Iron Powder (CIP) were chosen respectively to replace all fine aggregates and 1/10 filler of the basalt asphalt mixture. The electromagnetic characteristics, microwave heating rate and temperature field distribution of the steel slag asphalt mixture, CIP asphalt mixture and basalt asphalt mixture were studied and an electromagnetic software named CST was used to simulate the temperature field after microwave-heating. The results showed that the heating rates of the steel slag asphalt mixture and CIP asphalt mixture were 10°C higher than the basalt asphalt mixture. Laboratory experiment of the temperature field had good uniformity and was consistent with the CST simulation. Due to the better permittivity and permeability, steel slag and CIP asphalt mixture can be good microwave absorbing materials to apply in the pavement maintenance.

**Keywords:** steel slag; microwave heating; carbonyl iron powder; cst; asphalt mixture

### 1 INTRODUCTION

Early damage occurs in asphalt road due to environmental effects and heavy loads after a few years open to traffic. And it will accelerate if there is no repair in time. The majority of damage is the result of material properties themselves instead of the road structure. For this reason, a perfect timing to make preventive repairs can prolong the service life of road effectively. As an organic polymer, asphalt has reversible thermal properties of dissolution and precipitation, which explains the self-healing of asphalt. Study shows (Little & Bhasin 2007) that healing occurs after the load that generated the damage has been removed, because of the diffusion of the molecules between the two sides of the crack. It is also well known that the amount of healing increases when the material is subjected to a higher temperature during the rest period (Daniel & Kim 2001). Heating can lead to better healing of asphalt road. Conventional method is the infrared heating through heat conduction. The penetration depth is shallow and the temperature distribution is not uniform. The pavement surface may be overheated and result in fatal asphalt fumes (Terrel et al.1997).

Therefore, microwave energy is chosen to replace infrared energy. Microwave heating has a lot of advantages such as easy to control, good immediacy and rapidity. The idea of using microwave energy was initiated more than 40 years ago. Application of microwave heating in asphalt pavement

can be mainly divided into five aspects, microwave heating effects on the performance of asphalt mixture (Al-Ohaly & Terrel 1998, Al-Qadi et al.1991), microwave dielectric constants of asphalt mixture (Jaselskis et al.2003), microwave absorption efficiency of different asphalt mixtures (Hopstock & Zanko 2005, Gallego et al.2013), development of the microwave equipment for road (Hall 2008, Eliot 2013) and the mathematical model of microwave heating pavement materials (Benedetto & Calvi 2013). During the pavement rehabilitation, the time of closed traffic is as little as possible. But the heating rate of traditional asphalt mixture is not as effective as we needed. On the basis of predecessors' researches, two different methods are considered to improve the efficiency of microwave heating. One is to replace basalt or limestone with steel slag; the other is to replace mineral powder with Carbonyl Iron Powder (CIP).

As a kind of industrial waste, steel slag contains some metal oxides, especially transition metal oxide  $Fe_2O_3$ , and has strong microwave absorption ability. This not only can effectively improve the utilization rate of steel slag to avoid environmental pollution, but also can significantly enhance the absorbing ability of asphalt mixture. CIP is a kind of magnetic metal powder, obtained by pentacarbonyliron decomposition. CIP has the characteristics of high magnetic permeability, low coercive force and cheap price (Zivkovic & Murk 2012). Besides, CIP has large specific surface area and good temperature stability, so that it can guarantee the warming

of asphalt with good contact. In this paper, electromagnetic parameters and heating properties of steel slag asphalt mixture and CIP asphalt mixture were studied to verify the microwave heating effect. The analysis of the temperature distribution was carried out in CST MPHYICS STUDIO (MPS), a combined electromagnetic and thermal analysis tool integrated into CST STUDIO SUITE.

## 2 EXPERIMENTAL PROGRAM

### 2.1 Materials

90# asphalt was adopted as the binder. Basalt was used as the coarse aggregate and limestone as the fine aggregate and filler. Steel slag was used to replace all the fine aggregate to make the steel slag asphalt mixture specimen and CIP was used to replace 1/10 limestone filler to make the CIP asphalt mixture specimen. Detailed parameters of steel slag and CIP were described in Tables 1 and 2. The gradation was AC-13, a conventional continuously dense gradation.

### 2.2 Experimental method

Free-space method was used to measure the electromagnetic properties including permittivity and permeability. The measurement system included the vector network analyzer of Agilent E5071C, the waveguide input standard gain horn antenna of Hengda HD-26SGAH15 and the coaxial cable.

The microwave heating rate was measured via a 2450 MHz microwave oven. The surface temperature was tested by the infrared thermometer and the inner by the thermocouple. FLIR was used to obtain the temperature distribution in the speci-

Table 1. Chemical analysis of steel slag (%).

Material	Loss	SiO <sub>2</sub>	Al <sub>2</sub> O <sub>3</sub>	Fe <sub>2</sub> O <sub>3</sub>	CaO	MgO	Total
Steel slag	-1.95	15.6	2.04	25.55	41.87	11.68	94.79

Table 2. Carbonyl iron powder test report.

Index	Measured value	Standard value
Fe (%)	98.08	≥97.50
C (%)	0.74	≤0.9
O (%)	0.25	≤0.6
d50	3.762	—
Bulk density (g/cm <sup>3</sup> )	2.60	1.8~3.0
Tap density (g/cm <sup>3</sup> )	4.10	≥4.0
Average particle size (μm)	3.85	3.5~5.0

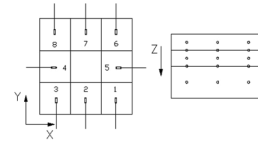


Figure 1. Temperature sensor arrangement diagram.

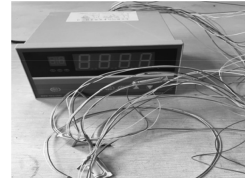


Figure 2. Sensor and the multipoint circuit detector instrument.

men surface. The specimens were dug by the core-drilling machine to create a hole in the center to measure the internal temperature immediately and accurately.

The laboratory experiment of temperature distribution was done to compare with the numerical simulation. The 30 cm × 30 cm × 20 cm slab of asphalt mixture was fabricated to simulate the pavement, by the combination of two 30 cm × 30 cm × 5 cm slabs and one 30 cm × 30 cm × 10 cm slab (Wang et al. 2011). They were stuck to each other by the asphalt, representing the top, middle and under layers, respectively. Five layers of temperature sensors were embedded in the mixture slab at 2.5, 5, 7.5, 10, and 15 cm depth from the slab surface. Eight temperature sensors were distributed into each layer of the slab, as illustrated in Figure 1. The temperature sensor is sealed in a 15 mm length and 4 mm diameter stainless steel tube, which can effectively block the microwave radiation from heating the sensor itself and inducing testing errors. The temperature sensor was linked to the multipoint circuit detector instrument (Fig. 2), whose working range is from 0 to 500°C.

## 3 RESULTS AND DISCUSSION

### 3.1 Electromagnetic property of the asphalt mixture at microwave frequencies

The electromagnetic parameters include the complex permittivity and permeability. The real part of the complex permittivity  $\epsilon'$  stands for the ability of electric field storage and the imaginary part  $\epsilon''$  stands for the ability of electric field loss. The real part of the complex permeability  $\mu'$  stands for the ability of magnetic field storage and the imaginary

part  $\mu'$  stands for the ability of magnetic field loss. They can be calculated by reversing scattering parameter  $S_{11}$  and phase angle in different conditions. The results were shown in Figure 3.

As shown in Figure 3, the value of  $\epsilon'$  remained basically unchanged while  $\epsilon''$  increased with the frequency. The value of  $\mu'$  decreased with the frequency while  $\mu''$  increased with the frequency except for the basalt asphalt mixture. The reason was that majority of the asphalt mixture were nonmagnetic materials and CIP took a very small proportion.

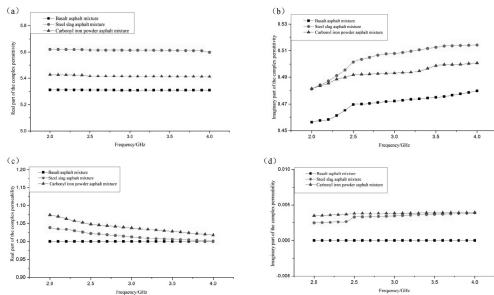
The microwave loss mechanism was mainly the dielectric loss in traditional asphalt mixture. For the other two kinds of asphalt mixture, the microwave loss mechanism included both the dielectric loss and the magnetic loss. It could be preliminarily ascertained that the microwave heating rates of the steel slag asphalt mixture and the CIP asphalt mixture were higher than the basalt asphalt mixture.

### 3.2 Microwave heating characteristics of the asphalt mixture

The compacted specimens were put in the microwave oven for heating. The temperatures were recorded every 20 seconds in 2 min. And FLIR took pictures in every minute. The results were showed in Figures 4 and 5.

As shown in Figure 4, both the surface temperatures and the internal temperatures were rising gradually versus elapse time. The microwave heating rates of the steel slag asphalt mixture and the CIP asphalt mixture were higher than the basalt asphalt mixture. The internal temperatures were 10°C above the surface.

As seen from Figure 5, the temperatures varied obviously in 0, 1 min and 2 min. But the difference among them was not that much, probably because



(a) Relationship between  $\epsilon'$  and frequency; (b) relationship between  $\epsilon''$  and frequency; (c) relationship between  $\mu'$  and frequency; (d) relationship between  $\mu''$  and frequency;

Figure 3. Relationship between complex permittivity and permeability of asphalt mixture and frequency.

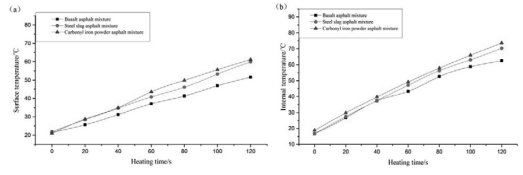


Figure 4. Temperature variation curve of microwave heating temperature on asphalt mixture: (a) surface temperature, (b) internal temperature.

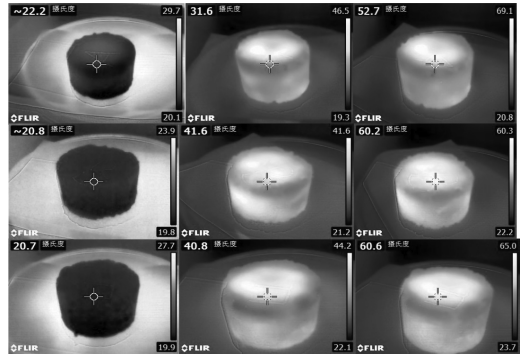


Figure 5. Infrared photos of microwave heating: 0 min (left), 1 min (middle) and 2 min (right).

the contents of steel slag and CIP were small. We can do further research to find the optimum content to obtain better microwave heating rate.

### 3.3 Temperature distribution of the asphalt mixture

The internal temperature distribution was detected to analyses the microwave heating mechanism so that it could provide the basic theory for the microwave heating technology in road maintenance. The temperatures of the mixture slab were monitored every five minutes for 15 min by a Witol industrial microwave oven. The results were shown in Figure 6. In this paper, we only considered the basalt asphalt mixture as a representative. And the numerical simulation was on the basis of actual pavement condition by the CST MPMYSICS STUDIO. The results were shown in Figure 7.

As seen from Figure 6, the temperature distribution was non uniform in each layer at different heating times. There was no temperature change at the beginning. With increasing time of microwave heating, the temperature variations in different depth layers showed more significant superimposing effects. Meanwhile, the temperature distribution also had some differences in the depth direction. Temperatures firstly increased and then

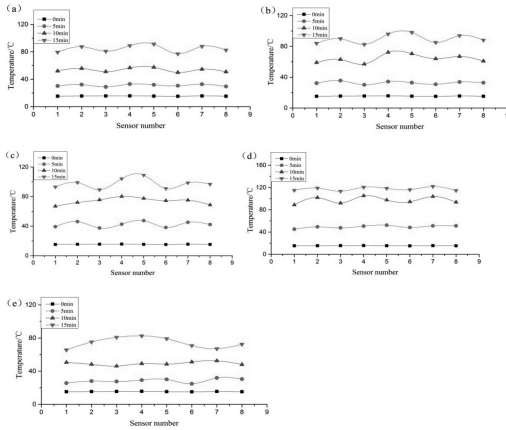


Figure 6. Temperature distributions in the mixture slab with different microwave heating time (a) 2.5 cm, (b) 5 cm, (c) 7.5 cm, (d) 10 cm, (e) 15 cm.

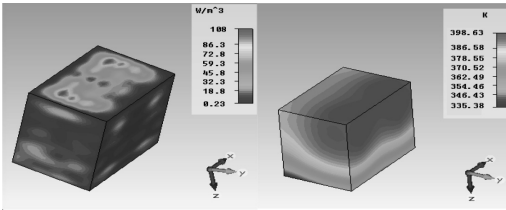


Figure 7. Power loss density and temperature distribution of microwave radiation on asphalt mixture for 15 min (the upper surface is 12 cm depth of the model).

decreased with the layer depth at the same heating moment. The asphalt mixture was a non-homogeneous and anisotropic material, which would inevitably cause some temperature variations under the microwave radiation. But the variation amplitudes were much smaller than the other heating methods. It can be considered that microwave heating has good uniformity.

As shown in Figure 7, the power loss density and the temperature were not uniformly distributed in the horizontal cross section. The temperature distribution is related to the power loss density, that is, where the loss power density is higher, the temperature is higher. The maximum temperature was 11 cm depth from the surface instead of the surface. The temperature firstly increased and then decreased in Z direction. Although the temperature distributions were non uniform in both horizontal and vertical direction, the temperature variations were acceptable.

The obtained model predictions were in good agreement with the laboratory experimental

results except for some deviations. It was feasible to analyze the microwave heating temperature field distribution of the asphalt mixture by numerical simulation method.

## 4 CONCLUSIONS

Steel slag and carbonyl iron powder were chosen respectively to replace all fine aggregate and 1/10 filler of the traditional asphalt mixture in this research. The electromagnetic characteristics, microwave heating rate and temperature field distribution of the steel slag asphalt mixture, CIP asphalt mixture and basalt asphalt mixture were studied. Some preliminary conclusions could be drawn as follows.

1. The electromagnetic properties and microwave heating rate of steel slag asphalt mixture and CIP asphalt mixture had a limited improvement compared to the basalt asphalt mixture, mainly because the small contents of steel slag and CIP in the asphalt mixture limited the ability of the microwave absorption. Therefore, it is of great significance to determine the optimum content of steel slag or CIP.
2. Microwave heating on the asphalt mixture had good integrity and uniformity, which had significant advantages compared to the infrared heating and direct contact flame. Numerical simulation was consistent with the experimental results, so it could be used to simulate temperature distribution in asphalt pavement with microwave heating, to better guide the microwave heating technology for pavement maintenance.

## 5 FURTHER STUDY

It has been proved that steel slag asphalt mixture and CIP asphalt mixture can be heated much faster with microwave energy than basalt asphalt mixture. However, work needs to be done to detect the main factors of heating rate, such as the gradation of steel slag and the content of CIP. Pretreatment also can be done to enrich the proportion of  $Fe_3O_4$  in steel slag. Fatigue performance can serve as an index to evaluate the healing effect.

## ACKNOWLEDGMENTS

This work was financially supported by the Fundamental Research Funds for the Central Universities and the Graduate Education Innovation Project of Jiangsu Province, China (KYLX15\_0145).



## REFERENCES

- Al-Ohaly, A. A., & Terrel, R. L. 1988. Effect of microwave heating on adhesion and moisture damage of asphalt mixtures (No. 1171).
- Al-Qadi, I. L., Ghodgaonkar, D. K., Varada, V. K., & Varadan, V. V. 1991. Effect of moisture on asphaltic concrete at microwave frequencies. *IEEE Transactions on Geoscience and Remote sensing*, 29(5), 710–717.
- Benedetto, A., & Calvi, A. 2013. A pilot study on microwave heating for production and recycling of road pavement materials. *Construction and Building Materials*, 44, 351–359.
- Daniel, J. S., & Kim, Y. R. 2001. Laboratory evaluation of fatigue damage and healing of asphalt mixtures. *Journal of Materials in Civil Engineering*, 13(6), 434–440.
- Eliot, M. 2013. U.S. Patent Application No. 13/887,828.
- Gallego, J., del Val, M. A., Contreras, V., & Páez, A. 2013. Heating asphalt mixtures with microwaves to promote self-healing. *Construction and Building Materials*, 42, 1–4.
- Hall, D. R. 2008. U.S. Patent No. 7,413,375. Washington, DC: U.S. Patent and Trademark Office.
- Hopstock, D. M., & Zanko, L. M. 2005. Minnesota taccinite as a microwave-absorbing road aggregate material for deicing and pothole patching applications.
- Jaselskis, E. J., Grigas, J., & Brilingas, A. 2003. Dielectric properties of asphalt pavement. *Journal of materials in civil engineering*, 15(5), 427–434.
- Little, D. N., & Bhasin, A. 2007. Exploring Mechanism of Healing in Asphalt Mixtures and Quantifying its Impact. In *Self healing materials* (pp. 205–218). Springer Netherlands.
- Terrel, R. L., Epps, J. A., & Sorenson, J. B. 1997. Hot-In-Place Recycling State-of-the-Practice. *Journal of the Association of Asphalt Paving Technologists*, 66.
- Wang, H. N., Xue, L., & Hao, P. W. 2011. Laboratory Evaluation of Microwave Heating Method for Hot In-Place Recycling. *Journal of Testing and Evaluation*, 39(6), 1–8.
- Zivkovic, I., & Murk, A. 2012. Extraction of dielectric and magnetic properties of carbonyl iron powder composites at high frequencies. *Journal of Applied Physics*, 111(11), 114104.



**Taylor & Francis**

Taylor & Francis Group

<http://taylorandfrancis.com>

# Numerical analysis of the influence range of a tunnel ventilation resistance grid

Yun-xiao Xin

*School of Highway, Chang'an University, Xi'an, China*

Ya-qiong Wang

*Shaanxi Provincial Major Laboratory for Highway Bridge and Tunnel, City, Chang'an University, Xi'an, China*

Kai Lai

*School of Highway, Chang'an University, Xi'an, China*

**ABSTRACT:** According to the equivalent design theory, resistance grids can effectively reduce the length of the tunnel ventilation model. In order to study the influence length of resistance grids in the model, this paper analyzes the distribution of fluid velocity and pressure in different grid types and wind speeds by numerical simulation. The results show that with the constant effective area, there are more holes in the resistance grid, the average flow function is more significant, and the influence length is significantly reduced, but it has little effect on the grid pressure drop. With the increase of wind speed, the pressure drop increases significantly. It is suggested that the number of resistance grid holes installed in the ventilation model be more than 500, and the total influence length of the model should be taken into account for about thrice smaller than the equivalent diameter of the model section.

**Keywords:** tunnel ventilation; resistance grid; model test; numerical simulation

## 1 INTRODUCTION

Tunnel ventilation is an important measure to ensure traffic safety and comfort during operation. In order to observe and study the distribution of ventilation in the tunnel, we usually take experimental means to observe it. Compared with the field test, model test, which can conveniently control variables, can directly reflect the characteristics and rules of the tunnel ventilation changes. Thus, it can enhance the understanding of tunnel ventilation problems and provide a reliable basis for the selection and optimization of the ventilation mode (Fang 2005; Tu 2007). At present, the method of numerical simulation has been used to study the tunnel ventilation, but the physical model tests to study the highway tunnel ventilation are still relatively few. Chongqing Communications Technology Research and Design Institute (1999) conducted several studies on tunnel ventilation, which established a more-than-100-m same-size tunnel model and organized the compilation of "Specifications for Design of Ventilation and Lighting of Highway Tunnel (JTJ 026.1-1999)".

In general, the length of the long highway tunnel is more than 3 km. If the test model adopts the original structure size, it is almost impossible

to achieve this length because of the limitation of the experimental area and condition. According to the similarity theory of the physical model, with the geometric similarity, the model is developed into a fully developed turbulent state, which is the only way to keep similarity relationship between the prototype and the model (Liu 1999), so we can construct equal proportion model with the similarity theory. Yan Zhiguo, Yang Qixin & Wang Mingnian et al. (2006), through the model test of Qinling Zhongnanshan highway tunnel, studied the longitudinal ventilation mode of vertical (oblique) wells. They used the air flow organization mode in the tunnel when the fire is generated in different ventilation sections from the model test.

Although establishing the equal proportion model can solve some problems based on the similarity theory, the length of the tunnel model sometimes is limited. Considering the ventilation physical model experiments is often to just study the complex local site, so the variable rate model can be used to decrease the length of the tunnel ventilation model with the similar resistance. In order to ensure the similarity in resistance between the prototype and model on the variable rate model test, we generally use the resistance grid to replace the flow resistance along the line. On the one hand, it adds roughness

of the model, which can make up for the decrease of the resistance coefficient along the line caused by model material. On the other hand, it can make up the decreased flow resistance along the line caused by decreasing the length of the model. Xie Yongli, Wang Yaqiong & Fang Lei et al.(2010) studied the combined longitudinal ventilation mode of the vertical (inclined) well on Qinling Zhongnanshan highway tunnel by model tests. In the process of model test, the 1:24 and 1:8 physical model test systems were established, and the resistance grid was used to replace the on-way resistance, which can effectively decrease the length of the model. Wang Yaqiong, Xia Fengyong & Xie Yongli et al. (2014) studied the two-hole complementary longitudinal ventilation mode on the Dabie Mountain highway tunnel by model test, established the 1:10 large-scale ventilation physical model, and used 14 resistance grids in the model to replace the on-way resistance, which decreased the model length to 72 m.

Because the installation of resistance grids can influence the local area in tunnel ventilation models, the scope of influence by resistance grid is analyzed by numerical simulation in this paper. There are many shapes of resistance grids, and different resistance grid types lead to different effect range. Therefore, we simulate the tunnel flow with the different number of holes in the grid and different wind velocity using FLUENT software to analyze the effect scope and draw the related conclusion that can provide reference in the future.

## 2 BASIC PRINCIPLE

### 2.1 Selection of similarity criteria

During the design of highway tunnel ventilation models, through the similarity criterion to establish the physical relationship between prototype and model, we can determine their proportional relationship, to ensure the similarity of the two flow systems. According to the fundamental hypothesis of tunnel ventilation, the air flow in the tunnel can be idealized as an incompressible viscous fluid flow, and the similarity criterion can be derived by the continuity equation and the dimensionless form of Navier–Stokes equations. In tunnel ventilation physical model tests, these two flow systems respectively follow the general differential equation:

$$\frac{C_u}{C_l} \left( \frac{\partial u_x}{\partial x} + \frac{\partial u_y}{\partial y} + \frac{\partial u_z}{\partial z} \right) = 0 \quad (1)$$

$$\begin{aligned} \frac{C_u}{C_l} \frac{\partial u_x}{\partial t} + \frac{C_u^2}{C_l} \left( u_x \frac{\partial u_x}{\partial x} + u_y \frac{\partial u_x}{\partial y} + u_z \frac{\partial u_x}{\partial z} \right) = \\ - \frac{C_p}{C_\rho C_l} \cdot \frac{1}{\rho} \frac{\partial p}{\partial x} + \frac{C_\nu C_u}{C_l^2} \cdot \nu \left( \frac{\partial^2 u_x}{\partial x^2} + \frac{\partial^2 u_x}{\partial y^2} + \frac{\partial^2 u_x}{\partial z^2} \right) \end{aligned} \quad (2)$$

$$\begin{aligned} \frac{C_u}{C_l} \frac{\partial u_y}{\partial t} + \frac{C_u^2}{C_l} \left( u_x \frac{\partial u_y}{\partial x} + u_y \frac{\partial u_y}{\partial y} + u_z \frac{\partial u_y}{\partial z} \right) = \\ - \frac{C_p}{C_\rho C_l} \cdot \frac{1}{\rho} \frac{\partial p}{\partial x} + \frac{C_\nu C_u}{C_l^2} \cdot \nu \left( \frac{\partial^2 u_y}{\partial x^2} + \frac{\partial^2 u_y}{\partial y^2} + \frac{\partial^2 u_y}{\partial z^2} \right) \end{aligned} \quad (3)$$

$$\begin{aligned} \frac{C_u}{C_l} \frac{\partial u_z}{\partial t} + \frac{C_u^2}{C_l} \left( u_x \frac{\partial u_z}{\partial x} + u_y \frac{\partial u_z}{\partial y} + u_z \frac{\partial u_z}{\partial z} \right) = \\ C_g \cdot g - \frac{C_p}{C_\rho C_l} \cdot \frac{1}{\rho} \frac{\partial p}{\partial x} + \frac{C_\nu C_u}{C_l^2} \cdot \nu \left( \frac{\partial^2 u_z}{\partial x^2} + \frac{\partial^2 u_z}{\partial y^2} + \frac{\partial^2 u_z}{\partial z^2} \right), \end{aligned} \quad (4)$$

where  $u_x, u_y, u_z$  = velocity components;  $p$  = air pressure;  $\rho$  = air density;  $\nu$  = fluid viscosity;  $g$  = gravitational acceleration;  $C_u$  = speed ratio;  $C_l$  = time ratio;  $C_l$  = length ratio;  $C_p$  = pressure ratio;  $C_\rho$  = density ratio; and  $C_g$  = gravitational acceleration ratio.

By the similarity theory, when the prototype and the model flow system are similar, the coefficients of the above equations should be equal; therefore,

$$\frac{C_u}{C_l} = \frac{C_u^2}{C_l} = C_g = \frac{C_p}{C_\rho C_l} = \frac{C_\nu C_u}{C_l^2} \quad (5)$$

From Equation 5, we can derive three similarity criteria: gravity similarity criterion, pressure similarity criterion, and viscous force similarity criterion. Because the tunnel ventilation flow system is an incompressible constant flow system, in order to make the prototype flow similar to the model, as long as the model satisfies the aforementioned three criteria, this similarity can be realized. Therefore, it requires that the corresponding closed force polygons, which are composed of gravity, viscous force, dynamic pressure, and inertia force of these two flow systems, are similar. By the similar polygons concept of theoretical mechanics, as long as the gravity, viscous force, and inertia force of the corresponding point are similar, the pressure will automatically be similar. Therefore, if the flow similarity condition between the model and the prototype is satisfied, both of them have equal Froude number and Reynolds number. In fact, these two similarity criteria are difficult to satisfy at the same time. Because only when the model is as large as the prototype, the speed ratio and length ratio can meet square and reciprocal relationship at the same time, which leads the model to lose its importance. As the viscous force is the main factor affecting the air flow rate, the viscous force similarity is chosen as the similar condition in the model test of tunnel ventilation, so the prototype and the model have the same Reynolds number.

### 2.2 The role of resistance grid

The similarity theory and the Nikuradse test show that the model flow state stay at the drag square area

with the geometric similarity is the only condition for the model to be similar to the prototype in flow system. However, the geometric similarity is generalized, which contains the absolute roughness of the wall surface, to make the model and the prototype have the same relative roughness and to achieve similar resistance. Because of the rough prototype surface, to achieve strict geometric similarity between the model and the prototype, the size, shape, and location of each bump on the model ought to be copied. In fact, this is almost impossible to achieve; even if these irregularities are accurately reduced to the model, its impact on fluid friction blocks will not be similar to the prototype.

As its inherent nature, the turbulent flow strictly is not constant, so the time-averaged flow field is more concerned in engineering design. Therefore, the ventilation of the tunnel is assumed to be steady flow, which uses the time-averaged flow field, and the flow does not change with time. Furthermore, the engineering model test is largely studying the macro overall law, such as the section average wind speed and average pressure. Even on a point, the law only reflects the time-averaged performance of a micro-mass turbulent. Therefore, we should give up strict geometric similarity in tunnel ventilation of the physical model test, maintaining the length geometric characteristics similar, to ensure that the resistance effects are similar, so as to achieve the engineering research purpose of flow approximate similarity of the model and the prototype. In the tunnel ventilation physical model experiment, adding resistance grids is to give up the strict geometric similarity and use the variable rate model, to maintain the approximate similarity of flow system study area between the model and the prototype, which leads the test model to achieve many study purposes in limit factors.

The practical fluid has certain viscosity, and the flow process overcomes the self-deformation movement to generate internal friction, which converts part of the mechanical energy into heat, thereby causing the loss of energy. According to the different boundary conditions of fluid motion, the energy loss is divided into frictional resistance loss  $h_f$  and local resistance loss  $h_j$ . In tunnel ventilation physical model experiment, from the resistance effect, the local resistance pressure drop of resistance grid can instead be part of the frictional pressure drop (the on-way frictional pressure drop), so as to achieve the effect similarity with the model and the prototype. According to the resistance equivalent theory  $h_j = h_f$ , we can derive that:

$$\lambda \cdot \frac{l}{D} \cdot \frac{\rho}{2} V^2 = \xi \cdot \frac{\rho}{2} V^2, \quad (5)$$

where  $\lambda$  = the on-way resistance coefficient and  $\xi$  = the local resistant coefficient.

In the simulation of tunnel ventilation, although the local resistance pressure drop of resistance grids can replace part of the on-way frictional pressure drop, the equivalent method is not applicable to all the problems of tunnel ventilation simulation. After all, this method ignores a large portion of the variation along the way. Therefore, the resistance grid model is generally used to study the tunnel local area, and it is not applicable to the physical model test, which requires the continuity of longitudinal length. In order to study the influence range of different grid types with different wind speeds, the following will introduce the numerical simulation of grids with different hole numbers.

### 3 CALCULATION MODEL ANALYSIS

#### 3.1 Model parameters

To facilitate the calculation, the length of the resistance grid numerical simulation model is set at 10 m, the equivalent diameter of model section is set at 0.845 m, and the resistance is located 2 m away from the entrance of the model. Model boundary condition is set to velocity-inlet, outlet boundary condition is set to outflow, and the resistance grid is set to the solid wall boundary. In order to study the effect of the resistance grid on the flow field, the surface absolute roughness is set to 0. The standard  $k$ - $\varepsilon$  model is adopted to the turbulence model, and the discrete solver is used to solve this model.

#### 3.2 Simulation results

According to the hole number of resistance grids, this test is divided into four working conditions: single-hole resistance grid, 46 holes resistance grid, 180 holes resistance grid, and 725 holes resistance grid. The effective area ratio of all the grids is 47% and the inlet wind speed is divided into two conditions: 3 and 6 m/s.

##### 3.2.1 Single-hole resistance grid

###### 1. The flow field distribution with 3 m/s wind speed

Figure 1 shows that, when the air flows through the single-hole resistance grid, it exhibits the characteristics of turbulent jet. Because of the decrease of section area, the wind velocity increases and the static pressure decreases obviously. The cross-sectional distribution of wind speed and pressure is uneven, and airflow varied significantly. After the air flow through the single-hole resistance grid, the section restores size, wind speed decreases, and static pressure increases gradually. After a certain distance, the wind speed restores to the previous value, static

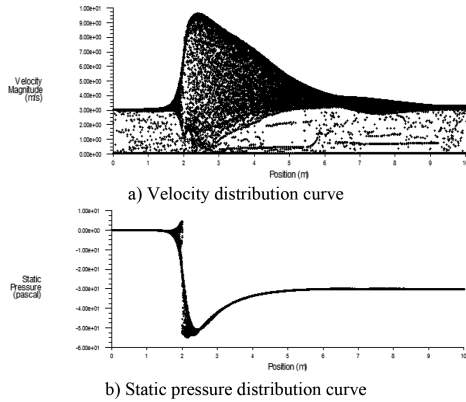


Figure 1. Flow field distribution of the single-hole resistance grid in tunnel model with 3 m/s wind speed.

pressure becomes stable, the distribution of wind speed and pressure in the cross-section becomes uniform, the impact of resistance grid disappears, and the resistance loss is mainly reflected in the static pressure loss. On the basis of comprehensive analysis of the wind speed and pressure, with 3 m/s wind speed, the influence upstream length of single-hole resistance grid is 1 m, the downstream length is 7 m, and the total influence length is about 10 times of the model section equivalent diameter. The pressure drop value is 30.36 Pa.

2. The flow field distribution with 6 m/s wind speed  
 Figure 2 shows that, with the 6 m/s wind speed, the influence upstream length of the single-hole resistance grid is 1 m, the downstream length is 7 m, and the total influence length is about 10 times of the model section equivalent diameter. The pressure drop value is 121.31 Pa.

### 3.2.2 46 holes resistance grid

1. The flow field distribution with 3 m/s wind speed  
 Figure 3 shows that, on the basis of comprehensive analysis of the wind speed and pressure, with the 3 m/s wind speed, the influence upstream length of 46 holes resistance grid is 0.5 m, the downstream length is 4 m, and the total influence length is about six times of the model section equivalent diameter. The pressure drop value is 34.38 Pa.

2. The flow field distribution with 6 m/s wind speed  
 Figure 4 shows that, with the 6 m/s wind speed, the influence upstream length of 46 holes resistance grid is 0.5 m, the downstream length is 4 m, and the total influence length is about six times of the model section equivalent diameter. The pressure drop value is 136.59 Pa.

### 3.2.3 180 holes resistance grid

1. The flow field distribution with 3 m/s wind speed

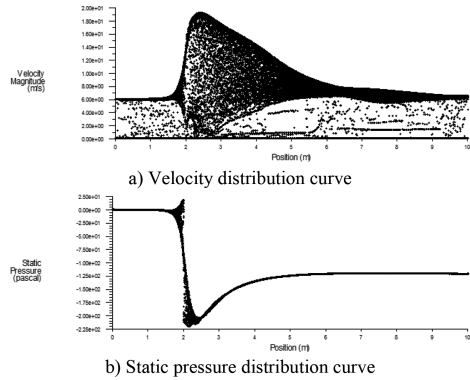


Figure 2. Flow field distribution of the single-hole resistance grid in tunnel model with 6 m/s wind speed.

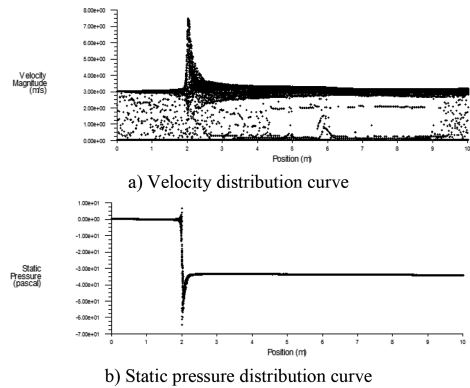


Figure 3. Flow field distribution of the 46 holes resistance grids in tunnel model with 3 m/s wind speed.

Figure 5 shows that, with the 3 m/s wind speed, the influence upstream length of 180 holes resistance grid is 0.5 m, the downstream length is 2 m, and the total influence length is about thrice the model section equivalent diameter. The pressure drop value is 34.49 Pa.

2. The flow field distribution with 6 m/s wind speed

Figure 6 shows that, with the 6 m/s wind speed, the influence upstream length of 180 holes resistance grid is 0.5 m, the downstream length is 2 m, and the total influence length is about thrice the model section equivalent diameter. The pressure drop value is 136.89 Pa.

### 3.2.4 725 holes resistance grid

1. The flow field distribution with 3 m/s wind speed

Figure 7 shows that, with the 6 m/s wind speed, the influence upstream length of 725 holes resistance grid is 0.5 m, the downstream length is 1.5 m,

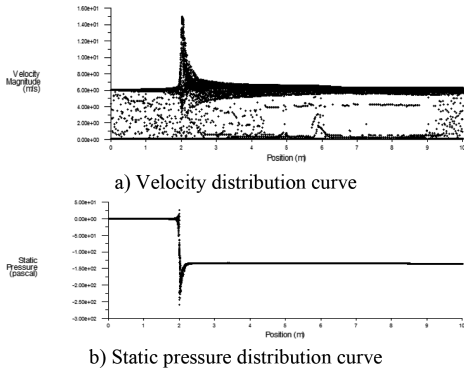


Figure 4. Flow field distribution of the 46 holes resistance grids in tunnel model with 6 m/s wind speed.

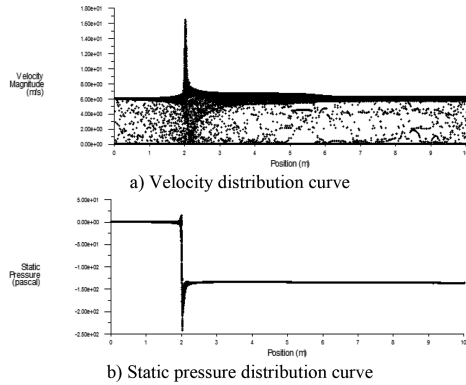


Figure 6. Flow field distribution of the 180 holes resistance grids tunnel model with 6 m/s wind speed.

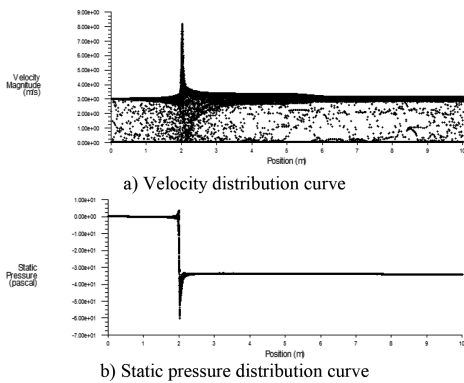


Figure 5. Flow field distribution of the 180 holes resistance grids in tunnel model with 3 m/s wind speed.

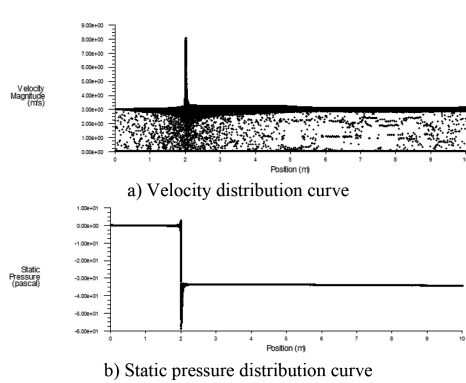


Figure 7. Flow field distribution of the 725 holes resistance grids in tunnel model with 3 m/s wind speed.

and the total influence length is about twice the model section equivalent diameter. The pressure drop value is 34.42 Pa.

## 2. The flow field distribution with 6 m/s wind speed

Figure 8 shows that, with the 6 m/s wind speed, the influence upstream length of 725 holes resistance grid is 0.5 m, the downstream length is 1.5 m, and the total influence length is about twice the model section equivalent diameter. The pressure drop value is 136.31 Pa.

### 3.3 General analysis

According to the numerical analysis results of these conditions, this paper respectively summarizes the pressure drop values (Fig. 9) and the influence length value (Fig. 10) in different grids types with 3 and 6 m/s wind speed.

As is shown in Figure 9, with the same wind speed and effective area ratio, the pressure drop

value of the single-hole resistance grid is lower, and the value of others is almost equal. Therefore, the number of holes on grids has little effect on the pressure drop. The wind speed can have a remarkable influence on the pressure drop; the higher the wind speed is, the higher the pressure drop value is.

Figure 10 shows that, with the same wind speed and effective area ratio, when the hole number of grid increases, the influence length of the resistance grid decreases. When the hole number is higher than 180, the decreasing trend of the upstream and downstream influence length tends to be gentle. The wind speed hardly affects the influence length of grid resistance. Therefore, it is suggested that the hole number of grids be higher than 500 with the constant effective area ratio, making more than 500 holes grid resistance, whose upstream and downstream influence length is less than 2.5 m, which is about thrice the diameter equivalent of the model.

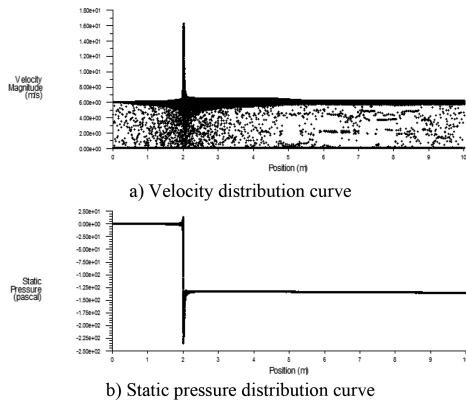


Figure 8. Flow field distribution of the 725 holes resistance grids in tunnel model with 6 m/s wind speed.

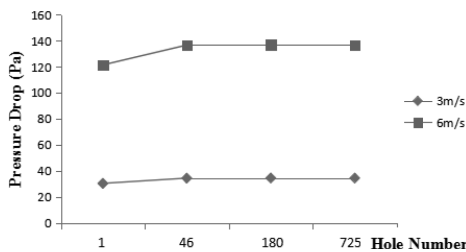


Figure 9. The pressure drop values of different resistance grids.

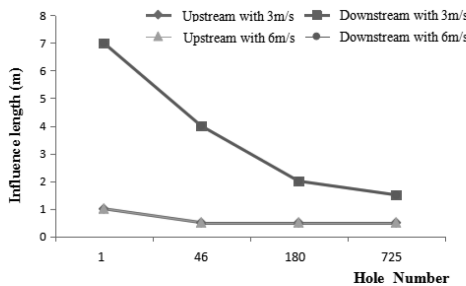


Figure 10. The influence range of different resistance grids.

#### 4 CONCLUSIONS

Through the numerical simulation research of the flow field with different number hole of resistance grid, we can obtain the following conclusions and suggestions:

When the air flows through the resistance grids, it exhibits the characteristics of turbulent jet. Because of the decrease of section area, the wind velocity increases and the static pressure decreases obviously. The cross-sectional distribution of wind speed and pressure is uneven, and airflow varied

significantly. After the air flow through the resistance grid, the section restores size, wind speed decreases, and static pressure increases gradually. After a certain distance, the wind speed restores to the previous value, static pressure becomes stable, the distribution of wind speed and pressure in the cross-section becomes uniform, the impact of resistance grid disappears, and the resistance loss is mainly reflected in the static pressure loss.

When the effective area ratio is constant, the hole number has little effect on the pressure drop, and the wind speed has a significant influence on the pressure drop. With the increase of wind speed, the pressure drop of the resistance grid increases significantly.

When the effective area ratio is constant, the hole number of resistance grids increases, the average flow function becomes more significant, the air flow fluctuation decreases, and the influence length significantly reduces.

With the constant effective area ratio, it is suggested that the hole number be more than 500 when we select the type of resistance grids, and we should consider that the upstream and downstream influence total length is less than thrice the model equivalent diameter.

#### REFERENCES

Chongqing Communications Technology Research and Design Institute. 1999. *Specifications for Design of Ventilation and Lighting of Highway Tunnel (JTJ 026.1-1999)*. Beijing: China Communications Press.

Fang, L. 2005. The physical model experiment research of long highway tunnel ventilation, *A Dissertation Submitted to Chang'an University for PhD Degree*. Xi'an: Chang'an University.

Liu, W. & Tu, Y. (eds) 1999. The similarity theory study on the highway tunnel operation ventilation model test, *Technology of Highway and Transport* (1): 27–29.

Ren, R. 2011. The study on application of the physical model experiment for long highway tunnel ventilation, *A Dissertation Submitted to Chang'an University for PhD Degree*. Xi'an: Chang'an University.

Tu, Y. & Chen, J.Z. 2007. The theoretical discussion on the physical model test of highway tunnel ventilation, *The Highway Tunnel* (4): 72–76.

Wang, S.T. 2010. The physical model experiment research of the HK-Zhuhai\_Macau undersea tunnel ventilation, *A Dissertation Submitted to Chang'an University for Master's Degree*. Xi'an: Chang'an University.

Wang, Y.Q. & Xie, Y.L.(eds) 2010. Physical model experiment on semi-transverse ventilation air inlet and outlet of subsea tunnel, *China Journal of Highway and Transport* 22(3): 76–82.

Wang, Y.Q. & Xia, F.Y.(eds) 2014. Physical model experiment on complementary ventilation of extra-long highway tunnel, *China Journal of Highway and Transport* 27(6): 84–90.

Yan, Z.G. & Yang, Q.X. (eds) 2006. Experimental study of shaft ventilation modes for road tunnels in case of fire, *Technology of Highway and Transport* (11): 101–106.



## Degradation of benzo[a]pyrene (BaP) in clay soil by electro-bioremediation

D.N. Huang

School of Municipal and Environmental Engineering, Shenyang Jianzhu University, Shenyang, China  
Institute of Applied Ecology, Chinese Academy of Sciences, Shenyang, China

Z.S. Ai, J. Tan, Y.J. Zhao & J.X. Fu

School of Municipal and Environmental Engineering, Shenyang Jianzhu University, Shenyang, China

**ABSTRACT:** Electro-bioremediation is an innovative technology for the cleanup of organic pollutant-contaminated soil. This study attempted to test the feasibility of the electrokinetic process for the bioremediation of soil contaminated with Benzo[a]pyrene (Bap) as a model Polycyclic Aromatic Hydrocarbon (PAH) at laboratory scale. The electric field significantly changed the soil pH and moisture content near the anode, which could be finely controlled by electrode polarity reversal. Over 40% of the initial 50 mg/kg Bap in clay soil could be removed under electric field with electrode polarity reversal in 40 days, around 88% higher than that with bacteria treatment only. The electrokinetic process stimulates the growth of bacteria and accelerates the decontamination efficiency of Bap. Hence, this study provides a promising electrokinetic technology for bioremediation of PAH-contaminated soils.

**Keywords:** bioremediation; electrokinetic; benzo[a]pyrene; clay soil

### 1 INTRODUCTION

Pollution of Polycyclic Aromatic Hydrocarbons (PAHs) has recently been paid a close attention because of their potential toxicity, mutagenicity, carcinogenicity, and ubiquitous distribution (Nieman et al., 2001). Moreover, because of their hydrophobicity, low volatility, and resistance to biological degradation, most PAHs are adsorbed strongly on soil particles and sediments, which make them less available for biological uptake, resulting in serious soil contamination problems. A total of 16 PAHs have been recognized as priority pollutants by the US EPA, of which, Benzo[a]pyrene (Bap), a five-ring PAH, was the first one to be identified as a carcinogen. It is generally used as an indicator for monitoring PAH-contaminated wastes.

The use of bioremediation technology for decontamination of PAHs in soils has been studied for many years. However, the long-time treatment period is a main shortcoming of this approach. Such low remediation rate is commonly due to the limited opportunities of interactions among pollutants, microorganisms, and nutrients (Wick et al., 2007). Particularly, in some low-permeability soils, the mobilities of bacteria and contaminants are further believed to be inhibited (Lahlou et al.,

2000). Thus, an associated operation of electro-bioremediation has been employed in the treatment of soil contaminated with PAHs in recent years. Several researches have revealed that the removal of some organic pollutants, such as Trichloroethylene (TCE), pentachlorophenol, and PAHs, can be improved by a proper application of electric fields (Harbottle et al., 2009; Niqui-Arroyo et al., 2006; Xu et al., 2010). Lear et al. found that the electrokinetic process has no serious negative effect on “soil microbial health”, thus they regarded this process as a viable soil remediation technology (Lear et al., 2004). Alshwabkeh and Bricka proved that the strength of electric field influenced the degradation of pollutants during *in situ* bioremediation (Alshwabkeh & Bricka, 2000).

However, soil characteristics such as pH and moisture content have a significant effect on biodegradation and contaminant behavior, which can be rapidly altered by the application of electric field (Aca & Alshwabkeh, 1993). The changed soil characters may also affect the health of the soil microbial community and its response to decontamination of pollutants. Too high electric field may have detrimental effects on the bacteria. Jackman et al. found that a current density of 200 A·m<sup>-2</sup> inactivated acidophilic bacteria (Jackman et al., 1999). Lear et al. reported that even a low electric

current ( $3.14 \text{ A}\cdot\text{m}^{-2}$ ) in soil detrimentally affected communities near the anode (Lear et al., 2004). The adverse effect on bacteria might be due to both the high electric intensity and extreme pH near the electrode. Further, the change in moisture content and contaminant distribution caused by electro dialysis might be another reason inhibiting the contaminant removal efficiency.

The control of soil pH and moisture content is of paramount importance for electro-bioremediation of organic pollutant-contaminated soils. When the electric field with periodic electrode polarity reversal is applied, the soil pH can be controlled, as the  $\text{H}^+$  and  $\text{OH}^-$  ions generated at the electrodes could be automatically neutralized by choosing an appropriate interval and the water can be distributed evenly with the changing direction of electro-osmosis flow (Lee & Yang, 2000; Luo et al., 2005). The feasibility of this strategy has been reported previously by Ho et al. (Ho et al., 1995). In their study, TCE-contaminated field was successfully decontaminated using hybrid techniques with electrode polarity reversal.

There have been several studies conducted on the decontaminants of phenanthrene in the soil by electro-bioremediation technology, but little is known to Bap because of its high persistence. The objective of this study is to test the effects of enhanced electro-bioremediation technology by reversing the polarity of electric field on the degradation of Bap. Using laboratory microcosms, this study examined the effects of electric current regime and subsequent soil pH and moisture content conditions on a clay soil artificially contaminated with Bap and inoculated with Bap-degrading bacteria.

## 2 MATERIALS AND METHODS

### 2.1 The tested soil and bacteria

Copy the template file B2ProcA4.dot. Natural clay soil samples were used for the experiment with some main properties as described in Table 1. The soil samples (0–15 cm) were collected from Shenbei New Area, Shenyang, China. The soil was air-dried at room temperature, and passed through a 2-mm-mesh sieve. The preliminary results indicated that the indigenous microorganism had a significant effect on the degradation of Bap. Hence, the soil samples were sterilized thrice by alternately using an autoclave ( $121^\circ\text{C}$  for 45 min) and a drier ( $105^\circ\text{C}$  for 30 min).

Bap was selected as the tested organic contaminant. The target concentration of Bap was  $50 \text{ mg kg}^{-1}$  (mass of contaminant/mass of dry soil). Bap was dissolved in acetone before being added to the

Table 1. Main physical and chemical properties of the tested soil.

N (%)	P (%)	Org.C	CEC	pH	Texture(%)		
					Sand	Silt	Clay
0.08	0.01	1.53	24.3	7.58	30.2	26.2	43.6

soil. After blending homogenously, a sample was taken to measure the initial concentration of Bap, as some of the contaminant might have been volatilized together with the acetone. The initial concentration of Bap was about  $41 \text{ mg kg}^{-1}$  dry soil.

A mixed culture of PAH-degrading bacteria was used as the experimental bacteria. By using basic mineral medium with Bap as the sole carbon source with components, the bacteria were isolated from a contaminated soil near a steel plant, which has long been exposed to the PAH air pollution. The bacterial cells were cultivated in the medium on a shaker ( $28^\circ\text{C}$ , 160 rpm), harvested in exponential growth phase by centrifugation, and resuspended in sterilized deionized water to obtain a highly concentrated bacterial suspension.

### 2.2 Electrokinetic cell and experiment design

The experiments were conducted in a Plexiglass chamber with dimensions  $18 \text{ cm} \times 14 \text{ cm} \times 5 \text{ cm}$ . Figure 1 shows the schematic view of the EK test setup. Approximately 600 g of the Bap-spiked soil with the initial moisture content about 25% w/w was carefully stacked into the chamber. Two cylindrical graphite electrodes (6 cm height and 1 cm diameter) were inserted into the soil at both ends of the soil chamber at a distance of about 1 cm from the wall of the chamber. Deionized water was selected as the processing fluid in both electrode chambers. A constant potential difference of 24 V ( $1.5 \text{ V cm}^{-1}$ ) was applied during the 40-day experimental period. The soil pH, moisture content, Bap concentration, and bacterial counts were analyzed periodically.

As summarized in Table 2, three tests, named Test1, Test2, Test3, were conducted to investigate the variation of soil character and Bap removal under different treatment. CK was used as a control test, without electricity or bacteria.

### 2.3 Analytical methods

The Bap concentration was determined using a HPLC Waters PAH C18 column ( $250 \text{ mm} \times 4.6 \text{ mm}$  i.d.,  $5 \mu\text{m}$ ) and Waters 2475Multi  $\lambda$  Fluorescence Detector. Before injection, the samples were filtered through a  $0.45 \mu\text{m}$  Teflon filter. The injection volume was set at  $10 \mu\text{L}$ . A mixture of acetonitrile

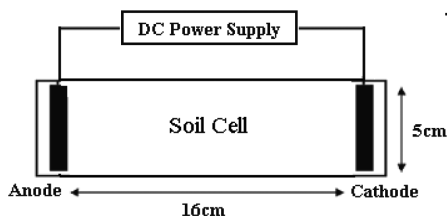


Figure 1. Schematic view of the setup used for electrokinetic experiments.

Table 2. The experimental summary.

Test code	Processing fluid	Electric field (V·cm <sup>-1</sup> )	Initial microbial count (CFU·g <sup>-1</sup> )	Polarity reversal time(h)
CK	Deionized water	0	0	0
Test 1	Deionized water	0	1.89 × 10 <sup>7</sup>	0
Test 2	Deionized water	1.5	1.97 × 10 <sup>7</sup>	0
Test 3	Deionized water	1.5	1.92 × 10 <sup>7</sup>	3

and water (90:10) was used as the mobile phase, at a flow rate of 1 ml min<sup>-1</sup>. The column temperature was maintained at 25°C. The Bap was detected by the excitation wavelength of 280 nm and emission wavelength of 410 nm.

The bacterial counts in soil were estimated by the plate counting method. For viable cell counting, 1 g of soil was diluted with 9 mL of sterile distilled water. After 10-fold serial dilution, 1 mL of final diluent was spread onto solid bacterial culture medium and incubated inverted in the dark at 28°C. The colony-forming units of bacteria were counted after 48 h. In addition, the moisture content was determined using the methods described by Lu (Lu, 2000).

### 3 RESULTS AND DISCUSSION

#### 3.1 Effect of electrokinetic process on soil pH

Test2 and Test3 were carried out to investigate pH changes under electrokinetic treatments with and without polarity reversal. In Test2, the pH values ranged from 3.4 to 8.7 at the end of the experiment, as shown in Figure 2. The acid or basic pH conditions near the electrode regions were due to the generation of H<sup>+</sup> and OH<sup>-</sup> ions in the anode and cathode during the electrokinetic process, respectively. The predomination of an acid front in the whole soil chamber was mainly due to the smaller size and faster movement of hydrogen ions (Jackman et al.,1999). The extreme pH near the electrodes produced adverse effects on the bacteria

and even slowed down the removal efficiency of contaminants.

In Test3, in which polarity reversal was performed, the pH was maintained in the range of 6.9–7.3 at the end of the experiment. The even distribution of pH resulted from mutual neutralization of H<sup>+</sup> and OH<sup>-</sup> ions generated from the anode and cathode, respectively. Compared with Test2, the anodic and alkaline pH in soil is finely controlled. The neutrality of soil was beneficial for the growth and activity of bacteria and removal of pollutants. Thus, polarity reversal was thought to be a simple technology to control the soil pH.

#### 3.2 Effect of electrokinetic process on soil moisture content

The soil moisture content distribution was analyzed throughout the soil cell after 10 days. As shown in Figure 3, the moisture content decreased near the anode and apparently increased near the cathode in Test2. The lowest moisture content (20%) was observed at 2 cm away from the anode, and the

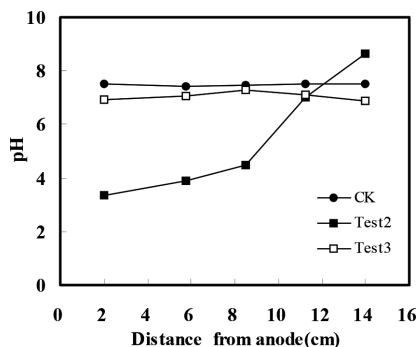


Figure 2. Change in soil pH after electrokinetic treatments.

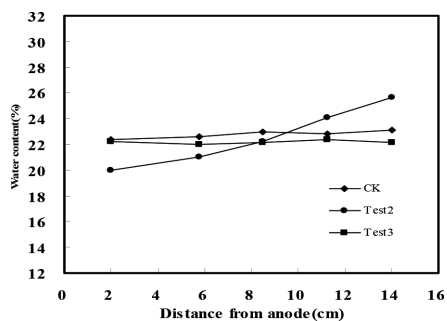


Figure 3. Change in soil water content after electrokinetic treatments.

peak moisture content (25%) was at 2 cm away from the cathode. The moisture content near the cathode was 28% higher than that near the anode. The change of soil moisture distribution was mainly attributed to the direction of migration of the electro-osmotic flow, resulting in the transport of water from the anode to the cathode. The uneven distribution of moisture content might cause the uneven distribution of bacteria and contaminants in soil, further inhibit the contact between contaminants and bacteria, and have a negative effect on the bioremediation of contaminants.

In Test3, the distribution of moisture content was even. The polarity reversal can change the direction of the electro-osmotic flow and further avoid the dryness in the anode (Xu et al.,2010). Therefore, the polarity reversal technology can help the soil moisture maintain at a stable level. It provided suitable conditions for the growth of bacteria and removal of contaminants.

### 3.3 Bap removal and bacterial counts

Bap removal is shown in Figure 4. It can be found that an obvious higher Bap removal efficiency was observed in Test2 and Test3 than that in Test1 and CK test during the whole experimental period.

In Test2, the Bap removal efficiency was 33% at the end of the experiment, while that in Test1 with bacteria treatment only was 21%. During the last 10 days, the slope of Test1 curve decreased to near zero. The decreased removal efficiency in Test1 might be due to the consumption of nutrients and the slowdown of biological metabolism. With application of electric field, the soil bacteria can maintain persistent activity in the bioremediation process. Some researchers have found similar results (Lu, 2000; Kim et al., 2010). However, the

Bap removal efficiency slightly decreased in Test 2 during the last 10 days compared with the initial stage. It might be due to the changes of soil characteristics (Figure 2 and Figure 3). In Test3, the maximum removal efficiency of Bap at the end of the experiment was 40%, around 1.9 and 1.2 times of that of Test1 and Test2, respectively. In contrast to Test2, the decreased removal efficiency was not observed in Test3, even during the last 10 days.

The changes in bacterial counts during different treatments showed that in the application of electric field, the Bap-degrading bacterial counts were generally higher than that without DC treatment. The most obvious advantages appeared on the 30th day, on which the density of the bacteria in Test2 ( $7.8 \times 10^8$  CFU/g) and Test3 ( $8.9 \times 10^8$  CFU/g) were 1.5 and 1.7 times of that in Test1 ( $5.2 \times 10^8$  CFU/g), respectively.

The change of bacterial counts favored the theory that a proper application of electric field might stimulate the growth of bacteria and further enhance the biodegradation of Bap in contaminated soils. Some previous studies have supported that the application of electric field has a positive effect on the bacteria. Lear (2004) and Kim (2010) respectively revealed that some kind of bacteria number and community structure can be increased after electrokinetic treatments. Our results are in good agreement with the previous studies.

Therefore, application of DC electric field can accelerate the organic contaminant bioremediation process; moreover, the electric field with reversed polarity could further enhance the removal efficiency by maintaining the soil pH and water content at a suitable level (Figure 2 and Figure 3) to benefit the growth of bacteria.

## 4 CONCLUSIONS

The electrokinetic process was found to induce significant pH and moisture content in soil. These parameters were significantly decreased near the anode without pH control. Using the polarity reversal, the soil pH was better controlled, ranging from 6.9 to 7.3, while the moisture content in the soil distributed evenly.

The proper application of electric field can stimulate bacterial growth and accelerate bioremediation of Bap in clay soil. Further, with polarity reversal, the Bap removal and bacterial counts were higher than those obtained by the electrokinetic process without polarity reversal. Therefore, periodically reversing the polarity of electric field was thought to be an effective technique to enhance the biodegradation of Bap in clay soil.

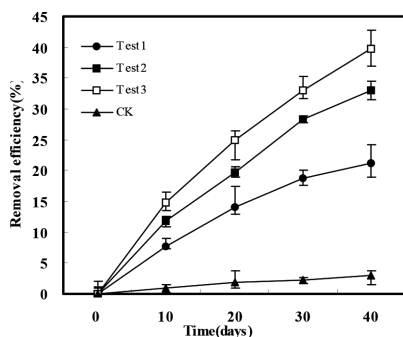


Figure 4. Change in Bap removal efficiency during the experiment.

## REFERENCES

- Acar Y.B. and Alshawabkeh A.N.1993. Principles of electrokinetic remediation, *Environ. Sci. Technol*, 27(13), 2638–2647.
- Alshawabkeh A.N. and Bricka M.2000. Basics and applications of electrokinetic remediation. In: Wise, D.L., Trantolo, D.J., Cichon, E.J., Inyang, H.I., Stottmeister, U.(Eds.). *Remediation Engineering of Contaminated Soils*, Marcel Dekker Inc., New York, 95–111.
- Harbottle M.J., Lear G., Sills G.C. and Thompson I.P. 2009. Enhanced biodegradation of pentachlorophenol in unsaturated soil using reversed field electrokinetics. *J Environ Manage*, 90(5), 1893–1900.
- Ho S.V., Sheridan P.W., Athmer C.J., Heitkamp M.A., Brackin J.M., Weber D. and Brodsky P.H. 1995. Integrated In Situ Soil Remediation Technology: The Lasagna Process. *Environ. Sci. Technol*, 29(10), 2528–2534.
- Jackman S.A., Maini G., Sharman A.K. and Knowles C.J. 1999. The effects of direct electric current on the viability and metabolism of acidophilic bacteria. *Enzyme and Microbial Technology*, 24(5), 316–324.
- Lahlou M., Harms H., Springael D. and Ortega-Calvo J.J. 2000. Influence of soil components on the transport of polycyclic aromatic hydrocarbon-degrading bacteria through saturated porous media. *Environ. Sci. Technol*, 34(17), 3649–3656.
- Lear G., Harbottle M.J., van der Gast C.J., Jackman S.A., Knowles C.J., Sills G. and Thompson I.P. 2004. The effect of electrokinetics on soil microbial communities, *Soil Biology and Biochemistry*, 36(11), 1751–1760.
- Lee H.H. and Yang J.W. 2000. A new method to control electrolyte pH by a circulation system in electrokinetic soil remediation, *J Hazard Mater*, 77(1), 227–240.
- Luo Q.S., Zhang X.H., Wang H. and Qian Y. 2005. The use of non-uniform electrokinetics to enhance in-situ bioremediation of phenol-contaminated soil, *J Hazard Mater*, 121(1–3), 187–194.
- Nieman J.K.C., Sims R.C., McLean J.E. and Sims J.L. 2001. Fate of pyrene in contaminated soil amended with alternate electron acceptors, *Chemosphere*, 44(5), 1265–1271.
- Niqui-Arroyo J.L., Bueno-Montesa M. and Posada-Baquero R. 2006. Electrokinetic enhancement of phenanthrene biodegradation in creosote-polluted clay soil. *Environ Pollut*, 142(2), 326–332.
- Lu R.K., *Analytic Methods for Soil Agricultural Chemistry*. China, Beijing: Agricultural Science and Technology Press, 2000, pp. 57–59.
- Kim S.H., Han H.Y., Lee Y.J., Kim C.W. and Yang J.W. Effect of electrokinetic remediation on indigenous microbial activity and community within diesel contaminated soil. *Sci Total Environ*, 2010, 408(16): 3162–3168, 2010.
- Wick L.Y., Shi L. and Harms H.2007. Electro-bioremediation of hydrophobic organic soil-contaminants: A review of fundamental interactions, *Electrochimica Acta*, 52(10), 3441–3448.
- Xu W., Wang C.P., Liu H.b., Zhang Z.Y. and Sun H.W.2010. A laboratory feasibility study on a new electrokinetic nutrient injection pattern and bioremediation of phenanthrene in a clayey soil, *J Hazard Mater*, 184(1–3), 798–804.



**Taylor & Francis**

Taylor & Francis Group

<http://taylorandfrancis.com>

# Study of the cable breaking effect on the structural characteristics of cable-stayed bridges

Wen-feng Tang

CCCC Second Highway Consultants Co. Ltd., Wuhan, China

**ABSTRACT:** Cable-stayed bridges are one of the main styles of long-span bridges, with cables playing a very important role in them. Cable corrosion is the most common and severe damage of cable-stayed bridges. It is necessary to study the mechanical behavior of cable breaking on these bridges. A finite element model of cable-stayed bridge is set up. The simulation of cable breaking on the finite element model and experiments in the laboratory were carried out simultaneously. Combining the theoretical and experimental analyses, the structural characteristics of cable breaking are obtained and the analysis result is useful to bridge health monitoring and bridge safety operation.

**Keywords:** cable-stayed bridge; model; cable breaking; structural characteristics

## 1 INTRODUCTION

Because of the long-term use, bad anchor, and poor antirust properties, the cables of cable-stayed bridges may break suddenly. There are many instances of cable breakage worldwide. Some cables of the Guangzhou Haiyin Bridge, built in 1988, broke suddenly in 1995 due to poor sealing anchor, and the government had to replace all the cables of it. When nearly one-tenth of the cable PE layer was found to be fractured in the 1999–2000 test, all the cables of the Sichuan Minjiang River Bridge, built in 1990, were replaced to ensure the normal operation of the bridge (Li, 2013; Lan, 2013). These not only significantly increased the later maintenance costs, but also had some negative social impacts. Therefore, it is necessary to study the effect of cable breaking on cable-stayed bridges, to guarantee the normal operation and improve the efficiency of the maintenance (Yu & Wang, 2010).

In order to explore force performance of cable breaking on cable-stayed bridges, this paper analyses the situation on a laboratory cable-stayed bridge model. By using finite element analysis software Midas and carrying out some related experiments, the mechanical behavior of the bridge was investigated.

## 2 FINITE ELEMENT MODEL

The cable-stayed scale model bridge was constructed using the Yangtze River Bridge as the prototype. The main bridge length is 780 m, and

the bridge span arrangement is 40 m + 130 m + 388 m + 130 m + 40 m. The main bridge structure is cable-stayed. According to the rigidity similarity theory, the design of the model bridge is simplified and the scale is 1:40 (Xiao, 2012). Its total length is 18.2 m and bridge span arrangement is 4.25 m + 9.7 m + 4.25 m. The towers are steel structures and the height is 3.50 m. The girder is a lightweight concrete beam. The cables are made of the same material as that of the Yangtze River Bridge and the number of cables is 56. The cable-stayed scale model bridge is shown in Figure 1.

The Finite Element Model (FEM) is build using the bridge finite element analysis software Midas. The girder is the beam element to simulate, the tower is the solid element, and the cable is the truss element. The space FEM of the bridge model is shown in Figure 2.



Figure 1. Cable-stayed scale model bridge.

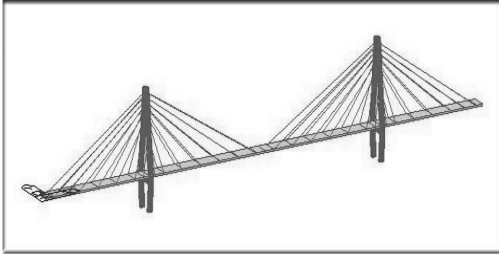


Figure 2. FEM of the cable-stayed bridge.

Single cable breaking is only considered in this paper and other situations are not considered. Considering the typical position of cable force, the cable breaking situations are: case 1 (the sidespan long cable breaks), case 2 (the sidespan middle cable breaks), and case 3 (the midspan long cable breaks). Considering the symmetry, all cases occurred in 6# tower.

### 3 RESULT ANALYSIS

#### 3.1 Change of cable force

The cable breaking causes the redistribution of full bridge cable force. Considering the symmetry, only one-fourth of the cables, that is, 14 cables in 6# tower are chosen, and the force change is shown in Table 1 (S is side span and M is middle span).

The cable force change is represented in histogram as shown in Figure 3.

From Table 1 and Figure 3, the following conclusions can be drawn:

The cable force near the broken cable increases obviously, the largest increment occurs in the adjoining cable, but in some cables, force decay occurs. Compared with all the cases, the effect of the longest cable breaking is maximum. Therefore, long cables should be paid more attention.

#### 3.2 Change of beam displacement

The beam vertical deformation in different cases is shown in Figure 4, and the change of beam vertical deformation after different cable breaking is shown in Figure 5.

The displacement of midspan is downward deflection of a maximum deformation of 0.34 mm. In addition, the maximum upward deflection is 0.09 mm. Therefore, the change of beam vertical deformation after cable breaking is very small.

#### 3.3 Change of dynamic property

The dynamic property of a bridge includes the natural frequency and the main vibration mode, which is an important index of bridge rigidity

and distribution (Xiao, 2012). For a cable-stayed bridge, a cable breaking will cause the redistribution of internal force of the whole bridge, which will lead to change of the bridge stiffness and distribution inevitably, thereby causing a corresponding change in the natural frequency and mode shapes. Through the modeling calculation, the first formal six modes of the cable-stayed bridge were obtained, as shown in Figure 6.

It has some influence on the dynamic property of cable-stayed bridge after cable breaking. The modal frequencies before and after cable break are shown in Table 2.

Table 1. Force change of stay cables under different cases (N).

Cables number	The original cable force	Case 1	Case 2	Case 3
S7	347.41	-347.41	22.50	-18.41
S6	308.98	64.80	23.71	-15.78
S5	267.79	53.41	24.54	-12.13
S4	220.63	39.03	-220.63	-8.46
S3	186.07	24.41	27.04	-5.07
S2	174.94	12.89	27.17	-0.74
S1	177.24	9.28	24.02	3.2
M1	189.56	2.21	17.98	7.72
M2	211.72	1.88	12.50	10.49
M3	254.26	3.98	5.17	14.37
M4	287.99	6.26	0.78	17.90
M5	301.43	4.52	-2.40	23.28
M6	290.48	-3.72	-4.95	30.7
M7	249.30	-18.00	-7.66	-249.30

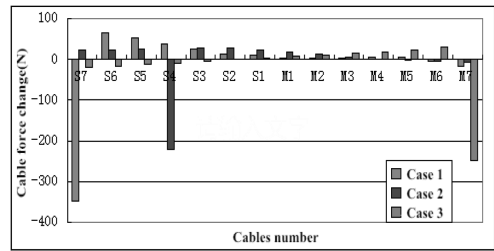


Figure 3. Cables force change of FEM simulation.

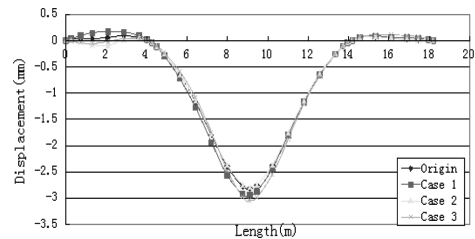


Figure 4. Beam displacement.



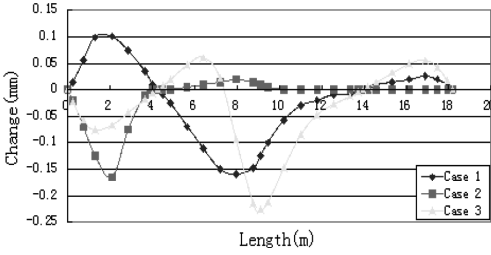


Figure 5. Change of beam displacement after cable breaking.

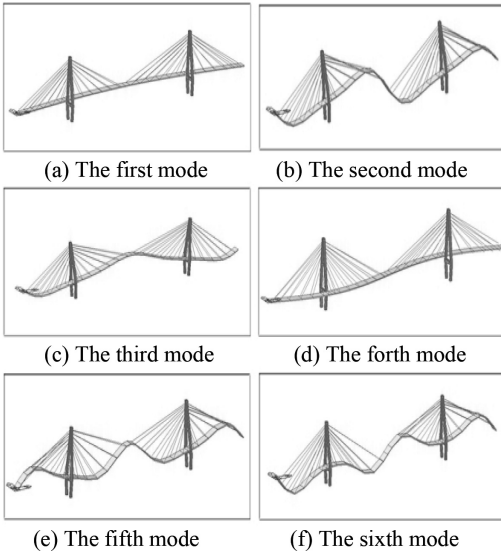


Figure 6. The first six mode shapes.

Table 2. The difference of each mode frequency.

Mode	The Original frequency (Hz)	Case 1	Case 2	Case 3
1	2.44	-0.04	-0.08	-0.04
2	6.49	-1.14	-0.26	-2.97
3	9.10	-1.30	-0.63	-1.58
4	9.63	-0.06	-0.01	-0.01
5	14.46	-3.84	-2.30	-0.10
6	16.66	-0.31	-2.40	0.72

Define:

$$difference = \left( \frac{frequency\ after\ breaking}{frequency\ before\ breaking} - 1 \right) \times 100\% \quad (1)$$

The order of vibration mode does not change and the value of frequency changes little.

## 4 THE EXPERIMENTAL TESTING RESULT

As to some analyses above, some related experiments were conducted in the laboratory. The situation was Case 3. The cable force, midspan displacement, and vibration mode were tested during and after the middle span long cable breaking. In the test, fiber Bragg grating sensors were used to measure cable force, and a dial indicator was arranged at the bottom of the girder center span. The dynamic property was tested by using the vibration dynamic signal test system.

### 4.1 Cable force change

Using the fiber Bragg grating sensor to measure the cable force, the measuring value was wavelength. The cable force was converted by the formula of wavelength (Hu, 2014). Figure 7 shows the force change of one cable during the breaking process. Through conversion, the force change of 13 cables is shown in Figure 8. There are some difference between the theoretical analysis and experimental test, but the force change trend is the same.

### 4.2 Displacement change of midspan

The maximum displacement of beam is the midspan in the process of cable breaking, whose displacement was tested by a dial indicator. The displacement change is shown in Figure 9. The

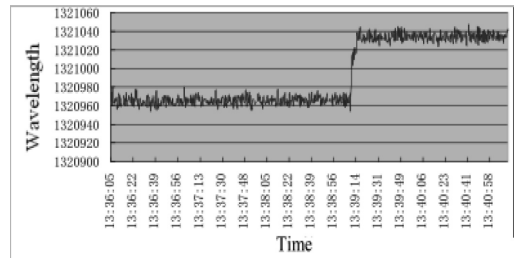


Figure 7. Cable breaking process.

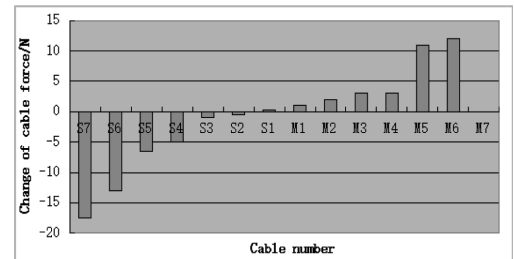


Figure 8. Force change of the other 13 cables.

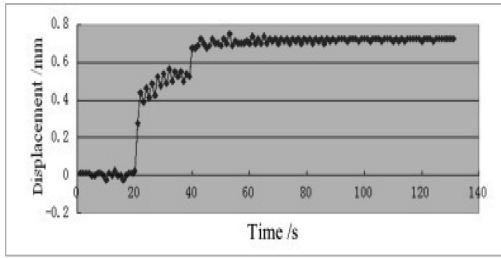


Figure 9. Displacement change of the midspan of the beam.

Table 3. The testing frequency before and after cable breaking.

Mode	Frequency before braking (Hz)	Frequency after braking (Hz)	Change of frequency (Hz)	Difference
1	2.44	2.45	0.01	0.41
2	6.07	6.05	-0.02	-0.33
3	8.32	8.30	-0.02	-0.24
4	10.75	10.80	0.10	0.47
5	14.72	14.60	-0.12	-0.82
6	18.80	18.60	-0.20	-1.06

displacement of the midspan is 0.73 mm after the cable breaking. The displacement change is higher than the finite element analysis. As the value is very small, it can be disturbed by the environment. However, the trend is correct.

#### 4.3 Modal result of test

The testing result of each modal frequency is shown in Table 3. The vibration mode orders of FEM analysis and laboratory testing are the same. The frequency changes before both the FEM analysis and experimental test are very small, and the effect on the modal result is minimal.

## 5 CONCLUSIONS

In this paper, a cable-stayed bridge scale model was constructed and analyzed using the Midas software. The cable force, beam displacement, and dynamic properties changed after different cables breaking. Some related experiments were conducted in the laboratory at the same time. Through the combination analysis of theory and experiment, the following conclusions were drawn:

1. Bridge cable force changes significantly before and after cable breaking. The changes of the beam displacement and dynamic property are small. The cable breaking causes the redistribution of the full bridge cable force, and the nearby cable force change is the largest.
2. The influence of breaking of long cables on the bridge is higher than the breaking of the short ones, so the long cables should be paid more attention in the engineering process.

## REFERENCES

- Anlin Hu. 2014. Analysis for Influence of Broken off Cables on Mechanical Properties of Some Low Tower Cable-stayed Bridge. *Technology of Highway and Transport* 5:91–95.
- Kai Xiao. 2012. Research on Design of Cable-stayed Bridge's Scale Model Based on Stiffness Similarity Theory. *Master's thesis, Wuhan University of Technology*.
- Tianlai Yu & Jinzhao Wang. 2010. Hazard Analysis of Cable-Stayed Bridges due to Cable Fault. *Journal of Northeast Forestry University* 38: 95–98.
- Xianliang Lan. 2013. Simulation Analysis of Extradosed Cable-Stayed Bridge Structure. *Western China Communications Science & Technology* 1: 45–49.
- Yanbing Li. 2013. Research of Broken Cable Hazard for Long Scale Cable-stayed Bridge. *Master's thesis, Chongqing Jiaotong University*.

# Passive and energy-efficient house design based on the climate of Tianjin

Y.F. Zhao, Z.R. Wang & Y.X. Tian

*School of Architecture, Tianjin University, Tianjin, P.R. China*

**ABSTRACT:** Passive and energy-efficient houses are drawing increasing attentions of scholars and practitioners in the field of architecture, which has been proved to be comfortable, sustainable, and attractive with economic benefits. This paper mainly focuses on the feasibility and design strategy of passive and energy-efficient houses located in Tianjin through the analysis of climate conditions of the area. However, the study of cold regions of North China such as Tianjin area is scarce in the literature. By analyzing climate data and the preliminary discussion on passive and energy-efficient house, the design strategies for Tianjin area with feasible and appropriate technologies are proposed, including external walls, insulation, thermal bridges, heat recovery ventilation system, airtightness, and shading design. In the end, the positive outlook of the future development is described and reasonable conclusion is provided.

**Keywords:** passive house; energy-efficient house; climate conditions; Tianjin

## 1 INTRODUCTION

In recent years, passive and energy-efficient house has played a more significant role in the research of architecture by scholars and practitioners in the field related to sustainability and energy conservation. The term passive house (German: “Passivhaus”) was originated in Germany and has been widely used in the concept of energy-efficient buildings. Wolfgang Feist, one of the scholars who set the standards of German passive house, described that the passive house proves the practicality of international energy-efficient construction standards, and is attractive, comfortable, and overall has economic sustainability<sup>[1]</sup>. By the end of December 2015, according to the index of passive house database website, there are more than 3,400 constructed passive houses with the verified standards and certification by the official Passive House Institute (PHI), of which China also has representative projects included in the database, such as Qingdao Sino-German Ecopark Passive House Demonstration Project—Passive House Technology Experience Center and Urumqi Sino-German Technical Cooperation Demonstration Project—“Happy Castle” Comprehensive Building<sup>[2]</sup>. The design and construction techniques of local China have reached the advanced level of the world. In addition, Sino-Singapore Tianjin Eco-city (SSTEC) is also in cooperation with the China Academy of Building Research Institute and the German Passive House Institute to promote pilot

projects with standards up to the level of German Passive House in the region of Tianjin area, and it is expected to be implemented in 2017<sup>[3]</sup>. The design, construction, and operation of a passive and energy-efficient house have close relationships with the local climate conditions and situations. Therefore, in this paper, we take Tianjin area as an example, and try to conduct a detailed analysis and discussion for the design of passive and energy-efficient house based on the climate conditions in different regions.

## 2 CLIMATE DATA

Tianjin is located in the north temperate, mid-latitudes, and the east coast of the Eurasian continent, mainly dominated by monsoon circulation, is the prevalent region of the East Asian monsoon, with warm temperate semi-humid monsoon climate. Tianjin is near the Bohai Bay, which is influenced by marine climate directly. The figure below shows the average condition of Tianjin’s climate data by Climatic Data Center of National Meteorological Information Center of China Meteorological Administration, in which the average statistical data are collected for 1981–2010 and extreme data for 1954–2014.

As the wind rose graph of Tianjin shows, with the reference of climate data and weather documentary, it can be concluded that Tianjin has four distinctive seasons with a large range of temperature.

Table 1. Average climate data of Tianjin area<sup>[5][6]</sup>.

Month	Extreme temperature		Average temperature (°C)
	High (°C)	Low (°C)	
January	14.3	-18.1	-3.4
February	20.8	-22.9	-0.1
March	30.5	-17.7	6.4
April	33.1	-2.8	14.7
May	40.5	4.5	20.5
June	39.6	10.1	24.8
July	40.5	16.2	26.8
August	37.4	13.7	25.9
September	34.9	6.2	21.1
October	30.8	-2.2	14.1
November	23.1	-11.4	5.2
December	14.4	-16.2	-1.2
Total	40.5	-22.9	12.9

\*Average data for 1981–2010; Extreme data for 1954–2014.

Table 2. Additional climate data of Tianjin area<sup>[5][6]</sup>.

Month	Precipitation (mm)	Relative humidity (%)	Sunshine duration (h)
January	2.4	57	170.1
February	3.6	54	170.2
March	8.1	51	202.4
April	22.1	50	223.8
May	37.3	55	249.0
June	80.6	64	226.9
July	148.8	75	206.4
August	124.1	76	204.4
September	44.6	69	205.3
October	26.3	64	196.1
November	10.7	61	163.0
December	2.8	59	157.6
Total	511.4	61.3	2375.2

The winter months mainly have multi northwest wind with low temperatures and less precipitation. Summer months have strong pacific warm subtropical high pressure with principal southerly winds, high temperatures, and precipitation. The average annual temperature of Tianjin is around 12–14°C, in which July is the hottest month. The annual average precipitation is between 360 and 970 mm (1949–2010), and 600 mm is the representative average figure of annual precipitation that many scholars and researchers summarized by multi-information.

Among resources of climate data and documentary, human comfort index is an indispensable factor which is determined by both personal factors and environmental factors. Human comfort index

can directly reflect the feeling degrees of human being as the user of the building in the studied area. Meanwhile, the index provides assistance and reference for the research of passive and energy-efficient house. On the basis of the fact that the human body has different feelings under the influence of different thermal sensation, the human comfort index can be divided into different levels: -4 to 4 denote cold to hot, respectively. The absolute value of the level indicates the level of comfort degree that human body feels from cold to hot<sup>[7]</sup>. Some literature studies also consider Wind Chill Temperature (WCT) as the impact factor under the condition of low temperature, and regard Temperature Humidity Index (THI) as the value of the combination of air temperature and relative humidity. Those index and figures can be the additional analysis results for the climate data from multiple perspectives.

When scholars from China analyzed the human comfort index of people in Beijing–Tianjin–Hebei area, they geographically divided the region into three classified regions, A, B, and C, where Tianjin region is regarded “Class B—cold comfort coastal zone”. The data collection method is described as follows: acquire the data of temperatures, wind speed, and humidity for the past few decades from local weather station in the region; calculate human comfort index within the year; and determine the distribution and leading factors<sup>[7]</sup>. The main climate characteristic of Tianjin for winter is cold and dry, with the longer length of heating time. Therefore, whether a house can rely solely on passive heating and insulation to reduce energy consumption and improve thermal performance and airtightness of the building envelope needs to be discussed and simulated. The solution of thermal comfort is also related to the project site. Therefore, during the process of energy-efficient implementation, for the cold area in which Tianjin is located, the main task in winter is to obtain solar heat and preserve heat, with sunshade of summer taking into account<sup>[9]</sup>. One of the main purposes of passive and energy-efficient house is to reduce thermal bridges by using appropriate technologies in order to meet the ecological construction concept and economic benefits.

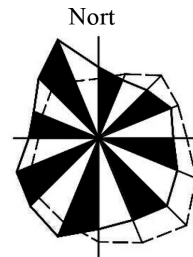


Figure 1. Average wind rose graph of Tianjin.

### 3 PRELIMINARY DISCUSSION ON PASSIVE AND ENERGY-EFFICIENT HOUSE

In recent years, the area of passive and energy-efficient house in China has considerably increased, but there are still some gaps compared with European countries such as Germany. The issue of “Passive and Energy-efficient Green Building Technical Guidelines (Trial)”, which was released in October 2015, can promote and improve the development of energy-efficient house in China to a certain extent<sup>[9]</sup>. Passive and energy-efficient house is not just a simple collection of advanced products and high-end technology, but reasonable design using appropriate technology. The common methods include promoting the thermal performance and airtightness of envelope and materials, meanwhile taking advantage of efficient new ventilation system and heat recovery technology<sup>[9]</sup>, so that the heating and cooling demand of the building could be decreased to a minimum, which may have significant effect on energy-saving and environmental sustainability. The airtightness is a key technical indicator that measures the effect of building energy consumption for passive and energy-efficient house, no matter in China or European countries. The standard of German passive house is to reduce the demand of building heating to below  $15 \text{ kWh}/(\text{m}^2 \cdot \text{a})$ <sup>[9]</sup>, in order to reduce energy consumption. For the cold area in which Tianjin is located, the “Guidelines” require that the average annual heating demand is also less than  $15 \text{ kWh}/(\text{m}^2 \cdot \text{a})$ . For tightness index, when the pressure difference of indoor and outdoor is 50 Pa, the Air Change (ACH) per hour for the building is less than or equal to 0.6. For indoor environmental parameters, the indoor temperature should not be less than  $20^\circ\text{C}$  in winter, and not higher than  $26^\circ\text{C}$  in summer. The relative humidity should be between 30% and 60%.

The aim of passive and energy-efficient house should be to reduce energy consumption. The early stage of the process should pay more attention to rational planning and spatial layout with energy solutions provided. The design of the project should be guided and oriented by the local climate characteristics and various conditions of the construction site, in order to make appropriate technical requirements. Each professional should coordinate with others and ultimately to generate optimization design and adaptation strategies for passive and energy-efficient house. A good passive and energy-efficient house should be designed and built with the best rationality in the following five aspects to coordinate with facades and external insulation, building envelope, thermal bridges, heat recovery fresh air system, and airtightness. The above five areas must be processed with the cooperation of all

professionals throughout the whole design process, in order to achieve the desired effect of passive and energy-efficient house.

### 4 DESIGN STRATEGIES OF PASSIVE AND ENERGY-EFFICIENT HOUSE LOCATED IN TIANJIN AREA

Considering the climate conditions of Tianjin area, when designing passive and energy-efficient house, the climate factors should be characterized as the main guide. Buildings should be mainly constructed toward the north-south or nearly north-south direction, and the main aim of the room or area should be to avoid winter dominant wind. By using Ecotect software, the climate data of Tianjin can be used for simulation. After the simulation of all year-round sunshine through the analysis module, the result of the best face and direction of the building can be generated. The building should be reasonably oriented on the project site. By improving the construction of walls, windows, and other components, the heat storage function of the building could be enhanced with the rational use of thermal properties of materials in order to achieve the purpose of passive heating. Meanwhile, the plan design should consider ventilation and sunshine to meet the minimum demand of sunshine. The layout design should be reasonable to create a favorable operating environment airflow. To develop the design strategies of passive and energy-efficient house located in Tianjin area, this study should be conducted in the following several technical indicators with reasonable exploration: the external walls and external insulation, thermal bridges, heat recovery ventilation system, airtightness, and shading design.

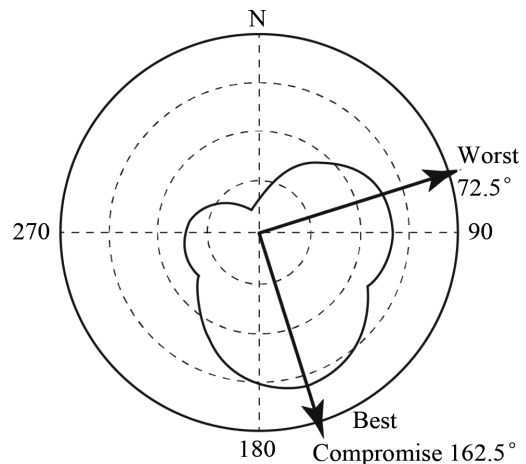


Figure 2. Sunlight analysis and best orientation.

#### 4.1 External walls and insulation

The insulation of retaining structure of passive and energy-efficient house should use high-performance insulation materials, while the thickness of the insulation layer should also be within the appropriate range. For the cold area in which Tianjin is located, it is appropriate to choose Expanded Polystyrene (EPS) with the thickness of the insulation layer around 240–300 mm. In recent years, Vacuum Insulation Panel (HVIP) has gradually been used with the thermal conductivity below  $0.006 \text{ W}/(\text{m} \cdot \text{K})$  and significant improvement of insulation performance. The chosen high-performance insulation materials should meet the standards of “Code For Fire Protection Design of Buildings—GB50016”.

For Tianjin area, the average heat transfer coefficient of roofing and facades should be between  $0.10$  and  $0.25 \text{ W}/(\text{m}^2 \cdot \text{K})$ . The average heat transfer coefficient of ground should be between  $0.15$  and  $0.35 \text{ W}/(\text{m}^2 \cdot \text{K})$  with reference to “Thermal Design Code For Civil Building”. The Window-to-Wall Ratio (WWR) should be reasonable when designing the plan, while the performances of exterior windows also have the following requirements: the heat transfer coefficient of windows should be in the range of  $0.80$ – $1.50 \text{ W}/(\text{m}^2 \cdot \text{K})$ . The range of Solar Heat Gain Coefficient (SHGC) should be  $\geq 0.45$  for winter, and  $\leq 0.30$  for summer. The temperature of the inner surface of the external window should be in the range of  $13$ – $17^\circ\text{C}$  with airtightness (no less than 8 degrees) and good resisting of wind pressure (no less than 9 degrees). Taking climatic factors into account, the external windows of the building are better to be installed with triple-glazed windows.

#### 4.2 Thermal bridges

Thermal bridges is an important factor affecting passive and energy-efficient house, which can be

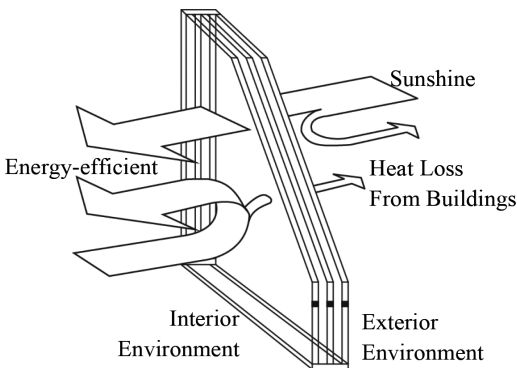


Figure 3. Demonstration of triple-glazed windows.

divided into geometric thermal bridges and structural thermal bridges. The thermal bridges should be avoided when designing the energy-efficient concept, because the external wall and building envelope cannot be penetrated. The insulation, walls, and connections should adopt the appropriate technical measures to prevent the loss of energy, while the insulation layer of roof and external wall should also be continuous components.

#### 4.3 Heat recovery ventilation system

Passive and energy-efficient house should adopt heat recovery ventilation system to meet the demand of the indoor cooling or heating, thereby reducing the operation of other systems to achieve energy-saving targets. The heat recovery varies according to the differences of energy recovery forms, heat recovery efficiency, and exhaust volume. The power consumption of heat recovery should be not more than  $0.45 \text{ W}/(\text{m}^3/\text{h})$ . The heat recovery ventilation system should also be optimized reasonably according to the local climate characteristics, use, and external environment of the building. The wind speed of the main air duct should be less than  $3 \text{ m/s}$ , and the speed of air delivery should be less than  $1.5 \text{ m/s}$ .

#### 4.4 Airtightness

Airtightness is a key technical indicator to achieve energy efficiency for a building. As mentioned previously, guidelines specify that the average annual heating demand should be less than  $15 \text{ kWh}/(\text{m}^2 \cdot \text{a})$ . When the indoor and outdoor pressure difference is  $50 \text{ Pa}$ , the ACH per hour for the building is less than or equal to  $0.6$ . The air barrier of a building should be continuous and without interruption in order to ensure that the operation of passive and energy-efficient house is not influenced by external factors, thus reducing the possibility of potential non-airtightness impact.

#### 4.5 Shading design

According to the total energy consumption of buildings located in cold regions such as Tianjin, the majority energy consumption in winter is due to heating, while the external heat gain can reduce energy consumption for heating in winter. However, it will affect the air conditioning energy consumption in summer. Therefore, in Tianjin area, apart from the north side, the other three sides of the building, east, west, and south, should be considered to set up appropriate shading measures. The shading design should be reasonably optimized according to the local climate characteristics, use patterns, and the external environment of the

building, in order to use the energy efficiently and meet the purpose of energy conservation. Shading measures may be taken or different materials of glass may be used based on the differences of reflectivity, which becomes a combined approach for energy saving.

## 5 CONCLUSION

The design and construction of passive and energy-efficient house is a complicated systematic task. Through the analysis and discussion of climate data in Tianjin, and the strategies of passive and energy-efficient house, research shows that the construction of a passive and energy-efficient house in Tianjin is feasible. However, the reality is still related to the site environment, specific conditions of use, or other individual differences between building locations. Therefore, the actual project practice in the region needs to be further evaluated objectively, with more theoretical model to conduct comparative analysis and obtain experimental results. In brief, the exploration and practice of passive and energy-efficient house has great practical significance in the development of energy-saving concept in Tianjin area.

For the outlook of future trend, it can be estimated that passive and energy-efficient house will play a more important role in the architectural area worldwide. It is common that the energy consumption of a normal building is nearly 30% of that of living energy consumption. Nearly 70% of the buildings that have already been constructed in Tianjin are high-energy consumption buildings. Although China has been promoting the standards of green building and energy-efficient house recently, the country still has gaps with advanced countries that have been practicing policies of passive houses for decades, such as Germany. However, because of the improvement in technologies worldwide, the area of passive and energy-efficient house has greatly improved. It is also closely related to the sustainability and energy-saving industry. At this moment, although several demonstration projects have already been conducted, this concept still has a long way to go to reach normal family. It is because of the higher cost of construction than the typical building. Therefore, the cost and price of a house is an important factor that influences

the development of passive house. Moreover, not all the developed estates prefer to choose passive and energy-efficient house when they consider building a house, while many scholars would like to conduct in-depth research in this area. Probably the development trend is oriented by the advanced technologies applied in this area, which is quite different from normal practice project. For passive and energy-efficient house, the appropriate technologies are as important as the design strategies, even more complicated. Hence, the industrial associations and governmental organizations cooperate to promote this concept. In conclusion, the idea of passive and energy-efficient house, green building, and sustainability will be the hottest trend in the future.

## REFERENCES

- [1] Feist, W. (2007). What is a passive house. *Passive House Institute*: 2–3.
- [2] Passive House Database. (n.d.). Retrieved January 9, 2016, from <http://www.passivhausprojekte.de/index.php>.
- [3] Sino-Singapore Tianjin Eco-city “Passive House” Demonstration Project. (2015, May 13). Retrieved January 9, 2016, from <http://finance.chinanews.com/house/2015/05-13/7274231.shtml>.
- [4] Tianjin Weather Report. (n.d.). Retrieved January 9, 2016, from <http://tianjin.tianqi.com/>.
- [5] Tianjin Geography. (n.d.). Retrieved January 9, 2016, from <https://zh.wikipedia.org/w/index.php?title=TianjinGeographT>.
- [6] China Meteorological Data Sharing Service Network. (n.d.). Retrieved January 9, 2016, from <http://www.nmic.gov.cn/web/index.htm>.
- [7] Sun, G. & Wang X., et al. 2011. Temporal-spatial characteristics of human comfort in Beijing-Tianjin-Hebei region. *Journal of Meteorology and Environment*. 27 (3): 18–23.
- [8] Kaufmann, B. & Feist, W. 2015. *Germany Passive House Design And Construction Guidelines*, Beijing: China Architecture & Building Press: 1–7.
- [9] Ministry of Housing and Urban-Rural Development (MOHURD). 2015. *Passive and Energy-efficient Green Building Technical Guidelines (Trial)*. Beijing: Ministry of Housing and Urban-Rural Development (MOHURD).
- [10] Beijing Municipal Commission of Urban Planning. 2006. *Evaluation standard for gTeen building*. Beijing: Beijing Municipal Commission of Urban Planning.



**Taylor & Francis**

Taylor & Francis Group

<http://taylorandfrancis.com>



# Location information provider framework using the open IoT technology

Nanju Kim, Joonwoo Park & Euiin Choi

*Department of Computer Engineering, University of Hannam, Republic of Korea*

**ABSTRACT:** Recently, crimes, lost stuff, and the like have been recognized as a social problem affecting the common people. To address this issue, location information technology has been developed. At present, various institutions have been providing location information service using mobile device. Furthermore, much research has been in progress to provide Location-Based Service (LBS) using the beacon in the IoT (Internet of Things). In this paper, we investigated the definition and technology of Seamless LBS and found that the accuracy of this technique is higher than that of the GPS in mobile environment. Also, we studied the Mobius platform for interworking with IoT. Finally, we proposed a new location lookup framework that complements the traditional location lookup techniques.

**Keywords:** seamless LBS; location information; mobius platform; beacon; IoT technology

## 1 INTRODUCTION

Crimes have been recognized as an important social issue. Accordingly, much effort has been made to provide the user location information. Thus, there is an increasing interest and need to develop techniques that provide accurate location information. Location-Based Service (LBS) grasp the location of a person or thing based on a mobile network. Then, it uses the advantages of the application systems and services. As such, LBS has emerged as a major key technology to determine the basic infrastructure with the development of wireless communication and the Internet. Also ranging from individual, business, and public sectors LBSs are utilized in a variety of forms. Therefore, recently, much research has been conducted to provide LBS using the beacon in the Internet of Things (IoT). In addition, in case of service, GPS is impossible to grasp the position of underground or inside buildings, and the Cell-ID method does not meet higher accuracy requirement of the user. In order to compensate for this problem, Seamless LBS has emerged [1], which uses location information technologies such as GPS and LBS to make users free from crimes. In this paper, we investigated the definition and technology of Seamless LBS and found that the accuracy of this technique is higher than that of the GPS in mobile environment. Also, we studied the Mobius platform for interworking with IoT. Furthermore, we proposed a new location lookup framework that complements the traditional location lookup techniques.

## 2 RELATED WORKS

### 2.1 Positioning services

We live in the era of technological change. IoT was developed for identification of objects, and it is being used in remote controls and product marketing [1,2].

#### 2.1.1 LBS (Location-Based Service)

The definition of LBS slightly differs for each institution. OGC (Open GIS Consortium) defines it as the integration all application software services to provide location information. The US FCC (Federal Communication Commission) defines it as the service providing geographical position of a material or person. The definition provided by the OGC is globally followed.

LBS is based on mobile communication technology. In other words, LBS technology tracks the location of mobile devices by using a variety of wired or wireless communication networks. The collected information are then processed for application in various private and public sectors. Briefly, LBS uses location detection (check) techniques to identify the location of an object [3].

#### 2.1.2 Seamless LBS

Seamless LBS was developed to overcome the drawbacks of the GPS and Cell-ID techniques mentioned earlier. It is commonly referred to as the next-generation LBS technology.

Implementation of this technique needs indoor positioning technologies such as WLAN and

Bluetooth. Also, mobile terminal tracking requires a network and GPS outdoor positioning technology. Integration of the above two technologies integrate provides position information continuously.

### 2.1.3 Beacon

Beacon uses non-audible frequency region machine-to-machine communication. It is a transmitter that uses low-energy Bluetooth as a short-range location-detecting technology that sends signals to the smart phones [4], tablets, PCs, and smart watches. In particular, the beacon provides complete details of the local area in the indoor or outdoor location with error less than 5 cm. It can automatically forward the required information through the application.

## 2.2 LBS platform

LBS platform is the one that performs the basic and critical function of LBS and it also provides a common component supporting a variety of LBSs. In this regard, many platforms have been developed such as MPC, GISP, AS, and AP [5].

### 2.2.1 Mobile Positioning Center

Mobile Positioning Center (MPC) is a server used for data retrieval, transmission, storage, and control in the network infrastructure[2, 7]. It uses a Position Determining Entity (PDE) to determine the position using a variety of technologies such as assisted GPS or observed time difference of arrival. MPC and MSC communicate with the emergency services network. The MPC also handles access restrictions to the position information.

### 2.2.2 Geographic Information Service Platform

Geographic information service platform is a content server providing Point of Interest (POI), traffic information, and electronic maps for LBS services. GISP uses spatial-temporal location as the key index variable for all other information. As a relational database containing text or numbers

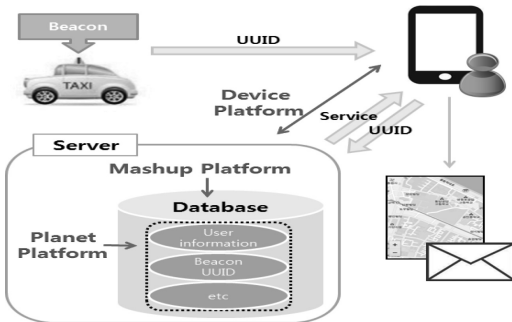


Figure 1. Proposed framework.

can relate many different tables using common key index variables, GISP can relate unrelated information by using location as the key index variable. The key is the location and/or extent in space time [8].

### 2.2.3 Application server and service provider

Application server and service provider act like LBS application service provider or client server based on the location information obtained from LBS platform or geographic information service platform. An application server can be either a software framework that provides a generalized approach to implement an application server, to determine the application functions, or the server portion of a specific implementation instance. In either case, the server's function is dedicated to the efficient execution of procedures (programs, routines, scripts) for supporting its applied applications [6, 9].

## 2.3 Mobius platform

With the increasing interest on IoT, research for IoT platform technology is continuing. This open IoT platform provides an Open API. Also, it supports the association and administration of external system for multiple-user service. Among the open IoT platforms, Mobius platform provides IoT service.

Mobius platform interconnects the things to the network. Therefore, it facilitates communication anytime and anywhere. Its working procedure is as follows: First, it collects data of objects. Then, it provides a service using those data, or provides a control method for the things. Through this, IoT platform can provide personal and social networks, smart health, and safety (advanced service).

### 2.3.1 Device platform

Device platform connects different things in the IoT infrastructure and provides interwork service with the IoT service platform. In other words, it is a software that provides IoT service. It can provide communication adapter using hardware communication module to provide ZigBee communication, mobile communication such as 3G and 4G, and IP communication such as Wi-Fi and Ethernet connection.

### 2.3.2 Planet platform

Planet platform registers profile information such as device ID, device name, and device location related the IoT device. Planet platform indexes the information and supports a variety of search based on it.

### 2.3.3 Mashup platform

The periodic data of the IoT device are received and stored, from which useful information is extracted by data fusion. Therefore, this plat-

form can provide useful information to the user. If network connection is difficult to direct, direct connection to the device can be realized using the Mashup platform.

#### 2.3.4 Store platform

The store platform includes registration, upload, and download data of the IoT device.

This platform involves a service application function that provides useful information to the user for interlocking with the device application and the device.

#### 2.4 Framework

Framework includes the standardized system execution environment of the application, the operating environment of the operator, and the development environment of the developer based on proven design and re-use of source code.

Development of high-quality system is possible, regardless of the ability to proceed application development based on the standard framework. Also, this saves the institutional and system construction costs. As the system is less complex, TCO and failures are reduced and the fundamental IT competitiveness can be possibly secured [10].

### 3 PROPOSED FRAMEWORK

It is difficult to face the increasing incidents of crime with the traditional location-providing technology. As described earlier, the development and research on detecting user location information is ongoing. Currently, position information services are provided GPS and Cell-ID techniques, which cannot grasp location inside buildings or underground. Furthermore, the accuracy of the information so obtained is not satisfactory. Seamless LBS technique was introduced to overcome these drawbacks, which can provide accurate indoor and outdoor location information.

The aim of this paper is to develop a framework for providing location information service based on beacon. The framework thus developed achieves this aim using mobile platforms such as Mobius platform, Seamless LBS, and beacon.

The framework is made from Mobius platform environment. In addition, beacon server is controlled and interlocked using the Mobius device platform. The beacon server stores information regarding code value of UUID, major and minor to differentiate all beacon information. Beacon first sends the code value to the application. Then, the application that connects to the server sends a beacon code value. Accordingly, the beacon server provides the application an appropriate service for the

code value. The information indexes and builds a database using the Mobius planet platform. Finally, the stored data are processed and combined using a Mobius mashup platform to provide useful information. For location information transmission, it uses the available location provider list, GPS status information, current status of the same location system, LocationManager class, which provides lately recorded location, and LocationListener interface, which manages location status change. The GCM, which supports service to send messages to the application, extracts GPS value and information received from beacon server to other users and itself.

### 4 CONCLUSION

LBS has been studied and developed in a wide variety of application area that has a close connection with our life. However, the scope for the development of technology or services for precise location information is still lacking. Therefore, studies on Seamless LBS should be conducted to grasp users' location information anywhere with high accuracy. Also, it may provide various associated services to meet the user requirements by data analysis based on this position information.

Problems with respect to various position information technologies in many fields should be analyzed. The various service and system research and developments facilitate providing high-accuracy position information from a variety of IoT environments.

### ACKNOWLEDGMENTS

This work (Grants No. C0300547) was supported by Business for Cooperative R&D between Industry, Academy, and Research Institute funded Korea Small and Medium Business Administration in 2015.

### REFERENCES

- [1] H. Choi, LBS, Location-Based Services trend Computer Software Research, Korea Electronics and Telecommunications Research Institute, No. 86, 2003.
- [2] Y. Cho et al, WARP-P: Wireless signal Acquisition with Reference Point by using simplified PDF—system concept and performance assessment, Proc. The ION 2013 Pacific PNT Meeting, Apr, 2013.
- [3] S.H Park, Location-Based Services (LBS) technology and market trends, Technical note, Surveying & Mapping Magazine, 3, 2011.
- [4] D. Tipper et al, Providing Fault Tolerance in Wireless Access Networks," IEEE Communication, Mag., Vol. 40, No. 1, Jan. 2002, pp. 58–64.

- [5] H. Choi, LBS, Location-Based Services trend Computer Software Research, Korea Electronics and Telecommunications Research Institute, No. 86, 2003.
- [6] Application server, [Wikipedia.org/wiki/Application server](http://Wikipedia.org/wiki/Application_server).
- [7] D. Tipper, Network architecture and protocols for mobile positioning in cellular wireless systems.
- [8] Geographic information platform, [Wikipedia.org/wiki/Geographic information platform](http://Wikipedia.org/wiki/Geographic_information_platform).
- [9] Y. Zhao, Standardization of mobile phone positioning for 3G systems, IEEE Communication. Mag, 40(7), pp. 108–116, 2002.
- [10] S.H Yoon, S.Y Cho, J.W Choi, A study on Frameworks for Platform of 3D Indoor Spatial Information, Korea Interior Design Journal, 14(1), pp. 210–213, 2012.

# Review of three-dimensional braided piezoelectric ceramic matrix composite

Xiao Ma & Gao-feng Wei

*School of Mechanical and Automotive Engineering, Qilu University of Technology, Jinan, China*

**ABSTRACT:** Three-Dimensional (3-D) braided piezoelectric ceramic matrix composite has excellent mechanical properties, good electrical properties and design control property. It has broad application prospects in the fields of acoustics, medicine, control, aerospace, etc. This paper briefly introduces the research progresses of piezoelectric ceramic composite and 3-D braided ceramic matrix composite. The several toughening methods of ceramics are discussed. The future research of 3-D braided piezoelectric ceramic matrix composite is prospected.

**Keywords:** piezoelectric ceramics; piezoelectric ceramic composite; ceramics toughening; 3-D braided

## 1 INTRODUCTION

Since the piezoelectric ceramics was found, it has attracted great attention of researchers in the material field at home and abroad. Due to its unique piezoelectric effect, piezoelectric ceramics has become an important information function structure material, which is widely used in high-tech fields such as sensing, driving, vibration control, structural health monitoring and so on (Park et al. 2001, Huang et al. 2001, Sodano et al. 2003). However, the inherent brittleness of the piezoelectric ceramic is very harmful to the stability and reliability of the smart devices in the harsh working conditions. To address this issue, the concept of piezoelectric ceramic composite was put forward. According to the role of piezoelectric ceramics in composite, piezoelectric ceramic composite can be divided into piezoelectric ceramic fiber composite and piezoelectric ceramic matrix composite.

3-D braided piezoelectric ceramic matrix composite is the perfect combination of the 3-D braided technology and the modern piezoelectric ceramic composite technology. It has great differences with conventional piezoelectric ceramic composite in microstructure and macroscopic properties. The fiber bundles are braided into preforms by the 3-D integral braided technology, and then the preforms and piezoelectric ceramics are compounded into 3-D braided piezoelectric ceramic matrix composite through the curing molding process. 3-D braided piezoelectric ceramic matrix composite combined the advantages of each component in one. It not only has the good performances of 3-D braided composites, such as high specific modulus, damage tolerance

and less sensitive to crack, but also has excellent piezoelectric properties of piezoelectric ceramics. It can realize the conversion between mechanical energy and electric energy. In order to make people more aware of the research work in this field. In this paper, the research progresses of piezoelectric ceramic composite and 3-D braided ceramic matrix composite are reviewed. The advantages and disadvantages of the existing piezoelectric ceramic composite are discussed. The future research ideas of 3-D braided piezoelectric ceramic matrix composite are given.

## 2 STUDY ON PIEZOELECTRIC CERAMIC COMPOSITE

### 2.1 *Piezoelectric ceramic fiber composite*

Under the tensile loads, metal material has an elastic deformation stage and plastic deformation stage before its fracture. However, the brittle fracture of piezoelectric ceramics occurred immediately at the end of elastic deformation stage. The hard and brittle characteristics of piezoelectric ceramics bring great difficulties to the forming process. It is hard to meet the requirements of the engineering field for the performance of intelligent material.

The concept of piezoelectric ceramic fiber composite was first proposed by Bent et al. (1995) who embedded the piezoelectric ceramic fibers into polymer matrix. Polymer matrix with good flexibility and impact resistance can improve the mechanical properties of piezoelectric ceramic fiber composite. Brei & Cannon (2004) put forward a novel piezoelectric ceramic fiber composite, which was made

of hollow piezoelectric fibers instead of solid fibers. The electric field can be applied through the thickness of the hollow fiber, so that the impedance of the material and the actuation voltage were reduced obviously. Through the representative volume element method, Berger et al. (2005) predicted the effective performance of orthotropic piezoelectric ceramic fiber composite. Lin & Sodano (2008) developed the active structural fiber, which was made of PZT thin film over the surface of carbon or SiC fiber. The stiffness and flexibility of fiber were improved, and the internal electrode for polarization was provided. Zhang et al. (2011) researched the 1–3 piezoelectric composites transducer by the theory of thickness vibration mode, transverse mode theory and finite element method.

With the development of piezoelectric ceramic fiber manufacturing technology, 3-D braided technology was applied to the fabrication of piezoelectric ceramic fiber composite. Ruan et al. (1999) studied the effective elastic constants, piezoelectric constants and dielectric constants of the 3-D two-step braided piezoelectric ceramic fiber composite by using 3-D connectivity model and an averaging technique. Based on an incompatible displacement finite-element method and the homogenization method, Feng & Wu (2001) examined the effective properties of 3-D four-step braided piezo-ceramic fiber composite.

## 2.2 *Piezoelectric ceramic matrix composite*

Although the piezoelectric ceramic fiber composite improved the toughness and reliability of the piezoelectric ceramics to a certain extent, simultaneously the piezoelectric properties of the composite are decreased (Zhang 2010). Therefore, some material researchers put forward a new composite with piezoelectric ceramic matrix. The mechanical properties of the piezoelectric ceramic matrix were improved by the methods of self-toughening, phase transformation toughening, particle toughening, whisker toughening and fiber toughening. Yamamoto et al. (1985) investigated the electrical and mechanical properties of SiC whisker reinforced piezoelectric ceramic composite. According to the changes of zirconia crystal structure at different temperature and pressure, Takahashi et al. (1994) researched the relationship between the volume fraction of zirconia fiber and the properties of zirconia fiber reinforced piezoelectric ceramic matrix composite. Chen & Yang (1998) developed a new approach for toughening PZT piezoelectric ceramics, in which some piezo-electric secondary phases tending to form plate-like or columnar structures were incorporated into piezoelectric ceramics to enhanced fracture toughness. Jin & Chen (2003) toughened BaTiO<sub>3</sub> ceramics by dispers-

ing coarse BaTiO<sub>3</sub> particles into the fine-grained matrix. In addition, the toughening mechanism was discussed. Ray & Batra (2007) proposed carbon nanotube reinforced piezoelectric ceramic matrix composite, the effective piezoelectric coefficient and elastic coefficient were discussed. Huang et al. (2010) prepared PMMA/PZT piezoelectric composite by in-situ polymerization method. The effect of the piezoelectric ceramics volume content on the piezoelectric and dielectric properties of the composite was researched. Zhang et al. (2011) studied the effect of metal phase volume fraction on the effective piezoelectric properties of metal particle reinforced piezoelectric ceramic matrix composite by using the effective medium theory of Green's function. Xu et al. (2015) prepared a three-phase piezoelectric ceramic matrix composite with CoFe<sub>2</sub>O<sub>4</sub> particles/epoxy embedded in piezoelectric ceramic matrix.

## 3 STUDY ON 3-D BRAIDED CERAMIC MATRIX COMPOSITE

In 1970s, fiber reinforced composite technology was first proposed. Now, the 3-D braided Preforms have become a hot research topic in the field of mechanics and materials, 3-D braided composite with excellent mechanical properties has become an important structural material in engineering field (Duan et al. 2014). The pure ceramics has excellent mechanical and physicochemical properties such as high specific strength, high specific modulus, good high temperature strength and high temperature stability. But the intrinsic brittleness of ceramics greatly limits the design and the use of ceramics parts.

To meet the needs of the aerospace industry for high stability and high reliability ceramics, the study of 3-D braided ceramic matrix composite has been carried out in many countries. Yang et al. (1988) synthesized 3-D braided nicalon fiber reinforced SiC matrix composite by chemical vapor infiltration. The fracture toughness and thermal shock resistance of the composites under different thermal loads were studied. Jenkins & Mello (1996) researched the tensile, compressive and flexural properties of 3-D braided SiC fiber reinforced ceramic matrix composite through experiment method. Pluvinae et al. (1996) investigated the effect of the size and shape of the hole on the damage of 3-D braided SiC fiber reinforced SiC matrix composite under the tensile loads. Li et al. (2004) considered the response of 3-D braided SiC fiber reinforced ceramic matrix composite under the action of the vertical impact of the super high speed projectile. Wang et al. (2006) discussed the shear and flexural properties of 3-D braided

C/SiC composite. Based on the random distribution theory of ceramic pore, Shi et al. (2014a, b) predicted the elastic properties, tensile strength and damage evolution of fiber bundles by using the microscopic model.

#### 4 RESEARCH IDEAS OF 3-D BRAIDED PIEZOELECTRIC CERAMIC MATRIX COMPOSITE

As an important intelligent structure material, piezoelectric ceramics has large piezoelectric coefficient, dielectric coefficient and electromechanical coupling coefficient. Due to the special chemical bond, piezoelectric ceramics lacks of plastic deformation process under large strain and impact loads, and it is prone to brittle fracture. Compared with piezoelectric ceramics, piezoelectric ceramic fiber composite has better dielectric properties and mechanical properties. However, the piezoelectric properties of piezoelectric ceramic fiber composite are reduced significantly, and the fabrication process of piezoelectric ceramic fiber is complicated. Although the existing piezoelectric ceramic matrix composite retains the excellent piezoelectric properties, its mechanical properties are not improved obviously.

Among the various toughening methods of ceramic matrix composite, the effect of continuous fibers toughening is the best. During the fracture process of continuous fibers reinforced ceramic matrix composite, crack deflection, fiber bridging and fiber pull-out failure can absorb fracture energy. This make the strength and toughness of the ceramic matrix enhanced effectively, the brittleness of the ceramics is overcome, and the fracture behavior of the ceramics can be changed radically. 3-D braided piezoelectric ceramic matrix composite is reinforced by 3-D braided preforms with overall space mesh structure. The mechanical properties and fracture toughness along the thickness direction of 3-D braided piezoelectric ceramic matrix composite are improved distinctly. The shortcomings of traditional piezoelectric composite, such as low strength and poor impact resistance, are avoided. Moreover, the piezoelectric effect and high sensitivity of piezoelectric ceramics are persisted.

At present, the theoretical research and experimental research on the 3-D braided piezoelectric ceramic matrix composite are in the initial stage at home and abroad. There is not a mature theoretical system that can be used to predict the effective elastic properties, piezoelectric properties and dielectric properties of 3-D braided piezoelectric ceramic matrix composite. Therefore, it is necessary to strengthen the research and application of 3-D braided piezoelectric ceramic matrix composite. The future research directions of 3-D braided pie-

zoelectric ceramic matrix composite are as follows. Based on the mature theoretical system of performances analysis on piezoelectric ceramic composite and 3-D braided polymer matrix composite, the effective elastic properties, piezoelectric properties and dielectric properties of 3-D braided piezoelectric ceramic matrix composite are analyzed and predicted. Furthermore, the analysis results are used to guide the design and fabrication of 3-D braided piezoelectric ceramic matrix composite. Experimental research is an indispensable method in material research. According to the existing fabrication process of 3-D braided carbon (SiC) fiber reinforced ceramic matrix composite, the process technology and electromechanical properties of 3-D braided piezoelectric ceramic matrix composite are the key point of the experimental study in further.

#### 5 CONCLUSIONS

In this paper, the research progress of piezoelectric ceramic composite and 3-D braided ceramic matrix composite is reviewed. The advantages and disadvantages of various piezoelectric ceramic composite are discussed. According to the existing research methods of 3-D braided ceramic matrix composite, the future research ideas of 3-D braided piezoelectric ceramic matrix composite are put forward.

3-D braided piezoelectric ceramic matrix composite has excellent mechanical properties and unique piezoelectric effect. Its macroscopic properties can be optimized through changing the microstructure of composite. Using 3-D braided piezoelectric ceramic composite instead of pure piezoelectric ceramics or traditional piezoelectric ceramic composite, the stability and reliability of intelligent device can be improved effectively.

#### ACKNOWLEDGEMENTS

This work is supported by the National Natural Science Foundation of China through grant 11271234.

#### REFERENCES

- Bent, A.A. Hagood, N.W. & Rodgers, J.P. 1995. Anisotropic actuation with piezoelectric fiber composites. *Journal of Intelligent Material Systems and Structures* 6(3): 338–349.
- Berger, H. Kari, S. & Gabbert, U. 2005. An analytical and numerical approach for calculating effective material coefficients of Piezoelectric fiber composites. *International Journal of Solids and Structures* 42: 5692–5714.

- Brei, D. & Cannon, B.J. 2004. Piezoceramic hollow fiber active composites. *Composites Science and Technology* 64(2): 245–261.
- Chen, X.M. & Yang, J.S. 1998. Toughening of PZT Piezoelectric Ceramics by In-Situ Complex Structures. *Journal of the European Ceramic Society* 18(8): 1059–1062.
- Duan, L.H. Lin, W.S. Yang, G.L. & Wang, J.L. 2014. Research Development of 3D-Cf/SiC Ceramic Matrix Composite. *Materials Review* 15: 40–43.
- Feng, M.L. & Wu, C.C. 2001. A study of three-dimensional four-step braided piezo-ceramic composites by the homogenization method. *Composites Science and Technology* 61(13): 1889–1898.
- Huang, S.F. Chang, J. & Qin, L. 2008. Properties of 1–3 cement based piezoelectric composite sensor. *Acta Materialia Composita Sinica* 25(1): 112–118.
- Huang, X.H. Zhang, L.L. & Xia, Y. 2010. Study on preparation and electrical properties of PMMA/PZT piezoelectric composites. *Journal of Ceramic* 31(3): 400–403.
- Jenkins, M.G. & Mello, M.D. 1996. Fabrication, Processing, and Characterization of Braided, Continuous SiC Fiber-Reinforced/CVI SiC Matrix Ceramic Composites. *Materials and Manufacturing Processes* 11(1): 99–118.
- Jin, D.Z. & Chen, X.M. 2003. BaTiO<sub>3</sub> ceramics toughened by dispersed coarse particles. *Ceramics International* 29(4): 371–375.
- Li, J.Z. Huang, F.L. & Zhang, Q.M. 2004. A study of hypervelocity impact on 3-DBC/SiC composite material dual-plate armor. *Chinese Journal of High Pressure Physics* 18(2): 163–169.
- Lin, Y. & Sodano, H.A. 2008. Concept and model of a piezoelectric structural fiber for multifunctional composites. *Composites Science and Technology* 68: 1911–1918.
- Park, G. Kim, M.H. & Inman, D.J. 2001. Integration of smart materials into dynamics and control of inflatable space structures. *Journal of Intelligent Material Systems and Structures* 12(6): 423–433.
- Pluvinage, P. Parvizi-Majidi, A. & Chou, T.W. 1996. Damage characterization of two-dimensional woven and three-dimensional braided SiC-SiC composites. *Journal of Materials Science* 31(1): 232–241.
- Ray, M.C. & Batra, R.C. 2007. A single-walled carbon nanotube reinforced 1–3 piezoelectric composite for active control of smart structures. *Smart Materials and Structures* 16(5): 1936–1947.
- Ruana, X. Safarib, A. & Chou, T.W. 1999. Effective elastic, piezoelectric and dielectric properties of braided fabric composites. *Composites. Part A: applied science and manufacturing* 30(12): 1435–1444.
- Shi, D.Q. Niu, H.W. & Jing, X. 2014a. Prediction method of elastic constants of 3-D braided ceramic matrix composites considering pores. *Journal of Aerospace Power* 29(12): 2891–2897.
- Shi, D.Q. Jing, X. & Yang, X.G. 2014b. Numerical prediction of tensile properties and damage evolution of three dimensional-four directional braided CMCs. *Acta Materialia Composita Sinica* 31(6): 1543–1550.
- Sodano, H.A. Park, G. & Inman, D.J. 2003. An investigation into the performance of macrofiber composites for sensing and structural vibration applications. *Mechanical Systems and Signal Processing* 18(3): 683–97.
- Takahashi, M. Baba, K. & Nishizato, O. 1994. Mechanical and electromechanical properties of monoclinic ZrO<sub>2</sub> fiber/PZT composites. *Journal of the Ceramic Society of Japan* 102(1): 65–70.
- Wang, B. Jiao, G.Q. Chang, Y.J. & Pan, W.G. 2006. Shear and Compress Experimental Study on 3-D Braided C/SiC Composites. *Journal of Aeronautical Materials* 26(6): 64–67.
- Xu, T.T. Wang, C.A. & Wang, C. 2015. Synthesis and magnetoelectric effect of composites with CoFe<sub>2</sub>O<sub>4</sub>-epoxy embedded in 3–1 type porous PZT ceramics. *Ceramics International* 41(9 A): 11080–11085.
- Yamamoto, T. Igarashi, H. & Okazaki, K. 1985. Electrical and mechanical properties of SiC whisker reinforced PZT ceramics. *Ferroelectrics* 63(1): 281–288.
- Yang, J.M. Chou, J.C. & Burklund, C.V. 1988. Fracture behavior of 3-d Braided Nicalon/Silicon Carbide Composite. *MRS Online Proceedings Library* 120.
- Zhang, K. Lan, Y. & Li, Q. 2011. Research on 1–3 piezocomposite broad-band underwater transducers. *ACTA ACUSTICA* 36(6): 631–637.
- Zhang, L.L. 2010. The preparation and the electric properties of polymer/piezoelectric ceramic composites. Wuhan: Wuhan University of Technology.
- Zhang, S. Qiu, H.M. & Zhang, H.L. 2011. Piezoelectric properties of metal-particle-dispersed piezoceramics composites. *Journal of University of Science and Technology Beijing* 33(6): 739–744.



# Analysis of deformation of a transmission tower by vacuum-combined surcharge preloading

B.B. Xu & W. Si

Tianjin Port Engineering Institute Ltd. of CCCC, Tianjin, China

Key Laboratory of Geotechnical Engineering of Tianjin, Tianjin, China

Key Laboratory of Geotechnical Engineering, Ministry of Communication, Tianjin, China

**ABSTRACT:** The widely distributed soft ground in Southeast China should be improved before construction of buildings. This paper analyzes the construction of a road embankment on the soft ground and the use of the vacuum-combined surcharge preloading method to reinforce the ground. In order to analyze the deformation of ground, a series of numerical analyses are conducted and the ground deformation is emphasized. The results show that the final settlement at the ground surface is nearly 3.5 m.

**Keywords:** Vacuum preloading; Surcharge preloading; Erected tower; Ground deformation

## 1 ENGINEERING BACKGROUND

With the increase of Chinese economy, there has been a significant progress in the development of the infrastructure, of which road construction has attracted much attention. The road construction plans mainly concentrate around the coastal area of East China, with the coastline containing silty soft soil due to river/sea erosion and sedimentation. Such soil types have high water content, high void ratio, high compressibility, low strength, and low permeability. Once the road is directly constructed on the soft ground, there would be significant deformation of uneven settlement due to the consolidation of ground, whose duration is usually very long, which may influence the servility of the road. In addition, low bearing capacity of the ground may result in the instability of the road. Therefore, it is very necessary to carry out ground improvement before road construction.

For the soft ground, the most frequently used method is vacuum preloading, considering its feasibility and economy.

The reinforcement mechanism of the vacuum preloading is mainly studied through indoor experiments and in-site engineering. Chen and Bao (1984) used one-dimensional negative pressure consolidometer to carry out the air exhaust experiments and found that if the differential pressure is zero, almost the same soil parameters can be obtained under both positive and negative pressures, that is, the consolidation effect is same.

Chen and Lin (1987) carried out a series of model tests to investigate the mechanism of

vacuum preloading. After the preloading, the water content of the top soil decreases significantly while the strength of the vane shear test increases to some extent.

Zhang (1990) studied the influence of the position of vacuum pressure and the distance between vertical drains on the improvement of reinforcement and found that the lower the position of the vacuum preloading is, the better the reinforcement effect is, and also that the influence of the distance between drains cannot be neglected.

Along the road to be improved, there are a series of high-voltage power transmission towers. The depth of the plastic vertical drain for vacuum preloading is 25 m and there is no enough clearance for the operation of the installation machine. Now the possible treatment is to dodge the power transmission tower, but the influence of horizon-

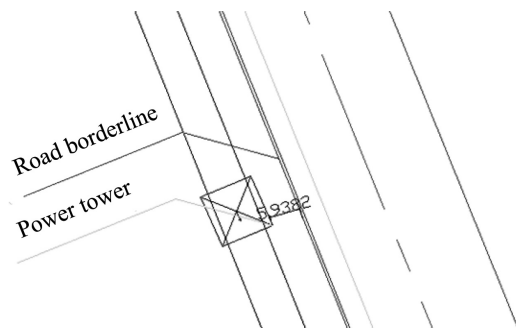


Figure 1. Relative position of the road and power transmission tower.

tal deformation of the ground during the vacuum preloading on the power transmission tower should be taken into consideration. Given this, double cement-mixed piles are installed at the borderline of the improved area. In this paper, the emphasis is put on the influence of the ground deformation during vacuum preloading on the power transmission tower.

## 2 IMPROVEMENT SCHEME

The total length and width of the road are 1578 and 20 m, respectively. The ground layers determined by the previous ground survey can be divided into silt, mucky clay, silty clay, and alluvium clay, sequentially.

The vacuum preloading method with plastic vertical drains of SPB will be adopted in the soil improvement of this road. The space of the drains is 1 m with a distribution of triangle. In order to reduce the influence of vacuum pressure on the surrounding environment, the cement-mixed pile is installed for isolation. The diameter of the pile is 700 mm with a space of 500 mm. The minimum embedment depth of the pile in the silty clay layer is 3 m. After 5–7 days of application of vacuum pressure, the degree of vacuum under the diaphragm seal reaches  $-80$  kPa. Then, the vacuum pressure is maintained for about 10–20 days before the addition of embankment. The embankment should be constructed within 60 days and the duration of vacuum-combined surcharge preloading should be at least 120 days.

## 3 NUMERICAL MODEL

According to the location of the road and the erected tower, a typical section is chosen to analyze, and the calculation model is shown in Fig. 2. Considering the asymmetry of the model, take the whole width of the road to be computed. The transmission tower is located at the right-hand side of the road to be improved and the distance between them is 2 m.

The ground is divided into four layers, including silt with depth of 28 m, mucky clay with depth of 10 m, silty clay with depth of 6 m, and clay with depth of 36 m. The left hand side, right hand side, and bottom layer of the model are impermeable. Besides, considering the transmission tower is three dimensional, the stiffness and volume weight of the tower are modified equivalently when it is used in the plane strain condition. The foundation of the tower is the cast-in-place pile.

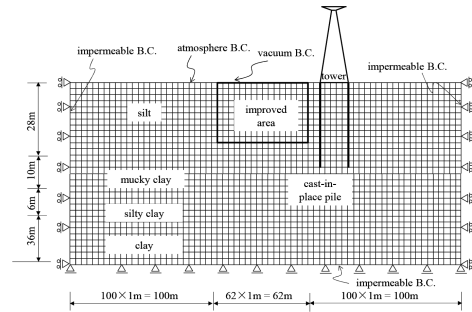


Figure 2. Numerical model and boundary conditions.

## 4 CALCULATION RESULTS

### 4.1 Settlement and horizontal displacement

Fig. 3 shows the layered settlement at the ground surface and the middle of the drains until 180 days. As can be seen, the maximum settlement at the ground surface is nearly 3.5 m, which is very close to the predicted value from the layer summation method. Before 90 days, the rate of settlement is relatively high under the combination of vacuum and surcharge loading, and then its value decreases gradually. Comparing with the settlement at the middle of the plastic vertical drain, that at the upper region is about 2.3 m, which accounts for about 66% of the total settlement. For the settlement at 180 days, the rate is almost zero and it can be regarded that the degree of consolidation is over 90%.

In the procedure of improvement of the road, the horizontal displacement outside the improved area and the deformation of tower are paid more attention. Figs. 4–7 show the horizontal displacements of the ground surface with distances of 1, 5, 10, and 15 m from the improved borderline at different depths. The maximum horizontal displacements are 0.3, 0.23, 0.22, and 0.17 m, respectively. The horizontal displacement of the ground surface with a distance of 1 m from the improved borderline is shown Fig. 4, which is located between the clay sealing wall and the cast-in-place pile foundation of the tower. As can be seen, the horizontal displacement gradually decreases from the ground surface toward deep ground. After the application of the surcharge load, there is positive horizontal displacement at the depth of 16–24 m, namely lateral deformation toward the outside of the improved area. Taking the deformation at the ground surface as example, at the initial stage of improvement, there is only vacuum preloading and the negative lateral deformation gradually increases. As the surcharge load is gradually applied, the rate of negative deformation decreases and the deformation is toward the outside of the improved area. After the four-stage

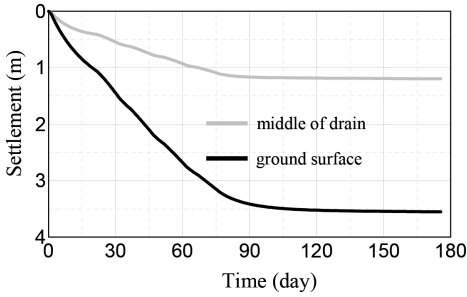


Figure 3. Curves of the layered settlement.

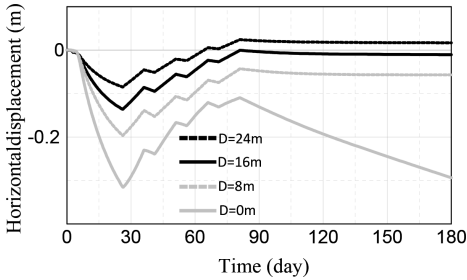


Figure 4. Horizontal displacement versus time at different depths (1 m distance from improved borderline).

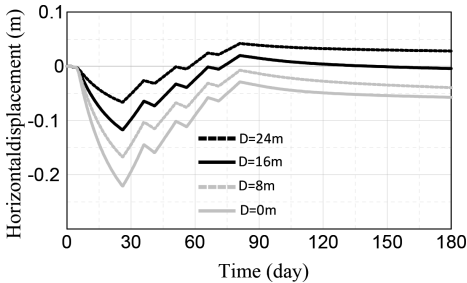


Figure 5. Horizontal displacement versus time at different depths (5 m distance from improved borderline).

surcharge load is added, the negative lateral displacement again increases under the vacuum pressure. Similar tendency of deformation can be seen at the distances of 5, 10, and 15 m from the borderline. The difference lies in that the variation of the negative displacement is not so significant, which can be attributed to the restriction of cast-in-place piles.

Fig. 8 shows the vertical deformation of the ground surface at different distances from the borderline. As can be seen, the final settlement at 1 m distance from the borderline is nearly 1 m, while the settlement at 15 m distance from the borderline is nearly 0 m. When the distance is between 5 and 10 m, the settlement at the ground surface increases continuously. When the

distance is between 10 and 15 m, the settlement at the ground surface initially increases under the action of vacuum pressure and then decreases because of the application of the surcharge load.

#### 4.2 Distribution of variables

Fig. 9 shows the distribution of the volumetric strain inside the ground at different stages. In the legend, blue indicates zero volumetric strain and red indicates 40% compressive volumetric strain. It should be clarified that in the tower, the volumetric strain is 40% due to the bug of post-treat program, but it should be zero. As can be seen, at the stage of vacuum preloading only, the mucky clay at the

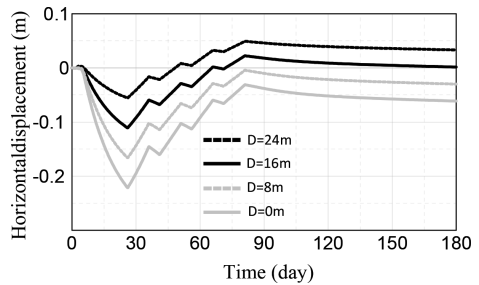


Figure 6. Horizontal displacement versus time at different depths (10 m distance from improved borderline).

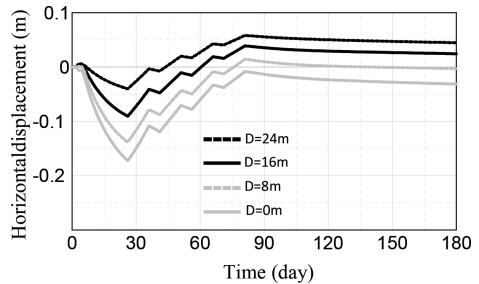


Figure 7. Horizontal displacement versus time at different depths (15 m distance from improved borderline).

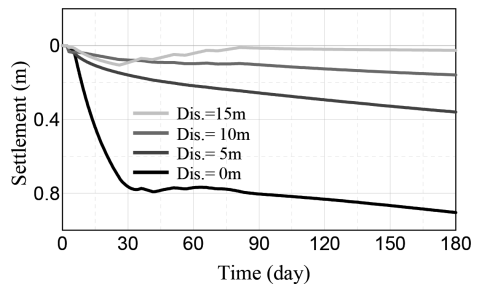


Figure 8. Uplift and settlement of the ground surface at different distances from the borderline.

ground surface is compressed rapidly and the volumetric strain reaches or exceeds the maximum. With the addition of each layer of the embankment, the volumetric strain gradually develops toward the deep ground. Meanwhile, there is obvious compressive strain at the ground near the cast-in-place piles. The tower inclines slowly toward the direction of the improved area and therefore the volumetric strain of the ground near the improved area is larger than that at the right-hand side of the tower.

Fig. 10 shows the distribution of the volumetric strain inside the ground at different stages. In the legend, blue indicates zero volumetric strain and red indicates 40% compressive volumetric strain. It should be clarified that in the tower, the volumetric strain is 40% due to the bug of post-treat program, but it should be zero. As can be seen, at the stage of vacuum preloading only, the mucky clay at the ground surface is compressed rapidly and the volumetric strain reaches or exceeds the maximum. With the addition of each layer of the embankment, the

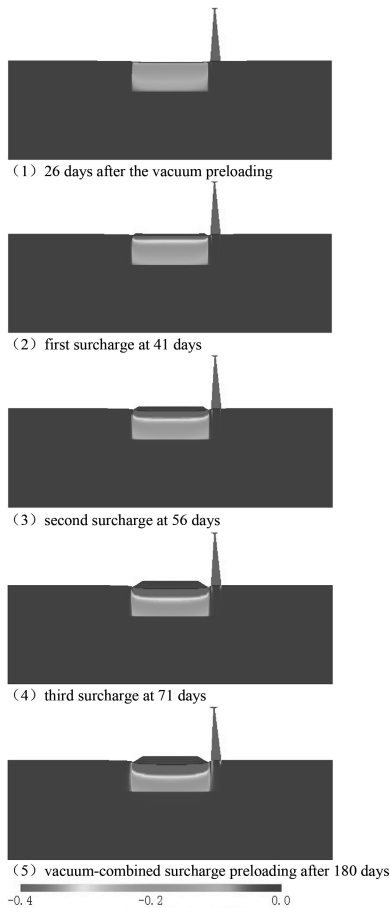


Figure 9. Distribution of volumetric strain.

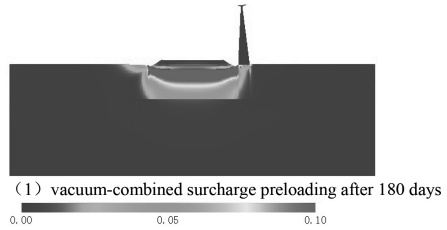


Figure 10. Distribution of shear strain.

volumetric strain gradually develops toward the deep ground. Meanwhile, there is obvious compressive strain at the ground near the cast-in-place piles. The tower inclines slowly toward the direction of the improved area and therefore the volumetric strain of the ground near the improved area is larger than that at the right-hand side of the tower.

## 5 CONCLUSIONS

In this paper, ground deformation during the vacuum-combined surcharge preloading is analyzed numerically. The emphasis is put on the horizontal displacement at different distances from the borderline of the improved area and the conclusions are as follows:

1. Initially, the rate of settlement increases due to the rapid consolidation of the ground, and then it decreases after 90 days. The final settlement is about 3.5 m.
2. Because of the surcharge effect, the negative displacement becomes smaller after the construction of each layer.
3. According to the distribution of volumetric strain, the tower inclines slowly toward the direction of the improved area and the volumetric strain of the ground near the improved area is larger than that at the right-hand side of the tower.

## REFERENCES

- Chen H. & Bao X.Q. 1984. Consolidation Effective Stresses in Soil under the Negative Pressure Condition, Chinese Journal of Geotechnical Engineering, Chinese Journal of Geotechnical Engineering, (5): 39-47.
- Chen H. & Lin F. 1987. Analysis of consolidation of ground installed with sand drains under loading and vacuum by boundary element method, Chinese Journal of Geotechnical Engineering, (4): 13-21.
- Zhang C.H. 1990. The influence of vacuum location and the spacing of drain well on the effect of preloading improvement, Chinese Journal of Geotechnical Engineering, (1): 56-60.

# Numerical modeling of air flow and pollutant distribution in industrial workshop with different solar chimney on the roof

Yu-feng Xue

*Shanghai Nuclear Engineering Research and Design Institute, Shanghai, China*

Xian-zhong Zhang

*Institute of Technology Innovation Co. Ltd., Zhejiang University, Zhejiang, China*

Ya-xin Su & Wen-yi Deng

*School of Environmental Science and Engineering, Donghua University, Shanghai, China*

**ABSTRACT:** Natural ventilation is a cost-efficient technology to apply to the industrial workshop with heat source. Four designs of Solar Chimney (SC), including an inclined design along the original roof, two vertical designs and a combination of vertical and inclined design, were proposed to install on the workshop roof to improve the indoor air quality in a heating-treatment workshop. The air flow behavior and pollutant distribution in the workshop were numerically calculated by CFD method. The fresh air exchange and Predicted Mean Vote (PMV), Predicted Percentage of Dissatisfied (PPD) indexes were used to evaluate the effect of the solar chimney configurations on the ventilation performance. Results showed that the natural ventilation and the indoor air quality were improved in various degrees when solar chimneys were installed on the workshop roof. The fresh air exchanges were increased about 39% as compared to the prototype when the solar chimney was vertically installed on the symmetric center of the workshop roof (as noted as SC-III). The SC-III solar chimney increased the averaged air velocity in the workshop, e. g., the averaged air velocity in the workshop working zone increased 43%. The thermal comfort was evaluated based on the index, PMV (Predicted Mean Vote) and PPD (Predicted Percentage of Dissatisfied). Solar chimney improved the thermal comfort in the working zone. The PMV index decreased when solar chimney was installed, e.g., PMV decreased from 1.503 for the prototype workshop to 1.282 for SC-III workshop, a 16.5% off, which indicated that the thermal comfort was improved. Solar chimney decreased the PPD, e.g., PPD decreased from 51.063% for the prototype workshop to 39.346% for SC-III workshop, a decrease of 22.9%.

**Keywords:** natural ventilation, solar chimney, industrial workshop, pollutant distribution, CFD

## 1 INTRODUCTION

Natural ventilation uses natural forces, such as wind and buoyancy, to deliver fresh air into buildings in order to limit the concentration of contaminations and to improve the indoor thermal environment (Khatami, 2013; Hussain & Oosthuizen, 2013). Generally natural ventilation is suitable for the workshop with heat sources due to the large temperature difference between the inside and outside of the workshop which forms the thermal pressure. Natural ventilation is usually adopted in some of the workshops; e. g., iron and steel processing workshop, due to its energy saving merit and the effect of geometrical parameters of the workshop on the ventilation performance have been previously studied via numerical method by the authors (Su & Wan, 2011, 2012a, 2012b; Su, et al, 2012). Solar Chimney

(SC) can enhance the natural ventilation by taking advantage of solar radiation to generate convective air flows, which pull air out of the interior of the building and replace it with fresh air from outside (Arce, et al, 2009; Mathur, et al, 2006). The authors applied solar chimney to workshop and found the ventilation rate was improved and the mean air velocity was increased, leading to the improved indoor thermal comfort as noted by the Predicted Mean Vote (PMV) and Predicted Percentage of Dissatisfied (PPD) indexes (Xue & Su, 2011).

In the industrial workshop, effective natural ventilation should improve not only the thermal comfort by increasing the ventilation rate and air velocity, but also the indoor air quality by driving the pollutants out. In this paper, the authors will present effect of solar chimney on the pollutant distribution inside the workshop.

## 2 MODEL AND METHOD

### 2.1 Physical model of the workshop with solar chimney

The original structure of the workshop with a heat source is showed by Figure 1, as noted to be prototype workshop. The workshop is  $40\text{ m} \times 20\text{ m} \times 24\text{ m}$  in length, width and height. There is a heat source in the center of the workshop along its length. The intensity of heat source is  $200\text{ W/m}^2$  according to the general requirement of industrial furnace for heating of metal materials and its surface temperature is  $573\text{ K}$ . The width and height of the heat source are  $3.2\text{ m}$  and  $2\text{ m}$ , respectively. There is one air inlet window on each side of the south and north wall of the workshop and one skylight (air outlet window) on each of the south and north side roof wall. The heights of the air inlet and outlet windows are  $3\text{ m}$  and  $2.4\text{ m}$  respectively.

Figure 2 shows one example of the typical SC configuration that is attached to workshop southern roof. Solar radiation enters into the SC channel through the transparent material and absorbed by the thermal storage materials. The air in the solar chimney is then heated and flows out of the SC at an increased speed due to the thermal force (buoyancy). The natural ventilation in the workshop is enhanced and indoor air quality is improved.

Generally, there are three types of SC, i.e., vertical type, inclined type and combination of both. Based on the structure of the workshop illustrated in Figure 1, four types of SC structures were designed, as showed in Figure 3. The air flow channel of the solar chimney is  $3\text{ m}$  for all of the 4 types of SC structure. The inclined angle is  $45^\circ$  for SC-I and SC-IV.

According to the weather record from 1971 to 2000 by Bureau of Meteorology of China, the mean solar flux is  $356.7\text{ W/m}^2$  in August in Shanghai, China. A glass cover is glazed on the solar chimney surface and the air flows in the channel between the glass glazing and the inner wall. The glass surface absorption coefficient is set as  $0.03$  and its transmissivity is  $0.92$ . The absorption coefficient of heat-storage wall is  $0.95$ . Therefore, the heat flux absorbed by the glass wall is  $356.7 \times 0.03 = 10.77\text{ W/m}^2$ , and the

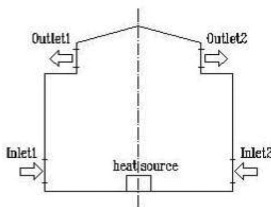


Figure 1. Prototype workshop.

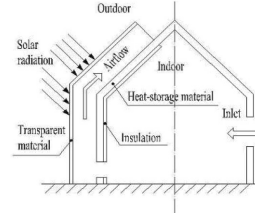


Figure 2. Principle of SC's operation.

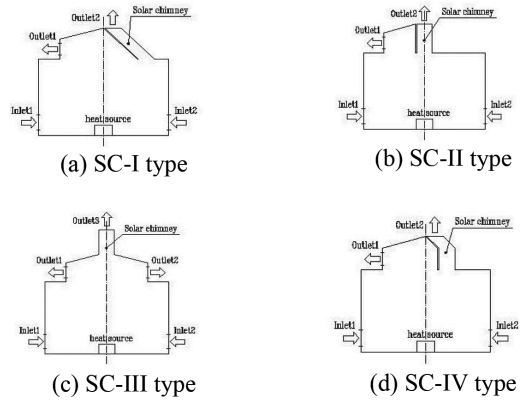


Figure 3. Workshop with different SC structures.

heat flux absorbed by the heat storage wall is  $356.7 \times 0.92 \times 0.95 = 311.8\text{ W/m}^2$ . The influence of wind pressure was neglected during the calculation. The ambient temperature of the open air is set  $304\text{ K}$  in Shanghai, which is the outdoor design temperature for ventilation given by the national standard. The operating zone is defined to be the zone that measures  $2\text{ m}$  from the ground, where most routine work is carried out.

### 2.2 Mathematical model and numerical method

Realizable  $k$ - $\epsilon$  model was used to calculate the turbulent flow in the workshop after several trial calculations and comparison to related experimental data. Standard wall function was adopted to calculate the near-wall flow. The transport equations of Realizable  $k$ - $\epsilon$  model are given as the following (Long, et al, 2007).

$$\frac{\partial(\rho\kappa)}{\partial t} + \frac{\partial(\rho\kappa u_i)}{\partial x_i} = \frac{\partial}{\partial x_j} \left[ \left( \mu + \frac{\mu_t}{\sigma_\kappa} \right) \frac{\partial \kappa}{\partial x_j} \right] + G_\kappa - \rho\epsilon \quad (1)$$

$$\frac{\partial(\rho\epsilon)}{\partial t} + \frac{\partial(\rho\epsilon u_i)}{\partial x_i} = \frac{\partial}{\partial x_j} \left[ \left( \mu + \frac{\mu_t}{\sigma_\epsilon} \right) \frac{\partial \epsilon}{\partial x_j} \right] + \rho C_1 E \epsilon - \rho C_2 \frac{\epsilon^2}{\kappa + \sqrt{V\epsilon}} \quad (2)$$

Hexahedral cell was used to mesh the whole workshop and the predicted results were validated by refining grid (when grid number increased twice, the difference of predicted results were less than 1%), which ensured the validity of simulation, i.e. the predict results were grid-independent. The workshop wall is set concrete and the hot wire material is aluminum. Air inlet velocity of eastern window is 1.58 m/s. In consideration of the existence of high temperature wire stock and heat resources, DO model is the suitable model to calculate the heat transfer and radiation. Second Order Upwind discretization scheme was used to discrete the equations and SIMPLIEC was used to solve the difference equations. The calculation was carried out by FLUENT 6.3 code (Fluent Inc., 2005). The validation of the present model was conducted according to experimental data in the previous studies (Xue & Su, 2011).

### 3 RESULTS AND DISCUSSION

#### 3.1 Air flow field in the workshop

Figure 4 presents the air flow field along the cross-section of the prototype workshop. When there is a heat source in the workshop, the fresh air entering from the open air through the inlets flows over the heat source and is heated, resulting to the rising flow. Local vortexes, as noted 1, 2, 3 and 4 in Figure 4, are formed under the ceiling. The heated air may undergo a recirculating flow in the upper workshop space before it leaves for the open air. Therefore the waste heat could not be directly and quickly exported to the open air.

When different solar chimneys are installed on the workshop roof, the air flow pattern is changed, as showed in Figure 5.

Figure 5 showed that when a solar chimney was used, the air flow velocity through the chimney channel increased, especially when the solar chimney was fixed at the center, e.g., the SC-III type and SC-II type. Once the rising flow above the heat source is enhanced, the natural ventilation is

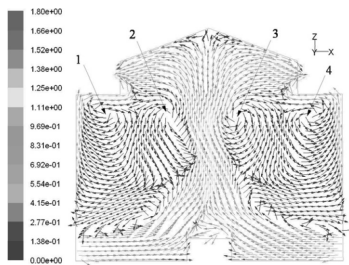


Figure 4. Air flow in the Prototype workshop (m/s).

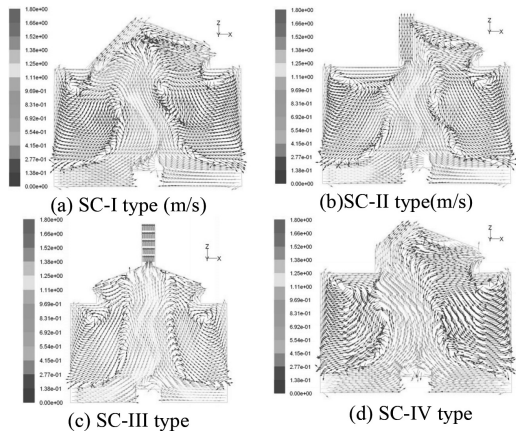


Figure 5. Air flow in the workshop with solar chimney (m/s).

improved and both the waste heat and any possible pollutant emission during the heating treatment could be quickly and directly drained away. When a declined solar chimney was fixed on the roof, such as SC-I type and SC-IV type, as showed in Figure 5(a) and Figure 5(d), a part of the heated air would accumulate under the ceiling and reside a longer time before it is drained out.

#### 3.2 Pollutant distribution in the workshop

Figure 6 and Figure 7 present the pollutant distribution along the central cross section of the prototype workshop and the workshops with 4 types of solar chimney.  $CO_2$  was used as the pollutant tracer in the numerical calculation. The original  $CO_2$  concentration (volume fraction) in the open air was 0.0314%.

In the workshop, the pollutant emissions formed during the heating manufacture process moved with the hot air to the ceiling and finally exited through the exhaust outlet, as showed in Figure 6. In the prototype of the workshop, the pollutant accumulated near the roof, the right and left corners. The local  $CO_2$  concentration was as high as 0.055%, about 1.75 times of the  $CO_2$  concentration in the open air, as showed in Figure 6.

The solar chimney on the ceiling of the workshop influenced the exhausting of the pollutant, as showed in Figure 7. When a solar chimney of SC-I type was installed on the workshop roof, the local pollution indexed by  $CO_2$  at the right corner was obviously improved, as showed in Figure 7(a), however, the pollutant concentration near the left corner was still high due to the local vortex of the air flow near the left corner below the roof. When the SC-II and SC-IV were used, the pollutant

concentration at the right side in the workshop was high, as showed in Figure 7(b) and Figure 7(d). When the SC-III type of solar chimney was used, the pollutant in the workshop could be easily exhausted outside the workshop, as showed in Figure 7(c).

Figure 8 presents the local pollutant concentration distribution along the workshop height at the cross section  $x = 5\text{ m}$  and  $x = 19\text{ m}$ . It was seen that the local pollutant distribution in the workshop with SC-III type of solar chimney was always lower than that in the workshop with other 3 types of solar chimney.

### 3.3 Actual fresh air exchange

The actual fresh air exchange was defined as the following:

$$n_e = n_x \cdot \varepsilon = \frac{Q_{inx}}{V} \cdot \frac{C_{out} - C_{in}}{C_{av} - C_{in}} \quad (3)$$

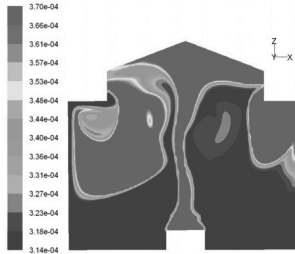


Figure 6. Pollutant distribution in Prototype workshop.

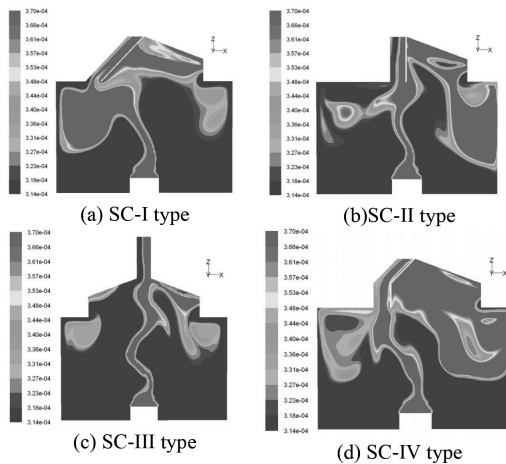
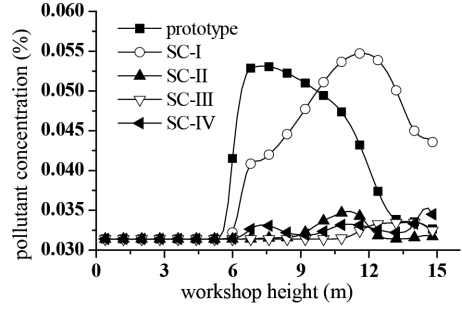
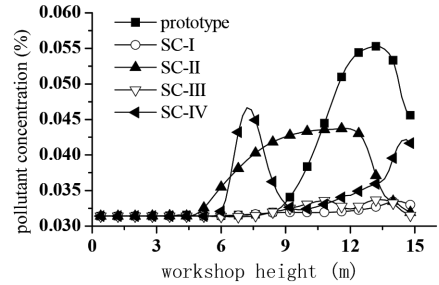


Figure 7. Pollutant distribution in workshop with solar chimney.



(a) At the cross section  $x=5\text{ m}$



(b) At the cross section  $x=19\text{ m}$

Figure 8. Local pollutant concentration distribution along the workshop height.

where  $n_x$  is the fresh air exchange and is defined as  $n_x = \frac{Q_{inx}}{V}$ , time per hour,  $Q_{inx}$  is the flow rate of the fresh air into the workshop,  $\text{m}^3/\text{h}$ ,  $V$  is the volume of the workshop,  $\text{m}^3$ .  $\varepsilon = \frac{C_{out} - C_{in}}{C_{av} - C_{in}}$ ,  $C_{in}$  and  $C_{out}$  are the pollutant concentration at the inlet and outlet,  $C_{av}$  is the averaged pollutant concentration in the building. The actual fresh air exchange was calculated and listed in Table 1.

When SC was installed on the workshop roof, the fresh air exchanges,  $n_x$  were increased, about 39% for SC-III and 24% for SC-II respectively as compared to that for prototype. The actual fresh air exchange  $n_e$  also increased when solar chimney was installed, e.g., an increase of 39% for SC-III and 29% for SC-II respectively. When SC-I and SC-IV were installed, the increase of  $n_e$ ,  $n_x$  and  $\varepsilon$  were relatively slighter as compared to those for SC-III and SC-II. Therefore, the solar chimney designs of SC-III and SC-II were more reasonable to exhaust the pollutant.

### 3.4 Predicted Mean Vote (PMV) and Predicted Percentage of Dissatisfied (PPD)

PMV (Fanger, 1970) is a synthetic index to evaluate the indoor thermal comfort which contains six main factors (temperature, relative humidity, wind speed, radiation temperature, clothing,



Table 1. Actual fresh air exchange.

	prototype	SC-I	SC-II	SC-III	SC-IV
$n_x$	29.57	30.61	36.69	41.18	32.42
$\epsilon$	1.03	1.08	1.07	1.03	1.06
$n_e$	30.46	33.06	39.26	42.42	34.37

Table 2. Corresponding level of PMV&PPD.

PMV	-3	-2	-1	0	+1	+2	+3
PPD (%)	99	77	26	5	26	77	99
Thermal sensation	Cold	Cool	Slightly cool	Neutral	Slightly warm	Warm	Hot

activity intensity). The main thermal comfort standard in the world is ISO 7730 which is based upon the PMV index (Olesen & Parsons, 2002). PMV predicts the mean value of the votes of a large group of people on the ISO thermal sensation scale. PPD predicts the percentage of a large group of people likely feeling ‘too warm’ or ‘too cool’ and it could be figured out through PMV. The corresponding relation between PMV and PPD is shown by Table 2.

The PMV & PPD is calculated by the following (Fanger, 1970):

$$PMV = (0.303e^{-0.036M} + 0.028) \times \{M - W - 3.05 \times 10^{-3} [5733 - 6.99(M - W) - P_a] - 0.42[(M - W) - 58.15] - 1.7 \times 10^{-5} M(5867 - P_a) - 0.0014M(34 - t_r) - 3.96 \times 10^{-8} f_{cl}[(t_{cl} + 273)^4 - (t_r + 273)^4] - f_{cl}h_c(t_{cl} - t_r)\} \quad (4)$$

$$PPD = 100 - 95 \exp[-(0.03353PMV^4 + 0.2179PMV^2)] \quad (5)$$

where  $M$  is the body's metabolic rate ( $W/m^2$ );  $W$  is the mechanical work by human ( $W$ );  $P_a$  is the partial vapor pressure of water in air (Pa);  $t_a$  is the air temperature ( $^{\circ}C$ );  $f_{cl}$  is the clothing covered coefficient (%);  $t_{cl}$  is the mean temperature of body surface ( $^{\circ}C$ );  $t_r$  is the mean radiant temperature of indoor space ( $^{\circ}C$ );  $h_c$  is the heat transfer coefficient of body surface ( $W/(m^2 K)$ ).  $M$ ,  $W$ ,  $P_a$ ,  $t_a$ ,  $f_{cl}$ ,  $t_r$  could be figure out directly.  $t_{cl}$  and  $h_c$  should be iterative computed by software such as Matlab 7.0.

PMV and PPD in working zone were calculated based on the CFD simulation results and listed in Table 3.

The data in Table 3 showed that the solar chimney had a very slight effect on the mean air temperature at the working zone ( $\Delta T < 0.04 K$ ) as compared to that in the prototype workshop. However, the mean air velocity in the working

Table 3. PMV/PPD.

	Prototype	SC-I	SC-II	SC-III	SC-IV
$T_h$ (K)	304.45	304.45	304.49	304.49	304.47
$V_h$ (m/s)	0.837	0.875	1.059	1.197	0.926
PMV	1.503	1.475	1.368	1.282	1.448
PPD(%)	51.063	49.544	43.814	39.346	48.085

$T_h$ : mean air temperature at working zone;  
 $V_h$ : mean air velocity at working zone.

zone was increased when different solar chimney was installed. The averaged air velocity in the working zone increased 43% and 27% when SC-III and SC-II was installed respectively. The calculated PMV showed that solar chimney also improved the thermal comfort in the workshop working zone and the PPD decreased. Among all of the 4 types of solar chimney, SC-III was demonstrated to have the best improvement on the thermal environment following by SC-II.

#### 4 CONCLUSION

Solar chimney improved the natural ventilation in the workshop and increased the actual fresh air exchange; as a result, the indoor air quality was improved obviously. The pollutant in the workshop could be exhausted much better when SC was installed on the workshop roof with a vertical design, SC-III and SC-II, than an inclined design, SC-I and SC-IV, as noted in the paper.

#### ACKNOWLEDGMENT

This work was supported by National Natural Science Foundation of China (No. 51278095), which are gratefully acknowledged.

#### REFERENCES

- Arce, J., Jimenez, M. J., Guzman, J. D. 2009. Experimental study for natural ventilation on a solar chimney. *Renewable Energy* 34:2928–2934.
- Clifford, M. J., Evcritt, P. J., Clarke R. 1997. *Build. Environ.* 32:305.
- Fanger, P. O. 1970. *Thermal Comfort*. Copenhagen: Danish Technical Press.
- Fluent Inc., 2005. *FLUENT User's Guide*. USA: New Hampshire.
- Hussain, S. & Oosthuizen, P. H. 2013. Numerical investigations of buoyancy-driven natural ventilation in a simple three-storey atrium building and thermal comfort evaluation. *Applied Thermal Engineering* 57(1–2): 133–146.

- Khatami, N., Cook, M. J., Firth, S. K., et al. 2013. Control of carbon dioxide concentration in educational spaces using natural ventilation. *International Journal of Ventilation* 11(4): 339–352.
- Long, T. Y., Su, Y. X., Xiang, W. Y., He, C. 2007. *Computational Fluid Dynamic*. Chongqing: Chongqing University Press.
- Mathur, J., Bansal, N. K., Mathur, S. et al. 2006. Experimental investigations on solar chimney for room ventilation. *Solar Energy* 80:927–935.
- Olesen, B. W. & Parsons, K. C. 2002. Introduction to thermal comfort standards and to the proposed new version of EN ISO 7730. *Energy and Buildings* 34:537–548.
- Su, Y. X. & Wan, X. 2011. Numerical simulation of the natural ventilation in workshop with different air inlet openings. *Advanced Materials Research* 250–253: 3187–3190.
- Su, Y. X. & Wan, X. 2012a. CFD simulation and retrofit of natural ventilation in a steel workshop. *Advanced Materials Research* 383–390:6608–6613.
- Su, Y. X. & Wan, X. 2012b. Natural ventilation in workshop with different horizontal arrangement of heat source. *Applied Mechanics and Materials* 229–231:2411–2414.
- Su, Y. X., Wan X., Su, A. L. 2012. Effect of skylight width on natural ventilation in industrial workshop. *Advanced Materials Research* 446–449:2904–2907.
- Xue, Y. F. & Su, Y. X. 2011. The improvement of natural ventilation in an industrial workshop by solar chimney Proceedings of 2011 International Conference on Computer Distributed Control and Intelligent Environmental Monitoring, 19–20 February, 2011, Changsha, China, 2302–2305. N Y: IEEE Computer Society.

# Test and analysis of hydration heat for the zero block of a continuous rigid frame bridge

H.B. Zhang & C.L. Lv

*The 5th Engineering Bureau Co. Ltd., of China Communications Railway Engineering Bureau Chengdu, Sichuan, China*

M. Ma, S.B. Chai & X. Ren

*College of Architecture and Civil Engineering, Xian University of Technology, Xi'an, Shaanxi, China*

**ABSTRACT:** Hydration heat of concrete materials was considered as one of the main reasons for some cracks in large-volume box girders. When zero concrete block of box girder from Anjiashan River Bridge was constructed, the sensors were installed in different areas of the zero concrete block, and temperature changes of hydration heat of concrete materials with increase of time were tested. As a result, changes of temperature of hydration heat of concrete materials with increase of time were obtained after a series of testing data on temperature of hydration heat of zero concrete block were analyzed. Finally, we put forward the corresponding manipulative measures to guide construction and provide a valuable reference for design and construction of concrete box girder.

**Keywords:** Temperature, hydration heat, large-volume concrete, zero block

## 1 INTRODUCTION

Continuous rigid frame bridges built of large volume, high strength concrete beams in the pouring process will produce much higher heat of hydration, resulting in a temperature gradient which will make the concrete produce uneven deformation and large temperature stress under the effect of constraint by itself. High-temperature stress will result in concrete structures producing cracks. Therefore, it is necessary to give full considerations to the influence of hydration heat on the process of pouring large volume concrete to prevent temperature cracks and improve the quality of the project.

Relevant studies had been conducted by many scholars: Kang (2008) carried out simulation analysis for hydration heat from bearing platform of large bridges by MIDAS/civil finite element calculation software, which guides the construction of large-volume concrete; Zang et al. (2007) conducted numerical simulation that effect from hydration heat of zero concrete block to long-span continuous rigid frame bridge and analyzed the temperature field of hydration heat and stress field distribution, which put forward reasonable suggestions for the control temperature and temperature stress; and Yuan et al. (2011) established finite element model of high pier of long-span continuous rigid frame bridge with the three-dimensional temperature field of the heat conduction theory.

Combined with the actual construction environment parameters, the model calculation results are compared with the data obtained by the analysis of hydration heat characteristics of box beam concrete. However, it is difficult to obtain the authentic change law of temperature field with time and space due to the complexity of temperature field and the difference of construction environment. In this paper, a zero concrete block is constructed using long-span continuous rigid frame railway bridge as the engineering background and testing and analyzing the change of temperature field of hydration heat and stress field distribution of zero concrete block poured.

## 2 PROJECT SUMMARY

The Anjiashan River Bridge is located in Luliang mountains, Baode County, Xinzhou City, Shanxi Province, China, with the control engineering of the Xingbao Railway. The bridge span arrangement for (81 + 130 + 81) m zero block is: length 13 m, width 22.8 m, bottom width 16.8 m, maximum height 9.2 m, roof thickness 80 cm, web plate thickness 130 cm, and base plate thickness 1.2 m. The main girder uses C55 concrete, and the concrete volume is 954.89 m<sup>3</sup>. Materials for the construction of concrete blocks are as follows: cement is 425, sand is 761, crushed stone is 1094, fly ash

is 75, admixtures is 5, water–cement ratio is 0.29, total plastic material is 1500.

### 3 THE BASIC THEORY OF HYDRATION HEAT

The temperature distribution analysis aims at analyzing the concrete condensation and hardening process of heating, convection, and conduction nodes caused by temperature change. The process condense sclerosis after concrete pouring, that is, the cement hydration fluid, releases a large amount of hydration heat. For the most part, because of the poor thermal conductivity of the concrete, heat is not dissipated in time during construction, focusing on casting a piece inside, which can increase the internal temperature of the concrete pouring piece quickly.

#### 3.1 Established heat conduction equations

After concrete pouring, under the influence of cement hydration, it can be seen that continuous homogeneous media has an internal heat source strength ( $c$ ) and transient temperature field ( $T$ ). The transient temperature field can be calculated by a three-dimensional unsteady heat conduction equation in a particular solution with known initial and boundary conditions. To simplify the problem, the concrete is assumed to be continuous, homogeneous, and isotropic casting with an internal heat source in order to calculate the transient temperature field of concrete box girders using the heat conduction equation:

$$\gamma \left( \frac{\partial^2 T}{\partial x^2} + \frac{\partial^2 T}{\partial y^2} + \frac{\partial^2 T}{\partial z^2} \right) + \frac{Q}{cd} = \frac{\partial T}{\partial t} \quad (1)$$

Node (1):  $\gamma$  – thermal conductivity;  $T$  – concrete transient temperature;  $Q$  – heat source density;  $c$  – concrete heat capacity;  $d$  – concrete density.

Due to the hydration heat effect, under the adiabatic condition, the increase of concrete temperature is

$$\frac{\partial \theta}{\partial t} = \frac{Q}{cd} = \frac{Wq}{cd} \quad (2)$$

Node (2):  $\theta$ —concrete adiabatic temperature rise;  $w$ —cement content;  $q$ —unit mass of cement in the heat released per unit of time.

The heat conduction equation can be rewritten as

$$\gamma \left( \frac{\partial^2 T}{\partial x^2} + \frac{\partial^2 T}{\partial y^2} + \frac{\partial^2 T}{\partial z^2} \right) + \frac{\partial \theta}{\partial t} = \frac{\partial T}{\partial t} \quad (3)$$

Node (3): The intensity of the heat source  $q$  can be obtained by accumulated hydration heat formula  $Q_t = Q_0(1 - e^{-mt})$ :

$$q = dQ_t / d\tau = mQ_0 e^{-mt} \quad (4)$$

Node(4):  $Q_t$ —cumulative hydration heat with age of  $t$ ;  $Q_0$ —total hydration heat of cement;  $m$ —coefficient of hydration;  $\tau$ —age of concrete.

#### 3.2 Determination of boundary conditions

Heat conduction equation established the general relationship of the temperature of the object with time and space. In order to determine the required temperature field, we need to know the initial and boundary conditions; boundary conditions are based on the interaction temperature between the concrete surface and surrounding medium (such as air or water). In general, there are four types of boundary condition, with the concrete structure surface contact with the air as the third type of boundary condition. When the concrete surface is exposed to air, heat flow density of the concrete becomes directly proportional to the difference between the surface temperature  $T_n$  and medium temperature  $T_a$ :

$$-\lambda \frac{\partial T}{\partial n} = \beta(T_n - T_a), \quad (5)$$

where  $\beta$  – exothermic coefficient of concrete surface,  $\text{KJ}/(\text{m}^2 \cdot \text{h} \cdot ^\circ\text{C})$  and the negative sign indicates outward radiating flow.

When  $\beta$  tends to 0, it indicates the second boundary condition; when  $\beta$  tends to  $\infty$ ,  $T_n = T_a$ , it indicates the first boundary condition; and  $0 < \beta < \infty$  indicates the third boundary condition.  $\beta$  depends on the solid surface roughness, viscous coefficient, and flow velocity of the fluid, and does not depend on the solid material itself. In the temperature control calculation, we commonly take  $\beta = 16\text{--}20$ .

## 4 TEST PLAN

For real data of hydration heat of the zero block, this study selected different research sections of the zero block and embedded temperature sensor and strain sensor, measuring that zero block casting after the completion of the hydration heat temperature changes with time. This study selected three typical sections, 1-1, 2-2, and 3-3; sensor number A-B, where A represents cross-section and B represents section number. The position of the test section and the sensor number inside the section are shown in Figure 1. The measurement points on the three cross-sections are shown in Figures 2 and 3.

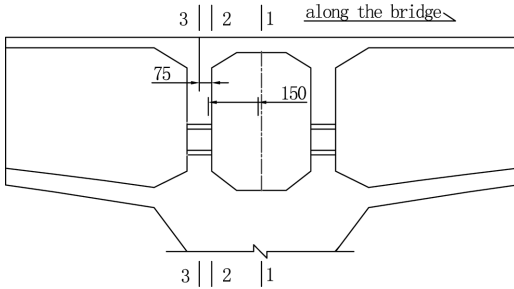


Figure 1. Main test section of 0 # block.

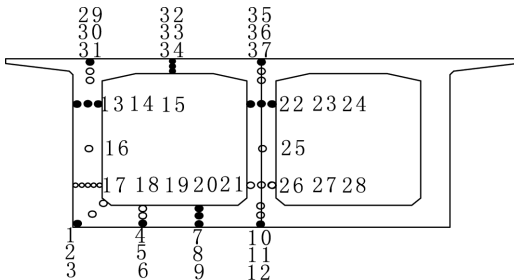


Figure 2. 1-1 cross-sectional layout of measuring points.

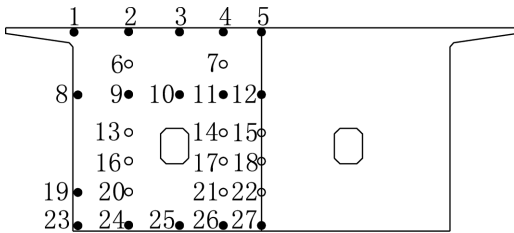


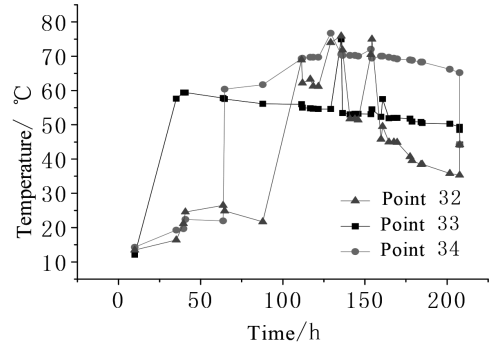
Figure 3. 2-2 3-3 cross-sectional layout of measuring points.

## 5 ANALYSIS OF CONSTRUCTION MEASUREMENT RESULTS

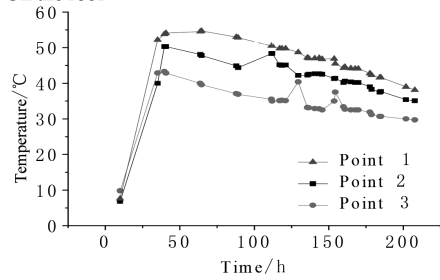
This paper presents part of the concrete hydration heat temperature measured curve, as shown in Figures 4–6:

### 5.1 1-1 Section temperature curve of time-varying

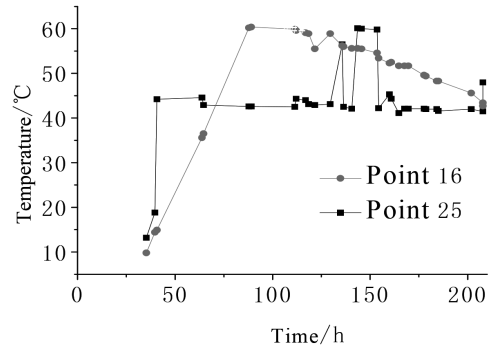
As shown in Figure 4, the temperature of the bottom plate is lower, about 50°C; peak temperature of the outer web is about 65°C; the surface temperature is up to about 55°C; the temperature of the inner web is about 65°C; and the temperature of roof is approximately 70°C.



(a) On the roof



(b) At the bottom



(c) On the web plate

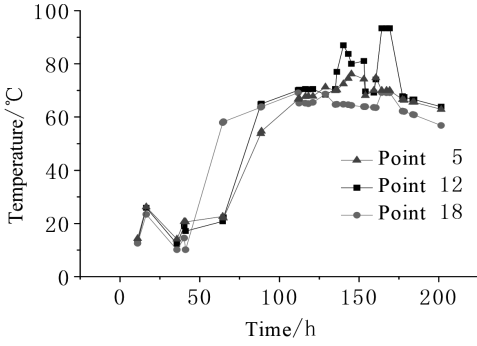
Figure 4. Time history curve of hydration heat temperature part of the measuring point.

### 5.2 2-2 Section temperature curve of time-varying

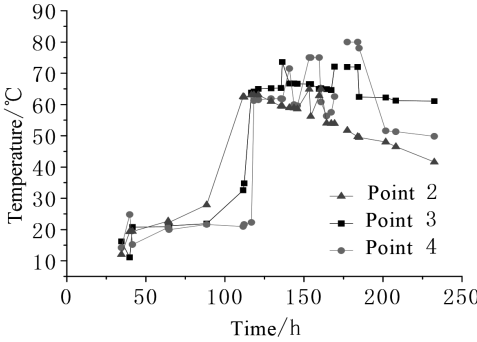
As shown in Figure 5, the peak temperature at the top and bottom plates is 70°C higher than that at other positions, and the heat dissipation is slower. This is mainly due to poor airflow inside the box of the zero concrete block.

### 5.3 3-3 Section temperature curve of time-varying

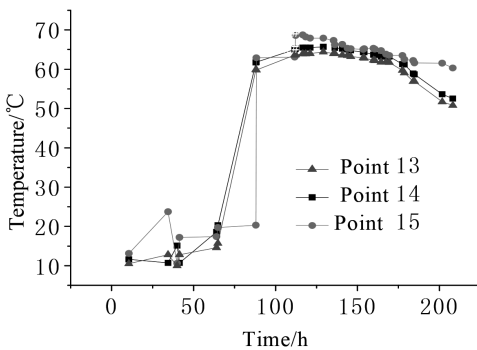
As shown in Figure 6, the peak temperature at the center of the diaphragm (3-3 section) is about 70°C higher than that at other positions, and the temperature of the outer surface is lower. Most of the measuring point temperature drop is slow, and



(a) On the roof



(b) On the web



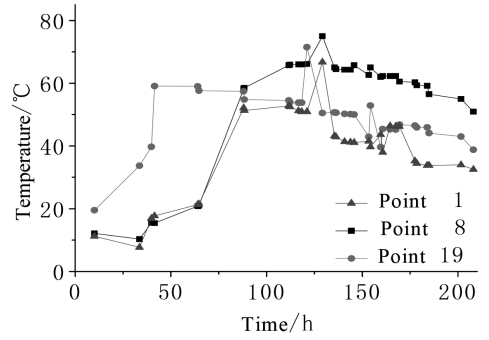
(c) On the manhole near section

Figure 5. Time history curve of hydration heat temperature part measuring point.

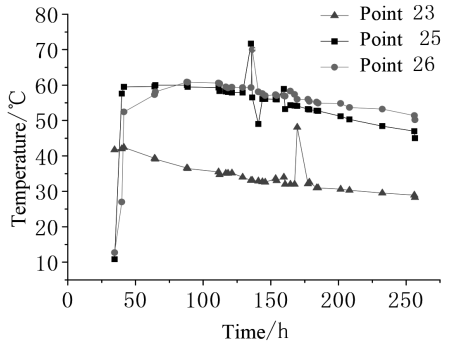
after 100 h of the completion of the construction, most of the measuring point temperature is still around 50°C.

## 6 CONCLUSION

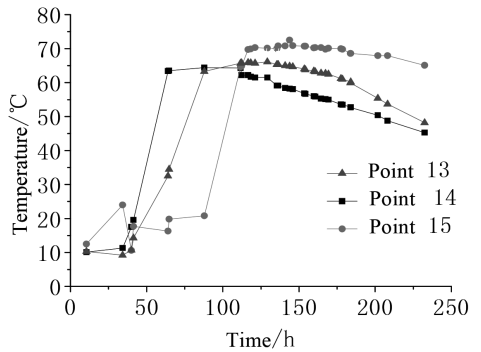
In this paper, the following conclusions are drawn from the research and analysis of the measured data: Inside the structure, the peak temperature of hydration heat is usually higher than that at other



(a) On the bottom



(b) On the lateral web



(c) On the manhole near section

Figure 6. Time history curve of hydration heat temperature part measuring point.

positions, where the temperature drop is slow, and the internal temperature field is less affected by the outside condition. However, the temperature field, the surface of the box beam, and the top plate and bottom plate are significantly affected by the outside condition. So the temperature gradient from the difference between inside and outside temperatures of zero concrete block should adopt preservation measures to reduce the temperature, which decreases the impact of the zero block stress and prevents the cracking of box girder.

## REFERENCES

- Feng, D.F. & Lu, W.L. 2006. Experimental study on the hydration heat temperature on the concrete box girder. *Journal of railway engineering* 8(98): 63–67.
- Kang, S.Z. 2008. Analysis and construction control of large volume concrete hydration heat. *World Bridge* (2): 42–44.
- Lu, W.L., Ji, W.Y. & Zhang, F.B. et al. 2002. Experimental study on hydration heat temperature and temperature strain of concrete box girder. *Northeast highway* 26(4): 62–65.
- Miao, C.Q., Sun, C.Z. & Li, A.Q. 2010. Concrete box girder bridge zero block process analysis and research of hydration heat. *Engineering journal of disaster prevention and mitigation* 30(4): 308–413.
- Yuan, M., Huo, H.J. & Yan, D.H. et al. 2011. High pier and long-span continuous rigid frame bridge box girder hydration research. *Chinese and foreign highway* 31(3): 138–142.
- Zhang, K.B., Zhu, Z.H. & Wang, D. et al. 2011. Large span continuous rigid frame bridge zero block temperature effect analysis during construction period. *Transportation science and engineering* 27(3): 30–34.
- Zhang, G. 2008. Hydration heat temperature damage fixed coupling method on the concrete box girder. *Journal of transportation engineering* 8(1): 55–60.
- Zang, H., Wang, K.B. & Liu, Z. 2007. Simulation and analysis of thermal effect of water in the auxiliary box girder of the bridge. *Bridge and tunnel engineering* 24(5): 95–98.



**Taylor & Francis**

Taylor & Francis Group

<http://taylorandfrancis.com>



# A review on load forecasting of town gas: Methods, applications, and analyses

H.Y. Tan, N. Li & C.Y. Tang

*University of Science and Technology Liaoning, Anshan, Liaoning, China*

**ABSTRACT:** Load forecasting is very promising for the gas balance between supply and demand. Given the complexity of load forecasting, the main challenge in its application is to determine appropriate methods to emulate the actual conditions of gas loading. This original work reviews the main steps of gas load forecasting. Several current methods are further discussed on mechanism and prospect. The factors affecting load forecasting results are summarized as result. On the basis of the observation made, it is possible to predict that combination of forecasting models will evaluate their potential better in the future.

**Keywords:** Gas load, forecasting, method

## I INTRODUCTION

Natural gas has caused great concerns and extensive utilization because it is clean and highly efficient. The growth rate of natural gas requirement has been estimated to reach 1.9% per year by 2035 and be higher than that of other fossil fuels globally<sup>[1]</sup>. Gas development in China has relevant increasing with the international gas requirement. Coal has been instated of renewable energy, natural gas, and nuclear power to optimize energy structure gradually in recent years<sup>[2,3]</sup>. This will accelerate natural gas production and improve the development of gas industry.

Gas transmission and distribution is an important part in the public utility, which relates to people's livelihood, economic development, and social operation. Because gas load significantly influence the reliability and efficiency of gas supply systems, it deserves an in-depth study in order to maximize the interest of the gas company<sup>[4]</sup>, based on gas supply or production.

Since the late 20th Century, many worthy references have been focused on gas load forecasting by statistical methods<sup>[5,6]</sup>. With the advances in computer technology and improvement of the forecasting performance requirements, more artificial intelligence forecasting methods are used in gas load forecasting<sup>[7-12]</sup>. Although several previous studies have been conducted on load forecasting<sup>[13-16]</sup>, the literature data on the factors affecting forecast

accuracy are still rare, which are important for future studies.

## 2 GENERAL STEPS OF GAS LOAD FORECASTING

### 2.1 *Collection and feature analysis of historical data*

The first step of gas load forecasting is to collect historical data and analyze their features using charts and graph. For example, in hourly load usually for a cycle of 24 h, there are three peaks, in the morning, afternoon, and evening, in a working day and two peaks, in the afternoon and evening, on holidays. And regularity of daily load is not very strong, but the weekdays and holidays are notably different. Then, monthly load is often influenced by seasonal factors, and it will show a variation of 12-month cycle. By contrast, randomness and seasonality of yearly load is not obvious and its trend is obvious. Thus, by analyzing load characteristics, we can determine the basic trends and the dispersion degree of data in order to select appropriate load forecasting method.

### 2.2 *Pretreatment of historical data*

System abnormality, human error, weather, or other factors may lead to abnormality in the historical data; thus, it is necessary to excavate,

judge, and correct them. Moreover, many models require standardized data before input to prevent non-convergence.

### 2.3 Correlation analysis of influencing factors

Correlation analysis represents correlation degree of influence factors and gas load. More influence factors can improve the prediction accuracy, but it also increases the difficulty of modeling. Correlation analysis can simplify the forecasting model without affecting the accuracy of the model, by selecting suitable factors.

### 2.4 Selection of gas load forecasting methods and model building

Load forecasting model reflects general characteristics of historical data. Thus, the selection of forecasting method should first consider load data and related information, then build the model with training data, and finally implement the resulting model to forecast. Finally, the model must be tested and evaluated.

Selecting appropriate load forecasting methods is the most important step. Currently, three categories of gas load forecasting methods have been used in the field. The first is the traditional mathematical statistical model such as regression analysis, time series method, and least square method. The second category consists of artificial intelligence methods such as wavelet analysis method, artificial neural network method, and gray theory prediction method. The third is a combination of various forecasting methods with their advantages.

## 3 OVERVIEW OF GAS LOAD FORECASTING METHODS AND THEIR APPLICATION STATUS

### 3.1 Time series method

Time series method is the earliest and most widely used traditional mathematical statistical method. Time series is constituted by historical load data, reflecting change characteristics, trends, and regular patterns of gas load; thus, we cannot forecast without analyzing historical data. Through mining the regular patterns from historical data, equations with appropriate parameters and model can be built. Furthermore, time series method ignores influence factors; thus, it cannot represent the relationship between influence factors and gas load. Furthermore, it has higher data requirements, and the specific performance is the larger change of historical data, the larger error. For this reason, many researchers believed that time series method is more suitable for short-term forecasting<sup>[14]</sup>.

The commonly used time series models include the Fourier series model, AR, and ARIMA forecasting

model<sup>[5,6,17]</sup>. Limited by the characteristics of time series method, stationary processing was necessary before forecasting<sup>[6]</sup>, in order to improve accuracy.

### 3.2 Gray theory forecasting method

Gray forecasting model was evolved in the 1980s from gray system theory, and it analyzes the change trend of gas load to explore the potential value, and then forecast quantitatively. Gray forecasting model is fixed, using cumulative data to build GM model and then obtaining forecasting data through inverse accumulated generating. In contrast with the mathematical statistical model built based on a large sample, the advantages of the gray forecasting model are more; as there are four historical data, it can establish the gray model by generating transformation. Furthermore, it builds the model by obtaining sequence rather than original data. It is worth noting that less data means much missing information, affecting the accuracy of load forecasting inevitably. Gray forecasting model in various cycle lengths are applicable, but it is used universally in the medium—and long-term forecasting for solving fragmentation of gas load records.

The GM (1,1) model is the first gray forecasting model applied<sup>[7,18]</sup>. Furthermore, this model of equi-dimensional filling vacancies addressed less availability of data by giving the new predictive value in complementary sequence to replace the original data<sup>[19,20]</sup>. Moreover, town gas consumption is usually associated with many other factors; simply considering historical data to predict was one-sided, so GM (1, N) model was applied to consider a variety of factors in the forecasting model<sup>[21]</sup>. However, several examples proved that when the gap between two adjacent data is large, the prediction error will be larger.

### 3.3 Artificial neural network method

Traditional mathematical models describe load by an explicit expression, but in fact it cannot represent completely. The artificial neural network model is a breakthrough in this aspect. Its input and output are the factors and gas load, respectively, and load forecasting process has been converted to a function mapping. The artificial neural network model may contain more factors, have a strong generalization ability, and the disadvantage is most input data of the artificial neural network model need to be pretreated to prevent non-convergence. For rapid development of gas, only considering the historical data in load forecasting is not feasible; therefore, artificial neural network has been used widely. However, to obtain weights and thresholds of artificial neural network, a large number of samples should be used in training, and hence medium—and long-term forecasting are not suitable.

At present, Back-Propagation (BP) neural network and Radial Basis Function (RBF) neural network are mainly used<sup>[8,9,22,23]</sup>. Several researchers have attempted to improve neural network, such as improving weights by genetic algorithm<sup>[24]</sup>, screening variable by step regression analysis<sup>[25]</sup>, neural network based on equi-dimensional filling vacancies<sup>[26]</sup>, and adaptive neural network based on fuzzy inference system<sup>[27]</sup>. Moreover, gas load has specificity influenced by region, which should be analyzed in specific circumstances, so we cannot obtain a generic model. At the same time, adaptive ability of the model should also be enhanced.

### 3.4 Support vector machine method

Artificial neural network model can easily attain the local minimum state, but support vector machine avoids this problem effectively, so it was also used in gas load forecasting after the artificial neural network and gray forecasting model<sup>[10]</sup>. The support vector machine maps input to high-dimensional feature space through a nonlinear function to give a linear optimization calculation, avoiding the problem of local teeny. And the SVM model training process obtains an optimum solution by solving the quadratic programming problem in essence. With the large samples, SVM model will take up a lot of memory and time, limited by its theory. However, it is undeniable that it has obvious advantages to solve fuzzy, stochastic, uncertainty, limited number of samples, and complex nonlinear problems.

In application, kernel function selection is an important part of improving effectiveness of the forecasting model. And many studies have established SVM models and modified models by selecting different kernel functions<sup>[28,29]</sup>. Moreover, optimization of model parameters is another important part of model building. Furthermore, meshing and cross-check were used commonly in gas load forecasting, but the specific methods are determined according to the actual need.

### 3.5 Wavelet analysis method

To further improve the accuracy of load forecasting, decomposing gas load sequence before forecasting is advisable. Wavelet transform is an ideal tool, overcoming some characteristic problems of capability after transforming, known as the “mathematical microscope”. Wavelet transform can carry out simultaneously domain and frequency domain analysis, possessing time–frequency localization and multi-resolution feature, making it appropriate to deal with non-stationary signals. In most time, gas load time series is an unstable sequence, so wavelet transform is usually applied to partial

decomposition of gas load sequence, laying the foundation for future forecasting.

Gas load sequence can be seen as the synthesis of the low-frequency component (regular part) and high-frequency components (unpredictable part). And selecting different load forecasting models based on wavelet division sequence could improve the accuracy of load forecasting and determine the error limit of the load forecasting<sup>[11]</sup>. Furthermore, wavelet transform decomposition sequence could be used as part of BP neural network input<sup>[30]</sup>.

### 3.6 Combination forecasting method

Currently, there are two combination forecasting method forms: one is horizontal cartel, combining several basic forecasting models by selecting different weight coefficient and the other is longitudinal combination, applying the nested forecasting outcomes in another forecasting method.

In the horizontal cartel, there are several combinatorial methods, such as genetic algorithm combined with the least squares method or gray forecasting model and BP neural network combined with SVM or gray forecasting model, then optimized commitment method was used to relate them<sup>[31,32]</sup>. In the longitudinal combination, artificial neural networks are favored by many studies. On the one hand, in the accumulative sequence or residual sequence of gray model, the output of fuzzy logic vector can be used as input neurons of artificial neural network<sup>[33]</sup>; on the other hand, wavelet base is commonly used in artificial neural network instead of the excitation function of the hidden layer<sup>[34]</sup>. Furthermore, using wavelet kernel as kernel function of SVM has also been affirmed<sup>[35]</sup>.

Combination forecasting method can be applied to a variety of gas load forecasting cycle lengths. And when a single model cannot function perfectly, we can consider using it. Moreover, we should not ignore the increased complexity and depressed precision of the model with better results. Even so, combination forecasting model still has obvious advantages in average error and reduces the error range.

## 4 CONCLUSION

Gas load forecasting has been developed for decades. Some worthy emulation models were built and used. Many studies investigated that gas load forecasting was seriously affected by prediction and data characteristics. And to some extent, the selection of forecasting methods determined the veracity of forecasting results. Because the gas load is varied with the development of industry and enterprises, many researchers realize that gas load is an integrated project which cannot be solved by single

mathematical model. Therefore, combined models could be more useful for complicated gas loading, and they improve the gas balance between supply and demand compared with single model.

## REFERENCES

- Azadeh, A., Asadzadeh, S. M., Saberi, M., Nadimi, V., Tajvidi, A. & Sheikalishahi, M. 2011. A Neuro-fuzzy-stochastic frontier analysis approach for long-term natural gas consumption forecasting and behavior analysis: The cases of Bahrain, Saudi Arabia, Syria, and UAE. *Applied Energy* 88(11): 3850–3859.
- BP 2035 World Energy Outlook[Online]. Available: [http://www.bp.com/content/dam/bp-country/zh\\_cn/Download\\_PDF/EnergyOutlook2035/EO%202035%20booklet%20FINAL.pdf](http://www.bp.com/content/dam/bp-country/zh_cn/Download_PDF/EnergyOutlook2035/EO%202035%20booklet%20FINAL.pdf).
- Chen Q M. 2014. Research on short-term gas-load forecasting based on combination methods. *M.S. thesis, Dept. Shanghai Normal University*. Shanghai.
- Chen R, Wang J, Wang L, Yu N & Zhang P. 2009. The forecasting of China natural gas consumption based on genetic algorithm. in *Proceedings of the 2009 Fifth International Joint Conference on INC, IMS and IDC. IEEE Computer Society*. Seoul, Korea: 1436–1439.
- Energy Development Strategy Action Plan (2014–2020 year) [Online]. Available: <http://baike.baidu.com/link>.
- Erdogdu E. 2009. Natural gas demand in Turkey. *Mpra Paper* 87(1):211–219.
- Fan X, Yang H, Kang X & Y Gao. 2011. Diameter of uneven-aged stand. in *Eighth International Conference on Fuzzy Systems and Knowledge Discovery*, Shanghai: 1550–1554.
- Fang J. 2012. Forecasting of Annual Gas Load Based on Grey Model. *Gas & Heat*32(5): 5–7.
- Guo W & Jiang D. 2013. Short-term gas load forecast based on support vector machine. *Gas & Heat* 33(3): B06-B09.
- Han X, Lai J B, Ma J F & Sun Z F. 2015. Forecast Method of Gas Consumption in Gas Planning. *GAS & HEAT* 35(8): B01–B04.
- Ismail M J, Ibrahim R & Ismail I. Adaptive neural network prediction model for energy consumption. in *Computer Research and Development (ICCRD), 2011 3rd International Conference on IEEE, 2011*: 109–113.
- Jiao W L, Lian L M, Cui J H & Yan M Q. 2002. Time series model of predicting short period city gas load. *Natural Gas Industry*22(1): 92–94.
- Jiao W L, Zhu B C & Feng Y G. 2006. Forecast of short-term town gas load based on BP neural network. *Gas & Heat* 26(12):12–15.
- Kizilaslan R & Karlk B.2008. Comparison neural networks models for short term forecasting of natural gas consumption in Istanbul. in *Applications of Digital Information and Web Technologies, 2008. ICADIWT 2008. First International Conference on the IEEE, 2008*: 448–453.
- Lai Z L. 2012. Research on gas load forecasting prediction based on SVM combined model. *M.S. thesis, Dept. Shanghai Normal University*. Shanghai.
- Li C J, Jiao W L & Zhao L B. 2007. A synthesis wavelet analysis method for short-term gas load prediction. *Natural Gas Industry*27(8):103–105.
- Li X Y. 2015. Studies of Town Gas Network Node Load Forecast and Storage Capacity. *M.S. thesis, Dept. Shandong Jianzhu University*. Jinan.
- Liu H, Liu D, Zheng G, Liang Y M & Song N L. 2002. Natural gas load forecasting based on least squares support vector machine. *Journal of Chemical Industry & Engineering* 55(5): 828–832.
- Luo Z P. 2016. Application of GM (1, 1) Method in Jin-gxi Natural Gas Pipeline Load Forecasting. *Pipeline Technique and Equipment* (1): 45–47.
- Ma X. 2015. Methods of City Gas Load Forecasting and Their Analysis. *Scientific and technological innovation and application* (15): 120.
- Peng S N, Su X H & Huang Q. 2005. Methods of city gas load forecasting and their analysis. *Journal of Chongqing Architecture University* 27(4): 137–141.
- Potočnik P, Soldo B & Šimunović G. 2015. Comparison of static and adaptive models for short-term residential natural gas forecasting in Croatia. *Applied Energy* 129: 94–103.
- Simshauser P, & Nelson T. 2015. The Australian east coast gas supply cliff. *Economic Analysis & Policy* 45, 69–88.
- Su X, Yuan Z M, Zhang L, Huang K & Xie Y. 2006. City gas load prediction based on grey theory. *Journal of Southwest Petroleum Institute* 28(6): 387–389.
- Tan H & Liu Y. 2006. Short-term gas load forecasting based on RBF neural network. *Energy for Metallurgical Industry* 25(5): 14–16.
- Tan Y F, Chen J X, Jiao W L & Yu Q Z. 2001. Applying BP artificial neural network to forecast urban gas short-term load. *Gas & Heat*21(3):199–202.
- Tan Y F. 2003. Establishment and Solution About Forecast Model of City Gas Seasonal Load. *Gas & Heat* 23(3): 131–133.
- The 13th Five-Year Energy Plan General Idea is Becoming Clear[Online]. Available: <http://wenku.baidu.com/link>.
- Wu S J, Wu X J & Liu X M. 2011. GM (1, 1) Grey Forecasting and Analysis on Energy Production and Supply in Shandong. in *Province Management and Service Science (MASS), 2011 International Conference on IEEE*: 1–4.
- Yang J & Weng W. 2014. Improved unbiased grey model for prediction of gas supplies. *Journal of Tsinghua University* (2): 145–148.
- Yao J, Zhou W G & Zhang Z X. 2010. Selection of input variables in daily gas load forecast based on artificial neural network. *Gas & Heat* 30(1): A28-A30.
- Yu F & Xu X. 2014. A short-term load forecasting model of natural gas based on optimized genetic algorithm and improved BP neural network. *Applied Energy* 134: 102–113.
- Zhang C, Liu Y, Zhang H & Huang H. 2014. Study on urban short-term gas load forecasting based on support vector machine model. *Journal of Tsinghua University* 54(3): 320–325.
- Zhang H Y. 2013. Research on daily gas load forecasting. *Journal of Henan Institute of Engineering* 25(2): 28–33.
- Zhou X L. 2015. Prediction of gas emission quantity based on GM-RBF neural network model combined by difference. *M.S. thesis, Dept. Anhui University of Science & Technology*. Huainan.

# Distributed temperature sensor- and fiber Bragg grating sensor-based method for gas pipeline leakage detection

Tuo Li, Hua-dong Gong, Li-chang Su & Qiang Li

*State Key Laboratory of Explosion and Impact and Disaster Prevention and Mitigation,  
PLA University of Science and Technology, Nanjing, China*

**ABSTRACT:** In most of the current natural gas pipeline leakage detection methods, traditional sensors are generally used to detect single parameter signal and then obtain the leakage information, which have higher non-response rates and false positive rate. The temperature distribution information along the pipeline can be obtained through distributed temperature sensor, and the vibration information acquired by Fiber Bragg Grating (FBG) sensor can be sorted out through the temperature information. By analyzing the test results, the temperature and vibration information of the pipeline obtained by these two optical fiber sensors are used to detect the leakage, which can effectively improve the positioning accuracy and reduce the false positive and negative rates.

**Keywords:** Distributed temperature sensor, FBG sensor, leakage, detection

## 1 INTRODUCTION

As a kind of important infrastructure, natural gas pipelines deliver energy to facilitate national economic development and bring convenience to the lives of residents. Until 2014, China had developed natural gas pipelines of nearly 85,000 km. In the future, more natural gas pipelines will be built and put into use. Because of various reasons, leakage often occurs in these pipelines, which not only causes great economic losses and waste of resources, but also triggers explosions and seriously threatens the social security. On 1 August 2014, a leakage occurred in the natural gas pipelines in Kaohsiung, Taiwan, triggering a series of explosions. The number of casualties was nearly 300, of which 22 died.

In order to obtain the leakage information of natural gas pipelines in a timely manner, leakage must be detected first. The detection methods include leakage noise detection method, leakage flux detection method, infrared imaging method, radioactive tracer leakage detection method, negative pressure wave method, pressure gradient method, mass or volume balance method, and acoustic test method. In these methods, sensors are discretely installed on the pipelines to receive a single parameter signal and then obtain the leakage information. Yet, these methods are generally plagued by low positioning accuracy and high false positive and negative rates.

Distributed optical fiber temperature sensors can not only obtain the temporal and spatial con-

tinuous temperature distribution information on the pipelines, but also have higher positioning and detection accuracies than the traditional detection methods, as the fiber has the following advantages: lightweight, small volume, anti-electromagnetic interference, resistance to high temperature, anti-corrosion, integration of information sensing, and transmission. By adopting the wavelength modulation method, Fiber Bragg Grating (FBG) sensor is not affected by light intensity, avoiding the problem of obscure phase measurement. The vibration information of the pipeline leakage can be acquired through the temperature information obtained from the temperature sensor. Distributed optical fiber temperature sensor and FBG sensor can be used to obtain the temperature and vibration information of the natural gas pipelines and then detect the leakage, thereby reducing the false positive rates.

## 2 DISTRIBUTED OPTICAL FIBER TEMPERATURE SENSING SYSTEM

Distributed optical fiber temperature sensor is a kind of optical fiber sensor that conducts temperature measurement and positioning in accordance with the Raman scattering effect produced by laser pulse in its transmission in the optical fiber and the principle of Optical Time Domain Reflection (OTDR). When laser pulses transmit in the optical fiber, reflection will occur, including Raman scattering. Raman scattering signal is related to

the temperature at the position where backscattering occurs. By demodulating the reflected signal, we can obtain the temperature at this position. It takes different times for the backscattering signals to return to the detector from different positions. By measuring the time taken by the signal from its launch to return as well as the speed of light in the optical fiber, we can determine the positions of light reflection. This is called OTDR technique, which can be used to determine the position of the corresponding temperature.

The distributed temperature sensing system adopts distributed optical fiber temperature sensors to obtain the temperature distribution information along the fiber, which includes temperature measurement host, sensing optical fiber cable, and application software.

### 3 QUASI-DISTRIBUTED FBG SENSING SYSTEM

#### 3.1 FBG sensor

The refractive index of FBG sensor's fiber core presents periodically distributed stripes. When they are under the action of external physical fields such as temperature and strain, their lattice spacing also changes, thereby changing the wavelength of the back-reflected laser. By detecting the Bragg wavelength spectrum of grating reflection or transmission, we can measure the strain and temperature values of the measured objects.

#### 3.2 Quasi-distributed FBG sensing system

Multiple FBG sensors are arranged in parallel to form a quasi-distributed FBG sensing system. The quasi-distributed FBG reflected light wavelengths

$\lambda_1, \lambda_2, \dots, \lambda_n$  are also different, which correspond to the detection points along the pipeline. When FBG is subject to stress and strain, its lattice spacing changes, and then the wavelength of its reflected light is also changed. The changed reflected light transmits to the optical fiber grating demodulator and the variation quantity of its wavelength is then obtained. From this information, we can calculate the vibration of each detection point.

In Figure 1, only four FBG sensors are marked. In real life, as long as the maximum range of the measured parameter and the light source spectrum bandwidth allow the use of multiple sensors in an optical fiber, hundreds of FBG sensors can be used for a single fiber.

Quasi-distributed FBG sensing system mainly consists of broadband light source, FBG optic cable, coupler, light detector, and software. It can obtain the duration, amplitude, and mean value of the grating reflection wave drift in real time.

### 4 PIPELINE LEAKAGE POSITIONING METHOD BY DOUBLE SENSORS

When natural gas pipelines leak due to material defects, corrosion, and cracking, the leaked gas will reduce the temperature of the leakage point. The temperature sensing fibers of distributed temperature sensors are located right above the pipelines, and the leaked gas flow will reduce the temperature of the leakage point. Thus, by obtaining the real-time temperature distribution information along the pipeline, we can obtain the locations of temperature decrease.

As natural gas pipelines are often in a complex environment and suffer much interference, distributed optical fiber temperature sensors have low temperature measurement accuracy and low reso-

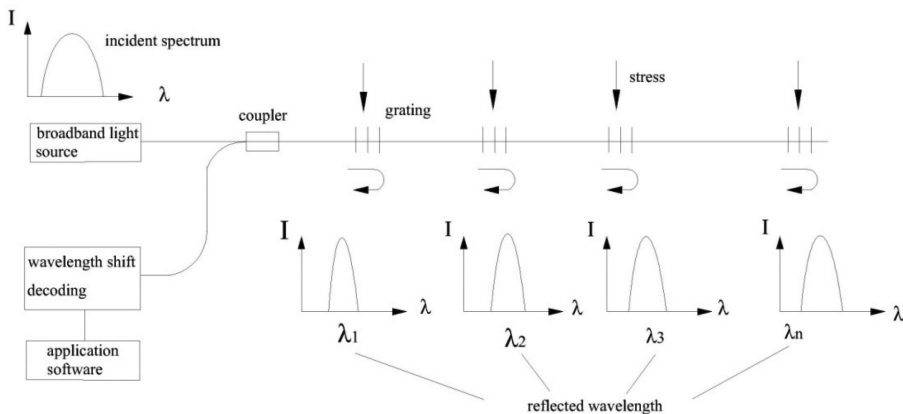


Figure 1. Principle of quasi-distributed FBG sensing.

lution. Besides, the Raman scattering light signal is very weak and the signal-to-noise ratio is very low. Thus, useful temperature information is nearly submerged in noise, causing high false positive and negative rates. The fibers of quasi-distributed FBG sensing system are located above the pipelines. When pipeline leakage occurs, the leaked gas will have an impact on the fiber, making it vibrate. The vibration then spreads to the surrounding FBG sensors. After the sensing of the stress and strain by the FBG sensors, the wavelength drifts. However, when the grating is located near the leakage points, its temperature also drifts.

The strain caused by vibration will stretch or compress the grating, so the variation quantity of FBG wavelength is

$$\Delta\lambda = \lambda_B(1 - P_e) \cdot \Delta\varepsilon = K_e \Delta\varepsilon, \quad (1)$$

where  $\Delta\lambda$  is the variation quantity of FBG reflected light wavelength,  $\lambda_B$  is the wavelength of the FBG sensor,  $K_e$  is the sensitivity of the measured strain,  $P_e$  is the effective photoelasticity coefficient of the optical fiber, and  $\Delta\varepsilon$  is the change in spacing.

The temperature-induced FBG wavelength variation quantity is expressed as

$$\Delta\lambda_T = K_T \Delta T = (\alpha + \xi) \Delta T, \quad (2)$$

where  $\alpha$  and  $\xi$  are the thermal expansion coefficient and thermo-optical coefficient of the fiber, respectively. The variation quantity of temperature can be obtained through distributed optical fiber temperature sensor, thereby eliminating the FBG wavelength drift caused by changes in temperature.

Distributed optical fiber temperature sensing system and quasi-distributed FBG sensing system are arranged on the pipelines as shown in Fig. 2. They are located above the pipelines, and the position of the FBG sensor is known. If leakage occurs, the leaked gas will produce a shock on the optical fiber and lead to the decrease of the surrounding temperature and the vibrating fiber. The vibration intensity will reduce with the increase of distance. More distant the grating is, the smaller the vibration and wavelength drift will be.

Distributed temperature sensing system can obtain continuously distributed temporal and spatial temperature along the optical fiber. A point detected with decreased temperature can be temporarily deemed as a leakage point. If quasi-distributed FBG sensing system observes that the FBG wavelength drifts on both sides of the point where the temperature decreases are the greatest ones, then we can determine that this point is the leakage point. Fig. 3 shows the distribution curve of temperature along the pipeline detected by the distributed temperature sensing system after the leakage. Fig. 4 shows the distribution of FBG wavelength drifts along the pipeline detected by the quasi-distributed FBG sensing system after the leakage.

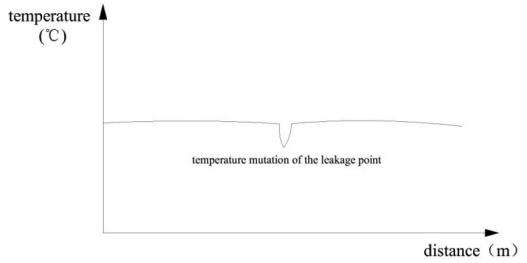


Figure 3. Distribution curve of temperature along the pipeline.

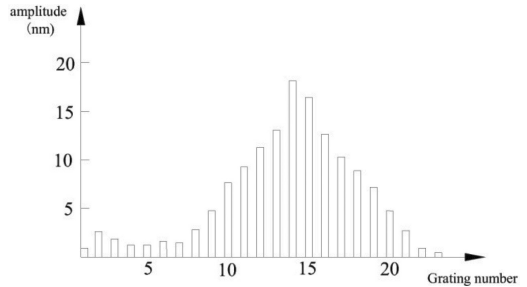


Figure 4. Distribution of FBG wavelength drifts along the pipeline after the leakage.

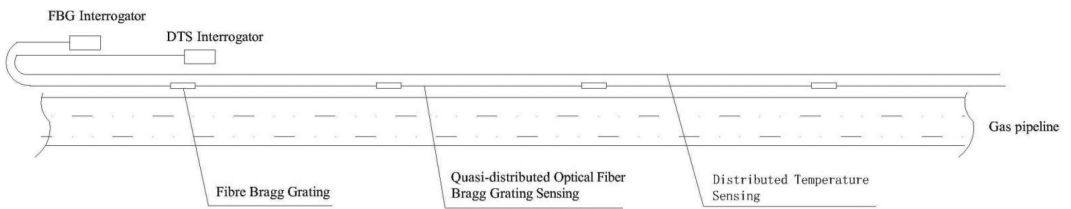


Figure 2. Layout diagram for distributed temperature sensing system and quasi-distributed FBG sensing system.

## 5 RESULTS

When distributed optical fiber temperature sensor detects a point with decreasing temperature (which is a concave point in the temperature curve) and the FBG wavelength drifts on both sides of the point are the greatest ones, then this point can be seen as a leakage point; if no FBG wavelength drifts are found on both sides of the point or the FBG wavelength drifts on both sides are not the greatest ones, then this point is not considered a leakage point.

When the temperature curve of distributed optical fiber temperature sensor has a concave point around the grating, the variation quantity of temperature at the grating can be obtained from the curve. Then, the variation quantity of FBG wavelength caused by stress and strain can be calculated using Eq.(1) and Eq.(2). If the FBG wavelength drifts on both sides of the point are the greatest ones, then leakage occurs at this point; if no FBG wavelength drifts are found on both sides of the point or the FBG wavelength drifts on both sides are not the greatest ones, then leakage does not occur at this point.

## 6 CONCLUSIONS

Gas pipelines require high leakage detection accuracy and low false positive and negative rates. Distributed optical fiber temperature sensor and FBG sensor can be jointly used to detect the leakage of pipelines. This method makes full use of optical fiber sensors' superior properties such as anti-corrosion, resistance to high temperature, and anti-electromagnetic interference, so it is suitable for natural environment. Compared with the

traditional detection methods, this method not only improves the positioning accuracy, but also reduces the false positive and negative rates.

## REFERENCES

- Chen Fuqiang, Li Xia. Fiber Bragg Grating Sensing System and Natural Gas Pipeline Leakage Detection. *Automation and Instrumentation*. 2009, 3:114–115.
- Chen Zhi gang, Zhang Lai bin, Wang Zhaohui. et. Method of Leakage Detection for Gas Pipelines Based on Distributed Optic Fiber Sensors. *Transducer and Microsystem Technologies*. 2007, 26, (7):108–110.
- Fang Weiwei, Jiang Desheng, Zhang Cui. Distributed Fiber Bragg Grating Demodulation System. *Optics & Optoelectronic Technology*. 2004, 2(5):37–39.
- Li Na. Fiber Bragg Grating Sensor Technology and The Study of Its Application in Inspection of Oil & Gas Pipeline Corrosion. [Hunan Industrial University master dissertation], zhuzhou: Hunan Industrial University: 2012:13–16.
- Li Sheying. Study on Reliability of Distributed Temperature Sensing System. [Hangzhou Dianzi University master dissertation]. Hangzhou: Hangzhou Dianzi University, 2010:19–23.
- Liao Kebing, Zhou Rongyi, Liu Aiqun. Discussion and Evaluation on Detection Methods for City Gas Pipe Leakage. *Industrial Safety and Environmental Protection*. 2007, 33(2):27–29.
- Rogers, A.J. Distributed Optical-fiber Sensing. *Optic Sensor. Engineering and Applications*, 1991, (11):2–24.
- Wang Dongyan, Zhang Yan. Leakage Detection for Natural Gas Pipelines Based on Fiber Grating. *Industrial Technology*. 2008, (32):79–80.
- Zhang Zaixuan, Guo Ning, Xu Xiangdong. Distributed Optical Fiber Temperature Alarming System. *Measuring Technology*. 2000, (2):264–267.
- Zhao Yong. Principles and Application Technology of Optical Fiber Sensors. [Tsinghua press]. 2007.



## Study on the re-utilization of wasted civil air defense project

Xin-yuan Zu & Li-chang Su

*Research Center of Underground Space, PLA University of Science and Technology, Nanjing, China*

**ABSTRACT:** The increasing concern on urban sprawl and environment deterioration has led to people paying more attention to space of low utilization and waste inside the city, in which the scale of civil air defense project is the largest. The adoption of appropriate measures on this sort of civil air defense project to perform re-utilization in the peacetime would bring out huge economic benefits hidden in civil air defense projects. Exerting the characteristics of the combination of peacetime and wartime and achieving flexible functional conversion from peace to war can realize the vision of making waste profitable.

**Keywords:** Wasted civil air defense project; underground space; re-utilization

### 1 THE NECESSITY OF RE-UTILIZATION OF SINGLE BUILDING TYPE CIVIL AIR DEFENSE PROJECTS

The Gulf War of the 1990s had exerted enormous influence on people's beliefs. Since the war ended, several countries had renewed their focus on the construction of civil air defense projects. The architectural types of civil air defense project back then were various, normally divided into two categories: single building type and attached type. To distinguish the two types, we should check whether there is solid ground building on the top of them. The one on the top of which there's no solid ground building is the single building-type civil air defense project.

Civil air defense projects are invested and constructed by the state with few commercial benefits. According to the status in China, however, re-utilization of civil air defense project or combining civil air defense project and underground space on the basis of civil air defense project's benefits could promote economic development while balancing social and economic benefits. The concept of the combination of peacetime and wartime is to make full use of finished or nearly finished civil air defense facilities to promote development and management by serving economic construction of the state and daily living and production of residents. Nowadays, however, problems like lack of maintenance, low utilization, and high vacancy rate still exist in the civil air defense project of China. In Beijing, for example, an investigation report shows that in September 2013, only 5,297 civil air defense projects of the total 12,217 ones were put in use, with the low utilization of 43.36%. Underground space resources in most of civil air

defense projects still remain idle instead of exerting their functions in the peacetime.

Civil air defense projects are usually built in urban and densely populated areas. From the aspects of social and economic benefits, the geographical locations of civil air defense projects are very favorable. Since wars require high-capacity projects, the architecture of civil air defense projects is advantageous. On the contrary, demolishing-abandoned civil air defense projects are complex and time consuming because of high cost and unimaginable impacts of the ground buildings and underground pipelines. Since the war ended, civil air defense project has gradually been losing its original functions, although its crucial effect had a significant impact on people. Under the background of the present combination of peacetime and wartime, appropriate reformation and re-utilization of civil air defense project could save resources and reduce waste, benefiting the society's sustainable development, promoting the process of urban modernization, and passing on civil air defense project as a historical symbol.

### 2 METHODS TO RE-UTILIZE CIVIL AIR DEFENSE PROJECT

Re-utilization of civil air defense project should be combined with reformation and construction of urban area. The methods can be grouped as follows:

#### 2.1 *Transform the functions of internal projects*

Since civil air defense projects in China have been designed nowadays for use in peacetime and

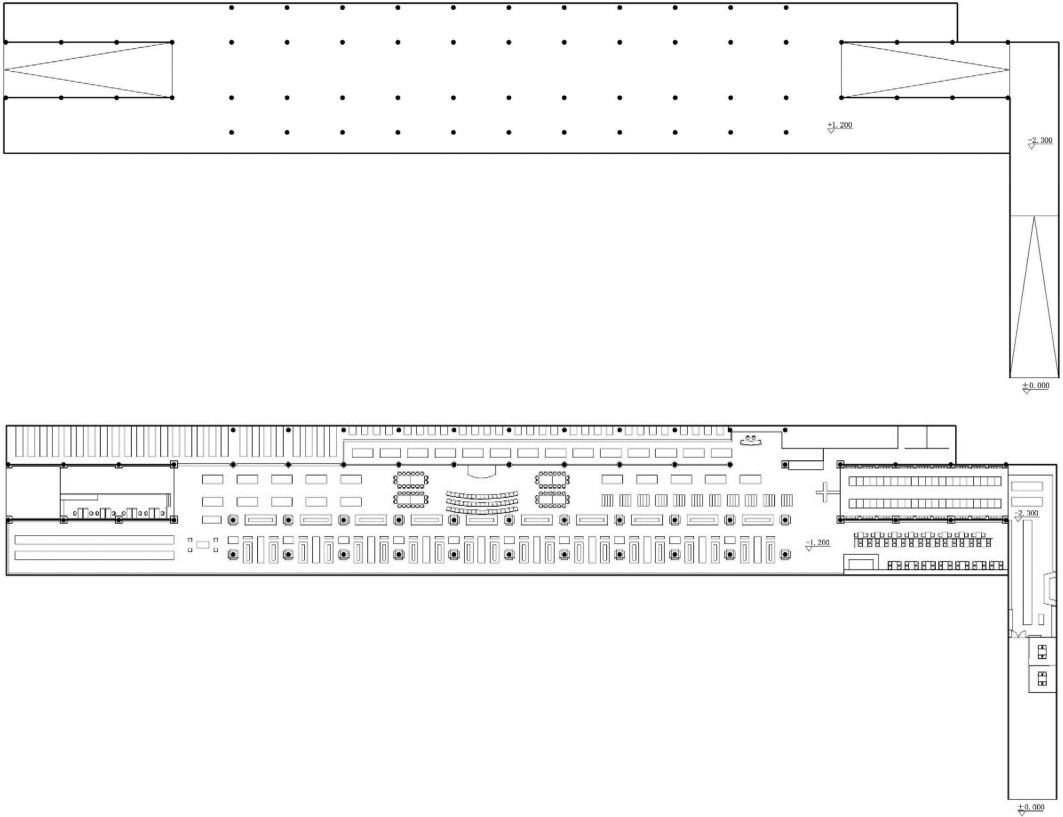


Figure 1. Original plane graph.

wartime, these projects equipped with professional facilities also possess conditions of parking, activity, and living and they are supposed to be made full use of. There are various functional places that can be transformed, such as resource storage site, parking lot, public transport, commercial place, and cultural and sporting place. Specific functions to be transformed should be decided based on the overall plan and the needs of the residents around the civil air defense project, and they are transformed according to the design specification of the transforming target. However, the prerequisite is that two layers of guard shields, air exhaust room, fire pipelines, and other facilities of civil air defense project must remain.

Take Pioneer Bookstore of Wutai Mountain in Nanjing as an example. The bookstore was made from a civil air defense project of 4,000 m<sup>2</sup>, fully utilizing the original space and architecture of the civil air defense project (see Fig. 1). For instance, the 40 m slope at the entrance of the civil air defense project has been transformed into art gallery (see Fig. 2) and the ventilation and drainage



Figure 2. Art gallery transformed from the slope at the entrance of the civil air defense project.



Figure 3. Pipelines full of industrial revolution flavour.

pipelines also add the bookstore an industrial and technological revolution atmosphere (see Fig. 3).

### 2.2 Connect to surrounding functional places

Another key method for re-utilization of civil air defense project is to connect one civil air defense project to its surrounding single building type and attached civil air defense projects and other underground space, achieving re-utilization of civil air defense projects. This method could provide more shield space and expand underground commercial space, promoting circulation of people and materials, creating organic network system, and hence increasing economic benefits. Connection between one civil defense project and its surrounding underground space refers to connecting civil defense project to other single building type and attached civil defense project or other underground space through civil defense main roads or passageways. The main connection mode is “point-plot-district-net”. “Point” is the most fundamental element of the form of underground space of each monomer. “Plot” refers to a section created by several “points” connecting each other through passageways, which means that all monomers are interlinked. The space connection is carried out by two methods: point connection and plane connection (see Fig. 4). “District” refers to underground area created by several “plots” connecting each other through underground passageways or underground walkways (see Fig. 5). “Net” means underground space system shaped by several “districts” connecting each other through subways, tunnels, underground expressways, and other main underground roads.

For example, Fashion Lady shopping mall located in the central commercial zone of Xinjiekou used to be the largest public civil defense project in Nanjing. In 2006, the second phase project was reformed to connect to subway No. 1 line (see Fig. 6), and this closely linked the shopping mall with the underground space of all surrounding shopping malls, multiplying passenger flow and hence creating more economic benefits.



Figure 4. Plot connection type.

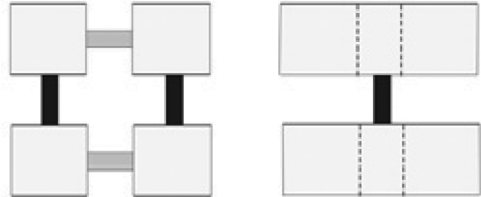


Figure 5. District connection type.



Figure 6. The linked entrance of the shopping mall and the subway.

### 2.3 Connect to traffic network

Combining civil defense project, subway, underground walkway, underground expressway, and others does not only realize re-utilization of civil defense project, save resources, and reduce waste, but also exerts the functions of shelter and evacuation.

Take the circular road (see Fig. 7) of Jiefangbei in Chongqing for example. Passageway of more than 1 km (see Fig. 8) within the project takes advantage of air-raid shelter dug in the anti-Japan war and is finished using it. The tunnel is about 15 m wide and 11 m high, having decreased the whole project’s construction capacity. The project also connects to the main underground parking in Jiefangbei, branching the ground traffic to ease traffic congestion.

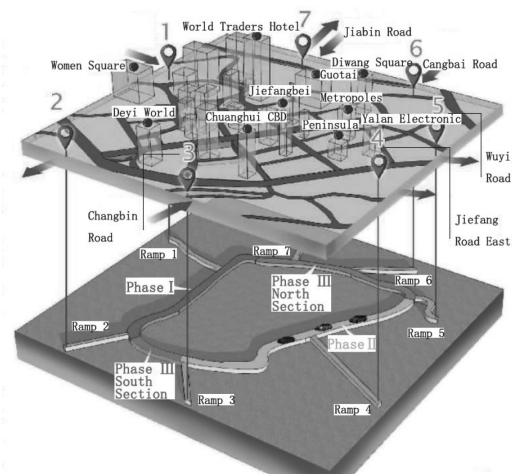


Figure 7. Underground circular road of Jiefangbei.



Figure 8. Reconstruction and extension of civil air defense project.

### 3 CONCLUSION

Since civil air defense project is of excellent architecture and high cost and is difficult to remove, considering its great historical value, re-utilization of wasted civil air defense projects conforms to the socialistic sustainable development concept of environmental protection, energy saving, and recycling. This paper concludes several methods of reforming wasted civil air defense project and offers reference value for other wasted civil air defense projects and even other types of waste underground space.

### REFERENCES

- Hongbo Li and Bocheng Li. Discussion of the civil air defense project's combination of peacetime and wartime. *Zhejiang architecture*, 2010, 27 (5): 8–9.
- Jing Tang. Both the development and application fortified in the underground projects. *Life and disaster*, 2009, (s1): 119.
- Qun Li. Civil air defense construction and urban sustainable development: [Tianjin University master dissertation]. Tianjin: Tianjin University, 2004, 50–52.
- Rong Zhang and Dongxia Liu. Analysis of planning and using of urban civil defense underground space. *Planning and design*. 2013 (06): 44–45.
- Zhilong He. Research on combining the civil air defense project with development and utilization of the underground space: [Hunan University master dissertation]. Changsha: Hunan University, 2009, 1–2.

# GPR scan assessment of pressure mortar quality in a tunnel vault

Sheng-long Tian

*School of Civil and Environmental Engineering, University of Science and Technology Beijing, Beijing, China*

Ming Cui

*CCCC Tunnel Engineering Company Limited, Beijing, China*

**ABSTRACT:** In order to evaluate the effectiveness of grout and the zone of defect, the landslide area of tunnel was detected in the longitudinal and transverse directions, with 900 and 1600 MHz radar antennae. Electromagnetic wave speed in the concrete was estimated by migration technique and linear time-history method. The wave velocity was 0.120 ns/m. Multiple reflections of subsurface anomalies, bad antenna coupling, and metal on wall surface were described in the detection images of radar. Thickness of shotcrete, spacing of joist steel, and layout of system bolt were scanned by geological radar technique. By analyzing color image and event image, the grout compactness, roof-contacted rate, and location of pumping area were judged and determined. Strong reflection in event image depicted the outline of ground arch at the concrete–rock interface. In the tunnel haunch of layered rock mass, there also existed strong reflection, wave distortion, and continuous wave with finite breaks, where the rock mass became obviously loose. The Ground-Penetrating Radar (GPR) detection was achieved through section information extraction to provide technical support for pressure mortar process.

**Keywords:** Tunneling engineering; grouting in the vault; scan assessment; waveform information

## 1 INTRODUCTION

Tunnels and underground space development in China has a long history. Naturally, layered structure of sedimentary rocks comprises two-thirds of mainland area, many metamorphic rocks also possess the characteristics of layered structure<sup>[1]</sup>, and a large number of civil workers in the construction of underground space face layered rock mass stability problems. By the end of 2013, 11,359 highway tunnels with the total length of 9.6056 million meters had been built. China ranks first in the number and total length of tunnels in the world. However, landslides are frequent. Grouting processes are carried out in landslide areas. Plumpness of grouting and degree of contact are important indicators that need to be detected strictly in non-destructive testing<sup>[2]</sup>. The mouth of the cave of the Qingling Tunnel is located in the Xing Long Elm Bay village. This is a two-way two-lane secondary highway tunnel with start–stop mileage of K16 + 660 ~ K18 + 460 and length of 1800 m. The rocks surrounding the layered rock mass are the breeze shale and dolomite.

## 2 WORKING PRINCIPLE OF GPR

### 2.1 *Technique of GPR*

Radar measurement principle is based on the reflection of electromagnetic waves in different media caused by their different velocity of propagation with different amplitudes and energy. When electromagnetic waves with a range of center frequency propagate from transmitting antenna, reflected electromagnetic wave of media interface was received by the receiving antenna. The different colors of the spectrum indicate the parameters of the received electromagnetic wave such as amplitude, energy, and frequency<sup>[3–4]</sup>. According to the theory of electromagnetic wave, when the radar pulse in the process of underground transmission meets different electrical media in the interface, electromagnetic waves produce refraction and reflection because of the electromagnetic properties of the upper and lower media<sup>[5–7]</sup>. Signal acquisition principle is shown in Figure 1.

The stratum depth of detecting is calculated by formula (1). Let us suppose formation interface for the horizontal interface, and the incident wave

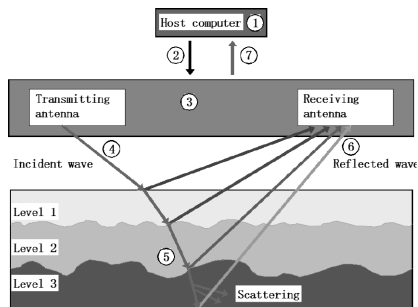


Figure 1. Principle of signal collection.

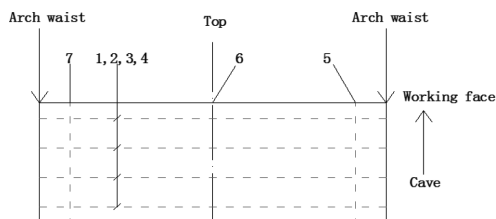


Figure 2. Survey line layout of 1600 MHz antenna.

and reflected wave follow the principle of optical geometry; however, the actual rock and soil layer interface is more complicated:

$$\sqrt{z^2 + \frac{x^2}{4}} = \frac{c \times t}{2 \times \sqrt{\epsilon_r}}, \quad (1)$$

where  $z$  is the depth of the formation bottom,  $c$  is the electromagnetic wave propagation velocity in air (300 mm/ns),  $t$  is the round-trip time for electromagnetic wave propagation in stratum medium,  $x$  is the center distance of the transmitting antenna and receiving antenna, and  $\epsilon_r$  is the relative dielectric constant of the material.

By the theory of electromagnetic wave reflection, reflection coefficient  $R$  mainly depends on the dielectric constant, as shown in formula (2). The stronger the reflection, the higher the amplitude of electromagnetic waves:

$$R \approx \frac{\sqrt{\epsilon_n} - \sqrt{\epsilon_{n+1}}}{\sqrt{\epsilon_n} + \sqrt{\epsilon_{n+1}}}, \quad (2)$$

where  $\epsilon$  is the dielectric constant of the material, subscript  $n$  indicates the overlying medium, and subscript  $n+1$  indicates the medium under the cover.

## 2.2 Radar detection scheme

According to the site conditions, line is divided into horizontal line (tunnel radial) and vertical line (tun-

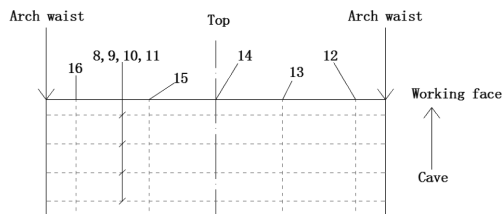


Figure 3. Survey line layout of 900 MHz antenna.

nel axial). Scan line layout is shown in Figure 2 and Figure 3. Using SIR3000 geological radar antenna, the grouting effect of the arch above the waist area was tested at the K18+170–K18+175 section.

## 3 INTERPRETATION OF GEOLOGICAL RADAR SPECIFICATIONS AND STANDARD

### 3.1 Electromagnetic interference

The aim of processing geological radar data is to suppress random and regular interference, displaying reflection wave with the greatest possible resolution on geological radar image. The extraction of reflected wave velocity, amplitude, and waveform parameters provides reliable basis for accurate geological interpretation of the information. The current data processing method of geological radar consists of pretreatment, filtering, convolution, migration homing processing, and other related signal processing methods<sup>[8-9]</sup>.

Identification of interference-affected target body is the basis for geological radar image interpretation. Interference signals can be due to many reasons, such as metal objects on the surface of wire, buildings, walls, bad antenna coupling, and multiples of the underground anomaly. Interference waves are easy to distinguish and confirm even with special shapes<sup>[10-12]</sup>.

In the process of radar detection, where the concrete cover layer of the beam is too thin, reflection interference wave will appear near the corresponding i-steel, as shown in Figure 4. The concrete cover thickness must meet the design requirements to ensure that the primary lining plays the supporting role.

During the operation of the radar, antenna surface should be close to the lining. The wavelength of the 1600 MHz antenna is 18.75 cm, and the distance between the lining and antenna surface is longer than  $\lambda/10$ , due to uneven lining surface. Figure 5 shows that the reflection interference wave existed from 0.20 m, within the scope of the whole level. Dispersed crescent strong reflected signal is distributed from 0.8 to 2.2 m in

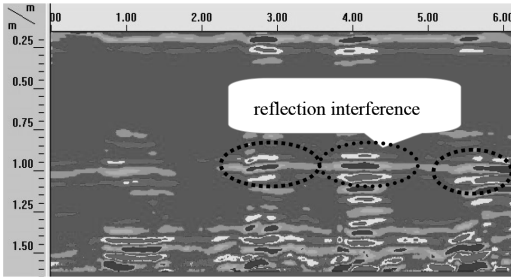


Figure 4. Electromagnetic interference of metal on wall surface (survey line 14).

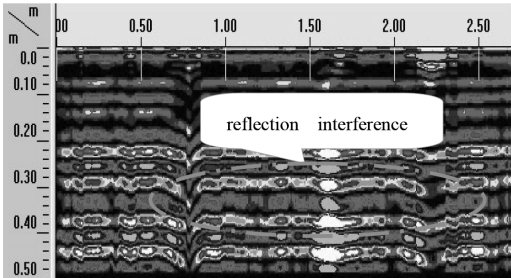


Figure 5. Electromagnetic interference of bad antenna coupling (survey line 5).

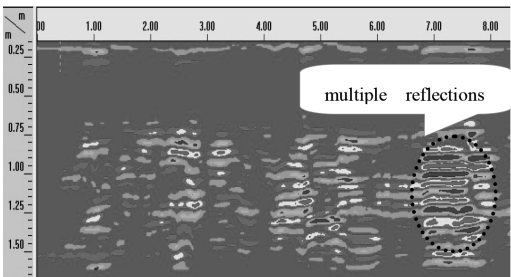


Figure 6. Electromagnetic interference of subsurface anomalies (survey line 12).

the horizontal direction, where i-beam spacing was 1.4 m. Independent anchor reflected signal was not found in the scan images. Figure 6 shows that multiple reflections of subsurface anomalies are due to i-beam interference.

### 3.2 Radar interpretation norms and standards

In the same way, the setting in the secondary heading for spacing should be changed from 20 pt to 7 pt. According to the non-destructive testing procedures for railway tunnel lining quality (TB10223-2004), Table 1 shows the backfill compactness behind the lining, steel frame, and reinforced loca-

Table 1. Relationship between lining quality of the tunnel and radar signal feature.

The actual situation	Radar signal characteristics
Rebar	A continuous strong reflection of small double-curved shape
Steel frame	Dispersed crescent strong reflected signal
Perfect	Weak signal amplitude, not even interface reflection signals
Imperfect	Lining of the interface is strong reflection signal in phase axis diffraction arc; discontinuous and relatively dispersed;
Cavity	Lining of the strong signal interface reflection and struck out phase are still strong in the lower part. The area of fire signal and the two groups of the signal path difference are larger.

Table 2. Relationship between pressure mortar quality and characteristic waveform.

Grouting quality	Perfect	Imperfect	Uncontacted
Energy change	Rule and slow attenuation	Poor regularity, fast attenuation	In accordance with fast attenuation
In-phase axis	Continuous	Intermittence	Discontinuous
Waveform	Uniform	More cluttered	Basic uniform
Amplitude	Low amplitude	High amplitude	High amplitude

tion distribution. Table 2 presents the relationship between the amplitude and energy change, synthetic axis, and grouting quality.

## 4 ELECTROMAGNETIC WAVE VELOCITY IN CONCRETE

Number determination for the target distance is very important for target localization. The factors affecting vertical underground target positioning accuracy are two-way travel time and electromagnetic wave propagation speed. Because computer is used for target search, the relative error of the round-trip time is small. The most influencing factor of the target localization accuracy is the electromagnetic wave propagation speed.

Concretes of grouting and second lining have similar symbols and ratio. The propagation speed of electromagnetic waves was determined in the grouting area by migration technique and time-history method. The thickness of the second lining

is 60 cm. Migration homing method of velocity measurement requires accurate horizontal distance, so a scan distance calibration car needs to be equipped with the measuring radar. In the time-history method, through the analysis of waveform, the location of the reflective surface is clear. It aims at calculating wave speed to find the origin of the signal.

It can be seen that the precision of electromagnetic wave propagation velocity in concrete directly affects the accuracy of the distance measurement:

$$h = v * \frac{t}{2} = \frac{c}{\sqrt{\epsilon_r}} * \frac{t}{2}, \quad (3)$$

where  $h$  is the distance from the object to surface,  $v$  is the electromagnetic wave propagation velocity in the concrete (300 mm/ns),  $t$  is round-trip time for electromagnetic wave propagation in stratum medium,  $c$  is the electromagnetic wave propagation velocity in air (300 mm/ns), and  $\epsilon_r$  is the relative dielectric constant of the material. The first wave of the electromagnetic wave is negative phase in SIR3000, as shown in Figure 7. Electromagnetic waves will produce strong reflection at the interface of concrete and air, where  $R$  is the positive phase constant. The electromagnetic wave velocity in concrete is 0.123 ns/m. The horizontal distance and vertical deep corresponding to the electro-

magnetic emission were accurately measured by 1600 MHz antenna and distance measuring car. Figure 8 shows that the electromagnetic wave speed is calculated by migration homing method as 0.117 ns/m. After averaging, the electromagnetic wave speed for C30 concrete is 0.120 ns/m.

## 5 VAULT GROUTING RESULTS

The surrounding rock at K18 + 170 ~ K18 + 175 is the  $x$  level. A small landslide occurred at the height 0.5–1 m. In order to avoid further development of the landslide, the first lining was strengthened. The length of the mortar anchor is 300 cm and the diameter is 22 cm. Form layout is plum flower, and spacing is 120 cm. The width of i-beam is 18 cm and spacing is 120 cm. Thickness of the sprayed concrete is 40–60 cm. A grouting hole was set up and three-segmented grouting was made. Radar detection started at 48 h after landslides.

As shown in Figure 9, in line 8 position, at the horizontal distance of 2–8 m and vertical depth of 0.6–0.8 m, high amplitude exists and phase axis is continuous. The reflection coefficient  $R$  is large at landslides, where rock is very loose. Figure 10 shows that, in line 9 position, at the horizontal distance of 4.5–9 m and vertical depth of 0.65–0.8 m, high amplitude exists and phase axis is continuous. Reflection exists at the interface of grouting.

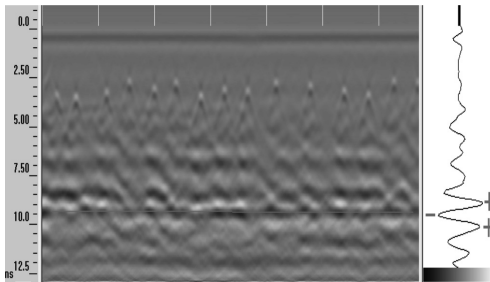


Figure 7. Linear time-history of electromagnetic waves.

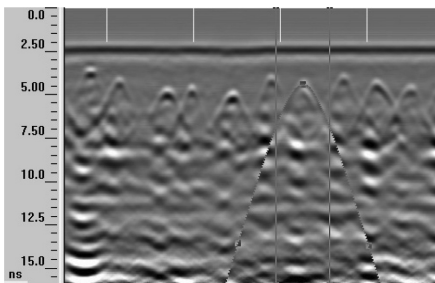


Figure 8. Migration of electromagnetic waves.

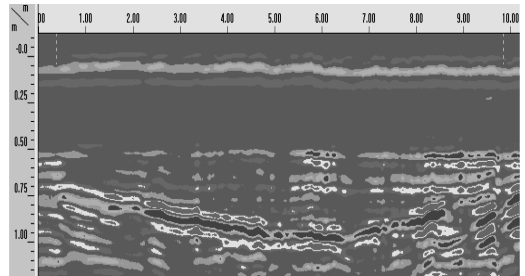


Figure 9. GPR record of section on line 8.

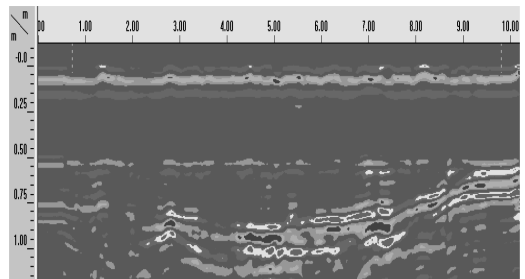


Figure 10. GPR record of section on line 9.



At horizontal distances of 0–1.5 and 8.5–10 m and vertical depth of 0.6–1.1 m, waveform is mixed and disordered, and reflection coefficient R is larger. The rock is loose because of landslides.

Figure 11 shows that, in line 10 position, at horizontal distances of 1.5–2.5 m, 5–6 m, and 8–10 m and vertical depth of 0.6–0.8 m, high amplitude exists and phase axis is continuous. The reflection at the interface of grouting and air is intense and coefficient R is large. Figure 12 shows that, in line 10 position, at the horizontal distance of 1–7 m and vertical depth of 0.6–0.8 m, high amplitude exists and phase axis is continuous. The reflection at the interface of grouting and air is weak and coefficient R is small.

Grouting did not touch the top at lines 8 and 9; however, grouting plumpness is better at lines 10 and 11. The less the surface domain and intensity of reflection, the better the plumpness of grouting and the top level. The reason for this phenomenon may be that the arrangement of vent holes and grouting holes is not reasonable. Figure 9 and Figure 10 show that strong reflection appears at the narrow interface of concrete, air, and rock. Figure 11 and Figure 12 show that reflection events draw the outline of vault cave. The arch foot area appears at different degrees of loosening in the tunnel. At the same time, the waveform is clutter and intermittent, and accompanied by strong reflection in radar map.

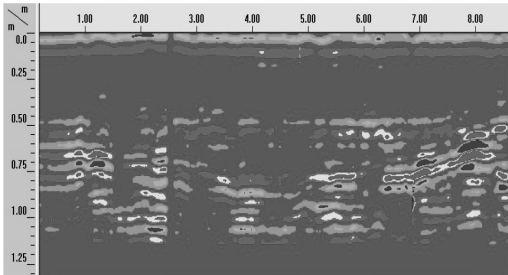


Figure 11. GPR record of section on line 10.

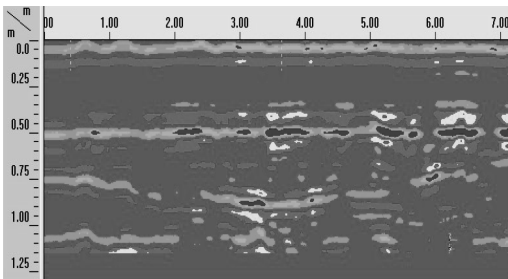


Figure 12. GPR record of section on line 11.

## 6 CONCLUSIONS

1. Using a two-way process and migration homing method, the electromagnetic wave speed of concrete was 0.117 and 0.123 ns/m, respectively.
2. When monitoring, antenna is close to the lining surface at less than  $\lambda/10$ . List three examples of reflected wave interference, metal objects, bad antenna coupling, and the underground abnormality.
3. Using 900 and 1600 MHz antennae, support quality and grouting effect of the caving zone were detected accurately. The thickness of sprayed concrete is 50 cm, and i-beam spacing is 1.2 m. Obviously, the system anchor arrangement has defects. Grouting did not answer the top at lines 8 and 9; however, grouting plumpness is better at lines 10 and 11.
4. Some conclusions are obtained by referencing radar detection results of lines 8 to 11. The less the surface domain and intensity of reflection, the better the plumpness of grouting and the top level.
5. In the arch waist position of the tunnel, radar waveform was clutter and reflection was strong, which were the loose characteristics significantly. In the vaults of the tunnel, the phase axis was continuous and the amplitude was lower, and the interface of grouting and rock mass was detected in the picture.

## REFERENCES

- [1] Xiong Liang. Layered Rock Stability and Bolt Support Parameter Optimization of Tunnel [D]. Chongqing: Chongqing University, 2010.
- [2] Wu Huo-zhen, Jiao Yu-yong, Li Hai-bo, Zhang Xiu-li. Technical method of ground penetrating radar for detecting grouting effect of air-raid shelter and its application [J]. Rock and Soil Mechanics, 2008, 29(S): 307–310.
- [3] Li Da-xin. Method and utilization of ground penetrating radar[M]. Beijing: The Geological Publishing House, 1994: 58–63.
- [4] Zeng Zhaofa, Liu Sixin, Wang Zhejiang, Principle and application of ground Penetrating radar method [M]. Beijing: Science Press. 2006.
- [5] H X J. Geological forecast for cavity at +978 of Malu-jing Tunnel on Yichang-Wanzhou Railway. Modern Tunnelling Technology, 2011, 48(1): 128–132.
- [6] Liu G, Li Z J, Shen W D. Integrated advance geologic prediction applied in Changleshan tunnel. Modern Tunnelling Technology, 2011, 2, 48(1): 123–126.
- [7] Liu Chuan-xiao, Jiang Jin-quan, Yang Yong-jie. Research on application of ground penetrating radar to detecting and identifying parameters of faults [J]. Rock and Soil Mechanics, 2004, 25(5): 832–838.
- [8] Xu xingang, LI dangmin, Zhou jie. Identifying inter-ferential wave in GPR and its countermeasure [J]. Chinese Journal of Engineering Geophysics, 2006, 3(2), 114–118.

- [9] Liu Z G, Qiao D H, Li Y W, Xu J Y. Application of karst hazard zoning to advance geological forecasting in tunnels. *Modern Tunnelling Technology*, 2013, 6, 50(3): 124–127.
- [10] Guo F Y. Applied Research of Ground Penetrating Radar in Tunnel Geological Prediction [D]. Guangzhou: South China University of Technology, 2011.
- [11] Deng Shi-kui. Application of ground penetrating radar to the quality supervision of soft soil improvement at Shen Zhen Wan [J]. *Chinese Journal of Geotechnical Engineering*, 2000, 22(1): 133–135.
- [12] Fu Zhifeng, Zhang Lei, Tang jianjun, et al. Exploration Techniques for the Bottom of Subway Tunnels and their Application [J]. *Modern Tunnelling Technology*, 2010, 47(4): 35–40.

# Research on existing residential building refurbishment in the urban area of cold climate region in China based on the aging population trend

Zi-Guang Chen

*Heilongjiang University, China*

Yu Zhang

*Harbin Institute of Technology, China*

**ABSTRACT:** This study is focused on the field of elderly oriented design for residential building, which is of paramount importance in China. In the northeast part of China, which is the heavy industry base, there are several existing residential buildings in the urban area. Facing the aging problem, this study analyzed the characteristics of existing buildings in this region, explored the possibility of elderly oriented refurbishment in this region, summarized the feasibility, including policy support, living feature of aging people, and inter-generational mutual and green sustainable development. These results will serve as reference for designing building for aging people in urban areas of cold climate region.

**Keywords:** Elderly oriented, residential building, refurbishment

## 1 INTRODUCTION

In the past two decades, the progress of urbanization has had a fast improvement in China. While the population largely grew and the family unit became smaller, the elderly population increased rapidly. According to the Sixth Nationwide Census, the proportion of people above 60 years of age is 13.26%, while that of people above 65 years of age is 8.87% in 2010, which were 2.93% and 1.91% increments compared with the data of 2000 [Li, 2013]. In China, aging of population is becoming an emergency problem. The total number of aging people was more than 200 million in China in September 2014, and it will peak in the 2030s. The northeast part of China locates in the cold climate region characterized by long time of cold weather, low temperature, and snow and wind in winter, which have negative effects on the outdoor activity of the people. The extreme difference in temperature also troubles the aging people.

In China, home-based care is the main living mode for aging people. The research on existing residential building refurbishment for aging people is a key point for improving the society in the northeast part of China. This paper aims at optimizing living environment for aging people in urban area in this region and improving livability, which is significant to social sustainable development.

## 2 THE DEMAND CHARACTERISTICS OF RESIDENTIAL BUILDING FOR AGING POPULATION TREND IN URBAN AREA IN THE NORTHEAST PART OF CHINA

### 2.1 *Supporting the aged in the existing residence*

Currently, there are three modes of old-age care in China: home-based, community service, and institution endowment. The home-based mode is the main old-age care mode supported by government according to the “National 12th five-years Plan”. In urban area of the northeast part of China, living in existing residence is the most practical old-age care mode, because of two reasons:

1. Low investment and easy popularization. In the urbanization process, both the number and scale of city had increased rapidly; in the mean time, the limit of territory and energy restrict the urban expansion in turn. In the northeast part of China, the traditional heavy industrial base of the country, in recent years, this region has been in the transition from extensive economic growth mode to sustainable intensive economic growth pattern of the historical period of reform. This region had slower economic growth than other regions, and the average per capita income is much lower (Table 1).

Table 1. Basic information of China and its three provinces in northeast.

	Area (m <sup>2</sup> )	Population (10 million)	Gross national product (billion)	Growth (%)	Lowest temperature (°C)
China	960	1,36,782	63,646.32	7.4	-27.4
Heilongjiang Province	45.48	3,835	1,503.94	5.6	-38.1
Liaoning Province	14.59	4,390	2,862.65	5.8	-32.9
Jilin Province	18.74	2,751	1,380.38	6.5	-35

Data sources: National Bureau of Statistics of China (2014).

After the foundation of the People's Republic of China, several industrial workers gathered in this region, almost all of them residing in concentrated apartments near the factory. Along with the transition of economic mode, majority of the workers were aged and had retired. The existing concentrated apartments, which had been built before decades, have become obsolete and needed refurbishment to cope with the development of the economy and living modes. In accordance with local regional development, refurbishing these existing apartments for aging people is better than building new residential buildings because of the following advantages: low investment, short construction time, and easy implementation. It also benefits by establishing pension systems and improving sustainable development of pension industry.

- Maintain the living mode conforming to the homing psychology of aging people. In the urban area of the northeast part of China, the majority of aging people are retired, who live in the apartment for staff and workers provided by the organization they worked for. These aging people, who have adapted with the surrounding environment and humanistic environment, would not like to change residence and living environment. Therefore, supporting the aging people living in the original apartment would maintain the original living mode, that is, refurbishment specific to aging people could not only improve the living environment, but also maintain the relationship between neighborhood and inter-generation, which would conform to the homing psychology of aging people. It would be a key point for completing comprehensive living support system for aging people in the background of aging society.

## 2.2 Improving the comfort level of existing residential building

In urban area of the cities in the northeast part of China, there are several existing residential communities in batches built from the 1970s to 2000s, which have complete service facilities. Because of the limit of material and construction technique in the past, these residential buildings need to be refurbished now. These residential buildings have the following limitations: too single unit type, unreasonable function division, too small kitchen and toilet, insufficient performance of insulation and water resistance, aging of equipment and pipes, and poor environment of community. The requirement of aging people is higher than others in the residential building. Therefore, through the elderly oriented refurbishment of existing residential buildings, their living environment could be improved; moreover, the comfort level of living could be improved.

## 2.3 Weakening the adverse impact of living environment for aging people from the severe cold climate

Cold climate region would have a huge impact on built environment. In the northeast part of China, during the low-temperature period, which would be for more than 4 months, there is thick snow cover and cold wind, which affect outdoor activity. According to relevant research, the education only takes 4.7% time of the normal aging people while activity takes 33.9%. [Liu et al. 2008] Therefore, through implementing special techniques in the building process, the light and wind environment could be adjusted to provide comfortable and convenient indoor and outdoor environment for aging people.

## 3 FEASIBILITY OF ELDERLY ORIENTED REFURBISHMENT OF EXISTING RESIDENTIAL BUILDING IN COLD CLIMATE REGION

On the basis of the analysis of the demand of elderly oriented refurbishment of existing residential building in cold climate region, we can note that the elderly oriented refurbishment of existing residential building is the most economic and effective solution for coping with the emergency trend of aging society in the northeast part of China. The aim of elderly oriented refurbishment of existing residential building is not meeting the special functional requirement of aging people, but conforms to finding the relationship between economy and policy, improving psychological health, supporting the intergeneration assisting mode, and improving sustainable development. The feasibility could be divided into four aspects: policy guiding, behavior

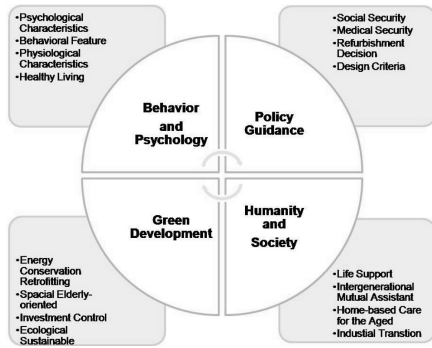


Figure 1. Influence factors of elderly oriented refurbishment of existing residential building in cold climate region.

and psychology, humanity society, and green development (Figure 1).

### 3.1 Making policy adjustment to support economic balance correspond to local economic development

The Chinese government has implemented existing residential building retrofitting project since the 1990s. Within the sustained and in-depth development of the retrofitting, a series of relevant policies were published. Taking Heilongjiang Province as an example, on the basis of the national policies, guidelines for existing residential community retrofitting in urban area of Heilongjiang Province had been published for implementing the retrofitting technique in 2013. In fact, the refurbishment of residential building in urban area of the northeast part of China could be summarized to three steps (Table 2). The stakeholder of the refurbishment changed from government to co-financing by government and company, and then to diversified multi-participants, including inhabitants, government, relevant administrators, architects, and constructors. We can find that within the policy support from the government, the composition of stakeholders of the refurbishment became more reasonable, the aim of refurbishment became more rational, and the investment mode became more complete. The relevant industry relates with aging form as pension industry. Existing residential building refurbishment is an economic industry with enormous development potential, and relates with multi-aspects. However, the research on elderly oriented refurbishment of residential building combines pension and refurbishment industry with great feasibility. As mentioned, there is great demand for refurbishment of existing residential building in urban area in the northeast part of China. Because this type of residential buildings were built as monetization housing distribution, the residential building has

Table 2. Basic information of China and its three provinces in northeast.

Stage	Aspects	Key points
1	<ul style="list-style-type: none"> <li>• Old dilapidated residential areas renovation</li> <li>• Squatter settlements renovation</li> </ul>	<ul style="list-style-type: none"> <li>• Structure security</li> <li>• Waterproofing and insulation of envelope</li> </ul>
2	<ul style="list-style-type: none"> <li>• Façade retrofitting</li> <li>• Insulation retrofitting</li> </ul>	<ul style="list-style-type: none"> <li>• Waterproofing and insulation of envelope</li> <li>• Unification of façade</li> </ul>
3	<ul style="list-style-type: none"> <li>• Comprehensive refurbishment</li> </ul>	<ul style="list-style-type: none"> <li>• Energy conservation performance of envelope structure</li> <li>• Optimizing living environment</li> <li>• Elderly oriented refurbishment</li> <li>• Barrier-free design</li> </ul>

clear property rights that the inhabitants have the right of use and proprietorship, but the company which developed the residential community has the right for the whole residential community. The clear property rights, together with the requirement for elderly oriented refurbishment of the residential building is the foremost reason for elderly oriented refurbishment of existing residential building in urban area in the northeast part of China.

### 3.2 Maintaining original neighborhood relations and saving investment would meet the expectations and economic affordability of aging people

China is in the very beginning of pension industry. Especially in the urban area of the northeast part of China, which is the national base of heavy industry, a large number of industrial workers are being transformed to aging people within the economic transition in this region. There is huge demand for living environment for aging people and residential building refurbishment. The refurbishment not only aims at optimizing the living environment for aging people, but also emphasizing their specific psychological characteristics during the whole process of refurbishment. Majority of the aging people would not leave the original residential community because they have high psychological demand on satisfaction of neighborhood relations and convenience to the residential community. The aging people in China organize several outdoor activities in groups, which would be limited in the long winter time, especially in the northeast part. Therefore, the aging people in this region usually organize outdoor activities in the area surrounding their residence. This means there is high demand for stable neighborhood relations. Meanwhile, existing building refurbishment would

take shorter time and lower cost than constructing new residential building or institutional care of the elderly, which would conform to the economic condition of aging people.

### 3.3 *Supporting intergeneration mutual assistant helping, optimizing living of aging people in cold climate region*

In the aspect of home-based care for the aged, there is common phenomenon including lack of resources for the elderly and obsolete facilities. The residential community environment and inner special environment need to be refurbished immediately. During the long winter time in cold climate region, not only the low temperature, but also the cold wind and snow would have negative impact on aging people by declining their outdoor activity. The benefits of refurbishing existing residential building for the aging people include minimal influence on the original family mode, maintaining stable neighborhood relations, and improving communication of aging people with other generations. The communication is quite flexible that not only reflecting in taking care of aging people by middle-young age, through the refurbishment, the “activity aging” concept would be implemented by letting aging people look after babies and children. By finding the conjunction point of different generations, the mutual intergeneration mode could be formed. It does not only improve comfort level of built environment, but also optimizes psychology environment for all inhabitants. There are already some effects on mutual intergeneration; for example, according to ABC news, there is one intergenerational learning center in one retirement home in Seattle, USA. Every Sunday, children would visit the center and conduct activities such as drawing and dancing with the aging people. It not only improves the vitality of aging people, but also helps the children to learn how to communicate with others. In China, problems exist in looking after children after school hours, as most parents are working. Therefore, it is a good idea to tap existing potential balance between demand and support ability of intergeneration.

### 3.4 *Improving energy saving and residential building sustainable development by construction material and land saving*

In the urban area of the northeast part of China, the form of buildings should adopt the intensive style as response to wind and cold climate. The distribution and form of residential buildings should be designed according to the wind direction and orientation in winter. Therefore, existing residential buildings usually occupy the best positions in the urban area and there are auxiliary facilities in the residential community. In the same time, the construction structure of existing residential buildings had been designed

for at least 50 years, which is much longer than the utilization time of the building. This means that it is advantageous if we carry out elderly oriented refurbishment of these existing residential buildings by saving construction materials and land for building. In the northeast part of China, the investment for existing residential building refurbishment is about 200 rmb/m<sup>2</sup> while that for constructing new residential buildings is at least 800 rmb/m<sup>2</sup>. Furthermore, limitations associated with heating and water pipe construction also exist. By the elderly oriented refurbishment of existing residential buildings, not only the aim of saving construction materials, energy, and land could be reached, but also there is significance for improving residential building sustainable development in the urban area of cold climate region.

## 4 CONCLUSIONS

In conclusion, the elderly oriented refurbishment of existing residential building is a research response to demands with times and social development, and it produced rich traditional region characteristics in urban area in the northeast part of China with cold climate. By analyzing the inner demand of elderly oriented refurbishment of existing residential buildings in urban area in cold climate region, the refurbishment is supported by national and local policies, in terms of the characteristics of aging people. There is also huge potential of green development for optimizing living environment for aging people in that region. Of course, the influence factors of elderly oriented refurbishment of residential building in urban area of cold climate region are rather complex. Therefore, this paper focused on the universality of existing buildings in the northeast part of China, which is the typical cold climate region. Further research should focus on the evaluation and techniques for implementing the strategy in the future.

## ACKNOWLEDGMENTS

This paper was supported by “the Fundamental Research Funds for the Central Universities” (Grant No. HIT.NSRIF. 2014073), “Heilongjiang Provincial Post-doctoral Research Funding” (Grant No. LBH-Z14110), and the Application Technology Research and Development Projects (Grant 2014 RFQXJ106).

## REFERENCES

- [1] J. Li, Some problems of design for elderly-oriented retrofitting in original residence, *Sichuan Architectural Science*, 2013(12):284–286.
- [2] M. Liu, N. Lou, J. Li, *development and management mode of residence for aging people*, Beijing: China Architectural & Building Press, 2008.

## Assessment of isolation methods for the erected tower near soft road embankment

B.B. Xu & W. Si

*Tianjin Port Engineering Institute Ltd. of CCCC, Tianjin, China*

*Key Laboratory of Geotechnical Engineering of Tianjin, Tianjin, China*

*Key Laboratory of Geotechnical Engineering, Ministry of Communication, Tianjin, China*

**ABSTRACT:** Near one road to be improved by the vacuum and surcharge preloading, there are a row of high-voltage towers. In order to reduce the influence of ground deformation on the erected tower, three schemes are adopted and it is necessary to evaluate the isolation methods. The results show that: 1) Under the effect of vacuum combined surcharge preloading, there is significant settlement at both the left and right top points; 2) There is nearly no influence of the installation of cement-mixed piles on the deformation of the tower; 3) It is an effective way to reduce the possible deformation of the tower during the improvement of the ground.

**Keywords:** isolation method; erected tower; deformation of tower

### 1 ENGINEERING BACKGROUND

For the soft ground, the most frequently used method is vacuum preloading method considering its feasibility and economy. The procedure of the vacuum preloading method is: 1) put a sand cushion with certain depth of 40 60cm on the surface of the soft ground; 2) insert vertical drainage such as sand drain or plastic vertical drain into the ground; 3) cover the entire ground to be improved with airproof plastic seal; 4) exert vacuum pressure using vacuum pump to the sand cushion and the vertical drains; 5) different pressure occurs between the vertical drains and the surrounding soils due to different permeability, under which the pore water is drained from the soft ground. For the vacuum combined surcharge preloading method, the fills for surcharge load is subsequently added on the top of the sealing cover after the vacuum pressure keeps stable for one or two weeks. If the ground is extremely soft, the addition of surcharge fill can be postponed.

One problem for the vacuum preloading method is the conversion from three dimensional sand drain to two dimensional sand wall. Because the deformation and seepage of the ground with sand drain are three dimensional, the suitable analyzing method is three dimensional. However, it is too

heavy to carry out the calculation and usually the calculation is based on the plane strain condition. How to transfer the three-dimensional sand drain to two-dimension is always the highlight.

Indraratna et al.(1997, 1999, 2000) research the method transferring from the single drain to unit length of sand wall. The method is that the average degree of consolidation of both sand drain and sand wall at arbitrary depth and time is equal through adjusting the permeability coefficient and space of the sand wall. The well resistance and smearing effect are also taken into consideration. But the equal-strain condition is only satisfied vertically, the horizontal deformation of the ground cannot be reflected using this method. Sanchez et al. (1990), Hird et al. (1992, 1995, 1998) gave the similar transferring method according to the equal horizontal degree of consolidation. However, Hird didn't consider the smearing effect, horizontal displacement and vertical seepage.

### 2 SOIL PROFILES

According to the design material, the total length of the road is 1578m and the width of the road is 20m. The ground layers can be determined by the

Table 1. Soil parameters used in the calculation.

Category	Silt	Mucky clay	Silty clay	Alluvium clay
Volume weight (kN/m <sup>3</sup> )	17.2	18.5	19.0	18.8
Void ratio	2.13	1.89	0.88	0.67
Modulus of compressibility (MPa)	2.1	2.4	3.6	7.3
Cohesive strength (kPa)	3	3	6	12
Frictional angle	2.0	3.1	6.5	15.4
Permeability (cm/s)	1.210 <sup>-7</sup>	1.810 <sup>-7</sup>	2.910 <sup>-7</sup>	3.510 <sup>-7</sup>

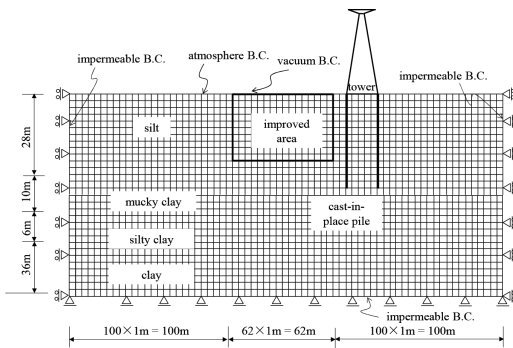


Figure 1. Numerical model and boundary conditions.

previous ground survey and it can be divided as silt, mucky clay, silty clay and alluvium clay sequentially. The soil parameters used in the numerical calculation are listed in the following table.

### 3 CALCULATION SCHEME

A typical section is chosen to analyze and the calculation model is shown in Fig. 1. Considering the asymmetry of the model, take the whole width of the road to be computed. The transmission tower is located at the right of the road to be improved and the distance between them is 2 m.

When the road is improved by the vacuum combined surcharge preloading, the depth of the clay sealing wall is only 6 m. There is neither cement-mixed pile to prevent the horizontal influence of the improved area, nor the ground under the tower is improved. In order to compare the effect of cement mixed sealing wall and the improvement of ground under the tower, the calculation schemes listed in Table 2 are carried out. Besides, the deformation of the ground and the tower is also analyzed when the tower is highest.

Table 2. Calculation schemes and contents.

Calculation conditions	Remarks
1 The height of the cast-in-place pile and tower is 34 m and 42 m respectively.	The worst-case as the benchmark
2 The height of the cast-in-place pile and tower is 34 m and 42 m respectively. In addition, add the cement-mixed pile with depth of 26 m.	Compare the influence of cement-mixed pile
3 The height of the cast-in-place pile and tower is 34 m and 42 m respectively. In addition, the ground of the tower is improved.	Compare the effect of improvement of the ground
4 Based on case 3, consider the effect of unloading on the deformation of tower.	Compare the effect of unloading

## 4 CALCULATION RESULTS

### 4.1 Deformation of tower

In order to evaluate the influence of ground deformation during the ground improvement on the tower, the settlement and displacement at the top of the tower are clarified in Figs. 2 and 3 respectively. According to Fig. 2, there is obvious settlement at both the left and right top point during the vacuum combined surcharge preloading. The settlements are 0.46 m and 0.29 m respectively and the uneven settlement is almost 0.17 m, which shows a configuration inclining to the left. As shown in Fig. 3, the horizontal displacement at the top of the tower gradually increases to 1.7 m due to the deformation of the ground. As the tower can be regarded as a rigid body, the displacements at the left and the right are equal. Considering the height of the tower is 42 m, the inclining angle of the tower is about 2.32°, which is towards the left. The deformation rate gradually decreases as the time elapses.

### 4.2 Assessment of supporting schemes

In order to reduce the deformation of tower, two schemes including the addition of cement mixed pile with 26m length and pre-improvement of the ground at the tower are considered. The effect of the pre-improvement can be quantized that the water content of the ground reduces from the natural water content to the liquid limit and the compression modulus of the ground increases three times. Figs. 4 and 5 show the vertical and horizontal deformation of the tower at the top under two schemes of improvement separately. It can be seen that after the installation of 26 m cement-mixed



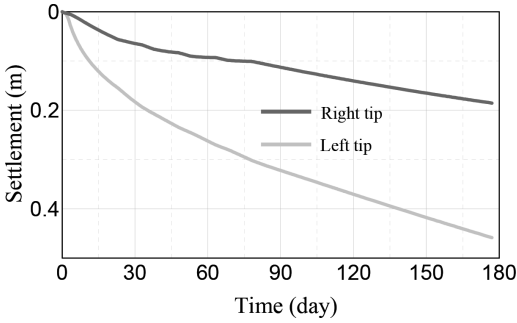


Figure 2. Settlement at the top of the tower.

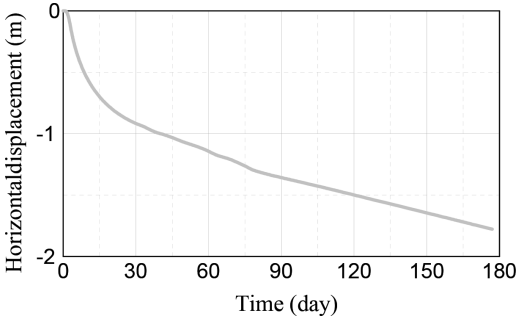


Figure 3. Horizontal displacement at the top of the tower.

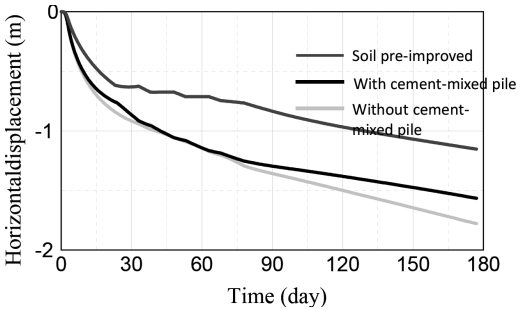


Figure 4. Horizontal displacement at the top tower under different schemes.

piles, there is no significant reduction in both horizontal and vertical directions before 90 d, and after 90 d the extent of reduction is also very small. Finally, the horizontal and vertical displacements decreases from 1.7 m and 0.46 m to 1.55 m and 0.44 m. The decreased degrees are only 8.8% and 4.3%, which shows that there is nearly no influence of the installation of cement-mixed piles on the deformation of the tower. However, when the ground at the tower is pre-improved, the deformation of the tower decreases obviously. The hori-

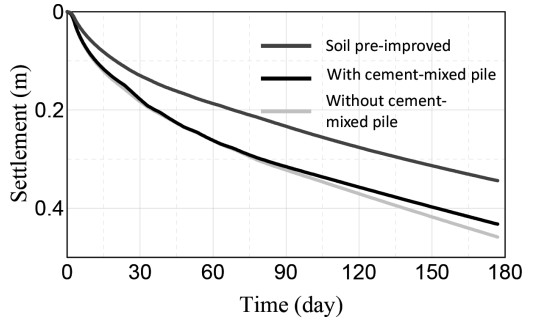


Figure 5. Settlement at the top tower under different schemes.

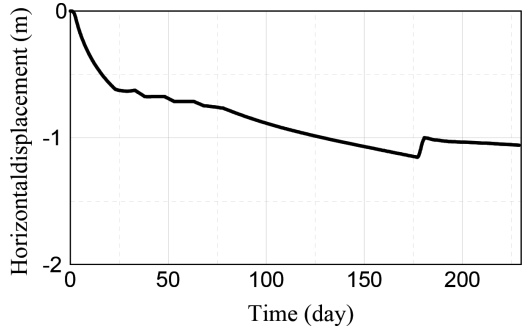


Figure 6. Horizontal displacement at the top of the tower considering the unloading of vacuum preloading.

zontal and vertical displacements decreases from 1.7 m and 0.46 m to 1.15 m and 0.36 m and the decreased degrees are as large as 32% and 26%, which means that the pre-improvement of the soft ground beneath the tower is an effective way to reduce the possible deformation of the tower.

Notice that there is no tendency of convergence for both the horizontal displacement and settlement at the top of the tower in Figs. 2 and 3, which can be understood that as long as there is vacuum pressure, the tower would deform continuously. In order to consider the deformation of the tower after unloading of vacuum pressure, the vacuum preloading after 180d is removed and at this moment there is still negative pressure inside the ground and the consolidation calculation is kept until 230d. The following deformation of the tower can be seen in Figs. 6 and 7. As can be seen, the horizontal displacement becomes smaller during the unloading stage and then gradually converges to about 1.05 m. For the settlement of the tower, the settlement at both left and right top points get convergent after unloading. In order to understand the deformation of the tower more clearly, Fig. 8 shows the sketch of the deformation at the top of the tower. Initially, there is no deformation at the

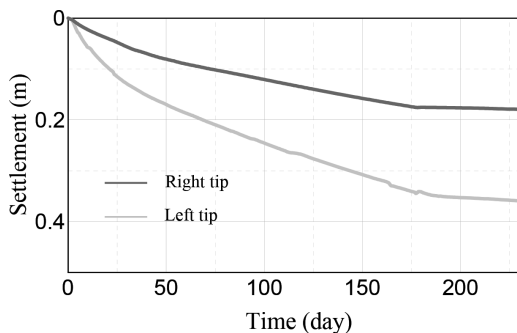


Figure 7. Settlement at the top of the tower considering the unloading of vacuum preloading.

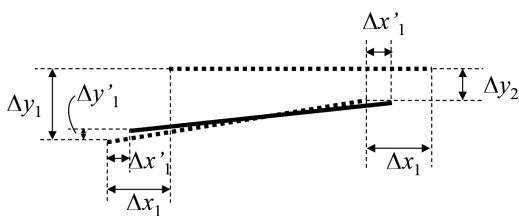


Figure 8. Schematic diagram of deformation at the top of the tower.

Table 3. Incremental deformation at the top of the tower.

Deformation	Vacuum + surcharge	Unloading	Remarks
$\Delta x_1$	-1.7	-	The negative represents the deformation toward the inside of the improved area in x direction and downwards in the y direction
$\Delta y_1$	0.46	-	
$\Delta x_2$	-1.7	-	The negative represents the deformation toward the inside of the improved area in x direction and downwards in the y direction
$\Delta y_2$	0.29	-	
$\Delta x'_1$	-	-0.11	The negative represents the deformation toward the inside of the improved area in x direction and downwards in the y direction
$\Delta y'_1$	-	-0.05	
$\Delta x'_2$	-	-0.11	The negative represents the deformation toward the inside of the improved area in x direction and downwards in the y direction
$\Delta y'_2$	-	0	

top. As the vacuum pressure is applied, the tower begins to subside and incline toward the improved area. The horizontal displacement and settlement at two ends are  $\Delta x_1$ ,  $\Delta x_2$  and  $\Delta y_1$ ,  $\Delta y_2$  respectively. After the remove of the vacuum pressure, the horizontal displacement and settlement in the reverse direction are  $\Delta x'_1$ ,  $\Delta x'_2$  and  $\Delta y'_1$ ,  $\Delta y'_2$  respectively. The detailed magnitudes can be seen in Table 3 and the solid line in Fig. 8 represents the final configuration of the tower.

## 5 CONCLUSIONS

In this paper, the deformation of tower due to the vacuum combined surcharge preloading is analyzed

numerically. The emphasis is put on the influence of ground deformation during the improvement stage on the transmission tower and the conclusions are as follows:

1. Under the effect of vacuum combined surcharge preloading, there is significant settlement at both the left and right top points. The magnitudes are 0.46 m and 0.29 m respectively and the uneven settlement is 0.17 m, which means that the tower inclines toward the left.
2. At the top of the tower, the horizontal displacement gradually increases to 1.7 m due to the influence of ground deformation. Considering the stiffness of the tower, there is the same displacement at both the left and right ends. Because the height of the tower is 42 m, the inclination angle of the tower is  $2.32^\circ$ .
3. When the cement-mixed piles with depth of 26m are installed at the borderline of the improved area, there is only slightly decrease of the deformation of the tower after 90d comparing with that without cement-mixed piles. And there is nearly no influence of the installation of cement-mixed piles on the deformation of the tower.
4. When the soil beneath the tower is pre-improved by other improvement methods, the horizontal and vertical displacements decreases significantly and it is an effective way to reduce the possible deformation of the tower during the improvement of the ground.

## REFERENCES

- Hird C. C. Pyrah I. C. and Russel D. 1992. Finite element modeling of vertical drains beneath embankments on soft ground. *Geotechnique*, (4):499-511.
- Hird C. C., Russel D. and Cinioglu F. 1995. Modeling the effect of vertical drains in two-dimensional finite element analysis of embankments on soft ground. *Can. Geotech. J. (S)*: 795-807.
- Indraratna B. and Redana I. W. 1997. Plane strain modeling of smear effects associated with vertical drains. *J. Geotech. and Geoenviron. Engrg. ASCE*. (5): 474-478.
- Indraratna B. and Redana I. W. 1999. Closure: Plane strain modeling of smear effects associated with vertical drains. *J. Geotech. and Geoenviron. Engrg. ASCE*. (1):96-99.
- Indraratna B. and Redana L. W. 2000. Numerical modeling of vertical drains with smear and well resistance installed in soft clay. *Can. Geotech. J.*, (1):132-145.
- Sanchez J.M. and Sagaseta C. 1990. Analysis of staged construction of embankments on soft soil, Proc.2nd European speciality conference on numerical methods in geotechnical engineering, Santander, 457-471.
- Zhao WB, Chen YH, Gong YP, 1998. A methodology for modeling sand-drain ground in plain strain analysis [J], *Journal of Hydraulic Engineering*, (6):53-57.

## Research on variable water volume collaborating with a variable water temperature operation scheme

H.Y. Tan & F. Cai

*University of Science and Technology Liaoning, Anshan, Liaoning, China*

**ABSTRACT:** Experts and scholars in the water system of energy saving technology have conducted several studies. Previous studies are mostly focused on minimizing energy consumption, but the water system has many energy-consuming parts. The air-conditioning water system must be, as a whole, to optimize operation conditions (i.e. minimum energy consumption). In this study, a mathematical model is built with the main energy consumption components of the water system through variable water volume collaborating with variable water temperature operation scheme and using the global search ability of genetic algorithm in 1st Opt to solve the optimal operation condition of air-conditioning water system under different load rates and conduct comparative analysis with variable volume system, which is widely applied for energy conservation. Experimental results show that the energy saving of the coordinated operation is higher than that with the variable water volume method only. This conclusion can be used as the theoretical basis of the actual project's coordination operation.

**Keywords:** Water system energy saving; mathematical modeling; genetic algorithm; variable water temperature collaborating with variable water volume

### 1 INTRODUCTION

With the pace of reform and opening up a huge rally in people's living standards, from the 1990s to the present, the proportion of building energy consumption in the total energy consumption increased about 60–70%. Therefore, reducing the running cost not only depends on controlling air-conditioning cost, but also responds to the national policy trend of "energy conservation and emission reduction". The energy consumption of water system taking up the whole air-conditioning system can reach 65–70%; thus, reducing water system operation energy consumption is significant. The load of air-conditioning system under the influence of the outside environment always varies, and because of the problems of design selection, system is often run below the rated conditions. In order to satisfy the real-time indoor cooling load, system must adjust the parameters of chilled water correspondingly.

Because the social requirement for energy conservation is increasing, the chilled water system on the control strategy has gone through variable water temperature and variable water volume. Yanshan Huang et al.<sup>[1]</sup> simulated the coefficient of performance (COP) of the chiller with the change of different external parameters through MATLAB and concluded that the unit's COP increases with the decrease of cooling water inlet temperature and increase of chilled water outlet tempera-

ture, and also increases with the increase of cooling water volume and chilled volume. On the basis of the above theory, by reducing the cooling water inlet temperature, increasing the chilled water outlet temperature, and increasing the cooling water and chilled water volume, the COP of the unit increases. In the air-conditioning water system, energy consumption of water chillers is generally over 50%. If the method of increasing the volume of chilled water and cooling water to improve the work efficiency of the unit is implemented, the energy consumption of the water pump increases, so there must be a best working point in the running process to minimize the energy consumption of water chillers, pumps, and cooling towers.

In this article, a mathematical model is built with the main energy consumption components in the water system, a coordinate regulation strategy is adopted, and the 1stOpt program is used to determine the optimal operation point under different load rates.

### 2 MATHEMATICAL MODELING OF WATER CHILLER BASED ON EXTERNAL PARAMETERS

There are two types of mathematical model of chiller: theoretical model and empirical model. The theoretical model involves the interior design

of the chiller, which is more complex. The error rate of the empirical model is slightly higher than that of the theoretical model, but completely meets the design and application of practical engineering.

In this study, we adopt the method of establishing empirical model, using the software 1stOpt to build the mathematical model of water chiller based on external parameters. On the basis of the study of Shizhong Yang<sup>[2]</sup>, the inlet and outlet temperatures of chilled water, inlet and outlet temperature of cooling water, chilled water volume and cooling water volume, and air-conditioning load rate are used to establish this multi-parameter nonlinear curve fitting of the unit energy consumption. Let us consider the following specific expression:

$$r_{cop} = a_1(a_2 * r_{Tci}^2 + a_3 * r_{Tei} + 1) * (a_4 * r_{Tco}^2 + a_5 * r_{Tco} + 1) * (a_6 * r_{Tci}^2 + a_7 * r_{Tei} + 1) * (a_8 * r_{Tco}^2 + a_9 * r_{Tco} + 1) * (a_{10} * r_{ew}^2 + a_{11} * r_{ew} + 1) * (a_{12} * r_{cw}^2 + a_{13} * r_{cw} + 1) * (a_{14} * r_Q^4 + a_{15} * r_Q^3 + a_{16} * r_Q^2 + a_{17} * r_Q + 1) + a_{18}$$

$$r_{cop} = \frac{cop}{cop_n}; \quad r_{Tci} = \frac{T_{ci} - T_{ci,n}}{T_{ci,n} - T_{eo,n}}; \quad r_{Tco} = \frac{T_{co} - T_{co,n}}{T_{ci,n} - T_{eo,n}};$$

$$r_{Tei} = \frac{T_{ei} - T_{ei,n}}{T_{ci,n} - T_{eo,n}}; \quad r_{Teo} = \frac{T_{eo} - T_{eo,n}}{T_{ci,n} - T_{eo,n}};$$

$$r_{ew} = \frac{W_e - W_{e,n}}{W_{e,n}}; \quad r_{cw} = \frac{W_c - W_{c,n}}{W_{c,n}}; \quad r_Q = \frac{Q - Q_n}{Q_n},$$

where  $r_{cop}$  = chiller energy consumption ratio;  $cop_n$  = chiller rated efficiency;  $cop$  = chiller actual efficiency;  $r_{Tci}$  = cooling water inlet temperature deviation rate;  $T_{ci}$  = cooling water inlet temperature;  $T_{ci,n}$  = cooling water rated inlet temperature;  $T_{eo,n}$  = chilled water rated outlet temperature;  $r_{Tco}$  = cooling water outlet temperature deviation rate;  $T_{co}$  = cooling water outlet temperature;  $T_{co,n}$  = cooling water rated outlet temperature;  $r_{Tei}$  = chilled water inlet temperature deviation rate;  $Tei$  = chilled water inlet temperature;  $Tei,n$  = chilled water rated inlet temperature;  $r_{Teo}$  = chilled water outlet temperature deviation rate;  $Teo$  = chilled water outlet temperature;  $r_{ew}$  = chilled water volume deviation rate;  $W_e$  = chilled water volume;  $W_{e,n}$  = rated chilled water volume;  $r_{cw}$  = cooling water volume deviation rate;  $W_c$  = cooling water volume;  $W_{c,n}$  = cooling water rated volume;  $r_Q$  = refrigerating capacity deviation rate;  $Q$  = actual refrigerating capacity; and  $Q_n$  = rated refrigerating capacity.

A mathematical model for 30HXY065 A chiller is constructed using genetic algorithm in 1stOpt to identify the parameters fitting the model. The rated working condition of chiller: refrigerating capacity 236 KW, electrical power 50 KW, chilled water volume 41 m<sup>3</sup>/h, cooling water volume 49 m<sup>3</sup>/h, temperature of chilled water inlet and outlet 12/7 °C, the temperature of cooling water inlet and outlet 30/35°C. According to the product sample man-

Table 1. Coefficients of the mathematical model for water chiller.

Coefficient	Value	Coefficient	Value
$a_1$	0.2356	$a_2$	-2.6998
$a_2$	0.8350	$a_2$	0.6794
$a_2$	-0.7362	$a_2$	-9.0107
$a_2$	0.2256	$a_2$	-0.0126
$a_2$	-0.5258	$a_2$	-6.6036
$a_2$	-0.4524	$a_2$	-0.0612
$a_2$	0.4961	$a_2$	-15.1342
$a_2$	17.8737	$a_2$	2.0333
$a_2$	0.9812	$a_2$	0.7638

ual, there are 24 groups of chiller operation data, of which 18 groups identify parameters and the remaining six sets of data check the coefficient of the model. The results show that maximum error is about 1.3%. Error rate meets the application standard of practical engineering; the coefficients of the mathematical model are shown in Table 1.

### 3 MATHEMATICAL MODELING OF WATER PUMP AND COOLING TOWER

It is now controversial whether cooling water system adopts variable frequency technology, but the author thinks that with the increase of building scale, the energy-conserving potential of the cooling water system has to be reckoned. Therefore, in this paper, cooling water system adopts frequency conversion technology. Now, the most energy saving technology of the pump focuses on increasing the pump shaft power or the effective power without considering the inverter and motor efficiency, so the energy consumption cannot reflect the actual energy consumption of water pump. From the aspect of the total energy consumption, the total input power of the pump can reflect actual energy consumption of the pump<sup>[4, 5]</sup>. Variable frequency pump is mainly composed of a frequency converter, motor<sup>[3]</sup>, and pump. Frequency converter is used to adjust the speed of the motor and then transform the operation energy consumption of the pump:

$$N_{in} = \frac{\rho g H Q}{3600 * 1000 * n_{VFD} * n_m * n_p}$$

$$n_m = 0.094187 * (1 - e^{-0.04X})$$

$$n_{VFD} = 0.5067 + 1.283 * X - 1.42 * X^2 + 0.5842 * X^3$$

$$X = \frac{n}{n'} = \frac{Q}{Q'}$$

where  $N_{in}$  = total input power, KW;  $\rho$  = density of water, kg/m<sup>3</sup>;  $g$  = acceleration due to gravity, m/s<sup>2</sup>;  $H$  = pump head, mH<sub>2</sub>O;  $Q$  = volume of water

pump, m<sup>3</sup>/h; Q' = rated volume of water pump, m<sup>3</sup>/h; n = pump speed; n' = pump rated speed; η<sub>p</sub> = efficiency of the pump; X = relative speed of the machine; and η<sub>VFD</sub> = inverter efficiency.

According to the unit parameters (chilled water and cooling water rated volume), two types of pumps are selected: SCP80-50 (chilled water pu) and SCP100-50 (cooling water pump). The parameters of the pumps are: (1) Type SCP80-50: rated vome 42m<sup>3</sup>/h, lift 50 mH<sub>2</sub>O, and pump efficiency 0.68; (2) Type SCP100-50: rated volume 50 m<sup>3</sup>/h/lift 50 mH<sub>2</sub>O, and pump efficiency 0.66.

Cooling tower theoretical mathematical model involves many factors such as the cooling water volume, the air volume of fan, and the influence of outdoor air parameters.

In this article, using the CFTOOL toolbox in MATLAB, a quadratic function relating power consumption and water volume is established<sup>[6]</sup>:

$$N_{\text{tower}} = 0.0002369 * W_c^2 + 0.03572 * W_c + 2.2$$

#### 4 VARIABLE WATER VOLUME COLLABORATING WITH VARIABLE WATER TEMPERATURE OPERATION SCHEME

Under the existing group control technology, air-conditioning water system with two (or more than two) water chillers, when load rate of both the chillers is lower than 50%, chillers will receive instruction of automatic control system to close a chiller. Therefore, under the existing group control technology, water chillers are usually run in their own more than 50% of the rated load<sup>[7]</sup>. Here, power consumption is compared with variable volume system at the load rate range of 50–100%. In variable volume systems, cooling water inlet temperature is 32°C, chilled water outlet temperature is 7°C, and inlet and outlet temperature of the water is higher than 2.3°C. In this study, 1stOpt<sup>[8]</sup> is used to calculate the minimum power under different load rates, whose programming interface is shown in Figure 1.

```

1 Parameter: x1(1:6) (5);
2 MinFunction: 236*(x1-72)^2+2354*(x1-72)+0.03572*(x1-72)^2+2.2;
3
4 (0.225*(x2-35)/(23)+2-0.525*(x2-35)/(23+1))*
5 *(17.2737*(x3-7)/(23)+2+0.3812*(x3-7)/(23+1)+(-2.8999*(x5-41)/(1)+2+0.679*(x5-41)/(1+1))*
6 (-9.0257*(x4-6)/(33)+(-0.2122*(x4-6)/(33+1)+7.9203)
7 +0.136*(x6)^2/(0.68*3600*(0.9428*(1-2.7183*(-9.04*66/50)))^(0.5067+1.283*(x6/50)-1.42*(x6/50)+2+0.3842*(x6/50)^3))+
8 0.277*(x7)^2/(0.66*3600*(0.9428*(1-2.7183*(-9.04*66/42)))^(0.5067+1.283*(x7/42)-1.42*(x7/42)+2+0.3842*(x7/42)^3))+
9
10
11
12
13
14
15
16
17
18
19
20
21
22
23
24

```

Figure 1. 1stOpt programming language of optimal operation parameters.

Table 2. Power consumption of two types of operation modes under different load rates (kW).

Load rate (%)	vwt & vwf	vwf
100	41.26	52.78
90	39.63	48.72
80	33.75	44.72
70	26.20	40.65
60	18.74	36.53
50	15.36	32.60

\* vwt&vwf refers to variable volume collaborating with variable water temperature and variable volume; vwf refers to variable water volume.

The objective function of the above mathematical model of power consumption of water chillers, pumps, and cooling tower, and constraint conditions of these parameters are as follows:

$$\begin{aligned}
 &25 < x_1 < 35; 30 < x_2 < 40; 7 < x_3 < 17; \\
 &2 < x_4 < 12; x_5 < 41; x_6 < 49; \\
 &x_2 - x_1 < 7; x_2 - x_1 > 2.3; x_3 - x_4 < 7; \\
 &x_3 - x_4 > 2.3; \\
 &4.1868 * (x_2 - x_1) * x_6/3.6 = 1.2 * x_7; \\
 &4.1868 * (x_3 - x_4) * x_5/3.6 = x_7;
 \end{aligned}$$

where x<sub>1</sub> = cooling water inlet temperature; x<sub>2</sub> = cooling water outlet temperature; x<sub>3</sub> = chilled water inlet temperature; x<sub>4</sub> = chilled water outlet temperature; x<sub>5</sub> = chilled water volume; x<sub>6</sub> = cooling water volume; and x<sub>7</sub> = water chiller load.

Under different load rates (50–100%), variable water volume collaborating with variable water temperature and variable volume, and two cases of optimal operation, the minimum power consumption is calculated using 1stOpt software, as shown in Table 2.

#### 5 CONCLUSION

As can be seen from Table 2, variable water temperature collaborating with variable water volume will save energy more than 20% compared with variable volume operation. In this paper, only considering the main energy consumption parts of air conditioning water system, there is discrepancy between using computer simulation and actual engineering methods. However, the energy saving of the variable water volume collaborating with variable water temperature operation scheme is indisputable. Although the equipment cost of variable water volume collaborating with variable water temperature operation scheme is slightly higher than the initial investment of the variable volume system, its low running cost is enough to make up for the defects.

## REFERENCES

- [1] Huang, Y.S. 2012. The dynamic optimization simulation research of air conditioning water system. *The master's thesis of Guangzhou university*:32–37
- [2] Yang, S.Z. 2015. The modeling and simulation of water chiller based on external parameters. *The computer simulation* 32(9):425–428.
- [3] Li, W. 2011. The mathematical model of water chiller used for building environment design. *The master's thesis of Wuhan textile university*:14–18.
- [4] Michel, A.B.B. 1999. Pumping Energy and Variable Frequency Drivers. *ASHRAE Journal*.
- [5] Liu, P. 2011. The modeling and optimization control of air conditioning cooling tower. *Journal of HVAC* 41(3):152–155.
- [6] Tang, J. et al. 2010. The simulation analysis of energy consumption of air conditioning system based on Matlab/Simulink. *Building Energy & Environment* 29(2):53–57.
- [7] Fu B. et al. 2008. Different refrigerating capacity chillers parallel running scheme and group control strategy. *Refrigeration & Air-Conditioning* 8(6):12–16.
- [8] 7D-Soft High Technology Inc. 2009. The manual of Istopt:16–61.

## Corrosion resistance of a plasma ion-implanted QC-10 alloy

Ming Hu, Xiao-xue Ren, Yun-long Zhang, Jing Gao & Pei-ling Ding

College of Materials Science and Engineering of Jiamusi University, P.R. China  
Institute of Applied Materials and Technology, Jiamusi University, P.R. China

**ABSTRACT:** The AlN-modified film was formed on the surface of QC-10 alloy by means of plasma injection technology successfully. The results showed that AlN films were formed as modified layer on the surface of QC-10 alloy. X-ray photoelectron spectroscopy (XPS) results showed that the AlN films have a depth higher than 12 nm from the surface. As the implantation voltage increased, the corrosion potential of QC-10 alloy after nitrogen implantation increased gradually and then decreased. Compared with the QC-10 alloy material, specimens had lower corrosion current density. The corrosion resistance of QC-10 alloy can be improved by plasma implantation.

**Keywords:** Plasma ion implantation, QC-10 alloy, AlN layer, Corrosion resistance

### 1 INTRODUCTION

Aluminum alloys have been widely used in automotive, aircraft, and ordnance industries because of their relatively high strength to weight ratio and low competitive price. Some metallic or ceramic films were utilized in aluminum alloys to improve their abrasion resistance or corrosion resistance, especially at room temperature [1–3]. The oxide films present on the surface of aluminum alloy quickly dissolve in acidic conditions, thereby reducing its corrosion resistance, which in turn limits its applications in the field of molding. In practical application, appropriate surface treatment methods are necessary to improve the corrosion resistance of aluminum alloys [4,5]. Recently, plasma ion implantation technology has been developed because of its stronger bonding force between the modified layer and matrix interface and potential to handle multi-directional complex shape components. At present, more studies are focused on the increase of wear resistance of aluminum alloy by plasma ion implantation technology. However, few studies lay emphasis on corrosion resistance of aluminum alloy. R.J Rodriguez [6] used this technology to modify aluminum alloy substrate, which resulted in the formation of AlN layer on the surface of the alloy and increment of its hardness and wear resistance. This paper dealt with the preparation of AlN-modified layer on the QC-10 surface by means of plasma ion implantation technology. The thickness of the modified AlN layer was controlled by implantation energy. Phase structure and corrosion resistance of AlN layer were also investigated.

### 2 MATERIALS FABRICATION AND CHARACTERIZATION

Commercial QC-10 alloy was introduced by Alcoa company in the United States. The experiment was carried out on the plasma ion implantation and deposition apparatus (FD-1200 K), whose parameters are as follows: pulse width 30  $\mu$ s, radio frequency power 400 W, implantation time ~ 4 h, injection dose  $2 \times 10^{17}$  to  $1 \times 10^{18}$  N<sup>+</sup>, Vacuum chamber pressure  $4 \times 10^{-3}$  Pa, and working gas pressure 0.8 Pa. Different values of electrical voltage such as 18, 21, 24, and 27 kV were used, and are defined as S18, S21, S24, and S27, respectively. Phase structure was investigated by Bruker D8 X-ray diffractometer (Germany), whose accelerated voltage and current are 40 kV and 40 mA respectively. Cu-K $\alpha$  radiation with grazing angle of 1°, step of 0.02°, and period of 0.2 s was used. The chemical valence state of AlN-modified layer was determined by electronic X-ray photoelectron spectroscopy (XPS, PHI5700 System, USA). Al target was chosen as the irradiation source and the denudation was conducted using 4 kV argon ion gun. The erosion area was 4  $\times$  4 mm and etching rate was 4 nm/min. At the same time, the element peak position was calibrated at C18284.6 eV. The corrosion was measured using Princeton electro-chemical apparatus. NaCl solution (3.5 wt%) was chosen as the corrosion medium. Surface morphology of QC-10 alloy before and after corrosion was observed by using a scanning electron microscope (SEM, JMS-6360 LV, Japan).

### 3 RESULT AND DISCUSSION

The small grazing angle in the X-ray diffraction pattern before and after plasma ion implantation of nitrogen in the QC-10 alloy is shown in Fig. 1. It is evident from the figure that the main peak of  $Al_2O_3$  and Al phase could be detected from the matrix QC-10 alloy, while other peaks of the AlN phase were found as main phase after the implantation of nitrogen in the QC-10 alloy. Meanwhile, the width of AlN diffraction peaks are broad, indicating the existence of polycrystalline cubic AlN phase in the surface of QC-10 alloy after plasma ion implantation. The presence of  $Al_2O_3$  peak was determined by insufficient vacuum degree during the plasma ion implantation process. The diffraction peak intensity of the AlN phase first increased and then reduced with the gradual increase of implantation electric voltage. The highest diffraction peak intensity was observed at the implantation electric voltage of 21 kV.

XPS peak of QC-10 alloy under 24 kV implantation voltage is shown in Fig. 2. The plasma ion-implanted QC-10 alloy was dealt with denudation about 120 s. The results showed that the binding energy of the  $Al_{2p}$  spectrum peak (73.8 eV) is

very close to that of the characteristic peaks of Al (72.7, 73.6, 74.8 eV). Similarly, the binding energy of  $N_{1s}$  spectrum peak (389.4 eV) was closed to that of XPS characteristic peaks of Al (397.4 and 381.4 eV). Therefore, the elements Al and N exist as AlN phase in modified films. Furthermore, the AlN phase existed even at the depth of 12 nm in the modified layer.

The dynamic polarization curves of the substrate QC-10 aluminum alloy and modified QC-10 alloy under different implantation voltages in NaCl solution are shown in Fig. 3. During corrosion process, hydrogen evolution process occurred

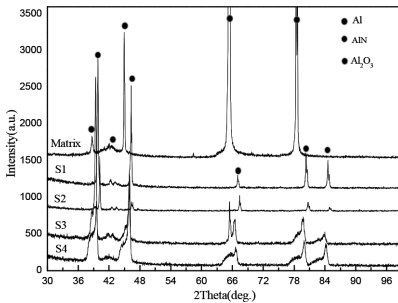


Figure 1. XRD pattern before and after plasma ion implantation of nitrogen in QC-10 alloy.

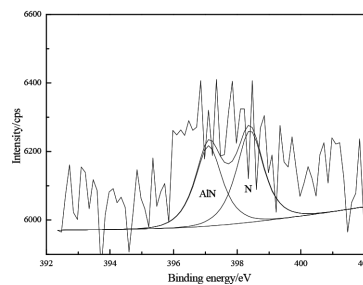
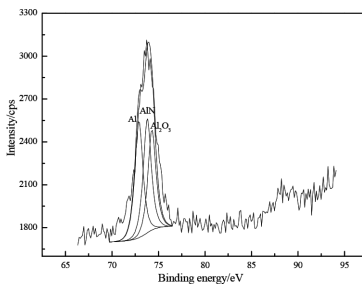


Figure 2. XPS fit spectra of  $Al_{2p}$  and  $N_{1s}$  after sputtering for 120 s.

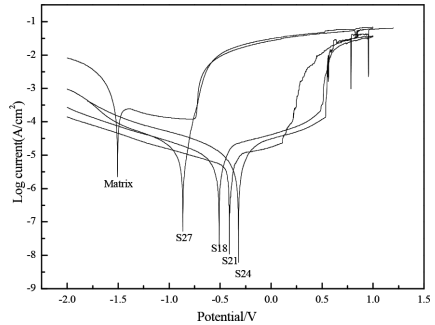


Figure 3. Polarization curves of QC-10 specimen under different implantation voltages.

Table 1. Corrosion parameters of QC-10 alloy under different implantation voltages.

Specimen	Current density (A/cm <sup>2</sup> )	Polarization resistance (Ω · cm <sup>2</sup> )
S0	$3.601 \times 10^{-4}$	157.20
S18	$4.282 \times 10^{-6}$	5,385.7
S21	$3.975 \times 10^{-6}$	9,923.8
S24	$3.056 \times 10^{-6}$	13,404.6
S27	$6.525 \times 10^{-6}$	9,902.9



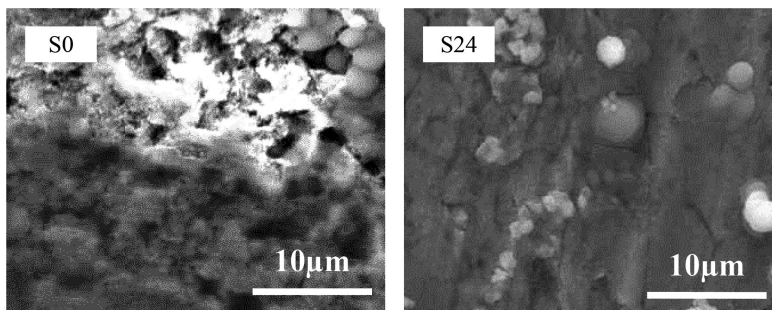


Figure 4. Surface morphologies of QC-10 alloy before and after chemical corrosion.

in the cathode and  $\text{Al}^{3+}$  ion was transferred from QC-10 matrix to NaCl solution in the anode. Thus, the corrosion rate of QC-10 alloy mainly depends on anodic reaction. The corrosion potentials at electric voltages 27, 24, 21, and 18 kV were about  $-0.851$ ,  $-0.627$ ,  $-0.417$ , and  $-0.305$  V, respectively. However, corrosion potential of the QC-10 matrix was about 1.5041 V. The thickness of AlN films on the QC-10 alloy surface increased with the increase of electric voltage, and the corresponding corrosion potential increased with further increase of AlN film thickness.

The corrosion current density and linear polarization resistance of QC-10 alloy before and after implantation are shown in Table 1. It is evident from the table that after implantation of nitrogen, the specimens showed much lower corrosion current density and corrosion current intensity (about two orders of magnitude) than the QC-10 alloy. Moreover, corrosion potential of the specimens varied from  $-1.504$  (for QC-10) to  $-0.305$  V (for S24). Therefore, it can be concluded that corrosion current gradually decreases with increase of electrode potential. According to Faraday's law, corrosion rate is proportional to corrosion current, which indicates that corrosion resistance of specimens significantly increases after nitrogen implantation. AlN films with appropriate thickness would effectively restrain corrosion reaction. The optimized QC-10 specimen with best corrosion resistance was found at the implantation electric voltage of about 24 kV.

The surface morphologies of QC-10 alloy before and after corrosion reaction are shown in Fig. 4. Deep corrosion crack and pit could be found on the surface of the QC-10 alloy substrate without nitrogen implantation. The corrosion crack was examined under nitrogen implantation in S24 specimen. The crack was found to be extended from the surface to the interior of the QC-10 alloy substrate. The modified AlN layer formed by nitrogen implantation could improve the corrosion resistance of QC-10 alloy.

#### 4 CONCLUSION

Modified AlN layer could be formed on the surface of QC-10 alloy after plasma ion implantation of nitrogen. The cubic AlN phase was detected as the main phase. The formation of AlN layer could improve the corrosion resistance of QC-10 aluminum alloy, and the corrosion current intensity of specimen decreased two orders of magnitude after plasma ion implantation of nitrogen. The optimized specimens of QC-10 alloy with best corrosion resistance were found at the electric voltage of about 24 kV.

#### ACKNOWLEDGMENT

The authors are grateful to the support of the Science and Technology Innovation Team of Jiamusi University (No. CXTD-2013-03).

Correspondence should be addressed to Yun-Long ZHANG; ylzhdr@126.com.

#### REFERENCES

- [1] Geory Merges. Injection mold manufacturing engineering. Chemical Industry Press.2003:17–20.
- [2] T. Yamanishi, Y. Hara, R. Morita, et al. Profile of implanted nitrogen ions in Al alloy for mold materials [J]. Surface and Coating Technology, 2001, 136: 223–225.
- [3] S.S. Kumari, U.T.S. Pillai, B.C. Pai. Synthesis and characterization of in situ Al–AlN composite by nitrogen gas bubbling method[J].Journal of Alloys and Compounds, 2011:2503–2509.
- [4] G.F. Iriarte, D.F. Reyes, D. González, et al. Influence of substrate crystallography on the room temperature synthesis of AlN thin films by reactive sputtering[J]. Applied Surface Science, 2011, 257: 9306–9313.
- [5] L.F. Xia, J.X. Liao. Tribological behavior of gradient modified layer on 2024 Aluminum alloy modified by plasma-based ion implantation. Wear, 2004, 256: 840–845.
- [6] R.J Rodriguez, A Sanz, A Medrano. Tribological properties of ion implanted Aluminum alloys [J]. Vacuum, 1999, 52: 187–192.



**Taylor & Francis**

Taylor & Francis Group

<http://taylorandfrancis.com>

# Exploring research theories and methods of rural settlement landscape from a multidisciplinary perspective

Nan-xi Wang & Qi Lu

State Key Laboratory of Subtropical Building Science, School of Architecture, South China University of Technology, Guangzhou, China

**ABSTRACT:** Rural settlement landscape, on the one hand, can provide various ecosystem services to human beings and, on the other hand, is an important cultural landscape. Thus, protection, preservation, and maintenance of rural settlement landscape are of great significance to a nation's benign development. On the basis of sorting out the research category and significance of rural settlement landscape, this paper reviews the research status of rural settlement landscape from the perspective of landscape architecture. Under such a background, it refers multidisciplinary research theories and methods of ecosystem service, ecological planning, landscape urbanism, and landscape gene with the purpose of raising multi-dimensional perspectives for the research on Chinese traditional rural settlement landscape and providing multivariable ideas for the protection and development of rural settlement landscape.

**Keywords:** Landscape architecture; rural settlement landscape; multidisciplinary perspective; research theories and methods

## 1 RURAL SETTLEMENT LANDSCAPE FROM THE PERSPECTIVE OF LANDSCAPE ARCHITECTURE

### 1.1 *Research category and significance of rural settlement landscape*

Traditional settlement, also called historical and cultural settlement, refers to ancient cities, towns, and villages that preserve obvious historical and cultural features and remain relatively intact in historical styles. Traditional settlement landscape is a generic term of people's visual perception and mental imagery brought by the internal and external forms of traditional settlements as well as their interactional settlement complexes<sup>[1]</sup>. Rural cultural landscape occupies a substantial proportion of research works on traditional settlement landscape, possesses strong continuity characteristics, and is full of human production atmosphere. Rural landscape is different from natural landscape with few human markings and is also distinct from cultural landscape designed with a purpose. Instead, it is a local symbol, accumulating the history of local development, recording ethnic historical and cultural information, preserving the essence of traditional community culture, and containing abundant landscape genes.

Traditional rural landscape reflects the adaptation of cultures and rural lands in different historical periods to the technologies of the time, and this

continuous change will go on in the current countryside evolution<sup>[2]</sup>. The connection between nature and the special spirit formed in rural cultural landscape is of great reference value in promoting sustainable modern land-use method and technology and can also maintain or strengthen natural environment value and ensure biological and cultural diversity in many regions around the world<sup>[3]</sup>.

### 1.2 *Research status of rural settlement landscape*

The research of rural landscape and rural settlement landscape has been launched in many subjects producing substantial results. In recent years, the research of rural landscape has developed rapidly in three fields: landscape ecology, human geography, and architecture & planning<sup>[4]</sup>.

For the rural settlements in rural landscape, especially the villages that preserve rich cultural relics of great historical value or commemorative significance and can reflect traditional historical characteristics and local ethnic features in a relatively comprehensive way, the domestic research on them has been increasing. It not only adopts some Western theories and methods, but also presents certain local research theories and methods. At present, researchers have been carrying out research mainly from perspectives such as morphology, typology, settlement, vernacular architecture, preservation and utilization of heritages, and tourism economics.

Landscape architecture is an interdisciplinary subject focusing on ecology, geography, and architecture. It also covers the range of philosophy, history, and art subjects and highlights practice. Currently, Chinese landscape architecture mainly focuses on landscape characters, cultural relics, ecological protection, and so on. It always starts from the macro-view of ecological planning and concentrates on natural patch and corridor conservation planning, land use, and rural landscape planning as well as rural human settlement environment and settlement planning<sup>[5]</sup>.

Landscape ecology theory and method is applied in natural patch and corridor conservation planning, which combines spatial analysis method that geography highlights and ecosystem function that ecology emphasizes. Rural land-use planning is carried out from land-use pattern, land suitability evaluation, and land-use planning. It seeks for optimal landscape utilization with the application of landscape suitability evaluation theory and method, and in the process of determining suitability, it transforms from only considering ecological factors to simultaneously considering the changing economic environments: demand and supply of land, human needs and change of value, political reality, and new technologies. The theories and methods of rural human settlement environment and settlement planning are relatively few. The rural human environment is improved mainly from the aspects of ecological courtyard and ecological community.

Whether some theories are applicable to the research of rural landscape remains to be further described systematically, such as the so-called patch-corridor theory and the status of landscape ecology that only obtains some results from the research of natural ecology. The ecology studied from the perspective of landscape ecology has some differences from artificial ecology, so the relationship between landscape ecology and human is very ambiguous. Hence, it should be further considered to apply them directly in living environment and agricultural production.

Compared with the above-mentioned subjects, although the research category of landscape architecture has a high contact ratio with rural landscape, the theories and methods of other subjects should be drawn upon at present stage due to immature development in this subject.

## 2 RESEARCH METHODS OF RURAL SETTLEMENT LANDSCAPE FROM A MULTIDISCIPLINARY PERSPECTIVE

The main purpose of this paper is to determine the view of landscape architecture on the complicated

research object of rural settlement landscape depending on its own characteristics and drawing support from theories and methods of other subjects as well as the general theories and methods within its own subject.

Rural settlement landscape has multiple values. Therefore, the ultimate purpose of rural landscape research is to properly conserve and reasonably utilize the values of rural settlement landscape and seek for theories and methods to improve its ecological and cultural values so that its resources can sustainably serve humankind. Therefore, the paper puts forward the following four theories and methods for its reference.

### 2.1 *Reference of ecosystem service theory and method*

The relationship between ecosystems as well as its services and human well-being has become the central point of the current ecology research. Ecosystem services mean the environmental conditions and effects for human to survive and develop and are the benefits people obtain from ecosystems in a direct or indirect way. Compared with city ecosystem, rural ecosystem is more functional in self-improvement and can provide diverse ecosystem services for human beings. Thus, the research core of rural settlement landscape is to continue and strengthen this service function.

The understanding of ecosystem service concept should be further improved. Ecosystem services come into being based on human beings, and the ecosystem service arisen from rural settlement landscape has certain differences from city ecosystem service. City ecosystem service focuses more on human needs, while rural ecosystem service not only centers on human needs but also considers nature much. Therefore, it will fail to understand the contents of ecosystem services comprehensively only by virtue of theories, but should go deep into countryside to conduct a long-term observation and investigation and acquire necessary information from the people closely linked with land.

Specific research methods can seek help from the value assessment of ecosystems in geography. According to the theories of environmental economics and resource economics, various methods can be applied to quantitatively assess the magnitude of ecosystem services. The method centering on survey is also called simulate market method, which directly or indirectly consults people's willingness to pay and then calculates the ecosystem value<sup>[6]</sup>.

Other traditional research methods such as field survey and interview that are often used in geography and sociology can also be applied. First-hand data about ecosystem services can be acquired through field observation, investigation, interview,

fixed spot observation, and sampling. Survey and interview play an important role in the research of ecosystem services, which can make up for the lack of information in humanities, emotions, behaviors, and information. For example, the influence of social, economic, and cultural factors on the perceptions and values of ecosystem services can be achieved through survey and review.

## 2.2 *Reference of ecological planning theory and method*

Since McHarg's first proposal, there have been many proposals about "integrating design into ecology" for landscape architecture. With the deepening knowledge of ecosystem concept and its functions in coordinating human activities with nature, the concept of ecosystem also flourishes as an organizational research principle. In fact, landscape planning based on ecosystems has become an academic consensus and has also formed an independent academic sector in Western countries. The contents of ecological planning have achieved a great depth and width, and its methods also bloom in radiant splendor. Especially after the 1980s, the rapid development of landscape ecology and human ecology promotes the understanding and application of ecology from the perspective of landscape architecture.

The landscape suitability evaluation method, humanity ecology planning method, and ecosystem and land classification method in ecological planning are another aspect that can be drawn upon, especially the humanity ecology method, as it offers careful study of landscape value, need, desire, and suitable mechanism under social structure. Oral narrative, text description, and qualitative analytical technique can be used to conduct structural matching by building model under the opportunities and limitations of natural and ecological environment<sup>[7]</sup>.

## 2.3 *Reference of landscape urbanism theory and method*

In recent years, the international exploration of landscape urbanism and ecological urbanism provides many new design ideas for landscape planning based on ecosystem services.

Landscape urbanism takes a dialectical thinking of the relationship between landscape architecture and ecology, just as James Corner advocated that landscape architecture should build a creative relationship with ecology in order to explore "a new possibility of cultural practice with more significance and imagination instead of only concerning improvement, compensation, aesthetics or taking commodity need as guideline"<sup>[8]</sup>. The discussion of landscape urbanism determines the great signifi-

cance of infrastructure and its related landscapes in modern urban development and public space. Landscape (ecological) urbanism not only pays attention to high-density city areas and public space, but is also involved in the whole landscape. However, its core ideas and design techniques can also be applied in rural areas, that is, rural settlement landscape is also one of the advocated infrastructure systems and public landscapes. Landscape (ecological) urbanism uses ecological methods to deal with sites, takes natural process as design forms, and respects the natural evolution of sites to solve problems. Relying on these core ideas, it applies landscape preference and ecological remediation, uses landscape to separate space, and reduces human intervention. All these are detailed methods of landscape urbanism theory.

Although this paper puts forward that the research of rural settlement landscape can use the theories and methods of landscape urbanism and landscape ecology for reference, their advent and development are not aimed at rural landscape and rural settlement landscape. The natural law and ecological base of rural landscape are quite different from city landscape, which is the research object of landscape urbanism and is also slightly different from the pure nature, which is the research object of landscape ecology. Therefore, those theories and methods cannot be applied mechanically but should be absorbed selectively according to the characteristics of rural settlement landscape. Similarly, there are many theoretical branches and issues about ecological planning, and many problems remain to be demonstrated or further discussed. While the implementation of continuous design is slightly difficult to proceed, feasible methods should be proposed according to the characteristics of rural landscape.

The digital landscape, computer simulation, and visualization methods in landscape architecture can offer an aid as well. Model simulation and computer simulation are important research methods, such as simulating ecosystem service related with water through SWAT (Soil and Water Assessment Tool), simulating ecosystem service about soil conservation and sediment deposition through RUSLE (Revised Universal Soil Loss Equation). Laypeople can also simulate hydrology dynamic, sediment scour and deposition, pollutant dispersion, and degradation as well as surface runoff and catchment through CFD software that is relatively mature at present, such as Flow3d, Xflow, Fluent, Urbanwind, and Vasari.

## 2.4 *Reference of human geography landscape gene theory and method*

It is difficult to acquire the humanistic value for the research object of rural settlement landscape.

Affected by the complicated natural and geographical conditions and diverse ethnic cultures, Chinese rural landscape presents a rich abundance, behind which always implies a special “soul” owned by Chinese traditional settlement landscape, so it has a sense of identity from the whole. The coexistence of identity and diversity in Chinese traditional settlement landscape needs to be explored, recorded, preserved, and succeeded through rational means. In order to explore landscape characteristics, it is necessary to dissect its cultural genes, recover its historical memories, and determine the relationship among landscapes. Landscape gene theory is one of the positive and effective guiding theories that has been demonstrated and gained certain effects.

The research about settlement history and geography in the field of geography is mainly concentrated on settlement selection, spatial layout, morphological characteristics, as well as its evolution rule. Indeed, besides traditional explanations and two-dimensional expressions, the research on spatial features, manifestation forms, and the inner connotations of historical and cultural landscape can also draw support from the concept of biological “gene”<sup>[9]</sup>. It is well known that gene originates from biology and carries genetic information passed by copying. However, genetic mutation may also occur, influenced by external environments. The biological gene concept can be promoted into the research category of settlement landscape in order to explore the original genes of cultural landscapes in different rural settlements and then build corresponding genetic maps, thus adding the scientific sense and expressiveness of research.

### 3 CONCLUSION

To conclude, rural settlement landscape possesses multi-dimensional values of ecology, culture, and so on. The research of rural settlement landscape also has strong comprehensive, intersectional, and exploratory characteristics; thus, it needs to integrate multidisciplinary research theories and methods to conduct a comprehensive demonstration to analyze and solve Chinese rural and traditional problems.

In the goal of sustainable development, this study puts forward using multidisciplinary

research theory and method in order to bridge the gap between ecology and design, playing efficacy to maximum, thinking from the perspective of planning and design as a whole cycle to deal with the issue of sustainable development of natural and human of rural settlement landscape, so as to provide new thoughts to research and development of the rural settlement landscape and finally create a sustainable landscape in favor of human well-being.

### ACKNOWLEDGMENT

This study is supported by Postdoctoral Science Foundation of China, Preferences for Rural Landscape in Lingnan Area of China Based on Ecosystem Culture Service Perspective (item number: 2015M582386); Fundamental Research Funds for the Central Universities in 2015, Study on the Value and Perceptual Evaluation of Rural Landscape in Lingnan Region (item number: x2 jz-D2155150).

### REFERENCES

- [1] Liu Peilin. Establishment and application research of traditional settlement landscape genome [D]. Beijing: Peking University, 2011: 1–240.
- [2] (Australia) Jane Lennon, (edited and translated by) Han Feng. Rural landscape [J]. Chinese Landscape Architecture, 2012 (3): 19–21.
- [3] Shan Jixiang. Walking into the world of cultural landscape heritage [M]. Tianjin: Tianjin University Press, 2010, 81.
- [4] Qian Yun. The Research Scope and Methodology of Vernacular Landscape with Practice in Landscape Architecture. 2014 (12): 31–35.
- [5] Wang Yuncai. Principles of landscape ecological planning [M]. Beijing: China Architecture & Building Press, 2014, 7.
- [6] Li Shuangcheng, etc. The Geography of ecosystem service [M]. Beijing: Science Press. 2014, 5.
- [7] Forster Ndubisi. Ecological planning: A historical and comparative synthesis [M]. Beijing: China Architecture & Building Press, 2013.
- [8] Charles Waldheim. The landscape urbanism reader [M]. Beijing: China Architecture & Building Press, 2010, 12.
- [9] Liu Peilin. Home landscape and gene—A deep interpretation of traditional settlement landscape gene [M]. Beijing: The Commercial Press, 2014, 3.

## Research on reinforced methods for a concrete structure

Mei-xiang Zhang, Bo Sun & Xiao-yi Zhang

*School of Architectural Engineering, Xinyu University, Xinyu, Jiang xi, China*

**ABSTRACT:** With the continuous development of building reinforcement technique, several reinforcement methods appear, with more advanced features. Experts and scholars worldwide have conducted several studies to put forward a new, high technical content, with an important social benefit and huge economic benefit reinforcement technique. This paper refers relevant studies on the concrete reinforcement techniques conducted worldwide to introduce several common reinforcement concrete methods; especially, the Fiber-Reinforced Polymer (FRP) reinforcement technique is reviewed. On this basis, the development trend of the reinforcement method is discussed finally.

**Keywords:** Concrete structure; FRP; Reinforcement; NSM; Prestressed reinforcement

### 1 INTRODUCTION

At present, reinforced concrete structures are widely used; however, because of improper design, usage, and maintenance; natural disorders such as earthquake, fire, and flood; and higher requirement, these buildings have many problems. Some problems endanger the safety of the structure. Structural strengthening requires low investment to repair and restore the bearing capacity of these structures. In addition, with the development of economy, to ensure the new requirements, such as the need to change the function or add layer building, these buildings should be reinforced. As strengthening technology has attracted increasing attention, the author combined the theoretical and experimental situations worldwide, summarized the common reinforcement methods, and provided the basis for future research.

### 2 RESEARCH ON TRADITIONAL REINFORCEMENT METHODS

Traditional reinforcement methods include increasing cross-section reinforcement, steel reinforcement, prestressing reinforcement, replacement of concrete reinforcement, increasing and support reinforcement. These construction processes are simple and have a mature design and construction experience. However, these traditional methods have many limitations such as large construction space, long duration, limited use, and poor corrosion resistance. Fiber-reinforced polymer (FRP) is a composite material, which is made of high-strength continuous fiber by following a certain

rule. Because of its advantages such as lightweight, high strength, simple construction, good design, good corrosion resistance, low thermal expansion coefficient, and wide application, it is considered the key to solve the problem of reinforcement corrosion. It is widely used in the field of civil engineering.

### 3 FRP REINFORCEMENT TECHNOLOGY

#### 3.1 *Externally bonded FRP reinforcement technology*

Externally bonded FRP reinforcement technology has been studied for more than 20 years with regard to its engineering application, and the related theory and technology is relatively mature. However, the fiber sheet strengthened by external material can be easily damaged because of the insufficient high-strength performance, possibility of easy damage of FRP paste by undesirable environmental conditions, easy wearing, poor fire resistance, and poor adjacent member. Therefore, this kind of reinforcement method is gradually replaced by externally prestressed FRP reinforcement technology and embedded reinforcement method.

#### 3.2 *Externally prestressed FRP reinforcement technology*

This technology combines the prestressed reinforcement method and the externally bonded fiber sheet reinforcement method. Although the structure of the ultimate load increases significantly with the externally bonded fiber sheet reinforcement method, the crack load and yield load

increase only slightly, because of the lag of FRP strain. In order to improve this situation, according to the principle of prestressed technology, externally prestressed FRP reinforcement method is proposed.

Owen Rosenboom and others[1] conducted research on six prestressed CFRP and SRP (steel fiber) reinforced concrete beams under static load and fatigue load and established the specification design of fiber material system with 16 other beams. Their result shows that the SRP structure efficiency is higher than that of CFRP materials.

Wei-chen Xue[2] from Tongji University studied the fatigue performance of the partial prestressed CFRP reinforced concrete beams. He Chao[3] from Southeast university conducted shear test on four CFRP prestressed model beams and studied the effect of different experimental factors on the shear properties of CFRP externally prestressed concrete beam, such as the arrangement of prestressed reinforcement and shear span-to-depth ratio.

Although this technology has many advantages, because of limitations such as improper measures of anchoring or improper paste quality, FRP is prone to strip damage and it is difficult to enhance the stiffness of the flexural member with large deflection or the concrete member with severe cracks, thereby reducing its serviceability limit. The embedded reinforcement technology has arisen at the critical moment.

### 3.3 *Embedded reinforcement technology*

Embedded reinforcement technique (near-surface-mounted, NSM) is developed in recent years as a new type of FRP reinforcement technology. This reinforcement technology involves the FRP reinforcement or FRP batten with epoxy resin embedded in the concrete cover of reinforced concrete members. Compared with externally bonded CFRP sheet method, this method has the advantages of high efficiency, high strength, corrosion resistance, good impact resistance, durability, fire resistance, and reducing surface treatment.

De Lorenzis and others[4] conducted a detailed analysis on the factors affecting reinforcement such as bending, shear, and bonding performance based on the results of existing research. They also concluded that the existing research is not sufficient and further studies are needed in the direction of long-term structure performance. Xue-jun He and Chao-yang Xhou[5] from Central South University studied the failure process, mechanical performance, strain distribution, and deflection deformation law of an embedded CFRP reinforcement beam on six full-scale experimental flexural reinforcement concrete beams. Zhao Jin[6] from

Henan Polytechnics University and others studied different experimental factors on the shear properties of embedded CFRP strip shear with concrete beams through nine embedded CFRP reinforcement beams, two externally bonded CFRP strip reinforced beams, and two concrete beams. The experimental factors include the amount of reinforcement, shear span-to-depth ratio, groove spacing, and slot size.

Test results show that failure of non-prestressed reinforcement beams is due to crushed concrete, damaged reinforcement material, and bonding failure. There is a reliable bond between reinforcement and concrete, which is the basic premise of the two types of materials that can work together. The embedded non-prestressed reinforcement has little effect on the cracking load of the component, and it cannot reduce the development of the crack, which can be solved by applying prestressed FRP tendons.

### 3.4 *Embedded prestressed reinforcement technology*

As the embedded prestressed CFRP reinforcement is less studied, a special anchorage needs to be developed, because of CFRP material anisotropy and low shear strength.

#### 3.4.1 *Embedded prestressed FRP reinforcement technology*

Hakan Nordin and Bjorn Taljsten[7] conducted a preliminary test and showed that prestressed reinforcement method is superior to other methods. Moataz Badawi and Khaled Soudki[8] conducted a monotonic loading test through four prestressed CFRP tendons embedded reinforcement concrete beams and found that the bearing capacity of reinforced beam increased by 90% on 40% prestressing degree, ultimate bearing capacity increased by 79% on 60% degree. They established an effective model, which forecasted flexural bearing capacity of prestressed reinforcement beam using the method of cross-section. Ya-hong Ding [9] from Henan Polytechnics University conducted a study on the bending performance of three CFRP tendons embedded reinforcement concrete beams and nine prestressed CFRP tendons embedded reinforcement concrete beams.

#### 3.4.2 *Embedded prestressed spiral rib steel wire reinforcement technology*

Ya-hong Ding first proposed the spiral rib steel wire as a new material, and in the same year, with Zhao Jin, she conducted experimental studies on embedded non-prestressed spiral rib steel wire reinforced concrete beams. The results showed that the technical effect is better than FRP reinforcement,



and the spiral rib steel wire is more likely to pre-stress. Then, Ya-hong ding, for the first time, studied monotonous static load for embedded prestressed spiral rib steel wire reinforcement concrete beams and showed that this effect is favorable. Furthermore, it can not only overcome the externally bonded FRP sheet debonding damage, but also can make up embedded non-prestressed spiral rib steel wire reinforced concrete beam, increase the cracking load and ultimate load of strengthened beams, and reduce beam crack propagation.

#### 4 SUMMARY AND OUTLOOK

This paper analyzed the traditional strengthening methods and FRP reinforcement technology in detail and arrived at the following conclusions:

1. The traditional reinforcement methods are directly reinforcing components, but not without limitations and deficiencies such as increased weight and expensiveness. With the development of the new reinforcement technology, the application of lightweight high-performance materials is the inevitable development trend of strengthening technology.
2. Fiber-reinforced composite materials are widely used; from externally bonded reinforcement, externally non-prestressed reinforcement, and embedded reinforcement to embedded prestressed reinforcement technology, strengthening technology is gradually becoming perfect and will be widely used in practice.
3. Experts and scholars carried out related experimental studies, but the experiment parameters and objects are different even for the same research direction. This makes the reinforcement technology research more comprehensive.

In order to make strengthening technology more mature, more widely in engineering practice, the following points need to be further studied:

1. Further research on theory and application of strengthening technology must be conducted. The current strengthening technology research shows that traditional strengthening methods have some defects. FRP reinforcement technology and embedded prestressed reinforcement techniques stand out, but the research on this kind of strengthening technique theory has just started, engineering practice is less, and hence the theory and application research on strengthening technology needs further research.
2. The development of composite methods is important. Combination of two or more

reinforcement methods, such as embedded prestressed spiral rib steel wire reinforcement method, increases the efficiency of the reinforcement by the combined advantages of the methods involved.

#### ACKNOWLEDGMENTS

1. "Experimental study and finite element analysis on RC beams strengthened with NSM prestressed spiral rib wires". Science and technology project in Jiangxi province education department in 2015 (GJJ151216).
2. "Research on the engineering application of reinforced methods for concrete structure". Field studies program of Xinyu University in 2015 (xj201505).

#### REFERENCES

- [1] Owen Rosenboom, Catrina Walter and Sami Rizkalla. Strengthening of prestressed concrete girders with composites: Installation, design and inspection [J]. *Construction and Building Materials* 23 (2009): 1495–1507.
- [2] Xue Weichen, Qian Wei, Tan Yuan. Studies on Fatigue Guidelines for Concrete Beams Partially Prestressed with CFRP Tendons [J]. *Journal of Tongji University (Natural Science)* 2008, 36(7):875–879.
- [3] He Chao. Shear Resistance Experiment Study for Externally Prestressed Concrete Beams[D]. Nanjing: Master Degree Thesis of Southeast University, 2007.
- [4] L. De Lorenzis, J.G. Teng. Near-surface mounted FRP reinforcement: An emerging technique for strengthening structures. *Composites: Part B* 38 (2007) 119–143.
- [5] He Xuejun, Zhou Chaoyang, Xu Ling. Experimental study on the flexural behavior of reinforced concrete beams strengthened with near-surface mounted CFRP laminates. *China Civil Engineering Journal*, 2008, 41(12).
- [6] ZHAO Jin, ZHANG Xue-li. Experimental study of shear characteristic of reinforced concrete beams strengthened with CFRP laminates. *Concrete*. 2007, 217(11):8–11.
- [7] Concrete Beams Strengthened with Prestressed Near Surface Mounted CFRP [J]. *Journal of Composites for Construction*. January/February 2006:60–68.
- [8] Moataz Badawi, Khaled Soudki. Flexural strengthening of RC beams with prestressed NSM CFRP rods—Experimental and analytical investigation [J]. *Construction and Building Materials* 23 (2009) 3292–3300.
- [9] Yahong Ding. Research on Flexural Behavior of Reinforced Concrete Beams Strengthened with Prestressed Near Surface Mounted Tendons [D]. Jiaozuo: Henan Polytechnic University Ph.D. thesis, 2009.



**Taylor & Francis**

Taylor & Francis Group

<http://taylorandfrancis.com>

# Analysis of the factors influencing energy consumption of a passenger transport station

Xing-kai Meng

*Research Institute of Highway MOT, Beijing, China*

Zhao Yan

*Chang'an University, Shanxi, China*

Wei-wei Heng

*Ji Lin University, Jilin, China*

Cheng Zeng

*Research Institute of Highway MOT, Beijing, China*

**ABSTRACT:** Passenger transport station is an important infrastructure that supports the development of the transportation industry, and reducing the energy consumption of such station is very important to realize the green, low-carbon transportation system. This paper focuses on the analysis of the factors affecting energy consumption of passenger transport station and puts forward the following suggestions: reasonable selection of passenger transport station site and scientific design functional area, active utilization of energy-saving materials and energy-saving design during station construction, use of energy-saving facilities, strengthening of passenger transport station internal energy-saving emission reduction management and energy consumption monitoring, and active application of energy-saving measures of information technology and new energy technologies.

**Keywords:** passenger transport station; energy consumption; influence factors; analysis

## 1 INTRODUCTION

The Chinese transportation industry is not only a basic and service industry for the development of national economy, but also an important energy-hungry industry. It significantly contributes to the national economy and industrial development. Statistics shows that transportation energy consumption accounts for about 10% of the total energy consumption in 2014. The main forms of consumed energy included gasoline, diesel, natural gas, and other non-renewable energy sources, which produced huge amounts of CO, HC, and other gas pollutants<sup>[1]</sup>. In 2009, the National Development and Reform Commission (NDRC) formulated and implemented the “guidance for promoting the development of low-carbon economy”, which proposed a developing pattern of “green economy and low-carbon economy” and put forward the goal of “by 2020, the carbon dioxide emissions of per unit of GDP will decline by about half of which in 2005”. In 2013, the Ministry of Transportation published the policy documents of “guidance for accelerating the development of green recycling low carbon transportation”; adopted plan

to establish a green recycling low-carbon transportation system in principle by 2020; enacted and enforced the evaluation index system of green recycling low-carbon transportation provinces, cities, roads, and ports; and promoted the construction and development of green, low-carbon transportation system. Passenger transport station is an important infrastructure to promote the development of transportation industry and establish the green recycling low-carbon transportation system<sup>[2]</sup>. Among the factors affecting energy consumption in passenger transport station operation steps, promoting and implementing the development of green, low-carbon environment and operation of highway transportation are of paramount importance.

## 2 ANALYSIS OF THE FACTORS AFFECTING ENERGY CONSUMPTION OF PASSENGER TRANSPORT STATION

Passenger transport station involves passenger transportation and other services. According to the national functional localization of passenger

transport station, electric energy, natural gas, and heating power are the main forms of energy consumed in passenger transport station operation steps. Electric energy is mainly used for architectural lighting, heating, ventilation, and other facilities, and natural gas is mainly used as fuel for vehicles. There are several other factors that affect passenger transport station operation steps. These mainly include reasonable selection of passenger transport station site and scientific design functional area, active utilization of energy-saving materials and energy-saving design during station construction, use of energy-saving facilities, strengthening of passenger transport station internal energy-saving emission reduction management and energy consumption monitoring, and active application of energy-saving measures of information technology and new energy technologies<sup>[3]</sup>.

### 2.1 Passenger transport station site selection

Site selection indirectly influences the energy consumption of a passenger transport station. The urban passenger transport station should be located near railway stations or public transport transfer junctions and the rural passenger transport station should be located near population centers, in order to reduce the energy consumption<sup>[4]</sup>. Thus, the passenger transport station site selection should comply with local conditions, mainly the harmony of urban master plan, comprehensive transportation and arterial road, vehicle access conditions, population distribution, and other factors affecting passenger transport station energy consumption.

### 2.2 Passenger transport station functional area design

According to the regulation of transportation industrial standard “grade division and construction requirements of passenger transport station”, a passenger transport station should include station square, park, departure area, waiting room, ticket lobby, service occupancy, office occupancy, production auxiliary rooms, life auxiliary rooms, and other facilities and buildings. Both general layout and site facilities and building room layout can influence the energy consumption of passenger transport station in operation. Division of station facilities area, design of flow of traffic and population, presence of circuitry in each streamline, and convenience of other means of transportation can indirectly affect the energy consumption of passenger transport station<sup>[5]</sup>, such as adding lighting and safety facilities. The layout of both service occupancy and office occupancy can influence the

patency of flow of passengers and luggage, which is also closely related to energy consumption of passenger transport station.

### 2.3 Passenger transport station buildings

Passenger transport station should include service occupancy (waiting rooms, ticket lobby, control room, driver and trainman retiring rooms, security room, etc.), office occupancy, production auxiliary rooms (switching room, vehicle safety detecting set), life auxiliary rooms, and other facilities and buildings. It should keep energy conservation and emission reduction and ensure green and low-carbon environment. In the design of passenger transport station buildings, energy conservation design methods, application of energy-saving materials, and application of related energy-saving measures can influence the energy consumption of passenger transport station operation steps<sup>[6]</sup>. Reasonable shape coefficient of passenger transport station, low window-to-wall ratio, external sunshade, window opening area, natural lighting in design, energy saving and insulation material in construction can also efficiently decrease the energy consumption of passenger transport station operation.

### 2.4 Supporting facilities and equipment of passenger transport station

Green and low-carbon passenger transport station cannot be realized without energy conservation and emission reduction of supporting facilities and equipment. These include tickets equipment, heating or refrigeration equipment, bulletin equipment, lighting equipment, water supply and drainage equipment, and energy measurement equipment. Selection and deployment of facilities and equipment should conform to the related energy-saving standards.

#### 2.4.1 Heating or refrigeration equipment

Data show that passenger transport station energy consumption is mainly composed of air-conditioning, refrigeration, and heating systems. There are three aspects of energy consumption: (1) choosing heating or refrigeration equipment without knowing its energy efficiency, which will result in high energy consumption; (2) the energy source of heating or refrigeration system chosen is not reasonable; and (3) the cooling or heating load of air conditioner was not calculated exactly in the design step, which will result in too high load and high energy consumption. Studies show that the chosen heating or refrigeration equipment should have at least 20% energy-saving potential<sup>[7]</sup> to increase energy efficiency. Moreover, solar energy or geothermal energy should be used for heating or refrigeration if possible.

#### 2.4.2 *Lighting electrical equipment*

Data show that in the course of operation of the passenger transport station, about 20–30% energy consumption is by lighting and other electrical equipment (except air-conditioning equipment)<sup>[8]</sup>. Therefore, energy saving in lighting and electrical equipment is of paramount importance. The high energy consumption of electrical equipment in passenger transport station is due to lighting in the building and parking areas of the station, security detection, and publicity notices with old equipment. On the contrary, the undesired design of lighting control mode requires unnecessary illumination of each area, contributing significantly to the energy consumption of electrical equipment. Therefore, the passenger transport station should choose energy-efficient lighting facilities and equipment, the conditional passenger transport station; using solar energy for lighting, heating, and automatic escalator and using frequency conversion or induction-type energy-saving escalator are some of the possible options.

#### 2.4.3 *Water supply and drainage equipment*

Passenger transport station has a large flow of personnel and cleaning passenger vehicles is compulsory. Therefore, water consumption is very high in passenger transport station. In order to save water resources, high-efficient water-saving vehicle-cleaning equipment and sanitary appliances should be chosen. To save water, the conditional passenger transport station should have the following facilities: solar energy for heating or preheating, rain-water collection device, landscape water for vehicle cleaning, and water recycling equipment.

#### 2.4.4 *Energy-measuring equipment*

Energy-measuring equipment used in passenger transport station itself consumes energy, thereby emphasizing the use of low energy consumption products. “Energy conservation law” clearly stated that energy-consuming units should strengthen the management of energy metering and passenger transport station. These units should achieve accurate measurement of energy consumption to facilitate the timely replacement of old equipment and other energy-saving measures.

#### 2.5 *Energy conservation management*

Energy conservation management is the process of passenger transport station energy management and is also an effective means of saving energy and realizing low-carbon green passenger transport stations. Passenger transport stations should establish and improve energy conservation organization, and have the corresponding

personnel. In order to reduce energy consumption of high-energy-requiring equipment, facility and equipment management and other enterprises are used to monitor and fine management. Passenger transport stations should reduce waste of energy and materials and optimize the structure of energy use. Reasonable incentive measures should be developed to reward people with good energy-saving effect and improve the energy conservation awareness of the passenger transport station management staff.

#### 2.6 *Energy monitoring*

Passenger transport station energy monitoring has indirect effects on its energy consumption. Energy consumption in the stations can be measured by using metering equipment, and statistics and analyses should be conducted to understand the level of energy consumption and the energy-saving potential of the equipment. According to the statistics and analysis of energy monitoring data, reasonable energy saving should be realized to have a positive effect on energy conservation of passenger transport stations.

#### 2.7 *Application of information technology*

With the development of information technology, online ticketing system, automatic bag storage system, self-ticketing system, automatic fare collection system, and other facilities have been developed in passenger transport stations. The application of information technology not only facilitated passenger travel and reduced the operation cost and energy consumption of the station, but also it made the operation and management of passenger transport stations convenient.

#### 2.8 *Application of new energy technologies*

In some cities, renewable energy sources such as solar energy, geothermal energy, and other renewable energy have been effectively applied in passenger transport stations to reduce the dependence on fossil fuels, thereby reducing the energy consumption of these stations and carbon dioxide emissions. The Wuxi Jiangsu central station serves as a good example by utilizing geothermal technology for its heating and cooling purposes.

### 3 CONCLUSION

Passenger transport station is an important infrastructure that supports the development of the

transportation industry. In order to realize green, low-carbon transportation system, it is important to reduce the energy consumption of the passenger transport stations. There are many factors affecting energy consumption of the passenger station: passenger transport station location, design functional area, passenger transport station buildings, facilities and equipment, passenger transport station energy-saving and emission reduction management, energy monitoring, information technology, and new energy technologies. To achieve energy saving and emission reduction, the passenger transport stations should select an appropriate site and scientific design functional area, utilize energy-saving materials and energy-saving design for station construction, use energy-saving facilities, strengthen passenger transport station internal energy-saving emission reduction management and energy consumption monitoring, and actively apply the energy-saving measures of information technology and new energy technologies, thereby developing the green, low-carbon transportation industry.

#### ACKNOWLEDGMENT

This study was supported by the Transportation Energy Saving and Emission Reduction Ability Construction Project.

#### REFERENCES

- [1] Meng Xing-kai, Zhang Zhi-fang, Yang Dong-bo, et al. Research the method of reduce fuel consumption on foreign medium and heavy duty vehicle [J]. *Energy Conservation & Environmental Protection in Transportation*, 2014, 10(1): 13–18 (In Chinese).
- [2] Meng Xing-kai, Zhang Zhi-fang, Zeng Cheng, et al. Analysis of influence factors of freight vehicle fuel economy [J]. *Energy Conservation & Environmental Protection in Transportation*, 2013, 9(6):78–82 (In Chinese).
- [3] Zeng Cheng, Meng Xing-kai. Study on the evaluation index system of green low carbon road transport station [R], Beijing: Research Institute of Highway MOT, 2014 (In Chinese).
- [4] Dai Guang-chao, Study on Saving-energy Assessment for Passenger Station and Freight Terminal of Road Transport [D], Shanxi: Chang'an University, 2012.
- [5] Ernest Forman, Kirti Peniwati. Aggregating individual judgments and Priorities with the Analytic Hierare Process [J]. *European Journal of Operational Research*, 1998, 108: 165–169.
- [6] Chen Wen-rui. Problem Analysis and Countermeasures Research on Operations Management Of Road Freight Station [D], Shanxi: Chang'an University, 2012.
- [7] Mei Ning, Janda K B, Busch J F. World wide status of energy standards for buildings. *Energy*, 1999, 19(1): 27–44.
- [8] Study on Low-carbon and Green Development of Road Transportation by AHP-Entropy Method [D], Niaoling: Dalian Maritime University, 201.

# Environmental development of the reading room in the university library based on human factors engineering

Chuan-jie Xu

Reader Service Center of Library, Jiangnan University, Wuhan, P.R. China

**ABSTRACT:** Environmental influence is one of the most important factors that have an impact on one's reading activity. According to the analysis of the environmental factors of the reading room in the university library, an environmental model is designed by using human factors engineering. Based on the model, the combined influence of lighting and noise is mainly studied and readers' proposals are gathered and analyzed. Using the proposed approaches, an environment evaluation method is presented to improve the service quality of the university library.

**Keywords:** environment development; human factors engineering; service quality; reading room

## 1 INTRODUCTION

Construction of a good library reading room environment so as to improve reader satisfaction and library service quality is a key task for a university library in the Internet period [1]. Because the reading room of the university library is one of the most frequently visited places where students, teachers, and social readers acquire knowledge, it is important to enhance environment quality management. Human Factors Engineering (HFE) is a scientific research discipline based on psychology, physiology, anatomy, anthropometry, and other disciplines. It studies how to design the man-machine-environment system in accordance with human body structure and the physiological and psychological characteristics [2]. Its purpose is to achieve the best match between man and the environment, so that in different environments, people can work effectively, safely, healthily, and comfortably. Today, HFE approaches are used to determine effective countermeasures to solve the problem. In this paper, some factors of physiological and psychological characteristics of the readers are researched by using HFE to achieve a comfortable and safe environment for the reading room arrangement of universities' libraries.

## 2 LAYOUT OF THE READING ROOM

Modeling of the reading room environment is the first step of this study. The influential factors of the reading room environment in the university library include many aspects. However, to simplify

the model, the most important factors such as lighting, sound, and arrangement of book shelves are analyzed and secondary factors such as temperature, humidity, and so on are neglected. The main steps of modeling are as follows:

1. The environmental factors are quantified.
2. The attribute weights and attribute values of lighting, sound, and arrangement are acquired.
3. The model is designed based on HFE.
4. The selected values are sorted through the method.
5. According to readers' proposals, the model is improved and optimized.

Figure 1 shows a library reading room with centralized layout. In the sampling test, readers are randomly selected. Their performances and reactions are recorded to provide the basis for

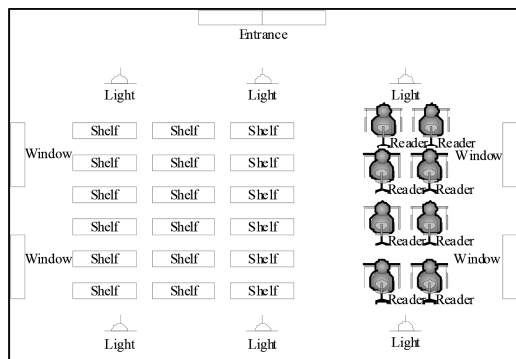


Figure 1. The model of a library reading room.

environmental modeling of the reading room. Moreover, through investigation of readers' proposals, valuable factors in the environment model can be determined, so as to provide decision-making advice for optimization of the model.

Assume that the attribute weights of the environment are  $\omega = (\omega_1, \omega_2, \dots, \omega_n)$ ,  $\omega_j \geq 0$ ,  $j \in M$  and the attribute values matrix is  $A = (a_{ij})_{n \times m}$ , then:

$$\sum_{j=1}^m \omega_j^2 = 1 \quad (1)$$

The comprehensive attribute value can be defined as follows:

$$z_i(\omega) = \sum_{j=1}^m r_{ij} \omega_j \quad (2)$$

The comparison of the comprehensive attribute values is as follows: if the difference between all attribute values is small, then the influence of the attribute is small; conversely, if an attribute can change all attribute values intensively, then it plays an important role.

Assume that  $V_{ij}(\omega)$  is the deviation, then:

$$V_{ij}(\omega) = \sum_{k=1}^n |r_{ij} \omega_j - r_{kj} \omega_j|, i \in N, j \in M. \quad (3)$$

Therefore, the model can be designed as follows:

$$\max V(\omega) = \sum_{j=1}^m V_j(\omega) = \sum_{j=1}^m \sum_{i=1}^n \sum_{k=1}^n |r_{ij} - r_{kj}| \omega_j. \quad (4)$$

$$\begin{cases} \max V(\omega) = \sum_{j=1}^m \sum_{i=1}^n \sum_{k=1}^n |r_{ij} - r_{kj}| \omega_j \\ s.t. \omega_j \geq 0, j \in M, \sum_{j=1}^m \omega_j^2 = 1. \end{cases} \quad (5)$$

### 3 ANALYSIS OF ENVIRONMENTAL INFLUENCE

Many researchers have studied the environmental influence of cleanliness, color, temperature, and humidity over the mental and physical effects of readers in the reading room [3–6]. It is concluded that measures such as maintaining cleanliness, choosing relaxing and vibrant colors, maintaining appropriate temperature and humidity can make readers comfortable and improve their satisfaction [7–10]. In this paper, the combined influence of lighting and noise is mainly studied.

Because it is difficult to quantify some environmental factors in environmental modeling, a

combined approach of quantitative and qualitative analysis based on scoring of readers is used. According to the established model shown in Fig. 1, the noise in the reading room was measured by sound level meters. It can be seen that the main noise sources are mobile phone ring, chatting, hauled noise when standing up or sitting down, and footstep noise of readers. Out of the different kinds of noise source, 66% of readers felt that the suddenly issued mobile phone ring greatly impacted them, 54% of readers found talking in the reading room unbearable, 48% of readers did not like the dragging noise of chairs, and 26% of readers complained that footstep pacing was bothering. Therefore, it is very necessary to minimize the noise in the reading room. In the library reading room, the readers' mobile phones should be placed in silent mode or switched off. Meanwhile, talking loudly should be forbidden in the reading room and readers should be instructed to stand up or down cautiously without any noise. When they walk in the reading room, they should be light-footed to avoid noise. At the same time, it is a good approach to put up posters in the reading room to prompt the reader to keep quiet.

Lighting directly affects the reader's visual sensibility. With the designed model, the reading room lighting is measured by using a photoelectric photometer. From the statistics of readers' focus and comfort under natural light, lamps, and their combination, it is found that, under conditions of enough natural lighting illumination, readers prefer natural light instead of lighting. Figure 2 shows

Table 1. The effects of various noise sources (%).

	Mobile phone ring	Chat	Hauled noise	Step	Others
Great	66	54	48	26	10
Normal	24	34	42	40	56
Neglected	6	16	16	28	38

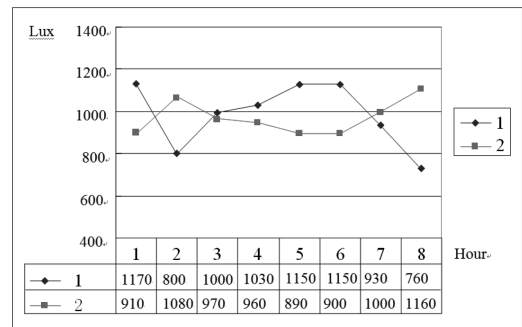


Figure 2. Effect of lighting.



the collected data about the combined light intensity of natural light and lamps. Curve 1 denotes the intensity of natural light and curve 2 denotes the intensity of lamps' light. To analyze the light effect, the light intensities of eight different hours are gathered. It is found that, under conditions of insufficient natural light illumination, even during daylight, lamps should be opened in time. Moreover, the combined intensity of the natural light and the lamps' light is about 2000 Lux, which indicates that the intensity of lamps' light should be adjusted on time according to the natural light's intensity and the total light intensity should be kept constant.

The arrangement of the lamps should be such that room illumination is even. Otherwise, visual fatigue will be caused easily. Therefore, in the reading room construction, attention should be paid to provide adequate natural lighting in the reading room and to avoid the usage of shielding windows. In this case, the use of natural lighting can be maximized. This not only improves the reader's level of comfort, but also saves electricity to achieve energy conservation and environmental protection. On the other hand, under the circumstance that lighting is not sufficient, even during daylight, all lamps should be opened if possible, so that the view of readers in the eyesight field is of the same brightness.

#### 4 THE PROPOSALS OF READERS

The purpose of collecting readers' proposals is to help in improving the reading room environment, which is the process of the model results and is not directly used in decision-making. As a stage summary, it can be used to assess the designed model and can be applied to optimize the model. In order to carry out environmental construction of the library reading room efficiently, timely collection of readers' feedback and suggestions is very necessary. Many good proposals were suggested by readers; the most frequently put forward eight proposals are chosen and shown in Table 2. It shows that readers focus on adding green bonsai, updating book tabs, arranging shelves, improving ventilation conditions, regulating circulation of books, cleaning dirty books, cleaning tables and chairs, and increasing interior decoration. The collected proposals from readers are necessary for continuous improvement of environmental construction. These suggestions are implemented in the environmental model. Through the adoption of these recommendations and to improve the reading environment and reading efficiency, the established model can reflect the quality of the library service better, as shown in Table 3. Three aspects of the environment namely, quietness, cleanliness, comfortableness are verified by the readers. It can

Table 2. The readers' proposals.

Item	Proposals
1	Add green bonsai
2	Update tabs
3	Arrange shelves
4	Improve ventilation conditions
5	Regulate circulation of books
6	Clean books
7	Clean tables and chairs
8	Increase interior decoration

Table 3. Satisfaction survey.

Readers' satisfaction	Quietness	Cleanliness	Comfortableness
Before improvement	73%	81%	82%
After improvement	89%	92%	91%

be seen that before the improvement, the percentage of satisfaction of quietness is 73%, cleanliness is 81%, and comfortableness is 82%. After the improvement, the percentage of satisfaction of quietness is 89%, cleanliness is 92%, and comfortableness is 91%. The total degree of satisfaction is increased obviously.

Under certain circumstances, such as the situation of multiple readers' decision-making, the problem of processing different readers' proposals will be met. In view of this situation, the opinions of different types of readers can be classified through a network and then information can be processed by using a computer with the designed model.

#### 5 CONCLUSIONS

Development of the reading room environment of the university library is the key factor of library service for reader's evaluation. Accurately obtained and efficiently analyzed environment information is of great significance in ensuring the positive effects of the environmental factors on reading activities in the college library. According to the built reading room model based on the HFE methods, readers' satisfaction is obviously improved by continuous enhancement of the reading room environment on a daily basis.

#### REFERENCES

- [1] Haider, S. J. 2004. Coping with change: Issues facing university libraries of Pakistan. *Journal of Academic Librarianship*, 30(3): 229-236.

- [2] Xu Chuanjie. 2013. Research on Implementation Plan of 5S Management in University Library. *Applied Mechanics and Materials*, 380–384: 4440–4443.
- [3] Ba Xiaoli. 2006. Discussion on the Humanist Service of Library's Circulation Department. *Sci-Tech Information Development & Economy*, 9: 39–40.
- [4] Lu Kezhi. 2006. How to improve circulation service quality in libraries. *Journal of library and information sciences in agriculture*. 2: 83–85.
- [5] Philipp Mayr. 2015. Recent applications of Knowledge Organization Systems: introduction to a special issue. *International Journal on Digital Libraries*. 17(1): 1–4.
- [6] Yi Jiangang. 2015. Modelling and Analysis of Step Response Test for Hydraulic Automatic Gauge Control. *Strojniški vestnik—Journal of Mechanical Engineering*. 61(2): 115–122.
- [7] Ying-Ming Wang, Celik Parkan. 2005. Multiple attribute decision making based on fuzzy preference information on alternatives: Ranking and weighting. *Fuzzy Sets and Systems*, 131(1): 101–106.
- [8] José Borbinha. 2005. Reference models for digital libraries: actors and roles. *International Journal on Digital Libraries*, 5(4): 325–330.
- [9] Tudhope, D., Lykke Nielsen, M. 2006. Introduction to Knowledge Organization Systems and services. *N. Rev. Hypermedia Multimedia*, 12(1): 3–9.
- [10] Zeng, M. and Chan, L. 2004. Trends and issues in establishing interoperability among knowledge organization systems. *Journal of American Society for Information Science and Technology*, 55(5): 377–395.

# A study on the optimization of green light sources in subway stations

Zhong-chao Zhao

Department of Environmental Design, Art School, University of Jinan, Jinan, Shandong, China

**ABSTRACT:** Light source performance has a great impact on energy-saving lighting of subway stations. Scientific and rational selection of an energy source is the key to achieve green lighting. In this paper, the advantages and disadvantages in the performance of three light sources that are commonly used in subway stations are compared, the differences in the performance of different types of fluorescent lamps are analyzed, and the prospect of LEDs' application in subway space is discussed.

**Keywords:** Subway Station; Green Light Source; Energy-saving Lighting

## 1 INTRODUCTION

In China, the most commonly used light sources in the subway space are fluorescent lamps, metal halide lamps, and LEDs. Out of these lamps, fluorescent lamps are largely used. The light source is an important part of energy-saving lighting for subway stations; therefore, how to make a more reasonable choice for light sources is the focus of this study.

## 2 PERFORMANCE ANALYSIS OF DIFFERENT LIGHT SOURCES

### 2.1 Fluorescent lamps

Fluorescent lamps are low-intensity gas discharge lamps. Compared with the traditional incandescent lamps, fluorescent lamps exhibit an advantageous performance due to the following factors: these lamps have a luminous efficiency that ranges from 60 to 90 l m/W, a color rendering index of above 80 and a life expectancy between 8000 h and 15000 h<sup>1</sup>. Based on the form of light source used, fluorescent lamps are classified into three types, namely straight tube fluorescent lamps, compact fluorescent lamps, and circular fluorescent lamps. Out of the above-mentioned light sources, straight tube fluorescent lamps and compact fluorescent lamps are largely used in subway stations. A straight tube fluorescent lamp falls into two length categories such as 600 mm and 1200 mm and four diameter categories such as T12, T8, T5, and T4. It also acquires many forms such as U-type, spiral-type, H-type, and so on (Figure 1). The advantages of a compact fluorescent lamp are as follows: small size, high luminous efficiency, and long life. It is suitable for downlight lighting. The disadvantage of fluorescent lamps is mercury population. Mercury



Figure 1. Compact fluorescent lamps.

may contaminate the living environment of human beings and affect human health.

### 2.2 Metal halide lamps

Metal halide lamps are high-strength gas discharge lamps. Their luminous efficiency ranges between 90 and 95 l m/W. The color rendering index of metal halide lamps can reach up to 80 at a color temperature of 3000 K and 90<sup>2</sup> at a color temperature of 4200 K. Their life expectancy is between 9000 h and 15000 h<sup>3</sup>. Metal halide lamps have been widely used in public buildings, because these have many advantages such as excellent light efficiency, good color rendering properties, and long life expectancy. However, metal halide lamps also have some

disadvantages such as long starting time, not being frequently opened, and large fading of light. These disadvantages limit their scope of application in subway stations and only those with higher space stations will choose to use metal halide lamps.

### 2.3 LEDs

LED stands for light emitting diode. Data show<sup>4</sup> that the luminous efficiency of LEDs can reach up to 2001 m/W in a laboratory (actually between 501 m/W and 1501 m/W) and their theoretical life can reach 50000 h or even longer (actually no less than 15000 h). LEDs exhibit relatively good color rendering properties. The color rendering index of white LEDs at warm temperatures can reach 90 or more and at cold temperatures can also be up to 75. These can meet the lighting needs for traffic space. In addition, the light source also has some advantages such as it is easy to control and easy to change the lighting illuminance by arbitrarily adjusting the electric current. In short, LEDs with properties such as high efficiency, safety, environmental protection, easy maintenance and other significant advantages are considered as the fourth generation of green light sources that are most likely to enter the general lighting arena.

By the basic performance analysis of commonly used light sources in subway stations, some laws can be found. The order of lamps in terms of luminous efficiency from the highest to the lowest is LEDs, metal halide lamps, and fluorescent lamps. In addition, the life of a LED is the longest, up to 50000 h. The life of a fluorescent lamp and a metal halide lamp can only reach up to 15000 h. From the above-mentioned information, the following conclusions can be drawn. Firstly, from the point of view of energy conservation, LED should first be selected, and then fluorescent lamp and metal halide lamp. Secondly, metal halide lamps are the most appropriate for high space of subway stations, because metal halide lamps not only have high brightness but also can cast light to a longer distance. Finally, although the performance of LEDs is more prominent, some problems such as high price, immature technology, lack of standards for design and testing, and so on still exist. These factors affected their widespread use in the subway space. Nevertheless, LEDs are the preferred light source for subway stations at present and will be so in future.

## 3 PERFORMANCE COMPARISON OF DIFFERENT FLUORESCENT LAMPS

Because fluorescent lamps have many advantages such as mature technology, affordable price, good energy efficiency, and so on, it is used more in

subway stations. However, there are many different types of fluorescent lamps. There are some even bigger differences in performance between the various types. Only by understanding these differences energy-saving fluorescent lamps can be better optimized. Therefore, what can advantages and disadvantages of different types of fluorescent lamps do? In this work, the Panasonic fluorescent lamp is taken as an example, the most commonly used three types of light sources are selected and their energy-saving effect is compared and analyzed.

From Tables 1 and 2, it can be found that, even though the three types of fluorescent lamps are very close to each other in properties such as power, color temperature, and color rendering, their luminous efficiency and service life are quite different. Firstly, the order of lamps in terms of luminous efficiency from the highest to the lowest is EHF efficient fluorescent lamps, trichromatic T8 fluorescent lamps, and compact fluorescent lamps. The efficiency of EHF efficient fluorescent lamps can reach while that of compact fluorescent lamps can only reach up to 66 lm/W. Secondly, the order of lamps in terms of life from the highest to the lowest is the same as that of luminous efficiency. However,

Table 1. Comparison of Panasonic fluorescent parameters.

Source name	Power	Flux	Luminous efficiency
	w	lm	lm/w
Trichromatic fluorescent tube (T8)	18	1380	76
Compact fluorescent lamp	18	1120	62
Compact fluorescent lamp	16	1400	88

\* Source: Panasonic official website information.

Table 2. Comparison of Panasonic fluorescent parameters.

Source name	CRI	Life	Color temperature
	ra	h	k
Trichromatic fluorescent tube (T8)	88	8500	3000
Compact fluorescent lamp	84	6000	2800
Compact fluorescent lamp	84	12000	3000

\* Source: Panasonic official website information.

the life of compact fluorescent lamps is only half of that of EHF efficient fluorescent lamps. It can be found that the energy saving parameters of different types of fluorescent lamps exhibit a considerable difference. When selecting a light source, its energy-saving parameters should be fully compared and the fluorescent lamp with long life and high efficiency should be preferentially chosen.

#### 4 LEDS' APPLICATION PROSPECT IN SUBWAY SPACE

The prospect of LEDs as a fourth-generation green light source is worth the wait. However, some problems that hinder their development still exist. For example, high price is one of the main reasons. Despite the initial price being higher, the final economic benefits are brighter than fluorescent lamps as their long-term use proceeds. This has been confirmed by some practical applications. Currently, LEDs can be used as the main light source in the subway station in two main ways. On one hand, in the simple lighting retrofit projects, in order to prevent the existing surface decoration from being destroyed, the specification of LED lamps should be the same as the original specifications of lamps. On the other hand, in a new project or indoor environment overall renewal project, any standard LED lamps can be used. Shenzhen Metro Line lighting, borrowed from Shekou<sup>5</sup>, is used to analyze the energy efficiency of LEDs in comparison with fluorescent lamps. Shekou's lighting design, Shenzhen Metro Line, abandoned some outdated design practices and first used LED lighting and intelligent control technology in a Chinese subway station, which is a bold reform and experiment for green lighting designs of underground space. The results also achieved the intended purpose. In this work, Keyuan station is taken as an example and a comparison of economic benefits between the use of a 105 lm/W LED light source and the use of a T8 trichromatic fluorescent light source is made (Table 3). Similar comparisons are made in the case of lighting effects and lighting conditions, where operating costs of two kinds of lighting solutions are compared. It can be found that 36 million was saved in the total cost of program 2 than that of program 1 in ten years. The savings rate is about 18%. In other words, the ten years' running costs are balanced between LED lighting and fluorescent lighting. However, after years of development, LED chip processing and packaging technology has been greatly improved and luminous efficiency and service life has also been significantly improved while the price has decreased substantially. It can be said that the current LED light source is more cost-effective and has the foundation and advan-

Table 3. Comparison of Panasonic Fluorescent Parameters.

Project	Scheme 1 (T8 Fluorescent lighting)	Scheme 2 (LED lighting)
Number of fixtures (Sets)	272	234
Lighting power (W)	76	65
Lamps price (Yuan)	183000	351000
Utilization factor	0.9	0.8
Light source life (h)	10000	35000
1-year electricity cost (Yuan)	172104.82	126630.92
10-year electricity cost (Yuan)	1721048.20	1266309.20
Light source replacement cost (Yuan)	10536.00	35167.86
Total (Yuan)	2009584.20	1652477.06

\* Source: compiled by the author based on paper information of Longtan

tage to replace fluorescent lighting. In addition, in terms of dimming, a LED exhibits more significant energy conservation than a fluorescent lamp. It also further laid LED lighting in the mainstream in subway space in the future.

At the same time, the use of high-power LEDs is also a noteworthy direction. There is a trend from small power toward high-power LEDs. When compared to low-power LEDs, the high-power LED has a smaller light-emitting area, larger luminous flux, and more concentrated light. Research shows that the highest-power LED light's efficiency can reach up to 170 lm/W and that of a common high-power LED is approximately between 120 lm/W and 150 lm/W. Clearly, high-power LEDs are more energy efficient than small-power LEDs, generate less heat, and light failure is also smaller. But, the small light area and high brightness power LEDs will bring serious glare problems. And so, a scientific optical design and a light diffusion panel with quality materials at light outlets are necessary, to prevent glare and improve illumination uniformity while not affecting the luminous efficiency. Guanzhou Station of Guangzhou Metro Line 4 is a classic example<sup>6</sup> of this case. The station lighting uses a 1 W high-power LED light source, a diffusion panel with a total light transmittance of 90%, and a silver reflective film inside the surface of the lamp used to improve the reflectivity. After product application, lighting solutions found that, in comparison with the original T8 grille fluorescent lamps, the average illumination has increased by about 36% and energy consumption has reduced by about 32%. Although this is only an attempt to the high-power LED, but its potential at social and

economic value is enormous and should be actively explored as a new direction in the subway station lighting design. If a lot of promotion, testing, evaluation, and improvement of LED should be completed in a series of application engineering.

In addition, with the development of control technology, intelligent lighting control, even Wisdom lighting control, has gradually become the mainstream. A very prominent feature of intelligent control is the ability to achieve real-time control of light and shade. And so, it not only saves energy efficiently, but also extends the life of the light source. In this aspect, the fluorescent lamp has no advantage. Although the light and shade of a fluorescent lamp can be changed by dimming ballast, this can also affect the service life of the fluorescent lamp. In contrast, the corresponding LED is controllable within microseconds, which is able to adapt to any power adjustment. It can be said, in terms of dimming, that LEDs have more significant energy-saving advantages than fluorescent lamps.

## 5 CONCLUSION

Based on the described analysis, in order to better implement energy-saving lighting, subway stations should prioritize usage of high-power and

long-life fluorescent lamps, while actively exploring and promoting the use of LED light sources in the subway space.

## ACKNOWLEDGMENTS

This work was financially supported by the Art Project of National Social Science Fund (13CB121).

## REFERENCES

- [1] Qiao Yuan, Qingxuan Zhan. Building lighting. Beijing, Chinese building industry press. 2006, 182.
- [2] Hong Liu, Jiangping Zhao. Introduction of green lighting. Beijing, Chinese power press. 2009.
- [3] Dan Wang. The research on energy saving and environmental protection of store lighting. Chongqing, Chongqing university school of architecture. 2006, 36.
- [4] Hui Xie, Bo Chai, Binbin Du. Office lighting design guide. Beijing, People Post Press. 2011, 28.
- [5] Tan Long, Shekou, Shenzhen Metro Line green lighting design. Metropolitan rapid transit. 2012, 25(3). 100–103.
- [6] Jiongsheng Shen, Optical design and application high-power LED lighting in subway station. China lighting. 2013, (8). 11–16.

# A study on the mechanical properties of mechanism sand mortars subjected to different temperatures

Hai-jing Xu & Cheng-xian Cen

Architecture and Traffic Engineering College, Guilin University of Electronic Technology, Guilin, China

**ABSTRACT:** The mechanical properties of mechanism sand mortars of different strength grades (M5–M15) were tested after being heated to different temperatures (100°C–1000°C). The influence law of temperature change on the mechanical properties of a mechanism sand mortar was analyzed in this paper. The results show that the strength of a mechanism sand mortar decreases with an increase in the heating temperature and the influence laws by heating of the mechanism sand mortars of different strength grades are basically identical. The degradation formula of mechanism sand mortars of different strength grades was obtained in this experiment.

**Keywords:** Temperature effect; mechanism sand; mortar; mechanical properties

## 1 INTRODUCTION

With the reduction of natural sand resources and damages such as farmland destruction, soil erosion caused by excessive sand mining has become worse. The advantage of mechanism sand is more obvious in the use of engineering. Many researchers study about using mechanism sand in engineering applications. But few people have investigated the properties of a mechanism sand mortar that is subjected to different temperatures. Xiaoyan Xu et al. [1] tested natural sand mortars. Xiaoyong Xu et al. [2, 3] tested high strength concrete. Natural sand replaced by mechanism sand as the main material in mortars is the trend of engineering. Therefore, the change rule of mechanism sand mortars subjected to different temperatures was studied in this paper.

## 2 EXPERIMENTAL STUDY

The masonry used in this experiment was stone masonry. M5, M7.5, M10, and M15 are the four strength grades that were selected as target strength grades.

### 2.1 Materials

#### 2.1.1 Cement

The strength 32.5 cement was produced by Xing-an Conch Cement Company Limited. Admixtures were not added to the cement.

#### 2.1.2 Sand

Sand was crushed by using Guilin's local pebbles. The sand grading parameters were obtained by performing the sieve experiment. Its fineness modulus was 3.17 and belonged to the coarse sand category.

#### 2.1.3 Water

Tap water was used to perform all experiments.

### 2.2 Specimen Production

The specimen was produced according to the "JGJ/T 70-2009 standard for test method of basic properties of construction mortar".

#### 2.2.1 Mixture ratio calculation

The calculation for the mortar mix was based on the "JGJ/T 98-2010 specification for mix proportion design of masonry mortar". The amount of cement and the amount of sand in one cubic of mortar depended on the strength of the mortar. The amount of water needed was selected in accordance with mortar consistency. The experimental results are shown in Table 1.

#### 2.2.2 Preparation of mortar specimens

The mortar mixture was prepared in a laboratory in standard plastic engineering test mode. Mixing and vibrating were performed manually. Mixing time was selected by using the "JGJ/T 70-2009 standard for test method of basic properties of construction mortar".

Table 1. Typical composition of the studied mortar.

Strength grade	Cement (kg/m <sup>3</sup> )	Water (kg/m <sup>3</sup> )	Sand (kg/m <sup>3</sup> )	Cement : Sand : Water
M5	207	300	1600	1:7.73:1.45
M7.5	260	300	1600	1:6.15:1.15
M10	290	300	1600	1:5.51:1.03
M15	363	300	1600	1:4.41:0.83

### 2.2.3 Conservation of mortar specimens

The specimens were protected in the standard plastic engineering test mode for 24 hours and then cured for one month (28 days) in the natural environment.

### 2.3 Specimen heating

The tests were carried out by using a heating control temperature box type of resistance furnace which is equipped with a heating capacity of 1000°C. The target temperatures were chosen, which include 25, 100, 200, 300, 400, 500, 600, 700, 800, 900, and 1000°C, where each increase by 100°C denotes a gradient. The same tests were carried out for all 11 groups. The temperature was maintained for 120 minutes after heating to the target temperature. The heating time schedule is shown in Table 2. The specimens were cooled naturally.

After heating the specimens to different temperatures, varying degrees of changes took place on the surface.

#### 2.3.1 Temperature: 100–200°C

No changes were detected in the specimens.

#### 2.3.2 Temperature: 300°C

Slight watermarks or water stains were observed on the surface of specimens.

#### 2.3.3 Temperature: 400°C

Minor marginal damage was observed in the specimens.

#### 2.3.4 Temperature: 700°C

It could be noted that the color of specimens had become darker, such as turning dark red or dark grey in color.

#### 2.3.5 Temperature: 900°C

M5 specimens had been broken to lose bearing capacity, while M7.5 and M10 specimens had small cracks.

#### 2.3.6 Temperature: 1000°C

Only M15 specimens' shape was retained. The rest of the specimens were broken.

Table 2. The time of heating and constant.

Temperature (°C)	Heating time (min)	Constant time/min
100	6	120
200	8	120
300	11	120
400	15	120
500	19	120
600	24	120
700	30	120
800	36	120
900	45	120
1000	54	120



Figure 1. Picture of M7.5 showing no detected changes.



Figure 2. Picture of the M5 specimen with watermarks.



Figure 3. Picture of the M5 specimen with marginal damage.

### 2.4 Compressive strength test

Specimens were loaded by using a hydraulic universal testing machine. The loading rate was 0.5 mm/min. Compressive strength tests were





Figure 4. Picture of the M10 specimen with slight cracks.

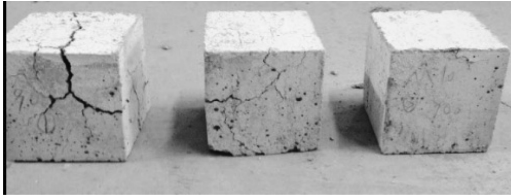


Figure 5. Picture of the M10 specimen with cracks.



Figure 6. Picture of the M15 specimen with slight cracks.

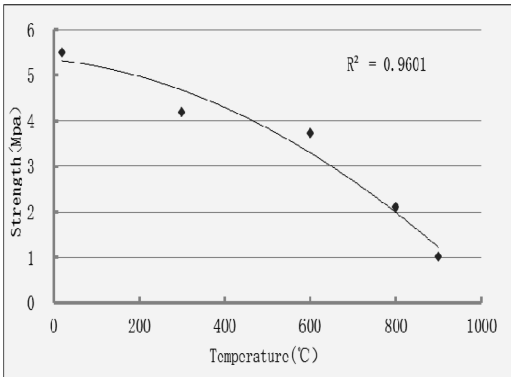


Figure 7. Graph showing the M5 experimental curve.

carried out on 120 specimens (4 strength grades) in this study. Test results are shown in Figures. 7–10.

As shown in the figures, with an increase of temperature, the strength of specimens show a declining trend. Different strength grade specimens have exhibited the consistent degradation law. Low strength specimens are sensitive to temperature changes. When the M5 mortar was heated to

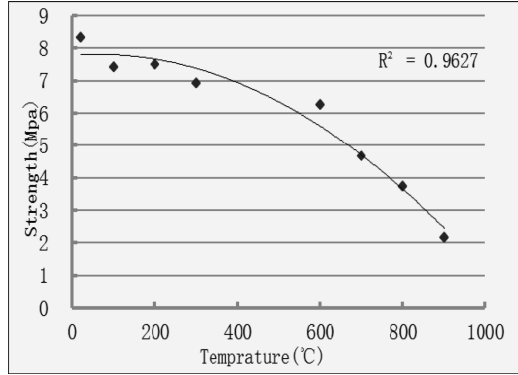


Figure 8. Graph showing the M7.5 experimental curve.

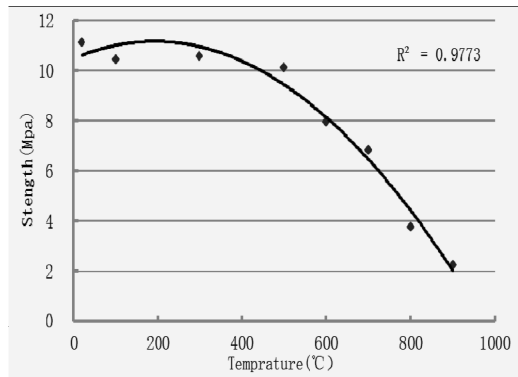


Figure 9. Graph showing the M10 experimental curve.

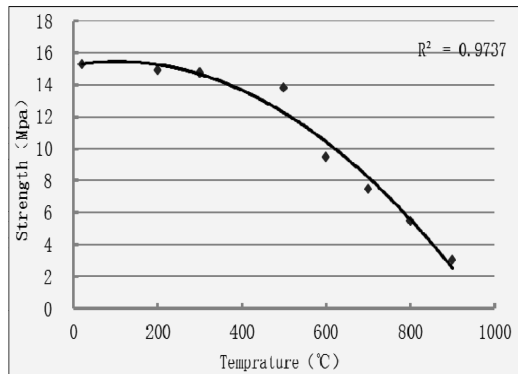


Figure 10. Graph showing the M15 experimental curve.

300°C, its strength declined by more than 20% and other high strength mortars will only lose 20% of their strength at 500°C or more. After being naturally cooled, the compressive strength of specimens exhibited a slight decline when heated to tempera-

tures between 100°C and 300°C. When the mortar was heated to more than 400°C, the compressive strength began to decline rapidly. When the temperature reached 800°C, the decline was worst and the mortars had lost almost all compressive strength.

The relationship between temperature and compressive strength is fitting by quadratic polynomial regression in this paper. Specific formulas are shown as follows:

M5 mortar:

$$P = -4E - 06T^2 - 0.0011T + 5.345 \quad (1)$$

$$20^\circ\text{C} \leq T \leq 900^\circ\text{C} \quad R^2 = 0.9601$$

M7.5 mortar:

$$P = -8E - 06T^2 + 0.001T + 7.7806 \quad (2)$$

$$20^\circ\text{C} \leq T \leq 900^\circ\text{C} \quad R^2 = 0.9625$$

M10 mortar:

$$P = -2E - 05T^2 + 0.0071T + 10.48 \quad (3)$$

$$20^\circ\text{C} \leq T \leq 900^\circ\text{C} \quad R^2 = 0.9773$$

M15 mortar:

$$P = -2E - 05T^2 + 0.0042T + 15.225 \quad (4)$$

$$20^\circ\text{C} \leq T \leq 900^\circ\text{C} \quad R^2 = 0.9737$$

The change formulas can be summarized as follows:

$$\sigma_i = aT^2 + bT + c \quad (5)$$

where  $\sigma_i$  represents compressive strength, T represents temperature, and a, b, and c are the constants obtained by the experiment.

### 3 CONCLUSIONS

Through this experimental study, the following conclusions were drawn:

1. With increasing temperature, the mechanism sand mortar's compressive strength decreases gradually. The pattern of the change is clear.
2. Mortar strength grades such as M7.5, M10, and M15 have similar variations in their compressive strengths after being subjected to different temperatures; when the temperature was less than 500°C, there was less decrease in the compressive strength, namely less than 20%. There was a rapid decline in the compressive strength when the temperature was more than 500°C. When the temperature reached 800°C, more than half of the compressive strength was lost.

### ACKNOWLEDGMENTS

The authors thank Mrs. Hui Jiang for her assistance in performing the compressive instrument operation and Mr. Zhaowen Chen for translation of literature.

### REFERENCES

- [1] Xiaoyan, Xu. & Guanglin, Yuan. 2009. Experimental study on the effect of high temperature on the strength of high-strength cement mortar. *Journal of Shandong University of Science and Technology* 28(5):35-48.
- [2] Xiao-yong, Xu. & Yan-fei, Ma. 2008. Experimental study on mechanical property of high strength concrete after high temperature. *Journal of Anyang Normal University* 28(5):149-152.
- [3] Min, Li. & Chun-xiang, Qian. 2002. The varying rule and the non-destructive measuring of high performance concrete after fire. *Industrial Construction* 32(10):34-36.
- [4] Qing-hai, Li. & Yan, Yao. 2008. Mechanism of effect of elevated temperature on compressive strength of cement mortar. *Journal of Building Materials* 11(6):699-703.

# Study on numerical simulation of three-dimensional viscoelastic mechanics for steel deck asphalt pavement

Wen-ke Huang, Xiao-ning Zhang, Hong-liu Rong & Shao-fan Cai

*School of Civil Engineering and Transportation, South China University of Technology, Guangzhou, China*

**ABSTRACT:** Three dimensional viscoelastic mechanics theory of asphalt mixture was used in this paper based on the UMAT function of ABAQUS and numerical analysis of three-dimensional viscoelastic constitutive applying on steel deck asphalt pavement was realized. A large piece of linear track accelerated loading facility MLS66 was used to conduct a two million times repeated loading test on the testing bridge. Three-dimension FE model of the bridge is used in simulation. Three-dimensional viscoelastic constitutive model was applied for the asphalt pavement and a static equivalent loading scheme was utilized for the two million times repeated loading. By comparing the accelerated loading test measured data with finite element numerical simulation results, a rather good agreement between measured and numerically predicted strains can be obtained that verifies the reasonableness and practicability of the FE model. This provides an effective method for further mechanical analysis of steel bridge deck asphalt layer.

**Keywords:** steel deck pavement; viscoelastic constitutive; numerical simulation; accelerated pavement test

## 1 INTRODUCTION

The asphalt mixture is mostly adopted as the pavement material for long-span orthotropic steel box girder deck pavement. Due to the different performances between asphalt mixture and steel material, the mechanical properties of pavement layer under traffic loading are very complex, and the problem of bridge deck pavement is a technical problem in highway construction. This makes bridge deck pavement be a technical problem in highway construction in the world.

The most direct means of steel bridge deck pavement structure design and mechanics analysis is to carry out the mechanical test of the real bridge [1, 2]. However, the actual experiment will be a major expenditure of time and effort, and also because the technical means is not perfect, the influence factors in actual design are not comprehensive. With the development of computer technology, the numerical simulation technique is applied as a supplementary means for the mechanical test of the real bridge to analyze the orthotropic steel bridge deck pavement structure.

For the mechanical analysis of steel bridge deck pavement structure, most of the literatures simplify the asphalt mixture into an ideal linear elastic material [3, 4]. The advantage of this method is that the simulated model is simple and the material

parameters are easy to obtain, but this assumption does not take into account the viscoelastic material properties of asphalt mixture. As a kind of thermo-rheological material, the mechanical behavior of asphalt mixture is mainly expressed by the viscoelastic properties, and the study of viscoelastic behavior has become the main research method in this field. Some literatures treated asphalt mixture as a viscoelastic body [5, 6]. In these literatures, steel deck asphalt pavement is analyzed based on one dimensional viscoelastic theory and finite element method, and some achievements have been made.

The stress state of steel deck asphalt pavement is different from general asphalt paving layer under the traffic load. For steel deck asphalt pavement, the stress mode is mainly in a complex three-dimensional stress state. In order to thoroughly study the mechanical response characteristics of steel bridge deck pavement, it is necessary to study the three dimensional stress of pavement layer. In this paper, the three-dimensional viscoelastic constitutive theory of asphalt mixture is used to realize the three-dimensional mechanical response of steel deck asphalt pavement by applying the ABAQUS finite element software.

A large piece of linear track accelerated loading facility MLS66 was used to conduct a two million times repeated loading test on the testing

bridge with a pavement structure used in the Hong Kong-Zhuhai-Macao Bridge. Three-dimensional FE model of the bridge is built and the equivalent loading test is carried out for 2 million times in details. Comparisons of simulation predictions and field measurements are presented.

## 2 THEORETICAL BACKGROUND

### 2.1 Linear viscoelastic constitutive model

For linear viscoelastic materials, including asphalt mixture, the stress-strain constitutive relation is expressed by convolution integrals. In the case of strain response at constant stress, the convolution relations is explained as follows for one-dimensional problems [7, 8]:

$$\varepsilon(t) = D_0 \sigma + \int_0^t \Delta D (\varphi^t - \varphi^\tau) \frac{d(\sigma)}{d\tau} d\tau \quad (1)$$

where the  $D_0$  is the instantaneous elastic compliance,  $\varphi^t$  is the reduced time and  $\Delta D$  is the transient compliance. It is given by:

$$\Delta D(\varphi) = \sum_{n=1}^N D_n (1 - \exp(-\lambda_n \varphi)) \quad (2)$$

where  $D_n$  is the  $n$ th coefficient of the Prony series and  $\lambda_n$  is the  $n$ th retardation time.

For three-dimensional problems, Eq. (1) can be decomposed into deviatoric and volumetric components, such that:

$$e_{ij}^t = \frac{1}{2} J_0 S_{ij}^t + \frac{1}{2} \int_0^t \Delta J (\varphi^t - \varphi^\tau) \frac{d(S_{ij}^\tau)}{d\tau} d\tau \quad (3)$$

$$\varepsilon_{kk}^t = \frac{1}{3} B_0 \sigma_{kk}^t + \frac{1}{3} \int_0^t \Delta B (\varphi^t - \varphi^\tau) \frac{d(\sigma_{kk}^\tau)}{d\tau} d\tau \quad (4)$$

$$\varepsilon_{ij}^t = e_{ij}^t + \frac{1}{3} \varepsilon_{kk}^t \delta_{ij} \quad (5)$$

where  $e_{ij}$  and  $\varepsilon_{kk}$  are the deviatoric strain and volumetric strain, respectively;  $\varepsilon_{ij}^t$  is the total strain and  $\delta_{ij}$  is the Kronecker delta;  $J_0$  and  $B_0$  are the instantaneous effective elastic shear and bulk compliances, respectively;  $\Delta J$  and  $\Delta B$  are the transient shear compliance and bulk compliance, respectively.

In most cases, the asphalt mastic Poisson's ratio  $\nu$  is assumed to be time independent leading that all the material properties in Eq. (3)–Eq. (5) can be determined from the data of compression tensile tests. Obviously, all the material properties in Eq. (3)–Eq. (5) can be determined by the uniaxial compression creep tests.

### 2.2 Finite element implementation for asphalt mixture

The Finite Element Method (FEM) is actually an incremental approach for numerical analysis. Current stress and strain at integration points of each element at every time increment are obtained from the stress and strain over the previous loading history. So the three-dimensional incremental deviatoric and volumetric strain formulations with constant stress rate can be derived using Eq. (3)–Eq. (5) with some algebraic manipulations. The results are expressed as:

$$\Delta e_{ij}^t = J(t) \Delta S_{ij} - \frac{1}{2} \sum_{n=1}^N J_n [\exp(-\lambda_n \Delta t) - 1] q_{ij,n}^{t-\Delta t} \quad (6)$$

$$J(t) = \frac{1}{2} \left\{ J_0 + \sum_{n=1}^N J_n \left[ 1 + \frac{1}{\lambda_n \Delta t} (\exp(-\lambda_n \Delta t) - 1) \right] \right\} \quad (7)$$

$$q_{ij,n}^t = \exp(-\lambda_n \Delta t) q_{ij,n}^{t-\Delta t} + \Delta S_{ij} \frac{1 - \exp(-\lambda_n \Delta t)}{\lambda_n \Delta t} \quad (8)$$

$$\Delta \varepsilon_{kk}^t = B(t) \Delta \sigma_{kk} - \frac{1}{3} \sum_{n=1}^N B_n [\exp(-\lambda_n \Delta t) - 1] q_{kk,n}^{t-\Delta t} \quad (9)$$

$$B(t) = \frac{1}{3} \left\{ B_0 + \sum_{n=1}^N B_n \left[ 1 + \frac{1}{\lambda_n \Delta t} (\exp(-\lambda_n \Delta t) - 1) \right] \right\} \quad (10)$$

$$q_{kk,n}^t = \exp(-\lambda_n \Delta t) q_{kk,n}^{t-\Delta t} + \Delta \sigma_{kk} \frac{1 - \exp(-\lambda_n \Delta t)}{\lambda_n \Delta t} \quad (11)$$

$$\Delta \varepsilon_{ij}^t = \Delta e_{ij}^t + \frac{1}{3} \Delta \varepsilon_{kk}^t \delta_{ij} \quad (12)$$

where  $\Delta e_{ij}^t$  and  $\Delta \varepsilon_{kk}^t$  are the incremental shear and bulk strains, respectively. The variables  $q_{ij,n}^t$  and  $q_{kk,n}^t$  are the shear and volumetric hereditary integrals for every Prony series term  $n$  at previous time  $t$ , respectively.  $\Delta \varepsilon_{ij}^t$  is the total incremental strain.

Then the three-dimensional constitutive model is implemented within the FE code. The ABAQUS user material subroutine (UMAT) is applied for this purpose.

## 3 ACCELERATED PAVEMENT TEST

Hong Kong-Zhuhai-Macao Bridge is a very large sea-crossing bridge under construction in China. The main construction of the bridge will include a 15.8 km-long continuous steel box girder span [9].

### 3.1 Testing bridge

The deck pavement structure of Hong Kong-Zhuhai-Macao Bridge intends to be “30 mm

thick mastic asphalt base course + 40 mm thick SMA-13 surface course". For full-scale experiments in the MLS66 facility, an orthotropic steel bridge test panel is available. The testing bridge has a dimension of 8000 × 3300 × 1680 mm in length, width and height respectively. Supporting length along the bridge span direction and supporting width along the width direction of the bridge are 250 mm and 2085 mm, respectively [10]. Earth anchorage supporting condition is applied to the end of the testing bridge. The testing bridge is shown in Figure 1. The main sizes of the testing bridge can be seen in Table 1.

### 3.2 Materials

Asphalt binder of mastic asphalt was obtained by blending the pure asphalt A-70 and Trinidad Lake Asphalt (TLA). Combination of the British standards (BS6925:1988)[11] and successful cases of steel bridge deck pavement in Hong Kong, the optimum ratio of A-70 to TLA is 3:7 (30%A-70+70%TLA). The mixture ratio of MA was determined by the graded mixture reports of Stonecutters' Bridge and Tsing Ma Bridge in Hong Kong provided by Anderson Asphalt limited.

### 3.3 Full-scale testing

MLS66 (Mobile Load Simulator 66) is a facility for full-scale accelerated pavement testing shown in Figure 2. There are two dual-wheel carriages landing on the pavement surface at every moment. The orthotropic steel bridge test panel was surfaced with a 30 mm thick mastic asphalt base course and a 40 mm thick SMA-13 surface course. The previous mechanical analysis shows that the bridge is in the most unfavorable loading state when the loading center locates above the web of testing bridge [12]. Strain for each layer of the deck pavement is accurately measured for every 50000 loading cycles. Figure 3 shows the top layer surface after loading for 200 million cycles.



Figure 1. Testing bridge before planted on the testing platform.



Figure 2. General view of MLS66.



Figure 3. The top layer surface after loading.

Table 1. Sizes of testing bridge and real bridge.

Parts	Cantilever height of Diaphragm (mm)	Section size of U rib (height × upper width × lower width) (mm)	Diaphragm density of mid-span (mm)	Thickness of top plate (mm)	Thickness of diaphragm/transverse rib (mm)	Thickness of U rib (mm)
Testing bridge	500	200 × 200 × 120	2500	18	16	8
Real bridge	1500	300 × 300 × 180	2500	18	16	8

## 5 FINITE ELEMENT MODEL AND MATERIAL PARAMETERS

### 5.1 Finite element model

To simulate the repeating loading of steel deck pavement, the developed FE model in ABAQUS is shown in Figure 4. Dimensions of the model are according to the full-scale testing bridge dimensions. Elastic modulus of steel is  $2.06 \times 10^5$  MPa with a density of  $7.85 \times 10^{-9}$  ton/mm<sup>3</sup>. The element type for steel is S4R and for asphalt mixture C3D8R is used. Thicknesses of mastic asphalt base course and SMA-13 surface course are 30 mm and 40 mm, respectively.

The wheel loading area is assumed as a circular shape with a diameter of 213 mm. Two dual-wheel groups are placed on the pavement surface of the FE model, and distance between the two wheel groups is 3080 mm. Stress magnitude of each wheel is 0.7 MPa. Boundary conditions of the model are according to the full-scale testing bridge.

The FE modeling of real loading mechanism in a full-scale accelerated pavement testing is a complex process and its detailed modeling needs lots of time to be consumed. Thus, a simple method introduced and applied by Hua and Uzarowski was used in this research [13, 14].

In this modeling scheme, the load is immediately and statistically applied to the model. Then, the cumulative time is calculated based on the number of wheel passes. The required time the wheel needs to pass the path, is calculated based on wheel velocity and diameter of the assumed circular shape. The wheel velocity of linear track accelerated loading facility MLS66 is 20 km/h. For circular diameter of 213 mm, the cumulative time in one loading cycle is about 0.0384 s.

### 5.2 Parameters determination

To determine the material parameters of mastic asphalt and SMA-13 in ABAQUS, a uniaxial static creep test was carried out on the asphalt concrete samples. The specimen has a diameter of 100 mm



Figure 4. Top view of the finite element model.

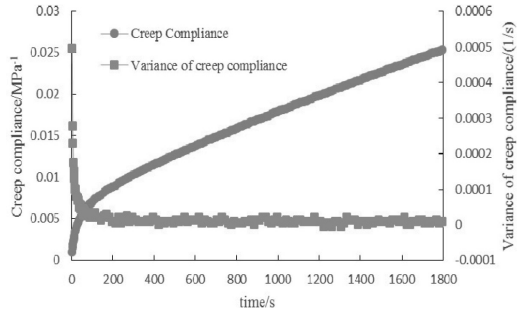


Figure 5. Creep curves of MA at 15°C.

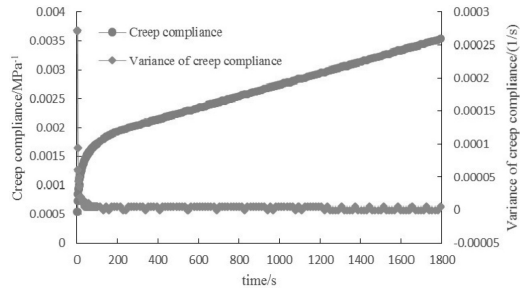


Figure 6. Creep curves of SMA-13 at 15°C.

Table 2. Creep parameters.

Number $j$	Reduced time $\tau_j/s$	MA Creep parameters $J_j/MPa^{-1}$	SMA-13 Creep parameters $J_j/MPa^{-1}$
1	$10^{-4}$	8.642E-2	6.680E-3
2	$10^{-3}$	5.290E-3	8.448E-4
3	$10^{-2}$	2.690E-3	2.398E-4
4	$10^{-1}$	2.770E-3	7.525E-4
5	$10^0$	3.129E-4	1.658E-4
6	$10^1$	2.122E-4	1.334E-4
7	$10^2$	2.122E-4	1.334E-4
8	$10^3$	2.122E-4	1.334E-4
$J_g/MPa^{-1}$		1.057E-4	6.842E-5
Correlation coefficient $R^2$		0.9994	0.9918

and specimen height is also 100 mm. The uniaxial static creep test was carried out at temperature 15°C. Creep curves with a stress level of 0.7 MPa are presented in Figure 5 and Figure 6.

The creep parameters in Eq. (2) can be developed from the uniaxial static creep test results through fitting Eq. (2). Creep parameters are shown in Table 2. As can be easily understood from the calculated values of correlation coefficient, approximations are accurate and acceptable.

## 6 RESULTS AND DISCUSSION

The experimental transverse strain data versus loading cycle curves of the SMA-13 surface layer on mid-span of the bridge above the web and across the edge web away from the middle span with a 3080 mm distance compared with the finite element numerical simulation results are presented in Figure 7 and Figure 8.

As can be seen from Figure 7 and Figure 8, both measured and simulated data show the trend of rheological behavior of asphalt mixture and the fitting of measured data has a high degree of agreement with the simulation data. Especially when the loading cycles are greater than 400 thousand times, the simulation data are almost coincident with the fitting curve of the measured data. This indicates that the presented three-dimensional viscoelastic constitutive model in this paper can be used to describe the material properties of the asphalt mixture accurately.

There are some tolerances between the full-scale results and the predicted results. The main reason is that dynamic load is applied to the full-

scale testing while immediate and statistical load is adopted for the FE prediction. Asphalt concrete is very sensitive to loading frequency. Elastic modulus of asphalt concrete varies a lot under different loading velocity. The elastic modulus adopted in ABAQUS, however, is a constant value, which leads to tolerances between the full-scale results and the predicted results. Furthermore, stress field simulated by finite element method is different from the realistic one tested at the accelerated pavement testing facility MLS66, which has an effect on the strains of steel deck asphalt pavement.

Although tolerances exist between the full-scale results and the predicted results, the errors are in the acceptable range. Therefore, we can use the numerical model to predict the tensile strain of steel bridge deck pavement. This will provide an effective method for the mechanical analysis of steel bridge deck pavement of asphalt mixture.

## 7 SUMMARY AND CONCLUSIONS

1. The asphalt mixture pavement of steel bridge deck is in a complicated three-dimensional stress state when under the action of traffic load. In this paper, the three-dimensional viscoelastic deviatoric strain increment and volumetric strain increment of asphalt mixture were derived based on the three dimensional viscoelastic constitutive theory. Combining with the ABAQUS finite element material users (UMAT) function, numerical analysis of three dimensional viscoelastic constitutive model can be achieved with FORTRAN programming language.
2. The uniaxial compression creep tests were applied to research on the creep characteristics of two adopted paving materials under the 0.7 MPa load level at temperature 15°C. The parameters of three dimensional linear viscoelastic constitutive model of asphalt mixture can be obtained by fitting test data.
3. By comparing the experimental data of accelerated loading test and the finite element numerical simulation results, it is found that the transverse strain of the SMA-13 surface layer in the numerical prediction is in good agreement with the measured results. Therefore, it is reasonable and practical to apply the three-dimensional viscoelastic constitutive numerical model as a means of verification to predict the tensile strain cracking failure control index of asphalt mixture steel bridge deck pavement which provides an effective method for further mechanical analysis of steel bridge deck asphalt layer.

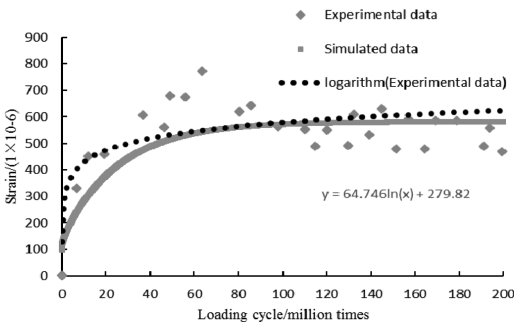


Figure 7. Surface layer transverse strain of SMA-13 across the edge web of the middle span.

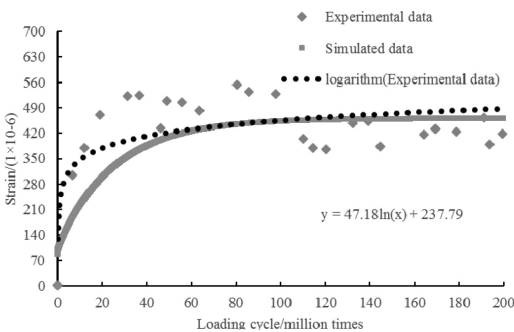


Figure 8. Surface layer transverse strain of SMA-13 across the edge web away from the middle span with a 3080 mm distance.

## REFERENCES

- [1] He G., Wong W. (2007). "Laboratory study on permanent deformation of foamed asphalt mix incorporating reclaimed asphalt pavement materials." *Construction and Building Materials*, 21(8): 1809–1819.
- [2] Medani T.O., Liu X, M. Huurman, Scarpas A, et al. (2008). "Characterisation of surfacing materials for orthotropic steel deck bridges. Part 1: experimental work." *Finite Elements in Analysis and Design*, 44: 552–563.
- [3] M. Huurman, T.O. Medani, A.A.A. Molenaar, C. Kasbergen, A. Scarpas. (2004). "APT testing and 3D finite element analysis of asphalt surfacings on orthotropic steel deck bridges." 83rd Annual TRB Meeting, Washington, D.C., USA.
- [4] Liu X., Medani T .O, Scarpas A, et al. (2009). "Characterisation of surfacing materials for orthotropic steel deck bridges. Part 2: numerical work." *International Journal of Pavement Engineering*, 11(3): 255–265.
- [5] ZHEN Xiao-xia, WANG Rong-hui, CHEN Yin-zhen.(2009). "Analysis of Viscoelastic Responses of Asphalt Mixture Pavements of Steel Bridge Deck." *Science Technology and Engineering*, 9(14):41–44.
- [6] ZHAO Guo-yun, YU Guo-xing, MO Lian-tong. (2013). "Mechanical Analysis for Viscoelasticity in Steel Deck Pavement." *Technology of Highway and Transport*, 2(3):69–73.
- [7] R.A. Schapery. (1968). "On a thermodynamic constitutive theory and its application to various nonlinear materials." *Proc. IUTAM Symp, East Kilbride*, 259–285.
- [8] R.A. Schapery. (1969). "On the characterization of nonlinear viscoelastic materials." *Polymer Engineering and Science*, 9(4):295–310.
- [9] South China University of Technology. (2011). "Research of steel deck pavement for Hong Kong-Zhuhai-Macao Bridge." Guangzhou: South China University of Technology.
- [10] South China University of Technology. (2012). "Accelerated loading test of steel deck pavement for Hong Kong-Zhuhai-Macao Bridge." Guangzhou: South China University of Technology.
- [11] BS 1447:1988, (1988). "Specification for mastic asphalt (limestone fine aggregate) for roads, footways and pavings in building."
- [12] South China University of Technology. (2011). "Research on mechanical analysis of steel deck pavement for Hong Kong-Zhuhai-Macao Bridge." Guangzhou: South China University of Technology.
- [13] Hua J. (2000). "Finite element Modeling and analysis of Accelerate Pavement Testing Devices and Rutting Phenomenon." Ph.D. Thesis, Purdue Univerdity.
- [14] Uzaowski L, Paradis M, Lum P. (2004). "Accelerated performance testing of Canadian asphalt mixes using three different wheel testers." Quebec: Transportation Association of Canada.



## Analysis of fluctuation in China's remaining recoverable oil reserves

L. Wang

*School of Energy, Xi'an University of Science and Technology, Xi'an, China*

J.S. Zhang

*School of Economy and Management, Yan'an University, Yan'an, China*

**ABSTRACT:** Oil resource is one of the major energy resources in China. Analyzing the variation law for its remaining recoverable reserves can reveal its level of assurance to energy supply security of China. Based on the Monte Carlo simulation methods, by selecting data of remaining recoverable reserves since 1980 as samples, we made an empirical study on their fluctuation. Historical data analysis showed that the changing process of China's oil-remaining recoverable reserves followed the geometric Brownian motion. In conclusion, a strategic oil reserve program and energy diversification strategy can not only relieve the supply risk of random fluctuation of oil reserves, but also is crucial to the energy supply security of China.

**Keywords:** oil resource; remaining recoverable reserve; fluctuation; Monte Carlo simulation; geometric brownian motion

### 1 INTRODUCTION

China is a big consumer of oil resources, and so accurately grasping the fluctuation of oil reserves can ensure China's energy supply security. Since its reform and opening, with rapid development of China's oil industry, explored reserves have been growing. The production of crude oil has increased steadily. Both these achievements have been making significant contributions to the economic and social development<sup>[1]</sup>. At the same time, demand and consumption of oil has also shown strong growth. According to the latest release of "Domestic and International Oil and Gas Industry Development Report 2014"<sup>[2]</sup>, China's apparent oil consumption (sum of production and net imports) has reached more than 518 million tons and its net imports are about 308 million tons. The oil external dependence has reached 59.5%, which far exceeds the internationally recognized warning line. Therefore, solving the issue of oil supply security in China is an urgent requirement because of the increasingly prominent contradiction between supply and demand and an increasingly complex geopolitical situation. However, to identify the root of the solution to this problem, we must clarify the long-term fluctuation of China's oil reserves, analyze the dynamic changes in growing potential oil resources, and then evaluate the oil resources and support capabilities quantitatively. In the new situation and new background, using an appropri-

ate method to carry out an empirical research to analyze the long-term change trend in oil reserves is helpful in grasping the status of occurrence of oil resources more accurately and in achieving better control over the level of security of oil resource supply. As a result, discovering a suitable mathematical model to describe the fluctuation trend of China's oil reserves is not only an important issue of China's energy supply security, but also is beneficial to the government and administrations which will evaluate the oil support capabilities accurately and make appropriate regulations and policies.

Reserves are dynamic concepts due to changes in technology, human cognitive abilities, exploration, exploitation capacity, and the economic capacity of a specific period<sup>[3]</sup>. Lory and some other scholars<sup>[4-8]</sup> used the geometric Brownian motion to describe the uncertainty of reserves in the beginning. Epaulard<sup>[9]</sup> summarized all kinds of factors and built a model of random fluctuation reserves based on the geometric Brownian motion. In recent years, Chinese scholars in related fields had also carried out some corresponding research work. K. Zhang<sup>[10-11]</sup> compared the oil reserves in different regions in recent decades, analyzed the reasons for changes, and forecasted their development trend. P.P. Shen<sup>[12]</sup> and Z. Y. Zhou<sup>[13]</sup> combined mathematical models with some other predicted data, and then performed a prediction of the growth trend of China's proven oil reserves in recent years. Y.X. Li<sup>[14]</sup> systematically analyzed the factors affecting

oil and gas reserves and production growth trends in China and then summarized them as the following three aspects: geology, theory technology, and demand and prices in oil and gas.

From all the above-mentioned studies, it is not difficult to see that foreign scholars are more inclined to directly assume the change of laws of energy reserves to the geometric Brownian motion or other random process models as a basis for the purpose of research. But they did not focus on energy reserves' long-term change process and have paid little attention to the empirical test of fluctuation in the oil reserves. Chinese scholars basically followed the achievements of Western scholars in this issue and focused on the theoretical analysis and lack of quantitative analysis of oil reserves' fluctuation, which will limit deeper research on oil resources supply security. On this basis, according to historical data of remaining recoverable reserves of oil resources in nearly 26 years, the statistical characteristics of the change process is analyzed and the Monte Carlo simulation method is used to test whether the geometric Brownian motion can fit its law of changes.

## 2 INDICATORS' SELECTION AND DATA SOURCES

### 2.1 *Indicators' selection of oil reserves*

According to the "oil and gas resources/reserves classification" of the Ministry of Land and Resources of PRC, considering the oil and gas reservoirs (fields) exploration and development stage, geology degree of reliability, and production capacity as the classification standards, oil reserves can be further subdivided into geological reserves and recoverable reserves (technically recoverable reserves and economically recoverable reserves) [15]. Although the Ministry of Land and Resources of PRC had made a detailed classification standard of oil reserves, many statistical agencies all around the world chose different indicators and periods to study the changing trend of oil reserves. Take the international community of "BP Statistical Review of World Energy" as an example; they chose the proven reserves of oil reserves to disclose some countries' long-term situation of fluctuation of oil reserves. In China, before 2006, the Ministry of Land and Resources was mainly based on remaining recoverable reserves to publish China's oil occurrence conditions. However, with the publication of the new standard "Oil and Gas Resources/Reserve Classification", China chose the oil-remaining recoverable technical reserves to present China's oil reserve conditions.

Because indicators of oil reserves lack uniform standards of measurement, choosing the

appropriate indicators to present their fluctuation laws is essential. With market economy under consideration, the current amount of resources (remaining recoverable reserves) should be more emphasized, rather than the total amount of oil underground speciation (reserves) or the cumulative amount of recoverable reserves (recoverable reserves). Thus, the remaining recoverable reserves of oil can truly reflect the status of a country's oil reserve conditions, forecast, and provide the potential production and availability for the future. In addition, although the remaining recoverable technical reserves can also reflect the current situation of China's oil reserves, given the limitations of a short period of data availability, their long-term laws of fluctuations could not be analyzed. Therefore, this article will use the remaining recoverable reserves data of oil resources since 1980 to carry out a study on the change trend of oil reserves.

### 2.2 *Data sources*

Statistical data are mainly obtained from "BP Statistical Review of World Energy", China's National Bureau of Statistics, and the Ministry of Land and Resources website. Wherein, to facilitate comparative analysis, proved reserves data which were based on "BP Statistical Review of World Energy" that transformed the unit from ten billion barrels into one hundred million tons was used. Besides, remaining recoverable reserves data are obtained from the Ministry of Land and Resources publications and annual reserves-related information. Remaining recoverable technical reserves data are collected from the China's National Bureau of Statistics website.

## 3 ANALYSIS OF FLUCTUATION IN OIL RESERVES

### 3.1 *Historical data analysis*

Comprehensively, when compared with the changing behavior of the proved reserves, the remaining recoverable reserves and the remaining recoverable technical reserves can help us grasp the linkages between these types of reserves. Figure 1 depicts the fluctuation of these types of reserves. The variations of remaining recoverable reserves and proved reserves were very similar, which showed a trend of random fluctuations, particularly in the years 1985 and 2000. In addition, from the year 2002, China's National Bureau of Statistics had used the remaining recoverable technical reserves to reflect oil resources; as a result, these data showed a clear upward trend.

Since the reform and opening up, China's remaining recoverable reserves of oil had gone through a very complex process of cyclic changes.



Figure 1. Fluctuation in China's oil reserves.

As can be seen from Figure 1, it could be roughly divided into three stages of change from 1987 to 2005. From 1978 to 1987, China's remaining recoverable reserves of oil were increasing substantially and especially peaked in 1984. From 1988 to 2005, remaining recoverable reserves data were more stable, although bottomed out in 1992 and began to rise rapidly in 1993. From 2006, remaining recoverable reserves started a new round of decline. Above all, the fluctuation of oil-remaining recoverable reserves in China showed a very obvious trend of random fluctuations.

In fact, we can infer from the formula that, as long as these are related to the proven recoverable reserves and production, these factors will directly lead to dynamic changes in remaining recoverable reserves. Specifically, the three factors that lead to changes are endowments, technological progress, and resource exploration investment. Resource endowments directly determine the size of discovery of the field-scale and almost every remaining recoverable reserve jumped was accompanied with discovered massive oil fields. If technology continues to advance, then we can break through the limitations of the original exploration, solve the technical problems which we could not overcome in the past, and explore unknown areas. A continuous increase in exploration investment can protect healthy development of the oil industry in terms of economy. Thus, the remaining recoverable reserves are the result of fluctuations in the dynamic interaction of many uncertain factors. Theoretically, the use of stochastic processes to characterize the fluctuation in remaining recoverable reserves of the oil is entirely reasonable.

### 3.2 The empirical analysis

From the theoretical analysis and graphical features, we can preliminarily judge that fluctuation of oil-remaining recoverable reserves has characteristics of random fluctuation. Since the geometric Brownian motion is the basic random process model and has good statistical properties,

an empirical analysis was made to see whether the geometric Brownian motion can fit the fluctuation in oil-remaining recoverable reserves. According to the standard model of the geometric Brownian motion, the following relations can be drawn:

$$dR(t) = \mu R_t dt + \sigma R_t dW_t \quad (1)$$

wherein,  $R(t)$  is the remaining recoverable reserves of oil,  $\mu$  is the parameter of rate of change obtained from proven data or exploitation of reserves,  $\sigma$  is the standard deviation of the remaining recoverable reserves, and  $W_t$  is a standard Wiener process.

On the basis of the geometric Brownian motion model, we can combine the unit root test with Monte Carlo simulation method to test the law of change of oil-remaining recoverable reserves. The specific test procedure is as follows:

1. Take the unit root test of the data of remaining recoverable reserves using EViews6.0 and judge their stability. The unit root test can be made of four classical methods, namely ADF test, DF-GLS test, PP test, and Elliott-Rothenberg-Stock test.
2. Use the maximum likelihood estimation method to estimate the parameters  $\mu$  and  $\sigma$  in the model by using MatlabR 2009a software.
3. Convert the geometric Brownian motion model into a function on  $R$  by Ito lemma and then use MatlabR 2009a software to perform Monte Carlo simulation of the data of the remaining recoverable reserves. In order to improve the accuracy of the simulation, we performed 10,000 times simulation. When comparing the actual residual recoverable reserves data and analog remaining recoverable reserves average error ( $E_M$ ) data to determine the accuracy of the model, the Ito lemma conversion process is obtained as follows:

If  $f(R(t)) = LnR(t)$ , then

$$\frac{\partial f}{\partial R}(R, t) = \frac{1}{R} \quad (2)$$

$$\frac{\partial f}{\partial t}(R, t) = 0 \quad (3)$$

$$\frac{\partial^2 f}{\partial R^2}(R, t) = -\frac{1}{R^2} \quad (4)$$

Based on Ito lemma, these can be written as follows:

$$df = \left[ \mu R_t \frac{\partial f}{\partial R} + \frac{1}{2} \sigma^2 R_t^2 \frac{\partial^2 f}{\partial R^2} + \frac{\partial f}{\partial t} \right] dt + \sigma R_t \frac{\partial f}{\partial R} dW_t \quad (5)$$

$$d(\text{Ln}R_t) = \left[ \mu - \frac{1}{2}\sigma^2 \right] dt + \sigma dW_t \quad (6)$$

Then, the formula can be obtained by integrating

$$\text{Ln}R(t+dt) - \text{Ln}R(t) = \left( \mu - \frac{1}{2}\sigma^2 \right) dt + \sigma\sqrt{dt}X \quad (7)$$

$R_t$  can be expressed as follows:

$$R_t = R_0 * \exp \left[ \left( \mu - \frac{1}{2}\sigma^2 \right) T + \sigma\sqrt{T}X \right] \quad (8)$$

wherein, T is the entire time and X is the Random standard normal distribution.

Besides, the average error ( $E_M$ ) is calculated as follows:

$$E_M = \frac{1}{N} \sum_{i=1}^N |R_i^s - R_i| \quad (9)$$

wherein,  $R_i^s$  is the simulated value of remaining recoverable reserves obtained using the Monte Carlo simulation method,  $R_i$  is the actual value of remaining recoverable reserves, and N is the number of samples.

### 3.3 Results

It is apparent from the results of the unit root test shown in Table 1 that, at the 5% significance level, the statistical value of each test method is greater than the critical value. It indicated that China's oil-remaining recoverable reserves and their logarithmic data could not reject the null hypothesis. That is to say, they both have unit roots. In addition, they do not have the stable characteristics. We can assume that their performances are random walk processes.

Based on this, the estimated results obtained by applying the maximum likelihood estimation method in MatlabR 2009a are as follows:  $\mu = 0.3519$  and  $\sigma = 0.4947$ . Furthermore, with the remaining recoverable reserves in 1980 as the base data, we can simulate remaining recoverable reserves of oil since 1980 by using the Monte Carlo simulation method. Then, in accordance with the

Table 1. Results of the unit root test.

Value	ADF	DF-GLS	PP	ERS				
R	-3.0	-1.7	-2.0	-1.4	-3.0	-1.8	3.0	12.4
LnR	-3.0	-1.6	-2.0	-1.3	-3.0	-1.8	3.0	12.6

Table 2. Statistical characteristics of the simulated data and the average error.

Statistics	Mean	SD	Max	Min
Simulated data	19.42	3.07	114.03	2.74
Average error	6.22	3.05	34.01	1.51

simulated data and the actual data, the average error  $E_M$  can be obtained. The statistical characteristics are given in Table 2.

As is apparent from Table 2, the value of average error ( $E_M$ ) is 6.2157. Thus, the geometric Brownian motion can fit China's remaining recoverable reserves of oil well. Besides, we can measure the kurtosis of the average error. If the kurtosis is smaller, that is to say, the model matches well.

Kurtosis is calculated as follows:

$$\text{Kurt}(E_M) = \frac{\sum_{i=1}^n (E_{M_i} - \overline{E_M})^4}{(N-1)S^4} \quad (10)$$

wherein, N is the number of samples and  $S^4$  is the fourth order center distance.

On using Eviews6.0 software to calculate the kurtosis of the average error, the value obtained is 7.0217. We can see that the geometric Brownian motion model could better match the data of China's oil resources remaining recoverable reserves.

## 4 CONCLUSIONS AND POLICY RECOMMENDATIONS

Due to the entire effect of the uncertainty of technology progress and exploration investment, China's oil resources remaining recoverable reserves will be in a normal state of random fluctuations. Therefore, stochastic processes are used to characterize the law of change. In this paper, the Monte Carlo simulation method is used to perform an empirical test of their fluctuations and the results showed that the dynamic changes of oil resources-remaining recoverable reserves followed the geometric Brownian motion. Additionally, the following policies were recommended:

1. To avoid the risk of oil supply security which is caused by random fluctuations of oil's remaining recoverable reserves, China should actively develop a specific and detailed strategic oil reserve plan. This strategy can gentle the lack of oil supply or oil crisis, and protect the security of oil supply from its roots.
2. Stochastic processes that are used to analyze China's oil reserves have increasing volatility

risk and imported risk is high. China should actively implement the strategic objectives of diversification of energy consumption. This will not only increase the proportion of alternative energy sources, but is also crucial for economic development and energy supply security.

## ACKNOWLEDGMENTS

This work was financially supported by the National Natural Science Foundation of China (No. 71273206).

## REFERENCES

- [1] Ping, W. & Yuwen, C. et al. 2011. Current situation and changing characteristics of oil reserves in China [J]. *Special oil and gas reseriors* 18(1):12–16.
- [2] 2014 domestic and international oil and gas industry development report [R]. 2014. Beijing: China Economic Research Institute of Oil Technology.
- [3] Jinsuo, Z & Qi, Q. 2013. Reviews on supply security of China's vital energy under uncertainties [J]. *Resources and Industries* 15(3):11–18.
- [4] Loury, G. C. 1978. Optimal exploitation of an unknown reserve. *Review of Economic Studies* 45:621–636.
- [5] Gibert, R. T. 1979. Optimal depletion of an uncertain stock. *Review of Economic Studies* 46:47–57.
- [6] Pindyck, R. S. 1980. Uncertainty and exhaustible resource markets. *Journal of Political Economy* 88(6):1203–1225.
- [7] Deshmukh, S. D., Pliska, S. R. 1983. Optimal consumption of a nonrenewable resource with stochastic discoveries and a random environment. *Review of Economic Studies* 50:543–554.
- [8] Brennan M, Schwartz E. 1985. Evaluating natural resource investment. *Journal of Business* 58:135–157.
- [9] Epaulard, A., Pommeret, A. 2003. Optimally eating a stochastic cake. *Resource and Energy Economics* 25:129–139.
- [10] Kang, Z. 2002. Analysis of oil remaining recoverable reserves variation in China since 1980 [J]. *China's Oil Exploration* 7(4):1–9.
- [11] Kang, Z. 2006. Change analysis of China's oil reserves in 1984–2004 [J]. *Oil & Petrochemical Today* 14(8):7–11.
- [12] Pingping, S. & Wenzhi, Z. et al.2000. Oil resource prospect and reserve forecast in China in next decade [J]. *ACTA Petrolei Sinica* 21(4):1–6.
- [13] Zongying, Z. & Kang, Z. et al. 2001. An introduction of common prediction methods and gas reserves, production rate and requirement [J]. *Xinjiang Oil Geology* 24(4):356–359.
- [14] Yuxi, L. & Daoyong, Z. et al. 2009. Factors that affect the increasing trends of China's oil and gas reserves and products [J]. *Acta Geoscientica Sinica* 30(6):855–867.
- [15] GB/T19492–2004 Oil and Gas Resources/Reserves Classification [S]. 2005. Beijing: China Standard Press.
- [16] Shaohui, Z & Jinsuo, Z. 2010. The empirical study on variable models of coal price in China [J]. *Journal of China coal society* 35(3):525–528.



**Taylor & Francis**

Taylor & Francis Group

<http://taylorandfrancis.com>

# Research on the recycled brick concrete technology

Mei-xiang Zhang, Xiao-yi Zhang & Bo Sun

*School of Architectural Engineering, Xin yu University, Xin yu, Jiang xi, China*

**ABSTRACT:** With the development of construction industry, construction waste recycling has become a topic of global concern. Research on recycled aggregate concrete at home and abroad fundamentally solves the problems such as aggregate resource scarcity and environmental degradation, but research on recycled brick aggregate concrete is less. Based on the domestic research results of recycled aggregate concrete, the technology of recycled brick aggregate concrete is studied in this article. This work aims to provide certain reference for future research on recycled aggregate concrete.

**Keywords:** Waste sintering brick; recycled aggregates; recycled concrete; engineering application

## 1 INTRODUCTION

Reinforced concrete structure is the most widely used form of building structure. With the continuous development of city construction in recent years, there is a continuous increase in consumption of concrete material. Of the several kinds of raw materials of concrete, aggregate accounts for 60%–70% of the total volume of concrete materials. But due to the expiry of service life, improper design, improper use, improper maintenance, and natural disasters such as earthquakes, many old buildings were torn down, in addition to the large volume of new buildings that produce waste concrete and waste aggregate. For a long time, it had caused serious resource depletion of sand and gravel and environmental pollution problems. Recycled aggregate or recycled concrete aggregate is defined as the aggregate that results from a certain proportion of interaction of waste concrete after cleaning, crushing, and grading. Recycled concrete is partly or fully made of recycled aggregates. Obviously, the development and application of recycled concrete not only uses a large amount of waste concrete and reduces the construction of natural aggregate consumption, but also fundamentally solves the natural aggregate shortage and the deterioration of ecological environment problems caused by large amounts of waste concrete. And therefore, it conforms to social sustainable development. Based on the domestic research results of recycled aggregate concrete, this article will analyze the technology of recycled brick aggregate concrete. This work aims to provide certain reference for future research on recycled aggregate concrete.

## 2 RESEARCH ON RECYCLED AGGREGATE CONCRETE AT HOME AND ABROAD

### 2.1 *Research on recycled aggregate concrete abroad*

Few studies by Malhotra V M [1], Buck AD [2], and Limbachiya MC [3] show that the laws of the compressive strength development of recycled aggregate concrete and ordinary concrete are similar. A study by B. C. S. J [4] shows that the compressive strength of recycled aggregate concrete is lower by 14%–32% than that of normal concrete.

Research carried out by Gupta S M [5] shows that the impact of the water–cement ratio on the compressive strength of recycled aggregate concrete is more obvious; a high water–cement ratio leads to higher compressive strength of recycled aggregate concrete than that of normal concrete of the same period and a low water–cement ratio leads to lowering of compressive strength of the recycled aggregate concrete than that of ordinary concrete of the same period.

A study by Ravindrarajah R [6] shows that, under the same water–cement ratio, contraction deformation increases the amplitude of recycled aggregate concrete at a larger rate than that of ordinary concrete. Another study by Eguchi K [7] shows that the drying shrinkage of recycled aggregate concrete is relatively larger.

### 2.2 *Engineering application of recycled aggregate concrete abroad*

After the Second World War, Germany, the Netherlands, Japan, and other countries studied about

the recycled waste concrete and held many special international conferences [8]. Construction waste processing in developed countries is divided into the following two stages: in the first stage, before the production of construction waste, they minimize wastes through scientific managements and effective control measures; in the second phase, after construction waste has been produced, they transform wastes into a renewable resource by using effective scientific methods.

The utilization rate of construction waste has reached 56% in Tokyo in 1988. Qingshui Construction Company and the Tokyo Electric Power Company in Japan developed the separation technology to separate waste concrete mortar and stones, to make more reasonable and effective use of these waste materials.

“Super fund law” enacted by the U.S. government regulates production enterprises with industrial waste to properly handle wastes, without giving approval to arbitrarily dump. In the United States, the scene of the asphalt pavement thermal regeneration technology is already quite mature; 50% of the road construction in the United States used asphalt concrete reworked material. As a result, direct construction costs fell by more than 20% on average, while indirect social benefits such as energy and environmental protection is huge.

The Netherlands is one of the earliest countries to carry out research and application of the recycled concrete. In the 1980s, The Netherlands made specifications about the use of recycled concrete aggregate to prepare plain concrete and reinforced concrete and prestressed reinforced concrete.

Denmark promulgated regulations that it allows the use of recycled aggregates in a suitable environment for certain specific structures in 1990.

German carbonization burning garbage disposal technology can clearly separate all kinds of renewable materials of the waste, recycle and use them. This technology effectively solves the problem of the waste land.

### 2.3 *Domestic research on recycled aggregate concrete*

Jian-zhuang Xiao [9] of Tongji University has carried out a study which shows that the same mixture ratio of recycled aggregate concrete, when compared with ordinary concrete, achieves lower compressive strength, but can fulfill the requirement of the specification.

Previous research carried out by Xingwen Luo [10] and Yan-dong Jia [11] shows that the elastic modulus of recycled aggregate concrete is lower when compared with normal concrete, but satisfies the requirement of the standard.

A study by Kun Li [12] of Dalian Science and Technology University shows that the quality of

the recycled concrete aggregate is closely related to the original concrete strength, the relationship of compressive strength of recycled aggregate concrete and absolute grey water is linear.

Research carried out by Chao Yi [13] of Jinan University shows that the replacement ratio of the recycled coarse aggregate affects the performance of recycled concrete; it also has the biggest replace rate.

Research carried out by Qiuyi Li [14] of Qingdao University of Science and Technology shows that, as the replace rate of recycled fine aggregate increases, the recycled concrete compressive strength decreases obviously. When equipped with low strength grade of concrete, the replace rate of fine aggregate should not be greater than 50%; when equipped with high strength grade of concrete, the replace rate of fine aggregate should not be greater than 20%.

### 2.4 *Engineering application of recycled aggregate concrete at home*

The Chinese government attaches great importance to construction waste recycling. Many related technologies and demonstration projects have funds and policy support; they also support comprehensive utilization of construction waste and production of new building materials.

An urban construction enterprise in Beijing recycled more than 800 t of construction waste, and successfully used it in the preparation of masonry mortar, interior wall and ceiling plaster, fine stone concrete floor, and concrete cushion layer.

Damaged concrete pavements have been widely used in highway construction in Xiangfan city in Hubei province and good economic and social benefits have been achieved. They used 30% recycled aggregates in cement stabilized base, leading to improved performance and reduced cost of the cement stabilized base.

## 3 RESEARCH ON RECYCLED BRICK AGGREGATE CONCRETE

Yong Cao's study [15] shows that the compressive strength of recycled brick coarse aggregate concrete is lower than that of natural aggregate concrete; the lower amplitude is obvious in the same age and the measured value of compressive strength of recycled brick aggregate concrete is low. But, it still meets the requirements of C20 and C25.

Research carried out by Handong Yan and Xiufeng Chen of Huaqiao University [16] shows that with the same aggregate amount and water phase ratio, increasing the dosage of cement can appropriately increase the compressive strength and elastic modulus of the recycled clay brick aggregate concrete.



A study by Lingjun Xie [18] of Shandong Agricultural University shows that the gradation, strengthening treatment, water–cement ratio, sand ratio, and water consumption per unit volume of recycled coarse aggregate are main influencing factors of the strength of recycled aggregate concrete. The replacement ratio of recycled brick coarse aggregate has a great effect on the strength of the recycled aggregate concrete; its compressive strength decreased with the increase of dosage of recycled brick coarse aggregate.

#### 4 CONCLUSION AND PROSPECT

Based on the research and engineering applications of recycled aggregate concrete at home and abroad, the following conclusions are drawn:

1. The factors influencing the compressive strength of recycled aggregate concrete are many; under the same proportions and water–cement ratio conditions, the performance of recycled aggregate concrete is lower than that of ordinary concrete, but it can still meet the requirements.
2. More and more construction wastes are developed and used, resource consumption is reduced, the ecological environment is protected, and ecological balance is maintained.
3. The replacement ratio of recycled aggregate impacts the performance of recycled concrete; it should not be greater than the maximum.

The following thrust areas need to be focused in further studies, to make recycled aggregate concrete technology more mature and more widely used in engineering practice:

1. Theoretical research needs thorough investigation; we should study properties such as flexural, impact resistance, durability and the bearing capacity of recycled aggregate concrete to make it more secure and to meet the engineering requirements, especially recycled waste brick aggregate concrete remains to be studied further.
2. Research on high strength recycled aggregate concrete.

#### ACKNOWLEDGMENT

1. Science and technology project titled “Experimental study and finite element analysis on RC beams strengthened with NSM prestressed spiral rib wires” in Jiangxi province education department in 2015 (GJJ151216).
2. Field studies program titled “Research on the engineering application of reinforced methods for concrete structure” of Xinyu University in 2015 (XJ201505).

3. Innovative training program for college students of Xinyu University titled “Research on the technology of recycled brick concrete” in 2015 (2015050).

#### REFERENCES

- [1] Malhotra V M. Use of recycled concrete as a new aggregate [R]. Rcpport. Canada Center for Mineral and Energy Technology. Ottawa. Canada. 1976: 76–18.
- [2] Buck A D. Recycled concrete as a source of aggregate [J]. Journal of ACI. 1977: 212–219.
- [3] Limbachiya M C. I.aelawat T.RCA concrete: A study of properties in the fresh state, strength development and durability [A]. Proceedings of International Conference on Sustainable Construction: Use of Recycled Concrete Aggregate [C], University of Dundee, Scotland, 1998: 227–237.
- [4] B.C.S.J. Study on recycled aggregate and recycled aggregate concrete [J]. Concrete Journal. 1978(16): 18–31.
- [5] Gupta S M. Strength Characteristics of concrete made with demolition waste as coarse aggregate [A]. Proceedings of the Intemational Conference on Recent Development in Structural Engineering [C], 2001: 364–373.
- [6] Ravindrarajah R. Tam C T. Properties of concrete made with crushed concrete as coarse aggregate [J]. Magazine of Concrete Research. 1985, 37(130): 29–38.
- [7] Eguchi K, Teranishi K, Narikawa M. Study on mechanism of drying shrinkage and water loss of recycled aggregate concrete [J]. Journal of Structural and Construction Engineering, 2003, pp: 1–7.
- [8] Yong-gang Chen, beibei cao. Development of recycled concrete at home and abroad [J]. Journal of building materials science and technology, 2004, 25(3): 4–6.
- [9] Jian-zhuang Xiao. Recycled concrete [M]. Beijing: China building industry press, 2008.
- [10] Xingwen Luo, chang-sheng guan. Experimental study on mechanical properties of recycled concrete [J]. Rock and soil mechanics, 2007, 11: 244.
- [11] Yan-dong Jia, Ling Li, Xiaohua Liu and so on. Experimental study on properties of different size recycled aggregate concrete [J]. Journal of transportation science and technology and economy, 2009, 5: 61.
- [12] Li Kun. Research on basic properties of recycled aggregate and recycled concrete [D]. Master degree theses of master of dalian university of technology. 2005.
- [13] Chao yi. Research on preparation of recycled aggregate concrete construction waste resource utilization [D]. Master degree theses of master of jinan university. 2014.
- [14] Qiu-yi li, Zhe Kong, Yuanxin Guo abd so on. Experimental research on the work performance and mechanical properties of recycled fine aggregate concrete [J]. Concrete, 2016, 1: 131–136.
- [15] Yong cao, bing-kang liu, Qin Xia. The drying shrinkage test on recycled concrete [J]. Journal of engineering and construction, 2009, 1: 47–49.

- [16] Handong Yan, xiu-feng Chen. Study on the impact of recycled waste clay brick aggregate on the properties of concrete [J]. Journal of sichuan building science, 2009, 35(5): 179–182.
- [17] Yaozong Zheng. Study on temperature control technology of guangzhou metro engineering concrete [J]. Journal of fujian building materials, 2006, 3:28.
- [18] Lingjun Xie. Preparation technology and performance study on recycled brick concrete [D]. Master degree theses of master of shandong agricultural university. 2012.

## A comprehensive information system for landslide monitoring based on a three-dimensional geographic information system

Mo-Wen Xie, Yan-Chang Jia, Fu-Xia Lv & Sheng-Xiang Chang

*School of Civil and Environmental Engineering, The University of Science and Technology Beijing, Beijing, China*

**ABSTRACT:** Landslide monitoring is an effective means of predicting a landslide's stability. Technology involving Three-Dimensional (3D) laser scanning and radar remote sensing have been applied to facilitate landslide monitoring. To process and analyze the 3D laser scanner and radar monitoring data, a geographic information system, 3D virtual reality, and Internet technology are required to improve the efficiency of the system. However, few studies have been conducted to explore a platform on which to perfectly combine these technologies. In this study, a comprehensive information system for landslide monitoring is proposed. Its main functions include 3D visualization of basic engineering geological data, secure monitoring of the landslide, monitoring data analysis, early warning, and network-based information release. The landslide monitoring system is a safety monitoring project on the Jinpingzi landslide. The results are very convincing and indicate that this study can improve the system reliability and provide a reference for relevant projects.

**Keywords:** landslide monitoring; comprehensive information system; 3D visualization; internet; GIS

### 1 INTRODUCTION

Landslide monitoring has always been an important subject in the study of landslides, and many recent studies have been conducted on related topics. Xie et al. (2011) developed a ArcGIS Server platform-based landslide safety monitoring network GIS. A 3D-analysis module has been developed to achieve graphical representation and interpolation of the monitoring data in the section plane and 3D view. Kunapo et al. (2005) developed a geotechnical engineering Web-GIS system to achieve the monitoring data query, for profile analysis, and to generate 3D images and soil distribution maps. Zhang et al. (2013) designed a landslide monitoring system based on a wireless network. He constructed the monitoring area of the mountain wireless sensor monitoring network and performed real-time monitoring of the mountain landslide natural disasters. Li et al. (2013) selected MAPGIS as a base platform whose basic functions are applied to manage the engineering geological information for Diao Zhongba and performed research on the secondary development library based on MAPGIS, and thus achieved early-warning of landslide. Wu et al. (2014) considered the limitations related to landslide monitoring by the Interferometric Synthetic Aperture Radar (InSAR) technique and proposed a method of integrating a Global Positioning

System (GPS) with Corner Reflector Interferometric SAR (CR-InSAR) techniques.

The studies mentioned above include all levels of fill and expansion of 3D visualization of the landslide and landslide monitoring. However, they have the following deficiencies: The monitoring system cannot keep pace with the times and does not have a unified platform to support GIS, 3D virtual reality, network, SAR, and 3D laser technology; The data management based on the relational data organization cannot adapt to the development requirements of landslide safety monitoring. For landslide monitoring, both the engineering geological conditions and the monitoring data should be considered. Because both are spatial data, data management based on a relational database for management, query, analysis, and processing spatial data appeared to be inadequate (Jia et al., 2012; Qiu et al., 2011). It cannot reflect the characteristics of the measuring point and the surroundings and will not be able to perform the visual query and analysis in the monitoring physical space; Fewer network-based landslide monitoring systems can meet the needs of the growing landslide monitoring work.

This paper proposes a landslide monitoring information system based on GIS, 3D virtual reality, network, SAR, and 3D laser technology. By means of 3D visualization and an Internet

platform, this system combines 3D visualization of engineering geological data integration, landslide safety monitoring, analysis, and forecasting, which integrates the space data acquisition, data organization, data processing, data results demonstration, and data analysis into a landslide monitoring information system.

## 2 THE SYSTEM REALIZATION

### 2.1 *Development framework and functions*

The system is based on component GIS technology, SQL server database, the Browser/Server (B/S) architecture, and Javascript+Vbscript and Asp.net+C# language. The component GIS is based on skyline TerraExplorer software. The system includes three modules that take into account the actual needs of landslide safety monitoring and the basic principles of GIS. The three modules include an engineering geological information module (solid modes), a monitoring data management module, and a data analysis and forecasting module. Based on these modules and landslide monitoring features, the system has a series of professional analysis functions, such as vector analysis, spatial analysis, correlation analysis, trend analysis, and threshold analysis. Based on these functions, users are able to more easily grasp the movement state of the landslide.

### 2.2 *Establish models*

To organize the combined data reasonably and achieve the system analysis functions and 3D display functions, we established a series of models. They can be divided according to their function into engineering geological solid models, monitoring data models, and data analysis models.

#### 1. Data Model

The system monitoring data were mainly obtained from monitoring instruments, including a drilling inclinometer, GPS, underground water level gauge, 3D laser scanner, and radar remote sensing satellites. The first three instruments are used to monitor point displacements, and latter two are used to monitor surface displacement.

**Point Data Model:** The data management module has three main methods of data management: file management, database management, and object-oriented management. In this system, the need to manage data mainly includes spatial data (such as landslide data for each monitoring point coordinate); nonspatial attribute data, such as the monitoring points of the category, number, description of nonstructured data, and a variety of digital pictures and sound files; and monitoring

information. Because the spatial data are unstructured and uncertain, the operation of spatial data needs to use the GIS function. Using the file (SHP file) storage landslide spatial data and attribute data of main part, with the help of relation database to manage the attribute data and monitoring information. Because the landslide spatial information and monitoring information are stored and managed separately, their relationship must be defined. In the SHP file, each monitoring point has a unique identifier; therefore, an identifier field was established in the tables in a relational database so the database can be linked by the monitoring points and the corresponding identifier. The association of attribute data is implemented by the GIS function. A variety of databases and file systems must be saved in the form of a project so it can be customized according to the specific landslide and monitoring project. Depending on the type of monitoring point data, some points only monitor displacement along a fixed direction, such as a drilling inclinometer. Some not only measure the size but also measure the displacement direction; for example, GPS monitors both the amount of displacement and the direction of the point movement. In the 3D system, we use a 3D arrow to represent these data points. The size of the arrowhead indicates the size of the measured values, the direction of the arrow denotes the direction in which the monitoring points move, and different colors represent different monitoring instruments. The attribute data, such as the point of monitoring time, size, and orientation, are stored in an SQL database, and the spatial data are stored in a spatial database, and the spatial and attribute databases are connected with a unified identification value. In 3D systems, a drilling inclinometer was used to measure data for display, lines are used instead of arrows, and the length of the line on behalf of the magnitude of displacement and the directions of lines denote the moving direction.

**Face data model:** GPS measurement is a kind of single-point monitoring that is based only on the important parts of the observation in pier landslide monitoring. GPS measurement has the advantage of high precision to the millimeter level. The disadvantages of this method include fewer monitoring points and difficultly obtaining the deformation; once destroyed it will seriously affect the continuity of data. The 3D laser scans to the grid scanning mode with high precision, high density, high speed, and nonprism measurement of surface, and has the characteristics of a high time resolution, high spatial resolution, and measuring accuracy of uniform. For a detailed understanding of the landslide deformation and overall change in detail, the 3D laser scanning technology is very meaningful. There is another way of monitoring—radar remote sensing monitoring. Monitoring data types

is also raster data. Unlike the optical remote sensing mechanism, radar remote sensing is an active remote sensing method; synthetic-aperture radar remote sensing works 24 hours a day in all weather, it can obtain a wide area deformation, its precision can reach the subcentimeter level, and it has broad application prospects for landslide monitoring. In 3D systems, laser scanners and radar remote sensing satellite monitoring data obtain the surface shape. The surface data of the displacement direction are fixed along the slope direction, but the data size varies, with different colors to distinguish different size data.

## 2. Data analysis model

One of the biggest advantages of GIS is to ability to unify spatial data and attribute data; based on the GIS function, data analysis seems to be an easy job. To show the monitoring data in an ideal way, the system developed different data analysis functions to enable users to master the landslide situation as much as possible through analysis of the spatial data and attribute data of the monitoring points. The functions include vector analysis, spatial analysis, correlation analysis, trend analysis, and conventional chart analysis.

Vector analysis model: For the GPS point data, the displacement is respectively along the XYZ direction component. To obtain the vector XYZ, the system developed vector analysis function. Displacement variation can be obtained by this model; For the surface data, such as laser scanner data and radar remote sensing satellite monitoring data, the displacement is usually along the slope direction. We can use a model to calculate the vertical and horizontal displacement. The main parameters of the model are the displacement size along the slope, the slope, and the aspect. We assume that for the surface coordinates of any point (x, y, z), the displacement value is S along the slope direction, the slope value is  $\theta$ , the aspect value is  $\beta$ , and the vertical and horizontal displacement of the point can be calculated by Eq. (1).

$$(1) \quad \begin{cases} \begin{cases} S_H = S * \cos\theta \\ S_V = S * \sin\theta \end{cases}, \beta \in (0, \pi/2) \\ \begin{cases} S_H = -S * \cos\theta \\ S_V = S * \sin\theta \end{cases}, \beta \in (\pi/2, \pi) \\ \begin{cases} S_H = -S * \cos\theta \\ S_V = -S * \sin\theta \end{cases}, \beta \in (\pi, 3\pi/2) \\ \begin{cases} S_H = S * \cos\theta \\ S_V = -S * \sin\theta \end{cases}, \beta \in (3\pi/2, 2\pi) \end{cases}$$

In Eq. (1),  $S_V$  is the vertical component of displacement and  $S_H$  is the horizontal component of displacement.

Spatial Analysis: Interpolation Analysis: The system provides Kriging and inverse distance interpolation. By interpolation, the system can continuously obtain face data from the limited point data. The system also can obtain the slope, aspect, mountain shadows, and the volume of a bad geological body.

Correlation Analysis: The model is used to analyze the correlation between the monitoring data and the environmental variables, such as analyzing the correlation between the surface displacement or movement speed and rainfall. As the conventional chart shows, the X-axis is the monitoring time, and the Y-axis represents the displacement value, rainfall, or rate of change of the displacement value.

Trend Forecast: The system can predict the trends of variables by polynomial fitting of the monitoring data. The highest degree of the polynomial is five polynomial.

## 3 SYSTEM APPLICATION

The Jinpingzi landslide is located on the right bank of the Jinsha River, and the Wudongde hydropower station is located approximately 900 m upstream. The Jinpingzi landslide is high in the Zhongshan landscape. The elevation of its leading edge is between 820 and 850 m, and its trailing edge is above 2200 m with an east-west trend. The results of remote sensing interpretation show that the landslide has a volume of about 620 million cubic meters. Its stable situation, deformation trends, and possible instability mode and scale relate to the development of the Wudongde hydroelectric station and have attracted attention from many circles.

### 3.1 Three-dimensional visualization

Three-dimensional visualization of engineering geological information includes comprehensive information on the engineering geological condition, bad geological phenomena, and the key points of the engineering geology.

### 3.2 Monitoring data 3D visualization

#### 1. Point data

Three-dimensional visualization of the point data can be a more intuitive representation of the measured value size and has significance for understanding landslide displacement. In the 3D system, monitoring point data are represented by arrows, the direction of the arrow indicates the direction of the monitoring point displacement, the size of the arrow represents the size of the monitoring values, green represents the X direction, and red represents the Y direction. To facilitate queries for attribute information of monitoring value while interacting

with the 3D terrain, the system developed a property information searching function. The function associates the measured values with the point in the map, so not only can we query the value of each point measured, we can also better understand the topography around the point. Combined with the engineering geological information, the system can make a comprehensive analysis of the monitoring results. Due to the directivity of the vector data, the traditional trend graphs cannot reflect the direction of its displacement. The system uses polar coordinates to visualize the measured values. Polar coordinates can indicate the size of the displacement values and represent the direction of displacement. When combined with the system's north modeling tools, a more intuitive understanding of the displacement and direction of the measured value can be obtained. The function can be seen from Fig. 1.

## 2. Surface data

Surface data, such as laser scanner data and radar remote sensing satellite monitoring data, are usually represented in the system by a surface form. Fig. 2 shows the 3D laser scanner monitoring result.

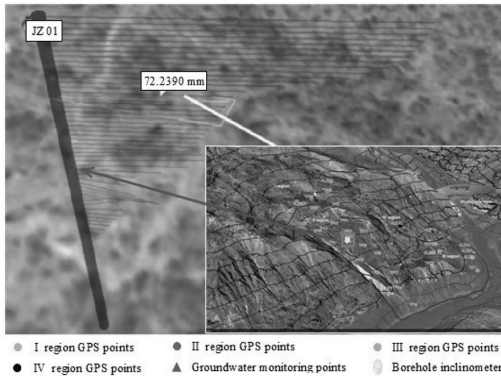


Figure 1. Value of borehole inclinometer.

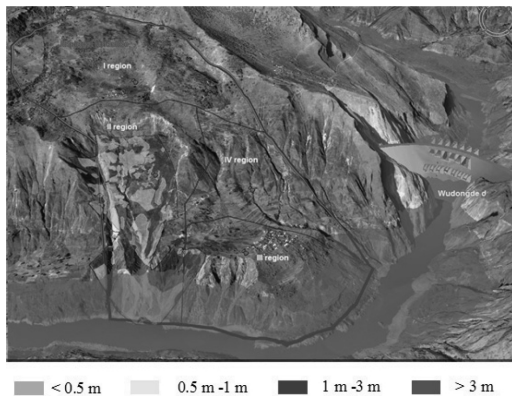


Figure 2. Monitoring results of laser scanner.

As shown in from the figure, the displacement of most of the Jinpingzi landslide is 3 to 5 mm.

## 3.3 Monitoring data analysis

### 3.3.1 Vector analysis

Fig. 3 shows the Jinpingzi landslide radar remote sensing vector analysis results. Graph a shows the monitoring results in the vertical direction of Radarsat-2 satellite between May 22, 2010, and June 22, 2010. Most of the vertical displacement is between 3 and 10 mm. In the eastern part of Region I, most of the monitoring value is between 1 and 3 mm. In Region IV, most of the vertical displacement is zero. Figure b shows the horizontal displacement of the Radarsat-2 satellite monitoring results between March 30, 2010, and May 30, 2010. The results in the monitoring time showed that most of the area of horizontal displacement was between  $-3$  mm and  $-10$  mm. The Region III monitoring value is between  $-6$  and  $-9$  mm, the vertical displacement value in Regions I and II is between  $-14$  and  $-20$  mm, and the horizontal displacement in most areas of Region IV is zero.

### 3.3.2 Spatial analysis

Fig. 4 shows the result of surface displacement by space interpolation in the Kriging method; with this method, we can obtain surface displacement from limited GPS monitoring points. The data were taken from January 2006 to July 2010.

As shown in Fig. 4 region II is the sliding body of the Jinpingzi landslide, which is the largest displacement sub in the Jinpingzi landslide, whose maximum value can reach 579.47 mm. The value in region I, the posterior wall of the landslide, is smaller than that in other zones. Region II is a slip tongue of the Jinpingzi landslide, which moves each year at a rate of about 60 mm to the Jinsha River.

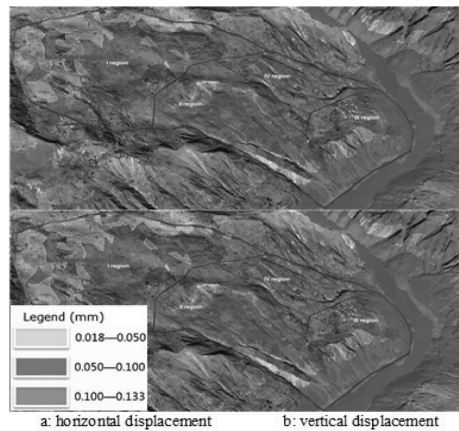


Figure 3. Remote sensing monitoring results.

Fig. 5 is the Jinpingzi landslide slope map obtained by surface analysis. As seen from the graph, the area of the larger slope belongs to the alpine and gorge region.

### 3.3.3 Correlation analysis

Correlation analysis is used to analyze the relevance between the monitoring amount and the environmental amount, such as the relevance between the surface displacement and the rainfall or the relevance between the surface displacement and the groundwater level.

Fig. 6 is a correlation analysis between rainfall and the displacement of the JY01 monitor-

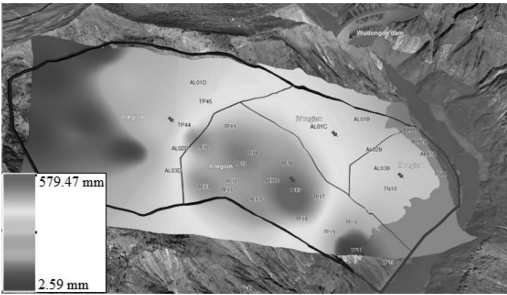


Figure 4. Spatial interpolation results.

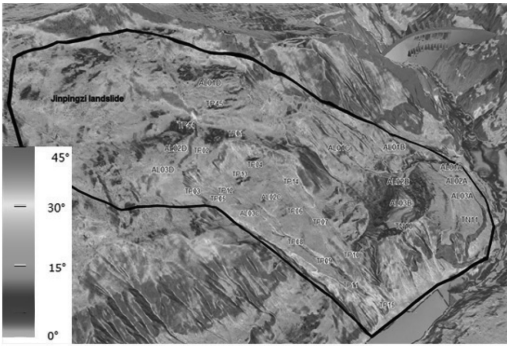


Figure 5. *Jinpingzi* landslide slope and aspect map.

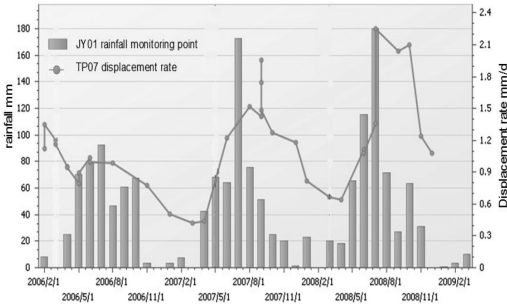


Figure 6. Surface displacement and rainfall rate curve.

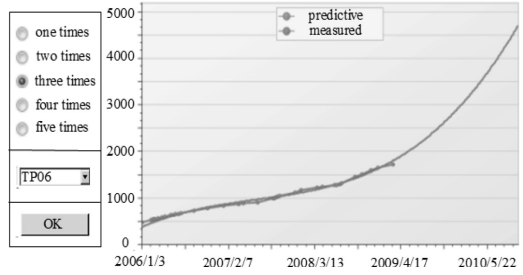


Figure 7. TP06 points polynomial fitting results.

ing point rate of the Jinpingzi landslide; it can be seen from the figure that May to October is the annual rainy season, that there is a large amount of rainfall, and that there is great variation in the displacement of the JY01 monitoring point. There is a positive correlation between the rate of change of the surface displacement and the rainfall: rainfall has a great influence on the movement of the Jinpingzi landslide.

### 3.3.4 Trend prediction

Fig. 7 shows the trend prediction result. The green line represents the measured values and the red line represents the predicted values; the two are in good agreement. From the predicted trend, displacement of TP06 was increasing.

## 4 CONCLUSIONS

In this paper, we present a comprehensive monitoring information system for landslides based on GIS, 3D virtual reality, network, SAR, and 3D laser technology. This system consists of 3D engineering and geological data, safety monitoring, and analysis and includes spatial data acquisition, data organization, data processing, demonstration of data results, and data analysis. Finally, the Jinpingzi landslide is used as an example to verify its feasibility, reliability, and practicality.

Integration of landslide monitoring systems is an inevitable direction. Systems need to add new and different methods and new technologies, such as 3D laser monitoring technology and deformation monitoring radar remote sensing technology. The system also requires the use of GIS technology for 3D visualization and analysis of the data obtained by the new technologies. Meanwhile, with the development of the information age, the network must be the direction of future information systems because it has great significance for data acquisition and sharing. This system must be widely used in landslide monitoring projects and other civil monitoring projects.

## REFERENCES

- [1] Xie Mowen, Chai Xiaoqing, Jia Ning, Wang Zengfu. "Development and application of real-time monitoring WEB-GIS for landslides," *Chinese Journal of Rock Mechanics and Engineering*, 2011, 30(10): 2090–2102.
- [2] Kunapo J, Dasari GR, Phoon KK, et al. "Development of a Web-GIS based geotechnical information system," *Journal of Computing in Civil Engineering, ASCE*, 2005, 19(3): 323–327.
- [3] Zhang Guirong, Yin Kunlong, Liu Liling, etc. "A real-time regional geological hazard warning system in terms of WEBGIS and rainfall," *Rock and Soil Mechanics*, 2005, 26(8): 1312–1317.
- [4] Li Xueping, Lia Yunan. "Design of GIS-based monitoring and early-warning system of landslide hazard in Diao Zhongba," *Energy Procedia*, 2012, 16: 1174–1179.
- [5] Zhu Wu, Zhang Qin, Ding Xiaoli, et al. "Landslide monitoring by combining of CR-InSAR and GPS techniques," *Advances in Space Research*, 2014, 53(3): 430–439.
- [6] Jia Ning, Xie Mowen, Chai Xiaoqing. Development and implementation of a GIS-based safety monitoring system for hydropower station construction. *Journal of Computing in Civil Engineering*, 2011, 26(1): 44–53.
- [7] Qiu Dandan, Lu Xinhai, Li Pei. "Monitoring and early-warning system of the high and steep slope in Daye mine based on GPS and GIS," *Journal of Wuhan Institute of Technology*, 2010, 32(1): 16–18.



# Study on the compatibility of the art design major and the Chinese language course in the colleges and universities of fine arts

Mei-ya Liang & Zheng-xi Ge

*Hebei Academy of Fine Arts, Shijiazhuang, Hebei, China*

**ABSTRACT:** In the colleges and universities of fine arts, the art design and the Chinese course construction is equally important and they both have the important significance for cultivating the art talents with the high skills and the high quality. However, now there exist various problems in the process of the compatibility between the art design major and the language course. In this paper, the main problem is how to explore the compatibility strategy conforming to the art design and the Chinese curriculum construction and how to make the teaching for the professional services and keep pace with the times, so as to realize the educational objectives of paying equal attention to the humanistic education and the art education.

**Keywords:** art design; Chinese language course; the compatibility strategy

## 1 INTRODUCTION

In the colleges and universities of fine arts, we put forward the compatibility between the art design major and the construction of the Chinese language course so that the art design and the creation of the students can be deeply rooted in the fertile soil of the Chinese culture courses in our country and their design and creation can bloom the real artistic spirit of the Chinese nation. This is the real innovation. Then the main problem discussed in the paper is how to explore the compatibility strategy conforming to the art design and the Chinese curriculum construction.

## 2 THE PROPOSAL AND THE TEACHING CURRENT SITUATION OF THE CHINESE LANGUAGE COURSE IN THE ART TEACHING

### 2.1 *The realistic significance of the Chinese language course in the college of fine arts*

In the college of fine arts, the realistic significance of the Chinese language course is to extract the classic literature works of the Chinese language course to study deeply and intensively and let the students know the essence of the Chinese literature, especially deeply understand the spirit of the Chinese culture. Only in this way, their art design and creation will have the cultural value and the artistic value. So we should study how to find the Chinese language course according with the characteristics of the students who learn the design arts, so as to

realize the education goals paying equal attention to the humanistic education and the art education. Such research has the realistic pertinence and it is naturally worthy of well study.<sup>[1]</sup>

### 2.2 *The teaching current situation of the Chinese language course in the colleges of fine arts*

Through the investigation and study we find that the present study of the design art and the Chinese language course in the college of fine arts commonly has the four aspects problems which need to be solved as follow.<sup>[2]</sup>

First of all, most of the students in the college of fine arts do not pay enough attention to the study of the Chinese language course on the concept. Most of the students in the college of fine arts can not realize that the culture is the base of the design art creation and simply think that the art is only the art and the design is just the design, and they have no direct relationship with the Chinese language. So they only learn the professional knowledge, but ignore the study of the Chinese language curriculum. The concept of one-sided understanding the art design has hindered their enthusiasm of actively learning the Chinese language curriculum. They only put the Chinese language course as the auxiliary course and have no occasion to invest a lot of energy to study. Especially the students who learn the western art are more reluctant to learn the Chinese language course, because they think that the Chinese language course has far distance with the western art and is not necessary to be learned. This idea is also the one of the reasons why they can not pay more attention to the study of the

Chinese language course. Without the enthusiasm of learning the Chinese language course, there is no fertile soil for the art design creation.

Secondly, the teaching level of the teachers in the college of fine arts is relatively weak. The college lacks the comprehensive teachers who both understand the art and the literature. The teachers usually are familiar with one aspect, but do not clearly understand the other aspect and even do not know it, which is the most urgent problem of reality at present. The teaching quality of the art design or the Chinese language course largely depends on the teaching level of the teachers. And at present in the college of fine arts, the teachers engaging in this aspect of teaching are the young and middle-aged teachers. On the one hand, the number of the teachers is relatively few, and on the other hand, the teaching level of the teachers needs to be improved. The college of fine arts relatively attaches importance to the introduction of the art talents and ignores the active introduction of the experts and scholars who are good at the construction of the Chinese language course, which is the fundamental cause of the relatively weak teaching level of the teachers in the college of fine arts.

Thirdly, the textbooks used by the college of fine arts can not completely conform to the reality of the students. Now, the situation in our country is that the textbook 《College Chinese language》 has so many editions. The textbook editions of 《College Chinese language》 totally have 1402 kinds which is published in the college Chinese teaching conference organized by the Ministry of Education. However, there are no the textbooks 《College Chinese language》 specially redacted for the students of fine arts. Most of the general and universal textbooks are written for the students in the higher colleges and universities and these textbooks mostly have no obvious characteristics, just repeat in low level and lack the necessary reference value. The articles selected by the textbooks tend to the literature masterpieces, especially the good poetry in the ancient China. The contemporary outstanding works of the humanities at home and abroad have very small percentage. Because of the diaphragm of the age and the difference of the major interests, a part of the students will not be interested in the selected title in the process of the study. So it is a worthy problem that how to select the suitable textbooks for the students of fine arts.<sup>[3]</sup>

The teaching concepts are traditional and the teaching methods are single in the college of fine arts. The situation of the Chinese teachers in many colleges and universities of fine arts is that the overall number of the course teachers is less and the young teachers whose professional titles and education backgrounds are low are more. The teachers have little learning and training opportunities

and their sphere of vision is not wide. The teaching situation is the behindhand teaching concept and the single teaching method. Many teachers still adopt the monotonous teaching method from the beginning when it comes to the end. In the class, the teacher speaks passionately, but the students are very vacant, such as falling in the clouds and the mist. The teacher speaks loudly, but the students are as silent as the grave. They maybe read an occasional book attentively, listen to the music or talk with each other in whispers. The students use the way of copying the homeworks of other students to cope with the teachers. How to do in the test? The teachers have to use the peacetime performances to save the students who failed in the final examination. So you can image the final teaching effect. The students are difficult to have the substantial gain and the teachers will laze away with the disappointed mood. We can't say it is not the sadness of the Chinese language education workers.

### 3 THE TOTAL IDEA OF THE COMPATIBILITY TEACHING REFORM OF THE ART DESIGN AND THE CHINESE LANGUAGE COURSE

The knowledge objective of the course is to make the students understand the historical development process of the major of the art design and the Chinese language course, master the basic rule and the main features of their development, define the historical trends of the cultural development and deeply understand the basic characteristics of the Chinese language course. The ability training goal of the course teaching is to make the students possess the following skills: the skill of discussion and communication; the language expression skill; the skill that can smoothly read and exactly understand the general articles, the academic works and the literary works and is able to understand the classical Chinese with the moderate difficulty and have the strong ability of the reading comprehension; the preliminary skill of mastering some basic literature knowledge and appreciating, analysing and evaluating the literary works. The emotional and value goal of the course teaching is to enhance the emotional understanding of the Chinese language curriculum, inspire the passion of expanding the national culture, establish the good positive attitude, get some enlightenments of planning the path of the life, improve the humanistic quality of the art students in our school, lead them to become the art designers with the cultural connotation and the high quality and provide the sustainable development power for their career.

#### 4 THE STUDY OF THE COMPATIBILITY COUNTERMEASURE OF THE ART DESIGN AND THE CHINESE LANGUAGE COURSE IN THE COLLEGE OF FINE ARTS

##### 4.1 *Positively make great efforts to the teaching textbooks construction in the college of fine arts*

The outstanding problem which need to be solved in the construction of the Chinese language course in the college of fine arts is the problem of the textbook. The specific opinion of our textbook construction is that we should establish the main ideas of redacting the textbooks starting from the teaching practice of the art colleges and universities. In the selected standards of the textbooks, we clearly put forward that the selected articles must be related to the majors in the colleges and universities of fine arts. The editorial board hopes that the selected titles can help the students improve the humanistic quality and enjoy the artistic life. It also hopes to promote the mother tongue literacy and the language expression ability, cultivate the interests in their majors and awaken the consciousness of the college students' independent thinking with the help of the professional related articles with the extremely strong literariness. The textbook is not only the carrier of the knowledge but also the partners of the students, and it can emotionally communicate with the students.

##### 4.2 *Positively improve the artistic culture of the professional teachers and the Chinese course teachers in the colleges of fine arts*

Training a team of the teachers with the high quality is an important task for the college. The colleges and universities of fine arts should have the consciousness to strengthen the training of the teachers and train the senior teachers who engage in the professional teaching and the Chinese language teaching at regular intervals. Meanwhile, they also should organize the young teachers to visit and learn and constantly improve the comprehensive quality of the teachers. No matter what majors the teachers belong to, they can not only focus on their own professional field of the research. According to the characteristics of the colleges and universities of fine arts, they should master the general rules of the art activities and positively improve the teaching contents, so that they can make the scientific research projects close to the fine arts and find the teaching contents which are the combination of the humanities and the arts.

Moreover, the teacher is not only the passer of the knowledge, but also has great enlightenment on the mind, the morality and the perfection of the

thoughts of the students. Therefore, in order to improve the comprehensive quality of the teachers, we should pay attention to the construction of the teachers' morality. Only the teachers' own soul is purified and their personality is perfected, they can edify and influence the students by their own noble personality and good virtue and help the students to shape their personality.<sup>[4]</sup>

##### 4.3 *Positively improve the teaching methods of the art design and the Chinese language course learning in the colleges of fine arts*

The teachers are actively to improve their own business level and humanity culture, at the same time, they should also actively explore the practical teaching paradigm which is suitable for the art design students combining with the actual needs of the art design students in our university. The Chinese language classes in the college are basically large classes, the duration of a class is ninety minutes and the theory is relatively strong, so the students are hard to avoid producing the feeling of fatigue at the latter half of the class. Therefore, in the Chinese language class, the teacher should ask more questions, walk around and design more interactive links to arouse the enthusiasm of the students.

We can improve the teaching methods from three aspects: Firstly, we should abandon the traditional pale knowledge teaching, such as the "force-feeding" way, and actively carry out the teaching methods of discussion, debate, enlightenment and interaction which give priority to the students. And we should give priority to the reading, thinking and discussion of the students not the explanation of the teachers and let the students really involved into the teaching process. Secondly, we should properly use the modern educational means. In class, the teachers should not only show the students the spirit charm of the traditional culture, but also fuse the teaching contents into the traditional culture using the multimedia equipments and improve the interests of the students using the modern teaching tools such as the audio and the video. Thirdly, the teachers should teach the students in accordance of their aptitude. When preparing the course, the teachers also need to carefully analyze the students and avoid the phenomenon of "one size fits all". The teachers should differently treat the students according to their different majors and different interests. Facing the undergraduate students and the junior college students with the different knowledge structures, the teachers should know what they need to teach and how to teach and timely adjust their teaching methods and contents according to the aptitude of the students.

#### 4.4 *Pay attention to the campus cultural construction of the Chinese language in the colleges of fine arts*

The construction of the campus culture can be achieved by holding a series of activities about the Chinese language courses. For example, we can invite the experts and scholars to hold the influential Chinese course lectures, and we can carry out the various exhibitions, the reading activities, the essay competitions, the speech competitions, the debate competitions and other activities which are about the theme of the Chinese language courses. If the fine forms and the coarse language expressions are not harmonious, the final communication effect must be directly affected. If the teachers can improve their various cultivation, collect the works of all kinds of students on campus and analyze them from the perspective of the language words in the classroom, we believe it still can cause the exploring interests of the students. In a word, we should build a full-bodied campus cultural environment and infect and guide the students in a process of the silent transforming influence, so as to improve the comprehensive cultural quality of the students.

### 5 HOW TO GRASP THE COMPATIBILITY FUTURE OF THE ART DESIGN AND THE CHINESE LANGUAGE COURSE

#### 5.1 *Set up the trinity course system of the schools, the teachers and the students*

For the art design students, the teaching time of the Chinese language course is limited, so most of the colleges and universities can open the class for only one academic year. In view of this situation, we put forward to establish the the trinity course system pattern of the schools, the teachers and the students. First of all, we put the Chinese language course as the important excellent course of the college and actively build the provincial excellent course. At the same time, we will blend the spirit of the Chinese language course into all aspects of the campus life, such as the campus construction, the classroom arrangement, the apartment culture and the class management, etc. And we should try our best to infiltrate the essence of the Chinese language course into the study and the life of the students, so as to realize the trinity course system pattern of the schools, the teachers and the students.

#### 5.2 *Building the assessment criteria integrating the knowledge capability and the quality-oriented education*

The universities and colleges of fine arts should not only actively reform the teaching contents

and the teaching methods, but also should constantly improve the assessment criteria of the course, so as to build the combining assessment standard of the knowledge ability and the quality-oriented education. Under the condition of mastering the knowledge reserve of the students, the colleges can reform the homework and the final exam grades of the students and make great efforts to transform from paying attention to the original knowledge to emphasizing the ability quality. For example, for the homework, the teachers used to let the students finish a small paper before, but the students maybe directly download it from the internet in the completing process and the significance is not big. We can let the students finish their homework in the form of speech and prepare the contents of the Chinese language course which the students are interested in, so that it can exercise the comprehensive ability of the students and improve the students' cultural quality. In the final examination tests, the teachers can give the short-answer questions and the essay questions which emphasize the examine of the ability quality instead of the traditional choice questions and the questions of filling in the blanks which pay attention to the knowledge points. At the same time, the teachers should also attach great importance to the the ideological guidance to the students and improve the learning interests of the students, so as to realize the training goal of the humanity quality education.

In a word, in the colleges and universities of fine arts, letting the art design and the Chinese language course combine well, we should combine their essence and make our art designs and art creations with the national style and the national customs of China, so that our art design works will have the basic spirit and the foundation of the Chinese culture.

### REFERENCES

- [1] Zhipu He, Min Jang. Art education. Beijing: People's Publishing House.2001.5. (In Chinese).
- [2] Xuejun Yue. The humanity quality education of higher art colleges. Social Science Front.1998(6). (In Chinese).
- [3] Hongfei Wei. Study on the compatibility of the Chinese language course and the modern design theory in the art design teaching in the colleges and universities. Education and Vocation. 2009(32). (In Chinese).
- [4] Yue Gu. Chinese language curriculum and the modernization of the higher education. Journal of North-western Polytechnical University. 2000. 6:20(2). (In Chinese).

## The calibration of refinery wastewater treatment process

Dong-le Cheng

*Qingdao Manda Industry & Trade Co. Ltd., Qingdao, China*

Lai-hong Yan

*China University of Petroleum, Qingdao, China*

**ABSTRACT:** In order to decrease shortages existing in the daily operation of some refinery Wastewater Treatment Plants (WWTP) and to maximize their overall treatment efficiency, in this study, through the calibration of a local WWTP for consecutive 40 days, we analyzed the removal efficiency of four typical water quality parameters, oil, COD,  $\text{NH}_3\text{-N}$ , and sulfide in petroleum refinery wastewater.

And the results showed that, through the quality of influent water was fluctuant, the quality of final effluent water was quite stable and met the discharge limits. Specifically, the concentration of oil in effluent was 3.6 mg/L and met its discharge standard; COD concentration was 83.3 mg/L, much lower than the design standard (350 mg/L); as for  $\text{NH}_3\text{-N}$ , the effluent concentration was 9.3 mg/L, and its design standard of effluent concentration was 17–30 mg/L, and the sulfide concentration in effluent was only 0.037 mg/L, also lower than the design standard. The total removal efficiency of oil, COD,  $\text{NH}_3\text{-N}$  and sulfide were 97.9%, 83.9%, 81.4% and 88.88%, respectively. So all actual results met the required demands, and the ultimate removal rates were also relatively high.

**Keywords:** refinery wastewater; calibration; A/O technology; removal efficiency

### 1 INTRODUCTION

Increasing industrialization, urbanization and enormous population growth in the worldwide have led to the generation of large quantities of wastewater, especially petroleum refining industries, since large quantities of wastewater are generated in petroleum refining processes of converting crude oil into various refined products (such as gasoline, liquefied petroleum gas, aviation fuel, and kerosene) [Fernando, S.G.E. 2011 & Yavuz, Y. et al. 2010]. Considering its toxicity and harmful to environment, the treatment of petroleum refinery wastewater before being discharged into coastal waters or other aquatic systems is rather essential. This is particularly true for developing countries where large amount of oil refinery wastewater with high amounts of hazardous pollutants was discharged into environmental without advanced treatment [Dimoglo A. et al. 2004, Diaz, E. et al. 2007 & Yuliwati, E. et al. 2012]. In China, for example, some refinery wastewater treatment plants are still using the traditional wastewater treatment process. And nowadays, WWTPs are facing new challenges to comply with more rigid wastewater discharge standards [Corona, F. et al. 2013]. In order to meet stringent discharge standards and cut running costs, instead of setting up

new treatment processes, the current processes should be optimized immediately [Yong S. et al. 2008].

The main goal of this research was to analyze the overall treatment efficiency of a local WWTPs and the removal efficiency of each treatment unit to decrease shortages existing in the daily operation to maximize the treatment efficiency.

### 2 MATERIALS AND METHODS

To achieve above goal, three sampling points from this WWTP were chosen for collecting wastewater samples: (1) raw influent; (2) anoxic-oxic (A/O); (3) final effluent. To ensure the comparison of wastewater collected every day, water samples were collected at the same time of each day, up to 40 days, and was stored in a cold room (4°C) before used.

This refinery WWTP has a treatment capacity of 100 m<sup>3</sup>/h and includes preliminary, primary, physicochemical and biological four treatment units, and the annual treatment capacity of wastewater is 876000t. And the final effluent is discharged into the sea after treatment and the sludge produced is removed from the facilities by an authorized contractor. The simplified treatment process of its treatment system is shown in Figure 1.

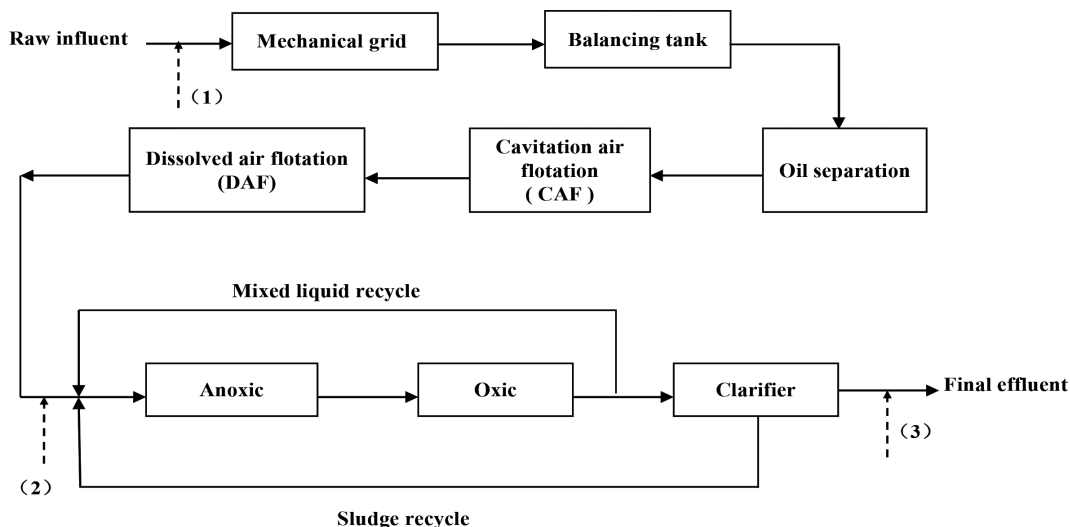


Figure 1. The Process of the local treatment plant and sampling sites ((1) raw influent, (2) A/O influent, (3) final effluent).

The biological treatment in this system is the conventional activated sludge process, which takes place in two separate units, for the removal of biodegradable organics.

Oil, Chemical Oxygen Demand (COD), Ammonia Nitrogen ( $\text{NH}_3\text{-N}$ ) and Sulfide were recognized as four most important parameters in this refinery wastewater treatment system. The contents of oil,  $\text{NH}_3\text{-N}$  and Sulfide were determined by Ultraviolet Spectrophotome, and COD values were determined by the potassium chromate method.

### 3 RESULTS AND DISCUSSION

#### 3.1 Oil

The oil concentration of raw influent, A/O influent and final effluent, and its removal efficiency of each unit in the consecutive 40 days were shown in Figure 2. The concentration of oil decreased gradually throughout the whole process. As showed in Figure 2(b), pretreatment phases have high removal efficiency to oil, the average value is up to 95.5%, since the Oil separation unit, Cavitation Air Flotation (CAF) unit and Dissolved Air Flotation (DAF) unit in the pretreatment phase play a key role in the removal of oil. Figure 2(a) indicates the average value of oil in DAF effluent was 8.5 mg/L, which met the demand of A/O influent quality (<20 mg/L). And although the oil value in raw influent was fluctuant, the effluent was rather stable. So this refinery wastewater treatment process has a high removal efficiency to oil if operate

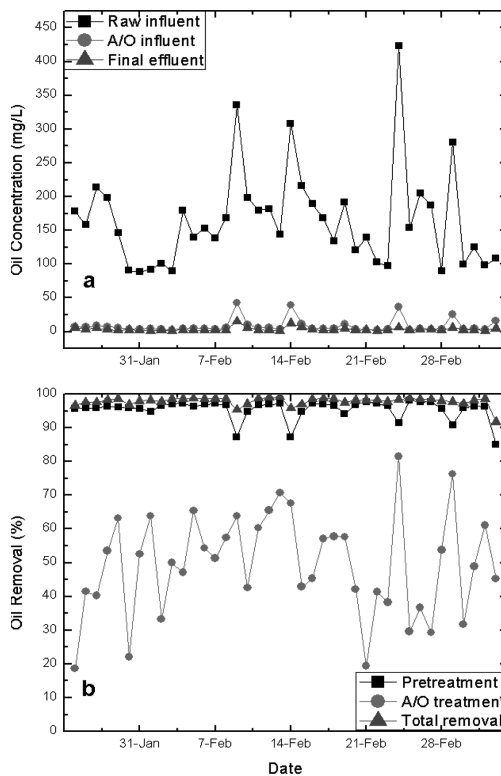


Figure 2. (a) Refers to oil concentration for raw influent, A/O influent and final effluent respectively; (b) Refers to oil removal efficiency for pretreatment, A/O treatment and total removal efficiency respectively.

correctly, and the final effluent value was under 5 mg/L meeting Grade I of the national standard.

### 3.2 Chemical Oxygen Demand (COD)

Figure 3 summarized the change of COD concentration in raw influent, A/O influent and final effluent during these 40 days, respectively, their removal efficiency were also shown in Figure 3(b). And from Figure 3(a), we can see the raw influent COD concentration fluctuated obviously, from 163 to 897 mg/L, the average value was 441.5 mg/L, which is below the range of design (600–1200 mg/L). By comparison, in final effluent, COD concentration became very stable, and achieved the national first level discharge standard (below 100 mg/L). So the whole system displayed better resistance to shock loads.

Figure 3 shows that the efficiency of A/O treatment units were better than that of pretreatment units for COD removal. Mainly because the existence of facultative anaerobes in A phase leads to

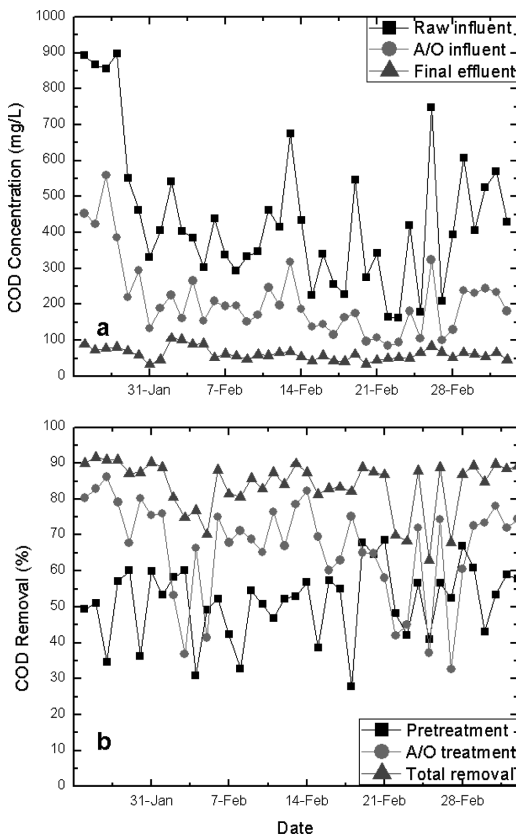


Figure 3. (a) Refers to COD concentration for raw influent, A/O influent and final effluent respectively; (b) Refers to COD removal efficiency for pretreatment, A/O treatment and total removal efficiency respectively.

the occurrence of hydrolysis and denitrification, so that the biochemical property of the refinery wastewater was improved, also, the COD concentration keep dropping during nitrification liquor recycling. As a whole, during the calibration period, the average value of COD removal efficiency was about 84%.

### 3.3 Ammonia Nitrogen ( $NH_3-N$ )

For  $NH_3-N$ , its changes of concentration and removal efficiency among different treatment units were presented in Figure 4. From Figure 4(a) we can see that, between Jan 24 and Jan 29 period, the concentration of  $NH_3-N$  in raw influent was very unstable (30–94 mg/L), meanwhile, Figure 4(b) indicates its removal efficiency was less than 60%. Through analysis, we found the main reason for lower removal efficiency during these days was the fluctuation of raw influent concentration, which resulted in the decrease of adaptability to environment and longer

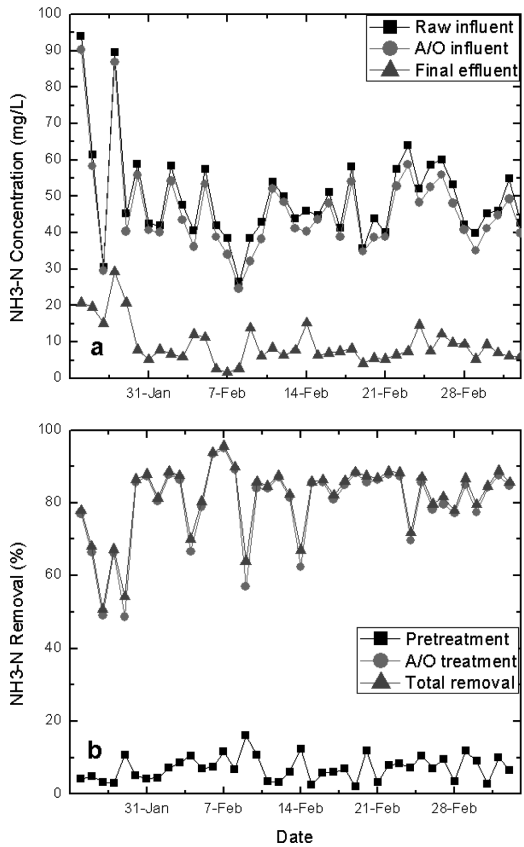


Figure 4. (a) Refers to  $NH_3-N$  concentration for raw influent, A/O influent and final effluent respectively; (b) Refers to  $NH_3-N$  removal efficiency for pretreatment, A/O treatment and total removal efficiency respectively.

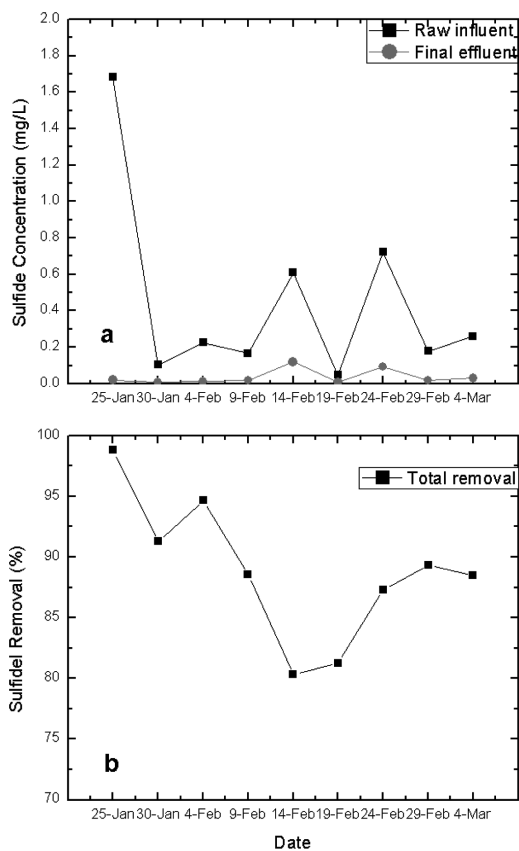


Figure 5. (a) Refers to sulfide concentration for raw influent, and final effluent respectively; (b) Refers to the total removal efficiency of sulfide.

growth cycle of autotrophic bacteria needed by  $\text{NH}_3\text{-N}$  removal. In that case, the proper regulating measure must be recommended to ensure relative steady influent concentration. After that, the total removal efficiency of  $\text{NH}_3\text{-N}$  was up to 80%.

From figure 4(b), the  $\text{NH}_3\text{-N}$  removal efficiency of pretreatment phases was quite low, the average value was only 7.1%, but its total removal efficiency is up to 80%, the removal process of  $\text{NH}_3\text{-N}$  mainly took place during A/O treatment processes.

### 3.4 Sulfide

The experimental results of sulfide is shown in Figure 5. From Figure 5(a) we can see the influent concentration of sulfide was relatively low, fluctuating from 0.048 mg/L to 1.683 mg/L, and the effluent concentration was more stable, and averaged about 0.037 mg/L. Figure 5(b) indicates the total removal efficiency of sulfide was around 89%.

## 4 CONCLUSIONS

- Overall, from the calibration results, we can see the concentration of all parameters meet the design standard and their corresponding discharge standards. Specifically, the concentration of oil in effluent was 3.6 mg/L, meeting its discharge standard; COD concentration in effluent was 83.3 mg/L, much lower than design standard (350 mg/L); as for  $\text{NH}_3\text{-N}$ , the effluent concentration was 9.3 mg/L, and its design standard of effluent concentration was 17–30 mg/L; and the sulfide concentration in effluent was only 0.037 mg/L. The total removal efficiency of oil, COD,  $\text{NH}_3\text{-N}$  and sulfide were 97.9%, 83.9%, 81.4% and 88.88%, respectively. So all actual results met the required demands, and the ultimate removal rates were also very high.
- According to calibration and analysis results, as for pretreatment units of this refinery wastewater treatment system, the removal efficiency of oil, COD and  $\text{NH}_3\text{-N}$  was 95.5%, 51.5% and 7.1% respectively. Obviously, the pretreatment unit, which contains Oil separation unit, CAF unit and DAF unit etc., was very effective for the removal of oil. In contrast, the COD removal efficiency of A/O treatment process was about 66.7%, and  $\text{NH}_3\text{-N}$  removal efficiency of this unit is up to 80%, close to its total removal efficiency. Since the wastewater went through anoxic phase and oxic phase alternatively, then organic pollutants and  $\text{NH}_3\text{-N}$  could be removed by nitrification and denitrification.

## REFERENCES

- Corona, F. et al. 2013. Monitoring nitrate concentrations in the denitrifying post-filtration unit of a municipal wastewater treatment plant. *Journal of Process Control* 23 (2): 158–170.
- Diaz, E. et al. 2007. Hydrogenation of phenol in aqueous phase with palladium on activated carbon catalysts. *Chemical Engineering* 131: 65–71.
- Dimoglo A. et al. 2004. Petrochemical wastewater treatment by means of clean electrochemical technologies. *Clean Technologies and Environmental Policy* 6: 288–295.
- Fernando, S.G.E. 2011. *The Book: Waste Water Treatment and Reutilization*. Intech Open Access Publishers.
- Yavuz, Y. et al. 2010. Treatment of petroleum refinery wastewater by electrochemical methods. *Desalination* 258 (1–3): 201–205.
- Yong S. et al. 2008. Treatment of petroleum refinery wastewater by microwave-assisted catalytic wet air oxidation under low temperature and low pressure. *Separation and Purification Technology* 62 (3): 565–570.
- Yuliwati, E. et al. 2012. Effects of process conditions in submerged ultrafiltration for refinery wastewater treatment: Optimization of operating process by response surface methodology. *Desalination* 287: 1–362.



## Relationship between microcell corrosion and macrocell corrosion of reinforcing steel in concrete structures

Zhong-Lu Cao

Tianjin Port Engineering Institute Ltd., CCCC First Harbor Engineering Company Ltd., Tianjin, China  
School of Civil Engineering, Hebei University of Technology, Tianjin, China  
Department of Civil Engineering, Kyushu Institute of Technology, Kitakyushu-shi, Japan

Sheng-Dong Mi, Hao-Yu Chen & Zhong-Chun Su

Tianjin Port Engineering Institute Ltd., CCCC First Harbor Engineering Company Ltd., Tianjin, China

Lian-Yu Wei

School of Civil Engineering, Hebei University of Technology, Tianjin, China

Makoto Hibino

Department of Civil Engineering, Kyushu Institute of Technology, Kitakyushu-shi, Japan

**ABSTRACT:** The relationship between microcell corrosion and macrocell corrosion of reinforcing steel embedded in chloride-free or contaminated concrete was investigated by comparing and analyzing the polarization curve and corrosion rate. The results indicated that the anodic/cathodic polarization curve of reinforcing steel in the microcell corrosion state could be used to predict the macrocell polarization behavior of cathodic steel or anodic steel in the macrocell corrosion state. There was a good relationship between macrocell and microcell corrosion current density, which was affected by the initial surface condition of steel. This relationship could provide a theoretical basis for predicting the magnitude of the macrocell corrosion rate from the calculated value of the microcell corrosion rate

**Keywords:** reinforcing steel; concrete; microcell corrosion; macrocell corrosion

### 1 INTRODUCTION

In the real reinforced concrete structures, macrocell current density ( $i_{\text{corr-ma}}$ ) of the current flowing between the actively corroding steel and the steel which was passive or had a lower corrosion rate usually cannot be measured directly due to the continuity and integrity of steel. The corrosion current density calculated by the Stern–Geary equation ( $i_{\text{corr-SG}}$ ) was widely used as the parameter to quantitatively evaluate the corrosion rate of steel. Technically, this corrosion current density was defined as microcell current density, because it was confined to a defined area under the counter electrode and was obtained based on the hypothesis that the oxidation current of an anode was equal to the reduction current of a cathode. Strictly speaking, this corrosion current density was not the real dissolution rate of steel, because it did not contain the macrocell current density ( $i_{\text{corr-ma}}$ ) of the current flowing from the measured area to another un-measured area. Therefore, in order

to better evaluate the corrosion rate of steel, it is necessary to investigate the relationship between  $i_{\text{corr-SG}}$  and  $i_{\text{corr-ma}}$  and to predict the possible magnitude of macrocell current density based on this relationship.

According to the literature, some work had been carried out to investigate the relationship between  $i_{\text{corr-SG}}$  and  $i_{\text{corr-ma}}$ . Andrade et al. (Andrade, Maribona, Feliu, González & Feliu, 1992) had analyzed the relative contributions of  $i_{\text{corr-SG}}$  and  $i_{\text{corr-ma}}$  and concluded that, if the anodic areas were 41 times larger than the cathodic areas, the value of  $i_{\text{corr-ma}}$  was about two orders of magnitude lower than that of  $i_{\text{corr-SG}}$ . If the anodic areas and cathodic areas were of the same size, the value of  $i_{\text{corr-ma}}$  was of the order of  $i_{\text{corr-SG}}$ . Only when cathodic areas were 41 times larger than the anodic area, the value of  $i_{\text{corr-ma}}$  was about 3–6 times greater than that of  $i_{\text{corr-SG}}$ . Hansson et al. (Hansson, Poursaeed & Laurent, 2006) investigated the macrocell and microcell corrosion of steels (the area ratio of the cathode to the anode was two) in ordinary and

high performance concretes and concluded that the  $i_{\text{corr-SG}}$  value was about 2 times greater than the  $i_{\text{corr-ma}}$  value in ordinary concrete, while the  $i_{\text{corr-ma}}$  in high performance concrete was between two and three orders of magnitude lower than the  $i_{\text{corr-SG}}$ . Poursaei et al. (Poursaei, Laurent & Hansson, 2010) found that for the specimens exposed to NaCl and MgCl<sub>2</sub> solutions, the  $i_{\text{corr-SG}}$  values were higher than the  $i_{\text{corr-ma}}$  values and this difference was greater for the specimens exposed to NaCl solution than for those exposed to MgCl<sub>2</sub>. The  $i_{\text{corr-ma}}$  and  $i_{\text{corr-SG}}$  values of the specimens exposed to CaCl<sub>2</sub> were similar.

As was mentioned above, the influence of the area ratio of the cathode to the anode, the admixtures, and different deicing salts on the relationship between  $i_{\text{corr-SG}}$  and  $i_{\text{corr-ma}}$  had been confirmed, but the data available in literature concerning the effect of steel's initial surface conditions on the relationship between  $i_{\text{corr-SG}}$  and  $i_{\text{corr-ma}}$  was scarce. Furthermore, for the given area ratio of the cathode to the anode, whether the value of  $i_{\text{corr-SG}}$  had an influence on the value of  $i_{\text{corr-ma}}$  also should be verified. Therefore, in this work, an experimental study was carried out to investigate the relationship between microcell and macrocell corrosion and the effect of steel's initial surface conditions on this relationship was also discussed.

## 2 EXPERIMENTAL

### 2.1 Materials

Plain round mild steel bars which were 19 mm in diameter and 180 mm in length were used; its chemical composition was as follows (wt%): 0.146 – C%, 0.223 – Si%, 0.521 – Mn%, 0.019 – P%, 0.010 – S% and remaining was comprised of Fe. To clarify the influence of steel's initial surface conditions on the relationship between microcell and macrocell corrosion, four typical initial surface conditions were artificially produced. They were mill-scaled or as-received Surface (SC), Polished surface (P), pre-Rusted surface by tap Water (RW), and pre-rusted surface by Seawater (RS). These surface conditions were usually generated during the processes of steel production, transportation, and fabrication and were very common for concrete structures just before the concrete was poured or cast. The pre-rusted surfaces, RW and RS, were obtained by spraying tap water and seawater on the surface of polished steels once in every two weeks for 104 days in a 20°C constant temperature room, respectively. Finally, RW was covered with yellow-brown oxides with a density of 8.3 mg/cm<sup>2</sup> and RS was covered with black oxides with a density of 42.0 mg/cm<sup>2</sup>.

The corrosion behaviors of steel were investigated in the cement mortar block with a dimension of 80 × 80 × 160 mm. For each cement mortar block, the mix proportion of water/cement/sand was 0.7:1:5. Ordinary Portland cement that met the specification requirements of JIS R5210 and had a density of 3.15 g/cm<sup>3</sup> was used. Sea sand that passed through JIS A 1102 sieve no. 4 (4.75 mm-opening) and washed by tap water was selected as the fine aggregate. Its density and water absorption were 2.58 g/cm<sup>3</sup> and 1.53%, respectively. For some blocks, chloride ions (3 wt% of cement) were added into the cement mortar at the time of casting as NaCl dissolved in the mixing water. All the blocks were allowed to set and harden in the mold for 1 day before being demolded and then cured for the next two weeks under water. After that, they were allowed to dry under a laboratory environment for another two weeks, prior to the beginning of experiment measurements.

### 2.2 Methods

The experimental design is shown in Table 1. Each case in Table 1 consisted of two blocks that were defined as A-side and B-side. For blocks in the A-side, steels with polished surface were used and the chloride content was 0 wt% of cement. While for blocks in the B-side, the surface conditions were changed from polished, scaled, and water-rusted to seawater-rusted and chloride was added with 0 or 3 wt% of cement. The experimental process is shown in Figure 1. Firstly the blocks in the A-side and B-side were disconnected for two weeks and then they were connected for another two weeks. These four weeks were defined as one cycle and 7 such cycles were carried out. During the whole process of experiments, the half-cell potential referred to the Ag/AgCl electrode and resistivity of steel and concrete were measured at set intervals by using a corrosion detection device.

The corrosion current density of steel in the disconnected periods is defined as the  $i_{\text{corr-mi}}$  value. It was calculated by the use of the following Stern-Geary equation:  $i_{\text{corr-mi}} = B/R_p$ , where  $R_p$  is the resistivity of steel and  $B$  is a constant which is commonly considered to be 26 mV for steel in the corroded state and 52 mV for steel in the passive state. In the connected periods of each cycle, the macrocell current flowing between the A-side and B-side was measured by using a zero resistance ammeter. The  $i_{\text{corr-ma}}$  value was calculated by using the following equation:  $i_{\text{corr-ma}} = I_{\text{ma}}/A_a$ , where  $I_{\text{ma}}$  is the macrocell current (unit: μA) and  $A_a$  (unit: cm<sup>2</sup>) is the surface area of steel acting as an anode specimen. The anode specimen was defined as the specimen that produced electrons and could be judged from the direction of current flow. In the disconnected

Table 1. Experimental design of this study.

Case no	A-Side	B-Side	Surface condition	
			A-Side	B-Side
1-1	P70-0-1	P70-0-2	P	P
1-2	P70-0-3	P70-0-4	P	P
2-1	P70-0-5	P70-3-1	P	P
2-2	P70-0-6	P70-3-2	P	P
3-1	P70-0-7	SC70-0-1	P	SC
3-2	P70-0-8	SC70-0-2	P	SC
4-1	P70-0-9	SC70-3-1	P	SC
4-2	P70-0-10	SC70-3-2	P	SC
5-1	P70-0-11	RW70-0-1	P	RW
5-2	P70-0-12	RW70-0-2	P	RW
6-1	P70-0-13	RW70-3-1	P	RW
6-2	P70-0-14	RW70-3-2	P	RW
7-1	P70-0-15	RS70-0-1	P	RS
7-2	P70-0-16	RS70-0-2	P	RS
8-1	P70-0-17	RS70-3-1	P	RS
8-2	P70-0-18	RS70-3-2	P	RS

\*Note: in this table, the initial surface condition of steel is marked as P, SC, RW, and RS. The w/c ratio is marked as 70. The chloride content is marked as 0 and 3. The serial number of block is marked as 1–18. For example, in P70-0-13, P means the steel had a polished surface, 70 means the w/c ratio is 0.70, 0 means the chloride content is 0 wt% of cement, and 13 means the serial number of the block is 13.

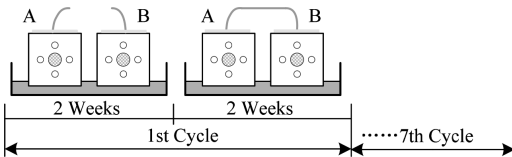


Figure 1. Experimental process of this study.

period of the 5th cycle, anodic/cathodic polarization curves of steel in both A-side and B-side for each case given in Table 1 were obtained by using a potentiostat. The reference electrode used here was Ag/AgCl electrode and stainless steel was used as the counter electrode.

### 3 RESULTS AND DISCUSSION

#### 3.1 Relationship between macrocell polarization and anodic/cathodic polarization curves

Figure 2 shows the anodic/cathodic polarization curves, corrosion potential, and corrosion current density of steels in the disconnected and connected periods of the 5th cycle. In the disconnected periods, the corrosion potential and corrosion current density of steels in the A-side (denoted using black filled squares) and B-side (denoted using

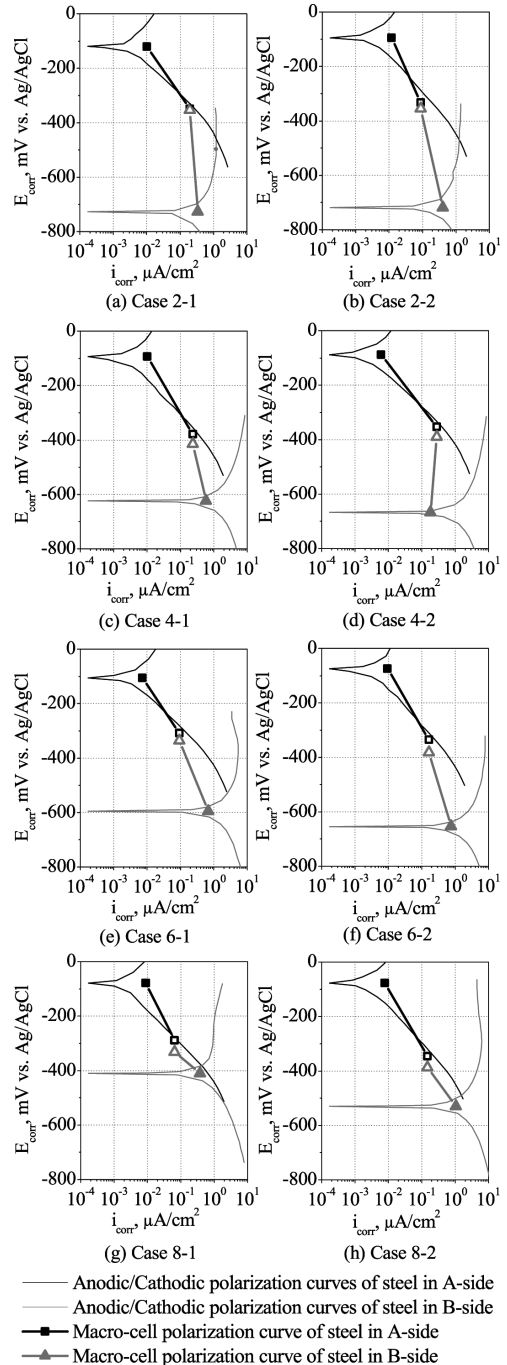


Figure 2. Relationship between macrocell polarization and anodic/cathodic polarization curves.

red filled triangles) were considered as the intersect point of the anodic polarization curve and the cathodic polarization curve of steels in the A-side

(black-thin lines) and the B-side (red-thin lines). When the steel in the A-side was connected with that in the B-side, due to the electrochemical driving force, the steel in the A-side was polarized cathodically to a lower potential point marked using black hollow square while the steels in the B-side were polarized anodically to a higher potential point marked using red hollow triangles, and an ohmic potential drop existed between the steels in the A-side and the B-side. The newly developed polarization caused the macrocell current flowing from steel in the A-side to steel in the B-side. Since the surface area of steel in the A-side was equal to that in the B-side, macrocell current densities of steel in the A-side and those in the B-side had the same values but opposite signs. The black thick line from the black filled square point to the black hollow square point is defined as the macrocell polarization curve of steel in the A-side while the red thick line from the red filled triangle point to the red hollow triangle point is defined as the macrocell polarization curve of steel in the B-side. Theoretically, the macrocell polarization of steel in the connected period was the result of further polarization of steel in the disconnected period due to the macrocell potential difference. This macrocell potential difference imposed a negative over-potential on the steel of the A-side and a positive over-potential on the steel of the B-side and therefore led to the polarization of steels and the generation of current. Due to the same principle of polarization, a relationship between the macrocell polarization and anodic/cathodic polarization curves of steels should exist.

It could be found that, irrespective of the initial surface conditions of steels in the B-side, the macrocell polarization curve of steel that acted as the cathode in the A-side was well consistent with its cathodic polarization curves while the macrocell polarization curve of the steel that acted as the anode in the B-side did not follow the same trend with its anodic polarization curve. In theory, the macrocell current that was induced by the macrocell polarization potential should be equal to the cathodic or anodic polarization current that was induced by the same over-potential imposed by the potentiostat. From the experimental results shown in Figure 2, it is observed that all the black hollow square points showing the macrocell corrosion state of steels in the A-side are very close to the cathodic polarization curves of steels in the A-side while all the red hollow triangle points showing the macrocell corrosion state of steels in B-side are far away from the anodic polarization curves of steels in the B-side. The macrocell current densities were much lower than the corrosion current densities of steels in the B-side

(red filled triangle points), which was not in agreement with the result of Gulikers (Gulikers, 1996) that for an anodic overpotential exceeding 50 mV, the magnitude of the macrocell current density might be considered to be nearly equal to the actual dissolution rate of the anode (steels in the B-side in this study) and also was not consistent with the macrocell corrosion model proposed by Maruya et al. (Maruya, Takeda, Horiguchi, Koyama & Hau, 2007) and Pergola et al. (Pergola, Lollini, Redaelli & Bertolini, 2013). The possible explanations for this result could be given from two aspects: the accuracy of anodic/cathodic polarization curve and the factors influencing macrocell current density. From the view point of the accuracy of the anodic/cathodic polarization curve, the anodic/cathodic polarization curve was greatly affected by the scan rate and the waiting time. If the scan rate was too rapid and the waiting time was too short, the result might not be representative of the system under the test. On the other hand, if the scan rate was too slow and the waiting time was too long, the system might change during the measurement. Therefore, an appropriate scan rate and a suitable waiting time were necessary to obtain the relatively accurate anodic/cathodic polarization curve. From another point of view, the macrocell current density shown in Figure 2 could be affected by various factors; but consideration should be given to the reasonability of the calculation of macrocell current density that referred to the total surface area of steels in the B-side. The steel in the B-side was embedded in a mortar containing 3% chloride (wt% of cement) and acted as an anode. This anode had both anodic and cathodic areas operating simultaneously in order to maintain the corrosion reaction. When this anode or corroded steel in the B-side was connected to the cathode or passive steel in the A-side, what was really happening was an extension of the cathodic areas which induced a decrease of the cathodic areas previously operating in the anode. And this redistribution of the area ratio of the cathode to the anode was greatly influenced by the oxygen concentration that varied with the moisture content of the mortar. Therefore, the corroded steel in the B-side was not usually a pure anode and had some cathodic areas still operating on its surface. These cathodic areas might be almost completely suppressed when the anode was effectively deaerated or when the area ratio of the cathode to the anode was very high. Only in this situation, the macrocell current density flowing between the steel in the A-side and the steel in the B-side would approach or equate the dissolution rate of the steel in the B-side.

### 3.2 Relationship between macrocell current density and corrosion current density calculated by the Stern–Geary equation

The values of  $i_{\text{corr-ma}}$  in each cycle were plotted against the values of  $i_{\text{corr-SG}}$  measured at the same cycle for the periods that the A-side steel was disconnected with the B-side steel in Figure 3-a and for the periods that the A-side steel was connected with the B-side steel in Figure 3-b.

As could be seen from Figure 3-a, the influence of the value of  $i_{\text{corr-SG}}$  on the value of  $i_{\text{corr-ma}}$  could be confirmed. When the value of  $i_{\text{corr-SG}}$  was higher than  $0.1 \mu\text{A}/\text{cm}^2$ , the corresponding value of  $i_{\text{corr-ma}}$  was equal to or slightly lower than the value of  $i_{\text{corr-SG}}$ . While the value of  $i_{\text{corr-SG}}$  was lower than  $0.1 \mu\text{A}/\text{cm}^2$ , the corresponding value of  $i_{\text{corr-ma}}$

was between one and three orders of magnitude lower than the value of  $i_{\text{corr-SG}}$ . The initial surface conditions of anodic steels played an important role in controlling the magnitude of macrocell current density. For the same  $i_{\text{corr-SG}}$  values, with reference to the initial surface conditions of anodic steel in the B-side, the macrocell current densities between steels were in the following sequence:  $\text{SC} > \text{P} > \text{RW} > \text{RS}$ . This indicated that the scaled surface was more prone to inducing macrocell corrosion when compared to the polished surface and the pre-rusted surface. The polished surface and pre-rusted surface seemed to provide a better resistance to inhibit the flow of macrocell current. However, attention should be paid to the macrocell potential difference that usually had a greater influence on the macrocell current. The macrocell potential difference for the case with seawater-rusted steel was  $100\text{--}200 \text{ mV}$  lower than that for the case with scaled steel (Cao, Hibino & Goda, 2014). Therefore, whether this potential difference resulted in the lower macrocell current density of seawater-rusted steel was worthy of consideration.

In Figure 3-b, the value of  $i_{\text{corr-SG}}$  was obtained from the connected periods, during which the macrocell corrosion had occurred. This condition was consistent with the practical situations in the field reinforced concrete structures. From the figure, the influence of  $i_{\text{corr-SG}}$  on  $i_{\text{corr-ma}}$  also could be confirmed. The ratio of  $i_{\text{corr-ma}}$  to  $i_{\text{corr-SG}}$  increased with increasing  $i_{\text{corr-SG}}$ . The effect of initial surface conditions of anodic steel on the macrocell current density also could be observed. With reference to the surface conditions of anodic steel in the B-side, when the  $i_{\text{corr-SG}}$  value was lower than  $0.1 \mu\text{A}/\text{cm}^2$ , the ratios of  $i_{\text{corr-ma}}$  to  $i_{\text{corr-SG}}$  were in the following sequence:  $\text{SC} > \text{P} > \text{RW} > \text{RS}$ , and the  $i_{\text{corr-ma}}$  value was between one and two orders of magnitude lower than  $i_{\text{corr-SG}}$ . While the  $i_{\text{corr-SG}}$  value was greater than  $0.1 \mu\text{A}/\text{cm}^2$ , the ratios of  $i_{\text{corr-ma}}$  to  $i_{\text{corr-SG}}$  were in the following sequence:  $\text{P} > \text{RW} > \text{SC} > \text{RS}$  and  $i_{\text{corr-ma}}$  was equal to or higher than  $i_{\text{corr-SG}}$ .

The relationships between  $i_{\text{corr-ma}}$  and  $i_{\text{corr-SG}}$  values were fitted by non-linear functions and the results are given in Table 2. It could be found that there was a good relationship between  $\log(i_{\text{corr-ma}})$  and  $\log(i_{\text{corr-SG}})$ , which was in the form of  $\log(i_{\text{corr-ma}}) = a * \log(i_{\text{corr-SG}}) + b$ , where  $a$  and  $b$  are the parameters varied with steel surface conditions. This relationship could provide a theoretical basis for predicting the magnitude of  $i_{\text{corr-ma}}$  from the value of  $i_{\text{corr-SG}}$ . It should be noted that this relationship was only suitable for the condition that the cathode area was equal to the anode area. If the area ratio of the cathode to the anode was greater or lesser than one, some changes on the fitted parameters ( $a$  and  $b$ ) would occur. Furthermore, other factors influencing the value of  $i_{\text{corr-ma}}$  or  $i_{\text{corr-SG}}$  might also have

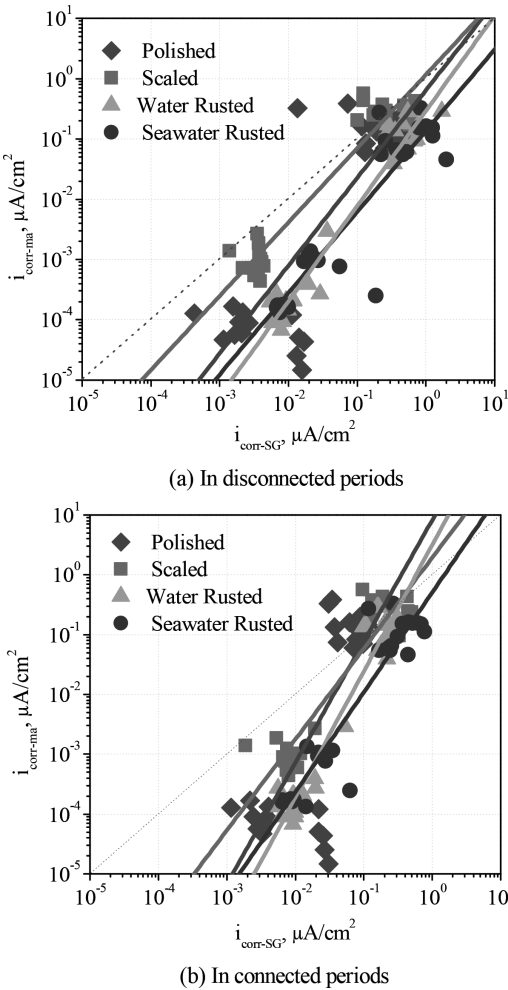


Figure 3. Relationship between macrocell current density and microcell current density.

Table 2. Functional relationship between  $i_{\text{corr-ma}}$  and  $i_{\text{corr-SG}}$ .

$\log(i_{\text{corr-ma}}) = a$ $*\log(i_{\text{corr-SG}}) + b$	$i_{\text{corr-SG}}$ in disconnected periods		
	A	b	R <sup>2</sup>
Polished	1.4559	-0.1901	0.7022
Scaled	1.2247	0.0668	0.9212
Water rusted	1.5792	-0.5323	0.9588
Seawater rusted	1.3478	-0.8631	0.8427
$\log(i_{\text{corr-ma}}) = a$ $*\log(i_{\text{corr-SG}}) + b$	$i_{\text{corr-SG}}$ in connected periods		
	A	b	R <sup>2</sup>
Polished	2.0189	0.8935	0.57
Scaled	1.5204	0.2881	0.8728
Water rusted	2.1057	0.4832	0.9327
Seawater rusted	1.67	-0.2936	0.8797

an influence on these relationships, which would be confirmed in future studies.

#### 4 CONCLUSIONS

The anodic/cathodic polarization curve of reinforcing steel in the microcell corrosion state can be used to predict the macrocell polarization behavior of cathodic steel or anodic steel in the macrocell corrosion state.

There was a good relationship between the macrocell corrosion rate ( $i_{\text{corr-ma}}$ ) and the microcell corrosion rate ( $i_{\text{corr-SG}}$ ), which was presented in the

form of  $\log(i_{\text{corr-ma}}) = a * \log(i_{\text{corr-SG}}) + b$ , where a and b are the parameters varied with the steel's initial surface conditions. This relationship would provide a theoretical basis for predicting the possible magnitude of  $i_{\text{corr-ma}}$  from the value of  $i_{\text{corr-SG}}$ .

#### REFERENCES

- Andrade C., Maribona I.R., Feliu S., González J.A., & Feliu Jr S. 1992. The effect of macrocells between active and passive areas of steel reinforcements. *Corrosion Science* 33(2): 237-249.
- Cao Z.L., Hibino M., & Goda H. 2014. Effect of Steel Surface Conditions on the Macro-Cell Polarization Behavior of Reinforcing Steel. *Applied Mechanics and Materials* 584-586: 1771-1779.
- Gulikers J.J.W. 1996. Experimental investigations on macrocell corrosion in chloride-contaminated concrete. *Heron* 41(2):107-124.
- Hansson C.M., Poursae A., & Laurent A. 2006. Macro-cell and microcell corrosion of steel in ordinary Portland cement and high performance concretes. *Cement and Concrete Research*, 36(11): 2098-2102.
- Maruya T., Takeda H., Horiguchi K., Koyama S., & Hau K.L. 2007. Simulation of steel corrosion in concrete based on the model of macro-cell corrosion circuit. *Journal of Advanced Concrete Technology* 5(3): 343-362.
- Pergola A.D., Lollini F., Redaelli E., & Bertolini L. 2013. Numerical Modeling of Initiation and Propagation of Corrosion in Hollow Submerged Marine Concrete Structures. *Corrosion* 69(12): 1158-1170.
- Poursae A., Laurent A., & Hansson C.M. 2010. Corrosion of steel bars in OPC mortar exposed to NaCl, MgCl<sub>2</sub> and CaCl<sub>2</sub>: Macro-and micro-cell corrosion perspective. *Cement and Concrete Research* 40(3): 426-430.

# The application of an active filter based on FPGA in a large building

Ying Lou

*School of Electronic and Information Engineering, Liaoning Science and Technology University, Anshan, Liaoning, China*

Xue-jie Wang

*School of Information and Electrical Engineering, Zhejiang University City College, Hangzhou, Zhejiang, China*

**ABSTRACT:** Along with the widespread use of various non-linear power electronic devices in the production and living environments, harmonic pollution has become an increasingly serious problem and the quality of the power grid has decreased. How to control the harmonic in power quality has become a matter of utmost concern. In this paper, an active filter device based on FPGA is introduced and the principle and method of harmonic control are expounded. FPGA is the main processing chip of the system; by processing a FFT algorithm, a harmonic will be generated to eliminate the grid harmonic. This active filter has been used in a large clothing wholesale market and the harmonic of the power grid was found to be well-controlled. FPGA has characteristics such as high speed, high reliability, and flexible reconfiguration. An active power filter with full digital control technology will be widely used in the harmonic control system.

**Keywords:** Active filter, FPGA, Harmonic control

## 1 INTRODUCTION

The methods of harmonic control mainly include the usage of a passive filter and an active filter; a passive filter is mainly composed of an inductor and capacitor. A passive filter device is simple, cost-effective, and can be operated reliably; but, the passive filter compensation characteristics are always influenced by the power grid impedance and running state, leading to the occurrence of parallel resonance which will lead to the harmonic being amplified and the LC filter being overloaded or even burned. In addition, it can only compensate the fixed frequency of the harmonic and the compensation effect is not very ideal. An active harmonic filter device is developed on the basis of the passive filter. An active filter unit is mainly composed of a power electronics circuit. It can produce a harmonic which has the same frequency and amplitude; with contrary phase as the grid harmonic [1], active filter is a dynamic compensation. In a large clothing wholesale market in Shenyang, the main loads are lighting equipment, central air-conditioning, elevators, etc. Because the market has many merchants, the use of power is uneven, which makes a three-phase load uneven. As a result, the three-phase four-wire power system is potentially threatened with neutral currents and harmonics,

leading to high temperature and loud noise in the transformer. The main harmonics are 3 times, 5 times, and 7 times. After adopting the active filter device which is introduced in this paper, harmonics have been well-eliminated.

## 2 DESIGN

An active filter system based on FPGA is introduced in this paper. The active filter system mainly includes the main circuit, drive circuit, control circuit, protection circuit, and the sampling circuit. The system principle's block diagram is shown in Figure 1.

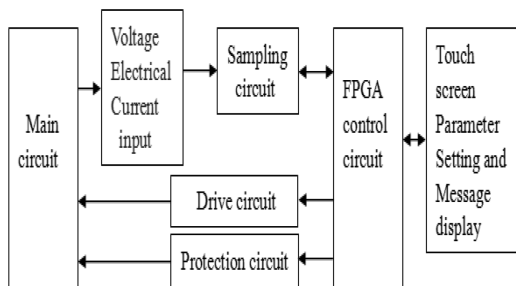


Figure 1. System principle's block diagram.

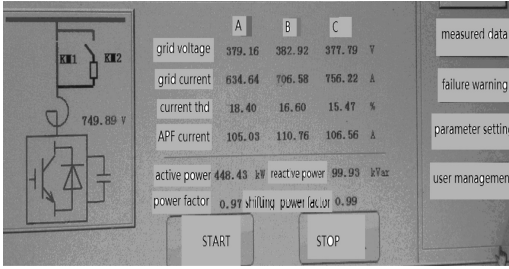


Figure 2. Running state display interface.

FPGA is the main processing chip of the control circuit. After collection of grid voltage and current, they are converted into digital signals by the ADC and sent to the FPGA. FPGA uses Fast Fourier Transform (FFT) algorithm to get the harmonic and then generate a corresponding modulation signal to the harmonic. Based on the principle of SPWM, we can get switch signals to control the IGBT single-phase bridge and finally, offset current will be sent to the grid. FPGA is in-charge of reading the current's discrete digital signals, realizing the FFT algorithm and the storage of harmonic analysis results, completing parameter set and information query by the touch screen, and setting filter harmonic sort and the size of the offset current according to the need. The system can show running status, measurement data, and fault alarm information. Figure 2 shows a running state display interface.

### 3 THE DESIGN AND IMPLEMENTATION OF FFT FOURIER ANALYSIS ALGORITHM

#### 3.1 Basic principle of algorithm

FFT is a transform form by which signal is transformed from the time domain to the frequency domain. It is an important analysis tool of signal processing. By using Fourier analysis, the non-sinusoidal function is decomposed into its harmonic. The waveform on the sinusoidal frequency  $\omega_0$  is known as the fundamental component and the waveform on frequency  $n \times \omega_0$  is called the harmonic component. FFT is a kind of efficient algorithm of the Discrete Fourier Transform (DFT), which is called the fast Fourier transform [2]. FFT is obtained by improving DFT based on the odd and even and virtual and physical features. Finite length sequences  $\{x(n)\}$  and frequency domain  $\{X(k)\}$  can be obtained from the DFT using the following equation:

$$X(k) = \sum_{n=0}^{N-1} x(n)W_N^{nk}, k = 0, \dots, N-1 \quad (1)$$

$W_N^{nk} = e^{-j\frac{2\pi}{N}nk}$  is named as the twiddle factor, generally  $x(n)$  and  $W_N^{nk}$  are complex numbers, and so  $X(k)$  is also plural. The computation work of completing a DFT is carried out by calculating  $X(k)$ 's value which needs  $N$  times of the plural addition and  $N-1$  times of the plural multiplication and calculating  $X(k)$ 's value of the  $N$  point needs  $N * N$  times of complex multiplication and  $N * (N-1)$  times of the plural addition. Complex number multiplication is more complex than the plural addition, and therefore when  $N$  is large, real-time processing requires high computing speed to complete the above calculation. FFT algorithm uses the symmetry and periodicity of  $W_N^{nk}$  to reduce the computational complexity [3].

Periodicity:

$$W_N^{nk} = W_N^{n(N+k)} = W_N^{k(N+n)} \quad (2)$$

Symmetry:

$$W_N^{n(k+N/2)} = -W_N^{nk} \quad (3)$$

In general, a FFT algorithm is Divided Into Time extraction (DIT) and the frequency extraction (DIF). In this design, the classic Radix-2 FFT algorithm of extraction in the time domain is chosen.

#### 3.2 Radix-2 FFT algorithm principle

Sequence  $x(n)$  is broken down into two  $n/2$  point subsequences according to the odd and even values of the number  $n$ ,

$$\begin{aligned} x(2r) &= x_1(r) & r = 0, 1, \dots, \frac{N}{2} - 1 \\ x(2r+1) &= x_2(r) \end{aligned} \quad (4)$$

Then, the following derivation can be obtained:

$$\begin{aligned} X(k) &= X_1(k) + W_N^k X_2(k) \\ k &= 0, 1, \dots, \frac{N}{2} - 1 \end{aligned} \quad (5)$$

Apparently,  $X_1(k)$  and  $X_2(k)$  only contain  $N/2$  point DFT, and so  $X(k)$  contains  $k = 0, 1, \dots, N/2 - 1$  point DFT [4]. By using the symmetry and periodicity of  $W_N^{nk}$ , the point obtained after the  $N/2$  point DFT is calculated using the following equation:

$$\begin{aligned} X(k + \frac{N}{2}) &= X_1(k) - W_N^k X_2(k) \\ k &= 0, 1, \dots, \frac{N}{2} - 1 \end{aligned} \quad (6)$$



By using the equation (5) and (6), as long as  $X_1(k)$  and  $X_2(k)$  of  $N/2$  point DFT are calculated, we can get the value of  $N$  points  $X(k)$  and the amount of calculation can be reduced to about half. Figure 3 shows the DFT decomposition process of an 8 points sequence extracted in time and the butterfly operation flow diagram.

The current signal is converted into digital signals after being sampled by the ADC and then FFT can be performed. The sampling frequency is 2 times larger than the signal frequency. Assuming that the sampling frequency is  $F_s$ , the signal frequency is  $F$ , and the sampling points is  $N$ , after FFT, we can obtain  $N$  point FFT results which are  $N$  points complex number; each point corresponds to a frequency point, the point (except the first) modulus value is  $N/2$  times the original signal peak. The first point is the DC component. Its value is  $N$  times the original DC component. The phase of each point is the phase of the frequency signal. The frequency of each point increases in turn and the frequency of the  $n$  points is calculated using the following equation:

$$Fn = (n-1) * Fs / N \quad (7)$$

From equation (7), it can be observed that  $Fn$  can be distinguished  $F_s/N$ . Similar to the realization of 512 points FFT processing, with signal frequency  $F$  (also known as power frequency) as 50 Hz and the sampling frequency  $F_s$  as 1024 Hz, by using equation (7), 3 times harmonic 150 Hz can be calculated and it should appear where  $n$  is 51. The DFT decomposition process of 8 points sequence and the butterfly operation flow diagram are shown in Figure 3.

### 3.3 The design of FFT

In this method, the FPGA chip is used to implement the FFT data processing functions. Altera's

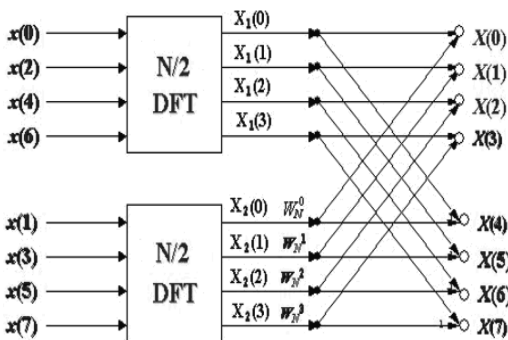


Figure 3. The DFT decomposition process of 8 points sequence and the butterfly operation flow diagram.

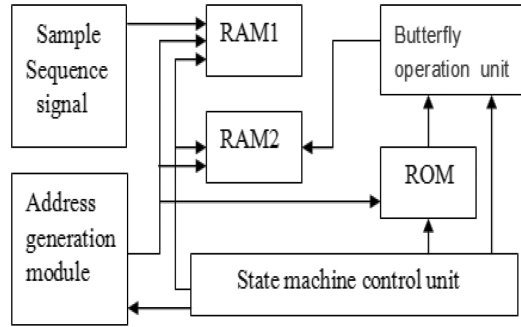


Figure 4. Block diagram of the FFT algorithm process.

FPGA Cyclone IV is chosen; it contains 360 18\*18 multiplier resources which can realize DSP processing intensive applications. VHDL hardware description language or LPM module is used to realize each function module of the FFT data processor. An FFT data processor includes the centre control module, the sampling sequence  $x(n)$  and  $X(k)$  storage module RAM [6], twiddle factor storage module ROM, the butterfly computing unit, address generation module, and so on. Using the state machine design pattern, the control module reads the sampling data and twiddle factors and completes the butterfly operation. LPM\_RAM was adopted to realize the data storage module and twiddle factor is calculated using Matlab and kept for .mif files. LPM\_ROM is customized as twiddle factor storage modules and each module is connected in a graphical editing mode to complete the FFT's top-level module design of data processing. Figure 4 shows the FFT algorithm processing block diagram.

## 4 THE COMPENSATION CURRENT GENERATION MODULE

The compensation current generation module is implemented on the basis of the principle of SPWM by using FPGA. A reference sine wave is generated by using the software method after a harmonic is detected by the FFT algorithm. According to the frequency and amplitude of the harmonic, the frequency and amplitude of the reference sine wave are changed in accordance with that of the harmonic wave and this is called modulation signal; then, the SPWM waveform is obtained by comparing the modulation signal with a triangle wave which has fixed frequency and amplitude. The triangle wave is generated with software and the SPWM wave is used to control the switching on and off of the IGBT switch device. In application, switch signals will connect the upper and lower



# Crouching suspicions, hidden potential: A literature review on US–China clean energy cooperation since 2009

Yi-Nan Ding

*Graduate School, International Business School, Beijing Foreign Studies University, Beijing, China*

Jing Shi

*Beijing Foreign Studies University, Beijing, China*

**ABSTRACT:** Since 2009, China and the US have exhibited increased cooperation in promoting clean energy and have achieved concrete results. In this paper, related scholarships from both countries are reviewed in terms of research agenda, characteristics, and shortcomings. It concludes that concerning the current situation, Chinese scholars focus on abstract cooperation mechanisms while Americans attend to specific initiatives and new progresses. Chinese scholars attribute intergovernmental frictions to the American fear of losing its major power status and catering to domestic politics while recognizing the Chinese IPR failure and inappropriate government subsidies. American scholars admit the influence of domestic politics but stress the disparity of technology development and deployment and the paradox between promoting clean energy and following global trade rules. Additionally, Chinese scholars recommend improving independent R & D capacity and learning how to “play with” WTO rules while facing trade frictions.

**Keywords:** China, the US, clean energy, cooperation.

## 1 INTRODUCTION

Since Obama Administration took office, the US–China cooperation on clean energy has become one of the major issues that have been shaping US–China relations. No matter when President Obama came to China for the first time or when his Secretary Clinton or Kerry visited Beijing in the past six years, clean energy has always been the centerpiece of their dialogues, including the US–China Energy Policy Dialogue (EPD) and US–China Strategic and Economic Dialogue (S & ED). While clean energy draws great attention from governments, businesses, and policy-makers, it has also become the hot spot of academic communities from both sides of the Pacific Ocean.

In this paper, the scholarships in relation to US–China clean energy cooperation from both China and the United States are reviewed and three parts are incorporated, including the origin of US–China clean energy cooperation, research agenda of Chinese and American scholars, and their characteristics and shortcomings.

## 2 THE ORIGIN OF US–CHINA CLEAN ENERGY COOPERATION

According to the US Environmental Protection Agency, clean energy includes energy efficiency and supplies options such as highly efficient combined

heat and power as well as renewable energy sources. Although it initially appeared in the cooperation between China and the United States in the late 1990s, it is after President Obama took office in 2009 that clean energy has begun to be the centerpiece in the US–China relations. The rising of clean energy cooperation is attributed to common challenges faced by China and the US, potential benefits, position change and complementation of the Chinese market, and American high technology.

Climate change has elevated the importance of clean energy in the bilateral relations between China and the United States. On one hand, climate change has become a prominent theme in the recently held international conference due to the potential influences it might bring about and consequently, the contest for resources including oil and energy diversity has pushed both countries to look for alternatives (Ma 2009; Zhu & Yang 2012). On the other hand, as the two largest greenhouse gas emitters, China and the United States have the responsibility to reduce carbon emission (Ma 2009, Cooke 2012; Lieberthal 2009). Many countries have regarded clean energy as alternatives to fossil energy and means of carbon emission reduction (Lieberthal & Sandalow 2008). For example, the United States and European Union (EU) have determined to replace 20% of fossil energy with clean energy by 2020, while China has also decided to replace 15% by then.

The international energy is in transition and clean energy is likely to become a new engine driving economic growth in future, especially after the Financial Crisis in 2008 (Zhu & Yang 2012; Cooke 2012; Yan 2012; Marsters & Turner 2001). As the two largest oil importers, China and the United States have the motivation to guarantee energy security and keep economy growing (Cooke 2012; Lieberthal 2009; Dreyer 2007). In the next place, China has also seen clean energy as an opportunity to adjust the industrial structure from a high pollution and high energy consumption economy to a low-carbon economy (Cooke 2012; Yan 2012; Pew Center & Asia Society 2009). Additionally, job creation in the construction of clean energy infrastructure and export is another bonus. More important benefits are the consolidation of political trust between the two countries and recognition of an international cooperation mechanism in addressing climate change (Yan 2012; Lewis 2012).

Changes in the political environment in both countries have provided an opportunity. Compared to President Bush's setbacks on climate change and energy, President Obama has a more agreeable attitude and takes climate change and clean energy seriously (Lieberthal 2009). On the Chinese side, the Chinese government has also attached importance to clean energy, institutionalizing and legalizing it in the Twelfth Five-Year Plan (Ma 2009; Lieberthal 2009). In the following years, the US-China Economic Policy Dialogue and US-China Strategic and Economic Dialogue will serve to close the distance between the two nations.

China and the United States are complementary in the clean energy field (Zhu & Yang 2012; Lewis 2012; Liu & Liu 2011). The United States has high technology on clean energy sources such as biomass, nuclear, coal, and wind, which China lacks while China has aggressive investment, strong manufacturing capacity, and a huge potential clean energy market, which the United States is desperately in need of (Zhu & Yang 2012; Lewis 2012; Liu & Liu 2011). Additionally, China is the largest coal consumer and its coal consumption is about twice that of the United States. The United States and China clean energy cooperation facilitates American economic growth and balances American trade deficit as well as helps China in achieving targets such as carbon emission reduction (Ma 2009; Zhu & Yang 2012; Lewis 2012).

### 3 MAJOR RESEARCH AREAS

Besides cooperation basis and potential benefits, Chinese and American scholars also devote themselves to the current situation, including cooperation mechanisms, existing problems, and their corresponding causes and solutions.

#### 3.1 Current situation

In the current situation of US-China clean energy cooperation, American scholars tend to focus on specific areas or initiatives. In their co-authored essay "Cooperative Competitors", Marsters and Turner introduce five areas for cooperation, namely scaled renewable development, soft tech and management, shale gas, carbon capture and sequestration, and intersection of water and energy issues (Marsters & Turner 2001). The Department of Energy presents recent developments of seven initiatives launched in 2009 in its progress report "US-China Clean Energy Cooperation" (U.S. Department of Energy 2011). Cooke introduces existing circumstances in USA and China in terms of technology and investment in his book *Sustaining U.S.-China Cooperation in Clean Energy* (Cooke 2012). In another journal, Cooke elaborates innovative "Urban Clean Energy Infrastructure" solutions of the US-China EcoPartnerships program in the Greater Philadelphia and Tianjin Economic-technological Development Area (TEDA) and describes three initial pilot projects, namely the Wetlands Urban Water Management project in the Nangang industrial zone, the Low-Carbon Built Environment project, and the Online Monitoring System project in the TEDA central business zone (Cooke 2015). By comparison, Chinese scholars like studying abstract structures. They spend a lot of energy on cooperation mechanisms and framework. The US-China Economic Policy Dialogue laid a solid foundation for bilateral cooperation in clean energy before both countries uplifted the issue in 2009 (Yan 2012). The US-China Strategic and Economic Dialogue has further elevated clean energy to the strategic level and made it an international issue (Yan 2012). In addition, bilateral agreements are made to produce concrete results (Jiang & Li 2013).

#### 3.2 Existing problems and causes

With respect to existing problems, both sides are prone to criticize each other. On the Chinese side, they summarize three main problems, namely export control of high technology on clean energy, trade frictions including green trade barrier, anti-dumping, and countervailing investigations and punitive tariffs, and lack of strategic mutual trust (Zhu & Yang 2012; Yan 2012; Dreyer 2007).

Some Chinese scholars criticize that it is the American fear of losing its major power status in clean energy and catering to domestic politics that result in its irrational action against China (Li & Wei 2011; Jiang & Li 2013; Tang 2009). The best example for the former is the frequent anti-dumping and countervailing investigation on solar and wind sectors, where Chinese manufacturers have an advantage. Meanwhile, other Chinese scholars also admit that China also plays a role in the bilateral conflict.

China fails to seriously uphold Intellectual Property Rights (IPR), which worries American counterparts about their patents; given directly to clean energy companies, Chinese government subsidies lower the price of Chinese products and make them more competitive; the Chinese policy of buying national clean energy equipment discriminates foreign competitors (Liu & Liu 2011). Although the intent to enlarge the clean energy industry is good, the method results in unfair international competition.

On the American side, they admit the existence of conflict, but stress that it is not subjective motivation but objective facts that result in conflict. First of all, promoting clean energy technologies contradicts with following the rules of the global trade system (Lewis 2012), which is similar to their Chinese counterparts. Due to immaturity of the clean energy industry and the new and expensive infrastructure, governments have to spend a lot to promote, which sometimes results in unfair competition. Secondly, disparity in clean energy technology development and deployment makes the conflict inevitable (Lewis 2012; Levi et al. 2010). The United States holds a high position in clean energy and wants to sell its high technology at a high price, while China expects the US to transfer its technology at a moderate price for promotion of clean energy. Furthermore, many American scholars admit that Sino-US politics also plays a role in the conflict, especially during leadership transition (Cooke 2012; Lieberthal 2009; Lewis 2012).

### 3.3 *Suggestions*

Chinese scholars offer some suggestions to eliminate their disadvantages. For example, China should focus on independent research and development, flexibly apply WTO rules, and change direct subsidies into companies and indirect subsidies into customers (Li & Wei 2012; Liu & Peng 2016). Facing the information asymmetry in the introduction of foreign technology, China should build a patent information bank to avoid the duplication of imports of patents and promote technology transfer in different areas of clean energy (Shen & Lv 2015). China and the United States should institutionalize technology transfer to resolve potential disputes and frictions by signing relevant agreements (Jiang & Li 2013; Liu & Peng 2016) and introducing private investors to promote the development of clean energy technology (Liu & Peng 2016), increase cooperation in international organizations (Tang 2009; Zhao 2015), and even establish an energy security shared mechanism in the Asia-Pacific area to decrease zero-sum competition by building an international energy channel in this region (Zhao 2015). Although various problems exist, both Chinese and American scholars believe that cooperation will prevail in the future (Zhu & Yang 2012; Cooke 2012; Lieberthal 2009).

## 4 CHARACTERISTICS AND SHORTCOMINGS

Chinese and American scholarships share some characteristics, but also differ in certain aspects. In common, they share similar research agendas, such as cooperation motivation, existing problems and corresponding causes, focus on conflicts of solar and wind sectors, and have the same publishing period (2009–2012). With respect to differences, firstly, American scholars focus on current affairs that happened after 2009, while Chinese scholars pay attention to the evolution of clean energy since late 1990s. Secondly, Chinese scholars have a macro view of clean energy and focus on abstract cooperation mechanisms, while their American counterparts have an eye on specific initiatives or sectors. Thirdly, Chinese scholars are willing to offer solutions to the existing problems by actively improving the current situation and improving themselves.

In this paper, contributions made by both Chinese and American scholars to research on clean energy are primarily appreciated. However, some gaps can be seen in these papers and need further analysis. In the first place, compared to Chinese scholarships, American scholarships are limited in quantity and most of them focus on specific areas and lack attention to the trends in clean energy. However, they have done a better job than their Chinese counterparts in terms of research methods used. Chinese scholars work on the issue only by means of qualitative analysis, while American scholars analyze both quantitatively and qualitatively, which can provide a more concrete result. Moreover, both Chinese and American scholarships were published between 2009 and 2012; therefore, they pay no attention to actions and policies adopted by new administrations of both nations.

## 5 CONCLUSION

Since the Obama Administration took office in 2009, clean energy has become one of the major issues that shape US-China relations. It draws academic attention from both sides of the Pacific Ocean while becoming a favorite area of study in the eyes of businessmen and policy-makers. In this paper, the author has reviewed both Chinese and American scholarships on US-China clean energy cooperation. First of all, the rising of clean energy appears as a result of common challenges faced by China and the US, potential benefits, political environment change and complementation of the Chinese market, and American high technology. In research areas, American and Chinese scholars share similarities as well as retain differences. When studying the current situation of clean energy, Chinese scholars pay more attention to abstract cooperation mechanisms while

American scholars think more about specific clean energy initiatives and new ongoing projects in different areas, like solar and wind sectors. Facing conflicts, such as high-tech export control, anti-dumping, and countervailing investigations, Chinese scholars differ in their opinions: some attribute it to the American fear of losing its major power status and catering to domestic politics, while others admit that the Chinese failure of IPR and inappropriate government subsidies also play a role. On the other hand, American scholars recognize the influence of domestic politics, but stress the disparity of technology development and deployment between the two and the contradiction between promoting clean energy and following global trade rules. Different from the American inaction, Chinese counterparts recommend improving independent research and development capacity and learning how to “play with” WTO rules when facing trade frictions.

Due to the novelty of the clean energy concept, scholarship is limited in quantity and most of them focus on the period between 2009 and 2012, while hardly paying attention to recent trends during new administrations in both countries. However, new administrations in the two countries have made a difference since the beginning. Last year, President Xi reaffirmed agreements on clean energy cooperation signed by China and the United States in 2008; both sides launched new cooperation initiatives in Fifth and Sixth US–China Strategic and Economic Dialogues. During the sessions of APEC, China and the United States released joint statements on climate change, setting new targets of carbon emission reduction such as 26%–28% to be achieved by the United States by 2025 and 20% to be achieved by China in 2030 (Minister of Foreign Affairs of PRC 2014). This action will facilitate the development and deployment of clean energy in both countries. Meanwhile, both sides have agreed to further deepen cooperation in clean energy, especially in clean coal technology, nuclear energy, fracking, and renewable energy. With the deepening of willingness and determination from the both sides of the Pacific Ocean, we can look forward to a bright future for US–China clean energy cooperation.

## REFERENCES

- Cooke, Merritt. 2012. *Sustaining U.S.-China Cooperation in Clean Energy*. Washington, D.C.: The Woodrow Wilson Center.
- Cooke, Merritt. 2015. “Greater Philadelphia and Tianjin Economic Development Area EcoPartnership on Urban Clean Energy Infrastructure”. *Journal of Renewable and Sustainable Energy* 7: 1–9.
- Department of Energy U.S. 2011. *U.S.-China Clean Energy Cooperation: A Progress Report*. U.S. Department of Energy.
- Dreyer, June Teufel. 2007. “Sino-American Energy Cooperation”. *Journal of Contemporary China* 16(52): 461–476.
- Jiang Shu & Li Qingsi. 2013. “From Photovoltaic to Wind Powers Disputes: A Game Theory Analysis of Sino-U.S. New Energy Cooperation”. *International Forum*. 15(2): 61–68. (in Chinese).
- Levi, Michael. Elizabeth C. Economy, Shannon K. O’Neil and Adam Segal. 2010. *Energy Innovation: Driving Technology Competition and Cooperation among the United States, China, India and Brazil*. New York: Council on Foreign Affairs.
- Lewis, Joanna. 2012. “Cooperation and Conflict in US-China Clean Energy Relations”. *China Environment Forum*. Washington, D.C.: The Woodrow Wilson Center.
- Li Dong & Wei Xiaosha. 2012. “Trade Frictions of US-China Clean Energy Cooperation, Causes and an Analysis of Solutions”. *Seeker* 11: 29–33. (in Chinese).
- Lieberthal, Kenneth G. 2009. “U.S.-China Clean Energy Cooperation: The Road Ahead”. *Energy Security Initiative* 5: 1–35.
- Lieberthal, Kenneth and David Sandalow. 2008. *Overcoming Obstacles to U.S.-China Cooperation on Climate Change*. John Thornton China Center at Brookings.
- Liu Qing & Liu Rongrong. 2011. “U.S.-China Clean Energy Cooperation”. *American Diplomacy and U.S.-China Relations* 2: 29–35. (in Chinese).
- Liu Yin & Peng Long. 2016. “US-China Cooperation on Climate Change: Achievements, Disagreements and Countermeasures”. *International Forum* 18(2): 46–52. (in Chinese).
- Ma Jianying. 2009. “US-China Clean Energy Cooperation”. *Modern International Relations* 12: 48–54. (in Chinese).
- Marsters, Peter V. & Jeniffer L. Turner. 2001. “Cooperative Competitors: Potential of U.S.-China Clean Energy Cooperation”. *China Environment Forum Brief*. Washington, D.C.: The Woodrow Wilson Center.
- Minister of Foreign Affairs. 2014. “Joint US-China Statement on Climate Change in 2014”. Minister of Foreign Affairs of the People’s Republic of China. (in Chinese).
- Pew Center and Asia Society. 2009. *A Roadmap for U.S. China Cooperation on Energy and Climate Change*. Pew Center and Asia Society.
- Shen Keyu & Lv Suyu. 2015. “Analysis of China’s Clean Energy Technology Introduction”. *Science and Technology Management Research* 4: 233–238, 2015. (in Chinese).
- Tang Yanlin. 2009. “Sino-US Energy Cooperation: Achievements, Differences and Solutions”. *Journal of Southwest Petroleum University* 2(6): 1–9, 2009. (in Chinese).
- Yan Shigang. 2012. “Problems and Prospects Analysis Facing U.S. China New Energy Cooperation and Sino-EU New Energy Cooperation”. *Practice in Foreign Economic Relations and Trade* 5: 18–23. (in Chinese).
- Zhao Qingsi. 2015. “Sino-US Energy Security Game in Asia-Pacific Area”. *International Review* 6: 130–143. (in Chinese).
- Zhu Caihua & Yang Mei. 2012. “Current Situation and Prospects of Sino-US Clean Energy Cooperation”. *International Economic Cooperation* 7: 17–24. (in Chinese).

# Research on the crack resistance ability of hybrid fiber reinforced concrete

Xiang-kun Liu, Zeng-qiang Du, Jian-xu Hui & You Gao

China Nuclear Building Materials Company, Wuhan, Hubei, China

**ABSTRACT:** Hybrid fiber reinforced concrete was prepared with the total volume fraction of the steel fiber, modified polypropylene fiber, and polypropylene fiber being not more than 1.1%. The basic mechanical properties and the crack resistance ability were tested on six groups of specimens. Based on the curves of CMOD–deflection, the effects of fiber volume fraction and hybrid mode upon the crack controlling ability of HFRC were investigated. The results are as follows: when the proportion of fibers is suitable, SF/HF/PPF HFRC can significantly improve the basic mechanical properties of the matrix concrete. The order of hybrid modes in terms of their crack resistance capacities is as follows: F > D > E > C > B > A; on the basis of the best crack resistance ability, the most suitable proportion of fibers in the study is as follows: 0.7% SF, 0.2% HF, and 0.11% PPF.

**Keywords:** hybrid fiber reinforced concrete; notched beam; crack resistance ability; curve of CMOD–deflection

## 1 INTRODUCTION

As a type of multiphase, multicomponent, and multi-level non-homogeneous material, plain concrete exhibits obvious brittleness. Once cracks emerge on its surface, it will undergo damage quickly. As is known to all, steel fibers exhibit excellent strengthening, toughening, and crack resistance properties. And also, adding steel fibers to plain concrete can significantly improve its strength and toughness. At present, there are many reported results of Hybrid Fiber Reinforced Concrete (HFRC) in China and abroad<sup>[1]–[7]</sup>. But the studies are mostly focused on flexural toughness, strength, and hybrid reinforcing effects and the fiber hybrid mode is limited to the Steel Fiber (SF) and modified Polypropylene Fiber (PPF). On the contrary, the crack resistance of HFRC and the performance of SF/HF/PPF hybrid fiber reinforced concrete are investigated in this work. Above all, a series of proportioning of SF/HF/PPF HFRC was designed and the flexural toughness test was performed on each group of notched specimens. Based on the curves of load–CMOD and CMOD–deflection obtained from the flexural toughness test, the effects of fiber volume fraction and hybrid mode upon the crack controlling ability of HFRC were investigated and the most suitable proportion of fibers was also determined.

## 2 EXPERIMENTAL DESIGN AND METHOD

### 2.1 Fiber prosperity

The steel fiber used in this study is flat steel fiber impregnated with Cu (SF). The modified polypropylene fiber (HF) is corrugated with excellent hydrophilic properties and the polypropylene fiber chosen for this work is Dura fiber. The main characteristics of each fiber are shown in Table 1.

### 2.2 Mixture ratio of the concrete

The design strength of the concrete is 60 Mpa with a water–cement ratio of 0.29 and a sand ratio of 42%. The fine aggregate used in this study is mid-course river sand (S) with a modulus of fineness of 2.8. The coarse aggregate chosen is limestone (L) with a maximum particle size of 25 mm and continual size distribution. Polycarboxylate concrete admixtures with 0.85%–1.05% cement dosage are also used.

In order to study the effect of fiber volume fraction and hybrid mode upon the crack controlling ability of HFRC, six different hybrid modes of fibers were designed and the details are summarized in Table 2.

Table 1. Main characteristics of each fiber.

Type	$\rho/\text{g}\cdot\text{cm}^{-3}$	$\sigma_b/\text{MPa}$	$E/\text{GPa}$	$l/\text{mm}$	$d/\text{mm}$
SF	7.85	1000	210	15	0.50
HF	0.92	392	9.80	30	0.60
PPF	0.91	276	3.79	12	0.03

Table 2. Hybrid modes of fibers.

Group	SF	HF	PPF
A	0	0	0
B	1.0%	0	0
C	0.9%	0.00%	0.11%
D	0.7%	0.2%	0.11%
E	0.5%	0.4%	0.11%
F	0.3%	0.6%	0.11%

### 2.3 The concrete mixing process and loading scheme

A forced mixer and the secondary material mixing technique were used to ensure even scattering of fibers in the concrete mixtures. Specimens and the test cubes were compacted by using a vibrating table with the square of  $1\text{ m} \times 1\text{ m}$ . After 24 hours' standing, the mold of the specimen was removed and taken to the standard curing room. With 28 days' curing, the tests were performed.

Based on the CECS: 13 2009<sup>[8]</sup>, the flexural toughness test was performed using deflection as the control signal at a rate of 0.20 mm/min. Deflection was measured by two LVDTs mounted between two rigid frames fixed at both sides of the test specimen and CMOD was measured by using a clip-gagger fixed at 2 mm from the bottom of the beam.

## 3 RESULTS AND DISCUSSION

### 3.1 Effects of fiber volume fraction and hybrid mode on basic mechanical properties

Based on the experimental results, Figure 1 shows the graphs of the compressive strength and splitting tensile strength of various hybrid modes of fibers.

From Figure 1, the following observations can be made:

- i. SF/HF/PPF HFRC can more significantly improve the compressive strength of plain concrete. But the strengthening effect will be not obvious when the proportion of the three fibers is not suitable. For example, the compressive strength of group D has improved by 23.88% with only 2.47% improvement of group F.

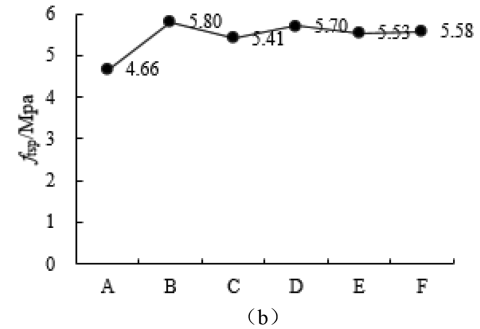
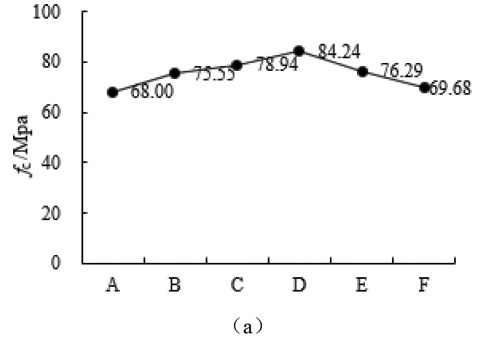


Figure 1. Graphs showing compressive strength (a) and splitting tensile strength (b) of various hybrid modes of fibers.

- ii. In contrast, the hybrid fiber can significantly improve the splitting tensile strength, which increased by 16.09% to 24.46%.

### 3.2 Analysis of HFRC's crack resistance capacity

#### 3.2.1 Correlation analysis of the CMOD and deflection

Figure 2 shows the calculation model of the CMOD and deflection ( $\delta$ ). In Figure 2, L stands for the length of the notched beam with H standing for height.

Based on Figure 2, It is observed that,

$$\begin{aligned} \delta &= L / 2 \cdot \tan \theta \\ \text{CMOD} &= 2 \cdot H \cdot \sin \theta \\ \tan \theta &\approx \theta, \sin \theta \approx \theta \\ \text{CMOD} &= (4H / L) \cdot \delta \end{aligned}$$

It is shown that there is a significant linear correlation between CMOD and  $\delta$  and the coefficient of proportionality is  $4H/L$ . Because the values of H and L are certain, the coefficient of proportionality is constant. By mixing fibers and concrete, its carrying capacity and its crack resistance ability will be improved because of fibers' excellent strengthening, toughening, and crack resistance properties. In other



words, HFRC's coefficient of correlation will change when compared to that of plain concrete. Therefore, it is entirely feasible to evaluate the crack resistance ability of the beam by using the coefficient.

### 3.2.2 Evaluation of HFRC's crack resistance ability

Based on Figure 2, the CMOD- $\delta$  curve can well-reflect the relationship between crack mouth opening displacement and deflection and the slope of the fitted curves can directly show the spending increase of CMOD to  $\delta$ .

When the value of  $\delta$  is certain, the greater the slope value, the greater is the CMOD value. In contrast, the smaller the slope value, the better is the crack resistance capacity HFRC exhibited. Figure 3 shows CMOD- $\delta$  curves from group A to group F. The fitted curves and the coefficients of correlation are shown in Table 3.

Table 3 supplies the fitted curves and the coefficients of correlation from A to F.

From Figure 3 and Table 3, the following observations can be made:

- i. The coefficient of correlation of each of the groups reached a stable level between 0.9925 and 0.9998. It is proved that the CMOD and  $\delta$  are linearly dependent, which is in agreement with the results of Section 3.2.1.
- ii. From Table 3, the order of hybrid modes of fibers in terms of the slope of curves is as follows: A > B > C > E > D > F. This means that the order of hybrid modes in terms of capacity of crack resistance is as follows: F > D > E > C > B > A. It proves that SF/HF/PPF HFRC exhibits more significant crack resistance ability than SF/HF HFRC and SF/HFRC.
- iii. The slope value of group F is the maximum. It is shown that group F has the best crack resistance ability. This is because of HF's excellent performance both in terms of toughening and crack resistance properties and group F also contains the maximum proportion. Although the slope of group F is the maximum, its compressive strength and splitting tensile strength obtained from Figure 1 are less than those of group D. Based on the basic mechanical and crack resistance properties, group D is more advantageous.

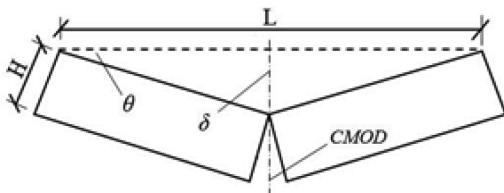


Figure 2. The calculation model of the CMOD and  $\delta$ .

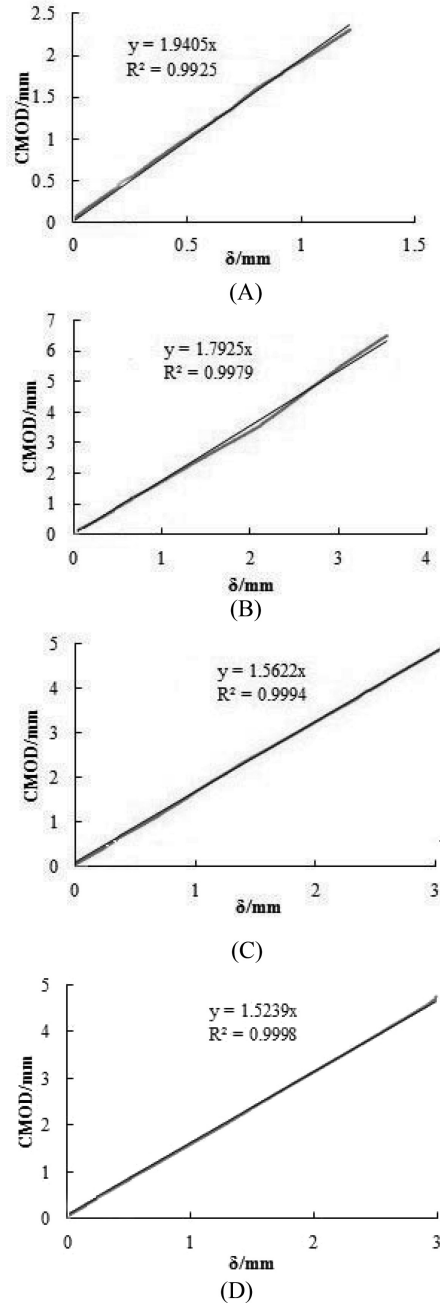


Figure 3. (Continued)

On the basis of the best crack resistance ability, the most suitable proportion of fibers in the study is as follows: 0.7% SF, 0.2% HF, and 0.11% PPF. Toughening and strengthening mechanisms are analyzed below. In SF/HF/PPF HFRC, the three fibers distribute disordered properties and

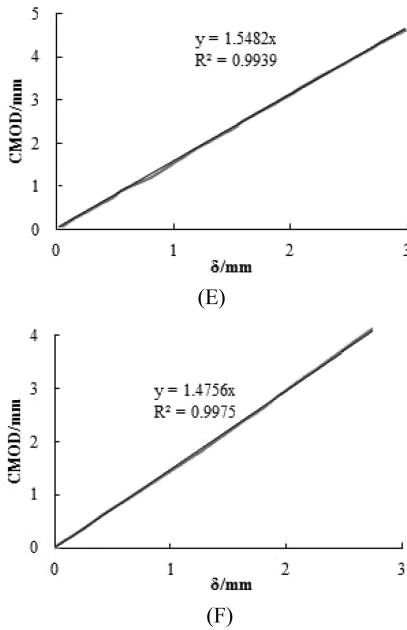


Figure 3. CMOD- $\delta$  curves of each of the groups (A-F).

Table 3. Fitted curves and the coefficients of correlation of each group of fibers.

Group	Fitted curve	R <sup>2</sup>
A	$y = 1.9405x$	0.9925
B	$y = 1.7925x$	0.9979
C	$y = 1.5622x$	0.9994
D	$y = 1.5239x$	0.9998
E	$y = 1.5482x$	0.9939
F	$y = 1.4756x$	0.9975

perform toughening and strengthening in turn with SF, HF, and PPF. Because the elastic modulus of SF is large, it can effectively improve the compressive strength<sup>[9]</sup>. But the effect of strengthening largely depends on the fiber's cohesive effect with the concrete. Once the steel fiber is pulled out from the concrete, the conventional concrete will undergo damage quickly due to its lower elongation. In contrast, the HF shows excellent tensile elongation properties with a suitable elastic modulus, so that it can exhibit significant toughening properties with better strengthening capacity. In addition to this, although the PPF has the lowest elastic modulus, it exhibits the largest tensile elongation and its quantity is high. It can effectively delay the destruction of the concrete while it also displays excellent crack resistance properties in the fresh state<sup>[10]</sup>.

#### 4 CONCLUSIONS

In this paper, the basic mechanical properties and the crack resistance capacity of SF/HF/PPF HFRC are investigated. Based on the experimental data and above discussion, the following conclusions can be drawn:

- i. SF/HF/PPF HFRC can significantly improve the basic mechanical properties of the matrix concrete. And the splitting tensile strength was largely improved by 24.26% with compressive strength by 23.88%.
- ii. The order of hybrid modes of the fiber in terms of the slopes of the CMOD- $\delta$  curves is as follows: A > B > C > E > D > F. This implies that the order of hybrid modes of the fiber in terms of their crack resistance capacities is as follows: F > D > E > C > B > A.
- iii. On the basis of the best crack resistance ability, the most suitable proportion of fibers in the study is: 0.7% SF, 0.2% HF and 0.11% PPF.

#### REFERENCES

- [1] Giaccio G et al. Use of small beams to obtain design parameters of fiber reinforced concrete [J]. *Cement & Concrete Composites*, 2008, 30:297-306.
- [2] Xia Dongtao, Liu Xiangkun, Zhou Boru. Flexural toughness of hybrid fiber reinforced high-performance concrete under three-point bending. *Applied Mechanics and Materials*, 357, pp.1110-1114, 2013.
- [3] Wang Haichao, Liu Jiaoyuan. The experiment of bending tension performance on the hybrid fiber reinforced concrete with higher toughness. *China Concrete and Cement Products*, (4), pp.46-49, 2011.
- [4] Deng Zongcai, Li Jianhui, Liu Guodong. Experimental study on mechanical properties of hybrid macro-fiber reinforced concrete. *Concrete*, (8), pp.50-55, 2006.
- [5] Zhao Liang-Ping, Gan Dan-Ying, Zhu Hai-Tang. Effect of the steel fiber on the strength and toughness on the concrete. *Journal of china university of water resources and electric power*, 33(6), pp.29-32, 2012.
- [6] Mei Guodong, Li Jixiang, Liu Xiao-Fan. Hybrid fiber reinforced concrete flexural behavior and hybrid effects. *Concrete*, (2), pp.21-24, 2013.
- [7] Wang Zhi-Jie, Meng Xiang-Lei, Wang Qi. Study on the flexural toughness of the steel fiber reinforced concrete. *Concrete*, (3), pp.71-74, 2014.
- [8] China Association for Engineering Construction. Standard test methods for fiber reinforced concrete, Beijing: China Planning Press, 2010.
- [9] Xia Dongtao, Liu Xiangkun, Xia Guangzheng. Research on the flexural toughness of hybrid fiber reinforced high-performance concrete. *Journal of huazhong university of science and technology (natural science edition)*, 41(6), pp.108-112, 2013.
- [10] Gao Dan-Ying, Zhao Liang-Ping, Feng Hu. Study on the flexural toughness and evaluating method of the steel fiber reinforced concrete. *Journal of building materials*, 17(5), pp.783-789, 2014.

## Fabrication and characterization of $B_4C$ ceramics with $Al_2O_3$ - $La_2O_3$ aids

Yun-long Zhang

*College of Materials Science and Engineering, Jiamusi University, Jiamusi, P.R. China*  
*Center for Composite Materials and Structure, Harbin Institute of Technology, Harbin, P.R. China*  
*Institute of Applied Materials and Technology, Jiamusi University, P.R. China*

Yu-min Zhang

*Center for Composite Materials and Structure, Harbin Institute of Technology, Harbin, P.R. China*

Xue-song Ding

*College of Materials Science and Engineering, Jiamusi University, Jiamusi, P.R. China*

Ming Hu

*College of Materials Science and Engineering, Jiamusi University, Jiamusi, P.R. China*  
*Institute of Applied Materials and Technology, Jiamusi University, P.R. China*

Chun-li Ma & Cheng-hai Li

*College of Materials Science and Engineering, Jiamusi University, Jiamusi, P.R. China*

**ABSTRACT:** In the present work, commercial  $B_4C$  powder were applied to fabricate  $B_4C$  ceramics by hot-press sinter technology by introducing  $Al_2O_3$  combined with  $La_2O_3$  served as sintering aids. Different amounts of  $Al_2O_3/La_2O_3$  aids were added to the  $B_4C$ -base material and hot-pressure sintering was conducted at  $1950^\circ C$  under argon atmosphere. Microstructure, crystal phases and density evolution were studied and correlated to  $Al_2O_3/La_2O_3$  aids content. The results showed that combination of  $Al_2O_3$  and  $La_2O_3$  aid was effective for promoting densification of  $B_4C$  ceramics. The influence of aids content on the phase constitution and sinter behavior of  $B_4C$  ceramics was investigated.

**Keywords:** hot-press sintering, sintering behavior, porosity, compound aids

### 1 INTRODUCTION

Boron carbide ceramics were important high-tech engineering materials mainly due to their outstanding physical, mechanical properties, high hardness and low density [1-3]. However, low fracture toughness and ultrahigh sintering temperature severely impede further development. Lots of attempts had been made to overcome these disadvantages, such as adoption of nano/submicron-sized powders as raw materials or introduction of a second phase into  $B_4C$  matrix composites. As for second phase, different materials such as  $TiB_2$ ,  $CrB_2$ ,  $ZrB_2$ ,  $SiC$ ,  $TiC$ ,  $Al_2O_3$ , etc. had been applied to improve fracture toughness and lowered sintering temperature, but improvement effects were limited [4-6]. More advanced sintering methods had been employed to produce more fully densified  $B_4C$  ceramics. Dense  $B_4C$  ceramics fabricated directly using only low temperature sinter method was rarely reported.

Other additives such as Fe, Ti, B, Mg, Co, Ni and Cu have also been used, with various degrees of improvement in sintering behavior and mechanical properties. Aluminum and Al-containing compounds such as  $AlF_3$  and  $Al_2O_3$  were also found to be effective for the densification of  $B_4C$ . In view of specific properties and potential applications of  $B_4C$  ceramics, it was meaningful to investigate whether dense  $B_4C$  ceramics can be fabricated through liquid-phase sintering under relatively low temperature. However, reports about  $B_4C$  ceramics with  $Al_2O_3/La_2O_3$  aids were scarce. In the present work,  $B_4C$  ceramics with high performance were fabricated with  $Al_2O_3/La_2O_3$  served as sinter additives. The main purpose of present work was to examine effectiveness of  $Al_2O_3/La_2O_3$  system served as densification sintering aids for  $B_4C$  ceramics. Another aim was to investigate how  $Al_2O_3/La_2O_3$  content influence relative density, micro-structure and sintering behavior of  $B_4C$  ceramics.

## 2 FABRICATION AND CHARACTERIZATION

$B_4C$  powder ( $D_{50} = 3.5 \mu\text{m}$ ).  $La_2O_3$  powder ( $D_{50} = 1 \mu\text{m}$ ) and  $Al_2O_3$  powder ( $D_{50} = 0.5 \mu\text{m}$ ) were used as sintering aids.  $Al_2O_3$  and  $La_2O_3$  were chosen as aids with molar ratio were 1:1. The total amount of sinter additions was varied from 3 wt% to 12 wt% in the mixture. The aids content of hot-pressed specimens were 3 wt%, 6 wt%, 9 wt% and 12 wt%, which were designated as S3, S6, S9 and S12, respectively. The mixture powders were weighed with an electronic balance, followed by a wet ball milling for 8h using a plastic bottle and SiC balls in absolute ethanol. After milling, ethanol was cleared by applying a co-evaporating method to decrease segregation during the process of drying. Then, the dried mixture powders were put into a graphite mold with an inner diameter of 40 mm and an outer diameter of 120 mm, and then sintered using a vacuum hot-press furnace, at  $1900^\circ\text{C}$  for 60 min under a pressure of 30 MPa in argon gas. The sintering temperature was measured by using an optical pyrometer. The heating rate was executed with  $20^\circ\text{C}/\text{min}$  from room temperature to  $1900^\circ\text{C}$ . The specimens together with the graphite mold were cooled to ambient temperature in the furnace. The specific mass was determined according to Archimedes method. The phase constitution was identified by XRD and macrostructure was investigated by Canon camera (60D). At least four bars were tested for each test condition. Fracture morphologies were observed by scanning electron microscope.

## 3 RESULTS AND DISCUSSION

### 3.1 Phase constitution analysis

Fig. 1 gave XRD patterns of the  $B_4C$  ceramic composites with S3, S6, S9 and S12. There existed diffractive peaks of  $B_4C$  and  $LaAlO_3$  phases in all sintered samples. While received  $La_2O_3$  phase was not detected.  $Al_2O_3$  phase was detected as minor phase due to  $Al_2O_3$  was excessive as received aids. Peak intensity of  $LaAlO_3$  phase in all samples increased with increasing content of mixture sintering additives.  $LaAlO_3$  phase was a new solid solution phase, formed by reaction of  $Al_2O_3$  and  $La_2O_3$  at reaction temperatures, which promoted densification of  $B_4C$  ceramic. The peak intensity of  $B_4C$  phase was not obviously varied as aids content increased.

### 3.2 Macrostructure observation

The macro-photograph of the sintered  $B_4C$  ceramics was listed in Fig. 2. All of the sintered materials were compact and their surface was smooth. The macro

dimension linear shrinkage of  $B_4C$  ceramics increased with sintered aids content increasing. As aids reached 12%, linear shrinkage of  $B_4C$  ceramics was about 7%. It can be attributed to that formation of eutectic phase, which promoted liquid phase sintering. The result was as similar with that in SiC ceramics with  $Y_2O_3-Al_2O_3$  system [7].  $La_2O_3-Al_2O_3$  aids were introduced into the  $B_4C$  ceramics, while it was difficult to avoid aforementioned problems of sintering shrinkage and weight loss. Under  $Al_2O_3/Y_2O_3$  aids system, introduced ways of aids and sintered temperature impacted weight loss and dimensional shrinkage rate. The higher sintered temperature was responsible for visible weight loss and dimensional shrinkage rate.

### 3.3 Densification behavior

Fig. 3 gave an overview of the measured density and porosity after liquid-phase sintering of materials investigated. The measured density of  $B_4C$  ceramics had similar evolvement rule with increase of sintered aids content. Measured density of  $B_4C$  ceramics varied from  $2.36 \text{ g/cm}^3$  to  $2.57 \text{ g/cm}^3$  when the sintered aids content enhanced from 3 wt% to 12 wt%. The measured density was not beyond  $2.6 \text{ g/cm}^3$  even if aids content was beyond 12 wt%. It was possible reason that volatilization of aids and formation of macro porosity played an critical role on reduction of measured density. As sintered

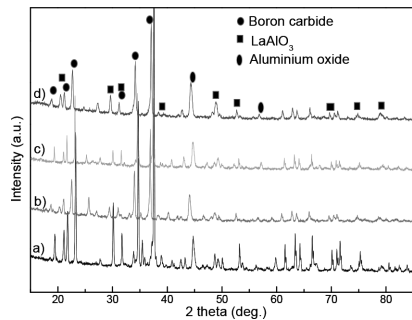


Figure 1. XRD pattern of  $B_4C$  ceramics, a), b), c) and d) represented S03, S6, S9, S12, respectively.

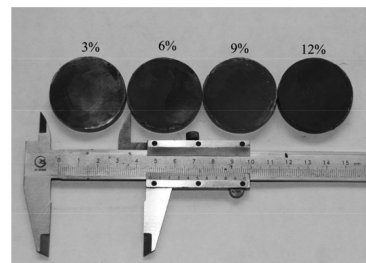


Figure 2. Macrostructure of sintered  $B_4C$  ceramics with different aids content.

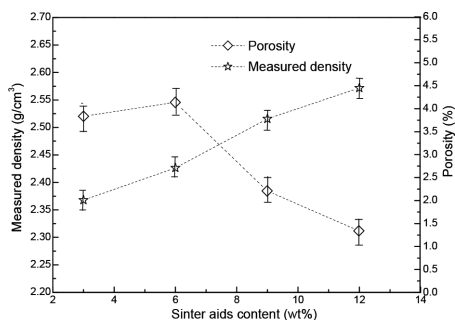


Figure 3. The curve of measured density and porosity against aids content of  $B_4C$  ceramics.

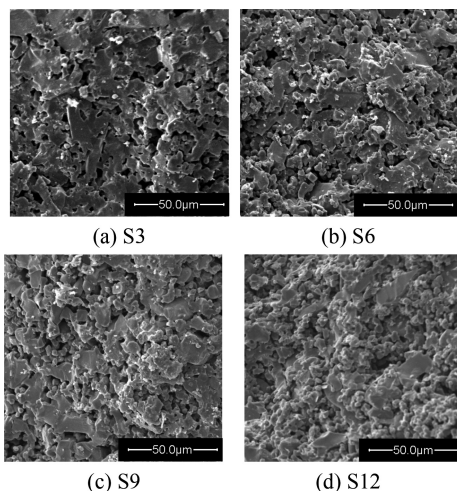


Figure 4. SEM photos of sintered  $B_4C$  ceramics with different aids content.

aids content increased, the porosity of  $B_4C$  ceramics increased first, then it decreased gradually, the maximum value of porosity was detected in the S6 sample (about 2.54%).

The micro-structures against sintered aids content of  $B_4C$  ceramics was represented in Fig. 4. It was obviously found that the volume of sintered aids content had an important effect on the porosity and micro-structures of  $B_4C$  ceramics. According to solution re-precipitation sintering mechanism<sup>[9]</sup>, small SiC grains may dissolve into liquid intergranular phase and re-precipitate on larger SiC grains when saturation of melt was reached. In present work, we found that coarse process of  $B_4C$  grains occurred during the hot-pressed sintering procedure.  $B_4C$  grains was finer ( $D_{50} = 0.5 \mu\text{m}$ ), while  $B_4C$  grains in sintered specimen had coarsen. As the sintered aids content was low (3 wt.% and 6 wt.%), the porosity of  $B_4C$  ceramics was obvious. With increasing aids, porosity of  $B_4C$  ceramics reduced. It can be attributed to volatilize and

decompose of aids along with inhibitory effect of hot pressing sintering. The interaction and balance of the above mentioned factors resulted in differences of micro-structure, sintering behavior and mechanical properties for  $B_4C$  ceramics.

## 4 CONCLUSION

$B_4C$  ceramics was fabricated by hot-press sinter technology at 1950°C by means of protective argon gas and  $Al_2O_3$  combined with  $La_2O_3$  served as sintering aids. Effect of  $Al_2O_3/La_2O_3$  aids content on the micro-structure, crystal phases and density evolution was surveyed. The results showed that  $Al_2O_3/La_2O_3$  compound sintering aid was effective for promoting densification of  $B_4C$  ceramics. The volatilize role and decompose behavior of aids along with inhibitory effect of hot pressing sintering would have a major impact on the micro-structure, crystal phases and density.

## ACKNOWLEDGEMENT

The authors were grateful for support by Chinese Postdoctoral Science Foundation (No.2012M520754), Major State Basic Research Development Program (No.2014CB46505) and the science and technology innovation team of Jiamusi University (No.CxtD-2013-03).

Correspondence should be addressed to Ming HU; jmsdxhuming@126.com

## REFERENCES

- [1] F. Thevenot, Boron carbide—a comprehensive review, *Journal of the European Ceramic Society*. 1990 (6): 205–225.
- [2] R.M. German, Pressure-assisted sintering, in: L.V. Interrant, M.J. Hampden-Smith (Eds.), *Sintering theory and practice*, John Wiley & Sons Inc., New York, 1996: 313–368.
- [3] A.K. Suri, C. Subramanian, J.K. Sonber, T. Murthy, Synthesis and consolidation of boron carbide: a review, *International Materials Reviews* 2010,(55): 4–40.
- [4] Vladislav Domnich, Sara Reynaud, Richard A. Haber, Manish Chhowalla. Boron Carbide: Structure, Properties, and Stability under Stress [J]. *J Am Ceram Soc* 2011, 94: 3605–3628.
- [5] Thévenot F. Boron carbide—a comprehensive review. *J Eur Ceram Soc*. 1990, 6: 205–225.
- [6] Levin L, Frage N, Dariel MP. A novel approach for the preparation of  $B_4C$  based cermets. *Int J Refract Met Hard Mater*. 2000, 18: 131–135.
- [7] A.K. Samanta, K.K. Dhargupta, S. Ghatak. Decomposition reactions in the SiC–Al–Y–O system during gas pressure sintering [J]. *Ceramics International*, 2001(27): 123–133.



**Taylor & Francis**

Taylor & Francis Group

<http://taylorandfrancis.com>

# An experimental study on eccentric compression reinforced concrete columns strengthened with HDPFs

Y. Qiao, C.Z. Sun, Z.B. Wang & G. Zuo

*Department of Architecture Engineering, Suqian College, Suqian, China*

**ABSTRACT:** In this paper, six reinforced concrete columns strengthened by high ductility polyester fibers and two reinforced concrete columns were used to perform the eccentric compressive test. The factors, including reinforcement form, fibers layers, and eccentricity, were studied. The test results show that the high ductility polyester fiber can obviously improve the bearing capacity of reinforced concrete and the polyester fibers can improve the deformation capacity of members and the reinforced concrete columns strengthened by high ductility polyester fibers avoid brittle failure, and the form and space affected the strengthening effect, and the bearing capacity and ductility of concrete columns reinforced by high ductility polyester fibers increased obviously with the increasing number of fiber layers. The results can provide reference for engineering applications for high ductility of polyester fibers.

**Keywords:** high ductility polyester fiber; reinforced concrete column; strengthen; eccentric compression

## 1 INTRODUCTION

At present, there are several kinds of fiber composite materials used for reinforced concrete columns in the field of civil engineering which are mainly made of glass fibers, aramid fibers, carbon fibers, and so on<sup>[1-3]</sup>. In particular, domestic and foreign scholars have carried out my studies on the application of carbon fibers. The study shows that although the bearing capacity of the strengthened members is increased, the ductility of the columns is limited and its brittle failure is because of the failure of the fiber.<sup>[4]</sup> Super Reinforcement with Flexibility (SRF) is a new seismic reinforcement technology in Japan after the year 2000. The technology uses High Ductility Polyester Fibers (HDPFs) as the reinforcing material.<sup>[5]</sup> At present, there is a small number of experimental studies and theoretical analysis overseas,<sup>[6-10]</sup> but there is no relevant experimental research and theoretical analysis in China.<sup>[11-13]</sup> Only some scholars have presented a brief introduction of the HDPF reinforcement technology. In this paper, a test was carried out to assess the axial bearing capacity of high ductility polyester fibers and two reinforced concrete columns in previous studies mainly aimed at the effect of reinforcement form, reinforcement spacing, length ratio, and concrete strength on the restraint performance, bearing capacity, and failure mode of reinforced concrete columns strengthened with HDPF.<sup>[14]</sup> In this paper, the eccentric compression test of reinforced concrete square columns

strengthened with high ductility polyester fibers was carried out firstly. Then, the failure characteristics, bearing capacity, and ductility of reinforced concrete columns strengthened with high ductility polyester fiber reinforced concrete columns under large and small eccentric loads are analyzed, which provides the necessary research foundation and reference for the application of HDPF reinforced concrete structures in future.

## 2 TEST SURVEY

### 2.1 Specimen design

In this experiment, eight eccentric specimens were designed, in which five were large eccentric specimens, and three were small eccentric specimens. Each group had a concrete column test piece as a contrast column, the initial eccentricity of the small eccentric concrete column specimens was 40 mm and the initial eccentricity of the large eccentric concrete column specimens was 150 mm. The section size of the specimen was designed as 200 mm × 200 mm,  $b = h = 200$  mm, in order to prevent the phenomenon of instability in the course of the test; the height of the test specimen was set to 1200 mm; that was to say that the long fine ratio is 6 and the parameters of the test specimen are shown in Table 1. The average strength of concrete is 36.5 MPa and the elastic modulus is 33.7 MPa. The elastic modulus of the HPB235 steel bar is 210

Table 1. General view of tested specimens.

Test piece number	Layer and package form of HDPF
DP I-1	Not strengthened
DP I-2	Horizontal one-layer 50 mm strip, with a spacing of 50 mm
DP I-3	Horizontal two-layer 50 mm strip, with a spacing of 50 mm
DP I-4	Horizontal one inclusive
DP I-5	Horizontal two inclusive
SP I-1	Not strengthened
SP I-2	Horizontal one-layer 50 mm strip, with a spacing of 50 mm
SP I-3	Horizontal one inclusive

GPa, the yield strength is 336 MPa, and the ultimate strength is 440 MPa. The elastic modulus of the HRB335 steel bar is 200 GPa, the yield strength is 405 MPa, and the ultimate strength is 532 MPa. The elastic modulus of polyester fiber ribbons is 6.25 GPa and the fracture strength is 600 MPa.

Reinforcement of the test column was performed using symmetric reinforcement, longitudinal reinforcement was carried out using four HRB335 rebars of 12 mm diameter, and stirrup was performed using circular reinforced HPB235 rebars of 6 mm diameter with 200 mm spacing. Stirrup spacing was provided at both ends of the range of the 300 mm encryption in the column, while the spacing was 200 mm. A test piece with reinforcement is shown in Figure 1.

### 2.2 Specimens loading and data acquisition

The experiment was carried out by using a 5000 kN electro hydraulic servo long cylinder pressure testing machine at the experimental center of Suqian College in Jiangsu province. The test specimens were hinged at both ends and a layer of fine sand was laid between the upper end of the test piece and the lower end of the column and the contact surface of the press plate to ensure that the stress applied on the specimen was uniform during the loading process. Application of local force on the surface will lead to local concrete premature crushing. Before loading, the test piece was required to carry out physics centering and geometric centering. Formal loading should be performed after completion of preloading. The loading device is shown in Figure 2.

According to relevant provisions of the concrete structure test method standard (GB/T50152-2012), the loading process was determined as follows: implementing the grading load formally after calibration of the test piece and the instrument. The displacement control method was adopted in this

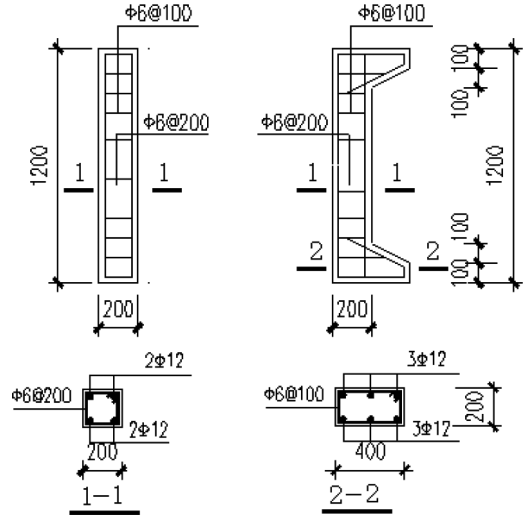


Figure 1. Reinforcement of specimens.



Figure 2. Picture of the loading apparatus.

experiment and the loading speed was 0.23 mm/s. At the beginning of the test, the load value of each level was 10% of the limit load, the test data was recorded 3 minutes after each stage of the loading, and the failure of the specimens was observed. Each load was held for 5–10 minutes, then the next level of load was added, and the process was repeated. Until the load reached 80%–90% of the ultimate bearing capacity, each load range was reduced to half of the original differential load and added. When the load reached the descending segment and the value reached 80% of the maximum load, the loading process was stopped and regarded as a specimen failure. The test load valued by using the 5000 kN electro-hydraulic servo long column pressure testing machine electronic control data acquisition system in a timely manner and the strain data were collected by using the DH3816 static stress and strain gauge measurement technique.



### 3 EXPERIMENTAL PHENOMENA AND TEST RESULT ANALYSIS

#### 3.1 Failure mode

Specimen DPI-2: when the load was increased to 45 kN, the concrete in the tension zone exhibited 3–4 fine transverse cracks, the deflection value of the column was 2.26 mm, and no obvious change of concrete was observed in the compression zone. When the load was increased to 120 kN, tension transverse cracks of concrete increased significantly, tiny longitudinal cracks accompanied with a fine crackle in concrete in the compression zone were observed. When the load was increased to 200 kN, the longitudinal crack in the compression zone of concrete increased significantly, the width became larger, and the crackle became obvious. When the load was added to 258 kN, the deflection value of the test piece was at 11.56 mm, the specimen showed obvious bending, the transverse crack of the concrete in the tension zone was very obvious, and the maximum crack width value was 8.9 mm. Compression zone concrete was crushed and expanded on the outside. But it was different from the failure phenomena of carbon fiber reinforcement of reinforced concrete columns. The HDPF ribbon did not exhibit the phenomena of fracture and crack and only in individual parts, the whitening phenomenon was observed due to stress. After stripping the HDPF ribbon, it can be observed that the internal compressive region of the concrete was crushed clearly. It can be seen that the tensile reinforcement was bent by artificial chiseling of concrete and the form of damage is shown in Figures 3 and 4.

Specimen DP-3: when the load was increased to 50 kN, there was no obvious change in the specimen. When the load was increased to 60 kN, the concrete in the compression zone was similar to that of DP I-3. When the load was increased to 170 kN, the longitudinal crack in the compression zone of concrete increased significantly, the width became larger, and the crackle sounded obviously. At this point, the deflection value of the test piece was increased to 5.48 mm, the specimen was bent,

and the longitudinal crack of the tensile zone became obvious. When the load was increased to 269.5 kN, the concrete in the middle area of the middle part of the compression zone was crushed and exhibited an outward expansion of the initial appearance. The load reached a peak and the form of damage is shown in Figures 5 and 6.

Specimen DP-4: due to wrapping of the component with HDPF, the internal cracks in the concrete cannot be observed in the process of loading, and development of the HDPF belt can only be observed by the load–deflection curve and the outsourced HDPF ribbon. When the load was increased to 70 kN, the strain value of concrete in the tension zone increased slightly and there was almost no increase in the tensile and compressive strains of the HDPF, which indicates that the HDPF ribbon has no effect at this point of time. When the load was increased to 70 kN, the tension compression strain of the HDPF ribbon had been gradually increasing, and the change of the deflection value was smaller in the test piece. When the load was increased to 210 kN, the specimen bent obviously accompanied with the fracturing sound of internal concrete and the ripping sound of the HDPF and concrete binder, and the tensile region of the fiber increased significantly, and the HDPF strip tension compressive strain values increased significantly. When the load was increased to 275 kN, the load reached the maximum value, and the bending of the test piece was more obvious, and the HDPF belt in the compression zone summoned up obviously, but no fracture and crack phenomena were observed and the form of damage is shown in Figures 7 and 8.

The failure process of specimen DPI-5 was similar to that of specimen DPI-4. Before the load was increased to 100 kN, the increase in the strain value of concrete in the tension zone was small and the change of tension and compression strain values of the HDPF was small. After the load was increased to 150 kN, the tensile and compressive strain of the HDPF gradually increased. The specimen bent obviously accompanied with the fracturing sound of internal concrete and the ripping sound of the



Figure 3. Failure pattern of column DP-2 (before stripping of bands).



Figure 4. Failure pattern of column DP-2 (after stripping of bands).



Figure 5. Failure pattern of column DP-3 (before stripping of bands).



Figure 6. Failure pattern of column DP-3 (after stripping of bands).

concrete binder, and the tensile area of the fiber increased obviously, and the concrete of the compressive region summoned up. When the load was increased to 295 kN, the load reached the maximum value and concrete cracks appeared in the tensile zone. The transverse crack of the inner concrete can be seen in the gap of the HDPF belt and the concrete in the compression zone was obviously pushed outward. The concrete restrained by the HDPF was also obviously pushed outward, but no fracture and crack phenomena were observed. The damage observed is shown in Figures 9 and 10.

SPII-2 and SPII-3 are test pieces with one layer of the whole layer of wrapped HDPF, with a spacing of 50 mm and an eccentric distance of the reinforcement specimen of 40 mm. The test status and failure state of the loading process of the two specimens were very similar and the damage started to appear at the core of the weak area. The outer surface of the HDPF appears with transverse folds and the bulging phenomenon. During the test, with the increase of the load, the strain of concrete and reinforcement increased gradually and the concrete tends to expand outward. When the load reached about 80% of the ultimate design value, the strain of the HDPF developed rapidly. The HDPFs of the compression face exhibit obvious bulging, accompanied with the fracturing sound of internal concrete and the ripping sound of the concrete binder during the loading process. When the SPII-2 specimen was loaded to about

480 kN, the compressive strain of concrete at one side of the axial load was far from the axial load required to achieve the ultimate strain. When loading to 630 kN, the compression zone side area concrete appeared to be crushed, pressed, crisp, and exhibiting broken shape and compression reinforcement yielding. When the SPII-3 specimen was loaded to the limit load of 680 kN, the concrete at one side of the compression zone was crushed, pressed, and exhibited compression reinforcement yielding. The member was declared to be damaged and the form of damage is shown in Figures 11–14.

### 3.2 Test results analysis

#### 3.2.1 Bearing capacity analysis

In this experimental study, the improvement of the ultimate bearing capacity of the concrete's eccentric columns before and after the reinforcement of the bonded HDPF strip is a very important index to measure the effect of the SRF method on the reinforcement of the reinforced concrete column, which improves the bearing capacity of eccentric compression concrete members, improves the ductility of concrete members, and also to fulfill important research purposes of the HDPF with constraint reinforcement. Table 2 shows the experimental results of HDPF fiber reinforced concrete eccentric columns.

By comparing the data in the table and analysis, the following conclusions can be drawn: (1) in the reinforced concrete members with HDPF reinforced concrete structures, the ultimate bearing capacity of concrete eccentric specimens strengthened by different reinforcement methods and wrapped layers is increased in different degrees. Among all the large eccentric components in the test, the maximum amplitude observed is 35.3% and the minimum is 18.4%; among all the small eccentric components, the maximum amplitude observed is 31% and the minimum is 22.1%. (2) The reinforcing effect of the HDPF with completely encased concrete columns is more significant than



Figure 7. Failure pattern of column DP-4 (before stripping of bands).



Figure 8. Failure pattern of column DP-4 (after stripping of bands).

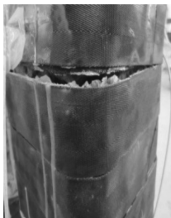


Figure 9. Failure pattern of column DP-5 (before stripping of bands).



Figure 10. Failure pattern of column DP-5 (after stripping of bands).



Figure 11. Failure pattern of column SP-2 (before stripping of bands).



Figure 12. Failure pattern of column SP-2 (after stripping of bands).

that of interval reinforcement, and the effect of the two layers of the HDPF is more than that of the one layer. However, the value of the ultimate bearing capacity increases with the number of HDPF layers; but they don't appear to support a proportional growth relation. (3) The bearing capacity of the specimens differs with the number of layers, the amount and the form of reinforcement of the HDPF, and the ultimate bearing capacity will be increased accordingly. But the increase of the bearing capacity of the specimens under small eccentric columns is not much larger than that of specimens under large eccentric compression columns.

### 3.2.2 Ductility analysis

In order to make HDPFs strengthen reinforced concrete members, their ductility should be analyzed. In this test, we study on the ductility of HDPF reinforced members by using the load–deflection (P–Δ) curve obtained during the test. The load–deflection curves of the bonded HDPF strip before and after the test column are shown in Figures 15 and 16.

The conclusions drawn through the analysis of the strain curve of the HDPF with the above loading are as follows: (1) compared to the column DPI-1 and SP II-1, there is no reinforcement, and therefore, no strain curve of load–HDPF is obtained. In the early stage of loading, because the values of the strain of concrete and steel are smaller, transverse and longitudinal strain values of the HDPF are very small, which indicates that the constraint effect of this HDPF on the specimen is very small. At this time, the strain rate is relatively slow, but the increase is stable with the increase of the load. The strain value corresponding to the ultimate load is relatively large and the maximum value is more than 9000, which shows that the value of HDPF elongation at this time is larger and the high ductility of the HDPF is also fully explained. (2) From the figure, the following observations can be made: with increase of reinforced layers, the descending strain value obtained from the load–strain curve will become more gentle, indicating that the increase in the number of reinforcement layers will lead to concrete damage



Figure 13. Failure pattern of column SP-3 (before stripping of bands).



Figure 14. Failure pattern of column SP-3 (after stripping of bands).

enhancement by the binding effect, and thereby lead to the development of concrete cracks more slowly, which will enable increase of ductility. In addition, with an increase in the distance between the HDPF reinforcements, the drop in the strain curve of the load–HDPF will become more and more steep, which indicates that the ductility of the specimens is getting worse. (3) As can be seen from the figure, when the reinforced column is destroyed, whether it is reinforced with HDPF spacing paste or HDPF package, the strain value of the HDPF belt is less than the limit strain value, which shows that the HDPF belt in the process of this experiment failed to play its role effectively.

Table 2. The main results of test members.

Test piece number	Eccentricity (mm)	Bearing capacity of specimen (kN)	Deflection value of the middle column of maximum load (mm)	Bearing capacity of reinforced columns/column bearing capacity
DP I-1	150	218.0	7.7	—
DP I-2	150	258.2	8.8	1.184
DP I-3	150	269.5	9.8	1.236
DP I-4	150	275.8	10.4	1.265
DP I-5	150	295	12.2	1.353
SP I-1	40	518	4.8	—
SP I-2	40	632.3	5.9	1.221
SP I-3	40	678.6	6.1	1.310

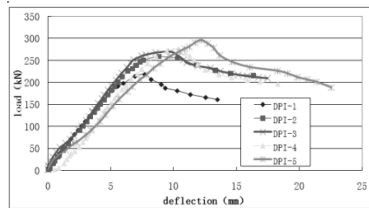


Figure 15. Load–deflection curve part specimens DPI-1 to DPI-5.

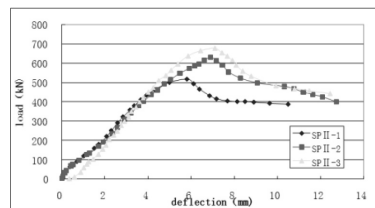


Figure 16. Load–deflection curve of part specimens SP II-1 to SP II-3.

## 4 CONCLUSIONS

In this paper, an eccentric compression test is performed on eight HDPF strengthening reinforced concrete columns, the specimens of the load–deflection and load–strain curves of eccentricity are collected, and the effects of size eccentricity, HDPF reinforcement form, and fiber layer number on the reinforced concrete columns under eccentric compression are studied. From the test process and test results, the following conclusions can be drawn:

1. HDPFs can not only improve the ultimate bearing capacity of the component, but can also improve the ductility of the component.
2. The reinforcement form and material dosage of the HDPF tape have an obvious effect on the reinforced concrete eccentric compression column. The effect of sticking two layers of the HDPF is more obvious than that of using one layer of the fiber. However, the increase of the value of the ultimate bearing capacity is not proportional to the increase of the number of HDPFs in the package.
3. When the reinforced column is destroyed, whether it is reinforced with HDPFs spacing paste or HDPF package, the strain value of the HDPF belt is less than the limit strain value, which shows that the HDPF belt in the process of this experiment failed to play its role effectively.
4. When the reinforced concrete's eccentric compression column is reinforced by using the HDPF ribbon, the bearing capacity increased significantly; but the large eccentric compression member's ductility increased even more.

## ACKNOWLEDGMENT

This work was supported by the Foundation of Jiangsu Educational Committee (12KJB560007).

## REFERENCES

- [1] Ouyang, Y., Huang, Y. & Qian, Z., et al. 2004. Analysis of flexural behavior of concrete beam restrained with glass fiber reinforced plastic sheet, *China Civil Engineering Journal* 37(3):26–34.
- [2] Lu, Z.d., Xie, Q. & Jiang, A.Q. 2005. Test on carbon-fiber-reinforced-polymer-wrapped RC column under eccentric loading, *Building Structure* 35(3):36–38.
- [3] Yan, J.H. & Yu, L. 2007. Limitation of axial-load ratio of reinforced concrete frame columns strengthened with AFRP sheets, *Industrial Construction* 37(6):104–106.
- [4] Ye, L.P. & Feng, P. 2006. Applications and development of fiber-reinforced polymer in engineering structures. *Chian Civil Engineering Journal* 39(3):24–36.
- [5] Qiu, B.X. 2008. Repair Reinforcement and reconstruction technology of post-earthquake building. Beijing: *China Building Industry Press*.
- [6] Kabeyasawa, T., Tasai, A. & Igarashi, S. 2002. An economical and efficient method of preventing old reinforced concrete buildings from collapse under major earthquake, *Proceedings of 7NCEE*, Boston.
- [7] Kabeyasawa, T., Igarashi, S. & Kim, Y-S. 2004. Shaking table test of reinforced concrete frames for verification of seismic strengthening with polyester sheet, *13th World Conference on Earthquake Engineering*, Vancouver, B.C., Canada, 1–6 August.
- [8] T. Kabeyasawa. 2005. Seismic evaluation and economical strengthening of reinforced concrete buildings. *Asian journal of civil engineering (building and housing)* 6(6):457–476.
- [9] Susumu Kono, Masato Doi, Jungyoon Lee, Hitoshi Tanaka. 2008. Seismic retrofit of RC members using FRP with very low young's modulus. *14th World Conference on Earthquake Engineering*. Beijing, China. 12–17 October.
- [10] Yousok Kim, Toshimi Kabeyasawa, Shunichi Igarashi. 2012. Dynamic collapse test on eccentric reinforced concrete structures with and without seismic retrofit. *Engineering Structures* 34:95–110.
- [11] Liu, X., Shi W.X. & Wang, J. 2012. Summary and comparison of traditional and innovative seismic strengthening technologies, *Structural Engineers* 2:101–105.
- [12] Yang, X.W. 2009. SRF, a Reinforcement technology for dilapidated building, *Time Architecture* 1:54–57.
- [13] Lv, Q.F., Zhu, H. & Zhang, J, et al. 2008. Innovative technologies for seismic retrofitting in Japan, *Construction Technology* 37(10):9–11+31.
- [14] Qiao, Y., Wang, Z.B. & Sun, C.Z. et al. Experimental study on axial compression reinforced concrete columns strengthened with SRF. *Industrial Building*. Accepted for publication.

## Road traffic conflict prediction model based on speed dispersion in mixed traffic environment

Xue Xia & Jing-yuan Gai

*Jiangsu Key Laboratory of Urban ITS, Southeast University, Nanjing, China*

*Jiangsu Province Collaborative Innovation Center of Modern Urban Traffic Technologies, Nanjing, Jiangsu, China*

**ABSTRACT:** With the development of economy and dramatic increase in private vehicle ownership, road traffic is becoming more and more congested in China. One of the most concerned side effects is the safety problem under mixed traffic flow. In order to evaluate the safety performance of mixed traffic flow, numerous studies have been done to analyze the dispersion characteristics and influencing factors of driving speed. In present studies, the relationship between the dispersion of driving speed and traffic conflicts was revealed based on traffic conflict technology. In this paper, regression models were developed from aspects of speed dispersion and influencing factors to estimate the severity of conflicts under various traffic and road conditions. With the result of this paper, we can predict the road traffic conflict and take steps in advance. The results of the study would be of great value and help to the evaluation of traffic safety under mixed traffic flow.

**Keywords:** mixed traffic environment; road speed dispersion; road traffic conflict; regression model

### 1 INTRODUCTION

In recent years, along with the steady and rapid growth of China's national economy and motor vehicles, modes of transportation have been developing hand in hand. The contradictions between the various elements of road traffic and the increasing traffic demand have become increasingly prominent. Because of the large speed discrete, the mixed traffic environment is becoming the concentrated area of traffic safety issues. The urban fringe, for example, has a complex traffic composition. Motor vehicles, non-motor vehicles and pedestrians are sharing the same road space, with large vans and small motor vehicles mixing together, which are typical features of mixed traffic. In addition, problems like dense township villages, heavy traffic, more entrances, inadequate transport facilities, the aggregation of markets, and illegal occupation of the lanes are more serious. These problems mainly increase the speed dispersion phenomenon in mixed traffic environment, which leads to increasing traffic conflict and brings about a major traffic safety problems. Thus, in connection with the reasons of traffic accidents in mixed traffic environments of urban fringe, it has become imperative to take appropriate measures to reduce casualties.

The current studies of road traffic safety evaluation are divided into two categories, namely direct

evaluation method based on accident statistics and indirect evaluation method with non-accident statistics. However, the results of the direct evaluation in practical applications are not enough satisfied, because of the barriers of obtaining the accident statistics, such as the rarity of accidents resulting in long safety evaluation cycle, the not completeness data causing low level of authenticity, and the statistical data with no uniform regulations leading to reduced data availability. In view of the above-mentioned drawbacks of direct evaluation method, Traffic Conflict Technique (TCT) come into being, as the primary method of indirect evaluation method.

Combined with the existing definition of TCT and characteristics of road traffic safety, the technique named as road traffic conflict technology, which is applicable to road traffic safety research is put forward. Therefore, the study of the relationship between speed dispersion and road traffic conflict is an important means of road traffic safety assessment.

### 2 ROAD SPEED DISPERSION

Speed dispersion is the essence of the current speed research. Back to 1950s, D. S. Berry, F. A. Haight and W. W. Mosher proposed that nor-

mal distribution, logarithmic—normal distribution and composite distribution can be used to describe the vehicle speed distribution (Wu, N, 2002). Leong found out that speed appeared to be normal distribution (Leong, 1968). Besides, Katti and Raghavachari worked out that the speed of bicycle appeared to be logarithmic-normal distribution (Katti, Raghavachari, 1986). In previous studies, various indicators to define the speed dispersion are put forward due to the differences of research purposes or methods and the limitations of data collection and process. Solomon studied the relationship between accident, vehicle speed and drivers and then put forward the concept of speed dispersion, which is defined as the difference between the speed of vehicles before accident and under normal conditions (Solomon, 1964). Grace and Potts introduced the mean and range of sectional speed distribution as a parameters of platoon dispersion theory (Grace, Potts, 1964). Helbing used section speed variance to quantify the speed dispersion (Helbing, 1996). Like this, there are many parameters used to describe speed dispersion, such as the standard deviation of the section speed, the root mean square coefficient of speed, the difference between the 85% speed and the average speed of a particular road section and so on (Saroach Boonsiripant, 2011).

The expressions of speed dispersion above are mostly used to research section speed dispersion. However the speed dispersion of the overall road is focused on now, so a new conception of road speed dispersion -  $\phi_L$  is put forward.

$$\phi_L = \frac{1}{n} \sum_{j=1}^n \frac{SL_j}{v_j}$$

$$SL_j = \sqrt{\frac{\sum_{i=1}^m (v_{i,j} - \bar{v}_j)^2}{m-1}}$$

where:

- $SL_j$  = Road speed standard deviation of vehicle  $j$ ;
- $V_{i,j}$  = Speed of vehicle  $j$  passing section  $i$ ;
- $\bar{v}_j$  = Average speed of vehicle  $j$  passing through the whole road;
- $m$  = Number of sections;
- $n$  = Number of vehicles passing through the road.

As can be seen by comparing the formula, after the treatment, the formula defined herein not only embodies the integrity of the road, but also ruled out the interference of different samples with different vehicle speed. which can effectively reflect the speed fluctuations of the road.

### 3 METHODOLOGY

#### 3.1 Data collection

As the mixed traffic environment is focused on here, the sample sections selected should try to cover complex road conditions and traffic characteristics, in order that more indicators can be considered when analyzing the speed dispersion factors. In addition, traffic conflicts should be collected to analyze the relationship between speed dispersion and traffic conflict.

Based on above principles, combined with the specific region information in Nanjing, 30 segments of G205, G312 and G104 are selected as samples. The UAV is used to shoot sample videos, when the weather is good in order to ensure the safety of UAV.

#### 3.2 Data processing

After getting samples, manual observation is used as main treatment to collect data we need, with following steps:

##### 1: Dividing sections

Several sections should be divided in order to calculate the distance. Road white lines and surrounding buildings are references when calculating, such as general road white lines are 6 m and the spacing between the white lines is 9 m in length.

##### 2: Table design

Good table design will help improve processing efficiency. The table should be designed to record the time of each car passing by each section, lane position, vehicle types, driving directions, changing lanes, conflict and so on.

##### 3: Manual observation

After preparing there is time for manual observation, during which time information the table mentioned should be collected.

##### 4: Data correction and processing

The speed between two sections can be calculated by the time the vehicle passing through nearby sections, which can be used to calculate the section speed of the vehicle roughly. Significant anomalies should be corrected to insure the accuracy of the data, in case of time recording errors, etc.

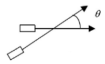
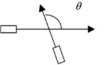
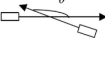
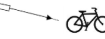

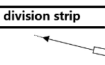
Due to the asymmetry of road traffic flow, each direction has different characteristics. So the two directions of each segment are selected to be two samples, therefore 60 samples are collected. Finally the road speed dispersion determined above is calculated.

#### 3.3 Model building

To complete the road traffic conflict prediction, the types of road traffic conflicts should be determined first. According to sample video, the road traffic

conflicts are divided into following categories, based on participants in conflict and conflict angle.

Table 1. Summary of road traffic conflict.

Conflict type		Conflict description	Conflict diagram
Conflict between vehicles	Rear-end conflict	Conflict angle $\theta \in [0, 45^\circ]$	
	Lateral conflict	Conflict angle $\theta \in [45^\circ, 135^\circ]$	
	Forward conflict	Conflict angle $\theta \in [135^\circ, 180^\circ]$	
Conflict between vehicles and non-motor vehicles	Motor vehicles and non-motor vehicles occupy each lane		
Conflict between vehicles and pedestrians	Pedestrians cross the vehicle lane		
Conflict between vehicles and road structures	Vehicles have collision with central median, division strip and other road structures		

Before building the logistics regression model, each conflict type should be classified into different grades, in order to determine the selection branches of the model response variable. The grades are shown in Table 2.

Before inputting the data, number 1, 2, 3 are used to replace level low, medium and high. Correlation analysis between variables is necessary before the logistic regression, in order to exclude factors completely unrelated to the dependent variable. Results are shown in Table 3.

In general, in order to avoid individual factors unrelated to the dependent variable in the univariate analysis, but have influence on the dependent variable with other factors, the selection region of significant will be relaxed to 0.4 or 0.6. When analyzing, factors whose significant more than 0.6 should be removed, so as not to influence the analysis results.

### 3.4 Results output

#### 1. Forward conflict

With the low level of conflict as a benchmark, excluding the average speed of vehicles and the

Table 2. Selection branches of the traffic conflict prediction model.

	Low (I)	Medium (II)	High (III)
Num. of forward conflict	10/km·h	10~20/km·h	>20/km·h
Num. of rear-end conflict	15/km·h	15~30/km·h	>30/km·h
Num. of lateral conflict	20/km·h	20~40/km·h	>40/km·h
Num. of conflict between vehicles and non-motor vehicles or pedestrians	50/km·h	50~100/km·h	>100/km·h
Num. of conflict between vehicles and road structures	20/km·h	20~40/km·h	>40/km·h

Table 3. Significance of correlation analysis between dependent variables and each factors.

	Forward conflict	Rear-end conflict	Lateral conflict	Conflict between vehicles and non-motor vehicles or pedestrians	Conflict between vehicles and road structures
Vehicle traffic	0.019	0.000	0.384	0.808	0.079
Average speed of vehicles	0.713	0.633	0.253	0.089	0.087
Proportion of non-motor vehicles	0.089	0.982	0.360	0.019	0.156
Proportion of large vehicles	0.039	0.435	0.233	0.977	0.847
Median strip	0.000	0.054	0.897	0.007	0.056
Non-motor division strip	0.627	0.022	0.005	0.213	0.000
Environment	0.001	1.000	0.187	0.172	0.463
Density of access port	0.132	0.737	0.322	0.000	0.907
Road speed dispersion	0.090	0.121	0.940	0.015	0.403

Table 4. Regression model of forward conflict.

Forward conflict	B	Standard error	Significance
2 Intercept	66.075	14.318	0.000
Vehicle traffic	-0.004	0.012	0.772
Proportion of non-motor vehicles	0.187	0.259	0.471
Proportion of large vehicles	1.885	1.315	0.152
Median strip	-76.081	2.151	0.000
Environment	9.548	8.621	0.268
Density of access port	-26.678	22.792	0.242
Road speed dispersion	-2.987	2.532	0.238
3 Intercept	74.917	14.847	0.000
Vehicle traffic	-0.012	0.013	0.363
Proportion of non-motor vehicles	0.036	0.265	0.893
Proportion of large vehicles	1.766	1.300	0.174
Median strip	-77.020	0.000	-
Environment	10.736	8.691	0.217
Density of access port	-27.183	22.827	0.234
Road speed dispersion	-2.998	2.549	0.240

\*Reference category: 1.

non-motor division strip, which are significantly not correlated, the regression model of forward conflict is shown below.

The conclusion can be drawn that the median strip has a very strong influence on forward conflict, followed by the density of access port and the environment. According to the actual situation, forward conflicts are divided into two categories, including conflicts when vehicles meeting, which is the most, and conflicts when vehicles retrograding, which is little there although. Thus, the deletion of the median strip will obviously lead an increase of the forward conflict level, from low to medium, even high. The increase of access port density will reduce the retrograding to find the exit, thus reducing the forward conflict level. With the development of the roadside environment, more vehicles are attracted, therefore the retrograding of vehicles is increasing.

### 2. Rear-end conflict

With the low level of conflict as a benchmark, excluding the average speed of vehicles, the proportion of non-motor vehicles, the environment and the density of access port, which are significantly not correlated, the regression model of rear-end conflict is shown below.

Table 5. Regression model of rear-end conflict.

Rear-end conflict	B	Standard error	Significance
2 Intercept	-3.799	1.979	0.055
Vehicle traffic	0.003	0.002	0.080
Proportion of large vehicles	0.008	0.069	0.907
Median strip	0.903	0.985	0.360
Non-motor division strip	-1.454	1.059	0.170
Road speed dispersion	0.067	0.118	0.573
3 Intercept	-8.380	4.153	0.044
Vehicle traffic	0.013	0.004	0.002
Proportion of large vehicles	0.015	0.100	0.884
Median strip	-0.047	1.506	0.975
Non-motor division strip	-5.623	2.611	0.031
Road speed dispersion	-0.007	0.227	0.974

\*Reference category: 1.

Table 6. Regression model of lateral conflict.

Lateral conflict	B	Standard error	Significance
2 Intercept	2.636	4.003	0.510
Vehicle traffic	-0.001	0.002	0.597
Average speed of vehicles	-0.038	0.056	0.493
Proportion of non-motor vehicles	-0.057	0.043	0.182
Proportion of large vehicles	-0.181	0.102	0.077
Non-motor division strip	-3.277	1.433	0.022
Environment	0.981	0.516	0.057
Density of access port	1.022	0.873	0.242
3 Intercept	-5.603	4.809	0.244
Vehicle traffic	0.003	0.002	0.171
Average speed of vehicles	0.006	0.068	0.930
Proportion of non-motor vehicles	0.017	0.052	0.744
Proportion of large vehicles	0.051	0.086	0.550
Non-motor division strip	-20.345	0.000	-
Environment	0.321	0.574	0.576
Density of access port	0.337	1.097	0.759

\*Reference category: 1.



Table 7. Regression model of conflict between vehicles and non-motor vehicles or pedestrians.

Conflict between vehicles and non-motor vehicles or pedestrians		B	Standard error	Significance
2	Intercept	-2.342	3.994	0.558
	Average speed of vehicles	-0.033	0.057	0.569
	Proportion of non-motor vehicles	0.037	0.043	0.383
	Median strip	1.000	1.149	0.384
	Non-motor division strip	-2.079	1.231	0.091
	Environment	-0.037	0.506	0.942
	Density of access port	1.085	0.919	0.238
	Road speed dispersion	0.036	0.195	0.853
3	Intercept	-54.493	13.134	0.000
	Average speed of vehicles	0.036	0.166	0.829
	Proportion of non-motor vehicles	0.248	0.116	0.033
	Median strip	27.898	0.000	-
	Non-motor division strip	-5.567	2.987	0.062
	Environment	-1.217	1.152	0.291
	Density of access port	-0.119	1.769	0.946
	Road speed dispersion	1.651	0.739	0.025

\*Reference category: 1.

Table 8. Regression model of conflict between vehicles and road structures.

Conflict between vehicles and road structures		B	Standard error	Significance
2	Intercept	-15.729	6.284	0.012
	Vehicle traffic	0.005	0.003	0.059
	Average speed of vehicles	0.106	0.090	0.240
	Proportion of non-motor vehicles	0.049	0.037	0.185
	Median strip	3.169	1.965	0.107
	Non-motor division strip	6.487	2.139	0.002
	Environment	1.302	0.640	0.042
	Road speed dispersion	-0.126	0.224	0.573
3	Intercept	-250.937	5.88E+5	1.000
	Vehicle traffic	0.148	83.677	0.999
	Average speed of vehicles	-1.512	7983.081	1.000
	Proportion of non-motor vehicles	0.239	3711.156	1.000
	Median strip	65.282	0.000	-
	Non-motor division strip	122.498	0.000	-
	Environment	52.827	3.24E+5	0.999
	Road speed dispersion	-4.597	6574.561	0.999

\*Reference category: 1.

Rear-end conflicts mainly arise from the sudden deceleration of the vehicle in front. In mixed traffic environment, the sudden deceleration of the vehicle mostly comes from the interference of non-motor vehicles and pedestrians, so the non-motor division strip is necessary for reducing the rear-end conflicts level, which can be reflected in the result. Other factors have little influence on rear-end conflicts level, while the road speed dispersion and the median strip may make the level increase to a certain degree, but reduce at a high level.

### 3. Lateral conflict

With the low level of conflict as a benchmark, excluding the road speed dispersion and the median strip, which are significantly not correlated, the regression model of lateral conflict is shown below.

Lateral conflicts mainly come from vehicles changing lanes and entering or leaving lanes, so the environment and the access port density are the main factors increasing the level from low to medium, due to the attraction coming with

these factors, which have little influence on the level when it is high. However, the deletion of the non-motor division strip may play a decisive role when the conflicts are at a high level. When there is no non-motor division strip, vehicles can enter or leave lanes anywhere they like, which may cause conflicts with vehicles in outside lanes.

#### 4. *Conflict between vehicles and non-motor vehicles or pedestrians*

With the low level of conflict as a benchmark, excluding the vehicle traffic and the proportion of large vehicles, which are significantly not correlated, the regression model of conflict between vehicles and non-motor vehicles or pedestrians is shown below.

In mixed traffic environment, the causes of these conflicts are diverse, due to the complex composition of traffic. Three reasons are summed up as below:

##### a. *The deletion of non-motor division strip leads to motor and non-motor vehicles mixing together.*

As we can see that the non-motor division strip can reduce this conflict level effectively, but cannot achieve complete isolation effect, due to the low level of law enforcement in mixed traffic environment.

##### b. *Non-motorized vehicles and pedestrians cross the road with casual.*

There are many people crossing the road where there are shopping, living or infrastructure areas. Mostly they cross the road with caution when there is no security facilities (such as median strip), while not so cautious when the security facilities are complete, because of the sense of security in their brains. So the median strip can increase the conflict level from the result.

##### c. *Vehicles have conflicts with non-motor vehicles and pedestrians when entering or leaving lanes.*

These are common conflicts when vehicles turning around, which are related to access port density. As we can see from the result, the access port density increases the conflict level to a certain degree, but cannot increase to high level.

#### 5. *Conflict between vehicles and road structures*

With the low level of conflict as a benchmark, excluding the proportion of large vehicles and the density of access port, which are significantly not correlated, the regression model of conflict between vehicles and road structures is shown below.

In mixed traffic environment, road structures include the median strip, the non-motor division strip, the curbs, etc. The two strips increase the conflict level for granted. In addition, when the level reaches high, the average speed of vehicles and the road speed dispersion would decline, which means the prone area of this conflict always has mixed traffic composition and big roadside interferences.

## 4 CONCLUSION

In this study, regression models were developed to predict the severity of conflicts under various traffic and road conditions. The values of pseudo R-squared in regression models are about 0.8, indicating that the model established can predict conflicts effectively. Moreover, the influencing factors identified based on the dispersion of driving speed was proved to be influential to traffic conflicts, which made it reasonable to evaluate the safety performance of road segment from a perspective of speed dispersion.

The results also showed that road conditions had more influence on traffic conflicts compared with traffic characteristics, which indicated that the psychological influence on traffic participants from road conditions could significantly affect their driving behavior and consequently lead to traffic accidents. However, it also made it easier to apply treatment according to road conditions and reduce traffic accidents.

## ACKNOWLEDGMENTS

This work was supported by National Natural Science Foundation of China under Grant No.51338003, the "Fundamental Research Funds for the Central Universities" and the "Research and Innovation Project for College Graduates of Jiangsu Province" No. SJLX\_0098.

## REFERENCES

- Grace, M.J., Potts, R.B. 1964. A theory of the diffusion of traffic platoons [J]. *Operations Research*, 12(2): 255–275.
- Helbing, D. 1996. Derivation and empirical validation of a refined traffic flow model[J]. *Physica A.*: 233, 253–282.
- Katti, B.K. and Raghavachari, S. 1986. Modelling of mixed traffic speed data as inputs for the traffic simulation models. *Highway Research Bulletin* 28, Indian Roads Congress, New Delhi, India, 35–48.
- Leong, H.J.W. 1968. The distribution and trend of free speeds on two-lane rural highways in New South Wales [J]. *Proc. Austr. Road Res. Board*, 4: 791–814.
- Saroch Boonsiripant, Michael O. Rodgers, Michael P. Hunter. 2011. Speed Profile Variation as a Road Network Screening Tool [J]. *Transportation Research Record: Journal of the Transportation Research Board*, Issue 2236, 83–91.
- Solomon, D. 1964. Accidents on main rural highway related to speed, drivers, and vehicle [R]. Washington: Bureau of Public Roads.
- Wu, N. 2002. A new approach for modeling of Fundamental Diagrams [J]. *Transportation Research A*, 36, 867–884.

# A review on the current development and debate of the global green new deal

Yi-Nan Ding

*Graduate School, International Business School, Beijing Foreign Studies University, Beijing, China*

Jie Tang

*School of English and International Studies, Beijing Foreign Studies University, Beijing, China*

**ABSTRACT:** Global Green New Deal (GGND) is a policy initiative established by the United Nations Environmental Program (UNEP) in 2008, which is aimed to resolve an array of economic, social, and ecological problems occurring in the recent years. With reference to the former US President Franklin D. Roosevelt's New Deal programs in the 1930s, it calls for strong will and actions of government leaderships across the international community, with the main focus on the role of green investment in helping shape a sustainable future development. Nevertheless, since being put forward, GGND has received no less doubts and criticisms than applause. This paper intends to review the GGND in practice and the debate around it—how the current major opinions converge and diverge.

**Keywords:** Crisis; global green new deal; ecosocialist

## 1 INTRODUCTION

The outbreak of the economic and financial crisis in 2008 has plunged the world into the worst global economic recession since the Great Depression of the 1930s. Moreover, while governments have been endeavoring to revitalize their economies, they also realize the risks from another brewing crisis with sweeping impacts—climate change. This combination of crises has been referred to by a non-governmental group as a “triple crunch”—including a credit-fueled financial crisis, dramatic climate changes, and disproportionately high energy price (Elliott, 2008).

To address these global threats, the existing systems and tools seem to have not worked satisfactorily. The double crisis of economy and ecology in the last few years has shown that “the old school way of doing business, i.e. based on finite fossil fuels and the exploitation of natural resources, is no longer possible” (Netzer, 2011). Hence, a new approach—Global Green New Deal (GGND)—has been promoted worldwide. It has become a buzzword in the political and academic debate nowadays. Originally advanced by the United Nations Environmental Program (UNEP), it is an economic policy strategy aimed to contribute to a more economically and environmentally sustainable world economic recovery.

In fact, this initiative is inspired by the former US President Roosevelt's New Deal programs.

During the Great Depression, many countries witnessed a dramatic decline in their gross national product and an unprecedented upsurge in unemployment rate. The current crisis demands the same strong leadership, though at the global scale and of a wider vision.

## 2 OBJECTIVES AND ELEMENTS OF GGND

According to the “Global Green New Deal: Policy Brief”, a report prepared by the UNEP, reviving growth and creating jobs should be essential objectives, but policies should also aim to reduce carbon dependency, protect ecosystems and water resources, and alleviate poverty. Otherwise, economic recovery will contribute only a little to avoid future economic and environmental crises. To achieve these objectives, three specific elements are put forward: (1) apart from the US \$3.0 trillion stimulus packages now being proposed, targeted fiscal stimulus should also be put in place; (2) the success of green investments should be advanced by domestic policy reforms; and (3) national actions should work together with international policy architecture and international coordination (Global Green New Deal, 2009).

A number of other international organizations such as International Labor Organization (ILO),

and non-governmental organizations such as the New Economic Foundation (NEF) and Green European Foundation (GEF) have published reports on GND. They have the same motive, that is, to meet the short-run challenges of reviving the worldwide economy while not sacrificing long-run economic and environmental sustainability.

### 3 GGND IN PRACTICE

Quite a few countries have conducted practical measures to achieve GGND goals. South Korea, for instance, has announced a Green New Deal plan in which many of the national actions of the proposed GGND have been well incorporated. At a cost of around US \$36 billion from 2009 to 2012, the initiative aims to create 9,60,000 jobs. The low-carbon projects include developing railroads and mass transit, fuel-efficient vehicles and clean fuels, energy conservation, and environmentally friendly buildings. These measures alone will make up more than 1.2% of GDP, whereas the full GND plan involves investments of around 3% of GDP (Barbier, 2009).

The European Union has specifically drawn a EU 20/20/20 program and a EU 2050 road map that seeks to: achieve a 20% emissions reduction; a 20% share of renewables in EU energy markets; a 20% improvement in energy efficiency in the EU; and reduce GHG emissions by 80–95% by 2050 (Hohler, 2009). In November 2010, the European Environment Agency (EEA) initiated a survey of resource efficiency policies and instruments in its member and collaborating countries, calling for actions conducive to sustain and enhance the well-being of current and future generations. It is a core element in creating a “green economy” in Europe and elsewhere.

China is also an increasingly active player in this endeavor. Green investment has become an important part of its GDP and expenditures on pollution control and transportation efficiency. According to the “Global Trends in Sustainable Energy Investment 2009”, a report released by UNEP, China’s investment on renewable energy projects has reached US \$15.6 billion, ranking the first in the Asia and Pacific region. China is now the largest producer of photovoltaic devices of solar energy and the second largest market of wind energy.

As the strongest economy as well as the largest energy consumer in the world, the United States can exert much influence in shaping the outcomes of GGND proposals. In fact, as early as in the 2008 presidential campaign, President Obama has embraced the core values of GGND. During the campaign, he pledged to cap carbon

dioxide emissions and to have more US energy come from renewable sources by 2025. In 2009, he signed American Recovery and Reinvestment Act (ARRC), with more focus put on renewable energy and smart grid.

There are other examples of efforts to effect sustainable structural changes. In 2010, the South African government, for example, presented the South African Renewables Initiative (SARI), which includes a staged plan for the establishment of a sustainable industrial policy: the percentage of renewable energies in the power supply is to be raised from under 1% at present to at least 15% by 2020 – primarily through wind power, solar energy, and photovoltaic devices. The government hopes that this will create 50,000 new jobs, help achieve more energy security, and strengthen the competitiveness of the country. Also worth noting is the Moroccan plan to increase the share of renewable energies in power production to 42% by 2020 through the construction of five solar thermal plants and expansion of wind energy (Netzer, 2011). India is well along the path to becoming a market leader in the area of renewable energies, in particular the generation of solar power. Green technologies are opening up a path for the country to reduce its own consumption of resources in a manner promoting its own growth objectives over the medium term.

### 4 ECOSOCIALISTS’ PERSPECTIVE OF GGND

Among the GGND theorists, perhaps the most striking and radical are the ecosocialists who are quite critical of GGND concepts. Ariel Salleh (2010) argues “the new green Keynesianism still rests on productivist assumptions”. Salleh points out that in the various green new deal programs, “socio-cultural analysis or political reflexivity” is absent. This approach is nothing but another attempt to save capitalism “without any deeper engagement with its real bottom line—healthy people in a healthy ecosystem”. Salleh elaborates her points by giving the example of the Transatlantic Green New Deal—how this plan, full of “psychological denial”, fails to represent “the basic incompatibility between capitalist accumulation and ecosystem integrity” (Salleh, 2010).

Salleh’s points are agreed by many other scholars who further regard the GND as “green capitalism”, and for them, profit-seeking and societal/environmental goals cannot be aligned within the same concept (Smith, 2011). The ecosocialist view rejects market-based mechanisms such as the “cap and trade” system and “clean development mechanisms”. Angus et al. argue that under the control of

these mechanisms, “capitalist interest groups can use carbon dioxide as a commodity, which explains the critical stance of ecosocialists against multilateral agreements such as the Kyoto Protocol”.

## 5 A SUPPORTIVE VIEW OF GGND

By contrast, GND supporters have a rather optimistic vision although they admit there can still be obstacles along the way. The ecosocialist stand is disputed by David Schwartzman who holds that GND can provide a transition to a post-capitalist society by environmentalists and labor joining with a program for green jobs. He disputes with those who reject the GND, because it does not call for the immediate creation of socialism; such a rejection lacks any strategy of class struggle (Salleh, 2010). Barbier believes that GGND is a necessary and a timely response with a bold initiative and a global vision by the way of ensuring that “the correct mix of economic policies, investments, and incentives reduces carbon dependency, protects ecosystems, and alleviates poverty while fostering economic recovery and creating jobs” (Barbier, 2009).

Sony Kapoor et al. compared the cost of a GGND proposal for EU and its positive effects on growth and employment. They concluded that “many of the investments that need to be made will generate positive rates of return with the profit potential for energy efficiency-related investments being particularly high” (Kapoor, 2011). By emphasizing policy designing and better coordination among different sectors, they also addressed the fear of financial and non-financial obstacles coming in the way of green investments, such as the under-pricing of carbon and the unpredictability of the climate regime. The GGND Group pays similar attention to the financial sector, but it seems to embrace a broadened definition of GGND. It claims that GGND is a “dual approach”: first, it proposes the renewal of the domestic and international financial system, including a changed regime of taxation; second, it calls for government intervention to allow higher public and private expenditure—targeted at environmental projects that will dramatically cut fossil fuel use and hence help to tackle climate change and peak oil (Elliott, 2008).

To achieve GGND goals, Nina Netzer suggests that to make progress along the path toward a GGND, “a dual thrust making it possible to move forward at both national and international levels is needed” (Netzer, 2011). An accommodation of interests between various actors must take place at both levels, forerunner coalitions need to be formed, and coherence should be established between various policy fields. Similarly, Barbier puts significant emphasis on global governance,

especially the role of G20. He thinks that although the United Nations works as an international forum for cooperation and coordination, the most likely as well as effective mechanism is the G20 forum of the world’s 20 largest rich and emerging economies. In his opinion, the G20 has played a significant role as a global forum for coordinating policy actions during the immediate economic crisis; and the coordinated actions by G20 economies will yield profound effects on “greening” the world economic recovery (Barbier, 2009).

## 6 FINAL REMARKS

Following the global crisis of 2008, the GGND concept has been garnering increasing public attention, and practical measures have been underway. However, in terms of its nature and the specific ways to realize its goals, scholars have shed varying views. Much opposition come from the ecosocialists. They think that GGND will not solve the current crisis in a fundamental way because the exploitative capitalist system is still predominant. Contrary to such a radical viewpoint, the GGND supporters applaud this concept as a promising way out of today’s multiple crises. They focus more on how to make good use of the concept and increase the policy efficiency of countries that are engaged in this global initiative. As they have mentioned, for individual countries, they should make wise policy decisions in terms of green investment: economic recovery should be aligned with ecological improvement. A strong leadership is needed to ensure the effectiveness of specific measures. And the government can mobilize resources in both public and private sectors to provide funding for their GGND plans. Also, national endeavors are not likely to succeed without international coordination, especially among those major countries with considerable economic and political clout in the international society.

## REFERENCES

- [1] Angus, Ian, Joel Kovel, & Michael Löwy. Belem Ecosocialist Declaration [ecosocialistnetwork.org](http://ecosocialistnetwork.org). 2009.
- [2] Barbier, B. Edward. Rethinking the Economic Recovery: A Global Green New Deal.” Report prepared for the Economics and Trade Branch, Division of Technology, Industry and Economics, United Nations Environment Programme, pp. 1–144, 2009.
- [3] Barbier, B. Edward. Global Governance: the G20 and a Global Green New Deal. *Economics E-Journal* August 21, pp. 1–26, 2009.
- [4] Elliott, Larry, et al. “A Green New Deal: Joined-up policies to solve the triple crunch of the credit crisis,

- climate change and high oil prices.” The first report of the Green New Deal Group, pp.1–46, 2008.
- [5] Global Green New Deal: Policy Brief. A report prepared by UNEP, pp. 1–33, 2009.
- [6] Hohler, Alice, et al. Global Trends in sustainable energy investment 2009: Analysis of Trends and Issues in the Financing of Renewable Energy and Energy Efficiency. A report prepared by UNEP, pp. 1–64, 2009.
- [7] Kapoor, Sony, et al. Funding the Green New Deal: Building a Green Financial System. A Policymaker Report from Re-Define, pp. 1–55, 2011.
- [8] Netzer, Nina. A Global Green New Deal: Response to crisis or paradigm shift towards sustainability? *International Policy Analysis*, pp. 1–11, 2011.
- [9] Salleh, Ariel. Green New Deal—or Globalisation Lite? *Arena Magazine*, pp. 15–19, 2010.
- [10] Sarkar, Saral. *Eco-socialism or Eco-capitalism?: A Critical Analysis of Humanity’s Fundamental Choices*. London, Zed Books, 1999.
- [11] Schwartzman, David. Green new deal: an ecosocialist perspective. *Capitalism Nature Socialism* 22, pp. 49–56, 2011.
- [12] Smith, Richard. “Green capitalism: the god that failed.” *Real-World Economics Review* 56, pp. 112–144, 2011.

## Toward a more compact and sustainable city—the use of underground space for Chinese mainland cities

Jia-yun Chen, Li-min Huang & Li-chang Su

*Underground Space Research Center of PLA University of Science and Technology, Nanjing, China*

**ABSTRACT:** With the rapid development of the Chinese economy and the urbanization process, recently population densities of core districts in many mainland cities have reached the levels of international cities, or even have surpassed them. However, the extensive and uneven development of urban spaces leads to traffic jams, dispersed city shape, and low land utilization level. In view of the above problems, the development of the compact city is a consensus in Chinese cities. Through the development and utilization of underground transportation, infrastructure, parking space, and so on, and through sophisticated development of urban land resources, it is feasible to achieve a compact city.

**Keywords:** Compact city; underground space; mainland city

### 1 INTRODUCTION

China is one of the countries in the world with vast land area; but excluding areas unfit for human habitation, there is not much land area per capita. Chinese cities are mostly built in relatively fertile and flat plains, which always conflict with the Chinese government's determination to protect arable land. Removing plateau, desert, and other areas inappropriate for human habitation, and considering the huge population base, per capita land area is even less than that in Japan. In addition, considering uneven regional development and other factors, many of the city's old towns have become the world's most congested areas. The rapid economic development of large cities brings problems which are quite common in China, namely high housing prices, traffic congestion, environmental pollution, and lack of pedestrian space and public space for activities. Representative cities are Beijing, Guangzhou, Shenzhen, Nanjing, and so on.

On the contrary, because of the uneven development of urban land, the current construction land area per capita is as high as 130 square meters, while the number is 82.4 square meters in developed countries and 88.3 in developing countries (Chou Baoxing, 2006); Hong Kong has an unimaginable 30 square meters per capita.

Considering the above problems, compact city development may be an effective solution. Compact city has numerous advantages: significantly saving land space, easier to build roads and

drainage, easy garbage collection, and other facilities. Furthermore, by limiting urban sprawl, we can reduce the cost of city public services. Representative cities are Tokyo and Hong Kong.

### 2 HIGH-DENSITY CHINESE CITIES

Old districts in some of China's major cities have high population density: the population density in Hongkou District of Shanghai has reached 36,307 persons/km<sup>2</sup>, more than the most intensive Tokyo district, Nakano, where the number is 20,504. The second-tier cities also have dense population, such as Gulou District in Nanjing, whose population density is 22,428 persons/km<sup>2</sup>. However, because of the unbalanced overall city development, the average population density of mainland cities is not high, which is still far from that of the developed cities. Taking Hong Kong as an example, it is an extreme case of compact development, with the density of the inner city as high as 1,16,531 persons/km<sup>2</sup> (Burgess, Rod, and Mike Jenks, 2002.) As of 2015, according to the Hong Kong SAR Census and Statistics Department, Hong Kong's population density reached 6,760 persons/km<sup>2</sup>, whereas that of Kowloon reached 47,040 persons/km<sup>2</sup>. Compared with these high numbers, the population density of Shanghai is only 3,700 persons/km<sup>2</sup> (<http://worldpopulationreview.com/countries/china-population/>), and the corresponding values for Guangzhou and Nanjing are 1,708 and 1,260.

Table 1. Population density of some large cities in the world.

City	Population	Land area (km <sup>2</sup> )	Population density	Highest population density	Highest density district
Hong Kong (2014)	7,152,000	1,079	6,626.8	56,779.1	Kwun Tong district
Shanghai (2010)	23,019,196	6,341	3,630.2	36,306.5	Hongkou district
Guangzhou(2010)	12,701,948	7,434	1,708.5	34,250.5	Yuexiu District
Nanjing (2013)	8,188,380	6,498	1,260.1	22,427.8	Gulou district
Tokyo (2010)	9,153,154	618	14,806	20,504	Nakano ward
New York (2010)	8,126,455	784	10,367.2	25,997.0	Manhattan borough

### 3 PROBLEMS CAUSED BY EXTENSIVE CITY DEVELOPMENTS

#### 3.1 Traffic congestion

From Table 1, we can see that the overall population density of Chinese first class cities is not high. This is because many Chinese cities have new districts, which have not been fully developed while occupying much land spaces. Extensive developments lead to massive outward expansion of the cities, resulting in longer travel distance for citizens to go to work. Crowded old cities always have high house prices, and people cannot afford buying houses in core districts and usually focus on buying in the suburbs, which leads to long-distance commuting to work every day, generating more cross-border traffic; by contrast, 67% of Hong Kong's Kowloon district public transport is local traffic, cross-border traffics are only minority ones (Mahtab-uz-Zaman, Q. M., Stephen SY Lau, and So Hing Mei,2000). Given the incomplete development or less frequency of urban public transport in some areas that are not yet fully covered, personal vehicles are preferred by citizens living in rural areas.

High volume of resident vehicle fleets occupies road resources. Vehicle fleet in cities with dense population is usually larger than cities with less population. However, large Chinese cities usually have higher motor vehicle ownership amount. Taking Dongcheng District in Beijing, China, and Nakano ward in Tokyo, Japan, as examples, the latter has a population density of 20,100 persons/km<sup>2</sup>, with vehicle ownership of 0.16 per person, while the former has a population density of more than 20,000 thousand persons/km<sup>2</sup> with vehicle ownership of 0.34 per person (Guo JF, Liu Y, Yu L, 2011). Private vehicles in Center City District take up valuable road resources, leading to insufficient parking space, which results in more on-street parking spaces, occupying the road spaces and further reducing the capacity of the road, and causing traffic jams and air pollution.

#### 3.2 City pollution

Urban public transport ought to cover vast majority of the urban areas in order to ensure the normal operation of the city, while low-density urban development brought about a significant increase of traffic demand in new districts. High-density urban form of Hong Kong allows urban infrastructure and transportation facilities run in a efficient way (Mahtabuz Zaman, Q. M., Stephen SY Lau, and So Hing Mei, 2000); on average, there are more people per kilometer using public transportation systems such as Hong Kong's MTR (Mass Transit Railway) so that it is economically affordable, and efficient for construction and operation, no wonder why the Hong Kong MTR is one of the few profitable systems in the city. By contrast, all Chinese city subways have usually negative earnings.

#### 3.3 City pollution

China's most large cities have large private vehicle fleets with cars becoming more affordable to citizens than houses in the central regions. Motor buses occupy a high proportion of public transport vehicles; considering the road congestion, these factors together bring a lot of exhaust emissions, which is an important source of urban air pollution. With the continuous expansion of cities, the phenomenon is becoming increasingly serious. Compared with the industrial structure of international cities such as Hong Kong, that of the mainland cities is at quite low level, and there are a large number of emitters in the new development zones, so industrial emissions are also a major cause of urban pollution in these developing cities. Public power supply is mostly via coal-burning power generation, also contributing to pollution in nearby city core districts.

#### 3.4 Fracture of urban texture

The construction of railways, highways, urban roads, and other transport routes leading to split textures of urban space have caused inefficient



transportation across them, and fault occurs within urban culture carrier, so that urban functions cannot be connected with each other, urban living space are not continuous, and so on. These features can be seen in Figure 2. As is evident from the figure, the railroad in the middle has lead to space separation between the upper and lower zones.

#### 4 REFINED DEVELOPMENT STRATEGIES THROUGH UNDERGROUND DEVELOPMENT

##### 4.1 Underground improving traffic system

Underground space can be an important part of public transportation and may even be the main

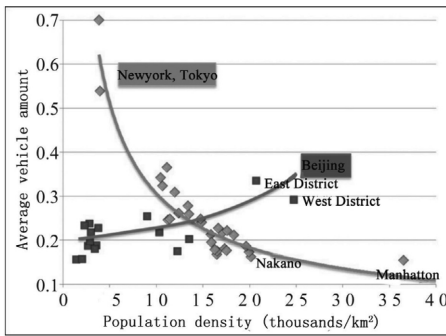


Figure 1. Relationship between population density and private vehicle numbers of many large cities in the world.

one. Compact city building makes fewer physical space isolation, thereby reducing the traffic demand throughout the city. A sound subway network structure can bear most part of the public transport. In addition, the construction of underground rapid transit road can divert the majority of car traffic, reducing the number of road intersections to improve traffic efficiency ground roads.

##### 4.2 Sewing segmented blocks

Construction of underground space can reconnect separated spaces, and create different city functions by pedestrian spaces. In 1994, Boston demolished the former elevated road and finished an underground 8–10 lane urban expressway system in 2004, the original lane was changed to the ground urban public green space, and sutured urban spaces were fragmented by the former expressway, as can be seen in Figure 3. Tokyo has also built a 40 m underground rapid central ring line as supplement of its public traffic system. In addition, similar transformations can also be seen in a number of cities such as Singapore, Madrid, and Moscow, with quite good results.

Underground space can also increase the vitality of the region by suturing functions in old city zones. As the land prices are always higher than new zones, low-rise buildings in these zones must be changed to high-rise ones to cover the costs, which always makes it difficult to renovate the old districts. Development of underground space can solve the problem by exploring underground space between the blocks, communicating with the surrounding land, and improving the economic value of the zone. Through a subway construction,



Figure 2. City space separated by railroad (Source: Google Earth).



Figure 3. Landscape before and after the Boston Big Dig (Resource: <http://tedxmanhattanbeach.com/>).

Nanjing Xinjiekou transformed the former central pedestrian overpass to an underground passage and communicated it with the surrounding underground structures, driving commercial activities in 1 million square meters of underground spaces, creating an ideal business value.

#### 4.3 Adding service facilities

Underground space development can add extra space without affecting the ground conditions, which is of paramount importance in old districts of many large cities, providing adequate accommodation for public infrastructure, parking, and so on. Construction of underground pipe gallery can centralize pipelines so that when people need to add a new pipeline, they do not need to excavate the ground; underground waste disposal plants, sewage treatment, electricity, and other facilities can free the ground space for public lawns, commuting spaces in the old city; construction of underground parking facilities can provide adequate parking space, which reduces occupancy of valuable floor space.

## 5 CONCLUSION

At present, many Western countries are experiencing depopulation process, so they are not keen at the concept of compact city. However, as China is still a developing country, cities in mainland

are all in the process of urbanization, large cities, with their unique advantages in resources, will attract people continuously for a quite long period of time, and gathering of people will be inevitable. The compact development mode is inevitable in avoiding urban sprawling. Some old districts in mainland cities have been more saturated, facing challenges to improve or upgrade, while new districts will expand their capacity and improve the supporting infrastructures and facilities. As an important measure, the underground space will play an essential role in urban development.

(Corresponding Author: Limin Huang, Lecturer, Underground Space Research Center of PLA University of Science and Technology, E-mail: 470224281@qq.com)

## REFERENCES

- Burgess, Rod, and Mike Jenks, eds Compact cities. Sustainable urban forms for developing countries Routledge, 2002.
- Chou Baoxing, Compactness and diversity- the core concept of sustainable city development, Urban Planning, 2006, 11: 18-24.
- Guo JF, Liu Y, Yu L. Understanding of traffic congestion in China's major cities, City Traffic, 2011, 02: 8-14+6.
- Mahtabuz Zaman, Q. M., Stephen SY Lau, and So Hing Mei. "The compact city of Hong Kong: a sustainable model for Asia?" Compact cities: sustainable urban forms for developing countries (2000): 255-268.

# Natural ventilation and seismic performance analysis of the special L-shaped spiral layout green building

Xiao-dan Li, Wen-jing Li, Hao Yang & Zhi-ting Chen

*China University of Mining and Technology, Beijing, China*

**ABSTRACT:** In this study, buildings with unique spiral layout are studied. The combination of L-shaped block units and facility floors can induce the natural ventilation of these buildings significantly; however, the special layout also brings great challenges to the structural design, in particular the structural seismic design. In this paper, the building airflow simulation and seismic performance analysis of a complex high-rise steel structure with both plane irregularity and vertical irregularity were conducted. The results show that the rational integrated design of green building's indoor space and structural system can be realized in this structure.

**Keywords:** Green building; complex high-rise steel structure; seismic sequence; aseismic analysis

## 1 INTRODUCTION

High-rise green buildings have been the focus of intensive research because of their design and performance. There are two main forces that drive the flow through the indoor space: external wind and buoyancy due to temperature difference. The effect of buoyancy is insignificant without an external airflow passage other than the structure itself. The addition of an external airflow passage such as a window in combination with buoyancy force increased the indoor ventilation by 47%. Moreover, it is found that buildings are restricted to transient draining flows in a space containing buoyant fluid, when the wind and buoyancy forces reinforce one another. Therefore, careful spiral positioning of windows in conjunction with external wind-driven forces and unique indoor space formed by spiral layout of L-shaped block units and facility floors has the potential to enhance natural ventilation. This complex high-rise steel structure with characteristic of plane irregularity and vertical irregularity is designed with integrated building airflow simulation, and then confirmed by anti-seismic performance analysis by an introduction to current systems and phenomenological modeling.

A 27 story complex high-rise green building model (including 21 standard floors with height 4 m; six mechanical floors with height 2 m) with fully glazed curtain wall is designed. A standard floor is divided into nine basic units, each with dimension of  $16.2 \times 16.2$  m. The total height and width (square) of the structure are 98 and 48.6 m, respectively. And the building is divided into seven L-shaped basic

blocks (the shaded area in Figure 1). Each of them contains three stories and has different functions. The seven L-shaped basic blocks present a clockwise spiral structure from bottom to top. Each of the upper block unit is seemed to rotate clockwise  $90^\circ$  relative to the block underneath the unit. Therefore, the L-shaped spiral structure forms a  $16.2 \times 16.2$  m courtyard in the middle of the building. Between adjacent block units, a 2-m-high mechanical floor is built with rooms to use as device rooms for each block unit and practice as the vertical transformation of the machine. They respectively lie in the 4th, 8th, 12th, 16th, 20th, and 24th floor.

A large spiraling portfolio of atrium ( $16.2 \times 16.2$  m) in the middle of the building is formed by L-shaped floors and designed based on fluid mechanics. For every block unit, a window in combination with outside is present as an addition to an external airflow passage, forming a spiral draining flow in the space containing buoyant fluid, because of the solar collector units set on the top of the building. This increased the indoor natural ventilation. In the large open space formed by three-story atrium combination, there are several platform functional units such as conference room, media center, international conference center, and leisure and other public entertainment units. Elevator shaft connected with the atrium facilitates the vertical functional connection with each unit.

Spiral viscous damping support system is used to coordinate the structure with building performance, which is a creative solution to the problem of L-shaped block element spiral twisting overrunning the structure rules. This also avoids the problem of

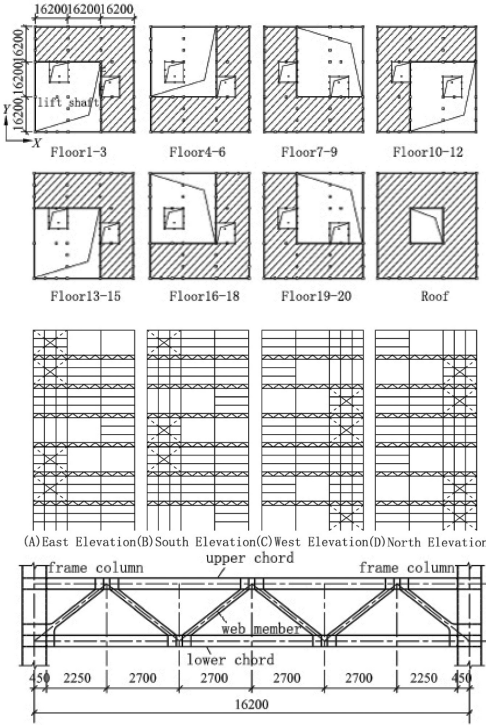


Figure 1. Structure diagram.

ordinary steel support systems, which make the floor lateral stiffness irregular. Thus, regular seismic response of irregular structural arrangement is achieved. Application of viscous damper brace can effectively reduce the torsional response of structures under horizontal seismic action. The structural mass distribution is in the periphery of the building function floor, and the effective control of the twist irregularity structure response under horizontal seismic action can be an effecting way for adjusting the lateral stiffness of the peripheral structure to enhance its torsional stiffness.

This paper is the additional step in the study being performed on different aspects of passive ventilation of the high-rise green building model, whose unique spiral layout induces natural ventilation, but poses significant challenges to the structural system selection and structural design, in which reducing the torsion effect from the spiraling layout of building block units is of paramount important during earthquakes. Structural analysis and shaking table test presented in this paper show that through the rational integrated design of green building indoor space and structural system, the problem of structural regularity beyond the code limit is solved effectively and operable and feasible natural ventilation is achieved.

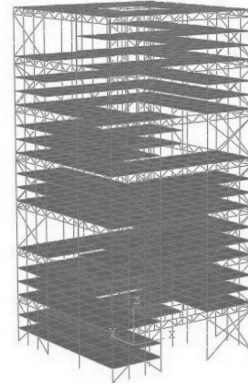


Figure 2. Finite element model of the complex high-rise steel structure.

## 2 STRUCTURE

### 2.1 Finite element model

The commercial finite element software Abaqus was used for the structural seismic analysis. The columns are square bar-reinforced concrete columns, whose section is  $900 \times 900 \times 22$  mm. The main beams are HN700  $\times$  300  $\times$  13  $\times$  24 with span of 16.2 m. The secondary beams are HN400  $\times$  200  $\times$  8  $\times$  13. The lower and upper chords of the outside truss are HN400  $\times$  200  $\times$  8  $\times$  13. The concrete is C40 and the steels are HPB335. The structure diagram is shown in Figure 1. In the Abaqus finite element model (FEM), beams and columns are simulated by B31 and floors and walls are simulated by S4R. The FEM is shown in Figure 2.

### 2.2 Material models

The Drucker–Prager model in Abaqus is used to simulate the nonlinear behavior of concrete. The PQ-Fiber USteel02 model, which was developed by Xinzhen Lu, is used herein to simulate the nonlinear behavior of steel. The Rayleigh damping is defined as:

$$C = \alpha[M] + \beta[K] \quad (1)$$

$$\alpha = \frac{2\omega_i\omega_j(\xi_i\omega_j - \xi_j\omega_i)}{\omega_j^2 - \omega_i^2}, \quad \beta = \frac{2(\xi_j\omega_j - \xi_i\omega_i)}{\omega_j^2 - \omega_i^2} \quad (2)$$

Where  $\omega_i$  and  $\omega_j$  are the  $i$ th or  $j$ th circular frequencies, respectively, and  $\xi_i$  and  $\xi_j$  are the  $i$ th or  $j$ th damping ratios, respectively.

The Newmark- $\beta$  numerical integration method is used in the time domain analysis. The basic dynamic equation is

Table 1. Natural periods of the structure.

No.	1	2	3	4	5
Period(s)	2.4234	2.2729	1.5257	1.3022	1.2760
No.	6	7	8	9	10
Period(s)	0.9176	0.8851	0.8433	0.8418	0.7817
No.	11	12	13	14	15
Period(s)	0.7106	0.6663	0.6354	0.6190	0.6142
No.	16	17	18	19	20
Period(s)	0.5576	0.5004	0.4936	0.4926	0.4903

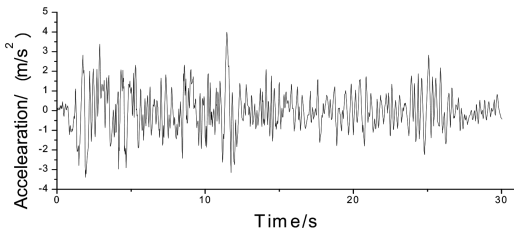


Figure 3. Acceleration time history curves of El Centro record.

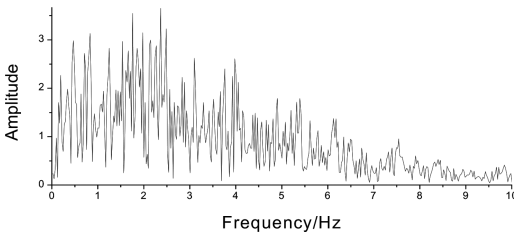


Figure 4. Fourier spectrum of seismic waves of El Centro record.

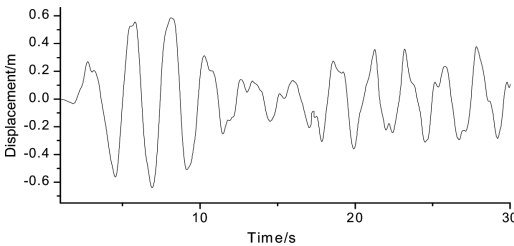


Figure 5. Horizontal displacement response at the structural roof corner.

$$[M]\{\ddot{u}\} + [C]\{\dot{u}\} + [K]\{u\} = -[M]\{I\}\ddot{u}_g, \quad (3)$$

where  $[M]$ ,  $[C]$ , and  $[K]$  are structural mass matrix, damping matrix, and stiffness matrix, respectively,

$\{u\}$ ,  $\{\dot{u}\}$ ,  $\{\ddot{u}\}$  are the node displacement vector, node velocity vector, and node acceleration vector, respectively,  $\ddot{u}_g$  is the ground acceleration, and  $\{I\}$  is the unit vector.

### 2.3 References

The model shapes and fundamental period of the structure are obtained through model analysis. The first 20 natural periods are listed in Table 1. The first horizontal period of the structure is  $T_1 = 2.4234$  s and the first rotation period is  $T_t = 1.5257$  s. Thus, the ratio of  $T_t$  to  $T_1$  is 0.6296.

In the time domain analyses, the El Centro wave was used. The data were recorded on ground, located at Imperial Valley, CA, USA. This record was obtained on 18 May 1940. The El Centro wave, whose amplitude is adjusted to 0.40 g, was considered as vertically incident S wave. The corresponding acceleration time histories, Fourier spectra, and the elastic acceleration response spectrum are shown in Figures 3–6.

Under strong shaking, structural materials will undergo inelastic deformation. After the seismic activity, the plastic deformation will remain. The horizontal residual inter-story deformation ratio along the height of the structure after seismic activity is shown in Figure 7.

## 3 CLOSURE

This paper presents the numerical simulation with Abaqus software to study the influence of seismic shaking on a building whose unique spiral L-shaped block unit layout and facility floors can induce natural ventilation, but, on the contrary, also bring significant challenges to the structural system selection and structural design. A three-dimensional FEM was built and corresponding analysis conducted. According to the FEM simulation, during an earthquake, the structural material will undergo inelastic deformation. After the seismic shaking, plastic deformation will remain.

Because the building is a “combination” of L-shaped units, the structural rotation response in

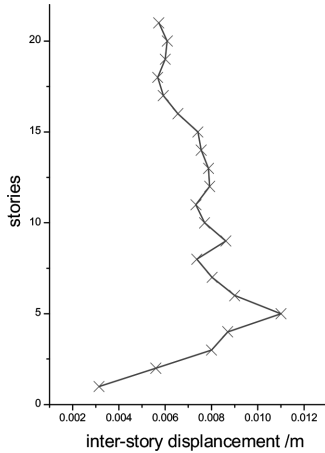


Figure 6. Inter-story horizontal deformation.

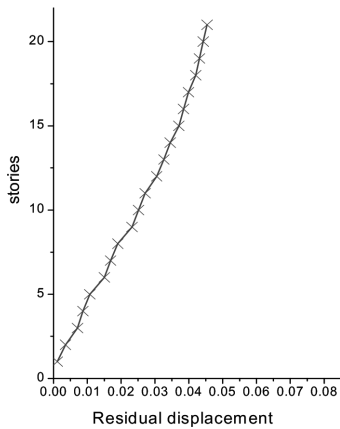


Figure 7. Horizontal deformation displacement.

an earthquake is not significant; furthermore, the structural horizontal deformation is acceptable.

#### 4 DISCUSSION

This paper is aimed to show that passive natural convection system design can be linked with structural analysis, and this “creation” of behavioral models of a building for an “as-designed” stage of its development can improve control and accuracy of special layout plans to enhance natural ventilation. Work on interoperability has made strides herein, but needs to be followed up by systems that harness interoperable tools in flexible systems that support a comprehensive dialogue between different actors in a building project team.

On the basis of the structural seismic response analysis using Abaqus, this study evaluated the seismic performance of the complex high-rise building for natural ventilation. Under strong shaking, the structural material will undergo inelastic deformation. During the entire shaking time, the structural rotation response is not significant and the structural horizontal deformation is acceptable.

The following are the limitations of this study, which should be addressed in future research:

- A successful structural study was presented in this paper for spiral cross-ventilation in a building with L-shaped block units and facility floors. For the optimum configurations, second-layer modeling using CFD to test in real situations and in more detail about structural joints would work with the pushover analysis to check whether they are feasible. And an overall cost optimization study would be followed up.
- In the future, it would be very valuable to have experimental data for complex high-rise green buildings to further enhance the validation of the computational model. Preferably, PIV measurements should be conducted to provide flow field data inside and around the building.
- This study only considered the structure verification and adjustment for seismic performance after completion of the ventilation and structural design. In the future, passive natural convection system design work should combine with structural analysis in an “as-designed” stage of its development to improve the control and accuracy of special layout plans to enhance natural ventilation. Work on interoperability has made strides herein, but needs to be followed up by systems that harness interoperable tools in flexible systems that support a comprehensive dialogue between different actors in a building project team.

#### REFERENCES

- [1] Augenbroe, Godfried (2011). The role of simulation in performance based design. In: J. Hensen and R. Lamberts (eds), *Building Performance Simulation for Design and Operation*. SponPress.
- [2] Ali Malkawi and Godfried Augenbroe (editors), *Advanced Building Simulation*. SPON Press, Taylor and Francis group, 2004. ISBN 0-415-32122-0.
- [3] Augenbroe, Godfried and Jan Hensen (editors). *Building Simulation 2003, IBPSA Conference Proceedings*, Eindhoven August 11–14, 2003.
- [4] Gueguen P, Bard P Y, Chavez-Garcia F J. Site-city interaction in Mexico City-like environments: an analytical study [J]. *Bulletin of the Seismological Society of America*. 2002, 92(2): 794–811.
- [5] Gueguen P. Seismic Interaction between soil and buildings: from soil-structure interaction to site-city

- interaction [D]. France: University of Grenoble, 2000.
- [6] Wirgin A, Bard P Y. Effects of buildings on the duration and amplitude of ground motion in Mexico city[J]. *Bull Seism Soc Am*. 1996, 86(3): 914–920.
- [7] S. Kazansky, V. Dubovsky. Chimney-enhanced natural convection from a vertical plate: experiments and numerical simulations [J]. 2003: 497–512.
- [8] Klaus Daniels. *Low-Tech Light-Tech High-Tech: Building in the information age*. English translation by Elizabeth Schwaiger. Berlin: Birkhauser Publishers, 1998
- [9] Chopra A K, Gutierrez J A. Earthquake response analysis of multistorey buildings including foundation interaction[J]. *Earthquake Engineering and Structure Dynamics*. 1974, 1(3): 65–77.
- [10] J B. Modal analysis for building-soil interaction [J]. *Engineering Mechanics Division*. 1976: 771-86102.
- [11] M I. Dynamic interaction of soil-structure with elastic rectangular foundation [Z]. Tokyo, Japan: 1978457-642.
- [12] Boutin C, Roussillon P. Assessment of the urbanization effect on seismic response [J]. *Bulletin of the Seismological Society of America*. 2004, 94(1): 251–268.
- [13] Chazelas J L, Guen P H G, Bard P Y, et al. Modeling of the site-city effect with centrifuge small scale model (instrumental techniques validation)[C]. Palaiseau, France: 2003.
- [14] Clouteau D, Ishizawa O, Mezher N. *Seismic wave propagation in a random city*[Z]. Boston: 2002.
- [15] Clouteau D, Aubry D. Modifications of the Ground Motion in Dense Urban Areas [J]. 2001, 4(9): 1659–1675.
- [16] Mezher N. Numerical modelling and quantification of the site-city seismic effect [D]. France: Ecole Centrale Paris, 2004.
- [17] Tsogka C, Wirgin A. Simulation of seismic response in an idealized city[J]. *Soil Dynamics and Earthquake Engineering*. 2003, 23(5): 391–402.
- [18] Kham M, Semblat J, Bard P, et al. Seismic Site–City Interaction: Main Governing Phenomena through Simplified Numerical Models[J]. *Bulletin of the Seismological Society of America*. 2006, 96 (5): 1934–1951.
- [19] Kuo-Tsang Huang, Wen-Pin Huang, Tzu-Ping Lin, Ruey-Lung Hwang. Implementation of green building specification credits for better thermal conditions in naturally ventilated school buildings [J]. *Building and Environment*, Volume 86, April 2015, Pages 141–150.
- [20] Sachinthaka Ravindu, Raufdeen Rameezdeen, Jian Zuo, Zhihua Zhou, Ravihansa Chandratilake. Indoor environment quality of green buildings: Case study of an LEED platinum certified factory in a warm humid tropical climate [J]. *Building and Environment*, Volume 84, January 2015: 105–113.
- [21] Nurul Sakina Mokhtar Azizi, Suzanne Wilkinson, Elizabeth Fassman. An analysis of occupant response to thermal discomfort in green and conventional buildings in New Zealand Original Research [J]. *Energy and Buildings*, Volume 104, 1 October 2015:191–198.
- [22] Augenbroe, Godfried (2011). The role of simulation in performance based design. In: J. Hensen and R. Lamberts (eds), *Building Performance Simulation for Design and Operation*. Spon Press.
- [23] Ali Malkawi and Godfried Augenbroe (editors), *Advanced Building Simulation*. SPON Press, Taylor and Francis group, 2004. ISBN 0-415-32122-0.



**Taylor & Francis**

Taylor & Francis Group

<http://taylorandfrancis.com>



## Effect of freezing and thawing on the physical properties of red sandstone

Hui-mei Zhang, Xiao-ning Liu, Chuan Peng & Xiang-zhen Meng

*Department of Mechanics, Xi'an University of Science and Technology, Xi'an, Shaanxi, China*  
*College of Architecture and Civil Engineering, Xi'an University of Science and Technology, Xi'an, Shaanxi, China*

**ABSTRACT:** For the growing engineering needs in cold regions, some red sandstone rocks were retrieved from the field and processed into samples with international standards, and then freeze–thaw cycle tests were performed under open water saturated state in this paper. The tests were conducted based on experimental research and in the background of major rock engineering in cold regions. By observing the process of freeze–thaw damage deterioration and the mechanism of freeze–thaw damage, variation of rock mass, volume, density, and longitudinal wave velocity with the freeze–thaw cycles was discussed and the mechanism of freeze–thaw damage deterioration was analyzed. Four deterioration models of freeze–thaw damage for red sandstone, particle spalling model, crack pattern model, shedding model, and fracture model, were developed. With the increase of freeze–thaw cycles, the rock mass, volume, and density decreased, and then P-wave velocity decreased.

**Keywords:** sandstone; freeze–thaw cycle; damage deterioration

### 1 INTRODUCTION

As a common natural material prone to damage, rock generates a large number of pores and micro-cracks, with high moisture even after a long time of geological processes. From the study of the freeze–thaw damage failure mechanism of rock, we find that the internal stress of rock changes with the high–low temperature and new cracks emerge. The local cracks grow into overall cracks gradually, thereby damaging the structure of rock. From the aspect of macroscopy, the rock strength decreases with the increase of deformation, rock cracking, and peeling<sup>[1–5]</sup>. These phenomena have certain influence on the construction, operation safety, and reliability of rock engineering in cold region. The analysis of physical properties of rock under freeze–thaw condition has a great practical significance for the engineering constructions in cold region.

At present, normal-, low-, and high-temperature variations of physical properties have been deeply studied and certain results achieved. In particular, the low-temperature freezing method has been widely used in tunnel excavation and coal mining<sup>[6–8]</sup>. Compared with the research methods of the above rock, the relative experiments on the physical and mechanical properties of water-bearing rocks under freeze–thaw cycles are few. In

this paper, red sandstone samples from Shaanxi Province, China, were used as the research object, freezing and thawing tests were conducted under saturated condition, and finally the effect of freezing and thawing on the physical properties of red sandstone was studied.

### 2 TEST INSTRUMENTS AND SOLUTIONS

The experiment was conducted on the red sandstone samples obtained from the same piece of large rock from Shaanxi to test data comparability. The raw sample was sent to a test chamber to undergo sleeve hole coring, cutting, polishing, and other processes, and finally international standard sample of  $\Phi 50 \times 100$  mm was obtained. After vacuum pump-forced saturation of the sample, rock quality, dimension, and longitudinal wave velocity were recorded. According to the longitudinal wave velocity measured, all the samples were divided into six groups of freeze–thaw cycles: 0, 5, 10, 20, 40, and freeze–thaw damage. Damage group is mainly used for measuring samples' longitudinal wave velocity under freeze–thaw cycles. All samples were sorted into the fast freeze–thaw test machine with temperature cycle of  $-20$  to  $+20^\circ\text{C}$  and  $+20$  to  $-20^\circ\text{C}$ . The freezing and thawing damage and failure behavior of the rock were observed

and recorded at 5, 10, 20, and 40 times of the wave velocity of all specimens in the freeze–thaw damage group.

### 3 TEST RESULTS AND ANALYSIS

#### 3.1 Analysis of the visual characteristics of freezing and thawing damage

The following results are obtained from the freezing and thawing process. After five times of the freezing and thawing process, free particles appear on the rock surface and edge, which increase with the number of freezing and thawing cycles. After 10 times of the freezing and thawing process, cracks appear on the sample surface, which increase with the number of freezing and thawing cycles, showing a deepening rift. After 40 times of the freezing and thawing process, surface layer of the rock breaks and tiny transverse crack appears in the middle of the rock. After 60 times of the freezing and thawing process, fracture appears, leading to collapse of the rock when gently pinched.

From the test, it can be found that freeze–thaw damage always occurs from outside to inside, and first appears on the rock surface and the edge. This is mainly because of the slow transmission of temperature inside the rock when the environment temperature is decreased, the higher internal temperature of rock than the outer surface temperature, and the large difference between the internal and external temperatures. According to the principle of thermal expansion and contraction, the lower surface temperature of the rock results in its contraction, and the higher internal temperature produces less shrinkage on the external surface of the rock, thereby resulting in a tensile stress on the surface of the rock due to the inhibition of shrinkage of the internal rock. When the tensile strength of the rock itself is less than the tensile stress on the surface, cracks appear on the surface of the rocks and the moisture inside the rock is condensed to ice by the continuous lowering of temperature, increasing the severity of the cracks further. Another reason is that in saturated specimens, in which average rock water content is less than its surface moisture, after many freeze–thaw cycles, the high moisture content results in softening, peeling, destruction of the rock surface gradually leading to internal damage, gradual expansion of internal fracture, formation of new cracks, and ultimate failure of the rock.

It was found that the samples have different forms of damage after different freeze–thaw cycles, which can be divided into four types, as shown in Figure 1:

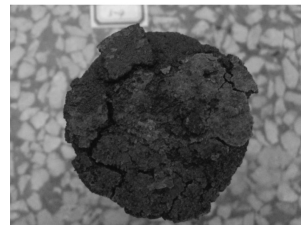
1. Particle spalling model: This is due to the high porosity, low rock strength, and low density of



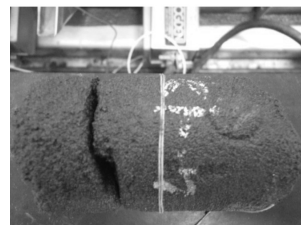
(a) particle spalling model



(b) crack pattern



(c) fall model



(d) fracture model

Figure 1. Deterioration model of freezing thawing damage of rock.

red sandstone. When the bond strength between water present in the rock and the rock particles decreases with the increasing number of freeze–thaw cycles, new damages occur and the surface particles of the rock become softened, leading to spalling phenomenon and eventual damage to the internal structure.

2. Crack pattern: During the freezing and thawing cycles, phase transformation from water to ice occurs repeatedly inside the rock, minerals produce non-uniform shrinkage, and the rock surface produces micro-cracks. With the increase in the number of freezing and thawing cycles, the cracks gradually expand, leading to deep cracks

connected into irregular net cracks to form tortoise shell-shaped structures.

3. Fall model: The original crack of the rock surface is constantly expanding, accompanied by the generation of new micro-cracks with the increase in number of freeze-thaw cycles. The micro-cracks in the rock surface develop into macro-cracks, together with the softening of the layer and the occurrence of the phenomena of falling, erosion and so on, ultimately leading to deepening of the damage.
4. Fracture model: With the increase in the number of freeze-thaw cycles, micro-cracks on the rock surface expand, confluence, coalescence, and become macro-cracks with internal migration. With further deepening freeze-thaw damage, cracks and spalling become more severe, finally breaking into two parts.

### 3.2 Changes of physical properties of the sample

Because the rocks are of discrete types, the test results only select representative rock samples as the research objects, and selected sample numerical experiments are average, which is more conducive to draw samples of each test index by changing freeze-thaw cycle rules. This section mainly selects the test results of the sample based on quality, volume, density, and wave velocity.

Tables 1 and 2 show that rock quality, the rate of change of rock quality, average quality, and the rate of change of average quality can be found from the first 10 freeze-thaw cycles. It is evident from the

tables that the rock quality increases sharply, the rock mass increases from 10.4700 to 17.1000 g, the average quality of 13.2100 g increases, the rate increases from 2.6180% to 4.2010%, and the average rate of increase of quality is 3.3010%. This is mainly due the following reasons: high porosity of the red sandstone, freezing and expansion of rock water, force caused by the initiation of the original and new cracks, migration of melt water to the rock, water filling inside the new crack, increase of rock mass, and increase of particle spalling. After 10 freeze-thaw cycles, particle peeling, cracking, freeze-thaw damage, and deterioration of model lead to higher mass loss and water migration, resulting in the decrease of the quality of the rock. After 20 freeze-thaw cycles, the quality of the specimen began to decline significantly. After 40 freeze-thaw cycles, a rock mass reduction of 7.6600–57.7200 g, quality decline rate of 1.9160–15.0630%, and average quality decline rate of 8.4100% were observed. This is mainly because of the increasing surface spalling and cracking of rock; rock mass damage rate is much higher than that due to water migration, leading to weight gain and significant quality decline.

Tables 1 and 2 show the sample volume, the rate of change of sample volume, average volume, and the rate of change of average volume. After five freeze-thaw cycles, because of the differences in individual properties of the samples, sample volume increases or decreases, but the average volume increases. The rate of increase of average volume is 0.0590%, which is mainly due to the freezing

Table 1. Sample mass, volume, density, and longitudinal wave velocity and its rate of change.

Rock specimen	Number of freeze-thaw cycles	Quality (change rate%)	Volume (change rate%)	Density (change rate%)	Longitudinal wave velocity (change rate%)
3-3	0	383.1900	189.6040	2.0210	1466.8000
	5	395.5200 (3.2180)	191.3490 (0.9200)	2.0670 (2.2760)	1184.4000 (-19.2500)
	10	395.2500 (3.1470)	188.7530 (-0.4490)	2.0940 (3.6120)	1051.2500 (28.3300)
	20	378.3800 (-1.2550)	184.1260 (-2.8890)	2.0550 (1.6820)	948.9000 (-35.3100)
	40	325.4700 (-15.0630)	155.2070 (-18.120)	2.0970 (3.7610)	737.6700 (-49.7100)

Table 2. Average mass, volume, density, and longitudinal wave velocity and its rate of change.

Rock specimen	Number of freeze-thaw cycles	Average quality (average rate of change)	Average volume (average rate of change)	Average density (average rate of change)	Average longitudinal wave velocity (average change rate%)
3-3	0	396.707	195.5380	2.0280	1485.1000
	5	408.1730(2.8910)	195.6530(0.0590)	2.0860(2.8600)	1164.2000(-21.6100)
	10	409.9170(3.3010)	194.3430(-0.6110)	2.1090(3.9940)	1047.2000(-29.4900)
	20	399.6830(0.7510)	190.0170(-2.8240)	2.1020(3.6490)	937.7000(-36.8600)
	40	30.584(-8.4410)	172.5030(-11.7800)	2.1010(3.5900)	754.3000(-49.2100)

and expansion of water in the rock, force caused by the initiation of original and new cracks, and volume expansion due to increase in water content. After 20 freeze–thaw cycles, the sample volume decreases, flaking and spalling occur on the rock surface, rate of change of average volume is reduced to 2.8240%, sample volume decreases rapidly, the shape of sample changes obviously, and the average volume reduction rate becomes 11.7800%. This is mainly due to the changes in the internal structure of the rock and flaking on the outer surface of the rock, resulting in the significant reduction in the volume of rock.

Rock density, average density, and their rates of change can be obtained from Tables 1 and 2. After 10 freeze–thaw cycles, the rock density increases, average density increased to 0.0580 g/mm<sup>3</sup>, and the rate of change of average density reached 3.9940%, mainly due to the presence of moisture in the original and new cracks, rock mass increase; however, the volume change in the early freeze–thaw cycles is small, which leads to the increase of rock density. After 20 freeze–thaw cycles, individual sample density continues to increase, the overall situation shows a gradually decreasing trend, and the rate of increase of average density of samples decreases to 3.6490%, which is due to the reduction of the mass of the rock. With the increase in the number of freeze–thaw cycles, rock density tends to become stable and the rate of change of rock density tends to be low. This is because the proportion of water and solid within the specimen remained stable, that is, fracture volume does not change significantly.

From Tables 1 and 2, we can observe that the longitudinal wave velocity of saturated rock decreases with the increase in the number of freeze–thaw cycles. With the increase of freeze–thaw cycles from 0 to 5, the rate of decrease of the longitudinal wave velocity is particularly significant, that is, 22%. When the number of freeze–thaw cycles is increased to 10, 20, and 40, the longitudinal wave velocity decreased to 29%, 37%, and 49%, respectively. This is mainly because, in the freeze–thaw cycle, by phase change from water to ice with different mineral particles of uneven contraction of the original crack expansion, large amounts of water enter into the rock. Because the wave propagation velocity in water is less than that in rocks and longitudinal in the presence of micropores and microfractures in rocks due to refraction, reflection, energy loss, and other unfavorable factors, the speed of the wave will be reduced.

## 4 CONCLUSIONS

1. For the red sandstone samples of freeze–thaw damage model to meet the international standard ( $\Phi 50 \times 100$  mm), four freeze–thaw damage deterioration models, particle spalling model, crack pattern model, shedding model, and fracture model, were developed.
2. Through the analysis of physical properties, it is concluded that the rock mass, volume, density, and longitudinal wave velocity change with the number of freeze–thaw cycles. With the increase in the number of freeze–thaw cycles, quality, volume, and density of the rocks first increased and then decreased; however, the longitudinal wave velocity of rock continued to decrease.

## REFERENCES

- [1] Zhang Jizhou, Miu Linchang, Yang Zhenfeng. Study on deterioration mechanism and mechanical properties of rock damage under freezing and thawing conditions [J]. Chinese Journal of rock mechanics and engineering, 2008, 27 (8): 1689–1694.
- [2] Liu Quansheng, Huang Shibing, Kang Yongshui, Cui Xianze. Development and thinking of the freezing thawing damage of fractured rock mass [J]. Chinese Journal of rock mechanics and engineering, 2015, 34 (3): 453–471.
- [3] Zhang Huimei, Yang Geng she. Rock under the freezing and thawing mechanics experiment and damage propagation characteristics [J]. Journal of China University of mining and technology, 2011, 40 (1): 140–145.
- [4] Zhang Huimei, Yang Geng she. Freezing and Thawing Environment red sandstone mechanical characteristics and damage analysis [J]. Mechanics and practice, 2013, 35 (3), 58–61.
- [5] Yang Geng she, Pu Yibin, Ma Wei. The damage propagation of [J]. experimental mechanics, the freeze-thaw environment of rock under the 2002, 17 (2): 220–226.
- [6] Sayles, F. H. Low temperature soil mechanics[R]. Hanover: US Army Cold Regions Research and Engineering Laboratory, 1966.
- [7] Jia Mi Xi, Yang P, Wang Lei and so on. Low temperature freezing under the action of sandy mudstone basic mechanical properties test [J]. Journal of China coal society, 2014, 39 (7): 1262–1268.
- [8] Xu Guangmiao, Liu Quansheng. Experimental study on basic mechanical properties of rock [J]. Chinese Journal of rock mechanics and engineering, under low temperatures of 2006, 12 (25): 2502–2508.

## Effect of surface microstructural features of injection-molded zirconia on the construction of dental implants

Chia-Ching Wang

*Department of Mechanical Engineering, National Kaohsiung University of Applied Sciences, Kaohsiung, Taiwan*  
*Department of Dental Laboratory Technology, Min-Hwei College of Health Care Management, Tainan, Taiwan*

Ming-Hong Lin & Sung-Long Chen

*Department of Mechanical Engineering, National Kaohsiung University of Applied Sciences, Kaohsiung, Taiwan*

Chien-Chang Lin

*Department of Mechanical Engineering, National Kaohsiung University of Applied Sciences, Kaohsiung, Taiwan*  
*Metal Industries Research and Development Centre, Kaohsiung, Taiwan*

Yau-Chia Liu

*Metal Industries Research and Development Centre, Kaohsiung, Taiwan*

Cen-Ying Lin

*ITRI Southern Region Campus, Industrial Technology Research Institute, Tainan, Taiwan*

**ABSTRACT:** In this study, a scanning electron microscope, a non-contact surface roughness tester, and a contact angle meter were used to investigate the surface microstructural features of zirconia samples, which were injected and printed by using the SM4Cr13 mold steel pretreated by femtosecond laser technology. The biocompatibility of the samples was assessed by performing an alkaline phosphatase test. The study results show that, as the scanning speed increased, the surface of the SM4Cr13 mold steel sample transformed from an island-like particulate structure into a relatively smooth and corrugated porous structure. Similar microstructural features were also observed on the surface of injected and printed zirconia samples. The printed zirconia sample obtained from the mold treated at 0.2 mm/s not only had a distinctly rough (1.156  $\mu\text{m}$ ) and hydrophilic (54.8°) surface, but also exhibited excellent biocompatibility. Therefore, zirconia printed by using this method has great potential for use in dental implants in future.

**Keywords:** femtosecond laser surface modification; microstructure; porous structure; biocompatibility

### 1 INTRODUCTION

Zirconia implants are mainly fabricated by the injection molding process. The molded implants have smooth surfaces; thus, sandblasting or acid etching is required to roughen the surfaces for easier adhesion of osteocytes. However, the sandblasting process makes it difficult to control the distribution and size of surface microstructures. Ceramic materials are brittle and tend to form unnoticeable fine cracks during the sandblasting process and sand grains are easily retained on the surface during cleaning [1]. Etching of the surface with hydrofluoric acid [2] can lead to environmental pollution and increased cleaning costs. In addition, improper control of parameters such as concentration, temperature, and soaking may cause intergranular corrosion, leading to the formation of a loosened structure with reduced

strength. Femtosecond laser technology has been widely used in industry and medical devices [3,4]. It not only directly fabricates microstructures on the surface of titanium implants [5–7], but also enables the formation of hydrophilic or hydrophobic microstructures on the surface of the mold [8]. In addition, it allows the formation of printing marks on the surface of the finished product or facilitates demolding [6]. Therefore, in this study, femtosecond laser technology was initially used to generate microstructures with different roughnesses on the surface of the mold cavity of the SM4Cr13 mold steel [9]. Following this, injection molding and printing were performed to fabricate zirconia implants with rough surfaces. Thereafter, the surface microstructural features that enabled the easy adhesion of osteocytes were investigated to provide reference information for zirconia implant design and development in future.

## 2 MATERIALS AND METHODS

### 2.1 Sample preparation

Polished SM4Cr13 mold steel materials of 10 mm diameter and 1 mm thickness were tested to perform surface modification. A SPIT FIRE Spectra-Physics femtosecond laser was used for surface modification and the operating parameters are shown in Table 1. After surface modification, the samples were cleaned for 15 minutes with ethanol in an ultrasonic vibrator and then air-dried. An injection and printing test was performed by using a KS-10 micro injector (Jakahashi, Japan) with zirconia containing 20 wt% binder and 3 mol.%  $Y_2O_3$ , and the detailed parameters are shown in Table 2. After injection and printing, the samples were cleaned for 15 minutes with ethanol in an ultrasonic vibrator and then air-dried.

### 2.2 Analysis of surface features

Surface microstructures were analyzed by using a JEOL JSM-6700F field emission scanning electron microscope at an operating voltage of 10–20 kV. A Bruker Contour GT-K non-contact surface roughness tester was used to measure the roughness of the material surface. Five measurements were taken and averaged for each sample. A surface hydrophilicity test was performed by using an FTA 125 contact angle meter by measuring the contact angle of deionized water to the surface of each sample and five measurements were averaged to obtain the result.

### 2.3 Alkaline phosphatase (ALP) test

Before testing, samples were autoclaved at 121°C for 15 minutes. After sterilization, samples were placed in a 24-well culture plate ( $n = 5$ ) and pre-

Table 1. Different laser process parameters for polished SM4Cr13 discs.

Parameters	Samples			
	Control	Fs-1	Fs-2	Fs-3
Repetition speeds (kHz)	0	1	1	1
Pulse energy ( $\mu J$ )	0	300	300	300
Laser wavelength (nm)	0	800	800	800
Pulse duration (fs)	0	120	120	120
Laser fluence ( $J/cm^2$ )	0	5.54	5.54	5.54
Scanning speed (mm/s)	0	0.2	0.6	3.5

Table 2. Injection process parameters for zirconia samples.

Injection parameters	
Mold dimension (mm)	50 × 6 × 3
Injection speed (cm/s)	5
Injection pressure (Zone 1/2/3/4) (Bar)	250/ 250/ 150/ 150
Injection temperature (Zone 1/2/3) (°C)	185/ 175/ 170
Mold temperature (°C)	42

osteoblasts (D1) were inoculated into the 24-well plate at an inoculation speed of  $1 \times 10^5$  cells/ml, and incubated at 37 °C under 5% carbon dioxide for 1, 4, 7, and 10 days, respectively. Afterwards, the culture medium was suctioned out and 0.5 ml of 0.1% Triton was added into each well at different time points and allowed to react for 1 h to allow for release of intracellular ALP. The content of each well was pipetted into a 96-well culture plate and 50  $\mu l$  p-nitrophenyl phosphate solution and 100  $\mu l$  Tris buffer solution were added into each well and allowed to react for 30 minutes at 37 °C. The optical density (OD) values at 450 nm were measured by using an ELISA Reader (BioTek-Epoch).

### 2.4 Observation of cellular morphology

Samples incubated for different time periods were observed under the SEM to check the cell adhesion and proliferation status on the surfaces. Incubated samples were fixed in 2% glutaraldehyde at room temperature for 1 h to preserve cellular morphology, cleaned with PBS solution twice, and then air-dried. Before performing SEM observation, the surface of each sample was coated with an approximately 20–30-nm thick Pt layer to increase its electric conductivity to obtain a clearer image.

### 2.5 Statistical analysis

Test data were analyzed by using student's test and ANOVA. A difference is considered significant if  $P < 0.05$ .

## 3 RESULTS AND DISCUSSION

### 3.1 Effect of femtosecond laser on the surface structure of the SM4Cr13 mold steel

Figs. 1 (a)–(d) show SEM images of SM4Cr13 samples processed by using femtosecond laser at different scanning speeds; Fig. 1 (a) shows the surface of an untreated sample, indicating that the polished sample had a highly smooth surface. On the contrary, after femtosecond laser treatment at different scanning speeds (Figs. 1 (b)–(d)), obvious changes in the surface microstructure were observed. At a scanning speed of 0.2 mm/s (Fig. 1 (b)), an island-like particulate structure with a particle size of approximately 5–10 nm was formed on the sample surface. As the scanning speed increased to 0.6 mm/s (Fig. 1 (c)), the size of the island-like particulate structure was increased to approximately 2–5  $\mu m$ . When the scanning speed increased to 3.5 mm/s (Fig. 1 (d)), the microstructure was converted into a relatively smooth and corrugated porous structure. These SEM results prove that femtosecond laser treatment at different scanning speeds effectively changed the surface microstructures of the SM4Cr13 mold steel.

An injection and printing test was performed by using a micro injector under identical conditions. Figs. 2(a)–(d) are the SEM images of individually injected and printed samples. Fig. 2 (a) shows the surface of the zirconia sample injected from the untreated mold and clearly the sample had a smooth surface with the same features as shown in Fig. 1 (a). However, the samples injected from the molds treated under the parameters of Fs-1 (Fig. 2 (b)) and Fs-2 (Fig. 2 (c)) formed concave surface microstructures with island-like particles with dimensions similar to that of the particulate structure. The sample injected from the mold treated under the parameters of Fs-3 (Fig. 2 (d)) exhibited no obvious surface structural features and displayed the same pattern as shown in Fig. 2 (a).

Figs. 3 (a)–(d) are images indicating the surface roughness of individually injected and printed samples. Fig. 3 (a) shows the surface of an untreated sample, where no obvious change in roughness was observed and the mean roughness (Rq) was approximately 0.252  $\mu\text{m}$ . As the scanning speed increased, obvious changes in surface roughness were observed, as shown in Figs. 3 (b)–(d), where the mean surface roughness of the printed sample was 1.156  $\mu\text{m}$ , 0.522  $\mu\text{m}$ , and 0.294  $\mu\text{m}$ , respectively. This result suggests that the scanning speed is inversely proportional to surface roughness.

Fig. 4 shows the contact angles of water droplets with the surfaces of the injected and printed samples, and the average contact angles were approximately

48.6°, 54.8°, 51.7°, and 49.5° for the untreated, Fs-1, Fs-2, and Fs-3 samples, respectively. This result indicates that there was no obvious change in the contact angle of the water droplet with the sample surface as the scanning speed increased. The surface hydrophilicity features show that a material is considered hydrophilic if the contact angle is less than 90°. On the contrary, a material is considered hydrophobic, if the contact angle is greater than 90°. Therefore, various zirconia samples obtained after injecting and printing are hydrophilic materials. Hydrophilic surfaces enable cell adhesion and proliferation, which in turn facilitate bone healing [10–12], biocompatibility, and cell morphology.

Fig. 5 shows average OD values for the ALP of individually injected and printed samples after incubation for different time periods. As shown in Fig. 5, no obvious difference in OD values was observed after incubation for one day. After a 4-day incubation period, OD values of various samples remarkably increased and the Fs-1 sample had the highest ALP content. After 7-day and 10-day incubations, the Fs-1 sample also had the highest OD value and exhibited a significant difference at D4 ( $p < 0.05$ ), D7 ( $p < 0.05$ ), and D10 ( $p < 0.05$ ) when compared with the untreated sample. The Fs-2 and Fs-3 samples displayed no obvious change or significant difference. Cell adhesion was further observed and the results are shown in Fig. 6. The cell growth status was observed at D4, and cells on the surfaces of four samples were adherent with pseudopodia, extending and attaching to the surface of the

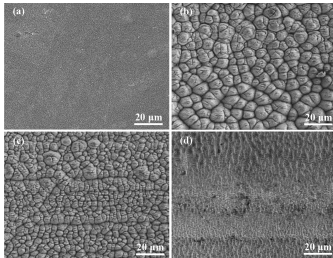


Figure 1. Topography SEM images of the (a) untreated, (b) Fs-1, (c) Fs-2, and (d) Fs-3 samples.

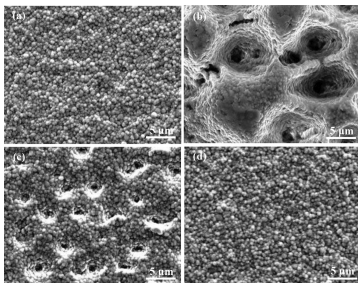


Figure 2. Topography SEM images of the printed (a) untreated, (b) Fs-1, (c) Fs-2, and (d) Fs-3 samples.

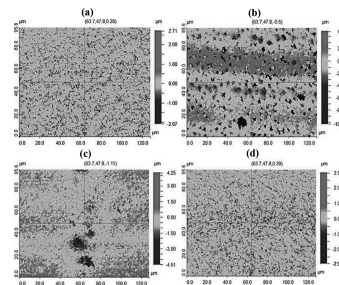


Figure 3. Average surface roughness of the printed zirconia samples.

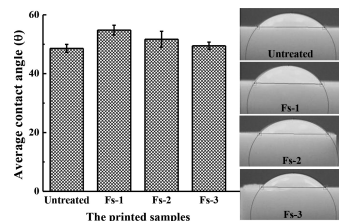


Figure 4. The wettability of zirconia printed with various speeds of laser scanning.

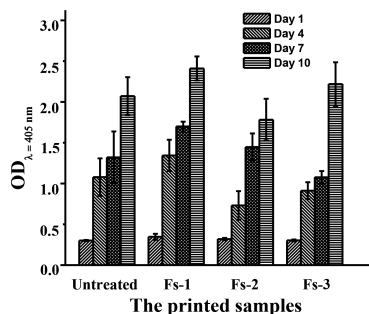


Figure 5. The cell cytotoxicity assay on control and printed zirconia samples.

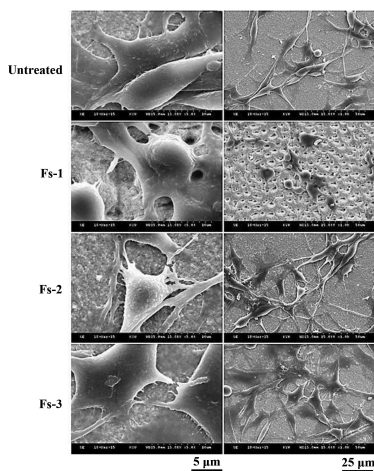


Figure 6. Cell morphologies of the printed zirconia samples after culturing with D1 cells for 1 day.

samples, indicating that the cells proliferated and started accumulating. Due to the presence of rough and porous surfaces, the Fs-1 sample exhibited sphere-like cell adhesion, whereas other samples displayed rod-shaped cell morphology. This phenomenon was also observed in samples after day-7 and day-10 incubations. This result proves that after being injected and printed from the mold and treated under different parameters, the samples did not release toxic substances into the cells and exhibited excellent biocompatibility. Therefore, zirconia printed by using this method has great potential to be used in artificial gums in future.

#### 4 SUMMARY

In this study, the mold was roughened by femtosecond laser technology instead of the sandblasting or acid-etching step in the conventional injection process and the desired surface roughness was directly obtained in one injection step. The test results show that the Fs-1 sample had the roughest (1.156 μm)

and most hydrophilic (54.8°) surface. In a cell adhesion test, the Fs-1 sample exhibited a better ALP value than samples treated under other parameters and might promote the re-mineralization of the implant surface and accelerate osseointegration.

#### ACKNOWLEDGMENT

The authors are deeply grateful to Innovation R&D and Medical Device Industrial Services (4/4) for their support with funding, experimental devices, and testing instruments.

#### REFERENCES

- [1] Bacchelli B., Giavaresi G., Franchi M., Martini D., De Pasquale V., Trire A., et al. Influence of a zirconia sandblasting treated surface on peri-implant bone healing: An experimental study in sheep. *Acta biomaterialia*. 2009;5:2246–2257.
- [2] Kohal R.J., Bachle M., Att W., Chaar S., Altmann B., Renz A., et al. Osteoblast and bone tissue response to surface modified zirconia and titanium implant materials. *Dental materials: official publication of the Academy of Dental Materials*. 2013;29:763–776.
- [3] Rapoport W., Khattak CP. Titanium sapphire laser characteristics. *Applied optics*. 1988;27:2677–2684.
- [4] Ranka M, Donnemfeld ED. Femtosecond laser will be the standard method for cataract extraction ten years from now. *Survey of ophthalmology*. 2015;60:356–360.
- [5] Vorobyev AY., Guo C. Femtosecond laser structuring of titanium implants. *Applied Surface Science*. 2007;253:7272–7280.
- [6] Tsukamoto M., Asuka K., Nakano H., Hashida M., Katto M., Abe N., et al. Periodic microstructures produced by femtosecond laser irradiation on titanium plate. *Vacuum*. 2006;80:1346–1350.
- [7] Ahmmed K.M.T., Ling E.J.Y., Servio P., Kietzig A.-M. Introducing a new optimization tool for femtosecond laser-induced surface texturing on titanium, stainless steel, aluminum and copper. *Optics and Lasers in Engineering*. 2015;66:258–268.
- [8] Bizi-bandoki P, Valette S, Audouard E, Benayoun S. Effect of stationary femtosecond laser irradiation on substructures' formation on a mold stainless steel surface. *Applied Surface Science*. 2013;270:197–204.
- [9] Lin H.G., SPH, S.E., Ma. *Mold Material Application Manual*. Machine Press. 2004;2:186–188.
- [10] Le Gu'ehennec L., Soueidan A., Layrolle P., Amouriq, Y. Review Surface treatments of titanium dental implants for rapid osseointegration, *Dental Materials*. 23 (2007) 844–854.
- [11] Gustavo Mendonca, Daniela B.S., Mendonca, Francisco J.L., Aragao, Lyndon F. Cooper, Review Advancing dental implant surface technology—from micron to nanotopography, *Biomaterials*. 29 (2008) 3822–3835.
- [12] Cho, S.A., Jung, S.K. A removal torque of the laser treated titanium implants in rabbit tibia, *Biomaterials*. 24 (2003) 4859–4863.



# Application of the catenary method and FBG sensors to monitoring ice thickness of power transmission lines

Lu-ming Li

*Information and Communications branch, Jiangxi Electric Power Company, Nanchang, China*

Zhi-ming Liu, Zhi-guo Zhang & Ci-lin Liu

*State Key Laboratory of Information Photonics and Optical Communications, Beijing University of Posts and Telecommunications, Beijing, China*

**ABSTRACT:** In this paper, real-time monitoring of the ice thickness problem of transmission lines is studied and modeling of the monitoring model with accurate equation of catenary linear state, which is based on Fiber Bragg Grating (FBG) sensors, is performed. It takes advantage of the conversion equation of overhead line lengths between different states. A comparative analysis of the performance is carried out between the results of this model and synchronous monitoring results by using a vernier caliper. Experimental measuring results show that, under the same conditions, the similarity of results between two methods is very high. The experimental results show that the average accuracy is about 0.5 mm.

**Keywords:** catenary line; accurate model; FBG; power transmission line; Ice

## 1 INTRODUCTION

Construction of a safe and reliable environmental protection and economy power system has become the common goal of the global power industry. Effective real-time monitoring for transmission lines is mandatory to ensure the safe operation of the power system. Thickness of ice coating on transmission lines is an important indicator of on-line monitoring, because thick sheets of ice coating can lead to the lines' fracture or the tower being collapsed. If it is a long distance transmission, it may cause widespread power outages and other serious consequences [1]. Therefore, many research units have started to look for effective ways to monitor and deal with icing.

Currently, the main methods of monitoring of ice thickness are divided into two categories. One is the weighing method [2], which directly measures line quality in a vertical span to calculate ice thickness. The other is the mechanics analysis method with axial stress or angle measuring [2–3], which is performed mostly by using an active instrument monitoring stress changes to calculate thickness. In the former method, the measured weight structure itself requires high precision. It is a complex and difficult operation. After implementation of the class method, the equipment is active to achieve initial information of the line. However, it will not only be affected by electromagnetic interference, but also will be affected by the relatively high cost.

At present, in the field of engineering, FBG is mainly used in monitoring points of high precision, a high speed real-time monitoring performance, suitable for engineering of the key parts of monitoring and at a moderate cost. A FBG sensor with OPGW or OPPC can constitute a communication network, provide a material basis [4] for real-time remote strain and temperature information monitoring and form an effective real-time remote monitoring system [5]. We propose a model of monitoring the power transmission line's icing thickness by using the temperature and strain of the line, and then give some experimental results.

## 2 FIBER BRAGG GRATING SENSING TECHNOLOGY

Photosensitive fiber Bragg grating is a section of the optical fiber with the fiber core refractive index in axial periodic modulation, which has the following two main parameters: the increment of the refractive index  $\Delta n$  and cycle  $\Lambda$ . When the cycle is equal to half of the wavelength, grating can couple the incident basal membrane and reverse phase transmission basement membrane and make it appear as a reflection of the wavelength selection function. Due to its mechanism which is in line with crystals in Bragg diffraction, it is called optical fiber Bragg grating (FBG). The basic equations of FBG are as follows:

$$\lambda = 2n_{co}\Lambda \quad (1)$$

where,  $\lambda$  is the wavelength and  $n_{co}$  is the effective refractive index of the fiber core. Change in outside temperature and stress will directly affect the two physical quantities, which affects the center wavelength of reflection,  $\lambda$  [6]. As shown below,

$$\frac{\Delta\lambda}{\lambda} = (1 - \rho_e) \cdot \varepsilon + (\alpha - \xi) \cdot \Delta T \quad (2)$$

In many practical applications, designing temperature insensitive fiber Bragg grating sensors to measure stress changes is very necessary and this technology has become very mature at present.

### 3 MODEL OF THE CATENARY METHOD

Transmission lines on the project can use the catenary equation for calculation. The catenary method is based on the conditions that its units' load should be uniformly distributed along the length of the overhead line to establish the principles and methods of calculation, in accordance with reality.

Known initial quantities of transmission lines are as follows:  $f_m$ —initial sag (m),  $l$ —Span (m),  $\Delta h$ —tower height difference (m),  $t_m$ —initial temperature ( $^{\circ}\text{C}$ ),  $E$ —Young's modulus of the line ( $\text{N}/\text{mm}^2$ ),  $\alpha$ —thermal expansion coefficient of line ( $^{\circ}\text{C}^{-1}$ ),  $d$ —the outer diameter of the line (mm),  $S$ —sectional area of the cable ( $\text{mm}^2$ ),  $G_0$ —mass per unit length of the line ( $\text{kg}/\text{m}$ ),  $g$ —acceleration of gravity ( $\text{N}/\text{kg}$ ), and  $\rho$ —the density of ice ( $\text{g}/\text{mm}^3$ ).

Here, the no-icing state is defined as  $m$  state.

The relative load of gravity  $g_m$  ( $\text{N}/\text{m}/\text{mm}^2$ ) under the initial non-icing conditions is given by the following equation:

$$g_m = \frac{G_0 g}{S} \cdot 10^{-3} \quad (3)$$

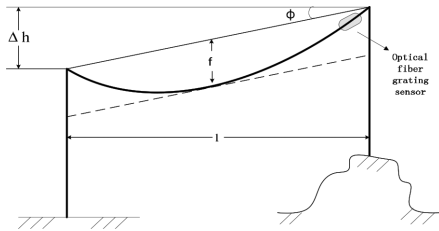


Figure 1. Principle diagram of transmission line modeling.

The initial horizontal stress  $\delta_m$  is given by the following expression:

$$f_m = \frac{2\delta_m}{g_m} \cdot sh^2\left(\frac{g_m l}{4\delta_m}\right) \quad (4)$$

The value of  $\delta_m$  is the same throughout in all expressions. The initial arc length  $L_m$  is given as follows:

$$L_m = \frac{2\delta_m}{g_m} \cdot sh\left(\frac{g_m l}{2\delta_m}\right) \quad (5)$$

The temperature ( $t_n$ ) is defined, under non-icing conditions (relative load of gravity is always denoted as  $g_m$ ), by the  $m1$  state solving the horizontal stress of the catenary ( $\delta_{m1}$ ), which is given as follows:

$$\begin{cases} L_{m1} = \frac{2\delta_{m1}}{g_{m1}} \cdot sh\left(\frac{g_{m1} l}{2\delta_{m1}}\right) \\ g_{m1} = g_m \\ L_{m1} = L_m \cdot [1 + (t_n - t_m) \cdot \alpha] \cdot \left[1 - \frac{\delta_m}{E} + \frac{\delta_{m1}}{E}\right] \end{cases} \quad (6)$$

Then, the corresponding axial stress is achieved using the following equation:

$$\delta_{Am1} = \delta_{m1} + g_m f_{m1} \quad (7)$$

The temperature ( $t_n$ ) is defined, under icing conditions, by the  $n$  state. The true value of real-time axial stress at the point of suspension ( $\delta_{An}$ ) is given as follows:

$$\delta_{An} = [e_n - (t_n - t_m) \cdot \alpha] \cdot E + \delta_{Am1} \quad (8)$$

where  $e_n$  ( $\mu\epsilon$ ) is the strain detected by FBG-based sensors. The true value of real-time horizontal stress at the point of suspension ( $\delta_n$ ) is given by the following expression:

$$\delta_n \approx \delta_{An} \quad (9)$$

The real-time relative load of gravity at the point of suspension ( $g_n$ ) is calculated as follows:

$$\begin{cases} L_n = \frac{2\delta_n}{g_n} \cdot sh\left(\frac{g_n l}{2\delta_n}\right) \\ L_n = L_m \cdot [1 + (t_n - t_m) \cdot \alpha] \cdot \left[1 - \frac{\delta_m}{E} + \frac{\delta_n}{E}\right] \end{cases} \quad (10)$$

The real-time ice thickness ( $b$ ) is given as follows:

$$\begin{aligned}
g_n &= g_m + g_{ice} \\
&= g_m + \frac{\mathbf{g} \left[ \frac{\pi(d+2b)^2}{4} - \frac{\pi d^2}{4} \right] \rho}{S} \times 10^{-3} \\
b &= \frac{\sqrt{\frac{4}{\pi\rho} \left( \frac{Sg_n}{\mathbf{g}} - G_0 \right) + d^2} - d}{2}
\end{aligned} \tag{11}$$

## 4 EXPERIMENTAL TEST AND DATA ANALYSIS

### 4.1 Experimental conditions

Table 1. Transmission line initial installation parameters.

$f_m = 3 \text{ m}$	$l = 78.8 \text{ m}$	$\Delta h = 3 \text{ m}$
$d = 12.8 \text{ mm}$	$S = 128.6 \text{ mm}^2$	$G = 578 \text{ kg/km}$
$E = 140000 \text{ N/mm}^2$		$C\alpha = 13.4(10^{-6}/^\circ\text{C})$



Figure 2. The experimental environment in Xuefeng Mountains.

### 4.2 Experimental measurement results analysis and performance comparison

Through installation of FBG sensors on the transmission line, the real-time strain and temperature of the installation point can be collected and applied in the catenary line method for computing real-time ice thickness results. At the same time, by using vernier calipers for synchronously and regularly measuring (it is the accurate reference), the corresponding ice thickness measuring results can be obtained. The results were compared between the two methods and are shown in Figure 3.

The average error is given as follows:

$$\bar{x} = \frac{1}{n} \sum_{i=1}^n (y_i - x_i) = 0.496(\text{mm})$$

In geometry, the angle cosine is used to measure the difference between the directions of two vectors. Therefore, the model uses this concept to

measure the difference between sample vectors. Two  $n$  sample points can use the similar concept of included angle cosine to measure the degree of similarity between them. The range of angle cosine values is  $[-1, 1]$ . The greater the included angle cosine value, the smaller will be the vector angle. The vernier calipers synchronously measuring the sample of ice is  $x_i$ , catenary line method measuring sample is  $y_i$ .

$$\cos(\theta_{xy}) = \frac{\sum_{k=1}^n x_k \cdot y_k}{\sqrt{\sum_{k=1}^n x_k^2} \cdot \sqrt{\sum_{k=1}^n y_k^2}} = 0.997392$$

It can be seen from the results that the angle between them is very close to zero.

Covariance is a measure of the linear independent dimensionless number and its value is in the range of  $[-1, +1]$ .

$$\rho_{xy} = \frac{\text{Cov}(x, y)}{\sqrt{D(x)} \cdot \sqrt{D(y)}} = 0.994371$$

It can be seen from the results that they are close to achieving completely positive linear correlation.

Under the same experimental conditions, the internal temperature results of the monitoring device and the external environment temperature results by the temperature special sensor are compared.

The temperature within the device is generally higher than the outside environment's temperature, especially when the outside environment's temperature is high. For the sensor, the fiber connection box is black in color; it absorbs the heat, making its internal temperature higher than the outside air temperature. But this model uses the relative temperature difference value as the amount of calculation, and thus the precision of the model is not affected.

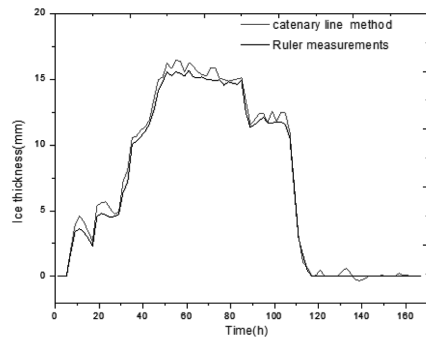


Figure 3. Comparison of the icing results.

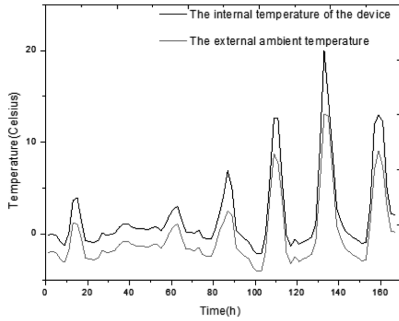


Figure 4. Graph showing the temperature inside the device and the temperature of the external environment.

## 5 CONCLUSIONS

An accurate catenary linear model is built on the basis of the different temperatures and different stress vales corresponding to different line lengths. There is an accurate conversion between different states. The model takes thermal expansion and contraction into consideration (caused by the temperature change only), which seriously affects the results for icing. Calculation results of the entire model and the results of the method using vernier caliper to monitor overhead line icing are very similar. The accuracy of the improved model already meets the engineering requirements; therefore, real-time monitoring of ice thickness of transmission lines can be effectively achieved.

## ACKNOWLEDGMENTS

This study is supported by the Project of JiangXi Electric Power Company (No. 201350807 and No. 201350808).

## REFERENCES

- [1] MA Guo-ming. A Novel Online Icing Monitoring System on Overhead Transmission Lines Based on Fiber Bragg Grating Sensor [D]. Baoding, North China Electric Power University, 2011.
- [2] LI Licheng, Yang Lin, HAO Yanpeng. Review of On-line Monitoring of Ice Coating on Overhead Transmission Line[J]. Power System Technology, 2012, 36(2): 237-243.
- [3] Huang Xinbo, Sun Qindong, Cheng Ronggui, Zhang Guanjun, Liu Jiabing. Mechanical Analysis on Transmission Line Conductor Icing and Application of On-line Monitoring System [J]. Automation of Electric PowerSystems, 2007, 31(14): 98-101.
- [4] Li Ming, Xu Yong-jun. Fiber Bragg Grating Sensor Technology for Status Monitoring of Overhead Transmission Line[J]. Telecommunications for Electric Power System, 2012, 33(241): 59-64.
- [5] Zhihang Xue, Qi Huang, Changhua Zhang, Yongxing Cao, Ran Zhang. Icing Monitoring System Based on Fiber Bragg Grating Sensor for Overhead Transmission Lines [C]. IEEE International Conference on Smart Instrumentation, Measurement and Application (ICSIMA), Kuala Lumpur, 2013: 1-4.
- [6] Ren Liang, Li Hongnan, Sun Li, et al. FBG sensor for on-line temperature measurements [C]//Proc SPIE Int Soc Opt Eng. San Diego, 2004: 94-99.

## Low temperature synthesis of CNTs on the micron-sized $\text{Cu}_p$ surface

Pei-ling Ding

*College of Materials Science and Engineering, Jiamusi University, Jiamusi, P.R. China*

Yun-long Zhang & Ming Hu

*College of Materials Science and Engineering, Jiamusi University, Jiamusi, P.R. China*  
*Institute of Applied Materials and Technology, Jiamusi University, Jiamusi, P.R. China*

Jing Gao

*College of Materials Science and Engineering, Jiamusi University, Jiamusi, P.R. China*

**ABSTRACT:** In order to improve the heat transfer performance of the copper matrix for the engineering application of electrical contact materials, an investigation was attempted to introduce carbon nanotubes (CNTs) onto the surface of copper micrometer particles. Fabrication for uniform growth of CNTs on the copper particles was executed by using the thermal CVD technique. The results showed that CNTs were distributed uniformly on the surface of copper microparticles at low reaction temperatures. The diameter of newly synthesized CNTs was within the range of 30–60 nm. Growth behaviors of CNTs determined by using the CVD method were considered to have adopted the “tip-growth” mechanism. The order degree of the graphitic structure in synthesized CNTs improved according to the results of Raman spectra of  $\text{CNTs}_{(\text{Cu})}$ .

**Keywords:** carbon nanotube, Ni/MgO catalyst, Catalytic CVD method

### 1 INTRODUCTION

For surface engineering applications such as electrical contact materials, investigated materials with high performance usually need to meet the following requirements: excellent electrical conductivity, low interception, etc.<sup>[1]</sup> However, it was difficult for pure metals or alloys to meet structure requirements. An electrical contact material was composed of a matrix phase and a reinforcement phase. The matrix material was made up of copper/silver metal, which exhibited excellent performance in terms of high thermal conductivity, low contact resistance, etc.<sup>[2]</sup> The reinforcement phase was composed of metal or compound or ceramics particles. The copper matrix was widely applied for electrical contact materials due to their electrical and thermal properties. Recently, CNTs were extensively researched, thanks to their superior mechanical properties and heat transfer performance.<sup>[3]</sup> More number of studies focused on CNTs/Cu composites.<sup>[4–5]</sup> However, density differences would result in heterogeneous distribution of above-mentioned two-phase materials. In this paper, the synthesis of Ni/MgO nanoparticles on the  $\text{Cu}_p$  surface by using the co-deposition method is discussed. The focus of this work is on fabrication for uniform growth

of CNTs on copper particles by using the thermal CVD technique. Inspecting the growth behaviors of CNTs was also aimed to be achieved in this work.

### 2 EXPERIMENTAL PROCESS AND MATERIAL CHARACTERIZATION

Industrial copper particles ( $D_{50} = 75 \mu\text{m}$ ) were used as received. The mixture solution of copper nitrate  $[\text{Cu}(\text{NO}_3)_2]$  and magnesium nitrate  $[\text{Mg}(\text{NO}_3)_2]$  were utilized to form the precursor. The mole ratio of  $\text{Cu}(\text{NO}_3)_2$  to  $\text{Mg}(\text{NO}_3)_2$  was 1:1. The  $\text{Ni}(\text{OH})_2/\text{Mg}(\text{OH})_2/\text{Cu}$  colloid was obtained by using the chemical co-precipitation method. Then, the mixture colloid was vacuum thermal treated for 8 h at 90 °C, which was then crushed into fine powder using a mortar. The obtained solid powders contained 7 wt% of the Ni catalyst. The CVD process was executed at atmospheric pressure in a horizontal alumina tube reactor that was connected to  $\text{N}_2$  and  $\text{CH}_4$  gas cylinders. About 500 mg of 7 wt% Ni/Cu catalyst was taken in a quartz boat and placed in the middle of the alumina tube as a reactor zone. Before 400°C, the heating rate was controlled at 5 °C/min and  $\text{N}_2$  was introduced as the protection

gas. The  $N_2$  gas flow rate was 400 SCCM. Within the range of 400 °C–670 °C,  $H_2$  gas was applied as the reduction gas. The gas flow rate was found to be 150–250 SCCM. After reaching 670 °C,  $N_2$  and methane began to purge to produce CNTs. During the reaction process, the gas flow ratio of  $N_2$  to  $CH_4$  was 1:1. Once the reaction was completed, methane flow was discontinued and  $N_2$  flow continuously purged the reaction chamber till room temperature was attained. The collected product was subjected to purification.

The yield of the carbon product after the reaction was calculated using the following expression<sup>[6]</sup>: Carbon Yield =  $\frac{m_{tot} - m_{cat}}{m_{cat}} \times 100\%$ , where  $m_{cat}$  and  $m_{tot}$  are masses of catalyst before and after the reaction, respectively. The phase composition of  $Cu_{(CNTs)}$  were identified by X-ray diffraction with scanning speed of 10°/min and a step length of 0.02°. A scanning electron microscope (JEOL, JSM-4700) was used to investigate the surface morphology of the sample after purification. Defects and graphitic nature were surveyed by Raman spectroscopy (Bruker RFS-27y) equipped with a liquid nitrogen cooled setup and with an output power of 10 mW

by means of a Nd:YAG laser source at a wavelength of 1064 nm.

### 3 RESULT AND DISCUSSION

The received copper powders are shown in Fig. 1. Electrolytic copper powder with dendrite shape structure had a rough surface morphology, and so it could acquire a high specific surface area. The hybrid powders obtained by chemical co-precipitation, vacuum drying, and grinding treatment processing are shown in Fig. 1 (b). A fine particle layer was coated on the surface of copper powder with micron grade.

The XRD patterns obtained after co-deposition (a) and after reduction treatment (b) for the copper powders are shown in Fig. 2. According to the analysis of Fig. 2, the copper powder was treated by using the co-deposition method and the diffraction peaks of  $Ni(OH)_2$  and  $Mg(OH)_2$  can be detected in the resultant product; here, the diffraction peak of  $Mg(OH)_2$  is not labeled in Fig. 2 (a).  $Ni(OH)_2$  and  $Mg(OH)_2$  had the

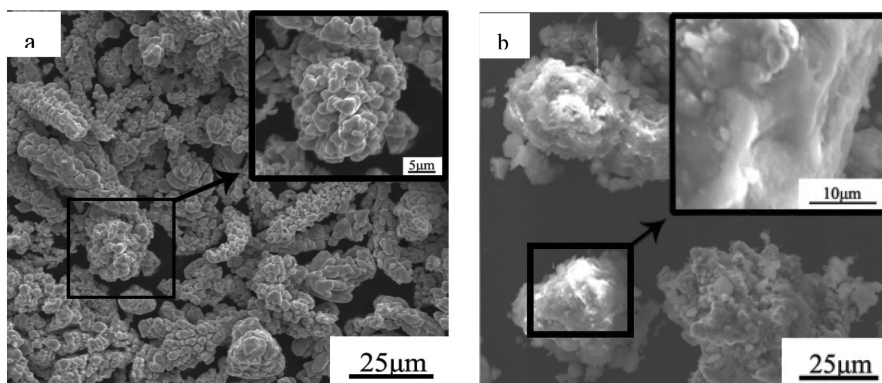


Figure 1. (a) Received copper powders and (b) precursor after co-precipitation.

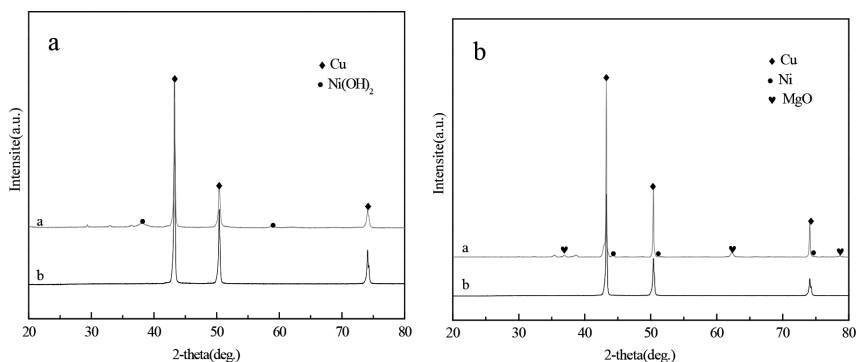


Figure 2. XRD patterns after co-deposition (a) and after reduction treatment (b).

same hexagonal structure, and so lattice parameters were similar for aforementioned two phases. Therefore, the XRD diffraction peaks of  $\text{Mg}(\text{OH})_2$  and  $\text{Ni}(\text{OH})_2$  would overlap. After heat reduction treatment, the MgO and Ni phase can be found. This implied that  $\text{Mg}(\text{OH})_2$  and  $\text{Ni}(\text{OH})_2$  would translate into the MgO and Ni phase after reduction treatment. It can be launched that the  $\text{Ni}(\text{OH})_2$  and  $\text{Mg}(\text{OH})_2$  phase can be formed after co-deposition treatment and the Ni/MgO catalyst can be formed on the copper powder surface after reduction treatment.

The morphology was detected for CNTs grown at  $670^\circ\text{C}$  from SEM images shown in Fig. 3 (a)–(d). These figures represented the product for CNTs at different magnification times, respectively. It can be observed that CNTs are distributed uniformly on the micron  $\text{Cu}_p$  surface. The diameter of newly

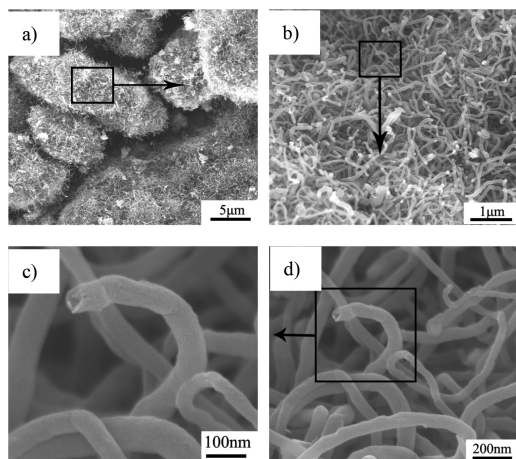


Figure 3. (a)–(d) Morphology of CNTs represented at different magnifications.

synthesized CNTs was within the range of 30–60 nm. Clear images of CNTs with smooth outer walls are shown in Fig. 3 (c) and (d).

The outer wall of CNTs was slightly rough. From observations made to study the end region morphology of CNTs with high magnification (Fig. 3 (d)), spherical catalyst particles can be detected on the end region of CNTs in some regions. Growth behaviors of CNTs synthesized by using the CCVD technique on the  $\text{Cu}_p$  surface were considered to follow the “tip-growth” mechanism.

XRD patterns of  $\text{Cu}_{(\text{CNTs})}$  products synthesized at  $670^\circ\text{C}$  are illustrated in Fig. 4. (a). The copper phase was the main crystalline phase. At the same time, Ni, MgO, and graphite were detected as minor crystalline phases. The carbon atom structure of the tube wall for CNTs was similar to that of the graphite lattice plane (002); the diffraction peak of the graphite (002) lattice plane could be observed at  $26.2^\circ$  from XRD patterns. The yield of CNTs reached 168% as the reaction temperature reached  $670^\circ\text{C}$ . Raman spectra of synthesized  $\text{CNTs}_{(\text{Cu})}$  at  $670^\circ\text{C}$  are shown in Fig. 4 (b). The broad peaks were detected within the region of  $1587\text{--}1598\text{ cm}^{-1}$ , which attributed to the graphitic structure with a certain degree of crystallinity as a result of in-plane vibrations of  $\text{sp}^2$  bonded carbon atoms in the graphitic layers which is called the tangential mode or G-band for CNTs. The high degree of symmetry and order of the structure of carbon materials would be characterized by the graphitic band (G-band) within the region of  $1550\text{--}1600\text{ cm}^{-1}$ , which was applied to identify well-ordered CNTs<sup>[7]</sup>. From Raman spectra of  $\text{CNTs}_{(\text{Cu})}$ , the intensity ratio of the D-band to G-band ( $I_D/I_G$ ) was low, which implied that there was a higher order degree of the graphitic structure for synthesized CNTs and the aforementioned results were in agreement with previous reports<sup>[8]</sup>.

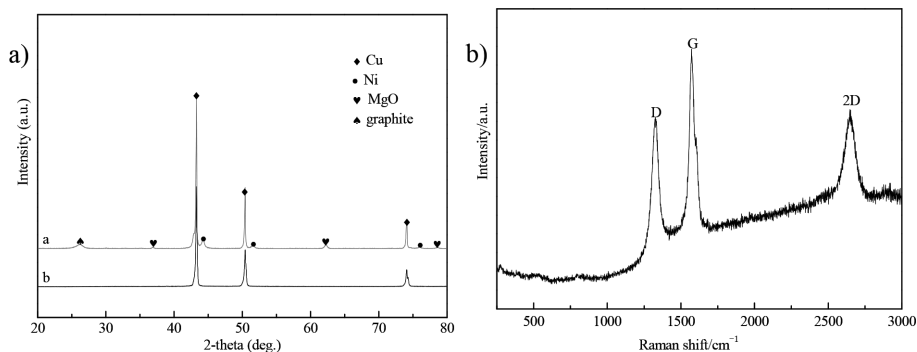


Figure 4. XRD pattern of  $\text{Cu}_{(\text{CNTs})}$  after CCVD treatment (a) and Raman spectrum (b).

#### 4 CONCLUSION

CNTs were introduced onto the  $\text{Cu}_p$  surface by using the CCVD technique. Ni/MgO catalyst particles were formed on the  $\text{Cu}_p$  surface by using co-deposition method. The growth behaviors of CNTs were surveyed. CNTs were distributed uniformly on the  $\text{Cu}_p$  surface at low reaction temperatures. The diameter of newly synthesized CNTs was within the range of 30–60 nm. The CNTs' growth process was considered as the "tip-growth" mechanism. Raman spectra implied that there was a certain degree of disorder of the graphitic structure in synthesized CNTs.

#### ACKNOWLEDGEMENTS

The authors extend their special thanks for the great support offered by the Postgraduate Technology Innovation Project for Jiamusi University (No. LZZ2015-004), Science and Technology Innovation Team of Jiamusi University (No. CXTD-2013-03), and National Science Foundation of China (No. 51271088).

Correspondence should be addressed to Ming HU; jmsdxhumming@126.com.

#### REFERENCES

- [1] Lungu M, Tsakiris V, Enescu E, et al. Development of W-Cu-Ni Electrical Contact Materials with Enhanced Mechanical Properties by Spark Plasma Sintering Process[J]. *Acta Physica Polonica A*, 2014, 125: 327–332.
- [2] Y. Champion, Y. Brechet. Effect of grain size reduction and geometrical confinement in fine grained copper: potential applications as a material for reversible electrical contacts, *Adv. Eng. Mater.* 2010,12: 798–802.
- [3] Berber S, Kwon YK, Tomanek D. Unusually high thermal conductive of carbon nanotubes[J]. *Physical Review Letter*, 2000, 84(20):4613–4613.
- [4] K.T. Kim, S.I. Cha, S.H. Hong, et al. Microstructures and tensile behavior of carbon nanotube reinforced Cu matrix nano composites, *Mater. Sci. Eng. A*, 2006, (430): 27–33.
- [5] W.M. Daoush, B.K. Lim, C.B. Mo, et al. Electrical and mechanical properties of carbon nanotube reinforced copper nano composites fabricated by electroless deposition process. *Mater. Sci. Eng. A*. 2009, (513): 247–253.
- [6] Bartosz Kruszka, Artur P Terzyk · Marek Wiśniewski, et al. Synthesis of carbon nanotubes and nanotube forests on copper catalyst. *Mater. Res. Express*, 2014: 1035040.
- [7] Yingxi Xie, Longsheng Lu\*, Yong Tang, et al. Grafting carbon nanotubes onto copper fibers using a one-step chemical vapor deposition process. *Materials Letters*, 2015(153): 96–98.
- [8] W.Z. Li, S.S. Xie, L.X. Qian, et al. Large-scale synthesis of aligned carbon nanotubes [J]. *Science*.1996, (274): 1701–1703.



# An experimental study on stiffness degradation of reinforced concrete columns strengthened with HDPF

Y. Qiao, C.Z. Sun, Z.B. Wang & G. Zuo

*Department of Architecture Engineering, Suqian College, Suqian, China*

**ABSTRACT:** In this paper, seven reinforced concrete columns strengthened by using high ductility polyester fibers and two reinforced concrete columns without high ductility polyester fibers were used to carry out the low reversed cyclic test. The factors, including reinforcement form and fiber layers, were studied and the load–displacement hysteretic curve and stiffness degradation were analyzed. The test results show that, because of the constraint function of the high ductility polyester fiber, the load–displacement hysteretic curve is fuller than the load–displacement hysteretic curve of reinforced concrete columns without high ductility polyester fibers, and the plastic deformation capacity increased obviously. The specimen had good energy dissipation capacity when compared with the specimen without high ductility polyester fibers, the rate of stiffness degradation was slower than that of the unstrengthened specimen, and the ductility performance was improved by high ductility polyester fibers.

**Keywords:** high ductility polyester fiber; reinforced concrete column; strengthen; stiffness degradation.

## 1 INTRODUCTION

In the field of structural seismic strengthening, because of their light weight, high tensile strength, durability, ease of construction, etc., common fiber-reinforced composite materials, comprising carbon fibers, glass fibers, and aramid fibers, have been widely used [1–3]. But there is one question worth noting that FRP materials', especially carbon fibers, performance of linear elasticity, low elongation until the destruction, causes brittle damage of confined concrete.

High ductility polyester fiber reinforcement technology (Super Reinforcement with Flexibility (SRF)) is used to strengthen the structure with High Ductility Polyester Fibers (HDPFs), originated in Japan after the year 2000. In 2001, Toshimi Kabeyasawa [5–7], Susumu Kono [8], Yousok Kim [9] published articles about HDPF reinforcement technology and carried out the shaking table test to reinforced concrete columns and shear walls strengthened with HDPF and verified the effect of strengthening the column and shear wall. The results prove that during earthquakes, the deformation and seismic ability of reinforced concrete columns and shear walls, strengthened with high ductility polyester fibers, can be improved substantially. There is no relevant experimental study and theoretical analysis, but some scholars have made a brief introduction for HDPF reinforcement technology. In this work, the load-carrying capacity test was carried out for reinforced concrete

columns strengthened with HDPF under axial compression, which includes analyzing the influence of reinforcement forms, reinforcement spacing, slenderness ratios, and concrete strength on constraining performance, load-carrying capacity, and damage mode of reinforced concrete columns strengthened with HDPF.

In this work, reinforced concrete columns strengthened with HDPF were designed, the cyclic loading test was conducted, and then the influence of high ductility polyester fibers on energy dissipation, stiffness, and ductility of reinforced concrete square columns was analyzed, thus providing a reference for high ductility polyester fibers used in the practical applications.

## 2 TEST SURVEY

### 2.1 Specimen design

Square cross-section and inverted T-shaped column specimens were divided into three groups. Seven members' concrete strength was C30 and the column dimension was 1000 mm, 200 mm, and 200 mm. All the members were symmetrically reinforced and constructed at the same time. Group Z I's reinforcement was carried out using four HRB400 A14 rebars, and the reinforcement ratio was 1.54. Group Z II's reinforcement was similar to that of group Z I and the reinforcement ratio was 3.08, but strengthened with eight HRB400 A14 rebars at the bottom of columns within 15 cm.

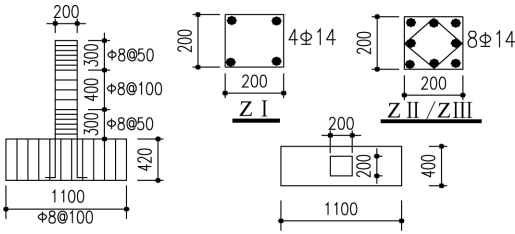


Figure 1. Reinforcement of specimens.

Specimen number	Layer number	Intensity (MPa)
Z I-1	Unstrengthened	36.5
Z I-2	One layer	33.2
Z I-3	Two layers	37.3
Z II-1	Unstrengthened	33.2
Z II-2	One layer	33.2
Z III-1	Unstrengthened	37.3
Z III-2	Two layers	36.5

Group Z III's reinforcement ratio was the same as that of Group Z II, but the reinforcement length was 30 cm and the stirrup was 8 mm of the HPB300 rebar. All members were strengthened with HDPF winding laterally. The parameters of the HPB300 rebar are as follows:  $E_s$ , 2.1 GPa; yield strength, 336 MPa; and ultimate strength, 440 MPa. The parameters of the HRB400 rebar are as follows:  $E_s$ , 2.0 GPa; yield strength, 465 MPa; and ultimate strength, 597 MPa. The parameters of HDPF are as follows:  $E_s$ , 2.1 GPa and cracking strength, 600 MPa.

## 2.2 Specimens loading and data acquisition

The cycle loading test was used to study the ductility performance of reinforced concrete columns strengthened with HDPFs in the Suqian College Architectural Engineering Structure Laboratory. An MTS hydraulic servo loading system provided the horizontal force and a 300 kN hydraulic jack with a pin joint at the head and a sliding device to guarantee the vertical force all the time provided the vertical force.

The loading system was designed according to the relevant provisions of "earthquake test methods for building regulations" (JGJ101-96). Firstly, the vertical force was loaded till the designed value was reached and the state was maintained for 30 minutes; Then, the horizontal force was loaded. During the horizontal force loading, at every step, there was a 10 kN increment until the specimens reached the yield stage, and data were collected every 5 minutes after each step. When it reached the yield displacement,  $\Delta$ , the loading was control-

led by displacement. When the horizontal loading reached its maximum of 85%, the specimens were considered to be damaged, and then the loading process was stopped. The strain of concrete, rebar, and HDPF would be collected by using Donghua 3816 strain gauges and force-displacement curves were obtained by using MTS.

## 3 TEST RESULTS AND ANALYSIS

### 3.1 Load-displacement hysteretic curve

The load-displacement hysteretic curve that recorded the loading process of reinforced concrete columns under cycle loading could also exhibit stiffness degrading and energy dissipation. Fig. 3 shows the load-displacement hysteretic curve of members without strengthening with HDPF and Fig. 4 shows the load-displacement hysteretic curve of members strengthened with HDPF.

Compared with each group of unreinforced specimens, the following can be observed: (1) the load-displacement hysteretic curve of column 1 in group Z II was fuller and more ductile than that of column 1 in group Z I and it was found that increasing the reinforcement ratios at the plastic hinge could improve columns' seismic performance. (2) The load-displacement hysteretic curve of column 1 in group Z III was fuller than that of column 1 in group Z II and it was found that increasing the length of the longitudinal reinforcement at plastic the hinge could improve columns' seismic performance.

When compared with group unreinforced specimens and group reinforced specimens, it can be observed that (1) the strengthened columns' load-displacement hysteretic curve was shuttle-shaped and fuller and it was found that strengthened columns' plastic deformation, ductility, and energy dissipation were better; (2) when compared with three columns in group Z I, the column's energy dissipation strengthened with two layers of fiber

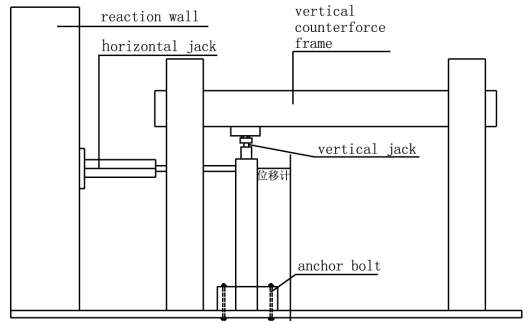


Figure 2. Sketch of the loading device.

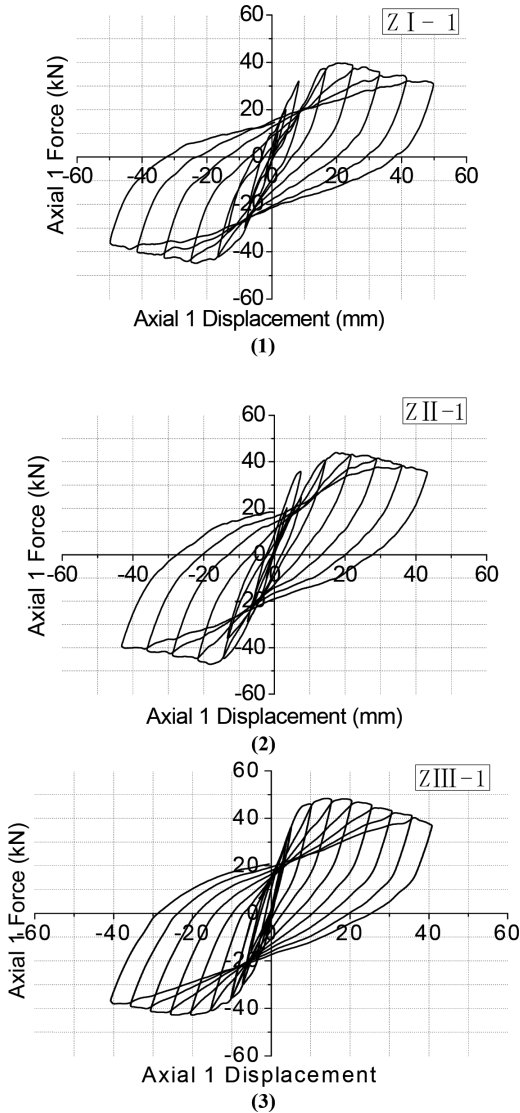


Figure 3. Hysteresis curves of unstrengthened specimens.

was better than the one strengthened with one layer of fiber and it was found that the more the number of fibers was, the better the seismic performance became.

### 3.2 Stiffness degradation

With the increment of loading displacement, damage accumulation would cause stiffness degradation. For determining the extent of stiffness degradation quantitatively after every cycle, secant stiffness was used to represent the stiffness degra-

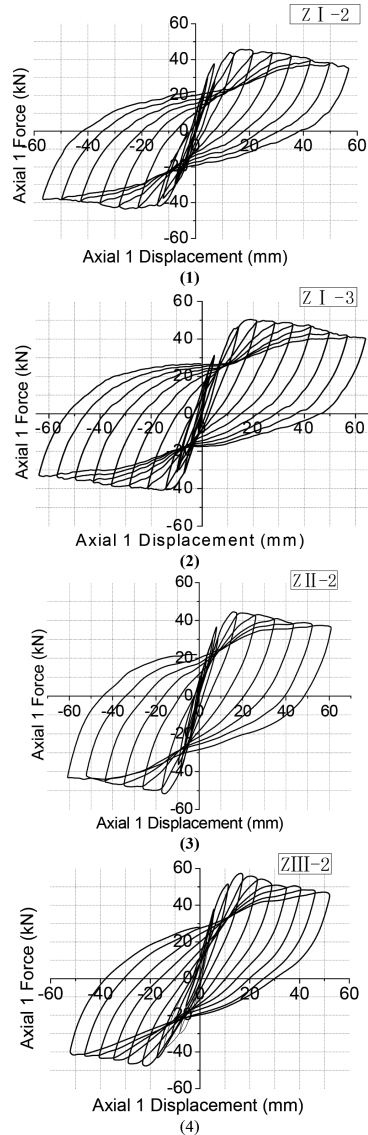


Figure 4. Hysteresis curves of strengthened specimens.

dation characteristic of the specimen under cyclic loading. Secant stiffness, as average stiffness after every loading cycle,  $K_i$ , was defined as the sum of the absolute values of positive and negative loading under cyclic loading that should be divided by the corresponding sum of absolute values of positive and negative displacements.

$K_i$  is calculated as follows:

$$K_i = \frac{|+F_i| + |-F_i|}{|+X_i| + |-X_i|} \quad (1)$$

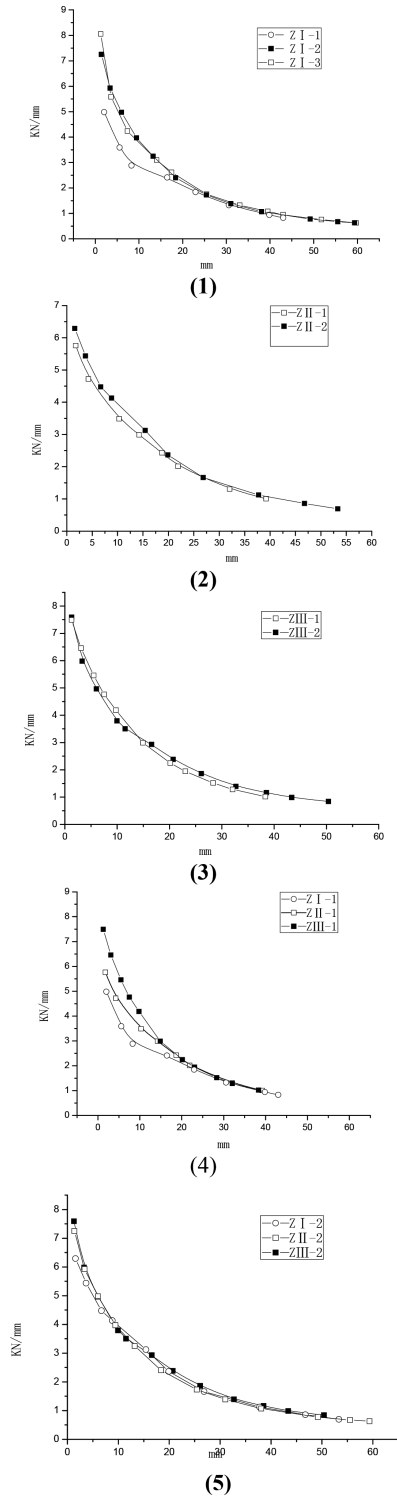


Figure 5. Comparisons of stiffness degradation curves.

where,  $F_i$  represents the  $i$ -th peak's horizontal load value;  $X_i$  represents the  $i$ -th peak's horizontal displacement value.

An important factor of influencing the displacement and stiffness on the top of column is the column's stiffness. With the increment of the displacement, the secant stiffness, representing the deformability of members, became more and more small gradually. This showed that the deformability of members was becoming better. The stiffness degradation curves are shown in Fig. 5-(1)–Fig. 5-(5).

Results were found and the following analyses were made from Fig. 5: (1) the stiffness degradation curve could be divided into the following three phases: stiffness dramatic degradation phase, from the beginning to the appearance of the first crack at the bottom of column; stiffness moderate degradation phase, from the cracking stage to the yield stage; and stiffness slow degradation phase, from the yield stage to the damage stage. Fig. 5 shows that the process of members' stiffness degradation was similar, such that the stiffness was at its maximum value, and with the appearance of cracks, the columns' stiffness degenerated dramatically. In this phase, the reinforcement ratios and the length of the longitudinal reinforcement at the plastic hinge had more influence on stiffness. When the plastic hinge appeared and columns came to the yield stage, the bond force between the concrete and rebar decreased theoretically, but because the fiber limited the development of cracks and improved the ductility, stiffness degenerated slowly and the columns could provide bearing capacity in spite of dramatic deformation. (2) From Fig. 5-(4), it was found that the length of the longitudinal reinforcement at the plastic hinge had more influence on initial stiffness. In the first phase, the longer the length of the longitudinal reinforcement was, the slower the stiffness degenerated will be. When the members yielded, the stiffness came to convergence nearly. It was found that reinforcement had more effect on the yield stage and before.

#### 4 CONCLUSIONS

Based on the results of the cycle loading test carried out on seven reinforced concrete columns, each specimen's load–displacement hysteresis curve was obtained and the influence of the layers of HDPFs and the length of the rebar in the plastic hinge zone on the reinforced concrete columns' stiffness was studied. The following conclusions can be drawn:

1. The hysteresis curve of reinforced concrete columns, strengthened with HDPF, was fuller

and exhibited more plastic deformation capacity. Moreover, with the increment of layers of HDPF, the hysteresis curve was fuller and showed an improved seismic performance. When compared with two layers of HDPF, the effect of one layer of HDPF was more ideal.

2. Because of the binding effect of HDPFs, the stiffness of strengthened columns degenerated slowly at the later stage of the loading and the ductility and bearing capacity can be improved dramatically in spite of severe deformation.

## ACKNOWLEDGMENT

This work was supported by the Foundation of Jiangsu Educational Committee (12 KJB560007).

## REFERENCES

- [1] Ye, L.P. & Feng, P. 2006. Applications and development of fiber-reinforced polymer in engineering structures. *Chian Civil Engineering Journal* 39(3):24–36.
- [2] Xiao, Y. 2004. Applications of FRP composites in concrete column. *Advance of Structural Engineering* 7(4):335–343.
- [3] Lelli Van Den Einde, Zhao Lei & Seible Frieder. 2003. Use of FRP composites in civil structural applications. *Construction and Building Materials*, 17(6–7):389–403.
- [4] Qiu, B.X. 2008. Repair reinforcement and reconstruction technology of post-earthquake building. Beijing: *China Building Industry Press*.
- [5] Kabeyasawa, T., Tasai, A. & Igarashi, S. 2002. An economical and efficient method of preventing old reinforced concrete buildings from collapse under major earthquake. *Proceedings of 7NCEE*, Boston.
- [6] K. Kabeyasawa, T., Igarashi, S. & Kim, Y.S. 2004. Shaking table test of reinforced concrete frames for verification of seismic strengthening with polyester sheet, *13th World Conference on Earthquake Engineering*, Vancouver, B.C., Canada, 1–6 August..
- [7] T. Kabeyasawa. 2005. Seismic evaluation and economical strengthening of reinforced concrete buildings. *Asian journal of civil engineering (building and housing)* 6(6):457–476.
- [8] Susumu KONO, Masato DOI, Jungyoon Lee, Hitoshi TANAKA. 2008. Seismic retrofit of RC members using FRP with very low young's modulus. *14th World Conference on Earthquake Engineering*. Beijing, China. 12–17 October.
- [9] Yousok Kim, Toshimi Kabeyasawa, Shunichi Igarashi. 2012. Dynamic collapse test on eccentric reinforced concrete structures with and without seismic retrofit. *Engineering Structures* 34:95–110.
- [10] Liu, X., Shi W.X. & Wang, J. 2012. Summary and comparison of traditional and innovative seismic strengthening technologies, *Structural Engineers* 2:101–105.
- [11] Yang, X.W. 2009. SRF, a Reinforcement Technology for Dilapidated building, *Time Architecture* 1:54–57.
- [12] Lv, Q.F., Zhu, H. & Zhang, J. et al. 2008. Innovative technologies for Seismic Retrofitting in Japan, *Construction Technology* 37(10):9–11+31.
- [13] Qiao, Y., Wang, Z.B., Sun, C.Z. & et al. Experimental Study on axial compression reinforced concrete columns strengthened with SRF. *Industrial Building*. Accepted for publication.



**Taylor & Francis**

Taylor & Francis Group

<http://taylorandfrancis.com>

# Architectural design strategies of zero-energy houses in a solar decathlon competition

Cheng Chen & Xin-pei Liu

Computer Network Emergency Response Technical Team, Coordination Center of China, Beijing, China

**ABSTRACT:** Solar Decathlon (SD) is an international multidisciplinary competition in which university teams design, construct and operate zero-energy solar houses by themselves. The SD Organization sets rules and regulations to promote a fair and interesting competition by regulating the basic characteristics and requirements that must fulfill building codes. From a research perspective, this paper presents the architectural design strategies of zero-energy houses competing in Solar Decathlon 2015. Architectural design strategies were analyzed based on the contest criteria that consisted of 10 separately scored contests. To obtain high points in the competition, first, architecture criteria were considered for the design strategies and then other criteria were considered for the architectural innovation. The grade of Photo-Voltaic (PV) integration, the architectural design approach and the placement of modules were observed to explore the methodology of PV integration in SD houses. Then, the local climate of target regions and the lifestyle of target residents were also taken into account to explore the innovational design of SD houses with respect to the local design strategies. In addition, the sustainable design of SD houses was described based on affordability strategies and the optimization of the interior and exterior space. In conclusion, the architectural design tendency of zero-energy houses was presented by discussing the PV integration, the local design strategies and the sustainable design strategies.

**Keywords:** solar decathlon 2015; contest criteria; PV; local design; sustainable design

## 1 INTRODUCTION

The energy consumed by buildings typically accounts for 40% of the total energy used worldwide, and it is accepted that modifications to building designs and operations can decrease substantial energy consumption. Moreover, buildings are increasingly expected to be sustainable, zero energy consumption and provide a healthy and comfortable environment that is economical to build and maintain [1]. Therefore, more policies are developed by governments to apply renewable energies, and architects and engineers are increasingly interested in constructing zero-energy houses to improve this management.

### 1.1 Zero energy building

A Zero-Energy Building (ZEB) is a residential or commercial building with greatly reduced energy needs through efficiency gains, such that the balance of energy needs can be met by renewable technologies (Fig. 1). A zero-energy building first needs to reduce its energy requirements, responding adequately to its environmental conditions, having an appropriated envelope and using passive design

strategies. Furthermore, high energy efficiency systems and equipment need to be selected [2].

### 1.2 Solar decathlon

Within this scenario, Solar Decathlon (SD) was created as an international competition among universities by the US Department of Energy [3–5]. During the competition, participating teams are required to design, build, and operate net zero-energy solar houses that consume as few natural resources as possible and produce minimal waste during their lifecycles. The SD competition has been held in America every two years since 2002, and the European edition and Asian edition were started in 2006 and 2013, respectively [6].

The rest of this article is organized as follows. Section 2 explains different contests on the architectural design of a prototype house. Taking the SD 2015 houses as examples, Section 3 describes two grades of photovoltaic (PV) system integration in buildings. Section 4 presents the design innovation of zero-energy houses based on the local climate of target regions and the lifestyle of target residents. Section 5 elucidates the sustainable strategies of zero-energy houses. Finally, Section 6 concludes this paper.

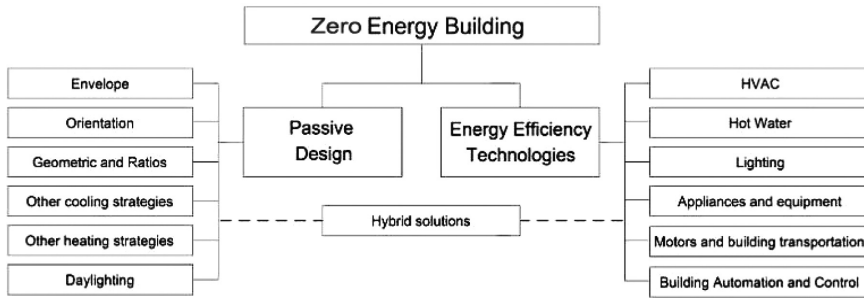


Figure 1. Zero-energy building.

Number	Contest Name	Available Points	Brief Description
1	Architecture	100	Architecture Jury reviews and evaluates the drawings, construction specifications, audiovisual presentation, architecture narrative, and final constructed project
2	Market appeal	100	Market Appeal Jury reviews and evaluates the drawings, construction specifications, audiovisual presentation, market appeal narrative, and final constructed project
3	Engineering	100	Engineering Jury reviews and evaluates the drawings, construction specs, energy analysis results and discussion, audiovisual presentation, engineering narrative and final constructed project
4	Communications	100	Communications Jury reviews and evaluates the team website, audiovisual presentation, communications narrative, onsite public exhibit, and public exhibit materials
5	Affordability	100	Cost estimator reviews the drawings, construction specifications, and final constructed project to estimate construction costs
6	Comfort zone	100	Keep zone temperature in 71°F – 76°F (22°C – 24°C) range, relative humidity below 60%
7	Appliances	100	Keep refrigerator temperature in 34°F – 40°F (1°C – 4°C) range; Keep freezer temperature in -29°C to -15°C range; Wash eight loads of laundry and five loads of dishes; Return eight loads of laundry to their original weight; Perform five cooking tasks
8	Home Life	100	All interior and exterior lights on at full levels at night; Conduct 16 water draws temperature within 10 minutes; Operate a TV and computer; Host two dinner parties for up to eight guest; Host neighbors to watch a movie on the home theater system
9	Commuting	100	Drive an electric vehicle at least 25 miles, eight times during contest week
10	Energy Balance	100	Produce at least as much electrical energy as is consumed during contest week; Consume less than 175 kWh of electrical energy during contest week
TOTALS		1000	

Figure 2. The 10 contest criteria.

## 2 CONTEST CRITERIA

The International Solar Decathlon (SD) competition is a high-level international competition that attracts outstanding universities and colleges from all over the world [6]. This competition requires that each team (university/college) design and construct an independent living house within 2 years, whose area should range from 60 m<sup>2</sup> to 100 m<sup>2</sup>

and whose energy supply must totally come from the solar energy. The competition is modeled after the Olympic decathlon competition: each home is evaluated for its overall performance in a total of 10 contests.

The contest is organized around 10 areas that are awarded by a total of 1000 points (Fig. 2). Some of the contests are evaluated by an external jury, while others are evaluated based on the completion of



some specific tasks to be scored. The 10 contests are described in Chart 1. Teams participating in the SD 2015 competition should concentrate on every contest in order to obtain the maximum points. According to the contest criteria, architecture is awarded by 100 points, and its evaluation is considered in two specific criteria by the jury: 1. architectural concept and design approach; 2. architectural implementation and innovation, both of which guide the architectural design of prototype houses directly. In addition, three other specific contests, namely market appeal, affordability and energy balance, influence the architectural design strategies. More particularly, market appeal is primarily related to the exterior and interior space of the house, the lifestyle of the target resident and the sustainability of the target climate. All the available points of affordability are earned within an estimated construction cost of \$250,000, which could impose restrictions on construction materials, structure designs and construction processes. To meet the energy balance, the integration of PV systems, which are the only source of electricity, is closely related to the house.

### 3 METHODOLOGY OF PV INTEGRATION IN BUILDINGS

Many authors have proposed different classifications and nomenclature for integrating PV technologies in buildings (7–9). In this study, all the houses are classified as either BIPV or BAPV, both of which have been widely accepted for the definition of PV integration in buildings. The houses were numbered from P01 to P14 (Fig. 3).

#### 3.1 Grade of integration

- BAPV, Building-Applied Photovoltaic: modules are used solely for generating energy, even as part of the architectural composition of the building, but do not replace or perform as a construction component. They may be assembled coplanar or not to the building envelope on roofs, facades, atria or shading devices.
- BIPV, Building-Integrated Photovoltaic: PV construction elements are part of the building envelope, not only acting as an energy generator, but also performing as an envelope function on roofs, facades, atria or shading elements.

Both grades of integration could be observed in SD houses, but BAPV applications have evident superiority. During the competition, 11 examples of BAPV and three examples of BIPV were presented.

#### 3.2 Architectural design approach

- Invisible application: modules are located out of the sight of the users, or are intentionally designed not to be distinguished from the rest of the building envelope;
- Added application: modules are applied to perform a function in the building, added to the construction, as in shading devices over windows;
- Highlighted application: modules are used to enhance the image of the building, without dominating it;
- Leading application: modules are preponderant, determining the image of the building.

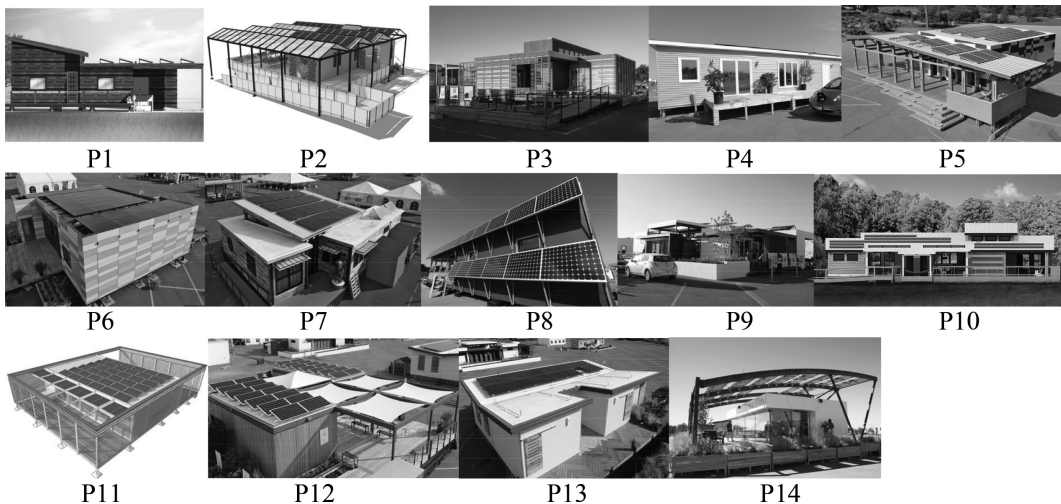


Figure 3. Houses from P1 to P14.

The most frequently used architectural design approach was the PV systems invisible to the users: this approach was observed in 10 applications, which was followed by the added approach with only two examples. The least used strategy was the highlighted application and the leading approach, both in one example.

### 3.3 Placement of modules

- Roofs: sloped roofs, flat roofs, atria (Fig. 4);
- Facades: cold facades, warm facades, window glazing (Fig. 5);
- Shading elements: canopies, louvers and brise-soleils (Figs. 6 and 7).

Sloped roofs have evident superiority to integrate PV modules in SD houses. The proportion between the sloped and flat roofs was 8 to 5 in this competition, while only one house applied PV integration in facades. It is worth noting that the use of non-optimal orientations in two houses with flat roofs responded to the design strategies to optimize the electrical energy profile according to the real energy demand, thus avoiding producing more energy than the house really needed, in order to make them net zero-energy houses. Furthermore, it was found that the placement of PV modules was not limited to the roof or facade, which means that PV could change the facade from the roofs as



Figure 4. Roofs.



Figure 5. Facades.



Figure 6. Louvers.

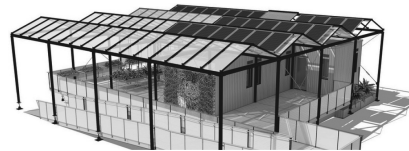


Figure 7. Canopies.

sliding panels, or assemble the facade in canopies as shadowing structures.

## 4 LOCAL STRATEGY OF ARCHITECTURAL DESIGN

Since the first SD in 2002, the local strategy of solar houses has attracted increasing attention. On the one hand, the local strategy meets contest criteria such as market appeal. On the other hand, the innovation of architectural design could be developed through local climate, local culture, local topography, etc.

Based on the local climate strategy, SD houses that tend to be residential buildings in normal conditions have developed the functions of disaster-resistant buildings in response to natural disasters. By taking the advantage of the PV system, the high thermal insulation envelope and the gray water system, SD houses can withstand certain extreme weather conditions, and they can also function as a disaster relief house with the capacity of providing power during electrical outages, expanding the market of zero-energy houses (Fig. 8).

The houses give an emphasis on the indoor-outdoor living space that offers a larger space for living and entering in SD 2015. Considering the

## 5 LOCAL STRATEGY OF SUSTAINABLE ARCHITECTURAL DESIGN



Figure 8. P11 with flood shutters.



Figure 9. P10 with sliding walls.

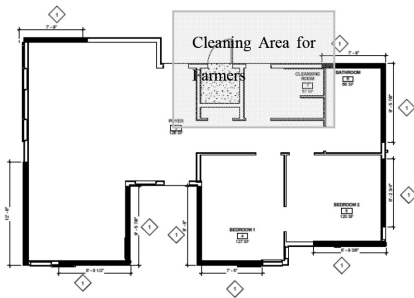


Figure 10. P13 for farm workers.

local climate, opening the sliding walls blends the public module into a generous outdoor area, doubling the public space, while keeping the footprint under 1,000 ft<sup>2</sup> (Fig. 9).

Finally, the lifestyle of target residents has an influence on the architectural design. The house is designed for farm workers who need a secondary entry and a cleaning room with shower to wash the clothes contaminated with dirt or work-related debris and to cleanse before entering the rest of the house. For saving land, the house is designed with a rectangular plan, which is adapted for New York where there are numerous rectangular street blocks (Fig. 10).

In the contest criteria “affordability”, participating teams should build a zero-energy house within \$ 250,000 to obtain full scores, while the expenses could be reduced substantially by using recycled materials. In SD 2015, two teams used refurbished shipping containers to form the structure of SD houses. On the one hand, recycled materials were used throughout the construction for affordability and to extend the lifecycle of the houses. On the other hand, shipping containers allowed the house to be pre-assembled quickly for easy transportation and assembly. In addition, a large amount of recycled materials were used in the exterior and interior space, such as wood siding reclaimed from shipping pallets, reprocessed fishing nets and recycled denim batting (Fig. 11).

Sustainable design could also be found in the optimization of the physical environment through passive design strategies in the shading, thermal environment and environmental greening. In particular, the adjustable shading component was used to control natural light and reduce the solar heat gain and cooling loads, and a passively conditioned space acted as a thermal buffer between the outside environment and the actively conditioned

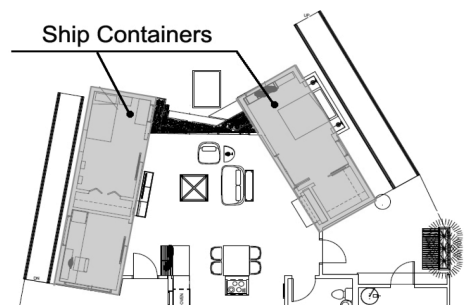


Figure 11. P7 with two ship containers.



Figure 12. P3 with adjustable shading.

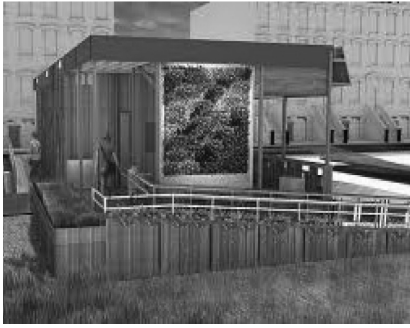


Figure 13. P8 with a living wall.

interior space, which served as a greenhouse during the winter. Moreover, a shade garden or a living wall was used to help stabilize the indoor environment while acting as landscaping of the home, which also had the potential to grow more food if the residents wished (Figs. 12 and 13).

## 6 CONCLUSIONS

In this article, it is worth noting that the houses described above were designed to participate in a competition, which means that the design strategies were more influenced by the contest criterion points, rather than by designing a commercial building. They were designed not only for the climatic conditions in California, but also to perform well in the original site. Nevertheless, the authors believe that they possibly represent tendencies of zero-energy building in the immediate future. Therefore, within the context mentioned above, the following tendencies can be pointed out:

- Compared with BIPV, the grade of BAPV integration played a dominant role in SD 2015. When the BAPV was used, the main design approach was the added application of modules, predominantly over the roofs, followed by the highlighting application on shading devices and roofs;
- The tendency of the local strategy is that zero-energy houses transform into disaster-resistant buildings in response to natural disasters by

using the specific design approach based on the local climate of the target regions. The interior and exterior space is designed for the lifestyle of local residents;

- Sustainable design is realized by using recycled materials and passive design strategies. Sustainable strategy enables architects to explore the innovation of zero-energy houses by considering the affordability of houses.

The SD has started in China since 2013. There are complicated climate zones in China, the largest developing country in the world. It could be seen that there is a promising market for zero-energy houses, especially for those with adaptive architectural design strategies.

## REFERENCES

- [1] Kolokotsa D, Rovas D, Kosmatopoulos E, Kalaitzakis K. a roadmap towards intelligent net zero and positive energy buildings. *Sol Energy* 2011; 85(12): 3067e84.
- [2] Edwin Rodriguez-Ubinas, Sergio Rodriguez, Karsten Voss, Marija S. Energy efficiency evaluation of zero energy houses. *Energy and Buildings* 83(2014): 23–35.
- [3] R.J. King, C. Warner, *Solar decathlon: energy we can live with*, Proceedings of the 3rd world conference on photovoltaic energy conversion, IEEE Press, Piscataway, NJ, 2003, pp. 2139–2142.
- [4] M.R. Wassmer, M.J. Brandemuehl, A. Jackaway, The simulation of a zero-energy residential building for the solar decathlon competition, Proceedings of the International Solar Energy Conference, American Society of Mechanical Engineers, New York, NY, 2003, pp. 45–53.
- [5] C.L. Warner, M.R. Wassmer, Solar decathlon 2005-PV system strategies and results, in: Proceedings of the 4th World Conference on Photovoltaic Energy Conversion, IEEE Press, Piscataway, NJ, 2006, pp. 2272–2276.
- [6] Information on <http://www.solardecathlon.gov/>
- [7] A.G. Hestnes, Building Integration of Solar Energy Systems, *Solar Energy* 67(4–6) (1999) 181–187.
- [8] T.H. Reijenga, PV in Architecture, in: A. Luque, S. Hegedus (Eds.), *Handbook of Photovoltaic Science and Engineering*, John Wiley and Sons, Great Britain, 2003, pp. 1005–1042.
- [9] S. Roberts, N. Guariento, *Building Integrated Photovoltaics: A Handbook*, Birkhäuser, 2009.

## Hot pressure sintering of BN-SiC composites with $\text{La}_2\text{O}_3$ - $\text{Al}_2\text{O}_3$ aids

Yun-long Zhang

*Center for Composite Materials and Structure, Harbin Institute of Technology, Harbin, P.R. China*  
*College of Materials Science and Engineering, Jiamusi University, Jiamusi, China*  
*Institute of Applied Materials and Technology, Jiamusi University, China*

Yu-min Zhang

*Center for Composite Materials and Structure, Harbin Institute of Technology, Harbin, P.R. China*

Zhong-huan Shao

*College of Materials Science and Engineering, Jiamusi University, Jiamusi, China*

Ming Hu

*College of Materials Science and Engineering, Jiamusi University, Jiamusi, China*  
*Institute of Applied Materials and Technology, Jiamusi University, China*

Yong Li, Jin-peng Gong, Bo Li & Yin-he Zhang

*College of Materials Science and Engineering, Jiamusi University, Jiamusi, China*

**ABSTRACT:** The hot-press sinter technology was applied under the condition of 1950°C by means of protective argon gas and  $\text{Al}_2\text{O}_3$  combined with  $\text{La}_2\text{O}_3$ , served as sintering aids in order to fabricate the full-density BN-SiC ceramics-based composites. Effect of  $\text{Al}_2\text{O}_3/\text{La}_2\text{O}_3$  aids on the micro-structure, crystal phases, density evolution, Vickers hardness and bending strength were surveyed in details. The results showed that  $\text{Al}_2\text{O}_3/\text{La}_2\text{O}_3$  aids were effective to promote densification of SiC/BN composites. The variation for Vickers hardness and bending strength of SiC/BN composites was not obvious under the condition of difference of sintering additives.

**Keywords:**  $\text{Al}_2\text{O}_3/\text{La}_2\text{O}_3$  aids, BN-SiC composites, Hot-press sintering

### 1 INTRODUCTION

Non-oxide ceramics, for example carbides and nitrides, had many advantageous mechanical properties under the room temperature and high temperatures condition owing to strong covalent bonding. In particular, Silicon Carbide (SiC) was a promising candidate for components in advanced gas turbines, piston engines, and heat exchangers thanks to their high strength and excellent creep resistance at elevated temperatures<sup>[1-3]</sup>. For multi-phase composites, either fibrous or particulate in nature, were employed to reduce probability of catastrophic failure. The mainly method to manage thermal stresses generated and simultaneously increase both crack initiation and propagation parameters was to use a high-low modulus composite. Generally, the addition of a low modulus phase to a strong, high modulus matrix decreases elastic modulus and flexure strength. Examples of these composites that use BN as the low modulus phase are  $\text{Al}_2\text{O}_3$ -BN<sup>[4]</sup>,

$\text{Si}_3\text{N}_4$ -BN<sup>[5]</sup>, SiC-BN<sup>[6]</sup> and AlN-BN<sup>[7]</sup>. The purpose of this work was to characterize SiC/BN ceramic with  $\text{Al}_2\text{O}_3/\text{La}_2\text{O}_3$  aids. The powder morphology of SiC/BN mixtures contained different  $\text{Al}_2\text{O}_3/\text{La}_2\text{O}_3$  content before and after ball-milling treatment was characterized. The microstructure and mechanical properties were measured.

### 2 FABRICATION AND CHARACTERIZATION

SiC powder ( $D_{50}=16\ \mu\text{m}$ ) and BN powder ( $D_{50}=3.5\ \mu\text{m}$ ).  $\text{La}_2\text{O}_3$  powder ( $D_{50}=1\ \mu\text{m}$ ) and  $\text{Al}_2\text{O}_3$  powder ( $D_{50}=45\ \mu\text{m}$ ) were applied as sintering aids. The weight ratio of SiC and BN were 6:4.  $\text{Al}_2\text{O}_3$  and  $\text{La}_2\text{O}_3$  were chosen as sintered aids for fabrication of SiC/BN ceramics with molar ratio were 1:1. The total amount of the sinter additions was varied from 6wt% to 15wt% in the mixture. The aids content of hot-pressed specimens were 6wt%, 9wt%, 12wt% and 15wt%, which were

designated as S6, S9, S12 and S15, respectively. The mixture powders were refined by a wet ball milling for 8 h using SiC balls in absolute ethanol. After milling, ethanol was cleared by applying a co-evaporating method to decrease segregation during the drying process. Then, the dried mixtures were put into a graphite mold with an inner diameter of 40 mm and an outer diameter of 100 mm, and then sintered by a vacuum hot-press furnace (Multi functioned 5000 type, in Japan), at 1900°C for 40 min under a pressure of 30 MPa in argon gas. The heating rate was executed with 15°C/min from room temperature to 1900°C. The specimens together with graphite mold were cooled to ambient temperature. The specific mass was determined according to Archimedes method. The phase constitution was identified by XRD and micro-structure was investigated by SEM. At least four bars were tested for each test condition. A minimum of fifteen indentation tests were performed for each condition of material and temperature. Vickers Hardness (HV) (in GPa) was calculated as:

$$HV = 0.0018544 \left( \frac{P}{a^2} \right)$$

where  $P$  is the load (in N) and  $d$  is the average length of the two diagonals (in mm).

### 3 RESULTS AND DISCUSSION

#### 3.1 Powder morphology before and after ball-milling

The received powders before and after ball-milling were given in Fig. 1. The SiC and Al<sub>2</sub>O<sub>3</sub> powders were

all big grains (Fig. 1a) and c)). While the BN and La<sub>2</sub>O<sub>3</sub> were small grains (Fig. 1b) and d)). After ball-milling treatment, SiC/BN/La<sub>2</sub>O<sub>3</sub>/Al<sub>2</sub>O<sub>3</sub> mixtures were homogeneous even if the aids were different. From SEM result, it can be seen that the ball-milling treatment would improve the uniformity of powder mixture and refine the powder granularity.

#### 3.2 Phase constitution analysis

Fig.2 showed XRD patterns of SiC-BN composites prepared by combustion synthesis under different aids content. It can be found that the main phases in the composites were h-BN and SiC. Small quantities of react-formed LaAlO<sub>3</sub> were found in the sintered specimens. The received materials were La<sub>2</sub>O<sub>3</sub> and Al<sub>2</sub>O<sub>3</sub>, so the LaAlO<sub>3</sub> was formed during the sintering process by means of the reaction between La<sub>2</sub>O<sub>3</sub> and Al<sub>2</sub>O<sub>3</sub>. At the same time, the received powders were not detected according to the analysis of the XRD pattern. As the molar

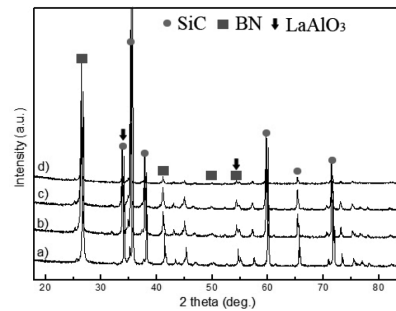


Figure 2. XRD patterns of SiC-BN composites with different aid content.

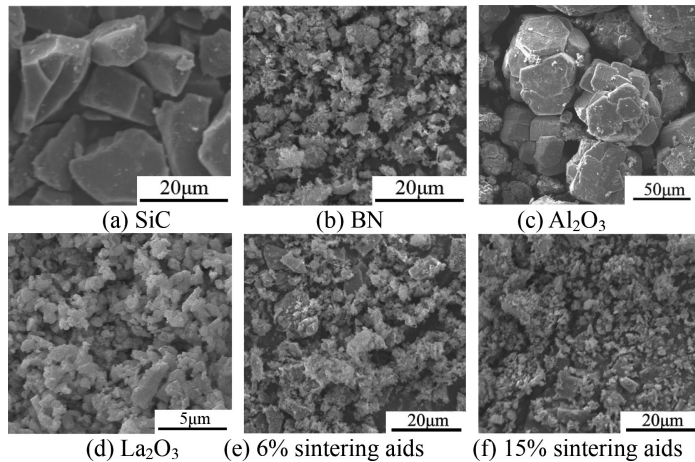


Figure 1.

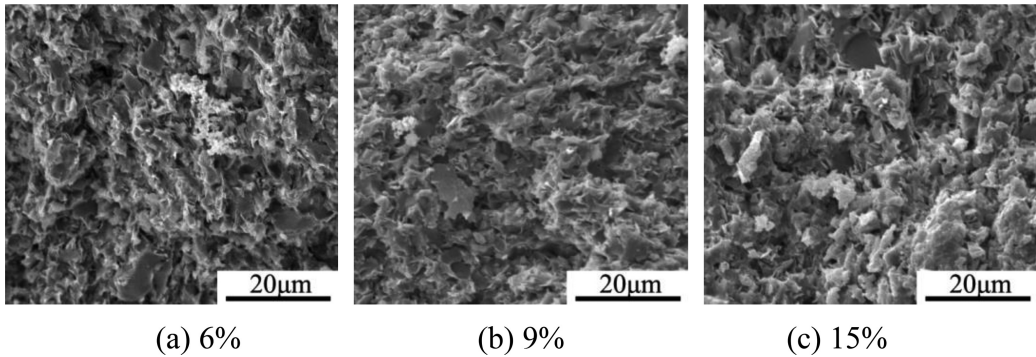


Figure 3.

Table 1. Comparison of properties of SiC/BN composites with different aids content.

Specimen denominated	Theoretical density (g/cm <sup>3</sup> )	Relative density (%)	Vickers Hardness (GPa)	Bending strength (MPa)
SA6	2.856	99.1	2.68 ± 0.11	204
SA9	2.895	98.8	2.84 ± 0.09	219
SA12	2.935	98.7	2.14 ± 0.05	208
SA15	2.975	97.8	1.87 ± 0.07	186

ratio of La<sub>2</sub>O<sub>3</sub> and Al<sub>2</sub>O<sub>3</sub> was 1:1, the reaction between La<sub>2</sub>O<sub>3</sub> and Al<sub>2</sub>O<sub>3</sub> can be formed LaAlO<sub>3</sub>. In this work, the additional Al<sub>2</sub>O<sub>3</sub> was excess in the original powders, nevertheless, Al<sub>2</sub>O<sub>3</sub> phase can not be detected from the XRD pattern. It was the possible reason that the gasification and evaporation process occurred during the sintering process.

### 3.3 Fracture morphology of SiC-BN composites

Fig. 3 showed fracture morphology of BN-SiC ceramic composites prepared with different aid content. Large amount of flake-like BN with diameter of about 2–10 μm and thickness of a few hundred nanometers can be observed. The equiaxed SiC grains embedded between the plate-like BN phases. Due to flake-like structure and strong covalent bond of BN phase, it was difficult to obtain full-density BN-SiC products. In general, high pressure, high temperature and/or sintering aids were applied to improve the density. There were mainly two reasons contributing to densification improvement of BN-SiC ceramic composites. Firstly, high loaded pressure and reaction temperature during the sintering process promoted sintering and densification behavior of the SiC-BN products. Secondly, formation of liquid eutectic phase LaAlO<sub>3</sub> during reaction synthesis process facilitated densification of BN-SiC ceramic.

### 3.4 Basic properties of SiC/BN composites

The comparison of properties of SiC/BN composites with different aids content of in the starting mixture was listed in Table 1. With increase of sintering aids, theoretical density enhanced, which varied from 2.856 g/cm<sup>3</sup> to 2.975 g/cm<sup>3</sup>. But the relative density reduced when the sinter aids increased. For all the specimens, relative density was higher than 97%, so hot press sintering method was benefit to promote densification in the sintering process. The Vickers hardness increased first and then reduced. The maximum value of the Vickers hardness for the SiC/BN composites was about 2.84 ± 0.09GPa. In the present work, the weight proportion between SiC and BN was constant, which was kept in 60:40. As the sinter aids reached at 9%, the optimal hardness can be obtained. The similar trend can be found in the bending strength property of SiC/BN composites. The maximum value of bending strength for SiC/BN composites was about 219 MPa. It was notable that the effect of aids content on the Vickers hardness and bending strength for the all sintered material was not obvious for SiC/BN composite. So we can draw to a conclusion that the variation for Vickers hardness and bending strength of SiC/BN composites was not obvious under the condition of the difference of the sintering additives.

## 4 CONCLUSION

SiC/BN ceramics composites were fabricated by hot-press sinter technology at 1950°C by means of protective argon gas and Al<sub>2</sub>O<sub>3</sub> combined with La<sub>2</sub>O<sub>3</sub> served as sintering aids in the present investigation. The effect of Al<sub>2</sub>O<sub>3</sub>/La<sub>2</sub>O<sub>3</sub> aids content on the micro-structure, crystal phases and density evolution, Vickers hardness and bending strength were surveyed. The results showed that Al<sub>2</sub>O<sub>3</sub>/La<sub>2</sub>O<sub>3</sub>

compound sintering aids were effective for promoting densification of SiC/BN composites. The interaction and balance of the aforementioned SiC/BN/La<sub>2</sub>O<sub>3</sub>/Al<sub>2</sub>O<sub>3</sub> mixtures resulted in the differences of micro-structure and sintering behavior for the SiC/BN composites.

#### ACKNOWLEDGEMENT

The authors were grateful for support by Chinese Postdoctoral Science Foundation (No. 2012M520754) and the science and technology innovation team of Jiamusi University (No. Cxt-d-2013-03).

Correspondence should be addressed to Yu-Min ZHANG; zhym@hit.edu.cn.

#### REFERENCES

- [1] Kim Y, Chun Y, Nishimura T, Mitomo M and Lee Y 2007 *Acta Mater.* 55:727.
- [2] Zhang X, Yang Q and Jonghe L 2003 *Acta Mater.* 51:3849.
- [3] Fernandez J, Munoz A, Lopez A, Feria F, Rodriguez A and Singh M 2003 *Acta Mater.* 51:3259.
- [4] D. Hasselman, P. Becher, K. Mazdizyani, *Z. Werkstofftech.* 11 (1980):82–92.
- [5] T. Kusunose, Y.-H. Choa, T. Sekino, K. Niihara, *Key Eng. Mater.* 161–163 (1999):475–480.
- [6] P. Valentine, A. Palazotto, R. Ruh, D. Larsen, *Adv. Ceram. Mater.* 1 (1986):81–87.
- [7] K. Mazdizyani, R. Ruh, E. Hermes, *Am. Ceram. Soc. Bull.* 64 (1985): 1149–1154.



# Optimization of electric vehicle charging infrastructure and model simulation through the Jeju electric vehicle demonstration project

Jauk Gu & Jongho Lee

Master's Course, Ajou University, Suwon, Korea

Jooyeoun Lee

Ajou University, Suwon, Korea

**ABSTRACT:** Electric vehicles have recently gained attention worldwide due to environmental issues. As such, technological trends are moving towards electric engines and away from combustion engines. Despite efforts in Korea to catch up with trends of electric vehicles, there is a long way to go. This study assumes the issue lies with the charging infrastructure and suggests the optimal number and location of charging stations by using the P-Median Algorithm. By reviewing the electric vehicle charging details in 2013 such as the location, major hubs, charging time and customer patterns (frequency of usage), the location of EV charging stations can be forecast through a model for simulation. Moreover, a comparative analysis of existing data and data since 2013 will help verify this algorithm.

**Keywords:** selecting location, p-median algorithm, EV infrastructure, model simulation

## 1 INTRODUCTION

### 1.1 Research background

To minimize global warming and climate change, regulations on carbon dioxide emissions have strengthened, leading to more awareness.

With recent trends in Smart Transportation, the auto industry paradigm is expected to drastically change due to environmental and energy issues. EV infrastructure such as Electric Vehicles, EV Charging Infrastructure and Total Operation Center is becoming important.

This can be seen in the EV trends at home and abroad. Trends in EV in Korea (Figure 1) show that in 2020, the distribution of EV is expected to have grown by 30 fold compared to 2015. EV trends overseas (Figure 2) show a year on year increase in distribution for Europe, USA, China and Japan, too.

Governments around the world set various subsidy plans for distribution which will promote penetration of EV further.

Many efforts were made in Korea to catch up with technology and supporting policies for EV, but without the establishment of an EV Charging Infrastructure, the benefits have been limited. Therefore, the location and number of charging stations must take into account the convenience of customers in order to promote further distribution.

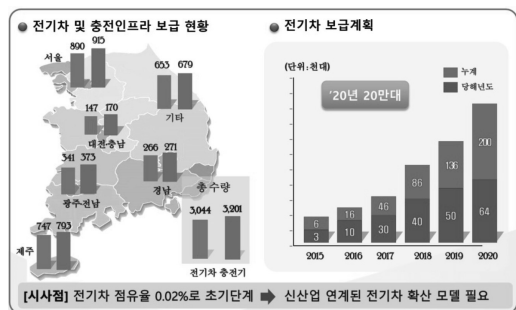


Figure 1. Domestic international electric vehicle supply situation and plans.



Figure 2. International electric vehicle supply situation and plans.

## 1.2 Research objectives

This paper suggests an optimization of charging infrastructure by removing unnecessary stations and re-allocating them to other areas by presenting an optimal number and type for charging stations.

As such, the data that analyzes the charging history in the 2013 Jeju empirical project and the p-median algorithm that determines the optimal location of the stations were used. The correlation between the charging history data and the location data was also analyzed for the optimal number and types of stations.

A comparison of the suggested charging station and actual charging stations since 2013 was used to measure the location accuracy of the Algorithm and verify the Algorithm.

After the study, the suggested data will be used for Arena simulation program to compare the simulation results and actual data, in order to verify the accuracy (customer usage quantity and pattern) of the Algorithm.

## 2 RELATED RESEARCH

Domestic studies on location selection are as follows.

Choi Seong-Beom, Han Tae-Yong. (2014) suggested heuristic algorithm for the p-median question to determine the optimal location of sports goods stores. The applicability of the suggested method was evaluated with a focus on cases.

Sang-Un Lee. (2015) used the P-median Algorithm to increase the node first before exchanging the node to address the shortcomings of the existing Myopic Algorithm.

Young-Hoon Kim. (2009), in association with the population census categorization issue, suggested the leading algorithm used for resolving the P-median issues and Cooper search heuristic. To that end, he set virtual blocks for census output areas to discuss the applicability and the results of the search using the P-median Algorithm.

Park Bora, Lee Kyu Jin, Choi Keechoo (2013) used the Heuristic P-median Algorithm in selecting the optimal location of bicycle parking lots and presented models in accordance with the presence or lack of a budget. Through a comparison with the actual location of bicycle parking lots, the Algorithm was verified.

Council, P. S. R. (2010) used cases where EV infrastructure was built to explain the technologies and characters needed for infrastructure establishment and charted a graph of the charging hours or inconveniences experienced by customers to visualize points that need to be considered when establishing an EV infrastructure.

Existing studies that use p-median algorithm minimized cost to find the optimal location. Cost here includes distance and number of residents. However, the information available on the Jeju project's charging stations is the charging details of customers. Therefore, to build an optimal charging infrastructure, the concept of variables, that is, the cost, must change. The variables of existing residents indicate the number of consumers or the consumption quantity. As such, in this study, it is defined as the usage quantity of the charging station (amount charged, frequency of charging). The usage quantity of charging station will have the weight adjusted through a correlation analysis between the amount charged and the charging frequency. The data will be standardized to make a uniform indicator. Distance is defined as the distance between existing charging stations and candidate charging stations so that the usage amount of existing charging stations can be minimized while the distance with the existing charging stations would be as close as possible. This would help distribute customers and help with more convenient services, while reducing the peak energy and distributing the power consumption to a more stabilized level.

The number and types of charging devices within the charging station will be concluded with an optimal value through an analysis of the customer charging pattern. Analysis of charging patterns will be done with a focus on the statistical data from customers over the one-year period of 2013.

In addition, establishing such an EV infrastructure is expected to help with energy distribution for V2G (Vehicle to Grid) infrastructure at a later date.

## 3 RESEARCH METHOD

### 3.1 Research directions

Before the study, there were a total of 17 charging stations for the Jeju EV empirical project in 2013, distributed across the entire Jeju Island. However, as seen in (Figure 3), the stations are mostly concentrated in 3 areas. As such, Jeju Do Province Office of Jeju City where there were a total of

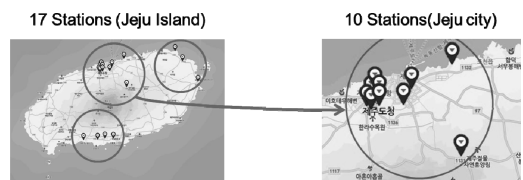


Figure 3. Set the range of data analysis.

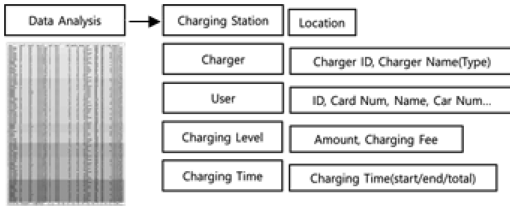


Figure 4. Data mining, standardization.

10 stations was selected as the study subject area. As seen in (Figure 4), the charging history data for the 2013 Jeju EV empirical project was categorized and standardized.

Basically, charging station refers to location. In addition, for charger and users, an identification card, name and type were standardized and only 'user' and 'charger ID' were used.

The correlation between the charging level of users and their charging time at a Charging Station was analyzed. Here, each charging station selects a nearby candidate location based on users' usage patterns.

### 3.2 Data analysis

Specifically, there were two categories for data analysis.

First, the selection of the location for a charging station. For this, the data needed to get the number of charging stations per region and the distance between each charging stations were extracted and the correlation between the data were analyzed. Since this paper only addresses one area (Jeju City), the number of charging stations per region may not be significant but it is nonetheless essential for comparing with data since 2013 and to expand the range. To conclude the optimal number of charging stations per region and the distance between stations, the charging time/duration pattern of the charging customer needs to be analyzed to see which charging stations are most used, which times they are most used (during work hours or after work on their way home) and how many number of charges were done. In doing so, the location of the charging station can be concluded. That is, the customer, charging time, location and number of charges were analyzed for each station and weights were given to each station for standardization. The data thus analyzed were used to select the optimal location through the P-median Algorithm.

Secondly, there is the issue of locating the charging device within the charging station. To determine the number of charging device per charging station and the type of charging device, the usage frequency for charging devices for a given station and charging time need to be analyzed. Rather

than use a special methodology for this, the usage frequency and charging time data since 2013 were used to forecast specific goals.

### 3.3 P-median algorithm

This study makes use of the correlation between existing customers and service providers to optimize the location selection while minimizing cost. However, if only the correlation between customer and service provider is used, regions that are highly populated there would automatically be a high number of service providers. Therefore, in order to select the location of new service providers that can minimize the demand for existing service providers and for distance, the algorithm was adjusted as seen in Figure 5. As such, hi can improve convenience by minimizing the indicator that was made with the customer data that we had analyzed earlier from charging stations and by distributing customers. The distance with existing service providers, too, is also minimized so that in areas where there is large demand the service provider would be located further apart to minimize unnecessary charging stations in advance. Based on the results of using this algorithm, that is, based on the selected location, Arena Simulation program will be used to reduce as much as possible the errors.

### 3.4 Research plans

Through this study, using the P-median method, the location selection of EV charging stations in Jeju city will be carried out. Studying heuristic methods that can resolve issues with the P-median will help improve the accuracy of selecting the

#### P-Median Algorithm

##### Inputs

- $h_i$  = Demand for existing stations
- $d_{ij}$  = Distance of an existing station with the new station
- $p$  = The number of new stations

##### Decision Variables

- $x_j = \begin{cases} 1, & \text{If the charging station has been installed in the node } j \\ 0, & \text{else} \end{cases}$
- $y_{ij} = \begin{cases} 1, & \text{When meeting the demands of the facility of node } i \text{ to node } j \\ 0, & \text{else} \end{cases}$

Subject to  $M \leq \sum_i \sum_j h_i d_{ij} y_{ij}$

$$\sum_j y_{ij} = 1 \quad (\text{for all } i)$$

$$\sum_j x_j = p$$

$$y_{ij} \leq x_j \quad (\text{for all } i, j)$$

$$y_{ij} \in \{0, 1\} \quad (\text{for all } i, j)$$

$$x_j \in \{0, 1\} \quad (\text{for all } j)$$

Figure 5. P-median algorithm.

optimal location. Moreover, a more detailed categorization of conditions that give weights to certain data or characteristics of variables will help increase the importance of correlation between data and thus increase accuracy.

In selecting the location of charging stations, data over one year may not be sufficient to guarantee accuracy. Therefore, based on the data from 2013 used in this study, the algorithm will be configured, but the data before 2013 and after 2013 will be compared and analyzed to further refine and revise the algorithm. The location selection results using the 2013 data will be applied to simulation to compare with the actual data since 2013 for verification of the algorithm. As a follow-up, an algorithm that takes into account other variables such as establishment costs and landmarks will also be developed.

#### 4 CONCLUSIONS

This study determined that one of the major issues in promoting further distribution of electric vehicles was the charging infrastructure that did not consider customer convenience. As such, using the engineering analytical method of the P-median Algorithm, it seeks to suggest a method of selecting the most optimal location for EV charging stations.

This study analyzes the EV operation data currently in use in Jeju City and sets the weights through a review of the correlation between the analyzed data so that the usage amount of each charging station can be seen as an indicator that

sets the demand quantity. Along with this demand quantity, the distance between the existing charging station and new charging station was minimized to select the optimal location.

By using a correlation between the existing service provider and the new service provider and not the P-median using the correlation between existing customers and service providers, the saturation or over-concentration of service providers can be resolved. It is also expected that relocation selection can be supported for unnecessary service providers.

A comparative analysis of this study's results and the data from after 2013 will help verify the algorithm, while follow-up simulation programs can be used to reduce the margin of error for the development of a more accurate algorithm.

#### REFERENCES

- [1] Choi, Seong-Beom, Han, Tae-Yong. (2014). Decision of p-Sports Shops Location Using p-Median Method. *The Korean Society Of Sports Science*, 23(3), 855–863.
- [2] Sang-Un Lee. (2015). A Constructive Algorithm for p-Median Facility Location. *Journal of the Korea Society of Computer and Information*, 20(6), 77–85.
- [3] Young-Hoon Kim. (2009). Applying a p-median algorithm to zone design problems. *Journal of the Korean Cartographic Association*, 9(2), 73–80.
- [4] Park Bora, Lee Kyu Jin, Choi Keechoo (2013). Optimum Location Choice for Bike Parking Lots Using Heuristic P-Median Algorithm. *KOREAN SOCIETY OF CIVIL ENGINEERS*, 33(5), 1989–1998.
- [5] Council, P. S. R. (2010). Electric Vehicle Infrastructure.

# Research on the impact of the fault's thickness on underground roadways

Man-hua Zhang & Pan Wang

*School of Civil and Environmental Engineering, University of Science and Technology Beijing, Beijing, China*

Li-li Shao

*College of Resources and Safety Engineering, China University of Mining and Technology (Beijing), Beijing, China*

**ABSTRACT:** Engineering geological conditions in underground mines are complex, which usually have fault zones at different scales. Some roadways have to be placed under the faults for mining a valuable ore. The thickness of faults is one of the important factors that control the stability of roadways. This paper tries to analyze the impact of the fault's thickness on underground roadways. For this purpose, 10 numerical models were designed and the thickness of the fault was varied from 2 m to 20 m, with an interval of 2 m. For comparison, the simulation of the model without fault was performed. The maximum displacements in these roadways were compared with each other. The results of the numerical simulation indicated that when the roadway was placed under the fault, the fault had an obvious impact on the displacement of the tunnel. However, when the thickness of the fault was greater than 10 m, the fault had a similar impact on the displacement of the roadway. The Z-displacement was more sensitive to the fault above the tunnel than the X-displacement, and the upper corners of the roadway had larger deformations. Therefore, when the roadway is designed under the fault, the roof of the tunnel should be strengthened to support.

**Keywords:** Fault; roadway; underground mines; displacement

## 1 INTRODUCTION

Faults are complex zones composed of linked fault segments, one or more high strain slip surfaces nested within regions of high and low strains, Riedel shears, splay faults, dilatational and constructional jogs, and relay ramps (D.R. Faulkner et al. 2010). Fault zones control a wide range of crustal processes, which have a controlling influence on the crust's mechanical property (Zoe.K. Shipton. 2010). Engineering geological conditions in underground mines are complex, which usually have fault zones at different scales (Xun Xi et al. 2015). To exploit a valuable ore more effectively and economically, mining engineers have to design some roadways under faults. When tunnels are arranged under the fault and the distance between the fault and the tunnel is short, the fault plays an important role in controlling the displacement of tunnels. Therefore, it is necessary to analyze the impact of faults on underground roadways in different scales. Some scholars have tried to analyze the stability of tunnels in fault zones by performing physical and

numerical simulations, geological structural surveys and direct monitoring (Dawers, N.H. & Anders, M.H. 1995, Cox et al. 2001, Sibon. 2001, Aydin et al. 2004, Seokwon et al. 2004, Zhong et al. 2008).

The thickness of faults is one of the important factors that control the stability of roadways. This paper tries to analyze the influence of the fault's thickness on underground roadways. To this end, 10 numerical models were designed and the thickness of the fault was varied from 2 m to 20 m, with an interval of 2 m. The maximum displacements in these roadways were compared with each other.

## 2 DESIGN OF SIMULATION MODELS

To analyze the impact of the fault's thickness on underground roadways, the roadway was designed under the fault and the distance between the fault and the roof of the tunnel was set as 2 m. The thickness of the fault was varied from 2 m to 20 m. The description of the fault and the roadway is shown in Figure 1.

The numerical simulation model was 60 m in height, 50 m in width and 50 m in length (Figure 2). It was divided into 124,299 zones and 23,296 grid points. The shape of the tunnel was a three-centered arch. The faults with different thicknesses were achieved by changing the mechanical parameters of zones in different locations. The parameters of the fault and the rock are described in Table 1. The stress condition in these models was set up as  $S_{XX} = 30$  MPa,  $S_{YY} = 25$  MPa, and  $S_{ZZ} = 20$  MPa.

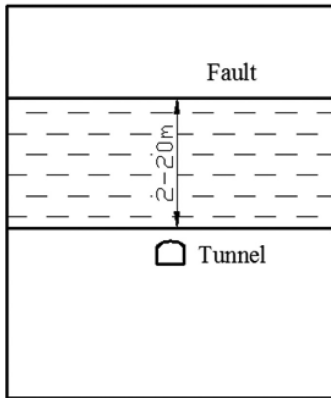


Figure 1. Description of the fault and the tunnel.

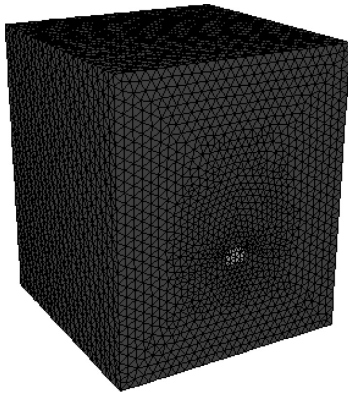


Figure 2. Numerical simulation model.

### 3 NUMERICAL SIMULATION AND ANALYSIS

A Mohr–Coulomb tunnel excavation model was built using the numerical software FLAC3D. FLac3D has become one of the most important tools for calculating rock mechanics problems since its introduction by ITASCA Company. The Mohr–Coulomb model is suitable for analyzing the mechanical behavior of normal soil and rocks.

The contour images of displacement can reflect the stability of the tunnels under the fault. The lateral displacement and vertical displacement are the most important index for analyzing the impact of the fault on underground roadways. So we show the contour images of the X-displacement and Z-displacement. For comparison, we also show the simulation results of the model without fault (Figure 3). Because of the space constraints, only two typical images of the 10 models are shown, in which the thickness of the fault are 2 m and 20 m (Figure 4 and Figure 5, respectively).

In the model without fault, the maximum Z-displacement of the roadway was nearly 1cm smaller than the maximum X-displacement. In the model with fault, both the maximum X-displacement and Z-displacement of the roadway became larger. However, the Z-displacement of the roadway had a great increase. In the model with fault, both the maximum X-displacement and Z-displacement of the roadway under faults were about 3 cm. The maximum Z-displacement of the roadway was a little larger than the maximum X-displacement. Thus, the Z-displacement was more sensitive to the fault. In other words, the faults had a greater influence on the vertical displacements of the roadway. From the contour images of the X-displacement, we can see that the faults existing above the roadways make the rock mass deform deeply and the upper corners of the roadway have larger deformations. The faults above the roadways have an obvious impact on the deformation of the roof of the tunnel.

As shown in Figure 6, with the increasing thickness of the fault, both the X-displacement and Z-displacement of the roadways are obviously increased, with the Z-displacement increasing more rapidly. The thickness of the fault has an

Table 1. Parameters of the rock and the fault.

Group	Density/ ( $\text{kg} \cdot \text{m}^{-3}$ )	Bulk modulus/ GPa	Shear modulus/ MPa	Internal friction angle/( $^{\circ}$ )	Cohesion/ MPa	Tensile strength/ MPa
Fault	1707	0.221	0.113	14.6	0.0901	0.0164
Rock	1595	2.33	1.18	28.1	33.2	5.11

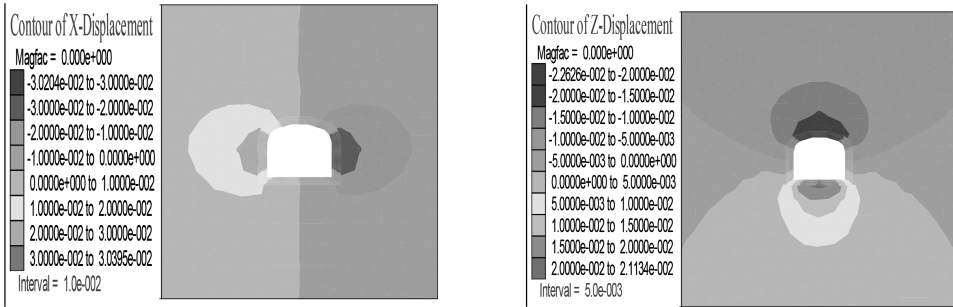


Figure 3. Contour images of the X-displacement and Z-displacement (no fault).

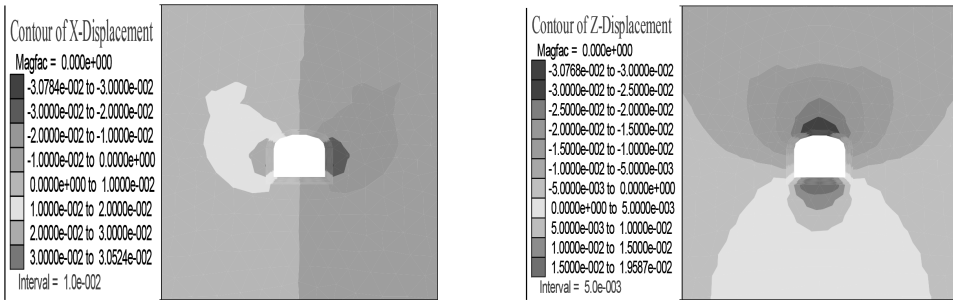


Figure 4. Contour images of the X-displacement and Z-displacement (the thickness of the fault is 2 m).

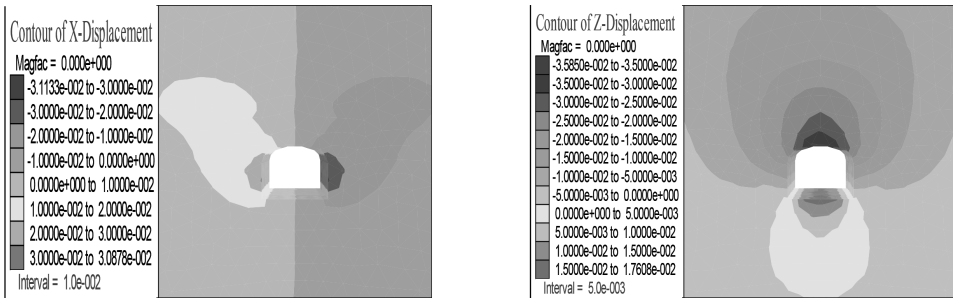


Figure 5. Contour images of the X-displacement and Z-displacement (the thickness of the fault is 20 m).

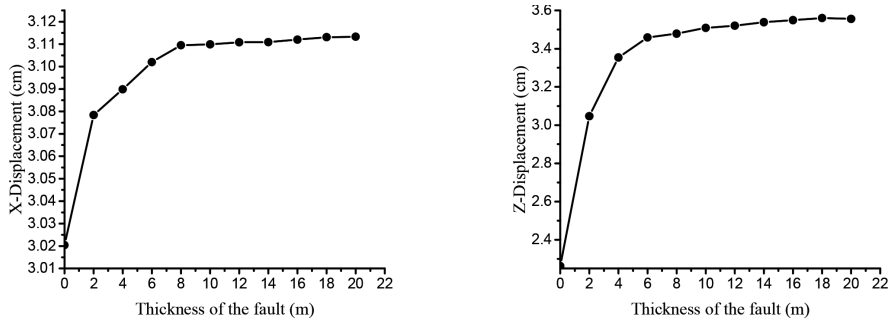


Figure 6. The maximum displacements of tunnel in different distances.

obvious impact on the roadways. However, when the thickness of the fault is greater than 10 m, the rate of increase of displacements becomes slow. We can see that large faults greater than 10 m have a similar impact on the stability of underground roadways.

#### 4 CONCLUSIONS

There are different scales of faults in underground mines, and some roadways have to be designed under the faults to exploit a valuable ore. To ensure that the roadways under the faults are stable, it is necessary to study the impact of the faults' thickness on roadways. By the numerical simulations of faults with different thicknesses and analyzing the displacements of roadways, the following conclusions can be summarized:

1. When the roadway was placed under the fault, the fault had an obvious impact on the displacement of the tunnel. The Z-displacement was more sensitive to the fault above the tunnel than the X-displacement.
2. The upper corners of the roadway had larger deformations when the fault was above the roadway. Therefore, when the roadway is designed under the fault, the roof of the tunnel should be strengthened to support.
3. With the increasing thickness of the fault, the displacement of the fault was also increased. However, when the thickness of the fault was greater than 10m, the fault had a similar impact on the displacement of the roadway.

#### ACKNOWLEDGMENTS

This work was financially supported by the Fundamental Research Funds for the Central Universities (FRF-TP-14-038A).

#### REFERENCES

- Aydin A., A. Ozbek., I. Cobanoglu. 2004. Tunneling in difficult ground: a case study from Dranaz tunnel, Sinop, Turkey. *Engineering Geology* 74(3-4): 293-301.
- Cox, S.F. et al. 2001. Principles of structural control on permeability and fluid flow in hydrothermal systems. *Reviews in Economic Geology* 14, 1-24.
- Dawers, N.H. & Anders, M.H. 1995. Displacement-length scaling and fault linkage. *Journal of Structural Geology* 17 (5): 607.
- Faulkner D.R. et al. 2010 A review of recent developments concerning the structure, mechanics and fluid flow properties of fault zones. *Journal of Structural Geology* 32(11): 1557-1575.
- Seokwon Jeon et al. 2004. Effect of a fault and weak plane on the stability of a tunnel in rock—a scaled model test and numerical analysis. *International Journal of Rock Mechanics & Mining Sciences* 41(S1): 486.
- Xun Xi et al. 2015. Comprehensive monitoring and stability assessment of roadway with water gushing in a fault zone. *Electronic Journal of Geotechnical Engineering* 20 (9): 9685-9700.
- Zhong Nong et al. 2008. Geological guarantee and construction controlling technique of main roadway crossing fault zone with 435 m fall. *Chinese Journal of Rock Mechanics and Engineering* 27 (Supp.1): 3292-3297 (In Chinese).
- Zoe K. Shipton. 2010. Fault zones: A complex issue. *Journal of Structural Geology* 32(11): 1554-1556.



## Study on the selection of adaptable plants in the area polluted with lead–zinc tailings in Hunan Province

Qiong Wang, Wei Sun & Liang-liang Wu

Beijing General Research Institute of Mining and Metallurgy, Beijing, China

**ABSTRACT:** Phytoremediation is a very effective way to remedy a heavy metal-polluted site. The investigations and tests conducted on the vegetation and plants of the Qiaokou & Yongxing Peng lead–zinc tailing area in Zixing City, Hunan Province shows that (a) herbs have a perfect ability to adapt to the area polluted with lead–zinc tailings, (b) the absorption capacity towards heavy metals by plants is mutually influenced by the genetic factor and environmental domestication; (c) *Caulis Fici Tikouae*, *Lespedeza bicolor* Turcz. and *Lolium perenne* L. have the perfect ability to migrate and absorb lead and zinc, and could be used for ecological restoration at the lead and zinc-polluted site.

**Keywords:** heavy metal pollution; lead–zinc tailings; plant selection; ecological restoration

### 1 INTRODUCTION

Some areas in which tailings left over by previous mining activities are stacked disorderly have serious heavy metal pollution. The content of heavy metals is high and the composition is complex; thus, selection of dominant plants that absorb and are tolerant to heavy metals in the tailing pollution site is of great significance. At present, the most widely used remedial measures for a heavy metal-polluted soil are mainly physical and chemical methods, such as the soil dressing method, the extraction method, the improvement method, the leaching method, etc. However, these methods have high costs and complex treatment processes, and are difficult for large-area pollution control. In contrast, the phytoremediation uses the plants ability to migrate and absorb some heavy metal elements, and transfer the heavy metal-polluted soil to plants for ecological recovery and pollution control<sup>[1-2]</sup>. As a safe, reliable, and low-cost ecological restoration method with a good effect, the phytoremediation technology has received more attention. Therefore, screening of plants that can absorb and be tolerant to heavy metals is of great significance.

Plants growing in the mining area, mineralization belt, and heavy metal-polluted site are highly tolerant to the pollution of heavy metals; therefore, an investigation on plants growing on an abandoned land in the mining area is one of the effective ways to look for plants that are tolerant to heavy metals. In this study, plants and soil of the Qiaokou & Yongxing Peng lead–zinc tailing area of Dongjiang Lake in Zixing City, Hunan Province

were measured and analyzed. Furthermore, tolerant plants in Hunan lead–zinc tailings area were preliminarily screened, in order to provide a reference for the ecological management of lead–zinc tailings in Hunan Province.

### 2 MATERIALS AND METHODS

#### 2.1 Summary of the investigation area

The field vegetation survey was conducted from the spring to the fall of 2015. The sampling area was the Qiaokou & Yongxing Peng lead–zinc tailing area of Dongjiang Lake in Zixing City, Hunan Province and the surrounding polluted area. The drainage basin of Dongjiang Lake has subtropical humid monsoon climate, four distinctive seasons and receives abundant rain. Its annual average temperature is 17.7°C and annual average rainfall is 1,487.6 mm. It usually rains from March through June and in the month of August. During summer, southern winds prevail, and in winter, northern winds prevail. Its annual average sunshine duration is 1,700 hours.

#### 2.2 Sampling and determination

According to the distribution of waste accumulation points in the mining area, the serpentine distribution method was used to set twelve 10 m × 10 m quadrats from the central area to the outside of the tailing pond. Plant samples in the quadrats were collected, and dominant plants were recorded. The overground and underground parts of herba-

ceous plants and small shrubs were collected. The leaves and branches of tall trees were also collected. Three repetitions were collected for each sample. At the same time, around the plant root system, soil samples from a depth of 0–20 cm were collected. The soil was dried indoor, and stones, plant roots and litters were removed from it. The soil was screened with a 0.6 mm sieve for the determination of heavy metal content. The plant samples were washed with water, leached twice with deionized water, dried in the oven at a temperature of 80°C, and crushed for the determination of heavy metal content. The soil samples were boiled with concentrated HNO<sub>3</sub>–H<sub>2</sub>O<sub>2</sub> (EPA 3050B), and the plant samples were boiled with HNO<sub>3</sub>–HClO<sub>4</sub>. Arsenic content was determined using atomic fluorescence spectrometry. The contents of Cu, Pb, Zn, Cr, Cd, and other heavy metals were determined using atomic absorption spectrometry. Furthermore, the national standard plant sample (GSV-3) and the national standard soil sample (GSS-1) were added for analysis and quality control.

### 3 RESULTS AND ANALYSIS

#### 3.1 Vegetation characteristics of lead–zinc tailing pollution site

Because of the low content of organic matter, total N, available P, and available K in lead–zinc tailings, poor soil and water retention ability, high pH value, high heavy metal content and other factors, it is very important to complete vegetation restoration and breed adaptable and tolerant plants on the tailing site. In the breeding process of tolerant plants, the investigation on natural colonized plants growing on the tailing site is of great significance [3–10]. In general, most natural colonized plants on the tailings pollution site are tolerant plants. This survey found that in the Qiaokou & Yongxing Peng lead–zinc tailing area, a total of 46 kinds of plants were collected, which belonged to 16 families and 43 genera (Table 1), including 14 kinds of gramineous plants, 15 kinds of composite plants, two kinds of Cyperaceae plants and Moraceae plants, and one kind of Moraceae, Abiatae, Anacardiaceae, Verbenaceae, Phytolaccaceae, Portulacaceae, Caprifoliaceae, Pteridaceae, Plantaginaceae, Oxalidaceae, Urticaceae, Commelinaceae, and leguminous plants. From the above survey, we can conclude that plants growing in and around the Qiaokou & Yongxing Peng lead–zinc tailing area are mainly gramineous plants and composite plants. Gramineous plants account for 31.11% of the total number of species, followed by composite plants accounting for 33.33%. Gramineous plants with strong reproduction ability are resistant to barrenness, drought and heavy metals, and composite plants have a good ability to adapt to the

environment and transmit their seeds. Therefore, both gramineous and composite plants are dominant plants in the Qiaokou & Yongxing Peng lead–zinc tailing area.

Among the 45 kinds of plants collected in the Qiaokou & Yongxing Peng lead–zinc tailing area, according to the relative density, relative frequency, relative abundance, and coverage of plants, 10 kinds of dominant plants in the sample area during the sampling were determined (Table 2). They include *Lolium perenne* L., *Vetiveria zizanioides* L., *Miscanthus floridulus* Schum., *Festuca arundinacea*, *Phytolacca americana*, *Coryza canadensis* (L.), *Artemisia lavandulaefolia* DC, *Ficus tikoua*, *Rhus chinensis* and *Lespedeza bicolor* Turcz. The 10 kinds of plants appeared in the sample field investigated. Their relative density and relative frequency are high. They generally exist in the tailing pond and are identified as the dominant plants. There are seven kinds of herbaceous plants that account for 70.0%. It has been shown that herbaceous plants have strong adaptability and stress resistance to the harsh environment prevalent in the Qiaokou & Yongxing Peng lead–zinc tailing area. They are native plants that adapt to local climate conditions. Even in the places near the tailing pond with high content of pollutants, these plants can grow well. They have strong tolerance to heavy metals.

#### 3.2 Content of heavy metals and distribution characteristics of dominant plants

According to the survey of natural vegetation, 10 kinds of dominant plants were selected in the Qiaokou & Yongxing Peng lead–zinc tailing area. The contents of Zn, Pb, and Cd determined in the 10 kinds of dominant plants are presented in Table 3.

A large difference was found in the content of heavy metals among the 10 kinds of plants. The overground part of *Caulis Fici Tikouae* had the highest content of Pb. The average content was up to 215.26 mg/kg. The overground part of *Artemisia lavandulaefolia* DC had the lowest content of Pb. The average content was 4.45 mg/kg. The root of *Caulis Fici Tikouae* also had the highest content of Pb. The average content was up to 57.35 mg/kg. The root of horseweed herb had the lowest content of Pb. The average content was only 3.12 mg/kg. The overground part of *Rhus chinensis* had the highest absorption of Zn. The average absorption was 96.15 mg/kg. The overground part of the horseweed herb had the lowest content of Zn, which was only 45.33 mg/kg. The root of *Vetiver grass* had the highest content of Zn. The average content was up to 113.21 mg/kg. The root of *Rhus chinensis* had the lowest content of Zn. The average content was only 5.64 mg/kg.

Table 1. Species of plants growing in the Qiaokou &amp; Yongxing Peng lead-zinc tailing area.

Family	Specific name	Latin name	Category	Vegetational form
Gramineae	Crab grass	<i>Digitaria sanguinalis</i> (L.) Scop.	Digitaria	Annual herb
	Miscanthus floridulus	<i>Miscanthus floridulus</i> Schum.	Miscanthus	Annual herb
	Bermuda grass	<i>Cynodon dactylon</i> (Linn.) Pers	Cynodon	Perennial herb
	Ryegrass	<i>Lolium perenne</i> L.	Lolium	Annual herb
	Imperata cylindrica	<i>Imperata cylindrica</i> (Linn.)	Miscanthus	Perennial herb
	Green bristlegrass	<i>Setaria viridis</i> (L.) Beauv.	Setaria	Annual herb
	Eleusine indica	<i>Eleusine indica</i> (L.) Gaertn.	Eleusine	Annual herb
	Eragrostis curvula	<i>Eragrostis curvula</i> (Schrad.)	Eragrostis	Perennial herb
	Festuca arundinacea	<i>Festuca arundinacea</i>	Festuca	Annual herb
	Arundinella anomala	<i>Arundinella anomala</i> Steud.	Arundinella	Annual herb
	Reed	<i>Phragmites australis</i> Trin.	Phragmites	Perennial herb
	Paspalum natatum	<i>Paspalum notatum</i>	Paspalum	Annual herb
	Chloris virgata	<i>Chloris virgata</i> Swartz	Chloris	Annual herb
	Vetiver grass	<i>Vetiveria zizanioides</i> L.	Vetiveria	Perennial herb
	Compositae	Artemisia lavandulaefolia	<i>Artemisia lavandulaefolia</i> DC	Artemisia
Horseweed herb		<i>Conyza canadensis</i> (L.)	Conyza	Perennial herb
Chrysanthemum indicum		<i>Chrysanthemum indicum</i>	Chrysanthemum	Perennial herb
Aster		<i>Aster tataricus</i> L. f.	Aster	Perennial herb
Senecio		<i>Senecio scandens</i> Buch.-Ham.	Senecio	Perennial herb
Artemisia annua		<i>Artemisia annua</i> Linn.	Artemisia	Annual herb
Artemisia scoparia		<i>Artemisia scoparia</i> Waldst. & Kit.	Artemisia	Perennial herb
Solidago virgaurea		<i>Solidago decurrens</i> Lour.	Solidago	Perennial herb
Erigeron annuus		<i>Erigeron annuus</i> (L.) Pers.	Erigeron	Annual herb
Sticktight		<i>Bidens pilosa</i> L.	Bidens	Annual herb
Sonchus brachyotus		<i>Sonchus brachyotus</i> DC.	Sonchus	Perennial herb
Kalimeris herb		<i>Kalimeris indica</i>	Kalimeris	Perennial herb
Bidens tripartita		<i>Bidens</i>	Bidens	Annual herb
Wormwood		<i>Artemisia argyi</i> H. Lév. & Vaniot	Artemisia	Annual herb
Xanthium sibiricum		<i>Xanthium sibmcum</i>	Xanthium	Annual herb
Cyperaceae	Tristachya	<i>Carex tristachya</i>	Carex	Annual herb
	Golden fimbriatylis	<i>Fimbristylis hookeriana</i> Bocklr	Fimbristylis	Annual herb
Moraceae	Paper mulberry	<i>Broussonetia papyrifera</i> Linn.	Broussonetia	Deciduous tree
	Ficus tikoua	<i>Ficus tikoua</i>	Ficus	Woody climber
Labiatae	Selfheal	<i>Prunella vulgaris</i>	Prunella	Perennial herb
Anacardiaceae	Rhus chinensis	<i>Rhus chinensis</i>	Rhus	Deciduous tree
Verbenaceae	Thorns	<i>Vitex negundo</i> L. var. Rehd.	Vitex	Deciduous shrub
Phytolaccaceae	Radix phytolaccae	<i>Phytolacca americana</i>	Phytolacca	Perennial herb
Portulacaceae	Purslane	<i>Portulaca oleracea</i>	Portulaca	Perennial herb
Caprifoliaceae	Honeysuckle	<i>Lonicera japonica</i> Thunb.	Lonicera	Annual herb
Pteridaceae	Ciliate desert-grass	<i>Nephrolepis cordifolia</i> (L.) Presl.	Pteris	Perennial herb
Plantaginaceae	Plantain herb	<i>Plantago asiatica</i> L.	Plantago	Perennial herb
Oxalidaceae	Creeping oxalis	<i>Oxalis corniculata</i> L.	Oxalis	Perennial herb
Urticaceae	Ramie	<i>Boehmeria nivea</i> (L.) Gaudich.	Boehmeria	Perennial root subshrub
Commelinaceae	Dayflower	<i>Commelina communis</i>	Commelina	Annual herb
Leguminosae	Indigofera pseudotinctoria	<i>Indigofera pseudotinctoria</i>	Indigofera	Deciduous shrub
	Lespedeza	<i>Lespedeza bicolor</i> Turcz.	Lespedeza	Deciduous subshrub

The overground part of *Caulis Fici Tikouae* had the highest absorption of Cd. The average absorption was 2.41 mg/kg. The overground part of *Les-*

*pedeza bicolor* Turcz. had the least absorption of Cd. The absorption was only 0.65 mg/kg. The root of *Lolium perenne* L. had the highest absorption of

Table 2. Relative density and frequency of the dominant plants growing in the tailing pond.

No.	Plant species	Relative density %	Relative frequency %
1	<i>Lolium perenne</i> L.	11	16
2	<i>Vetiveria zizanioides</i> L.	10	7
3	<i>Miscanthus floridulus</i> Schum.	15	22
4	<i>Festuca arundinacea</i>	12	15
5	<i>Phytolacca americana</i>	4	3
6	<i>Conyza canadensis</i> (L.)	3	1
7	<i>Artemisia lavandulaefolia</i> DC	4	2
8	<i>Ficus tikoua</i>	8	5
9	<i>Rhus chinensis</i>	13	15
10	<i>Lespedeza bicolor</i> Turcz.	9	6
11	Other plants	11	8

Table 3. Content of heavy metals in plants Unit: mg • kg<sup>-1</sup>.

Plant species	Part	Pb	Zn	Cd
<i>Phytolacca acinosa</i>	Overground part	26.11	45.45	1.30
	Underground part	33.65	37.96	0.63
<i>Festuca arundinacea</i>	Overground part	7.21	55.22	0.65
	Underground part	4.33	71.12	0.98
<i>Artemisia lavandulaefolia</i> DC	Overground part	4.45	50.6	1.64
	Underground part	12.94	80.32	0.77
<i>Lolium perenne</i> L.	Overground part	12.45	47.24	1.03
	Underground part	27.04	85.70	1.16
<i>Caulis Fici Tikouae</i>	Overground part	215.26	78.12	2.41
	Underground part	57.35	32.32	2.09
<i>Rhus chinensis</i>	Overground part	17.60	96.15	1.54
	Underground part	8.32	5.64	0.42
<i>Miscanthus floridulus</i>	Overground part	18.64	76.28	1.08
	Underground part	4.05	64.52	0.74
<i>Vetiver grass</i>	Overground part	7.56	51.47	0.76
	Underground part	32.72	113.21	1.87
<i>Lespedeza</i>	Overground part	5.32	76.43	0.65
	Underground part	21.54	43.11	1.04
<i>Horseweed herb</i>	Overground part	5.43	45.33	1.62
	Underground part	3.12	35.54	1.04

Cd, which was up to 64.9 mg/kg. The root of *Rhus chinensis* had the least absorption of Cd, which was only 0.42 mg/kg.

A large difference was found in the content of heavy metals among the dominant plants. The overground part of the plants had the highest content of Zn. The average content was 63.01 mg/kg, ranging between 45.33 and 96.15 mg/kg. The overground part of the plants had a relatively high content of Pb. The average content was 34.76 mg/kg, ranging from 4.45 to 215.26 mg/kg. The average content of Cd in the overground part

of the plants was 1.34 mg/kg, with the range of 0.65–2.41 mg/kg. The roots of the plants had the highest content of Zn. The average content was 55.37 mg/kg, ranging from 5.64 to 113.21 mg/kg. This was followed by Pb, whose average content was 22.30 mg/kg with the range of 3.12–57.35 mg/kg. The roots of the plants had the lowest content of Cd. The average content was 1.08 mg/kg, ranging from 0.42 to 2.09 mg/kg.

The research showed that normal heavy metals of general plants included Pb (0.1–41.7 mg/kg), Zn (1–160 mg/kg), and Cd (0.2–3 mg/kg). Among the 10 kinds of dominant plants, the overground part of *Caulis Fici Tikouae* had a very high content of Pb. It showed that *Caulis Fici Tikouae* had a very strong absorbing ability towards Pb. Zn and Cd contents in the other dominant plants were positive, which showed that these plants had a strong ability to adapt to the environment, grow well in the environment with severe heavy metal pollution and had a certain heavy metal tolerance.

### 3.3 Transfer and absorbing characteristics of dominant plants towards heavy metals

Transfer Factor (TF) is defined as the ratio of heavy metal content in the overground part to the underground part of the plant. It is used to measure the plant's ability to transfer heavy metals. When the TF is greater than 1, it indicates that the plant can absorb an element from the underground part and transfer it to the overground part, so that the underground part absorbs a large amount of such heavy metal. This shows the plant's tolerant growth<sup>[11]</sup>. In a sense, the polluted soil can be treated with the plant extraction method. When the TF is less than 1, the plant will reduce toxicity through its own rejection mechanism and prevent the transfer of heavy metal elements absorbed by the underground part to the overground part.

From Table 4, we can see that the transfer factor of Pb in six kinds of plants is greater than 1, including *Lolium perenne* L., *Miscanthus floridulus*, *Festuca arundinacea*, *Caulis Fici Tikouae*, *Lespedeza*, and *Vetiver grass*; the transfer factor of Zn in seven kinds of plants is greater than 1, including *Phytolacca acinosa*, *Festuca arundinacea*, *Lolium perenne* L., *Caulis Fici Tikouae*, *Miscanthus floridulus*, *Vetiver grass*, and *Lespedeza*. The transfer factor of Cd in seven kinds of plants is greater than 1, including *Festuca arundinacea*, *Lolium perenne* L., *Caulis Fici Tikouae*, *Miscanthus floridulus*, *Vetiver grass*, and *Lespedeza*. In the lead–zinc tailing area with high content of Pb and Zn, six kinds of native plants whose Pb and Zn transfer factors are greater than 1 can be selected as the tolerant plants, including *Festuca arundinacea*, *Lolium perenne* L., *Caulis Fici Tikouae*, *Miscanthus floridulus*, *Vetiver grass*, and *Lespedeza*.

Table 4. Transfer factor and absorbing factor of heavy metal elements in plants Unit: mg • kg<sup>-1</sup>.

Plant species	Pb		Zn		Cd	
	TF	BCF	TF	BCF	TF	BCF
<i>Phytolacca acinosa</i>	0.82	0.06	0.20	0.22	0.18	0.01
<i>Festuca arundinacea</i>	1.13	0.17	1.54	0.68	1.11	1.23
<i>Artemisia lavandulaefolia</i> DC	0.60	0.03	0.84	0.25	0.65	0.05
<i>Lolium perenne</i> L.	1.42	1.10	1.60	1.02	1.92	0.10
<i>Caulis Fici Tikouae</i>	2.60	2.16	1.23	0.89	0.76	1.30
<i>Rhus chinensis</i>	0.68	1.05	0.78	0.22	1.73	0.09
<i>Miscanthus floridulus</i>	1.51	0.12	1.16	0.21	0.87	0.07
<i>Vetiver grass</i>	1.11	0.25	0.21	0.44	0.39	0.10
<i>Lespedeza</i>	1.18	0.24	1.10	1.28	1.10	0.09
<i>Horseweed herb</i>	0.73	0.22	0.95	0.42	0.18	0.02

Bioaccumulation Factor (BCF) is defined as the ratio of corresponding heavy metal content in the overground part of the plant and soil. It is used to measure the plant's ability to absorb and accumulate heavy metal elements in soil. It is one of the indices for evaluating the plant's ability to absorb heavy metals<sup>[12-17]</sup>. When the BCF is greater than 1, it shows that the heavy metal content in the overground part of the plant is greater than that in the soil environment where it grows, so the plants can be used for the restoration and control of heavy metal pollution in soil. It can be seen from Table 4 that *Caulis Fici Tikouae's* BCF of Pb is 2.16, and *Lespedeza's* BCF of Zn is 1.28. The BCF and TF of *Caulis Fici Tikouae*, *Lespedeza*, and *Lolium perenne* L. for Pb and Zn are greater than 1, which shows that *Caulis Fici Tikouae*, *Lespedeza*, and *Lolium perenne* L. have a strong ability to migrate and absorb Pb and Zn. They can be used for the ecological restoration of Pb and Zn-polluted area.

#### 4 CONCLUSION AND DISCUSSION

1. A total of 10 kinds of dominant plants growing in the Qiaokou & Yongxing Peng lead-zinc tailing area could be used as the plant restoration resources of the region. Herbaceous plants accounted for 70% of the dominant plants. They had a strong ability to adapt to the harsh environment prevalent in the Qiaokou & Yongxing Peng lead-zinc tailing area.
2. In the same sampling area, different plants obviously had different abilities to absorb heavy

metals, and the same kind of plants absorbed heavy metals differently in different sampling fields. It was shown that plant's absorption ability of heavy metals was mainly controlled by its own genetic mechanism, but the polluted environment could often domesticate plant species with strong tolerance or super-accumulation characteristics towards pollutants.

3. *Caulis Fici Tikouae*, *Lespedeza bicolor* Turcz., and *Lolium perenne* L. had a perfect ability to migrate and absorb Pb and zinc, and could be used for ecological restoration at the Pb and zinc-polluted site.

#### ACKNOWLEDGMENTS

This project was financially supported by the International Technology Cooperation Special Project (2012DFA90500); Research on Key Technology Cooperation for Comprehensive Improvement to Acidic Pollution in Metallic Mine Dump.

#### REFERENCES

- [1] He Xiaoyan. Soil Microbes—Plant Combined Repairment Technology of Heavy Metal Pollution in Industrial Zone [D]. Central South University of Forestry and Technology, 2005, 6. (In Chinese).
- [2] Chen C M, Liu M C. Ecological Risk Assessment on a Cadmium Contaminated Soil Landfill—A Preliminary Evaluation Based on Toxicity Tests on Local species and site-specific information [J]. Science of the Total Environment, 2006, 359(1/3): 120–129.
- [3] Tan Guie. Research of *Rychofragmus Violaceus* Restoring Cd-Zinc Polluted Soli and reinforcer effect by exogenous bacterium [D]. Shanghai University, 2007, 6. (In Chinese)
- [4] Eduardo Moreno-Jiménez, Jesús M. Peñalosa, Rebeca Manzano. Heavy metals Distribution in Soils Surrounding an Abandoned Mine in NW Madrid and Their Transference to Wild Flora [J]. Journal of Hazardous Materials, 2009, 162(2/3): 854–859.
- [5] Fairbrother A, Wenstel R, Sappington K.. Framework for Metals Risk Assessment [J]. Ecotoxicology and Environmental Safety, 2007, 68(2): 145–227.
- [6] Whiting SN, de-Souza MP, Terry N. Phizosphere Bacteria Mobilize Zn for Hyperaccumulation by *Thlaspi caerulescens* [J]. Environmental Science & Technology, 2001, 35:3144–3150.
- [7] Zhang XH, Lin AJ, Gao YL. Arbuscular mycorrhizal colonisation increases copper binding capacity of root cell walls of *Oryza sativa* L. and reduces copper uptake [J]. Soil Biology & Biochemistry, 2008, 26:1–6. (In Chinese).
- [8] Hao DAC, Ge GB, Yang, L. Bacterial diversity of axusrhizos here: culture-independent and culture-dependent approaches [J]. FEMS Microbiollet, 2008, 284(2):204–212.
- [9] Zhong Weizhen, Ecotoxicological Effect of Manganese Mine Tailings and Mn-Cd Combined Pollution on Plants [D]. Guangxi Normal University, 2008. (In Chinese).

- [10] Dong Sheqin, Li Bingwen, et al. Probe into the Mechanism of Hyper-accumulator Plants Absorbing the Heavy Metals in the soil [J]. *Taiyuan Science & Technology of China*. 2004, 1:64–66. (In Chinese).
- [11] Fang Hui, Cao Min, et al. Assessment of Heavy Metals Pollution in Abandoned Lead-Zinc Mine Tailings in Huize of Yunnan Province. [J]. *Chinese Journal of Ecology*, 2009, 28(7):1277–1283.
- [12] Cao H C, Luan Z Q, Wang J D, Zhang X L. Potential Ecological Risk of Cadmium Lead and Arsenic in Agricultural Black Soil in Jilin Province, China [J]. *Stoch Environ Res Risk Assess*, 2009, 23(1): 57–64. (In Chinese).
- [13] Fan Nimai. Lead Absorption and Physiological and Ecological Characteristics of *Buddleja Officinalis* Maxim [D]. Kunming University of Science and Technology, 2008, 3. (In Chinese).
- [14] CAO De-ju, WANG Guang-yu, et al. Accumulation of Heavy Metals in Dominant Plants Growing on Mineral Areas in Anhui Tongling [J]. *Journal of Agro-environment Science China*, 2005, 24(6):1079–1082. (In Chinese).
- [15] Sun Qingye, Lan Chongyu, et al. Natural colonized plants on tailings of Lead-Zinc mine [J]. *Acta Ecologica Sinica of China*, 2001, 21(9):1457–1462. (In Chinese).
- [16] Jiang Xianjun, Luo Yongming, et al. Study on Phytoremediation of Heavy Metal Polluted Soils [J]. *Acta Pedologica Sinica of China*, 2002, 39(5): 664–670. (In Chinese)
- [17] Zhang Hanbo, Duan Changqun, et al. Dynamic of Heavy Metals in a Lead-Zinc Tailings Deposited in Different Years [J]. *Journal of Agro-environment Science (China)*, 2003, 22(1): 67–69.

# Research on development and utilization of the empty layer space of Nanjing Weisanlu Yangtze River Tunnel

Li-chang Su, Xing-ping Zhu, Xin-yuan Zu & Wei-na Hou

Research Center of Underground Space, PLA University of Science and Technology, China

**ABSTRACT:** The empty layer space of the city traffic tunnel is an important part of the underground space resources. The development and utilization of these empty layer spaces is of great significance to the sustainable development of a city. It is a meaningful practice to build the empty layer space of Nanjing Weisanlu Yangtze River Tunnel and the surrounding underground space into an underground parking garage. The characteristics of the empty layer space of Nanjing Weisanlu Yangtze River Tunnel are analyzed, and the key points for its planning and design as well as its optimization are described in an attempt to provide reference for future development and utilization of the empty layer space of city traffic tunnels.

**Keywords:** The empty layer space; development and utilization; the city traffic tunnel

## 1 INTRODUCTION

When excavating foundation pits, building retaining walls and constructing loops in city traffic tunnels, a lot of supporting building spaces and abandoned structures that are not used for tunnel traffic will be produced, namely, the empty layer space of traffic tunnels. After the construction of traffic tunnels is completed, the empty layer space is often filled with debris, which not only causes a waste of large underground space, but also leads to irreversible consequences and security risks. This is not in line with the overall goal of environmental protection and low carbon construction for modern cities. If the empty layer space of traffic tunnels is not reasonably developed and utilized for a long time, it will cause an immeasurable waste of urban underground space resources.

With the popularization of the idea of sustainable urban development, people gradually realize the importance and urgency of developing and utilizing the empty layer space of traffic tunnels. In the construction process of Nanjing Weisanlu Yangtze River Tunnel, to build its empty layer spaces and the surrounding underground space into an underground parking garage not only realizes the reuse of empty layer space resources of traffic tunnels, but also satisfies the surrounding area's needs for public parking facilities.

## 2 EMPTY LAYER SPACE OF WEISANLU YANGTZE RIVER TUNNEL

### 2.1 Site analysis copy the template file copying old text onto new file

The empty layer space of Nanjing Weisanlu Yangtze River Tunnel is located in the intersection of Dinghuaimen Street and Yangziji Jiang Avenue. As shown in Fig. 1, the Tunnel connects to Yangziji Jiang Avenue, Dinghuaimen Street, Zhenghe South Road, Lijiang Road, Jiangdong North Road and



Figure 1. Location map for the empty layer space of Weisanlu Yangtze River Tunnel.

Longyuan West Road. The riverside scenery belt to the west of the Tunnel is a golden riverside line in the Nanjing section of Yangtze River, which is characterized by the most representative façade features of main urban zone and the functions of waterside zone. It is planned that a comprehensive orbit transfer hub will be built, namely, Public Transit Hub of Treasure Ship Ruins Park. In the future, it will integrate the functions of modern business, leisure and sightseeing, tourism and shopping, as well as high-grade residence, and will become the most distinct industrial development belt along the Yangtze River and one of the most important living and recreational zone in Nanjing.

## 2.2 Spatial composition

The empty layer space of Weisanlu Yangtze River Tunnel consists of abandoned space, the nearby space to be filled and the nearby additional space, as shown in Fig. 2.

### 2.2.1 Abandoned space

Abandoned space refers to the empty layer space of the traffic tunnel in the narrow sense. It is located right above the Yangtze River Tunnel space and has two layers: upper layer and lower layer. Seeing from the floor plan, the empty layer space is rectangular. As it shares the retaining walls with the Tunnel, it has the same width with the Tunnel.

### 2.2.2 Nearby space to be filled

The nearby space to be filled refers to the empty layer space of the Tunnel in the broad sense. The excavation space for the open excavation section of Weisanlu Yangtze River Tunnel is greater than the width of the Tunnel, so the excavation will produce the spaces on both sides of the abandoned space

right above the Tunnel, which are to be filled with debris.

### 2.2.3 Nearby additional space

Nearby additional space also refers to the empty layer space of the Tunnel in the narrow sense. Such space is near to the Tunnel space, but is not within the excavation scope of the Tunnel. It is generally located below the open ground plane next to the Tunnel and easily connects to the above abandoned space and nearby space to be filled.

## 3 KEY POINTS FOR PLANNING & DESIGN AND ITS OPTIMIZATION TEXT AND INDENTING

### 3.1 Layout plan

Restricted by the Yangtze River Tunnel and Ground Overpass, the underground parking garage for the empty layer space of Weisanlu Yangtze River Tunnel is irregularly triangle. As shown in Fig. 3,

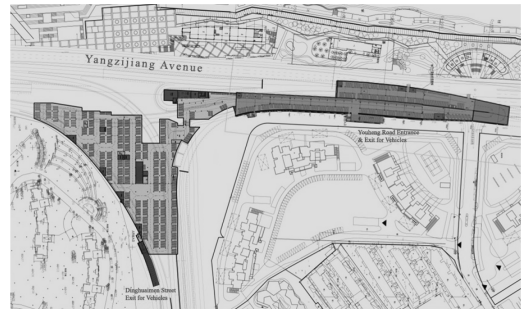


Figure 3. Floor plan for underground parking garage.

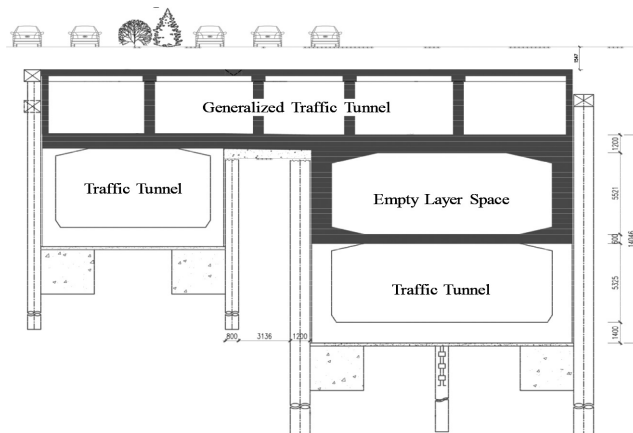


Figure 2. Spatial composition of the empty layer space of Weisanlu Yangtze River Channel.



the parking garage is 454.30 m from north to south and 157.53 m from east to west. The garage is a two-floor underground building and has a construction area of 22449.18 m<sup>2</sup>. The newly built garage has an area of 12,409.76 m<sup>2</sup>; the construction area of the empty layer space used is 3,363.57 m<sup>2</sup>; the construction area of the overhead part of the empty layer space is 5,892.29 m<sup>2</sup>; the construction area for the entrance and exit of the garage is 783.65 m<sup>2</sup>; The top of the triangle garage is covered by green vegetation.

### 3.1.1 The parking garage at the first floor underground

The parking garage at the first floor underground is built on the 6–8 m overburden layer between Yangzijiang Avenue and Weisanlu Yangtze River Tunnel, whose average storey height is 5.2 m with a construction area of 6,055.8 m<sup>2</sup>. There are 180 parking spaces, and two of them are designed for the disabled. In the north of the garage, there are the entrance and exit to the parking garage at the second floor underground, the management room and the supporting facilities. In the south of the garage, there are a fire-water pool and a water pump house.

### 3.1.2 The parking garage at the second floor underground

The parking garage at the first floor underground is built by using the empty layer space of Weisanlu Yangtze River Tunnel and the underground space of the triangle greening belt connecting Yangzijiang Avenue and Dinghuaimen Street. It has a construction area of 19,605.24 m<sup>2</sup>. There are 460 parking spaces, and three of them are designed for

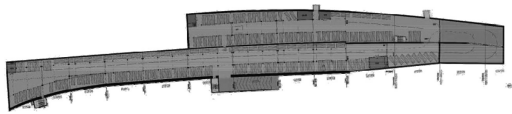


Figure 4. Floor plan for the parking garage at the first floor underground.

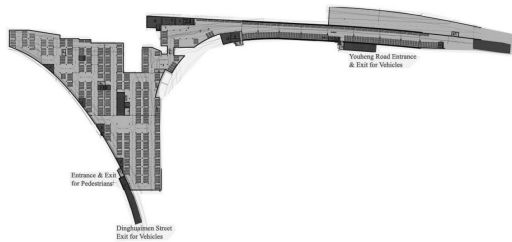


Figure 5. Floor plan for the parking garage at the second floor underground.

the disabled. In the north of the garage, there are the entrance and exit to the parking garage at the first floor underground. The vehicles can directly get to the intersection of Yangzijiang Avenue and Youheng Road through the garage at the first floor underground. In the limited space area, the management room and supporting house are rationally built so that the irregular underground space is well-designed.

## 3.2 Space form combination

### 3.2.1 External SpaceForm

To some extent, the internal functions of the underground parking garage built from the empty layer space of Weisanlu Traffic Tunnel affect its external spatial form. As shown in Fig. 6, as the upper part of this underground garage is an urban trunk road, attention should be paid to the guarantee of smooth ground traffic. On the one hand, the urban trunk road should meet urban traffic's demands for external form and structure; on the other hand, the urban truck road can also be seen as the external form of the underground parking garage made from the empty layer space. The irregular triangular part is located below the Overpass, and the external space form is restricted by the traffic roads, so it has been planned as a greening belt.

### 3.2.2 Internal space form

The floor plan of underground parking garage also affects the internal space form. The Yangzijiang Avenue section of the underground parking garage made from the empty layer space of Weisanlu Traffic Tunnel has two underground floors, which form a three-layer space together with the Yangtze River Tunnel. As the parking garage in this section is consistent with the Yangtze River Tunnel below it, a narrow space form comes into being. The three-layer space connects to each other through



Figure 6. Aerial view of external form of underground parking garage.

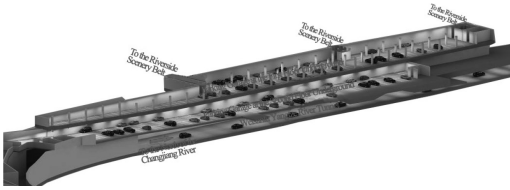


Figure 7. Perspective view for the underground parking garage in the northern section of Yangzijiang Avenue.



Figure 8. Perspective view for the underground parking garage below the Overpass.

the staircases on both sides and the motor vehicle ramps on both ends, breaking the enclosed underground space and providing comfortable internal space of underground parking garage for the users.

### 3.3 Planning and settings for entrance and exit

To develop and utilize the empty layer space of Weisanlu Yangtze River Tunnel into an underground parking garage, we should not only take into account the motor vehicle flow on the external trunk roads, but also consider how to bring convenience to the pedestrian flow in the surrounding residential communities. Only in these ways can we design appropriate entrance and exit for vehicles and pedestrians. Based on the analyses of the surrounding vehicles and pedestrians, three entrances and exits are designed for vehicles, while 10 entrances and exits are designed for pedestrians.

#### 3.3.1 Entrance and exit for vehicles

The main body of this underground parking garage is located at the Jiangnan Untwining Overpass of Weisanlu Yangtze River Tunnel, namely, the intersection of Dinghuaimen Street and Yangzijiang Avenue, the northern part of Haideweicheng to the south. The Yangzijiang Avenue is west to Jiajiang and Riverside Scenery Belt. Therefore, the parking requests of the underground parking garage mainly come from three directions: north,

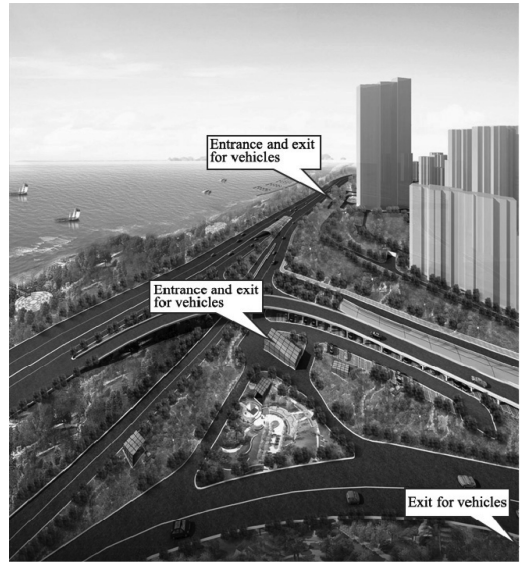


Figure 9. Entrance and exit for vehicles in the underground parking garage.

east and south. In the north of the parking garage, limited by the external Qinghuai River, the traffic flow mainly comes from Xiaguan Bridge and Sancha River Bridge; the traffic flow in the east mainly comes from Dinghuaimen Street; the traffic flow in the south mainly comes from Yangzijiang Avenue.

According to the parking space construction scale and relevant construction standards of the underground parking garage, two double-lane entrances and exits and one single-lane exit are designed for motor vehicles, namely, the Youheng Road Entrance and Exit for parking requests from the north, the Greening Belt Entrance and Exit for parking requests from the east and the south, and the Exit to the east of the northern Haideweicheng.

#### 3.3.2 Entrance and exit for pedestrians

In accordance with the people-oriented principle, the setting of entrance and exit for pedestrians should facilitate their fast access to the underground parking garage and the ground destination, as shown in Fig. 10. People come out of the underground parking garage in order to reach the surrounding residential and office buildings or the Riverside Scenery Belt. The distance between neighboring entrances and exits for pedestrians is no more than 100 m, which effectively shortens the distance between the underground parking garage and the ground destination. In addition, as the greening belt for the Overpass has a

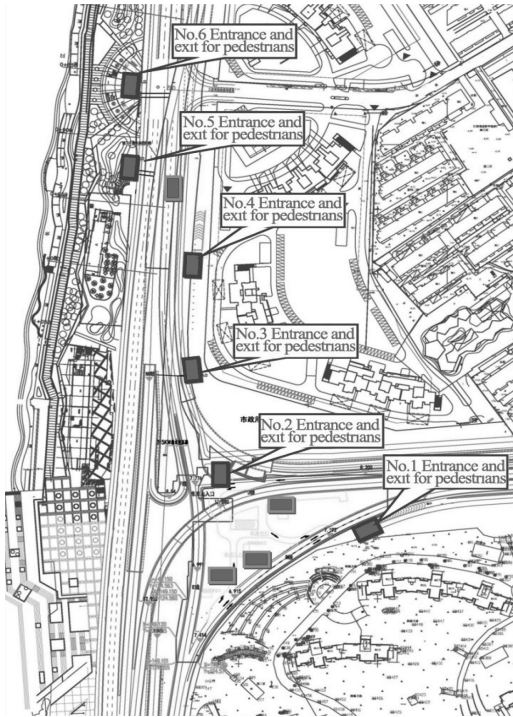


Figure 10. Entrance and exit for pedestrians in the underground parking garage.

large area, four entrances and exits for personnel evacuation are designed to meet the evacuation needs.

#### 4 CONCLUSIONS

The construction of the empty layer space of Nanjing Sanweilu Yangtze River Tunnel and the surrounding underground space into an underground parking garage accords with the city's sustainable development requirements, avoids the simple non-recoverable abandonment behavior that just pursues short-term economic benefits, effectively enhances the development level and utilization rate of urban underground space, and facilitates the city's future development.

#### REFERENCES

John Zacharias (2007). A Decision Support System for Planning Underground Space. *Urban Planning International*, 2(22):45–48.

John Zacharias (2011). Planning Future Cavern Development in Hong Kong. *Proceedings of the Joint HKIE-HKIP Conference on Planning and Development of Underground Space*, 9:25–28.

Parriaux (2004). The hidden side of cities—towards three-dimensional land planning. *Energy and Buildings*, 12(36):123–126.

Raymond L. Sterling (2005). *Underground Space Design*. Louisiana: John Wiley & Sons Inc.

Tsutomu Ikeda, Masami Yokotsuka (2009). Study of Underground Space Utilization for Urban Renaissance Tokyo's Yaesu District. *Proceedings of 12TH International conference of the Associated Research Centers For Urban Underground Space*, 11:456–458.



**Taylor & Francis**

Taylor & Francis Group

<http://taylorandfrancis.com>

## Study of rural landscape design ideas

Xin-yue Zhang

*Art and Design Department, Lijiang River College of Guangxi Normal University, Guangxi, China*

**ABSTRACT:** In this paper, Guilin Dongjiang River Basin was taken as the research object. New ideas of current rural landscape design were searched from the perspective of studies based on the types of rural landscape. This paper was gradually expanded from the aspects of scale, ecology, and humanity with the gradual deepening of the problem. Each aspect is provided with different corresponding design methods. The author tried to expand the new space of the landscape aesthetic field by the design method of the countryside landscape.

**Keywords:** rural landscape; sustainable; design method

### 1 INTRODUCTION

Urbanization and industrialization are inevitable trends of historical development, which provide a brilliant prospect for constructing and developing towns and villages. However, Lao-tzu states that “misfortune might be a blessing in disguise, and vice versa, picturesque villages and towns are changed into the same pattern like products produced on the same production line due to standard construction of ‘forming field into square shape, making roads into network, connecting channels as a whole, and planting trees into rows’ in urbanization”. Local culture that makes us proud also disappears with the environmental inorganic and simplification process.

Rural tourism acts as an important complement and extension in the Guilin tourism industry. Rural tourism landscape design, as a complement to Lijiang’s characteristic tourism landscape, has strong territorial and appreciative features. It has been proposed to aim at gradually and manually solving the environment without consideration of humanity in the rural urbanization process. It is an expanded and well-accepted tourism resource, which has become popular among the majority of tourists. Rural tourism landscape design has the most prominent characteristic such as quietness, dignified sense and sense of ease different from the city. Laozhai located in the Dongjiang River Basin is a typical representative.

### 2 COUNTRYSIDE LANDSCAPE FEATURES—INSIDE AND OUTSIDE INTERACTION

Magic Yao Nationality Laozhai is located in the east of Guilin, intersecting between Lingchuan

Town, Xing’an Town, and Longsheng Town. Xiaodongjiang River is so clear that its bottom can be clearly seen, and it winds from the east and north along Qingshitian. The village road alongside the river also winds along the direction of the water flow, which is more than 70 kilometers long. A village called Dongyuan is located near the Xiaodongjiang River. There are two stockaded villages at Dongyuan Village, respectively, located in two columns, one is called Laozhai and the other Xinzhai. The stockaded villages are built on the hillside, which are composed of more than 100 households and 400 villagers. Every household has a hibiscus, which belongs to the wooden structure pile-dwelling building with the characteristics of a Yao nationality folk house and is well preserved. When the stockaded village is observed from the hillside or from the bottom of the hill, hibiscuses stand on the hillside orderly, which are surrounded by tall trees and bamboos as well as gurgling rivers.

The mountainous countryside landscape is completely different from the urban landscape as follows: First, the mountainous countryside landscape is mostly completely created by labor with few machines, thereby avoiding fatal damage to the nature; second, the countryside landscape refers to the terrace, living, and labor landscape of Yao nationality. Such a mountainous countryside landscape is not modified, which focuses on residents’ participation. Villagers do not create them painstakingly according to the visual experience, who are linked with the surrounding environment through life and labor. Such an intimate involvement interaction is an important feature of the countryside landscape. The countryside landscape only belongs to “an empty symbol, a dead event

and meaningless experience with deep aesthetics” without the above-mentioned inside and outside interaction.

### 3 CREATION OF THE COUNTRY LANDSCAPE

Countryside landscape design learning from villages should be a direction that should be applied to urban design and rural urbanization construction. However, the city has its own characteristics and many facts that cannot be avoided. Therefore, it is very important to apply some design means of countryside design to create the urban landscape.

#### 3.1 *Affinity*

##### 3.1.1 *Humanity scale*

Cultivated land scale and stone wall height can be basically formed within the human labor scope in the village area. For example, orchards created in Laozhai along the hillside are mostly constructed along the contours. Generally, the piled stone wall cannot be as high as the human stature. Fields are also divided according to the daily cultivable area of the farmer as the unit. It can be summarized that the human spatial scale is important to create the affinity landscape.

Therefore, it is critical to change “generalized” inertia thinking. Human intervention should be minimized on the basis of meeting the required conditions. For example, the bottom load-bearing parts are made up of stones or bricks on the external wall of many old buildings in the town, and the upper parts are made up of soil, tiles, or timber. Currently, similar conditions are also discovered on the treatment of some water supply channels. Soil under the outfall can be easily eroded, and some scattered stone or iron networks are placed under the soil. The natural base is still kept in other places. We have a lesson to be learnt from such a vivid and prudent method.

##### 3.1.2 *Blur function*

Function mobility and diversity are pursued in the countryside landscape. For example, the shrine is used as a venue for the banquet during weddings and funerals. Farm equipment can be used in the shrine during the spare time. Farmland not only acts as a venue for drying fodder and grains, but also provides the best playground for children during the harvest season. Such a landscape design with multiple functions is more worthy of promotion and promotion in the modern city with increasingly insufficient land.

#### 3.2 *Ecology*

##### 3.2.1 *Diversified terrain*

Soil has multiple relationships with humans. Soil, as the environment of an organism’s growth, can be observed everywhere. However, soil is covered under thick stones and cement in the city. The design and application of soil cannot be ignored in the creation of the landscape with beautiful ecology in the urban environment.

First, application of soil to a large area is a foundation for reconstructing a sound ecological environment in the city. Ground surface water can be easily eroded without land and micro-topographical change. It is not easy to form a rich vegetation. Second, a rich terrain can be easily formed by land accumulation, and a unique and flat urban landscape can become more vivid and vibrant. Therefore, creation of a diversified terrain by soil and formation of the landscape with countryside fun depend on the method with a prominent effect on the city with complex functions. Schwartz shaped soil humps in different sizes on the landscape by a bulldozer in front of a Minneapolis federal court. Soil lump shapes become organic and diversified due to better fabricability of the soil.

##### 3.2.2 *Permeable base surface*

Rural areas are basically composed of porous materials. For example, there are many holes on the surfaces of roads, rivers, and arable land. Many gaps are formed at the joints of materials. Therefore, rainwater can penetrate into these gaps naturally. Plants can grow freely, and manual landscape can be integrated into a natural environment. But that does not mean a complete avoidance of artificial materials; the originally compacted materials can be provided with porous and permeable surfaces for plant growth through proper processing and transformation.

#### 3.3 *Spirituality*

##### 3.3.1 *Quietness—conversion of heart*

Several conditions are required for creating the beauty of quietness in the countryside landscape. First, it requires the availability of rich biological communities. Wild birds, fish, and shrimps appearing from time to time provide people with the opportunity to contact with a variety of creatures in the countryside. They arouse pity and sympathy in the human mind from instinct. We produce the same emotion as that of Miyazaki’s “Farewell Firefly”. The firefly in the film is important for creating such a warm and poignant visual experience. Second, landscapes with gentle and small undulating

curve forms in the countryside are beneficial for calming down mood and making people quiet. In addition, fruit trees and agricultural environment strongly stimulate people's taste experience. They can meet the basic dependence of humans on food to a certain extent.

### 3.3.2 *Comfortableness*

Kevin Lynch states that: "neighborhoods, markers or roads should be easily identified in a readable city", and then she added that: "a high-quality environment image can make the owner to emotionally produce very important sense of security...". It is a sense of country to the sense of fear after disorientation. In fact, the countryside landscape is composed of a number of readable images. For example, river and road directions form a stark direction; therefore, it is easy to understand geographical regions. The entrance to the village is always surrounded by leafy trees as markers. In the city, creation of a readable and understandable regional marker landscape is beneficial for increasing the ease of sense in the urban space.

### 3.3.3 *Dignity*

A person's life is short. However, the nature is broad and far-reaching so that the object in nature can form a kind of beauty with an ancient sense along time and accumulation. They can be integrated into the surrounding natural environment, although they can be gradually extinguished. Humans are unable to retain their calm in face of such deep and intriguing vicissitudes in nature. This is dignity which is produced in the countryside landscape.

Beauty may be created by roadside mossy stones, a section of weathered fence in the field, a mottled lime wall or a wood-side desert melon outside the house. Natural stones, bricks, wood, and other organic materials are mainly used for producing such beauty of dignity. They constantly change with time. Therefore, some tiny landscapes with historical significance should be added to the

urban landscape for evoking a historical sense of the places, which can be created by an old stone, a dead tree or some old photos in the city.

## 4 CONCLUSION

Some features of the rural landscape are adopted as a reference for aiming at the pursuit of a landscape design on the harmonious coexistence between human and nature, originating from reality. This paper started with excessively radical and extensive reality in the urbanization process, "landscape morphology" – a graduate course of environment art in the Chinese Academy of Fine Arts School of Architecture—which was combined for primarily discussing the basic methods of the countryside landscape design, and some design strategies and ideas were provided for the city landscape design.

## ACKNOWLEDGMENT

1. This study was funded by the 2015 Guangxi College and University Research Project "Research on Guilin Rural Tourism Planning and Designing under Human Habitat and Humanity Spirit—with Guilin Jiuwu Bojitang as Example". Project number: KY2015 LX759;
2. This article was funded by the 2016 Teaching Reform Project of Guangxi College and University Education "A Research on the Value of Ancient Dwelling in the Northern Guangxi". Project number: (YB2014603).

## REFERENCES

- [1] Zhang Lin. Planning Research Theory of Agricultural Sightseeing Garden. Heilongjiang. Northeastern University, 2006.
- [2] Wang Xiangyun. On Revelation of Traditional Folk Houses on Modern Residential Architecture Culture. South Architecture, 2004 (6).



**Taylor & Francis**

Taylor & Francis Group

<http://taylorandfrancis.com>



## Author index

- Ai, Z.S. 175
- Cai, F. 241  
Cai, S.-F. 273  
Cao, Z.-L. 19, 303  
Cen, C.-X. 269  
Chai, S.B. 209  
Chang, S.-X. 289  
Chen, B. 107  
Chen, C. 373  
Chen, F.-L. 81  
Chen, G.-S. 71  
Chen, H.-Y. 19, 303  
Chen, J.-Y. 341  
Chen, L.-L. 5  
Chen, S.-L. 355  
Chen, S.-Y. 145  
Chen, W.-G. 71  
Chen, Z.-G. 233  
Chen, Z.-T. 345  
Cheng, D.-L. 299  
Choi, E. 191  
Cui, M. 227
- Deng, W.-Y. 203  
Deng, X.-S. 159  
Ding, P.-L. 141, 245, 363  
Ding, X.-S. 321  
Ding, Y.-N. 313, 337  
Dong, F.H. 133  
Dong, X.-M. 151  
Du, Z.-Q. 317
- Fan, L. 37  
Fu, J.X. 175
- Gai, J.-Y. 331  
Gao, J. 141, 245, 363  
Gao, M. 93, 125  
Gao, Y. 317  
Ge, Z.-X. 295  
Geng, Y.-Z. 15  
Gong, H.-D. 219  
Gong, J. 31  
Gong, J.-P. 379  
Gu, J. 383
- Guo, K. 31  
Guo, M.-L. 1
- Hao, L.-S. 5  
He, W.-L. 151  
Heng, W.-W. 257  
Hibino, M. 19, 303  
Hou, W.-N. 397  
Hu, M. 141, 245, 321, 363, 379  
Huang, D.N. 175  
Huang, L.-M. 341  
Huang, S.-P. 1  
Huang, W.-K. 273  
Hui, J.-X. 317
- Jia, Y.-C. 289  
Jiang, S.-C. 15  
Jiang, X.-L. 85
- Kim, N. 191
- Lai, K. 169  
Lao, Y.-C. 145  
Lee, J. 383  
Lee, J. 383  
Li, B. 379  
Li, C.-H. 321  
Li, L.-M. 359  
Li, M.-H. 145  
Li, N. 215  
Li, Q. 219  
Li, T. 219  
Li, W.-J. 345  
Li, X.-D. 345  
Li, Y. 379  
Liang, M.-Y. 295  
Lin, C.-C. 25  
Lin, C.-C. 355  
Lin, C.-Y. 355  
Lin, M.-H. 355  
Liu, C.-L. 359  
Liu, J. 49  
Liu, W. 163  
Liu, X.-K. 317  
Liu, X.-N. 351  
Liu, X.-P. 373
- Liu, Y.-C. 355  
Liu, Z.-M. 359  
Liu, Z.-Z. 15  
Lou, C.H. 133  
Lou, Y. 309  
Lu, B. 65  
Lu, H.-L. 107  
Lu, J. 77  
Lu, Q. 249  
Luo, W. 37  
Lv, C.L. 209  
Lv, F.-X. 289
- Ma, C.-L. 321  
Ma, M. 209  
Ma, X. 195  
Mei, S.-Q. 31  
Meng, X.-K. 257  
Meng, X.-Z. 351  
Mi, L. 45  
Mi, S.-D. 19, 303  
Miao, P.-H. 163
- Ni, Y.-B. 59  
Niu, G. 71  
Niu, J.-T. 151
- Pang, B. 37  
Park, J. 191  
Peng, C. 351
- Qian, J.-Q. 107  
Qiao, Y. 325, 367  
Qiu, J. 99
- Rao, X.-C. 65  
Ren, X. 209  
Ren, X.-F. 119  
Ren, X.-X. 141, 245  
Rong, H.-L. 273
- Shao, L.-L. 387  
Shao, Z.-H. 379  
Shen, Q. 59  
Shi, J. 313  
Si, W. 199, 237

Su, L. 31  
 Su, L.-C. 219, 223, 341, 397  
 Su, Y.-F. 137  
 Su, Y.-X. 203  
 Su, Z.-C. 19, 303  
 Sui, X.-P. 15  
 Sun, B. 155, 159  
 Sun, B. 253, 285  
 Sun, C.Z. 325, 367  
 Sun, H.-B. 103  
 Sun, W. 391  
  
 Tan, H.Y. 215, 241  
 Tan, J. 175  
 Tang, C.Y. 215  
 Tang, J. 337  
 Tang, W.-F. 181  
 Tian, S.-L. 227  
 Tian, Y.X. 185  
  
 Wan, C.-Y. 107  
 Wang, C.-C. 355  
 Wang, C.-H. 55  
 Wang, J.-J. 37  
 Wang, L. 279  
 Wang, N.-X. 249  
 Wang, P. 137, 387  
 Wang, Q. 65  
 Wang, Q. 391  
 Wang, S.-Y. 163  
 Wang, X.-J. 309  
 Wang, Y.-F. 31  
  
 Wang, Y.-Q. 169  
 Wang, Z.B. 325, 367  
 Wang, Z.R. 185  
 Wei, G.-F. 195  
 Wei, L.-Y. 19, 303  
 Wei, Z.-Z. 151  
 Wu, J. 11, 41  
 Wu, L.-L. 391  
 Wu, S. 15  
 Wu, W.-T. 25  
 Wu, Z.-B. 85  
  
 Xia, X. 331  
 Xie, H.-B. 31  
 Xie, J.-H. 159  
 Xie, L.-F. 113  
 Xie, M.-W. 289  
 Xin, Y.-X. 169  
 Xu, B.B. 199, 237  
 Xu, C.-J. 261  
 Xu, H.-J. 269  
 Xu, W.-Q. 71  
 Xue, Y.-F. 203  
  
 Yan, L.-H. 299  
 Yan, Z. 257  
 Yang, H. 345  
 Yang, Y. 85  
  
 Zeng, C. 257  
 Zeng, S. 155  
 Zhai, J. 137  
 Zhang, H.B. 209  
  
 Zhang, H.-M. 351  
 Zhang, J. 65  
 Zhang, J. 155  
 Zhang, J.S. 279  
 Zhang, M.-H. 387  
 Zhang, M.-X. 253, 285  
 Zhang, S.-Q.-Y. 159  
 Zhang, X.-N. 273  
 Zhang, X.-Y. 253, 285  
 Zhang, X.-Y. 403  
 Zhang, X.-Z. 203  
 Zhang, Y. 233  
 Zhang, Y.-H. 379  
 Zhang, Y.-L. 141, 245, 321, 363, 379  
 Zhang, Y.-M. 321, 379  
 Zhang, Y.-R. 37  
 Zhang, Y.-X. 37  
 Zhang, Z.-G. 359  
 Zhang, Z.-H. 129  
 Zhao, J.-F. 119  
 Zhao, T.-L. 99  
 Zhao, Y.F. 185  
 Zhao, Y.J. 175  
 Zhao, Z.-C. 265  
 Zhou, J.-L. 113  
 Zhou, Q.-H. 59  
 Zhou, W. 65  
 Zhou, X.-L. 107  
 Zhu, S.-B. 107  
 Zhu, X.-P. 397  
 Zu, X.-Y. 223, 397  
 Zuo, G. 325, 367